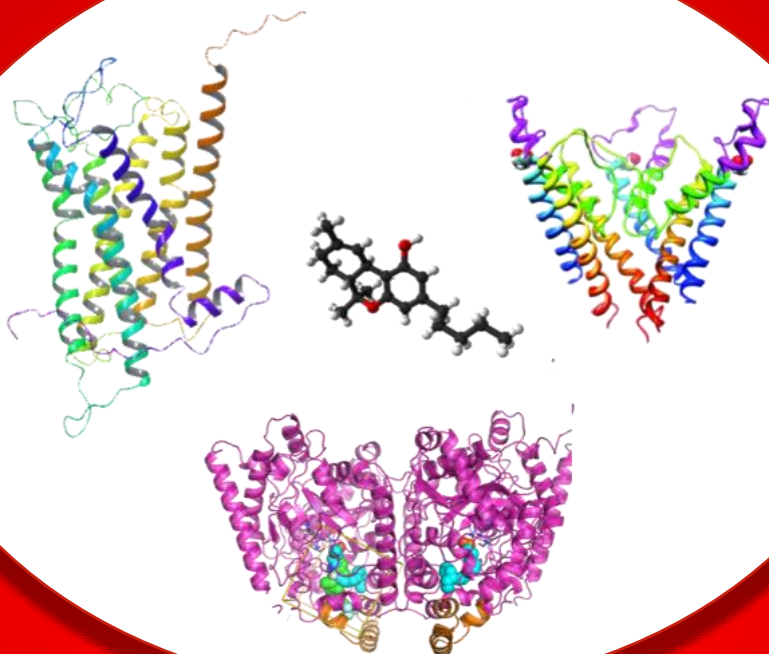# PhD Program in Pharmaceutical Science and Technology

Design, synthesis and SAR of small molecules acting on pain pathways

PhD Student: Dr. Alessandro Deplano
Supervisor: Prof. Valentina Onnis

University of Cagliari
Department of Life and Environmental Sciences

Università degli Studi di Cagliari

DOTTORATO DI RICERCA

Scienze e Tecnologie Farmaceutiche
Ciclo XXVIII

TITOLO TESI

Design, synthesis and SAR of small molecules acting on pain pathways

Settore scientifico disciplinare di afferenza
CHIM-08
Settori ERC
LS7_3; PE5_7

Presentata da	Dott. Alessandro Deplano
Coordinatore Dottorato	Prof. Elias Maccioni
Tutor	Prof.ssa Valentina Onnis

Esame finale anno accademico 2014 – 2015

University of Cagliari

PhD Course in

Pharmaceutical Science and Technology

XXVIII Cycle

PhD Thesis

Design, synthesis and SAR of small molecules acting on pain pathways

SSD

CHIM-08

ERC

LS7_3; PE5_7

Presented by   Dr. Alessandro Deplano

Supervisor   Prof. Valentina Onnis

PhD Coordinator   Prof. Elias Maccioni

Final Exam of academic year 2014 – 2015

Index

5   Full Papers   321

I.   Acknowledgements

II.   Abstract

Pain is a pathological disease that constitutes one of the most important problems of public health. Epidemiological studies showed that about 20% of the Europe population is affected by moderate or chronic pain. This data highlighted the gigantic impact of this problem not only in the suffering people but also in term of costs for public health. The classes of drugs most used today in the treatment of pain are NSAIDs and opioids. Unfortunately, both have important side effects specially when used in chronic treatment. Therefore, the research of new drugs which exploiting new targets that have an analgesic effect without the side effects is important.

This thesis describes the design, synthesis and biological activity of compounds which have potential analgesic activity by their action on three different pathways involved in pain information transmission.

1. The first class of compounds, are amide derivatives of the principal NSAIDs or correlated molecules, they are designed to be able to interact with the endocannabinoid system. In particular, described compounds were designed and tested as inhibitors of FAAH, the principal enzyme involved on the metabolization of endocannabinoids. The aim was to cause an increase of the endocannabinoids concentration which leads to analgesic effect by the potentiation of the endocannabinoid tone. Some of the studied compounds showed inhibitory activity against FAAH at micromolar to nanomolar concentrations.

2. The second class of compounds were designed to interact with prokineticin system. Numerous studies highlighted the involvement of this system in different physiological processes including nociception. Activation of these receptors on the neurons on the pain pathways produces hyperalgesic effects. Therefore, the development of prokineticin receptor antagonists could be a new strategy for pain therapy. Compounds described in this thesis are endowed with triazinedione structure. A new synthetic procedure was set up allowing yields up to 50% higher than reported for analogue compounds. The triazinediones showed in vivo

analgesic activity at picomolar concentrations and demonstrated antagonistic activity on prokineticin receptors.

3. The third target on which the compounds reported in this thesis act is the channel-receptor TRPV1, which is an important component of pain information transmission pathways. TRPV1 opening causes an influx of positive ions inside the cell that lead to its depolarization and consequent propagation of the information on the upper levels. In this case then the block of this channel with antagonist or molecules that cause receptor desensitization could result in an analgesic effect. The above mentioned triazinediones demonstrated a modulatory activity component against TRPV1 receptor, which may explain at least in part their in vivo analgesic activity.

III. Riassunto

Il dolore inteso nella sua forma patologica quindi non come strumento utile alla sopravvivenza dell'uomo è uno dei più importanti problemi legati alla salute pubblica. Studi epidemiologici hanno mostrato che il dolore, da moderato a cronico, è presente in circa il 20% della popolazione Europea. Questo dato mette in luce il grosso impatto che ha questo problema non solo sulla persona affetta da queste patologie ma anche in termini di costi per la sanità pubblica. Le classi di farmaci utilizzate al giorno d'oggi per questo problema sono principalmente due, i FANS e gli oppioidi, purtroppo entrambe presentano importanti effetti collaterali soprattutto legati al loro utilizzo in terapie croniche. Quindi la ricerca di nuovi target coinvolti nella mediazione dell'informazione dolorosa riveste un ruolo molto importante.

In questa tesi vengono descritte la progettazione, la sintesi e l'attività biologica di composti che possiedono potenziali attività analgesiche in quanto agiscono su tre diverse vie implicate nella trasmissione del dolore.

1. I primi composti, derivati ammidici dei principali FANS o di molecole correlabili, sono stati studiati per essere in grado di interagire con il sistema cannabinoide. In particolare i composti descritti sono stati progettati e testati come inibitori del principale enzima deputato alla metabolizzazione degli endocannabinoidi, la FAAH, con lo scopo di ottenere un effetto analgesico dovuto all'aumento dell'attività del sistema cannabinoide. Alcuni dei composti studiati hanno mostrato un'attività inibitoria nei confronti della FAAH variabile da micromolare a nanomolare.

2. I secondi invece sono stati progettati per interagire con il sistema delle prokineticine. Numerosi studi hanno evidenziato il coinvolgimento di questo sistema in diversi processi fisiologici tra cui la nocicezione, infatti l'attivazione di questi recettori a livello dei neuroni delle vie del dolore ha effetti iperalgesici. Quindi lo sviluppo di antagonisti di questi recettori può essere una nuova strategia per il trattamento del dolore. I composti descritti in questa tesi aventi struttura triazinodionica sono stati ottenuti con

una nuova procedura sintetica che consente di ottenere i prodotti con rese fino al 50% superiori rispetto a quelle ottenute nella preparazione di composti analoghi. Nei saggi biologici questi composti hanno mostrato attività analgesica in vivo a concentrazioni picomolari. I triazinodioni hanno dimostrato attività antagonista nei confronti dei recettori della prokineticina.

3. Il terzo target su cui agiscono i composti riportati in questa tesi è il recettore canale TRPV1, importante componente delle vie di trasmissione dell'informazione dolorosa, la sua apertura causa infatti un influsso di ioni positivi all'interno della cellula che porta alla sua depolarizzazione e conseguente propagazione dell'informazione ai centri superiori. In questo caso quindi il blocco di questo canale con antagonisti o agonisti-desensitizzanti può risultare in un effetto analgesico. I triazinodioni sopra menzionati hanno dimostrato una componente di attività modulatoria nei confronti dei recettori TRPV1 che potrebbe almeno in parte essere responsabile dell'effetto analgesico mostrato nei saggi in vivo.

IV. Publication list

I. Congiu, C.; Onnis, V.; **Deplano, A**.; Salvadori, S.; Marconi, V.; Maftei, D.; Negri, L.; Lattanzi, R.; Balboni, G., A new convenient synthetic method and preliminary pharmacological characterization of triazinediones as prokineticin receptor antagonists. *European Journal of Medicinal Chemistry* 2014, *81*, 334-340.

II. Lattanzi, R.; Congiu, C.; Onnis, V.; **Deplano, A**.; Salvadori, S.; Marconi, V.; Maftei, D.; Francioso, A.; Ambrosio, C.; Casella, I.; Costa, T.; Caltabiano, G.; Matsoukas, M.; Balboni, G.; Negri, L., Halogenated triazinediones behave as antagonists of pkr1: in-vitro and in-vivo pharmacological characterization. *International Journal of Pharmaceutical Sciences and Research* 2014, *5*, 5064-5072.

III. De Petrocellis, L.; Schiano Moriello, A.; Byun, J. S.; Sohn, J. M.; Lee, J. Y.; Vázquez-Romero, A.; Garrido, M.; Messeguer, A.; Zhang, F.-X.; Zamponi, G. W.; **Deplano, A.**; Congiu, C.; Onnis, V.; Balboni, G.; Di Marzo, V., Inhibitory effect of positively charged triazine antagonists of prokineticin receptors on the transient receptor vanilloid type-1 (TRPV1) channel. *Pharmacological Research* 2015, *99*, 362-369.

IV. Gouveia-Figueira, S.; Karlsson, J.; **Deplano, A.**; Hashemian, S.; Svensson, M.; Fredriksson Sundbom, M.; Congiu, C.; Onnis, V.; Fowler, C. J., Characterisation of (R)-2-(2-Fluorobiphenyl-4-yl)-N-(3-Methylpyridin-2-yl)Propanamide as a Dual Fatty Acid Amide Hydrolase: Cyclooxygenase Inhibitor. *PLoS ONE* 2015, *10* (9), e0139212.

V. Karlsson, J.; Morgillo, C. M.; **Deplano, A.**; Smaldone, G.; Pedone, E.; Luque, F. J.; Svensson, M.; Novellino, E.; Congiu, C.; Onnis, V.; Catalanotti, B.; Fowler, C. J., Interaction of the N-(3-Methylpyridin-2-yl)amide Derivatives of Flurbiprofen and Ibuprofen with FAAH: Enantiomeric Selectivity and Binding Mode. *PLoS ONE* 2015, *10* (11), e0142711.

Reprints of the published papers were made with permission from the respective publisher.

V. Abbreviations

1-(3-Dimethylaminopropyl)-3-ethylcarbodiimide hydrochloride (EDC)
15-(S)-Hydroperoxyeicosatetraenoic acid (HPETE)
1-Hydroxybenzotriazole hydrate (HOBt)
2-(4-((2-(Trifluoromethyl)Pyridin-4-yl)amino)phenyl)propanAmides (TPA)
2-Arachidonoylglycerol (2-AG)
2-Arachidonoylglycerolether (2-AGE)
2-Propanol (2-PrOH)
Acetonitrile (MeCN)
Acetylcholine (ACh)
Acyl chain binding (ACB)
Adenylate cyclase (AC)
A-Kinase anchor proteins (AKAP)
Amidase signature (AS)
AMPA receptors (AMPAR)
Anandamide (AEA)
Arachidonic acid (AA)
Arachidonoyl serotonin (AA5HT)
β-1 Adrenergic receptor (β1)
Bioluminescence Resonance Energy Transfer (BRET)
Ca^{2+} Activated K+ channel (CAKC)
Ca^{2+}-Dependent trans-acylase (NAT)
Calcitonin gene-related peptide (CGRP)
Cannabinoid receptors (CB)
Central nervous system (CNS)
Chemokine receptor type 4 (CXCR4)
Cyclooxygenase (COX)
Diacylglycerol (DAG)
Dichloromethane (CH_2Cl_2)
Diethyl ether (Et_2O)
Diisopropylethylamine (DIPEA)
Dimethylformamide (DMF)
Dorsal root ganglia (DRG)
Endocannabinoid (EC)
Endocannabinoids membrane transport (EMT)
Endocrine gland-derived vascular endothelial growth factor (EG-VEGF)
Endoplasmic reticulum (ER)
Endovanilloids (EV)
Ethanol (EtOH)
Ethoxy oleoyl fluorophosphonate (EOFP)
Ethyl acetate (AcOEt)
Fatty acid amide hydrolase (FAAH)
G Protein coupled receptors (GPCRs)

Human TRPV1 receptor (hTRPV1)
Hydrochloric acid (HCl)
Hyperpolarization-activate current (Ih)
Hyperpolarization-activate cyclic nucleotide-gate channels (HCN)
Inositol 1,4,5-triphosphate (IP$_3$)
International Association for the Study of Pain (IASP)
Iodomethane (MeI)
Isopropyl ether (iPr$_2$O)
Lipoxygenase (LOX)
Magnocellular nucleus of Raphe (MNR)
Mammalian Bv8 (mBv8)
Mechanosensitive/osmosensitive K$^+$ channel (TREK-1)
Melting points (m.p.)
Membrane access channel (MAC)
Methanol (MeOH)
Methylarachidonoyl fluorophosphonate (MAFP)
Mitogen-activated protein kinases (MAPK)
Molecular dynamics (MD)
Monoacylglycerol lipase (MAGL)
N,N-Dimethylformamide dimethyl acetal (DMF-DMA)
N-Acylphosphatidylethanolamine (NAPE)
N-Arachidonoyl dopamine (NADA)
N-Arachidonoyl ethanolamine (Anandamide, AEA)
N-Arachidonoyl-phosphatidylethanolamide (NAr-lysoPE)
Neurokinin receptors (NK)
Neurotensin receptor 1 (NTS1)
Nitric oxide (NO)
NMDA Receptor (NMDAR)
Non-steroidal anti-inflammatory drug (NSAID)
Oleylethanolamide (OEA)
Palmitylethanolamide (PEA)
Periaqueductal grey (PAG)
Phenylmethylsulfonyl fluoride (PMSF)
Phosphatidylcoline (PC)
Phosphatidylinositol (PI)
Phosphatidylinositol 4,5-bisphosphate (PIP$_2$)
Phosphodiethanolamine (PE)
Phospholipase A2 (PLA2)
Phospholipase C (PLC)
Potassium carbonate (K$_2$CO$_3$)
Potassium cyanate (KOCN)
Prokineticin 1 (PK1)
Prokineticin 2 (PK2)
Protease-activated receptor 1 (PAR1)
Protein kinase C (PKC)

Receiver operating characteristic (ROC)
Resiniferatoxin (RTX)
Rhodopsin receptor (RHOR)
Rostral ventral medial medulla (RVM)
Sodium bicarbonate (NaHCO$_3$)
Sodium borohydride (NaBH$_4$)
Sodium hydride (NaH)
Sodium hydroxide (NaOH)
Sodium methoxide (NaOMe)
Sodium sulfate (Na$_2$SO$_4$)
Stretch-activated nonselective cation currents (SACC)
Substance P (SP)
Superior cervical ganglia (SCG)
Tetrahydrofuran (THF)
Tetramethylsilane (TMS)
Tetrodotoxin-resistant and sensitive voltage-gated Na+ channel (TTX-R)
Transient Receptor Potential (TRP)
Transient receptor potential cation channel subfamily M member 8 (TRPM8)
Transient receptor potential cation channel subfamily V member 1 (TRPV1)
Transient receptor potential cation channel, subfamily A member 1 (TRPA1)
Triacetoxyborohydride (NaBHAc$_3$)
Triethylamine (TEA)
Trifluoroacetic acid (TFA)
Type D Ca^{2+}-dependent phospholipase (NAPE-PLD)
Voltage-gated K$^+$ channel (VGKC)
Δ^9-Tetrahydrocannabinol (THC)
κ-Opioid receptor (κ-OPR)

1. PAIN

1. Pain

1.1 Pain: Definition and physiological role

An "unpleasant sensory and emotional experience associated with actual or potential tissue damage" is the definition of pain given by the International Association for the Study of Pain (IASP).[1] This unpleasant sensation is also a fundamental component of animal lives. Without pain people would not be able to detect injurious stimuli, and would lose the ability to protect themselves from punctures of sharp objects or the heat of a flame. Also people would lose the ability to feel a body problem like the discomfort of bruising or a more important problem in a vital organ. A clear example of how pain is important for life is given by the greatly reduced life expectancy of people affect by the rare occurrence of congenital insensitivity to pain, in some of these people it has seen as they fail to engage in protective behavior against injuries they inflict on themselves.[2]

Pain is not useful like an alert system only, the activation of the nociceptors by noxious stimuli, which is followed by alteration at several levels in the nociceptive pathways is fundamental for protecting the injured area. Such as increased blood flow and vascular permeability caused by the release of some neuropeptides from peripheral nerves activated by mechanism in the injured tissue which contribute to the healing process. Also the central nociceptive pathways may cause a temporary hyper-sensitization which produces enhanced pain and focused attention to the injured area.[3] For example, after sunburn the affected area is subjected to a temporary sensitization, as results normally painful stimuli elicit pain of greater intensity (this phenomenon is call hyperalgesia). Even normally innocuous stimuli, such as warmth or light touch, are perceived as painful (this phenomenon is call allodynia). Allodynia is also present as component of the symptoms in the 15-50 % of patient affected by

neuropathic pain (that will be better explain below in section 1.2).

This just described it is the "good" pain, the one needed to live safely and to avoid dangerous situations. But there is another one, the "bad" pain, that is generated by a wrong adaptation response to a nervous or not nervous tissue injure, in this case pain is no longer a defense mechanism but it became a pathology called Pain Syndrome.[4]

The most representative type of "bad pain" is chronic pain, which is defined as pain experience for a period of about three to six months, which it is felt every day or almost every day. Actually this definition is not really exhaustive because it is not true that any pain that is not chronic is acute, there are some cases where either or neither are entirely satisfactory.

The temporal aspect, alone, does not define entirely the difference between acute and chronic pain, their difference is more correlated to the body capacity or incapacity to restore the physiological conditions. Chronic pain is self-perpetuating because resulting from alterations in nociceptive pathways induced by a starting injure, and persists even when the noxious stimuli finish.

Pain is one of the most important problems for public health; epidemiologic data indicate that in Europe about one person in five suffers from moderate or severe chronic pain; also almost 90% of these people have suffered of chronic pain for over two years, and about one in five for much longer periods even more than twenty years.[5,6] Today in Europe and USA only neuropathic pain afflicts fifteen million.

These numbers indicate the gigantic impact of pain not only for the afflicted people, but also for the society in term of costs for public health (about two hundred billion for year in Europe only).[7]

In this sense it is evident that the research of new pain treatment has fundamental importance for several reasons, such as, first of all for the preclinical research to find more accurate and effective new therapeutic strategies to improve the life of the affected person, but

also for public health in the perspective of reduce costs of pain therapy, and last but not least for basic research focalized in understanding of pain mechanism.

1.2 Pain: Classification

On the base of its causes pain can be defined nociceptive, neuropathic, inflammatory or somatoform type.

Nociceptive pain is the most common; it is the classic pain caused by tissue damage or by thermic, chemical or mechanical stimuli; it is generally proportional activation of nociceptors. Nociceptive pain can be divided in visceral or somatic pain; the first one concerns thoracic and abdominal organs, usually it is stronger than somatic pain and it can be delocalized respect to the organ, which causes pain, such as the arm pain during myocardial infarction. While somatic pain involves the nociceptors located in the musculoskeletal system, in the skin or in the joints; unlike that visceral it is well localized at the lesion site.[8,9]

Neuropathic pain is caused by an injury or by a malfunction of nervous transmission. It can be provoked by an ectopic neuronal firing in the soma or axons, or it can be caused by peptides released after a nerve injury contributing to the inflammatory response. Lastly neuropathic pain can be caused by the inhibition of neuronal system involved in the transmission and modulation of peripheral stimuli.[8]

Inflammatory pain, caused by a hyper-sensitization is due to an injury or an inflammatory process. The nerves of the sensory afferent pathways are sensitive to some inflammatory mediators such as bradykinin, prostaglandins and leukotrienes. The prolonged stimulation, by these mediators, of the nerves can cause peripheral and central sensitization, and modifications of the neuronal function that can results in chronic pain. Often is very difficult distinguish

between neuropathic and inflammatory pain because prolonged inflammation can cause neuronal damage that result in neuropathic pain. Likewise a neuronal damage can cause an inflammatory response that contributes to the appearance of inflammatory pain.[10]

Somatoform pain has an important psychological component; patients feel a severe pain without the presence of a real injurious stimulus that causes it.[11]

1.3 Pain transmission

The pain transmission system is divided in two pathways; the ascending path, which sends the information of the pain stimulus to the brain, and the descending path, which can have either an antinociceptive and/or pro-nociceptive effect on the nociceptive afferents.[12]

The two pathways are controlled by numerous chemical mediators, which can act directly on ionic channels and/or on metabotropic receptors that are connected with intracellular second messengers. These processes regulate the activation of nociceptors, favoring or disfavoring, the progression of the pain information.

Moreover, the excitability of the afferent fibers can be modified also by DNA regulation, resulting in receptors, ionic channels and enzymes synthesis and expression. In fact their gene transcription is regulated by the information sent to the cell soma of sensory neurons.[13]

1.3.1 Ascending pathways

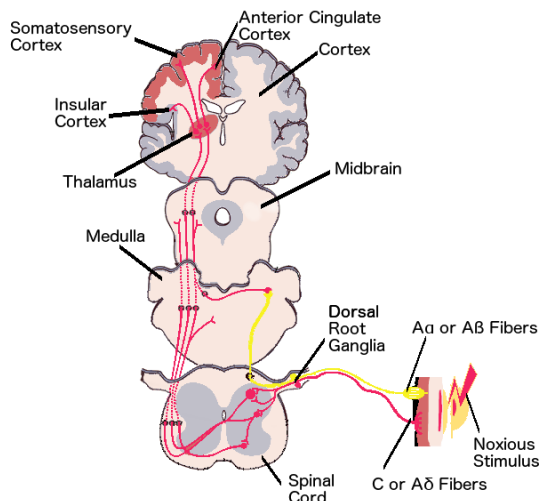The pain sensation, like others, begins by the activation of a specific kind of peripheral nerves. These nerves are located under the skin and in the internal organs. There are different afferent fibers; some respond to stimuli at low intensity to mediate innocuous sensations like a touch or a feeling of sensations of heat and cold. Others, those have a higher activation threshold, respond to more intense stimuli coding for the noxious information. The fibers mediating the painful information are called nociceptors, they respond quickly and selectively to different kind of stimuli, mechanic, thermal and chemical, that have a sufficient intensity to cause tissue damage (Figure 1).

Figure 1. Ascending Pathways.

Nociceptors can be classified in two major classes based on physiological criteria such as the conduction speed.[3] One type, fast conducting myelinated, called A fibers, the other type slow conducting with small caliber and un-myelinated, called C fibers. These can be further divided on the basis of the response characteristic and receptors involved.[14]

The C fibers respond to severe mechanical and thermal stimuli (CMHs) such as temperatures higher than 45° C. The majority of these fibers also respond to chemical stimuli, for this reason they are considered polymodal.

The A fibers are divided in two major classes, Aδ with medium diameter axons that mediate acute, well-localized pain. The Aβ with larger diameter and rapid conductivity respond to innocuous mechanical stimuli.

The Aδ fibers are divided in two main classes. Type I, high-threshold mechanical nociceptors (HTMs), which respond to both mechanical and chemical stimuli and have high heat thresholds (>50°C), it is important to note that they sensitize in the site of tissue injury. Conversely Type II Aδ nociceptors have much lower heat threshold, but very high mechanical threshold.[15]

From the nerve terminals the pain sensation is sent to the cell body located in the dorsal root ganglia (DRG) of the spinal cord. In particular C fibers ending in the upper layers at the level of laminas I and II; whereas A fibers ending more in depth, up to lamina V.[16]

The depolarization of these fibers produces immediate release of glutamate, which binding its postsynaptic inotropic receptor, AMPA, causes in turn depolarization of the next neuron on the dorsal horn. Then the information is distributed by projection neurons, mainly located in laminas I, II and V, to supraspinal centers by five major ascending pathways[17]:

1. *Spinothalamic*. It includes axons coming from laminas I and V and terminate in thalamic nuclei after crossing the midline of the spinal cord and ascending in the anterolateral white matter. Evidence suggests that this pathway mediates information about intensity and location of pain.[18]

2. *Spinoreticular*. It consists in the axons of projection neurons in laminas VII and VIII, it terminates in both the reticular formation and the thalamus after passing through the anterolateral quadrant of the spinal cord, without crossing the midline.[19] This tract may be involved in the affective-motivational aspect of pain; it can also be involved on the nervous activity related on somatic and autonomic motor reflexes. Moreover, the descending projection of reticular formation

of the raphe nuclei may have effect on the inhibitory control of the incoming painful information.

3. *Spinocervical.* This tract begins in laminas III and IV of the dorsal horn, passes through the lateral white matter of the upper two cervical segments of spinal cord. The majority of the axons crosses the midline and ascends in the medial lemniscus of brainstem, ending in midbrain nuclei and in the ventroposterior lateral and posteromedial nuclei of thalamus. Some other neurons send their axons into the dorsal columns and terminate in the cuneate and gracile nuclei of the medulla. This pathway for the majority mediates tactile stimuli and just a few noxious stimuli.

4. *Spinomesencephalic.* Neurons of laminas I and V project to the lateral part of periaqueductal grey (PAG) and to other mesencephalic structures. The axons of this tract pass through the anterolateral quadrant of the spinal cord. They also project to parabrachial nucleolus, which projects, in turn, to the amygdala, an important nucleus of the limbic system that regulates emotional states.[20,21]

5. *Spinohypothlamic.* It includes the axons of neurons with soma in laminas I, V and VIII of the dorsal horn, these axons project to hypothalamic nuclei. It mediates the autonomic control of neuroendocrine and cardiovascular response that accompanies pain syndromes.[22]

   Another important supraspinal center is rostral ventromedial medulla, that as well as PAG, is a connection point between ascending and descending pathways. [23]

   This extensive distribution of pain information in the brain is the reason of the pain experience complexity, which included sensory, emotional, and motor components.[17]

   On dorsal horn, thalamus, medulla, reticular and cortical there are numerous neurotransmitter systems implicated on the regulation of the excitatory inputs. Evidences suggest that electrical stimulation of the ascending pathways, causes the release of mediators of

nociception: encephalin,[24] norepinephrine and serotonin[25] on both spinal and brainstem.

Interneurons releasing peptides or monoamines and peptides operated medulla-spinal pathway are activated by afferent inputs and can modulate the peptides release from C fibers. Some other modulators implicated in this circuit are prostanoids and nitric oxide (NO) that caused an increase of the Ca^{2+} conductance on the dorsal horn and consequent increase release of substance P (SP).[26-28]
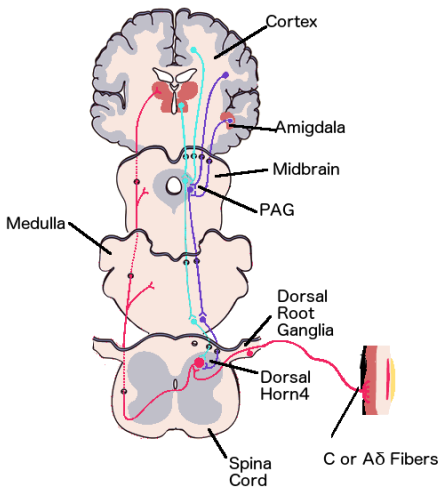
1.3.2 Descending pathways

Figure 2. Descending Pathways**.**

These pathways have modulatory role of the pain sensation (Figure 2), in the spinal cord acting both on the postsynaptic projected neurons and on the dorsal horn interneurons. They are also responsible of the integration among sensitive, cognitive, emotional and motivational sensation with afferent nociceptive information.[29] Direct and indirect circuits from hippocampus, cortex, thalamus, rostral ventral medial medulla (RVM) and PAG are involved in this system.

This system is critical to regulate the pain sensation and can have both excitatory and inhibitory effect.

From a long time the importance of PAG nucleus is well known, in 1969 Reynolds demonstrated that electric stimulation of this area has enough analgesic effect allowing to perform an abdominal surgery without the animal showing any distress sign.[30]

PAG projects pain information in an area of the brainstem called magnocellular nucleus of Raphe (MNR), from here the nerve pathways end in the spinal cord. Here the projected neurons, by serotonin secretion, modulate the inhibitory activity of encefalinergic interneurons at the gelatinous substance. At this level the activity of inhibitory interneurons is regulated by the "gate control theory". This control mechanism is influenced by fibers of small and large caliber; in particular Aβ fibers inhibit the transmission (close the gate), conversely Aδ and C fibers facilitate the transmission (open the gate).[31] PAG is also connected to another important structure, the locus ceruleous, where noradrenergic neurons come from. These project their axons on the dorsal horn and here, by the activation of α_2 presynaptic receptors, cause the inhibition of pain transmission.[32]

1.4 Pain: Modulators involved in pain transmission

In each of the nucleolus mentioned above many mediators are involved in the modulation of pain information transmission.

1.4.1 Glutamate

Subsequently to the activation of the nociceptors, glutamate is released on the dorsal horn, here it binds AMPA receptors (AMPAR) on the projected neurons membrane and causes diffusion of the pain information. If the single noxious stimuli is prolonged in time or the stimuli are more than one the dorsal horn neurons became more responsive. This process is caused by increased depolarization of the postsynaptic membrane and consequent removal of the block of the NMDA receptor (NMDAR) by the action of glutamate, on both inotropic NMDA and metabotropic MGluR receptors.[33]
Both AMPA and NMDA are also present in further positions of the nociceptive pathway; NMDARs have been identified on both unmyelinated and myelinated axons in peripheral somatic tissues,

after their activation and consequent influx of ions (Na^+ and Ca^{2+}) the pain information is sent to spinal cord.[34]

The central sensitization is caused mostly by the increased excitability of the dorsal horn neurons and, as a consequence, its response to sensory input is facilitated. Then even low-intensity stimuli generate pain (allodynia) and noxious stimuli result in pain response that is augmented in duration and amplitude (hyperalgesia). Evidences have demonstrated the involvement in allodynia and hyperalgesia of dorsal horn NMDAR, suggesting a role for NMDAR even in supraspinal sensitization mediation. Indeed, increase NMDAR activity caused hyper-excitability of brainstem circuit.[35]

Also AMPA receptor is expressed in DRG cell bodies and in both unmyelinated and myelinated sensory nerves,[34,36] suggesting that glutamate release acting on peripheral AMPARs may contribute to the initiation of nociceptive signaling.[37]

On the dorsal horn of spinal cord, in particular on laminas I e II, evidences suggest the dual activity of glutamate receptors, one mediated by NMDA receptors located on the postsynaptic neurons which send the pain information on the brainstem,[38] the other mediated by the AMPARs located on primary afferents which inhibit glutamate release.[39]

As for NMDARs also AMPA receptors are expressed ubiquitously in brain regions associated with nociception.[40] These receptors, probably, mediate the rapid excitatory transmission between many nodes within the ascending nociceptive pathways, such as input from sensory neurons in the spinal cord to brainstem and thalamus, as well as from thalamic neurons to sensory cortex. They are implicated also in descending pathways from amygdala and anterior cingulate cortex to PAG and RVM. Descending inhibitory inputs to sensory neurons in the spinal cord come from PAG and RVM.[41]

1.4.2 Bradykinin and Kallidin

Two potent pro-nociceptive agents derive from a precursor protein termed kininogen, they are the nona-peptide bradykinin and its related deca-peptide kallidin. Two receptors have been identified for these peptides, namely B_1 and B_2.[42] B_1 and B_2 receptors belong to the family of G protein coupled receptors (GPCRs), most of knowledge about the biochemical mechanism of these receptors are related to the B_2 but they appear to utilize similar signal transduction mechanism.
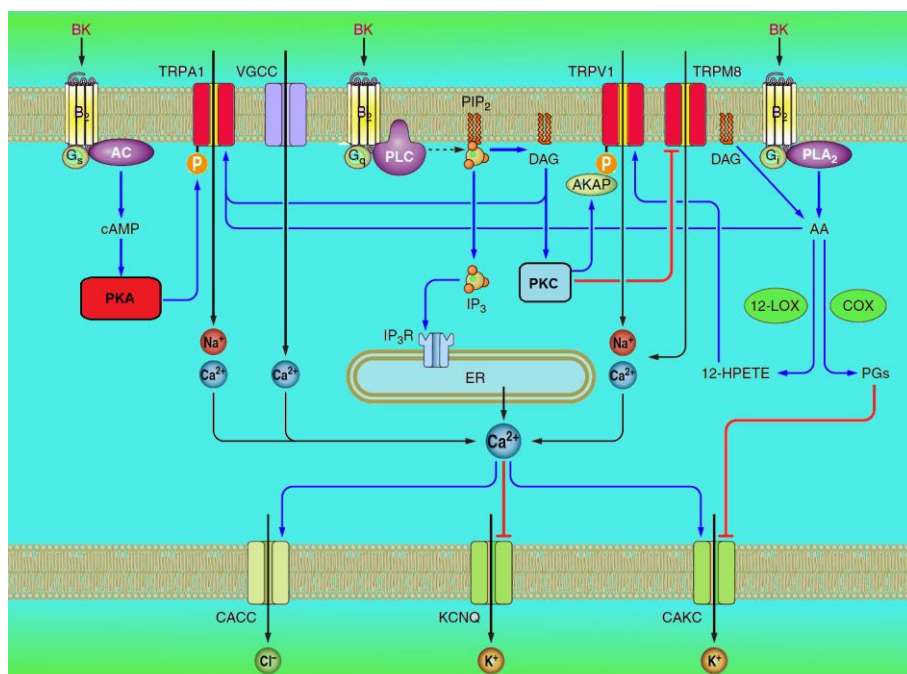
Figure 3. Schematic representation of bradykinin (BK) most important signal transduction mechanism in nociceptive sensory neurons.

There are two major differences between these receptors; the first regards the affinity of the peptides, they act preferentially on the B_2, the other is that B_2 receptors are largely constitutive instead the B_1 are induced by tissue trauma, inflammation and nerve injury.[43] Studies demonstrated the presence of these receptors also in the

spinal cord and even in higher center, which contribute with those in periphery to generate pain and hyperalgesia.[44]

The bradykinin signaling mechanism system is very complicated and connected with various other systems as shown in Figure 3.

With the activation of the receptor by bradykinin and subsequent activation of the G protein, different intracellular processes begin, one signaling mechanism is mediated by the activation of phospholipase C (PLC), which by the cleavage of phosphatidylinositol 4,5-bisphosphate (PIP_2) produces an increase of the levels of the second messengers inositol 1,4,5-triphosphate (IP_3) and diacylglycerol (DAG). The last one activates the protein kinase C (PKC), which causes, through PKC-mediated phosphorylation of ion channels, an influx of ions like Na^+, K^+ and Ca^{2+}, these ion influxes on DRG neurons result in membrane depolarization and subsequent signal transmission to the next level. [45] The increase of intracellular Ca^{2+} concentration is mediate also by PLC-activation, that by interaction between IP_3 and its endoplasmic reticulum (ER) receptors produces Ca^{2+} release from the intracellular stores.[46]

Another effect of the influx of extracellular Ca^{2+} is DAG metabolization of by DAG lipase with consequent release of arachidonic acid (AA)[45], additionally the binding of bradykinin to B_2 receptors causes the activation of phospholipase A_2 (PLA_2), through G_i protein, that result in further AA formation in sensory neurons.[47] AA release leads to production of prostanoids and leukotrienes by specific enzymes; the hyper-sensitization effect of these AA metabolites will be discussed in the next section.

Activation of B_1 and B_2 receptors has also effects on some TRP channels, which have considerable importance in pain transmission. In particular, the activity of three channel receptors is mediated by bradykinin, Transient receptor potential cation channel subfamily V (Vanilloid) member 1 (TRPV1), Transient receptor potential cation channel, subfamily A (Ankyrin) member 1 (TRPA1) and Transient

receptor potential cation channel subfamily M (Melastatin) member 8 (TRPM8).

TRPV1, also known as capsaicin receptor, is located on polymodal nociceptive primary afferent neurons; it is a nonselective cation channel that can be activated also by noxious stimuli, like heat (temperature > 43°C), and low pH. TRPV1 is activated also by endogenous compounds such as N-arachidonoyl dopamine (NADA)[48] and anandamide (AEA)[49] or exogenous molecules like capsaicin.[50] The channel activation results in two mainly important events, one is the membrane depolarization, the other is the release of neuropeptides like SP and calcitonin gene-related peptide (CGRP), caused by the Na^+ and Ca^{2+} influx respectively.

In the cascade of second messengers induced by the activation of bradykinin receptor two are the pathways that interact with TRPV1; one is related to the conversion of the AA by the enzyme lipoxygenase (LOX) in products that active the TRPV1,[51] the other is mediated by the B_2 receptor-PLC-PKC signaling pathway.[52]

Contrary to the TRPV1, TRPM8 is activated by cold (temperature < 25°C) and chemicals like menthol and eucalyptol, which induce a cool/soothing sensation.[53] The activation of bradykinin receptor has inhibitory effect on TRPM8, probably due to dephosphorylation of the channel by a PKC-activated protein phosphatase.[54]

Cold is also responsible of the TRPA1 channel activation, as well as endogenous substances and exogenous chemicals like mustard oil. Also bradykinin, with its second messengers cascade,[55] can activate channels and allow the influx of Na^+ and Ca^{2+} ions producing the same effects due to the TRPV1 activation.

Different second messengers produced by the activation of B_2 may cause up-regulation of TRPA1. DAG, produced by the breakdown of PIP_2 PLC-mediated, and AA are two of these. Another pathway leading to the activation of TRPA1 is mediated by the cAMP-PKA cascade due to the activation of receptor B_2 coupled with G_s protein.[56]

These are just some of the most important bradykinin mediate pain information pathways.

1.4.3 Prostanoids

AA is converted into prostaglandins (such as PGE_2, PGI_2, PGD_2 and $PGE_{2\alpha}$) and thromboxanes (like TXA_2) by cyclooxygenase (COX) enzymes. A pro-nociceptive role has been reported for these AA derivatives in particular for PGE_2 and PGI_2.

On the base of the relative agonist affinity numerous prostanoid receptors have been cloned and classified: PGE_2 binds EP receptors, PGI_2 binds preferentially IP, TXT_2 binds TP and PGD_2 binds DP.

Not all these receptors are implicated on the mediation of the pain information, just some of these were revealed in DRG neurons (EP_1, EP_2, EP_{3A}, EP_{3B}, EP_{3C}, EP_4, DP_1, DP_2 and IP).
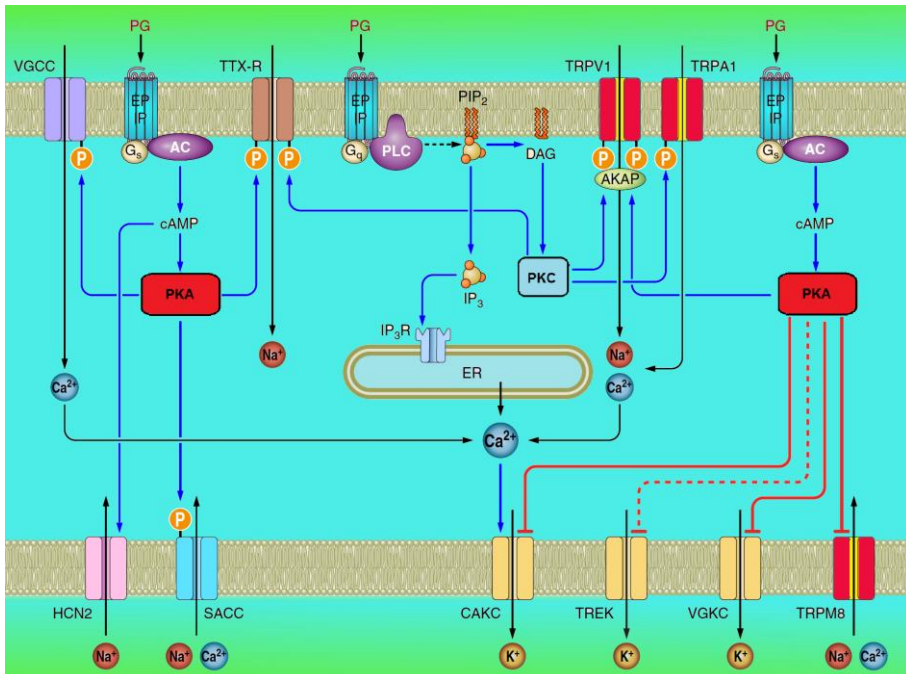
Figure 4. Schematic representation of prostanoids (PG) most important signal transduction mechanism in nociceptive sensory neurons.

As for bradykinin the transduction mechanism of prostanoids is very complex and involves several second intracellular messengers (Figure 4), the result of these pathways is the depolarization and the transmission of the pain information to the next nucleus.

Binding of PGE_2 and PGI_2 to their receptors induces cAMP and IP_3 accumulation in DRG neurons. This means that the depolarization evoked by PGE_2 or PGI_2 begins with the activation of PLC or adenylate cyclase (AC) mediated by G_s and G_q proteins respectively.[57]

The accumulation of cAMP and the consequent activation of PKA causes influx of Ca^{2+} mediated by the phosphorylation of voltage-gated Ca^{2+} channels.[58] One of the results of the intracellular Ca^{2+} concentration increasing is the release of SP and CGRP from sensory nerves of various organs.[59]

Tetrodotoxin-resistant and sensitive voltage-gated Na^+ channel (TTX-R), located in DRG, is positively modulated by PGE_2 causing increase Na^+ current and inducing a hyperpolarizing shift. [60] cAMP-PKA signaling pathway is the major responsible for the activation by phosphorylation of this channel, the activation by this pathways induced leftward shift in its conductance-voltage relationship. Although even the PKC causes an enhanced TTX-R Na^+ current it appears more likely that modulation of this channel is mediated by PKA than PKC. Furthermore inhibitors of either PKA or PKC reduce PGE_2 effects.[61]

TRPV1 is another channel modulated by the activation of both EP (in particular EP_1 for PKC pathway and EP_4 for PKA pathway) and IP. Conversely to TTX-R, PKA and PKC do not directly phosphorylate vanilloid channel, but probably the effects of the activation of prostanoids receptors are mediated by the phosphorylation of regulatory proteins associated with TRPV1, known as A-kinase anchor proteins (AKAP). On DRG neurons prostaglandins modulate TRPV1, in particular the activation of EP_1/IP-G_q-PLC-DAG-PKC-AKAP-TRPV1 pathway has the predominant role, only a minor contribution arrives from EP_4/IP-G_s-AC-cAMP-PKA-AKAP-TRPV1 pathway.[57,62]

As described for bradykinin, prostanoids display effects on TRPM8 and TRPA1 also. The activation of PKA pathway by PGE_2 causes inhibition of the TRPM8 channel.[63] Conversely in TRPA1, PGE_2 through PKC pathway phosphorylates the channel resulting in increase of intracellular Ca^{2+} concentration.[64]

Hyperpolarization-activate cyclic nucleotide-gate channels (or HCN) are a family of channel permeable to both Na^+ and K^+ that are responsible of hyperpolarization-activate current (I_h). In particular HCN2 and HCN4 channels are expressed on small sensory neurons in DRG.[65] These channels are positively modulated by PGE_2, forskolin, cAMP and cGMP, which promote depolarization and increase the maximum amplitude of ionic current.[66]

SACC (stretch-activated nonselective cation currents) are channels permeable to Na^+, K^+ and Ca^{2+} located in DRG neurons, their activity is mediated by cAMP-PKA pathway.[67]

Some channels are down-regulated by prostanoids signaling. Voltage-gated K^+ channel (VGKC) is one of these. PGE_2, through cAMP-PKA pathway, suppresses outgoing K^+ current that caused decrease of after-hyperpolarization by reducing voltage-dependent K^+ conductance.[68,69]

Other two channels are down-regulated through cAMP-PKA pathways; Ca^{2+} activated K^+ channel (CAKC) and mechanosensitive/osmosensitive K^+ channel (TREK-1), both are implicated in the decrease of after-hyperpolarization.[70,71]

1.4.4 Prokineticin

Prokineticin 1 and 2 (PK1 and PK2) are two small peptides implicated in numerous physiological processes including nociception.[72]

These peptides exert the activity binding two GPCRs known as PKR1 and PKR2. It is important to emphasize that the activation of prokineticin system do not cause directly pain but it is responsible for lowering pain threshold and hyperalgesic effect. It is possible

distinguish two phases on the prokineticin hyperalgesic signaling, the first caused by the PKRs on the nociceptors near the injury, the secondary caused by central action due to activation of the prokineticin receptors located on the DRG and spinal cord.[73]

Evidences suggest that PKRs are located in some DRG C and Aδ fibers, which present CGRP (one-third) and SP (one-fifth).[74]
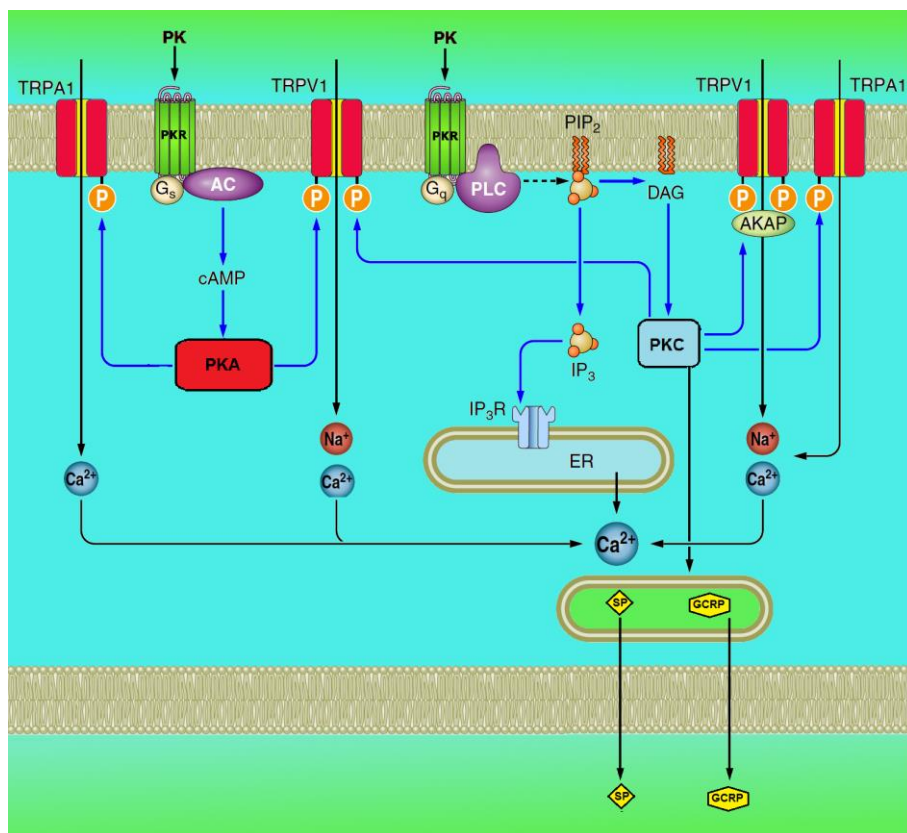

Figure 5. Schematic representation of prokineticin (PK) most important signal transduction mechanism in nociceptive sensory neurons.

At the present time the entire intracellular pathway consequent to the activation of the PKRs, which lead to hyperalgesic effect, is not completely known.

Evidences show that PKRs are coupled with G_s, G_q and G_i proteins that, when activated, begin a cascade of second messengers leading to sensitivity increase to pain stimuli (Figure 5).

Probably the activation of G_q proteins stimulates the Ca^{2+} mobilization from intracellular store through IP_3-PLC pathways.[73]

The increasing of the intracellular Ca^{2+} concentration is not mediated by the release from intracellular stores only, but the activation of TRPV1 channel seems to be the major cause of Ca^{2+} influx. This hypothesis is supported by numerous experiments, which showed the high co-expression percentage on the same DRG neurons of vanilloid channels and PKRs.[75] Probably the activation of PKRs coupled with G_q and/or G_s proteins lead to the phosphorylation of TRPV1 through PKC, PKC_ε and PKA respectively. This is important because, experiments highlighted that phosphorylated-TRPV1 is more sensible to thermal, mechanical and chemical stimuli.[76]

TRPV1 is not the only channel co-expressed with PKRs in nociceptors and DRG neurons, TRPA1, although with a lower percentage, is co-expressed with prokineticin receptors in particular with PKR1. This means that the activation of PKRs caused hypersensivity to high and low temperatures.[77]

Another pathway connecting PKRs to pain information transmission is mediated by the release of CGRP and SP on the DRG and spinal cord neurons. Some evidences show that these substances are released in response to PKC_ε translocation caused by PKRs activation.[74,77]

Furthermore the prostanoid system appears to be involved in prokineticin signaling, in particular some experiments showed that the activation of PKRs promotes eicosanoid pathway probably by PLC-DAG and/or by directly activation of PLA2.[78]

These just described are the most important known mechanisms relating prokineticin system and nociception.

1.4.5 Substance P

Bradykinin, prostanoids and prokineticin, as just described, are all involved on the release of substance P, an undecapeptide belonging

to the peptide family called tachykinins (neurokinin-A and neurokinin-B are other two members of this family).

SP is synthesized in the DRG (where the soma of C fibers is located) and it is transported to the *substantia gelatinosa* of the spinal dorsal horn and peripherally to the nerve endings. In response to signal of an above described mediator, SP is released at the level of the first synapse of primary neurons in the superficial layers of the spinal dorsal horn (I-III).[79] SP was also detected in lamina V[80] and in lamina X surrounding the central canal.[81]
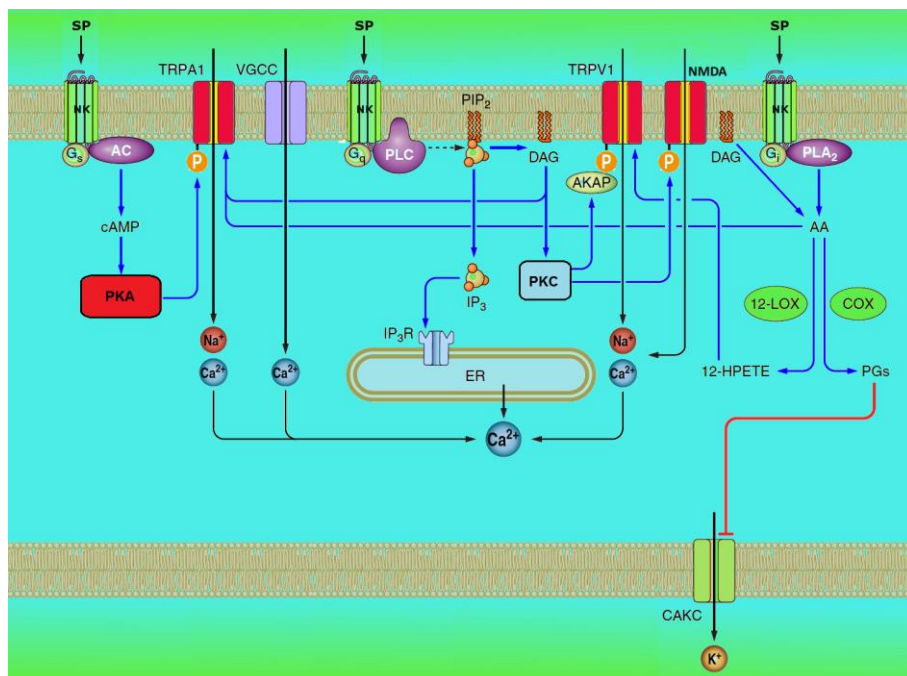
Figure 6. Schematic representation of substantia P (SP) most important signal transduction mechanism in nociceptive sensory neurons.

SP is one of the mediators responsible for nociceptive transmission to the central nervous system (CNS); after its release and receptor binding, SP, causes alterations in cell membrane excitability and consequent sending information to the next step.

SP and the other peptides of the tachykinins family exert their function binding three neurokinin receptors (NK-1, NK-2 and NK-3); in particular, SP has the best affinity to NK-1. All NK are GPCR; NK-1 is

coupled with G_i, G_0, and G_{q11}.[82] NK activation generates various second messengers responsible of trigger a wide range of effector mechanisms (Figure 6), which regulated the cellular excitability and different other functions. In particular it has been reported that the activation of NK-1 is responsible of the Ca^{2+} mobilization from intra- and extracellular sources mediated both by PLC that hydrolyzes PIP_2 into DAG and IP_3. The first one is responsible, at least partially, of the influx of the extracellular Ca^{2+} by potentiation of NMDA receptors via PKC. While IP_3 is responsible of the release of Ca^{2+} from intracellular stores.[83,84]

Other two important pathways cause, one the mobilization of AA via PLA_2,[85] the other the cAMP accumulation via AC and consequent activation of PKA.[86]

All the mediators described until now explicate predominantly pro-nociceptive role, but there are numerous mediators which have inhibitor activity, some already mentioned, the majority of these acts on the descending pathways.

1.4.6 Neurotransmitters (Noradrenaline, Serotonin and Acetylcholine)

1. Noradrenaline.

Noradrenergic neurons originate in the locus ceruleous and project their axons to the spinal dorsal horn; the noradreline binding with α_2 receptor on the presynaptic neurons causes suppression of pain signals by reduction of both the release of excitatory glutamate from primary afferent fibers and the activity of the excitatory interneurons.[87-89] The α_2 receptor is a GPCR associated with G_i protein its activation causes inhibition of the AC, reduction of the cAMP intracellular concentration and consequent block of the progression of the pain information.

Noradrenaline may promote suppression of pain signals in spinal dorsal horn by activation of the α_1 receptor located on the inhibitory GABAergic interneurons.[90,91]

Furthermore evidences suggested that noradrenaline has pain modulatory role even in CNS.[92,93]

2. Serotonin.

Serotoninergic neurons originate on RVM nucleus (including raphe magnus and the nucleus reticularis magnocellularis)[33] and project their axons to the spinal dorsal horn. This pathway that is classically considered inhibitory, actually, has both pro- and anti-nociceptive effects. RVM contains two types of cells: the OFF cells that are inhibited by noxious stimulation and excited by opioids, and the ON cells that are excited by noxious stimulation and inhibited by opioids. The OFF circuit has inhibitory effect on ascending nociceptive transmission; conversely, ON cells facilitate pain information transmission through activation of descending pathway to spinal cord.[94,95]

Different receptor subtypes in the dorsal horn are activated by serotonin.[33] 5-HT$_1$ receptors exert anti-nociceptive effect, in particular, postsynaptic 5-HT$_{1A}$ receptors inhibit the excitability of the spinothalamic neurons and the excitatory interneurons, while presynaptic 5-HT$_{1B/D}$ receptors inhibit neurotransmitter release from primary afferents.

Conversely, the pronociceptive effects are mediated by 5-HT$_2$ and 5-HT$_3$ receptors.[29,96] 5-HT$_3$ receptors are cation channel, those located on presynaptic membrane facilitate the depolarization and consequent neurotransmitters release from primary nociceptive afferents, while those located on the postsynaptic neuron increase the excitability of the spinothalamic tract.

As for noradrenaline, also serotonin is present in further brain nuclei involved in nociception.[97]

3. Acetylcholine.

Acetylcholine (ACh) major activity in nociception signaling is in the spinal cord. ACh is released from the cholinergic interneurons in dorsal horn, activated by inhibitory descending noradrenergic and serotoninergic pathways.[98] Cholinergic somas on spinal cord are located prevalently in laminas III and IV, from here axons are projected both in deep and in superficial laminas.[99] ACh inhibitory effect in dorsal horn predominantly involves muscarinic receptors located in both primary afferent fibers terminal (M_2 and M_3 predominantly) and on dorsal horn projected neurons (M_2 and M_4).[100]

Activation of nicotinic receptors contribute to the noradrenergic antinociceptive activity in dorsal horn.[101] ACh can activate directly noradrenergic neurons on the spinal cord acting on nicotine receptors located on the terminus.[102]

1.4.7 Opioid peptides

Endorphins, encephalin, dynorphins, endomorphins are a series of endogenous peptides involved in pain modulation, named endogenous opioids. These peptides are located mainly in the brain, spinal cord and in the peripheral nervous system.

The targets of endogenous opiods are three GPCRs, μ (mu), δ (delta) and κ (kappa). The μ receptors are located mainly in brain and spinal cord, including many areas involved in nociception such as medial thalamus, PAG and MNR, confirming their role in modulating pain information. The μ receptors have been also localized in the nucleus accumbens, cerebellar trunk, thalamus and striatum.[103]

The distribution of δ receptors is quite similar to that of μ. Moreover, they have been located in the olfactory area and substantia nigra too. Conversely, κ receptors have a quite different localization. They were found in the amygdala, hypothalamus, and pituitary as well as in the striatum.[104]

The three opiod receptors are coupled with G_i/G_o proteins, which have overall inhibitory effects, in fact they cause a membrane stabilization with consequent decrease of the discharge frequency and inhibition of neurotransmitter release.

The activation of these G proteins opens K^+ channels, potassium ions come out of the cell causing hyperpolarization. Opioids cause inhibitory effect also via closure of the Ca^{2+} voltage-dependent channels on the presynaptic terminal producing action potential decrease and consequent reduction of the neurotransmitters (like glutamate and/or SP) release.

G_i proteins coupled with opioid receptors also inhibit AC, then the cAMP reduction and consequent decrease of the activity of related PKA may be responsible of change of ion channels permeability. Despite the signal transduction details are not entirely known, the cAMP cascade is clearly involved in the long term effects of the opioids like tolerance, dependence and abstinence.[105]

Opioid peptides exert their inhibitory action at three levels:

- in *spinal cord* through small inhibitory interneurons that releasing the endogenous opioids inhibit the activation of the spinal projection neurons;
- through *descending pathway from PAG* in three different ways, directly inhibiting the projection neurons, stimulating neurons opioid inhibitors and/or inhibiting excitatory interneurons;
- in *brain*, which explain the connection between opioid effects on emotional and hormonal aspects of pain.

1.4.8 Endocannabinoids

The endocannabinoids (ECs) are a class of endogenous compounds endowed analgesic mechanism and action site similar to opioids peptides.

The main representative compounds of this class are anandamide (*N*-arachidonoyl ethanolamine or AEA) and 2-arachidonoylglycerol (2-AG), they exert their activity binding two GPCRs, CB1 and CB2.

Evidence suggests that CB1 are localized prevalently in the presynaptic terminal. CB1 are coupled with G_i/G_o proteins and their activation, as for the opioid receptors, cause cAMP concentration diminution, Ca^{2+} channels closing and K^+ channels opening, causing reduction of neurotransmitters release as final consequence.

AEA and 2-AG are formed starting from AA, and released by the postsynaptic neurons as consequence of Ca^{2+} intracellular concentration increasing.

As opioid peptides, ECs act at different levels of nociceptive pathways, supraspinal, spinal and peripheral.

ECs exert their antinociceptive proprieties in PAG, thalamus, RVM, MNR and amygdala *supraspinal areas*.[106] In RVM it has been revealed that cannabinoids inhibit the firing of ON cells, whilst promoting the firing of OFF cells.[107]

In *dorsal horn neurons* it is not yet completely clear ECs action mechanism; evidences suggest that CB1 are located in this area prevalently on the presynaptic of nociceptive primary afferents and on populations of excitatory interneurons.[108]

At *peripheral level* the ECs antinociceptive effect has been described as mainly CB2 mediated.[109] The analgesic effect involves different mechanisms, inhibition of the production and release of pro-inflammatory and pro-nociceptive mediators,[110] and cytokines by peripheral immune cells.[111]

It is important to underline that AEA, but not 2-AG, can have pro-nociceptive effect because it can bind TRPV1 in an intracellular site. This binding can cause channel opening and consequent neurons depolarization. The affinity AEA RRPV1 affinity is lower as compared to the receptors CB1 and CB2.[112]

1.5 Pain: The nowadays pain therapy

Because the pain information transmission involves numerous pathways, systems, mediators, receptors etc. the analgesic drugs can act on different way.

For a proper pain therapy it is essential a correct diagnosis of the disease causes since, as previously described, there are many different types of pain. In general acute pain does not represent a problem because it accurately responds to opioid or non-steroidal anti-inflammatory drugs (NSAIDs).

Treatment of chronic pain is more difficult, because the emotional and subjective conditions represent fundamental components of the pathologic state. The 50% of chronic pain patients suffer of depression, while the 40% of anxiety disorders.[6]

The different classes of drugs used in pain:
-   act on the site of inflammation or injury (NSAIDs);
-   block the activity of the primary afferent neurons (local anesthetics);
-   enhance the inhibitory system (opioids);
-   stimulate the inhibitory descending pathways (tricyclic antidepressants).

NSAIDs and opioids are the most used analgesic drugs. NSAIDs have anti-inflammatory, antipyretic and analgesic properties. As well as for the treatment of acute pain (such as headache and acute backache), NSAIDs are indicated for treatment of rheumatologic diseases, arthrosis and musculoskeletal pain; but they are less useful for neuropathic pain.

NSAIDs activity is due to the inhibition of the COX enzymes and consequent inhibition of the prostaglandins formation in particular PGE_2. At least two different isoforms, COX-1 and -2, exist, the first is constitutively expressed, and it is responsible to the normal physiological function. While the COX-2 is generally inducible and is synthesized during inflammatory processes causing prostaglandin

concentrations increase at the site of inflammation. Some NSAIDs are non-selective COX-1 and COX-2 inhibitors, some are preferential COX-2 inhibitors and some other are selective COX-2 inhibitors.

The problem of the prolonged use of the NSAIDs is related to their side effects. In particular the non-selective NSAIDs may cause stomach ulcers by inhibition of gastric COX-1, blocking the synthesis of the prostaglandins that in turn stimulate the production of the gastric wall protective mucus and inhibit the secretion of hydrochloric acid. Another important adjunct effect of NSAIDs is the inhibition of platelet aggregation by, especially, the inhibition of COX-1 mediated thromboxane formation.

Although the selective COX-2 inhibitors do not have the gastric side effect, their use is limited because they have some important cardiovascular side effects due to lack of anti-platelet activity.

Analgesic Opioids mimic the effects of opioid peptides binding opioid receptors (μ and δ in particular) at the three above described levels, spinal cord, the inhibitory descending pathways and brain, according to their ability to cross the blood brain barrier.

Opioids are used for treatment of acute pain, post-operative pain and in palliative care; while their use for chronic pain is not very common. Also this class of compounds has numerous important side effects, especially related to their chronic use. Short period major toxic effect is respiratory depression caused in particular, but not only, by an increase threshold of CO_2 necessary to the centers of the brainstem to stimulate respiration. Short period side effects include nausea, constipation and sedation. Long-term side effects included addiction, tolerance to the analgesic effect and abstinence.

NMDA antagonists like ketamine, memantine and dextromethorphan display significant analgesic effects counteracting the pro-nociceptive activity of glutamate. In addition, in this case there are significant systemic side effects, which greatly limit the use also they easily develop tolerance.

Anticonvulsant drugs like gabapentin, which inhibits Ca^{2+} and Na^+ voltage-dependent channels, are mainly used to treat pain in diabetic neuropathy and postherpetic neuralgia. Other anticonvulsants like carbamazepine and phenytoin are used for treatment of trigeminal neuralgia. These drugs may cause hepatotoxicity and show cognitive impairment, confusion, drowsiness, dizziness and nausea.

α_2-*Agonists,* like clonidine, behave as anti-nociceptive agents binding the adrenergic presynaptic receptors that causes reduction of the release of catecholamines. The problem with this class of compounds is the lack of selectivity for the α_2-receptors in the nociceptive pathways.

Triptans such as sumatriptan and its analogs are selective agonist of serotonin receptor (5-HT$_{1B/1D}$) used for the treatment of primary migraine.

Ergot alkaloids like ergotamine or dihydroergotamine, are used for migraine treatment.

Antidepressants in particular the tricyclic antidepressants cause a potentiation of the noradrenaline and serotonin inhibitory pathways by the inhibition of the reuptake of nordrenaline and serotonin in the spinal cord. The problems of this class of drug are the long on-set time and their toxicity.

For all the problems of the current pain therapies, the research of new drugs endowed with better therapeutic efficacy and fewer side effects, also taking advantage of new targets is actually very active.

1.6 References

1   Fishbain, D., Johnson, S., Webster, L., Greene, L. & Faysal, J. Review of Regulatory Programs and New Opioid Technologies in Chronic Pain Management: Balancing the Risk of Medication Abuse with Medical Need. *Journal of Managed Care Pharmacy* **16**, 12 (2010).

2   Nagasako, E. M., Oaklander, A. L. & Dworkin, R. H. Congenital insensitivity to pain: an update. *Pain* **101**, 213-219, doi:http://dx.doi.org/10.1016/S0304-3959(02)00482-7 (2003).

3   Basbaum, A. I., Bautista, D. M., Scherrer, G. & Julius, D. Cellular and Molecular Mechanisms of Pain. *Cell* **139**, 267-284, doi:http://dx.doi.org/10.1016/j.cell.2009.09.028 (2009).

4   Mannion, R. J. & Woolf, C. J. Pain Mechanisms and Management: A Central Perspective. *The Clinical Journal of Pain* **16**, S144-S156 (2000).

5   Breivik, H., Eisenberg, E., O'Brien, T. & OPENMinds, o. b. o. The individual and societal burden of chronic pain in Europe: the case for strategic prioritisation and action to improve knowledge and availability of appropriate care. *BMC Public Health* **13**, 1229 (2013).

6   Breivik, H., Collett, B., Ventafridda, V., Cohen, R. & Gallacher, D. Survey of chronic pain in Europe: prevalence, impact on daily life, and treatment. *European Journal of Pain* **10**, 287 - 333 (2006).

7   van Hecke, O., Torrance, N. & Smith, B. H. Chronic pain epidemiology and its clinical relevance. *British Journal of Anaesthesia* **111**, 13-18, doi:10.1093/bja/aet123 (2013).

8   Christo, P. J. & Mazloomdoost, D. Cancer Pain and Analgesia. *Annals of the New York Academy of Sciences* **1138**, 278-298, doi:10.1196/annals.1414.033 (2008).

9   Sikandar, S. & Dickenson, A. H. Visceral Pain – the Ins and Outs, the Ups and Downs. *Current opinion in supportive and palliative care* **6**, 17-26, doi:10.1097/SPC.0b013e32834f6ec9 (2012).

10 Omoigui, S. The biochemical origin of pain: The origin of all pain is inflammation and the inflammatory response. Part 2 of 3 – Inflammatory profile of pain syndromes. *Medical Hypotheses* **69**, 1169-1178, doi:http://dx.doi.org/10.1016/j.mehy.2007.06.033 (2007).

11 Zunhammer, M., Halski, A., Eichhammer, P. & Busch, V. Theory of Mind and Emotional Awareness in Chronic Somatoform Pain Patients. *PLoS ONE* **10**, e0140016, doi:10.1371/journal.pone.0140016 (2015).

12   Morgan, M. M. & Fields, H. L. Pronounced changes in the activity of nociceptive modulatory neurons in the rostral ventromedial medulla in response to prolonged thermal noxious stimuli. *Journal of Neurophysiology* **72**, 1161-1170 (1994).

13   Woolf, C. J. & Salter, M. W. Neuronal Plasticity: Increasing the Gain in Pain. *Science* **288**, 1765-1768, doi:10.1126/science.288.5472.1765 (2000).

14   Weidner, C., Schmelz, M., Schmidt, R., Hansson, B., Handwerker, H. O. & Torebjörk, H. E. Functional Attributes Discriminating Mechano-Insensitive and Mechano-Responsive C Nociceptors in Human Skin. *The Journal of Neuroscience* **19**, 10184-10190 (1999).

15   Handwerker, H. O., Kilo, S. & Reeh, P. W. Unresponsive afferent nerve fibres in the sural nerve of the rat. *The Journal of Physiology* **435**, 229-242, doi:10.1113/jphysiol.1991.sp018507 (1991).

16   Lorenzo, L.-E., Ramien, M., St. Louis, M., De Koninck, Y. & Ribeiro-Da-Silva, A. Postnatal changes in the Rexed lamination and markers of nociceptive afferents in the superficial dorsal horn of the rat. *The Journal of Comparative Neurology* **508**, 592-604, doi:10.1002/cne.21691 (2008).

17   Treede, R.-D., Kenshalo, D. R., Gracely, R. H. & Jones, A. K. P. The cortical representation of pain. *Pain* **79**, 105-111, doi:http://dx.doi.org/10.1016/S0304-3959(98)00184-5 (1999).

18   Willis, W. D., Jr. in *Spinal Cord Monitoring and Electrodiagnosis* (eds Koki Shimoji, Takahide Kurokawa, Tetsuya Tamaki, & WilliamD Willis, Jr.) Ch. 1, 1-7 (Springer Berlin Heidelberg, 1991).

19   De Broucker, T., Cesaro, P., Willer, J. C. & Le Bars, D. Diffuse noxious inhibitory controls in man. *INVOLVEMENT OF THE SPINORETICULAR TRACT* **113**, 1223-1234, doi:10.1093/brain/113.4.1223 (1990).

20   Yezierski, R. P. & Broton, J. G. Functional properties of spinomesencephalic tract (SMT) cells in the upper cervical spinal cord of the cat. *Pain* **45**, 187-196, doi:10.1016/0304-3959(91)90187-3 (1991).

21   Gauriau, C. & Bernard, J.-F. Pain Pathways and Parabrachial Circuits in the Rat. *Experimental Physiology* **87**, 251-258, doi:10.1113/eph8702357 (2002).

22   Zhang, X., Kostarczyk, E. & Giesler, G. Spinohypothalamic tract neurons in the cervical enlargement of rats: descending axons in the ipsilateral brain. *The Journal of Neuroscience* **15**, 8393-8407 (1995).

_____

23   Tracey, I. & Mantyh, P. W. The Cerebral Signature for Pain Perception and Its Modulation. *Neuron* **55**, 377-391, doi:http://dx.doi.org/10.1016/j.neuron.2007.07.012 (2007).

24   Le Bars, D., Bourgoin, S., Clot, A. M., Hamon, M. & Cesselin, F. Noxious mechanical stimuli increase the release of Met-enkephalin-like material heterosegmentally in the rat spinal cord. *Brain Research* **402**, 188-192, doi:http://dx.doi.org/10.1016/0006-8993(87)91066-3 (1987).

25   Hammond, D. L., Tyce, G. M. & Yaksh, T. L. Efflux of 5-hydroxytryptamine and noradrenaline into spinal cord superfusates during stimulation of the rat medulla. *The Journal of Physiology* **359**, 151-162, doi:10.1113/jphysiol.1985.sp015579 (1985).

26   Nicol, G., Klingberg, D. & Vasko, M. Prostaglandin E2 increases calcium conductance and stimulates release of substance P in avian sensory neurons. *The Journal of Neuroscience* **12**, 1917-1927 (1992).

27   Meller, S. T. & Gebhart, G. F. Nitric oxide (NO) and nociceptive processing in the spinal cord. *Pain* **52**, 127-136, doi:http://dx.doi.org/10.1016/0304-3959(93)90124-8 (1993).

28   Malmberg, A. & Yaksh, T. Hyperalgesia mediated by spinal glutamate or substance P receptor blocked by spinal cyclooxygenase inhibition. *Science* **257**, 1276-1279, doi:10.1126/science.1381521 (1992).

29   Gebhart, G. F. Descending modulation of pain. *Neuroscience & Biobehavioral Reviews* **27**, 729-737, doi:http://dx.doi.org/10.1016/j.neubiorev.2003.11.008 (2004).

30   Reynolds, D. V. Surgery in the Rat during Electrical Analgesia Induced by Focal Brain Stimulation. *Science* **164**, 444-445 (1969).

31   Melzack, R. Gate control theory: On the evolution of pain concepts. *Pain Forum* **5**, 128-138, doi:http://dx.doi.org/10.1016/S1082-3174(96)80050-X (1996).

32   Westlund, K. N., Bowker, R. M., Ziegler, M. G. & Coulter, J. D. Noradrenergic projections to the spinal cord of the rat. *Brain Research* **263**, 15-31, doi:http://dx.doi.org/10.1016/0006-8993(83)91196-4 (1983).

33   Millan, M. J. Descending control of pain. *Progress in Neurobiology* **66**, 355-474, doi:http://dx.doi.org/10.1016/S0301-0082(02)00009-6 (2002).

34   Coggeshall, R. E. & Carlton, S. M. Ultrastructural analysis of NMDA, AMPA, and kainate receptors on unmyelinated and myelinated axons in the periphery. *The Journal of Comparative Neurology* **391**,

_____

78-86, doi:10.1002/(SICI)1096-9861(19980202)391:1<78::AID-CNE7>3.0.CO;2-O (1998).

35   Miki, K., Zhou, Q.-Q., Guo, W., Guan, Y., Terayama, R., Dubner, R. & Ren, K. Changes in Gene Expression and Neuronal Phenotype in Brain Stem Pain Modulatory Circuitry After Inflammation. *Journal of Neurophysiology* **87**, 750-760 (2002).

36   Kinkelin, I., Bröcker, E.-B., Koltzenburg, M. & Carlton, S. M. Localization of ionotropic glutamate receptors in peripheral axons of human skin. *Neuroscience Letters* **283**, 149-152, doi:http://dx.doi.org/10.1016/S0304-3940(00)00944-7 (2000).

37   Omote, K., Kawamata, T., Kawamata, M. & Namiki, A. Formalin-induced release of excitatory amino acids in the skin of the rat hindpaw. *Brain Research* **787**, 161-164, doi:http://dx.doi.org/10.1016/S0006-8993(97)01568-0 (1998).

38   Popratiloff, A., Weinberg, R. J. & Rustioni, A. AMPA Receptor Subunits Underlying Terminals of Fine-Caliber Primary Afferent Fibers. *The Journal of Neuroscience* **16**, 3363-3372 (1996).

39   Lee, C. J., Bardoni, R., Tong, C.-K., Engelman, H. S., Joseph, D. J., Magherini, P. C. & MacDermott, A. B. Functional Expression of AMPA Receptors on Central Terminals of Rat Dorsal Root Ganglion Neurons and Presynaptic Inhibition of Glutamate Release. *Neuron* **35**, 135-146, doi:http://dx.doi.org/10.1016/S0896-6273(02)00729-8 (2002).

40   Monaghan, D. T., Yao, D. & Cotman, C. W. Distribution of [3H]AMPA binding sites in rat brain as determined by quantitative autoradiography. *Brain Research* **324**, 160-164, doi:http://dx.doi.org/10.1016/0006-8993(84)90636-X (1984).

41   Guan, Y., Terayama, R., Dubner, R. & Ren, K. Plasticity in Excitatory Amino Acid Receptor-Mediated Descending Pain Modulation after Inflammation. *Journal of Pharmacology and Experimental Therapeutics* **300**, 513-520, doi:10.1124/jpet.300.2.513 (2002).

42   Marceau, F. & Bachvarov, D. Kinin receptors. *Clinical Reviews in Allergy & Immunology* **16**, 385-401, doi:10.1007/BF02737658 (1998).

43   Ahluwalia, A. & Perretti, M. B1 receptors as a new inflammatory target. Could this B the 1? *Trends in Pharmacological Sciences* **20**, 100-104, doi:http://dx.doi.org/10.1016/S0165-6147(99)01321-8 (1999).

44   Ferreira, J., Campos, M. M., Araújo, R., Bader, M., Pesquero, J. B. & Calixto, J. B. The use of kinin B1 and B2 receptor knockout mice and selective antagonists to characterize the nociceptive responses

caused by kinins at the spinal level. *Neuropharmacology* **43**, 1188-1197, doi:http://dx.doi.org/10.1016/S0028-3908(02)00311-8 (2002).

45   Burgess, G., Mullaney, I., McNeill, M., Dunn, P. & Rang, H. Second messengers involved in the mechanism of action of bradykinin in sensory neurons in culture. *The Journal of Neuroscience* **9**, 3314-3325 (1989).

46   Kozaki, Y., Kambe, F., Hayashi, Y., Ohmori, S., Seo, H., Kumazawa, T. & Mizumura, K. Molecular cloning of prostaglandin EP3 receptors from canine sensory ganglia and their facilitatory action on bradykinin-induced mobilization of intracellular calcium. *Journal of Neurochemistry* **100**, 1636-1647, doi:10.1111/j.1471-4159.2006.04320.x (2007).

47   Gammon, C. M., Allen, A. C. & Morell, P. Bradykinin Stimulates Phosphoinositide Hydrolysis and Mobilization of Arachidonic Acid in Dorsal Root Ganglion Neurons. *Journal of Neurochemistry* **53**, 95-101, doi:10.1111/j.1471-4159.1989.tb07299.x (1989).

48   Huang, S. M., Bisogno, T., Trevisani, M., Al-Hayani, A., De Petrocellis, L., Fezza, F., Tognetto, M., Petros, T. J., Krey, J. F., Chu, C. J., Miller, J. D., Davies, S. N., Geppetti, P., Walker, J. M. & Di Marzo, V. An endogenous capsaicin-like substance with high potency at recombinant and native vanilloid VR1 receptors. *Proceedings of the National Academy of Sciences* **99**, 8400-8405, doi:10.1073/pnas.122196999 (2002).

49   Smart, D., Gunthorpe, M. J., Jerman, J. C., Nasir, S., Gray, J., Muir, A. I., Chambers, J. K., Randall, A. D. & Davis, J. B. The endogenous lipid anandamide is a full agonist at the human vanilloid receptor (hVR1). *British Journal of Pharmacology* **129**, 227-230, doi:10.1038/sj.bjp.0703050 (2000).

50   Immke, D. C. & Gavva, N. R. The TRPV1 receptor and nociception. *Seminars in Cell & Developmental Biology* **17**, 582-591, doi:http://dx.doi.org/10.1016/j.semcdb.2006.09.004 (2006).

51   Hwang, S. W., Cho, H., Kwak, J., Lee, S.-Y., Kang, C.-J., Jung, J., Cho, S., Min, K. H., Suh, Y.-G., Kim, D. & Oh, U. Direct activation of capsaicin receptors by products of lipoxygenases: Endogenous capsaicin-like substances. *Proceedings of the National Academy of Sciences* **97**, 6155-6160, doi:10.1073/pnas.97.11.6155 (2000).

52   Cesare, P., Dekker, L. V., Sardini, A., Parker, P. J. & McNaughton, P. A. Specific Involvement of PKC-ε in Sensitization of the Neuronal Response to Painful Heat. *Neuron* **23**, 617-624, doi:http://dx.doi.org/10.1016/S0896-6273(00)80813-2 (1999).

53   Reid, G., Babes, A. & Pluteanu, F. A cold- and menthol-activated current in rat dorsal root ganglion neurones: properties and role in cold transduction. *The Journal of Physiology* **545**, 595-614, doi:10.1113/jphysiol.2002.024331 (2002).

54   Premkumar, L. S., Raisinghani, M., Pingle, S. C., Long, C. & Pimentel, F. Downregulation of Transient Receptor Potential Melastatin 8 by Protein Kinase C-Mediated Dephosphorylation. *The Journal of Neuroscience* **25**, 11322-11329, doi:10.1523/jneurosci.3006-05.2005 (2005).

55   Bandell, M., Story, G. M., Hwang, S. W., Viswanath, V., Eid, S. R., Petrus, M. J., Earley, T. J. & Patapoutian, A. Noxious Cold Ion Channel TRPA1 Is Activated by Pungent Compounds and Bradykinin. *Neuron* **41**, 849-857, doi:http://dx.doi.org/10.1016/S0896-6273(04)00150-3 (2004).

56   Yu, S. & Ouyang, A. TRPA1 in bradykinin-induced mechanical hypersensitivity of vagal C fibers in guinea pig esophagus. *American Journal of Physiology - Gastrointestinal and Liver Physiology* **296**, G255-G265, doi:10.1152/ajpgi.90530.2008 (2009).

57   Smith, J. A. M., Amagasu, S. M., Eglen, R. M., Hunter, J. C. & Bley, K. R. Characterization of prostanoid receptor-evoked responses in rat sensory neurones. *British Journal of Pharmacology* **124**, 513-523, doi:10.1038/sj.bjp.0701853 (1998).

58   Smith, J. A. M., Davis, C. L. & Burgess, G. M. Prostaglandin E2-induced sensitization of bradykinin-evoked responses in rat dorsal root ganglion neurons is mediated by cAMP-dependent protein kinase A. *European Journal of Neuroscience* **12**, 3250-3258, doi:10.1046/j.1460-9568.2000.00218.x (2000).

59   Kopp, U. C., Cicha, M. Z. & Smith, L. A. PGE2 increases release of substance P from renal sensory nerves by activating the cAMP-PKA transduction cascade. *American Journal of Physiology - Regulatory, Integrative and Comparative Physiology* **282**, R1618-R1627, doi:10.1152/ajpregu.00701.2001 (2002).

60   England, S., Bevan, S. & Docherty, R. J. PGE2 modulates the tetrodotoxin-resistant sodium current in neonatal rat dorsal root ganglion neurones via the cyclic AMP-protein kinase A cascade. *The Journal of Physiology* **495**, 429-440 (1996).

61   Gold, M. S., Levine, J. D. & Correa, A. M. Modulation of TTX-R I Na by PKC and PKA and Their Role in PGE2-Induced Sensitization of Rat Sensory Neurons In Vitro. *The Journal of Neuroscience* **18**, 10345-10355 (1998).

---

62   Moriyama, T., Higashi, T., Togashi, K., Iida, T., Segi, E., Sugimoto, Y., Tominaga, T., Narumiya, S. & Tominaga, M. Sensitization of TRPV1 by EP1 and IP reveals peripheral nociceptive mechanism of prostaglandins. *Molecular Pain* **1**, 3 (2005).

63   Linte, R., Ciobanu, C., Reid, G. & Babes, A. Desensitization of cold- and menthol-sensitive rat dorsal root ganglion neurones by inflammatory mediators. *Experimental Brain Research* **178**, 89-98, doi:10.1007/s00221-006-0712-3 (2007).

64   Bang, S., Kim, K. Y., Yoo, S., Kim, Y. G. & Hwang, S. W. Transient receptor potential A1 mediates acetaldehyde-evoked pain sensation. *European Journal of Neuroscience* **26**, 2516-2523, doi:10.1111/j.1460-9568.2007.05882.x (2007).

65   Mayer, M. L & Westbrook, G. L. A voltage-clamp analysis of inward (anomalous) rectification in mouse spinal sensory ganglion neurones. *The Journal of Physiology* **340**, 19-45, doi:10.1113/jphysiol.1983.sp014747 (1983).

66   Ingram, S. L. & Williams, J. T. Modulation of the hyperpolarization-activated current (Ih) by cyclic nucleotides in guinea-pig primary afferent neurons. *The Journal of Physiology* **492**, 97-106, doi:10.1113/jphysiol.1996.sp021292 (1996).

67   Cho, H., Shin, J., Shin, C. Y., Lee, S.-Y. & Oh, U. Mechanosensitive Ion Channels in Cultured Sensory Neurons of Neonatal Rats. *The Journal of Neuroscience* **22**, 1238-1247 (2002).

68   Grega, D. & Macdonald, R. Activators of adenylate cyclase and cyclic AMP prolong calcium- dependent action potentials of mouse sensory neurons in culture by reducing a voltage-dependent potassium conductance. *The Journal of Neuroscience* **7**, 700-707 (1987).

69   Jiang, X., Zhang, Y. H., Clark, J. D., Tempel, B. L. & Nicol, G. D. Prostaglandin e2 inhibits the potassium current in sensory neurons from hyperalgesic kv1.1 knockout mice. *Neuroscience* **119**, 65-72, doi:http://dx.doi.org/10.1016/S0306-4522(03)00073-3 (2003).

70   Fowler, J. C., Wonderlin, W. F. & Weinreich, D. Prostaglandins block a Ca2+-dependent slow spike afterhyperpolarization independent of effects on Ca2+ influx in visceral afferent neurons. *Brain Research* **345**, 345-349, doi:http://dx.doi.org/10.1016/0006-8993(85)91014-5 (1985).

71   Fink, M., Duprat, F., Lesage, F., Reyes, R., Romey, G., Heurteaux, C. & Lazdunski, M. Cloning, functional expression and brain localization of a novel unconventional outward rectifier K+ channel. *The EMBO Journal* **15**, 6854-6862 (1996).

---

72   Giannini, E., Lattanzi, R., Nicotra, A., Campese, A. F., Grazioli, P., Screpanti, I., Balboni, G., Salvadori, S., Sacerdote, P. & Negri, L. The chemokine Bv8/prokineticin 2 is up-regulated in inflammatory granulocytes and modulates inflammatory pain. *Proceedings of the National Academy of Sciences* **106**, 14646-14651, doi:10.1073/pnas.0903720106 (2009).

73   Negri, L., Lattanzi, R., Giannini, E., Metere, A., Colucci, M., Barra, D., Kreil, G. & Melchiorri, P. Nociceptive sensitization by the secretory protein Bv8. *British Journal of Pharmacology* **137**, 1147-1154, doi:10.1038/sj.bjp.0704995 (2002).

74   Vellani, V., Colucci, M., Lattanzi, R., Giannini, E., Negri, L., Melchiorri, P. & McNaughton, P. A. Sensitization of Transient Receptor Potential Vanilloid 1 by the Prokineticin Receptor Agonist Bv8. *The Journal of Neuroscience* **26**, 5109-5116, doi:10.1523/jneurosci.3870-05.2006 (2006).

75   Hu, W.-P., Zhang, C., Li, J.-D., Luo, Z. D., Amadesi, S., Bunnett, N. & Zhou, Q.-Y. Impaired pain sensation in mice lacking prokineticin 2. *Molecular Pain* **2**, 35 (2006).

76   Negri, L., Lattanzi, R., Giannini, E., Colucci, M., Margheriti, F., Melchiorri, P., Vellani, V., Tian, H., De Felice, M. & Porreca, F. Impaired nociception and inflammatory pain sensation in mice lacking the prokineticin receptor PKR1: focus on interaction between PKR1 and the capsaicin receptor TRPV1 in pain behavior. *The Journal of Neuroscience* **26**, 6716 - 6727 (2006).

77   Negri, L., Lattanzi, R., Giannini, E. & Melchiorri, P. Bv8/Prokineticin proteins and their receptors. *Life Sciences* **81**, 1103-1116, doi:http://dx.doi.org/10.1016/j.lfs.2007.08.011 (2007).

78   Negri, L., Lattanzi, R., Giannini, E. & Melchiorri, P. Modulators of Pain: Bv8 and Prokineticins. *Current Neuropharmacology* **4**, 207-215 (2006).

79   Hökfelt, T., Kellerth, J.-O., Nilsson, G. & Pernow, B. Experimental immunohistochemical studies on the localization and distribution of substance P in cat primary sensory neurons. *Brain Research* **100**, 235-252, doi:http://dx.doi.org/10.1016/0006-8993(75)90481-3 (1975).

80   Ljungdahl, Å., Hökfelt, T. & Nilsson, G. Distribution of substance P-like immunoreactivity in the central nervous system of the rat—I. Cell bodies and nerve terminals. *Neuroscience* **3**, 861-943, doi:http://dx.doi.org/10.1016/0306-4522(78)90116-1 (1978).

81   Lamotte, C. C. & Shapiro, C. M. Ultrastructural localization of substance P, met-enkephalin, and somatostatin immunoreactivity

_____

in lamina X of the primate spinal cord. *The Journal of Comparative Neurology* **306**, 290-306, doi:10.1002/cne.903060206 (1991).

82   Quartara, L. & Maggi, C. A. The tachykinin NK1 receptor. Part I: Ligands and mechanisms of cellular activation. *Neuropeptides* **31**, 537-563, doi:10.1016/S0143-4179(97)90001-9.

83   Mitsuhashi, M., Ohashi, Y., Shichijo, S., Christian, C., Sudduth-Klinger, J., Harrowe, G. & Payan, D. G. Multiple intracellular signaling pathways of the neuropeptide substance P receptor. *Journal of Neuroscience Research* **32**, 437-443, doi:10.1002/jnr.490320315 (1992).

84   Mochizuki-Oda, N., Nakajima, Y., Nakanishi, S. & Ito, S. Characterization of the substance P receptor-mediated calcium influx in cDNA transfected Chinese hamster ovary cells. A possible role of inositol 1,4,5-trisphosphate in calcium influx. *Journal of Biological Chemistry* **269**, 9651-9658 (1994).

85   Garcia, M., Sakamoto, K., Shigekawa, M., Nakanishi, S. & Ito, S. Multiple mechanisms of arachidonic acid release in Chinese hamster ovary cells transfected with cDNA of substance P receptor. *Biochemical Pharmacology* **48**, 1735-1741, doi:http://dx.doi.org/10.1016/0006-2952(94)90459-6 (1994).

86   Nakajima, Y., Tsuchida, K., Negishi, M., Ito, S. & Nakanishi, S. Direct linkage of three tachykinin receptors to stimulation of both phosphatidylinositol hydrolysis and cyclic AMP cascades in transfected Chinese hamster ovary cells. *Journal of Biological Chemistry* **267**, 2437-2442 (1992).

87   Kawasaki, M. D. Y., Kumamoto, P. D. E., Furue, P. D. H. & Yoshimura, M. D. P. D. M. α2Adrenoceptor–mediated Presynaptic Inhibition of Primary Afferent Glutamatergic Transmission in Rat Substantia Gelatinosa Neurons. *Anesthesiology* **98**, 682-689 (2003).

88   Pan, Y.-Z., Li, D.-P. & Pan, H.-L. Inhibition of Glutamatergic Synaptic Input to Spinal Lamina IIo Neurons by Presynaptic α2-Adrenergic Receptors. *Journal of Neurophysiology* **87**, 1938-1947, doi:10.1152/jn.00575.2001 (2002).

89   Olave, M. J. & Maxwell, D. J. Neurokinin-1 Projection Cells in the Rat Dorsal Horn Receive Synaptic Contacts from Axons That Possess α2C-Adrenergic Receptors. *The Journal of Neuroscience* **23**, 6837-6846 (2003).

90   Baba, M. D. P. D. H., Shimoji, M. D. P. D. K. & Yoshimura, M. D. P. D. M. Norepinephrine Facilitates Inhibitory Transmission in Substantia Gelatinosa of Adult Rat Spinal Cord (Part 1) Effects on Axon

_____

Terminals of GABAergic and Glycinergic Neurons. *Anesthesiology* **92**, 473-473 (2000).

91   Baba, M. D. P. D. H., Goldstein, M. D. Peter A., Okamoto, M. D. P. D. M., Kohno, M. D. P. D. T., Ataka, M. D. T., Yoshimura, M. D. P. D. M. & Shimoji, M. D. P. D. K. Norepinephrine Facilitates Inhibitory Transmission in Substantia Gelatinosa of Adult Rat Spinal Cord (Part 2) Effects on Somatodendritic Sites of GABAergic Neurons. *Anesthesiology* **92**, 485-485 (2000).

92   Maruo, K., Yamamoto, H., Yamamoto, S., Nagata, T., Fujikawa, H., Kanno, T., Yaguchi, T., Maruo, S., Yoshiya, S. & Nishizaki, T. Modulation of P2X receptors via adrenergic pathways in rat dorsal root ganglion neurons after sciatic nerve injury. *Pain* **120**, 106-112, doi:http://dx.doi.org/10.1016/j.pain.2005.10.016 (2006).

93   Howorth, P. W., Teschemacher, A. G. & Pickering, A. E. Retrograde adenoviral vector targeting of nociresponsive pontospinal noradrenergic neurons in the rat in vivo. *The Journal of Comparative Neurology* **512**, 141-157, doi:10.1002/cne.21879 (2009).

94   A I Basbaum, a. & Fields, H. L. Endogenous Pain Control Systems: Brainstem Spinal Pathways and Endorphin Circuitry. *Annual Review of Neuroscience* **7**, 309-338, doi:doi:10.1146/annurev.ne.07.030184.001521 (1984).

95   Mason, P., Gao, K. & Genzen, J. R. Serotonergic Raphe Magnus Cell Discharge Reflects Ongoing Autonomic and Respiratory Activities. *Journal of Neurophysiology* **98**, 1919-1927, doi:10.1152/jn.00813.2007 (2007).

96   Suzuki, R., Rygh, L. J. & Dickenson, A. H. Bad news from the brain: descending 5-HT pathways that control spinal pain processing. *Trends in Pharmacological Sciences* **25**, 613-617, doi:http://dx.doi.org/10.1016/j.tips.2004.10.002 (2004).

97   Zhao, Z.-Q., Chiechio, S., Sun, Y.-G., Zhang, K.-H., Zhao, C.-S., Scott, M., Johnson, R. L., Deneris, E. S., Renner, K. J., Gereau, R. W. & Chen, Z.-F. Mice Lacking Central Serotonergic Neurons Show Enhanced Inflammatory Pain and an Impaired Analgesic Response to Antidepressant Drugs. *The Journal of Neuroscience* **27**, 6045-6053, doi:10.1523/jneurosci.1623-07.2007 (2007).

98   Detweiler, D. J., Eisenach, J. C., Tong, C. & Jackson, C. A cholinergic interaction in alpha 2 adrenoceptor-mediated antinociception in sheep. *Journal of Pharmacology and Experimental Therapeutics* **265**, 536-542 (1993).

99   Gillberg, P.-G., Askmark, H. & Aquilonius, S.-M. in *Progress in Brain Research* Vol. Volume 84 (eds Aquilonius Sten-Magnus & Gillberg Per-Göran) 361-370 (Elsevier, 1990).

100   Höglund, A. U. & Baghdoyan, H. A. M2, M3 and M4, but not M1, Muscarinic Receptor Subtypes are Present in Rat Spinal Cord. *Journal of Pharmacology and Experimental Therapeutics* **281**, 470-477 (1997).

101   Xu, Z., Chen, S.-R., C. Eisenach, J. & Pan, H.-L. Role of spinal muscarinic and nicotinic receptors in clonidine-induced nitric oxide release in a rat model of neuropathic pain. *Brain Research* **861**, 390-398,   doi:http://dx.doi.org/10.1016/S0006-8993(00)02051-5 (2000).

102   Khan, I. M., Stanislaus, S., Zhang, L., Taylor, P. & Yaksh, T. L. A-85380 and Epibatidine Each Interact with Disparate Spinal Nicotinic Receptor Subtypes to Achieve Analgesia and Nociception. *Journal of Pharmacology and Experimental Therapeutics* **297**, 230-239 (2001).

103   Thompson, R. C., Mansour, A., Akil, H. & Watson, S. J. Cloning and pharmacological characterization of a rat μ opioid receptor. *Neuron* **11**, 903-913, doi:http://dx.doi.org/10.1016/0896-6273(93)90120-G (1993).

104   George, S. R., Zastawny, R. L., Brionesurbina, R., Cheng, R., Nguyen, T., Heiber, M., Kouvelas, A., Chan, A. S. & Odowd, B. F. Distinct Distributions of Mu, Delta and Kappa Opioid Receptor mRNA in Rat Brain. *Biochemical and Biophysical Research Communications* **205**, 1438-1444, doi:http://dx.doi.org/10.1006/bbrc.1994.2826 (1994).

105   Al-Hasani, R. & Bruchas, M. R. Molecular Mechanisms of Opioid Receptor-Dependent Signaling and Behavior. *Anesthesiology* **115**, 1363-1381, doi:10.1097/ALN.0b013e318238bba6 (2011).

106   Walker, J. M. & Hohmann, A. G. in *Cannabinoids* Vol. 168 *Handbook of Experimental Pharmacology* (ed RogerG Pertwee) Ch. 17, 509-554 (Springer Berlin Heidelberg, 2005).

107   Meng, I. D. & Johansen, J. P. Antinociception and modulation of rostral ventromedial medulla neuronal activity by local microinfusion of a cannabinoid receptor agonist. *Neuroscience* **124**, 685-693, doi:http://dx.doi.org/10.1016/j.neuroscience.2003.10.001 (2004).

108   Hegyi, Z., Kis, G., Holló, K., Ledent, C. & Antal, M. Neuronal and glial localization of the cannabinoid-1 receptor in the superficial spinal dorsal horn of the rodent spinal cord. *European Journal of Neuroscience* **30**, 251-262, doi:10.1111/j.1460-9568.2009.06816.x (2009).

109   Guindon, J., Desroches, J. & Beaulieu, P. The antinociceptive effects of intraplantar injections of 2-arachidonoyl glycerol are mediated by cannabinoid CB2 receptors. *British Journal of Pharmacology* **150**, 693-701, doi:10.1038/sj.bjp.0706990 (2007).

110   Hao, M.-x., Jiang, L.-s., Fang, N.-y., Pu, J., Hu, L.-h., Shen, L.-H., Song, W. & He, B. The cannabinoid WIN55,212-2 protects against oxidized LDL-induced inflammatory response in murine macrophages. *Journal of Lipid Research* **51**, 2181-2190, doi:10.1194/jlr.M001511 (2010).

111   Cencioni, M. T., Chiurchiù, V., Catanzaro, G., Borsellino, G., Bernardi, G., Battistini, L. & Maccarrone, M. Anandamide Suppresses Proliferation and Cytokine Release from Primary Human T-Lymphocytes Mainly via CB$_2$ Receptors. *PLoS ONE* **5**, e8688, doi:10.1371/journal.pone.0008688 (2010).

112   Tóth, A., Blumberg, P. M. & Boczán, J. in *Vitamins & Hormones* Vol. Volume 81   389-419 (Academic Press, 2009).
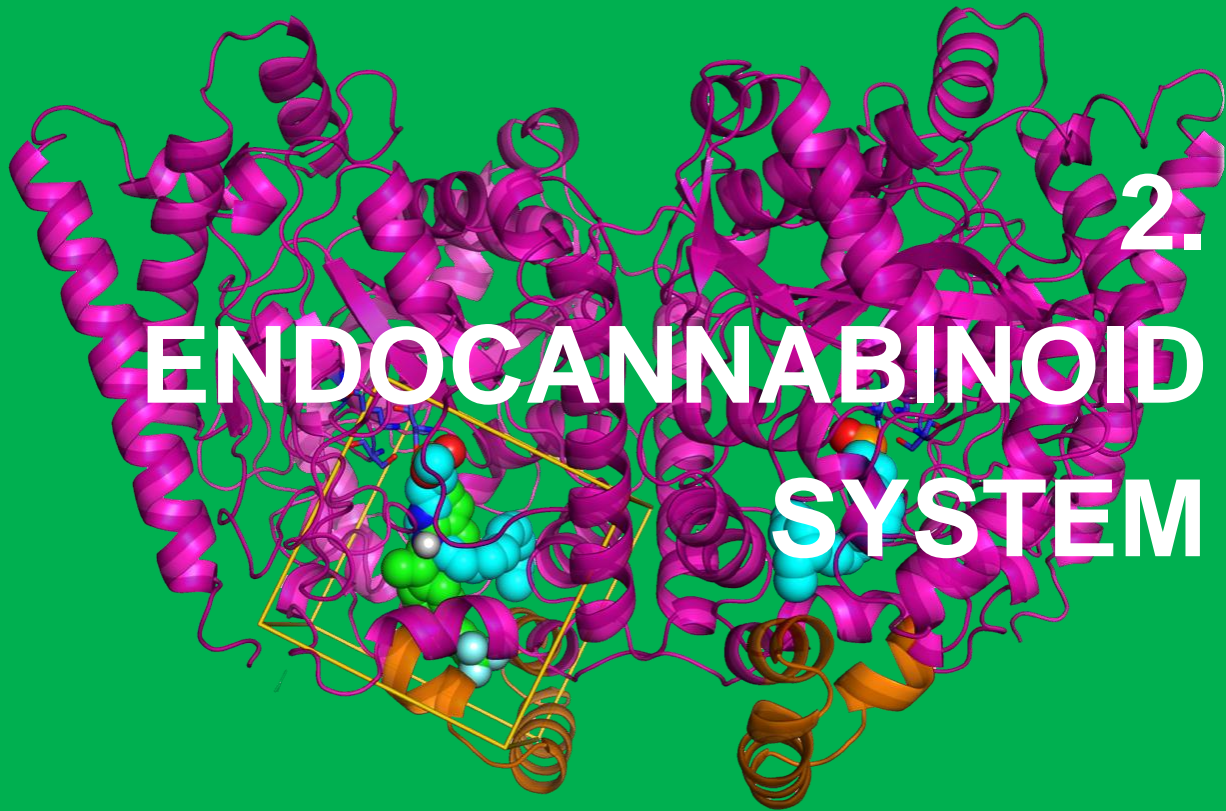
2.
ENDOCANNABINOID
SYSTEM

2. Endocannabinoid System

2.1 Endocannabinoid System: History
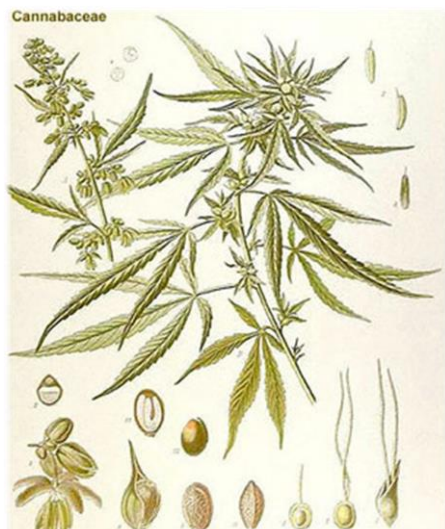
Figure 1. Cannabis Sativa.

Cannabis sativa (Figure 1) is an annual herbaceous plant, belonging to the family of *cannabaceae* of the *urticales* order, which contains over than 400 chemical compounds. Of these 66 compounds endowed with terpene-phenolic structure are cannabinoids. This term refers to all compounds of plant origin (phytocannabinoids), endogenous (endocannabinoids) or synthetic capable of binding cannabinoid receptors (CB). Phytocannabinoids can be found in all parts of the plant, and are concentrated in the yellowish resin secreted primarily from the far inflorescence of female plant.

Medical history of this plant in very old and spread all over the world, Pen T'sao Chin, the oldest Chinese book about medicinal herbs (Figure 2), dating back to 3000 BC, is the first that treats on the cannabis curative effect, recommending cannabis for the treatment of diseases such as malaria, rheumatism, gout, constipation and others. Subsequently the cannabis therapeutic indications were extended to the treatment of fever, anxiety, and as wounds healing promoter.

Figure 2. Pen T'sao Chin's book.

Cannabis, in India in approximately 1000 BC, was considered "one of the five sacred plants", it was indicated for the treatment of diarrhea, digestive disorders and lack

of appetite. There are evidence of the use of cannabis by other cultures like Egyptians, Assyrians, Romans and Greeks.

Herbarium of 70 A.D. and Galen (100 A.D.) indicate cannabis for the treatment of earaches, jaundice and edema.

During the XIIth century, the use of cannabis as medicinal plant greatly diminished because the Inquisition considered it as witch grass. For this reason in some countries, such as France and Spain, its use was prohibited, even as medication.

Only in XIXth century, when some Napoleon's soldiers return in France from Egypt cannabis began to spread in Europe, both for recreational and medicine purposes, it was adopted as the official medicine to treat pain, convulsions and nausea. In those years there has been a growing interest of scientists in the therapeutic properties of cannabis.

In the XXth century, first in USA and then in Europe, the increasing of the recreational use and the growing interest in the opium derivatives and other synthetic drugs led to ban the use of cannabis as medicine.
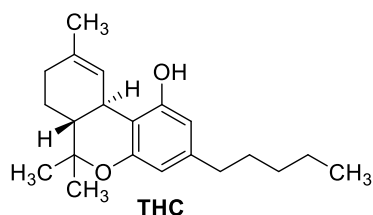
Figure 3. Δ^9-tetrahydrocannabinol structure.

In the last decades, since the discovery and isolation of the most potent active ingredient of cannabis, the Δ^9-tetrahydrocannabinol (THC) (Figure 3), the interest of the scientific community on cannabis is back.[1] This interest was increased by the discovery of membrane receptor capable to bind THC.[2,3]

2.2 Endocannabinoid System: Components

2.2.1 Cannabinoid receptors

In 1988 the receptor responsible of the pharmacological and behavioral effect of cannabinoids was individuated,[2] this receptor was called CB_1 because shortly after another receptor was discovered

and called CB_2.[4]

These receptors, which have 44% structural homology, belong to the A class (or rhodopsin class) of GPCR family and are coupled with inhibitory G proteins (G_i and G_o). CBs activation causes the inhibition of AC and the activation of mitogen-activated protein kinases (MAPK).[5] The activation of CB_1, but not CB_2, causes also the inhibition of N, P/Q type voltage-dependent Ca^{2+} channels[6] and the activation of the inwardly rectifying K^+ channels.[7]

Some evidences suggested that CB_1 is also able to activate the PLC indicating that it is also coupled with a G_q or a G_s protein.[8]

Numerous studies indicate the implication of the cannabinoid system on several physiological processes, both in the peripheral nervous system and in the CNS.

CB_1 receptors are present in peripheral and central nervous system, reproductive system, gastrointestinal tract, eyes,[9] liver, bladder and adrenergic system. In peripheral nervous system CB_1 located on DRG interneurons, superior cervical ganglia (SCG) and pre-junctional bladder fibers mediate nociception, vascular and gastrointestinal functions.[10,11]

Cannabinoid system is implicated in modulation of memory, learning, locomotor activity, posture and motor coordination, by CB_1 receptors located in basal ganglia, olfactory bulb, hippocampus and cerebellum.[12]

Furthermore CB_2 are present on immune system,[13] microglia cells[14] and in small concentrations in the brainstem.[15]

The most important receptors for nociception are located on amygdala, PAG and the dorsal horn of the spinal cord.[16]

Pharmacological evidences suggest the existence of other cannabinoid receptors, but these have not yet been characterized.[17,18]

2.2.2 Endocannabinoids
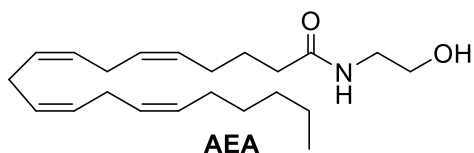
Figure 4. Anandamide structure.

The discovery of cannabinoid receptors in the early 90s promted the researchers to individuate the endogenous ligands of these receptors; the first molecule able to bind the CB identified was the N-arachidonoylethanolamine (Figure 4) also known as anandamide, it is the amide originated by two common compounds, AA and ethanolamine.[19]
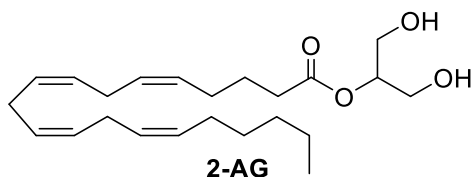
Figure 5. 2-Arachidonoylglycerole structure.

Some years after a monoacylglycerol derivative, the 2-AG (Figure 5), was identified as CBs ligand.[20]
In subsequent years numerous other CBs ligands have been identified, such as the 2-arachidonoylglycerolether (2-AGE) an analogue of 2-AG, endowed with CB_1 better affinity.[21]
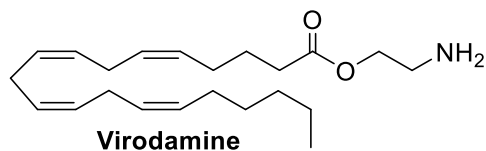
Figure 6. O-arachidonoylethanolamine structure (Virodamine).

A compound similar to AEA is virodamine also known as O-arachidonoylethanolamine (Figure 6). In this molecule the AA is connected to the ethanolamine by an ester bond. Virodamine acts as CB_1 agonist/antagonist and CB_2 agonist.[22]
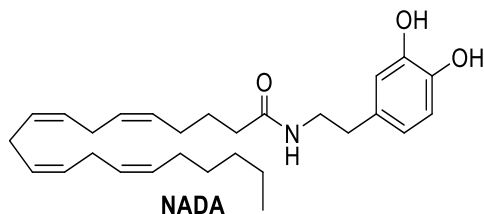
Figure 7. Arachidonoyl dopamine structure.

Further three amides, the oleylethanolamide (OEA),[23] palmitylethanolamide (PEA) and the *N*-Arachidonoyl dopamine (NADA) (Figure 7) were identified. The last one is forty times more selective on

CB_1 than CB_2[24] and is able to activate TRPV1 as AEA.[25] All these endogenous compounds capable of binding the CBs are called endocannabinoids (EC).

ECs are synthesized from AA coming from membrane phospholipids. Conversely to other neurotransmitters, ECs, are too fat-soluble and they cannot be stored in vesicles. Thus they are synthesized and released when necessary. A plausible mechanism that could lead to ECs production is the intracellular level increase of Ca^{2+}, this hypothesis is based on the fact that some enzymes of the biosynthetic pathways are influenced by Ca^{2+} (Figure 8).
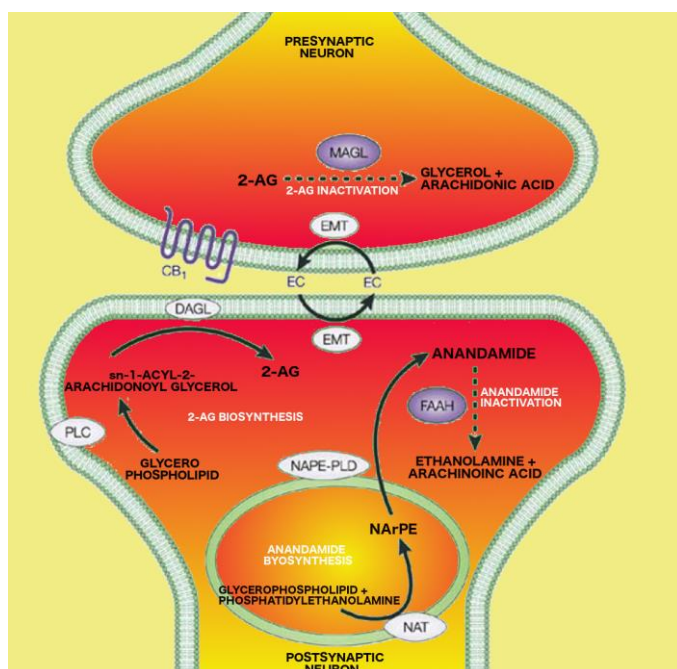
Figure 8. Endocannabinoid system.

After their release in extracellular matrix by a specific membrane transport protein ECs spread by a retrograde way to the same cell or on neighboring cells, acting as autocrine or paracrine mediators. In particular on neurons, generally, the CB_1 receptors are located on the

presynaptic terminal and after activation cause neurotransmitters release reduction (Figure 8).[26]

Evidences suggested that AEA, in an extended conformation, spread with the ethanolamine portion at the level of the polar heads of the membrane phospholipids and the hydrophobic portion within the bilayer. AEA, diffuses laterally in one of the two layers of the membrane and reaches CB_1 binding site located in the hydrophobic pocket formed by helices 3 and 6, causing receptor activation.[27]

The ending of EC signaling begin with the reuptake of the compound from the extracellular matrix by the same transporter which bring it out, the endocannabinoids membrane transport (EMT) (Figure 8).[28]

After being internalized in cells ECs are enzymatically hydrolyzed, the principal hydrolytic enzymes for the degradation of AEA and 2-AG are fatty acid amide hydrolase (FAAH), which is able of hydrolyzing both AEA and 2-AG,[29] and monoacylglycerol lipase (MAGL), selective for 2-AG. MAGL can be found both in membrane and cytosol, in those brain areas where the CB_1 are expressed (Figure 8).[30]

When the activity of FAAH and MAGL is suppressed both AEA and 2-AG are metabolized by COX-2.[31,32]

2.3 Endocannabinoid System: Biosynthesis of the most important endocannabinoids

AEA and 2-AG are the most known ECs and were the first to be discovered; AEA is able to bind both CBs as partial agonist,[33,34] while 2-AG is a full agonist of the two receptors.[20] The synthetic processes that lead to the formation of these two ECs are well known.

2.3.1 Biosynthesis of Anandamide

AEA is produced according three synthetic pathways.

1
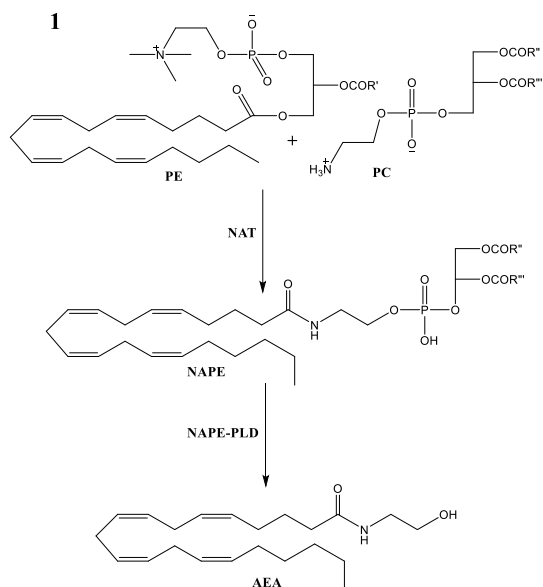
1. The first involves the formation of N-acylphosphatidylethano-lamine (NAPE), by a Ca^{2+}-dependent *trans*-acylase (NAT), which transfers an AA unit from position one of the membrane phospholipid (phosphatidylcoline, PC) to the amino group of phosphodiethanolamine (PE). Then NAPE is hydrolyzed to AEA by a specific type D Ca^{2+}-dependent phospholipase (NAPE-PLD).[35]

2
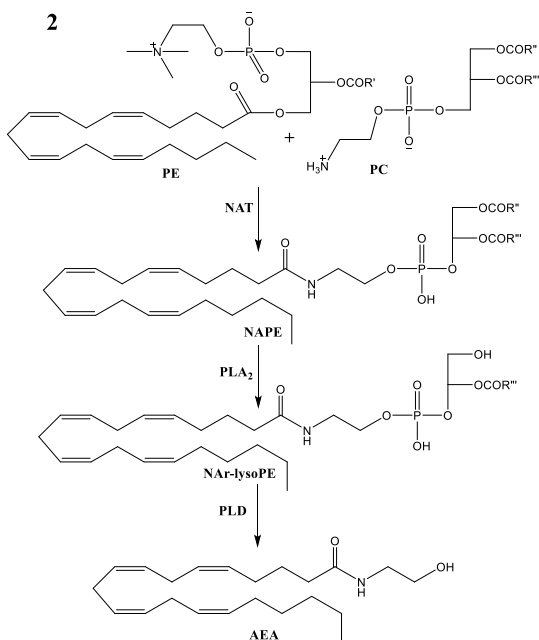
2. The second involves PLA2, which hydrolyses NAPE forming N-arachidonoyl-phosphatidylethanolamide (NAr-lysoPE). Then a specific phospholipase releases anandamide.[36]

3
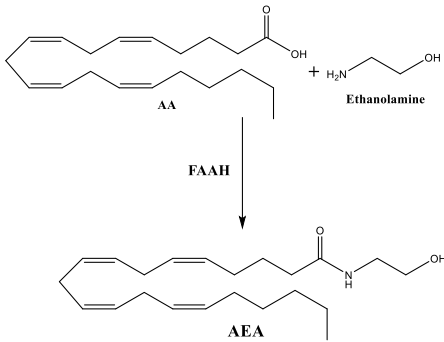
Figure 9. Anandamide biosynthetic pathways.

3. In the third the precursor are AA and ethanolamine, which are condensed by FAAH, to form AEA. This synthetic pathway needs high levels of the two substrates, necessary to allow the enzyme to work on contrary. This event is unlikely within the cell.[37]

2.3.2 Biosynthesis of 2-Arachidonoylglycerol
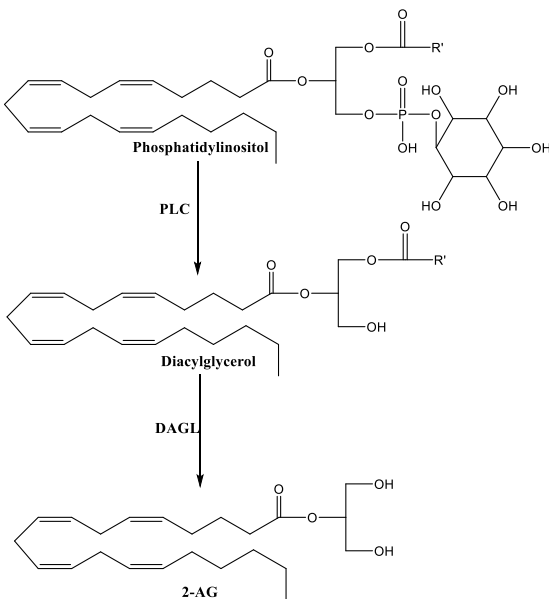
Figure 10. 2-Arachidonoylglycerol biosynthetic pathway.

Biosynthesis of 2-AG is very complex and diversified. This EC is in part produced by the enantioselective hydrolysis of DAG, operated by a DAG-lipase.[38,39]

DAG is necessary to synthesize 2-AG and derived or from the hydrolysis of phosphatidylinositol (PI) by a specific PLC Ca^{2+}-dependent[39] or from the hydrolysis of phosphatidic acid catalyzed by a specific phosphohydrolase Ca^{2+}-dependent (Figure 10).[40]

2.4 Endocannabinoid Degradation: FAAH

As mentioned above the most important enzyme for the metabolization of AEA is FAAH (Figure 11), that was characterized in 1996.[29]

FAAH is localized on the postsynaptic membrane and is mostly expressed in brain areas rich in CB_1 receptors. FAAH weighs 64 kDa and is a homodimer constituted by 579 amino acids whose amino acids sequence is highly conserved.[41]
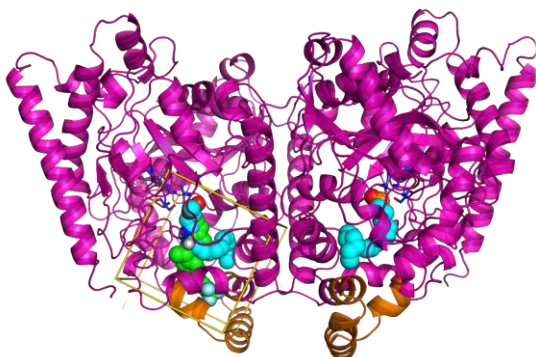
Figure 11. FAAH.

FAAH belongs to the serine hydrolase superfamily even if it utilizes a different hydrolytic mechanism from the typical triad serine-histidine-aspartic acid. FAAH is the first known member of a family known as *amidase signature* (AS).[42] These enzymes have a 56 amino acids region highly conserved, known as *amidase consensus sequence*, rich in glycine, alanine and serine residues.

FAAH is an integral membrane enzyme with a transmembrane N-terminal domain, absent in other members of AS. The central portion is constituted by a β-sheet surrounded by a series of α-helix.

In the enzyme numerous channels are present; one of these is located near the hydrophobic domain α-18 and α-19 and it is probably useful to facilitate the movement of the substrate polar groups to the active site. Another channel is located near the active sites and have the Ile-491 residue important to recognize the substrate.[43]

An additional channel emerges from the active site and forms a pocket exposed to the cytosol, probably with the function to

guarantee the access of the water molecule necessary for the de-acylation of the reaction intermediate.

2.4.1 Hydrolytic mechanism
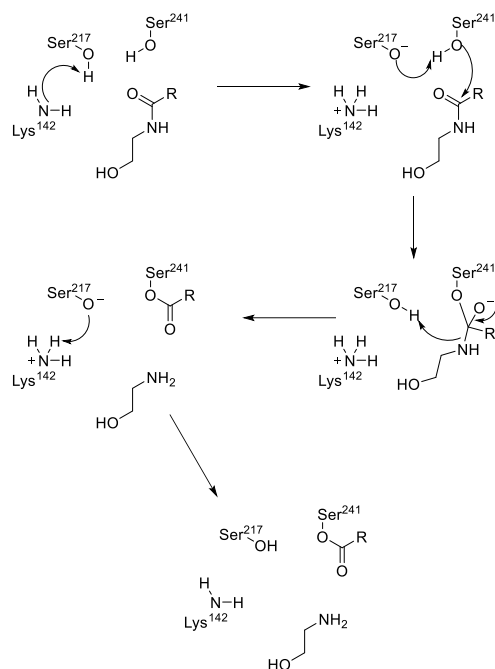
Figure 12. FAAH Hydrolithyc Mechanism.

FAAH hydrolyze AEA and the other substrates by the activity of its characteristic triad, Ser-241, Ser-217 and Lys-142. Mullholland[44] and Jorgensen[45] propose a hydrolytic mechanism that provides initial deprotonation by the Lys-142 on Ser-217 and subsequent formation of a zwitterionic intermediate. The formed alkoxide removes a proton of Ser-241; this binds the carbonyl carbon of substrate (e.g. AEA) forming a tetrahedral intermediate. The transfer of the proton from Ser-217 to the amino group of AEA leads to the breaking of the amide bond, with consequent release of ethanolamine.

Then Lys-142 returns the proton to Ser-217, while the Ser-241 remains linked to the rest of the substrate as ester, which will be successively released as AA restoring the enzyme (Figure 12).

2.5 Endocannabinoid System: Exogenous modulators

Endocannabinoid system is involved on regulation of numerous physiological activities such as cognitive function, food consumption, blood pressure, heart rate, body temperature, mood, memory, inflammation, pain perception, neurodegenerative diseases and others.[46-49]

2.5.1 CBs agonists

The Δ^9-THC and the other CB ligands (both natural and synthetic) could be good analgesic compounds for the antinociceptive and anti-inflammatory effects mediated by CBs located on the nociceptive pathways.[50,51]

Compounds that bind both CB_1 and CB_2 belongs to four classes, the classic cannabinoids (such as THC (Figure 3)), not classic cannabinoids (CP55940 (Figure 13A)),[52] aminoalkyl indoles (WIN55212-2(Figure 13B))[53] and eicosanoids (AEA (Figure 4), 2-AG (Figure 5) and methanandamide (Figure 13C)).[54]
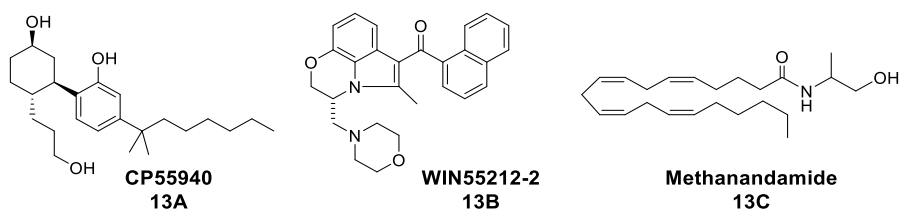
Figure 13. CBs agonists.

Nevertheless their clinic use is limited for the side effects caused by the direct and non-selective activation of CBs, such as psychotropic manifestations, dysphoria, dizziness, altered perception, effects on motor coordination and memory, depression of the immune system and their potential for abuse.[55-57]

2.5.2 AMT inhibitors

A possible way to profit by the healthy effects of the activation of the cannabinoid system but avoiding the side effect may be to enhance the activity of endocannabinoids, like AEA. This is possible in two ways. One option is by the inhibition of AMT with compounds like AM404 (Figure 14A), VDM11 (Figure 14B), UCM707 (Figure 14C), OMD-1 and -2; the problem of these compounds is the low selectivity, they are also CB agonists and FAAH inhibitors, furthermore the AM404 is able to activate TRPV1. Therefore it is not clear, if the AMT inhibitors activity is due to the direct transporter inhibition or if it is mediated by the activity on CBs and/or FAAH.
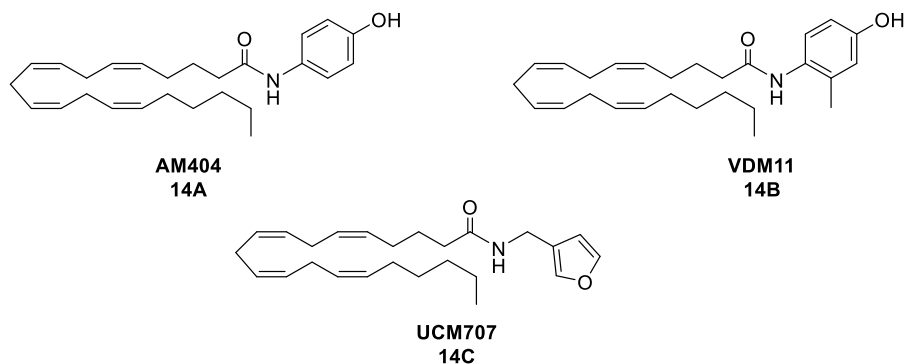
Figure 14. AMT inhibitors.

2.5.3 MAGL inhibitors

The other possibility to increase the levels of ECs is by the inhibition of the enzyme responsible for their degradation. In this way the ECs levels are increased and in turn all their biological effects could be prolonged and enhanced, without the risk of incurring in the psychotropic effects and/or other side effects, due to the activation of the global CBs from direct agonists.

Some MAGL inhibitors have been reported, their activity leads to increase the concentration of 2-AG, but not AEA. Examples of these compounds are the OMDM169 (Figure 15A), URB-602 (Figure 15B), NAM (Figure 15C) and chloropyrifos (Figure 15D).[58]
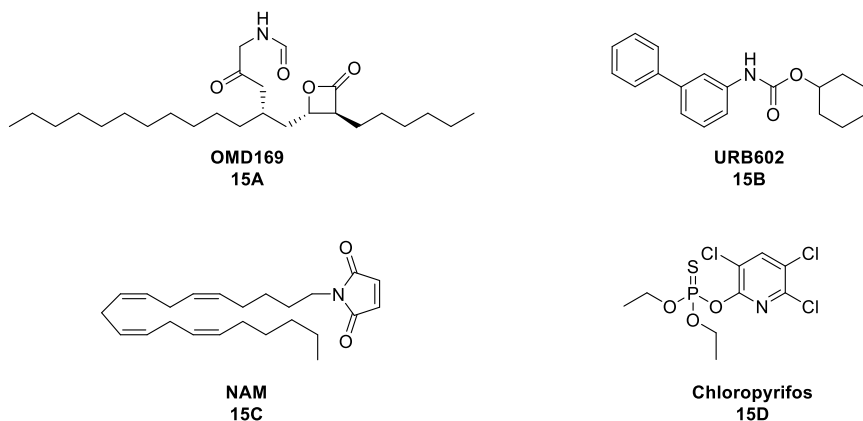
Figure 15. MAGL inhibitors.

2.5.4 FAAH inhibitors

Numerous compounds able to inhibit FAAH have been reported. Phenylmethylsulfonyl fluoride (PMSF) (Figure 16A), the first FAAH inhibitor described was accidentally discovered when it was added to rat brain homogenate to inhibit protease activity. Unexpectedly PMSF was found to inhibit FAAH.[59]
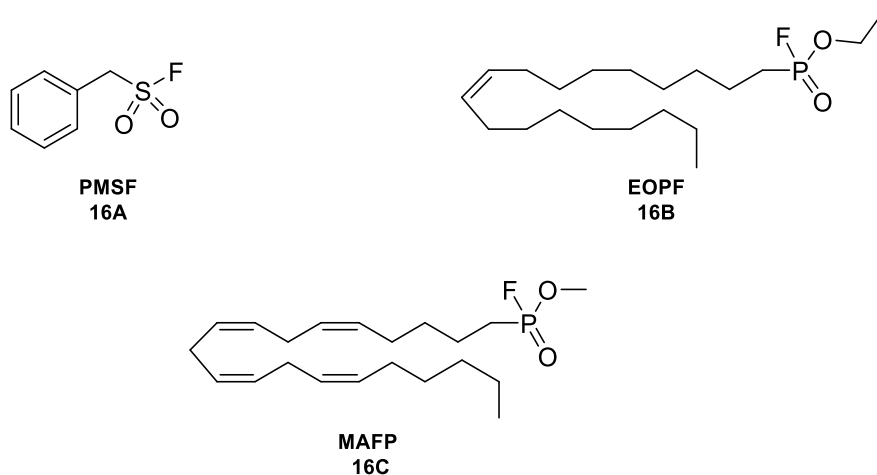
Figure 16. Early FAAH inhibitors.

The next step of FAAH inhibitor discovery was the insertion of the sulfonyl fluoride group on fatty acids. This combination led to the discovery of inhibitors more selective and potent such as laurylsulfonyl fluoride, ethoxy oleoyl fluorophosphonate (EOFP)

(Figure 16B), methylarachidonoyl fluorophosphonate (MAFP) (Figure 16C). The last was found to inhibit FAAH with an IC_{50} value of 2.5 nM,[60] it was also used to obtain the crystal structure of the enzyme.[61] The problem of these compounds is their significant agonist affinity for the CB_1 receptor that makes them poor drug candidates.

2.5.4.1 α-ketoheterocycle

Studies conducted before the FAAH was fully characterized and the catalytic mechanism understood led to design compounds that use activated carbonyl group as putative active sites trap. Amides, α-ketoamides, α-ketoesters and trifluoroketones were prepared and tested against FAAH for this purpose. The most potent of these was arachidonoyl trifluoromethyl ketone (Figure 17A).[62]

A paper published in 2000 suggested that AEA and oleamide were degraded by the same enzyme, which was later revealed to be FAAH.[63] On this base, the corresponding oleoyl trifluorometyl ketone was prepared and it showed an IC_{50} value of 0.082 μM (Figure 17B).

17A   **17B**
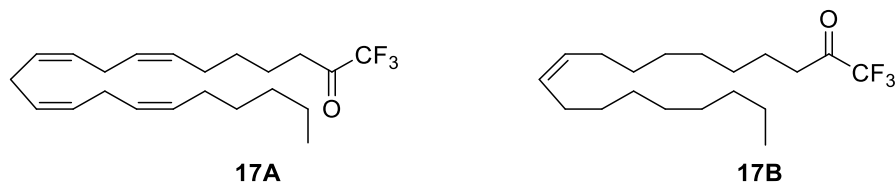
Figure 17. Trifluoromethyl ketoneFAAH inhibitors.

As extensions of this study new series of compounds endowed with α-ketoheterocycle structure were prepared. In these new series the trifluoromethyl group of compound **17B** was replaced by various heterocycles designed to activate the ketone to nucleophilic attack.[64] These compounds exert their inhibitor activity forming a hemiketal bond with Ser-241.[65,66] These potent and selective FAAH inhibitors have been shown to be reversible, competitive and some of these showed efficacies on preclinical models of pain also.

More is the ability of the heterocycle to activate the ketone to nucleophilic attack more potent is the inhibitor, in fact oxazoles were found to be superior to thiazoles or imidazoles.
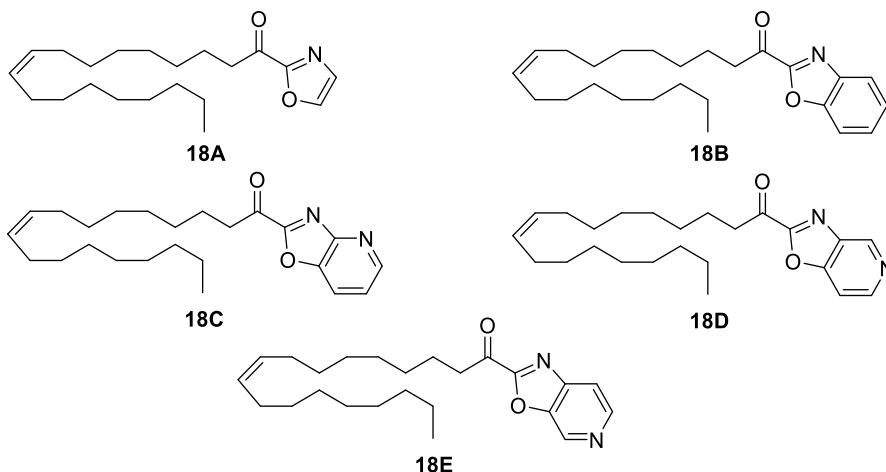
Figure 18. Other α-ketoheterocycle FAAH inhibitors.

The substitution of the trifluoromethyl group with oxazole (Figure 18A) caused about five times increase in activity (IC$_{50}$ from 0.082 μM of **17B** to 0.017 μM of **18A**). The conversion of oxazole into benzoxazole (Figure 18B) caused reduction in activity (IC$_{50}$ 0.37 μM), however the conversion in pyridinoxazoles caused significant activity increase, in particular for compounds **18C**, **18D** and **18E** (Figure 18) (IC$_{50}$ 2.3 nM, 7.2 nM and 3.7 nM respectively). The authors suggested that this activity improvement is probably due to the involvement of the pyridine nitrogen in hydrogen bond with two or more FAAH residues or/and to its ability to enhance the ketone electrophilicity.

Starting from compound **18C**, which shows the better activity, the attention was focused on modifications on the alkyl tail. In this way it was discovered one of the most potent and selective FAAH inhibitors known, OL-92 (Figure 19A) which show an IC$_{50}$ value of 0.2 nM; however, probably due to its poor pharmacokinetics, in vivo studies this compound did not showed analgesic activity.[67]

Further modification of oxazol-ketone inhibitors led to the design of a large number of new compounds with different substituents in

oxazolyl ring, including the OL-135 (Figure 19B), which is one of the best characterized FAAH inhibitor.[65] Furthermore OL-135 demonstrated its analgesic property in different in vivo assays.[67]
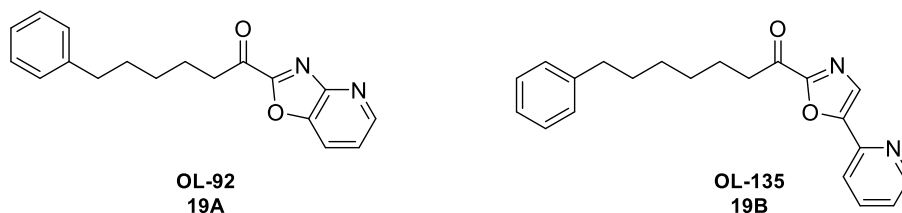
Figure 19. Other α-ketoheterocycle FAAH inhibitors.

The idea that modification of endogenous substrates may lead to create FAAH inhibitors brought to design different compounds such as arachidonoyl serotonin (AA5HT) (Figure 20A),[68] which was initially described as FAAH inhibitor and later as TRPV1 antagonist also, AM404[69] (Figure 14A) and Arvanil (Figure 20B).[70] AA5HT probably for its dual activity against FAAH and TRPV1 showed high efficacy on both acute and chronic pain.[71]
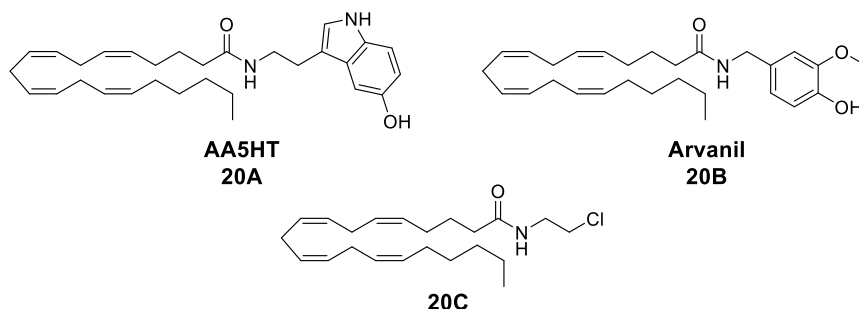
Figure 20. Example of FAAH inhibitors.

The manipulation of the ethanolamine portion of AEA led to the discovery of some FAAH inhibitors, the most potent of which was the alkyl chloride derivative (Figure 20C) with an IC_{50} value of 0.9 μM, these results suggested that small aliphatic and aromatic groups were better tolerated than larger lipophilic groups.

Studies conducted by Fowler on the influence of the length of the fatty acid chain highlighted that the decreasing of FAAH inhibition

property was directly related with the diminution of chain length below 12 carbon atoms.[72]

Preparing derivatives of Arvanil, in 2001 Di Marzo reported a SAR study describing the urea compound, O-1987 (Figure 21), which showed an IC_{50} value of 2.0 μM.[73]
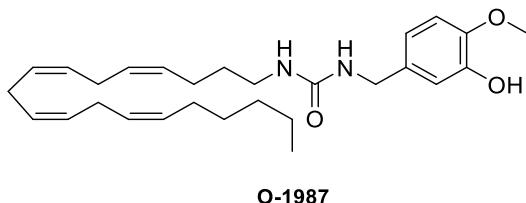
O-1987

Figure 21. FAAH inhibitor O-1987 structure.

2.5.4.2 Carbamates

Starting from knowledge about carbamate AChE inhibitors, a new large class of FAAH inhibitors was studied. In particular starting from the compound **22A**, which did not inhibit FAAH, improvement of lipophilic property by replacement of the methylamine with a cyclohexylamine led to a compound with an IC_{50} value of 300 nM (Figure 22B). Further modification led to the potent FAAH inhibitor URB-524 (Figure 22C) and then to the analog URB-597 (Figure 22D), showing IC_{50} values of 0.063 and 0.0046 μM respectively.[74]

Kinetic studies showed that these compounds behave as non-competitive inhibitors and were non-dialyzable, suggesting that they are irreversible inhibitors binding covalently FAAH.

Alexander and Cravatt proposed an URB-597 FAAH inhibition mechanism where the O-aryl carbamate moiety acylates the residue Ser-241 on the catalytic site.[75]

Arylcarbamates are both extremely potent and selective against FAAH respect to other serine hydrolases. URB-597 and its analogs showed good activity as painkillers and anxiolytics.[76,77]

22A   **22B**

URB-524   **URB-597**
22C   **22D**
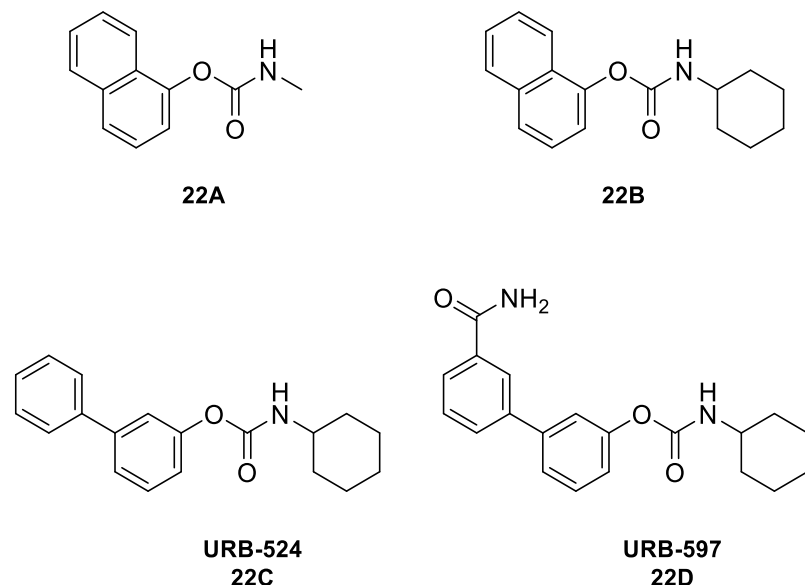
Figure 22. Carbamate FAAH inhibitors.

2.5.4.3 Ureas

As well as carbamates, also aryl urea derivatives have been explored as FAAH inhibitors.
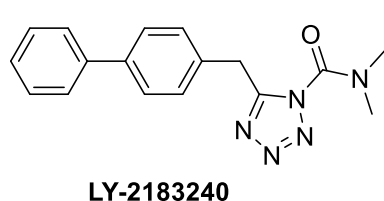
LY-2183240

Figure 23. FAAH inhibitor LY-2183240 structure.

One of the first urea inhibitor was the compound LY-2183240 (Figure 23), originally described as anandamide transport inhibitor,[78] just later it was found to be a potent FAAH inhibitor with an IC_{50} value of 12 nM.[79] Evidences suggested that this compound inhibit FAAH by covalent binding of the Ser-241, in a similar way such as carbamate inhibitors.

In 2006 Takeda (Figure 24A) and Janssen in 2007 (Figure 24B) published patent applications on piperazine arylurea FAAH inhibitors.[80,81] Mass spectra analysis of Janssen's compound JNJ-1661010 (Figure 24) bound to rat FAAH indicated that the carbonyl of the urea was acting as an electrophile covalently modifying the active site with the aniline fragment functioning as the leaving group upon binding to the enzyme.[82]
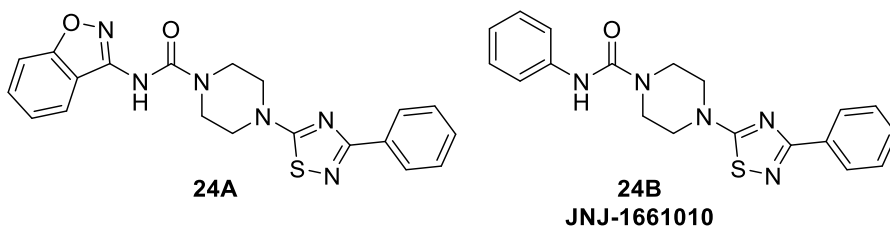
Figure 24. Piperazine arylurea FAAH inhibitors.

In 2007 Cravatt *et al.* reported very selective FAAH inhibitor compounds founded by screening of Pfizer chemical library;[83] PF-750 (Figure 25A), which is a piperidinyl urea and piperazinyl urea derivative PF-622 (Figure 25B), both are more potent than URB-597 with IC$_{50}$ values of 16.2 nM and 33 nM respectively. Covalent bonding mode to FAAH was proven by several methods, e.g. time-dependent inhibition and the rapid dilution studies. Another important difference between URB-597 and PF-750/622 is about their selectivity. In fact the two PF compounds did not show any activity against other serine hydrolases conversely to URB-597 and other compounds of this class.[84]
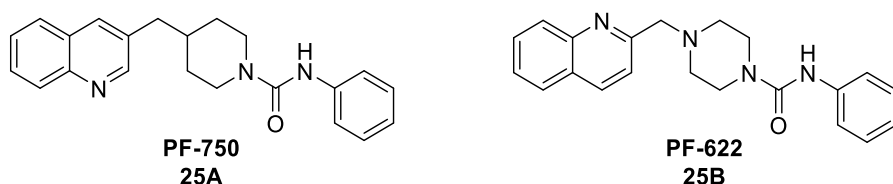
Figure 25. Structure of two urea FAAH inhibitors.

Some of the most promising FAAH inhibitors reached the early stage of clinical trial for treatment of different diseases such as anxiety, depression and pain. These FAAH inhibitors are substituted ureas endowed with irreversible enzyme inhibition profile. The clinical trials on PF-04457845[85] **(26A)**, BIA-10-2474[86,87] **(26B)** and JNJ-42165279[88] **(26C)**, (Figure 26) have been discontinued due to pharmacological activity similar to NSAID used as positive control, severe off target effects or voluntary suspension.
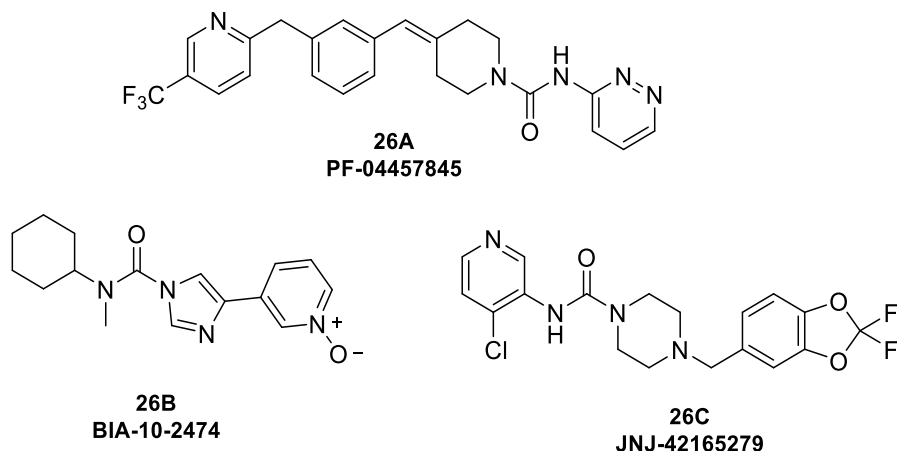
Figure 26. Structure of three FAAH inhibitors in clinical trials.

2.6 Endocannabinoid System: AEA as COX substrate

Despite FAAH is the main enzyme responsible for the metabolism of AEA, it is also substrate of other enzymes such as COXs, in particular COX-2.[31] The different activity of COX-1 and COX-2 on AEA may be due to the absence of an arginine residue on the active sites of the first enzyme.[89]

COX-2 converts AEA in prostaglandin-endoperoxid-ethanolamine, which in turn is converted in prostaglandin-ethanolamide.[90]

These compounds are bad agonists of prostanoid receptors but they cannot be metabolized by FAAH.[91]

2.6.1 COXs

COXs also known as prostaglandin-endoperoxide synthase, as mentioned above, are enzymes devoted to formation of prostaglandins, thromboxane and prostacyclin starting from AA.

COXs exist in two isoform, namely COX-1 and COX-2; the first is constitutively expressed in numerous tissues and it is responsible of the formation of prostanoids necessary to the normal physiological activity. Conversely, COX-2 that is generally inducible, is produced

during inflammatory process and leads to increase of prostanoids at the inflammation site.

The two isoforms have about 63% structure homology and are dimer integrated in cell membranes with a globular structure.

COX-2, in addition to produce the inflammatory mediators, induces, through production of PGE$_2$, a hypersensitivity of the nociceptive fibers increasing the sensitivity to pain.

2.7 Endocannabinoid System: A new analgesic strategy

It has been demonstrated that in pain state the ECs synthesis is increased prevalently in areas involved in pain control (such as PAG). Therefore the administrations of substances that inhibit the ECs metabolization cause increase of EC concentrations and in turn enhancement of the activation of CB1 receptors mostly on PAG.

Several in vivo studies showed that the co-administration of a FAAH inhibitor and a NSAID has synergic effect. As example the same analgesic effect showed by diclofenac as single drug was obtained by co-administration of the FAAH inhibitors URB-597 and a dose significantly lower of the NSAID. Moreover the typical ulcerogenic effect was significantly reduced compared to treatment with only diclofenac.[92,93]
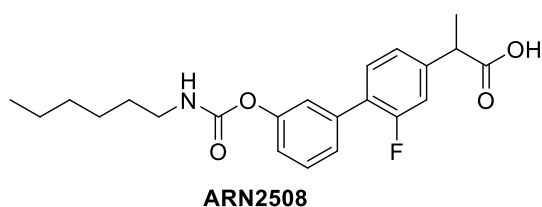
ARN2508

Figure 27. FAAH inhibitor ARN2508.

Another example of the useful addictive effect of the dual inhibition of FAAH and COX was highlighted by studies on the compound ARN2508 (Figure 27), which is a hybrid between the covalent FAAH inhibitor URB-597 and the NSAID flurbiprofen both sharing a biphenyl core. This compound showed antinociceptive propriety without the classical gastrointestinal side effects of NSAIDs.[94,95]

Given the structural similarities between AEA and AA, COX and FAAH and being AEA a substrate of COX also, it is no surprise that NSAIDs partially inhibit FAAH; however this inhibitory effect is so slight that they are not able to increase ECs concentrations.[96,97] For example ibuprofen and flurbiprofen showed FAAH inhibitory IC_{50} values of 270 and 29 µM respectively.[98,99]
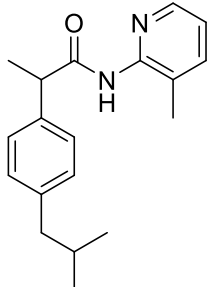
Figure 28. Ibu-AM5

Concluding, a strategy for the treatment of pain could be to design compounds targeting both COX and FAAH. For this purpose it was designed the N-(3-methylpyridin-2-yl)-2-(4'-isobutylphenyl) propionamide or **Ibu-AM5** (Figure 28), an amide analogue of ibuprofen where the carboxylic group is functionalized with 2-amino-3-methylpiridine. This compound has demonstrated activity as FAAH inhibitor 300 times higher than the parent Ibuprofen, moreover without giving ulcerogenic effects.[100,101]

Ibu-AM5 showed mixed inhibition behavior suggesting the presence of more than one binding site on the enzyme.

2.8 Endocannabinoid System: Results and Discussion

Based on these considerations in this thesis it is discussed the design, synthesis and pharmacological activity of new derivatives of profens and **Ibu-AM5** designed as dual inhibitors of FAAH and COX.

Are proposed two series of compounds, the profen series and the TPA series. The first derived by the modification of the different portion of **Ibu-AM5**. While, the second series derived from the modification of the isobutyl moiety of **Ibu-AM5** into trifluoromethylpyridine.

All synthesized compounds were tested as FAAH inhibitors; the pharmacological assays were performed at the Prof. Christopher Fowler laboratories, University of Umea, Sweden. The ability to inhibit the FAAH was measured in rat brain homogenates using tritiated AEA as substrate.

All these modifications were based on analysis of the inhibition kinetic of **ibu-AM5** with the double aim to make SAR and to determinate the requirements for the FAAH inhibition keeping in mind the putative presence of multiple binding sites.

2.8.1 Results and Discussion: Profens

Based on the **Ibu-AM5** structure and with the aim to discover the better modification improving the activity as FAAH inhibitors, we made modification to all moieties of the molecule (Figure 29). As showed in Figure 29 we evaluated the influence on FAAH inhibitory activity of the distance between the carbonyl and the aromatic ring, the position and type of the substituents on the ring of the amide portion, the presence and the chirality of the methyl in α to the carbonyl group. Furthermore analogs of Ibu-AM5 were prepared using as parent acid different profens.
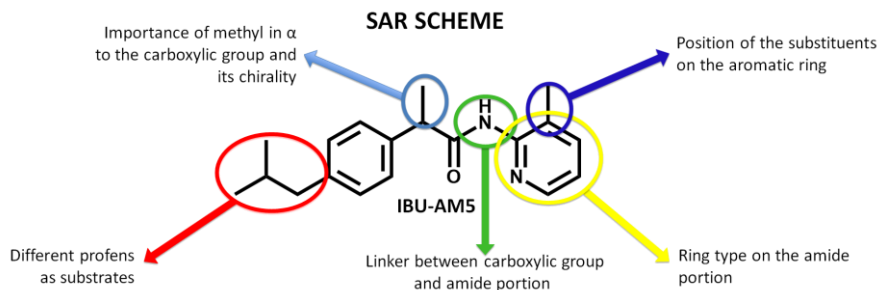
Figure 29. SAR scheme of the **Ibu-AM5** modifications.

The **Ibu-AM5** is characterized by a three atoms linker between aryl and pyridine rings. To evaluate the effect on FAAH inhibitory activity of the distance between the two rings, some amides bearing a 4 or 5 atoms linker were prepared. The synthetic pathway to obtain these amides started from the condensation of ibuprofen with ethyl glycinate hydrochloride or ethyl-3-aminopropionate using the condensing agent 1-(3-dimethylaminopropyl)-3-ethylcarbodiimide hydrochloride (EDC). The reactions were performed in acetonitrile solution (MeCN) in the presence of 1-hydroxybenzotriazole hydrate (HOBt). The obtained esters were hydrolyzed under basic conditions to obtain the (2-(4-isobutylphenyl)propanoyl)glycine **(4)** and 3-(2-(4-isobutylphenyl)propanamido) propanoic acid **(5)**. These two acids were then condensed with 3- and 6-methyl-2-aminopyridine and picolylamines using the EDC method to obtain the amides **Ibu-AM9-13** (Scheme 1).[102,103]
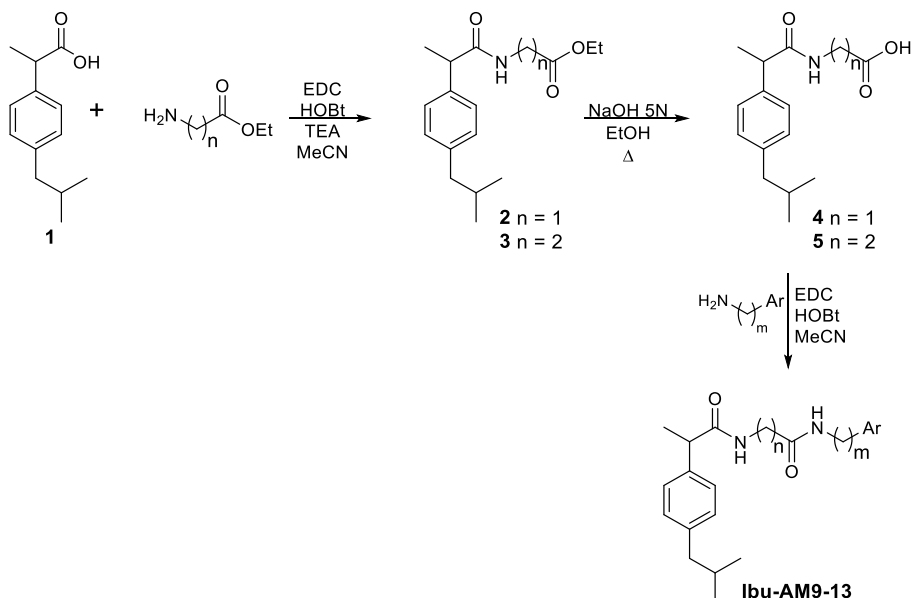
Scheme 1. Synthesis of **Ibu-AM9-13**.

All the amides **Ibu-AM9-13** showed FAAH inhibition percentage in the 81-100% range (Table 1). The increase of the distance between the carboxylic group and the pyridine caused a decrease in activity. This is highlighted by the reduction in the activity of the compounds **Ibu-AM11**, **Ibu-AM12** and **Ibu-AM13** as compared to **Ibu-AM9**, and of **Ibu-AM9** as compared to **Ibu-AM5**. The difference in activity of the compounds **Ibu-AM12** and **Ibu-AM13** might be due to the displacement of the pyridine nitrogen.

Also the displacement of the methyl on the pyridine from the 3-position of **Ibu-AM9** to 6-position (**Ibu-AM10**) caused an important reduction in inhibitory activity confirming what already described with the 6-methylpyridine analog of **Ibu-AM5**.[101]
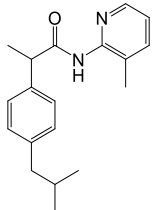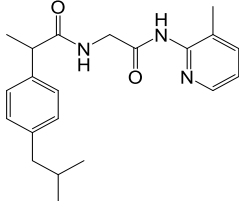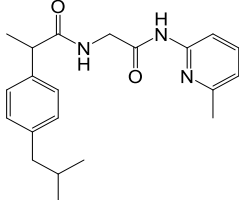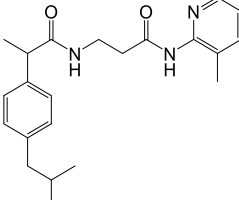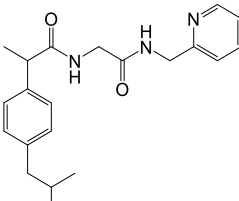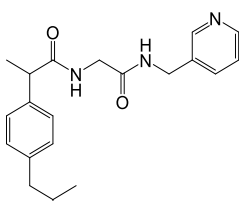
Compound	Formula	Max inhibition (%)	IC$_{50}$ (µM)
Ibu-AM5		100	0.52
Ibu-AM9		100	3.2
Ibu-AM10		100	150
Ibu-AM11		90±3	93
Ibu-AM12		100	90
Ibu-AM13		81±8	37

Table 1. Maximum percentage and IC$_{50}$ values for inhibition of rat brain AEA hydrolysis by compounds **Ibu-AM9-13**, ibuprofen and **Ibu-am5**.
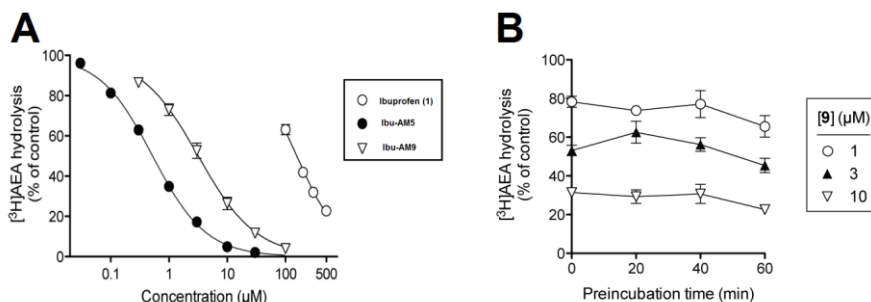
Chart 1. Mode of inhibition of rat brain FAAH by Ibuprofen (**1**), **Ibu-AM5**, and **Ibu-AM9**. Panel A: AEA hydrolysis at the substrate and inhibitor concentrations shown (means and s.e.m, n=3). Panel B: homogenates were preincubated with the compounds for the times shown prior to addition of 0.5 µM [3H]AEA and assay for FAAH activity (means and s.e.m., n=3-4).

Ibu-AM9, which completely inhibits the enzyme with an IC_{50} value of 3.2 µM is the best of this group of amides, for this reason it was selected for further studies. Its inhibitory profile is time-independent, probably due to the formation of a non-covalent bond with the enzyme. The V_{max} and K_m values indicated that **Ibu-AM9** is a competitive inhibitor (Chart 1A and B). [102,103]

Ibu-AM5 and **Ibu-AM9** were tested also for their activity against COXs (Ovine COX-1 and human COX-2 obtained by recombinant DNA). AA was used as substrate for both the isoforms, COX-2 was also tested using AEA as substrate because it was reported that different substrates may influence the inhibitor activity.[104]

As showed on table 2 **Ibu-AM5** and **Ibu-AM9** display COX-1 inhibitory activity similar to the reference compound ibuprofen. The COX-2 inhibition depends on the substrate used: when the substrate is AA Ibuprofen and its amides display weak activity. Conversely ibuprofen, **Ibu-AM5**, **Ibu-AM9** showed a better inhibitory activity when the substrate is the AEA.[102,103]

Compound	pI$_{50}$ [IC$_{50}$, µM]		
	COX-1 (AA)	COX-2 (AA)	COX-2 (AEA)
Ibuprofen (1)	4.53±0.11 [29]	<3.5 (36±8% inhib at 300 µM)	5.22±0.09 [6.0]
Ibu-AM5	4.22±0.06 [60]	<3.5 (41±4% inhib at 300 µM)	4.72±0.09 [19]
Ibu-AM9	4.30±0.05 [50]	<4 (18±5% inhib at 100 µM)	>5 (17±8% inhib a 3 µM, complete inhib a 50 µM)

Table 2. IC$_{50}$ Values for COX-1 and -2 inhibition by ibuprofen (**1**) **Ibu-AM5** and **Ibu-AM9.**

To further study the effect on activity of the linker, the second carbonyl group was removed and a new series of ibuprofen benzylamides was designed. To synthesize the benzylamide series, ibuprofen was condensed with adequately substituted benzylamines by EDC method (Scheme 2).
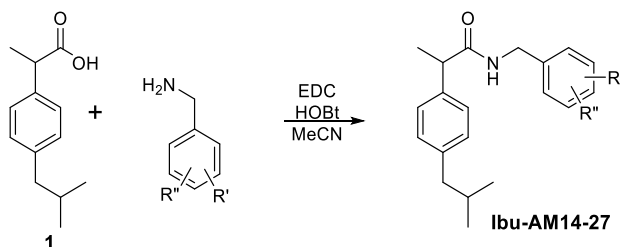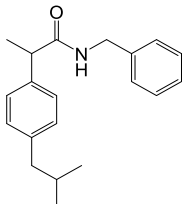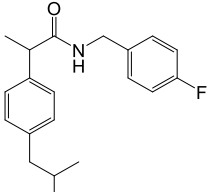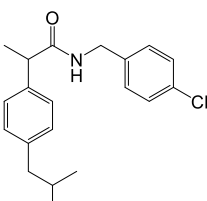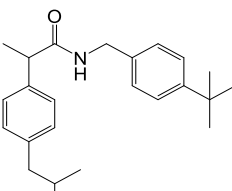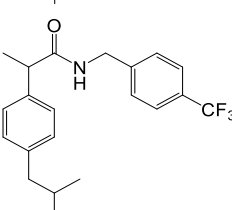
Scheme 2. Synthesis of **Ibu-AM14-27**.
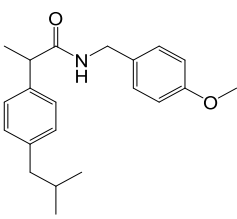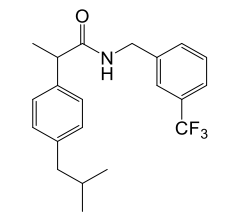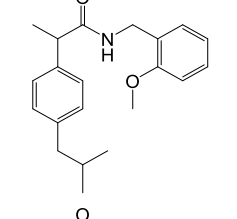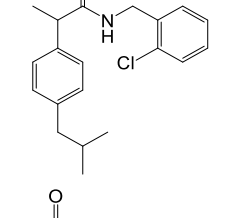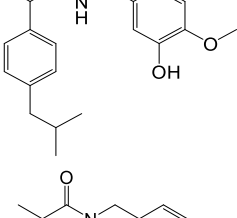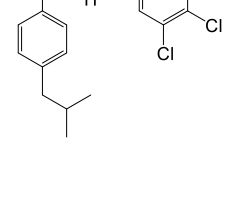
In general benzylamide derivatives did not show particularly interesting activity (IC$_{50}$ values ranging 18 and 51 µM) with the exception of **Ibu-AM22**, and **Ibu-AM26**. **Ibu-AM22** and **Ibu-AM26** showed FAAH inhibitory activity with IC$_{50}$ values of 4.1 and 4.4 µM, respectively (Table 2).

As showed in table 3, the position and the kind of substituent on benzyl moiety affect the inhibitory activity. The presence of 4-substituent is not tolerated. Conversely, substituents in 2-position are well tolerated, as showed by the 2-chloro **(Ibu-AM22)** and 2,5-dichloro **(Ibu-AM26)** derivatives. Moreover, the displacement of chlorine atom from 5-position of **Ibu-AM26** to 6-position **(Ibu-AM27)**

lead to a complete loss of activity. A mild activity was showed by the 2,4-dichlorophenyl substituted amide **Ibu-AM25** (IC$_{50}$ 21 μM).

Compound	Formula	Max inhibition (%)	IC$_{50}$ (μM)
Ibu-AM14		100	21
Ibu-AM15		100	27
Ibu-AM16		100	27
Ibu-AM17		100	25
Ibu-AM18		100	51

Ibu-AM19		100	43
Ibu-AM20		100	28
Ibu-AM21		100	18
Ibu-AM22		100	4.1
Ibu-AM23		100	18
Ibu-AM24		100	36
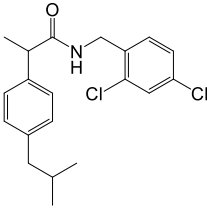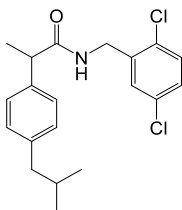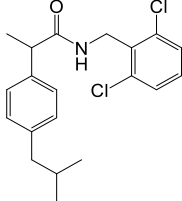
Ibu-AM25		100	21
Ibu-AM26		54±4	4.4
Ibu-AM27		19±6% inhibition @100 µM	

Table 3. Maximum percentage and IC$_{50}$ values for inhibition of rat brain AEA hydrolysis by compounds **Ibu-AM14-27.**

With the aim to increase the hydrophilicity of the amides and to reduce the flexibility of the amide chain a new series of phenylpiperazinamides was designed. Also ibuprofen phenylpiperazine derivatives were prepared using the same conditions described for the benzylamide series (Scheme 3).
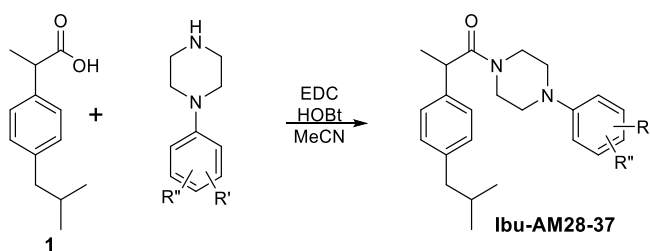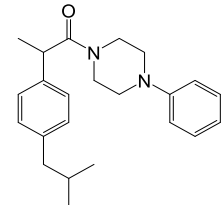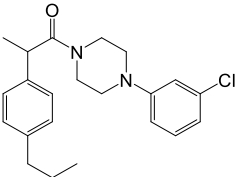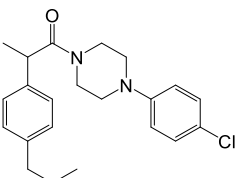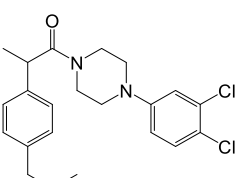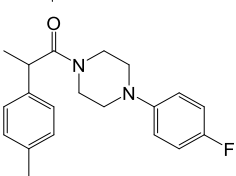
Scheme 3. Synthesis of **Ibu-AM28-37**.

In general all the phenylpiperazine derivatives displayed FAAH inhibitory activity better than benzylamide series. As shown in table 4 the 3- and 4-chlorophenyl amides **Ibu-AM29** and **Ibu-AM30** were the best compounds of this series. Starting from these results we designed the 3,4-dichlorophenyl substituted amide **Ibu-AM31** that,

contrary to the expectation, showed inhibitory activity about 10 times lower. The substitution of 3-chlorine of **Ibu-AM29** with the methyl group to afford **Ibu-AM35** cause a clear reduction in activity. The introduction of second methyl group in 2-position **(Ibu-AM36)** restored the activity, while the displacement of 3-methyl into 2-position produced loss of activity **(Ibu-AM37)**.

Compound	Formula	Max inhibition (%)	IC$_{50}$ (μM)
Ibu-AM28		100	4.7
Ibu-AM29		100	1.7
Ibu-AM30		100	1.7
Ibu-AM31		100	16
Ibu-AM32		100	17
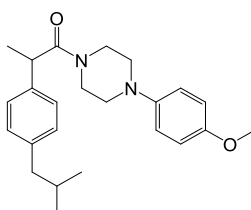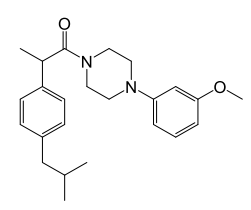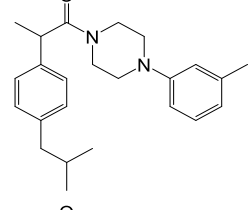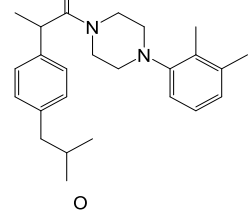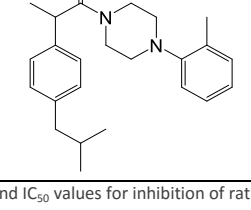
Ibu-AM33		100	4.5
Ibu-AM34		41±3% inhibition @100 µM	
Ibu-AM35		65±3	16
Ibu-AM36		89±4	1.7
Ibu-AM37		33±3% inhibition @100 µM	

Table 4. Maximum percentage and IC_{50} values for inhibition of rat brain AEA hydrolysis by compounds **Ibu-AM28-37**.

The further modification made was the insertion of a methylene bridge between the piperazine and the aromatic ring. These amides were prepared by condensation of ibuprofen with N-BOC-piperazine, using the same methods of condensation described above. After BOC-deprotection, a benzyl group was added by reductive alkylation, treating the intermediate **7** with the suitable substituted benzaldeyde in presence of sodium bicarbonate (NaHCO₃), sodium borohydride (NaBH₄) in dichloromethane (CH₂Cl₂) solution (Scheme 4).

Unfortunately, this modification afforded the poor active analogs **Ibu-AM38-42** (Table 5).
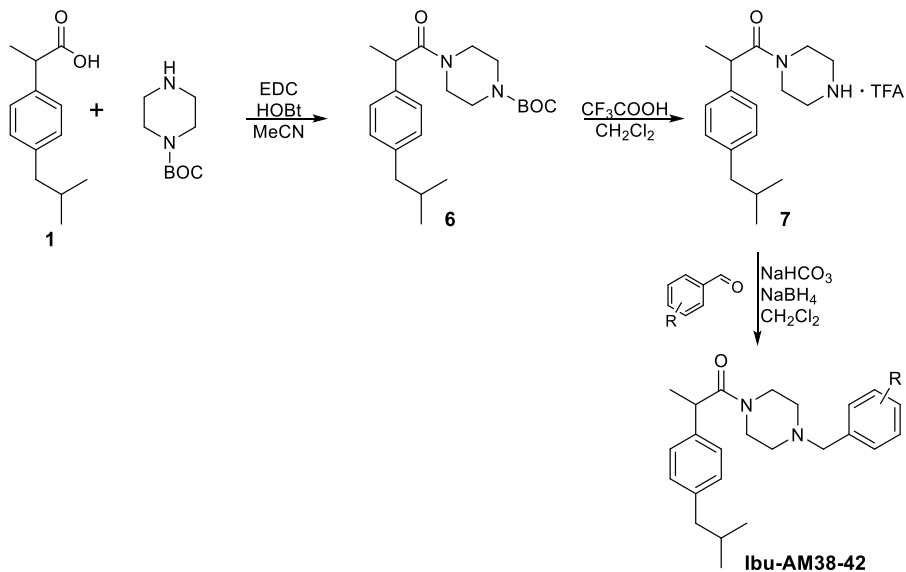
Scheme 4. Synthesis of **Ibu-AM38-42**.
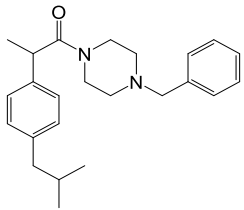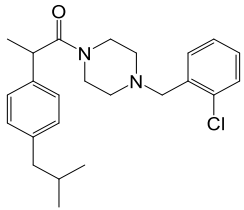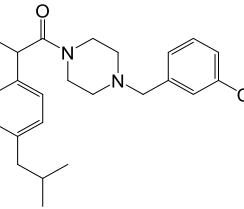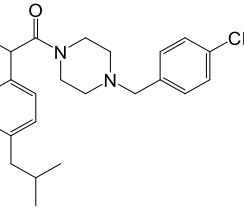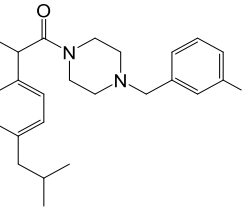
Compound	Formula	Max inhibition (%)	IC$_{50}$ (µM)
Ibu-AM38		18±5% inhibition @100 µM	
Ibu-AM39		no inhibition @100 µM	
Ibu-AM40		8±1% inhibition @100 µM	
Ibu-AM41		no inhibition @100 µM	
Ibu-AM42		no inhibition @100 µM	

Table 5. Maximum percentage and IC$_{50}$ values for inhibition of rat brain AEA hydrolysis by compounds **Ibu-AM38-42.**

As extension of the paper published in 2007,[101] where ibuprofen amides with different methylaminopyridines were prepared to evaluate the better position of pyridine nitrogen and methyl group, we prepared **Ibu-AM43** where ibuprofen is condensed with 3-amino-2-metylpiridine (Scheme 5). This compound showed an IC$_{50}$ value of 9.5 µM, confirming that the best activity is related to the presence of

both methyl and pyridine nitrogen in *ortho* positions to the amide nitrogen as in **Ibu-AM5** (Table 6).
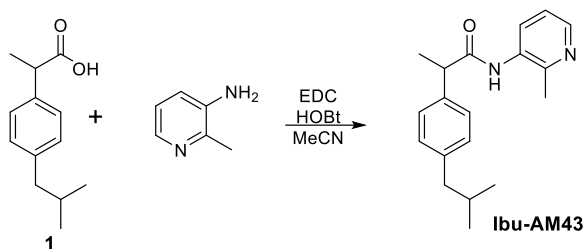
Scheme 5. Synthesis of **Ibu-AM43**.

Compound	Formula	Max inhibition (%)	IC$_{50}$ (μM)
Ibu-AM5		100	0.52
Ibu-AM43		100	9.5

Table 6. Maximum percentage and IC$_{50}$ values for inhibition of rat brain AEA hydrolysis by compound **Ibu-AM43.**

To evaluate the activity changes produced by replacing of the pyridine ring with other heterocycles, compounds **Ibu-AM44-47** were designed. These four compounds were prepared through the above described EDC procedure (Scheme 6). The inhibitory activity results shown in table 7 indicate that the substitution by a methylindole **(Ibu-AM44)** or a thiazole **(Ibu-AM45)** causes complete loss of activity. While compounds bearing a thiadiazole ring **(Ibu-AM46** and **Ibu-AM47)** showed weak inhibitor activity, with IC$_{50}$ values of 26 and 36 μM respectively.
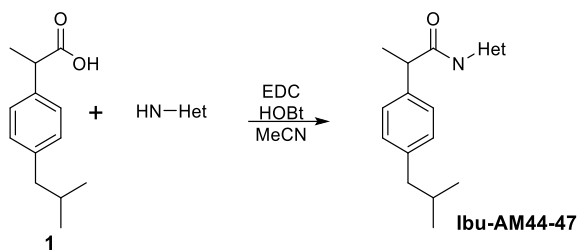
Scheme 6. Synthesis of **Ibu-AM44-47**.

Compound	Formula	Max inhibition (%)	IC$_{50}$ (μM)
Ibu-AM44		36% inhibition @100 μM	
Ibu-AM45		43% inhibition @100 μM	
Ibu-AM46		100	26
Ibu-AM47		100	36

Table 7. Maximum percentage and IC$_{50}$ values for inhibition of rat brain AEA hydrolysis by compounds **Ibu-AM44-47.**

As mentioned above the importance of the methyl on the pyridine ring was established, the methyl absence or its moving in a position different from *ortho* to the amide nitrogen results in activity

decrease. On this basis to evaluate the influence on the activity of the pyridine nitrogen we changed pyridine ring with a phenyl (Scheme 7). With this purpose we prepared **Ibu-AM48,** which is the 2-methylphenyl analog of **Ibu-AM5**, and **Ibu-AM49**, where the methyl group is substituted by fluorine. As reported in table 8 the replacement of pyridine ring with a phenyl produced activity decrease even more pronounced when methyl group is substituted with fluorine.
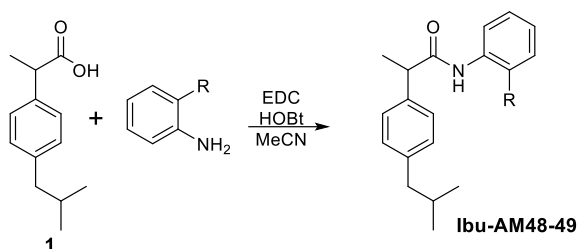
Scheme 7. Synthesis of **Ibu-AM48-49.**

Compound	Formula	Max inhibition (%)	IC$_{50}$ (μM)
Ibu-AM5		100	0.52
Ibu-AM48		100	2.0
Ibu-AM49		100	2.4

Table 8. Maximum percentage and IC$_{50}$ values for inhibition of rat brain AEA hydrolysis by compounds **Ibu-AM48-49.**

As further evaluation a group able to establish hydrogen bond with the enzyme was inserted on amide phenyl ring. With this purpose the 2-hydroxy **(Ibu-AM50)** and the 4-hydroxy **(Ibu-AM51)** derivatives were designed. As indicated by their IC_{50} values the presence of the hydroxy group in 4-position caused an increase in activity. Next step was the integration of this activity enhancement with the presence of a 2-methyl group, with this purpose the compound **Ibu-AM52** was prepared by condensation of ibuprofen with 2-methyl-4-hydroxyaniline. **Ibu-AM52** showed very good activity with an IC_{50} value of 0.35 µM. With the aim to study the influence on the inhibitory activity of hydrogen bond donor or acceptor group **Ibu-AM52** was modified by introduction of a 4-methoxy for the 4-hydroxy group to afford **Ibu-AM53** (Scheme 8). The result was decrease in activity, indicating that a hydrogen bond donor is better than an acceptor (Table 9).
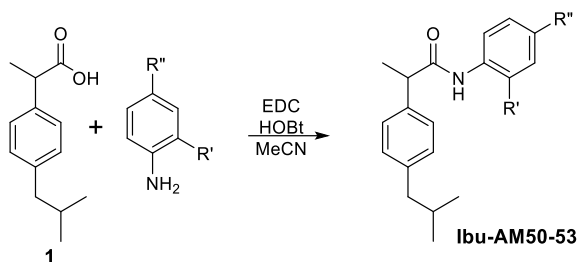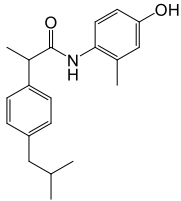

Scheme 8. Synthesis of **Ibu-AM50-53.**
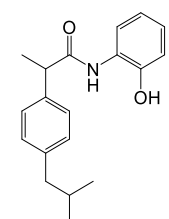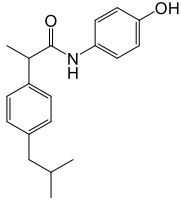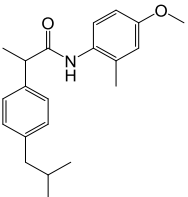
Compound	Formula	Max inhibition (%)	IC$_{50}$ (µM)
Ibu-AM50		100	8.5
Ibu-AM51		100	3.8
Ibu-AM52		100	0.35
Ibu-AM53		100	4.6

Table 9. Maximum percentage and IC$_{50}$ values for inhibition of rat brain AEA hydrolysis by compounds **Ibu-AM50-53.**

The most active amides bear a pyridine substituted with methyl group in *ortho* to amide nitrogen, while the importance of both position and chemical properties of the substituent were not cleared. With aim to extend SAR study we designed some **Ibu-AM5** analogs. As showed in the table the 3-methyl group was replaced with 3-chlorine **(Ibu-AM54)**, 3-trifluoromethyl **(Ibu-AM55)**, 3-bromine **(Ibu-AM56)**, 3-iodine **(Ibu-AM57)** and 3-hydroxyl **(Ibu-AM58)** substituents (Scheme 9).
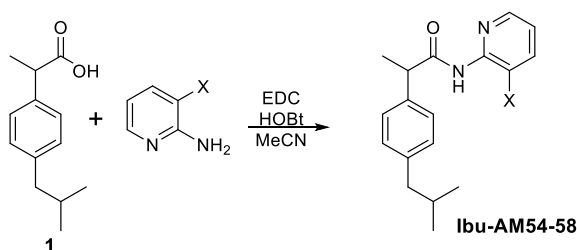
Scheme 9. Synthesis of **Ibu-AM54-58.**

The 3-chlorine derivative showed small reduction in activity as compared to **Ibu-AM5**, while the replacement of the chlorine with bromine, iodine and trifluoromethyl groups produced improvement of activity. Among these, the 3-bromopyridine analog **Ibu-AM56** is the most potent FAAH inhibitor of the Ibu-AM series with an IC_{50} value of 0.083 µM. On the contrary, the introduction of the 3-hydroxy group is not favorable for the activity. The comparison of **Ibu-AM58** with **Ibu-AM5** reveals that the replacement of the methyl with a hydroxyl group produces about 4 times activity decrease, confirming the trend showed by the aryl analogs **Ibu-AM48** and **Ibu-AM50**. However, the comparison of **Ibu-AM58** and **Ibu-AM50** activities indicates that the presence of pyridine nitrogen increased the inhibitory activity about 4 times (Table 10).

Compound	Formula	Max inhibition (%)	IC_{50} (µM)
Ibu-AM5		100	0.52
Ibu-AM54		100	0.91
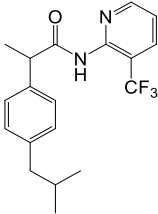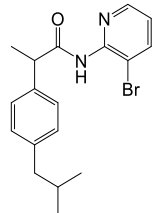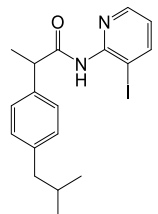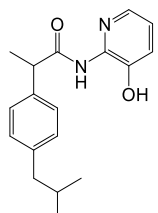
Ibu-AM55		100	0.36
Ibu-AM56		100	0.083
Ibu-AM57		100	0.12
Ibu-AM58		100	2.1

Table 10. Maximum percentage and IC_{50} values for inhibition of rat brain AEA hydrolysis by compounds **Ibu-AM54-58.**

Successively the effect on activity of the methyl group at the C-α to the carbonyl group was taken into consideration. The unmethylated **Ibuf-AM1** was obtained by the condensation between ibufenac **(8)** and 2-amino-3-methylpyridine **(9)** (Scheme 10). The deletion of methyl group **(Ibuf-AM1)** resulted in drastic activity reduction of about 130 times as compared to **Ibu-AM5**, highlighting the methyl group considerable influence for the inhibitory activity against FAAH (Table 11).
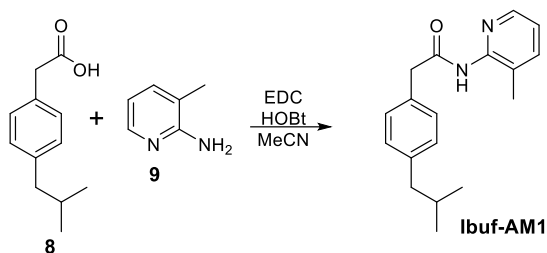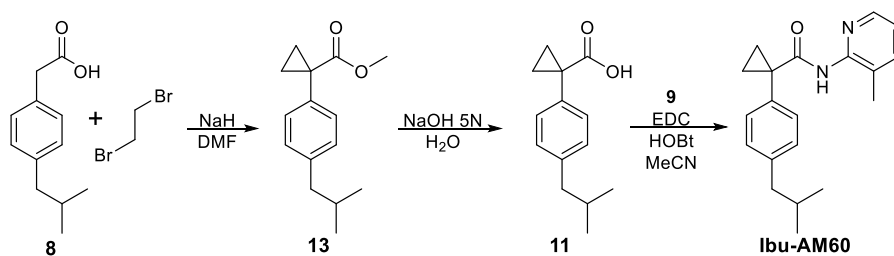
Scheme 10. Synthesis of **Ibuf-AM1**.

To better understand SAR of the C-α position further two derivatives were designed, the dimethyl derivative **Ibu-AM59**, and the cyclopropyl analog **Ibu-AM60**. To prepare **Ibu-AM59**, **8** was converted into its methyl ester **10**, which was treated with iodomethane (MeI) in dimethylformamide (DMF) solution in presence of sodium hydride (NaH) to obtain compound **11**. The ester **11** was hydrolyzed into the acid **12**, which was finally condensed with the 2-amino-3-methylpyridine (**9**) using EDC procedure (Scheme 11). In a similar manner, **Ibu-AM60** was obtained by amidation with **9** of acid **14**, in turn obtained upon treatment of **10** with 1,2-dibromoethane and NaH in DMF solution, followed by basic hydrolysis (Scheme 12). Both these compounds showed a lower activity than **Ibu-AM5**, in particular the insertion of second methyl causes about a doubling of the IC$_{50}$ value, while the cyclopropyl to even almost eight times (Table 11).
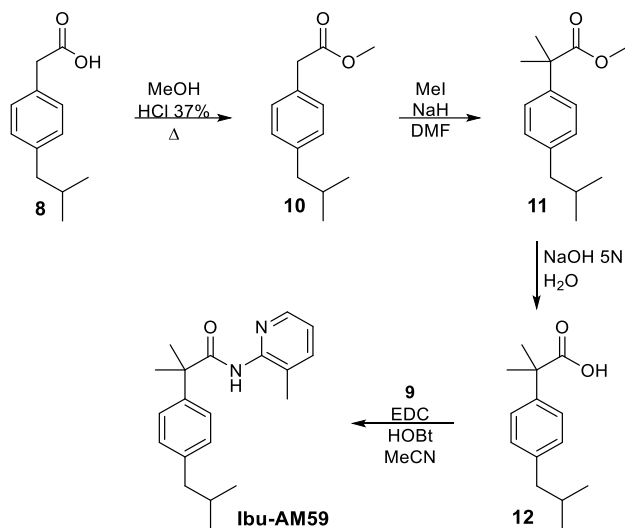
Scheme 11. Synthesis of **Ibu-AM59.**

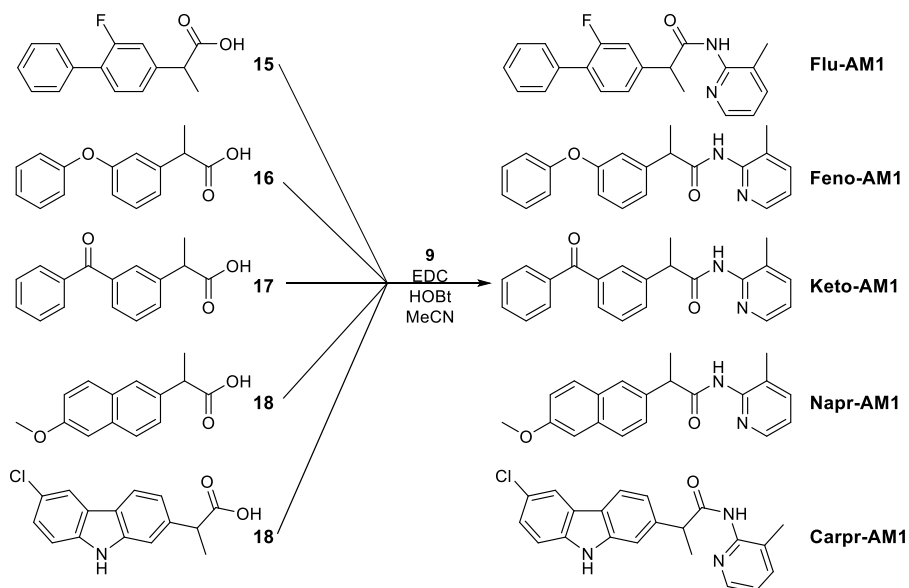**Scheme 12.** Synthesis of **Ibu-AM60.**

Compound	Formula	Max inhibition (%)	IC$_{50}$ (µM)
Ibu-AM5		100	0.52
Ibuf-AM1		100	68

Ibu-AM59	100	1.0
Ibu-AM60	100	4.1

Table 11. Maximum percentage and IC$_{50}$ values for inhibition of rat brain AEA hydrolysis by compounds **Ibuf-AM1, Ibu-AM59-60.**

Given the reported small FAAH inhibitory activity of other NSAIDs,[98,99,105] we synthesized the amides of flurbiprofen **(15)**, fenoprofen **(16)**, ketoprofen **(17)**, naproxen **(18)**, and carprofen **(19)** with **9** (Scheme 13).

Scheme 13. Synthesis of **Flu-AM1**, **Feno-AM1**, **Keto-AM1**, **Napr-AM1** and **Carpr-AM1**.

As shown by the results reported in table 12 the amides of fenoprofen and ketoprofen are weak FAAH inhibitors and **Napr-AM1** has an IC$_{50}$ value similar to **Ibu-AM5**. While, amides of flurbiprofen

and carprofen have better activity than **Ibu-AM5**, in particular **Carpr-AM1** has an IC$_{50}$ value of 0.034 μM almost fifteen times better than **Ibu-AM5.**
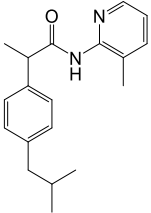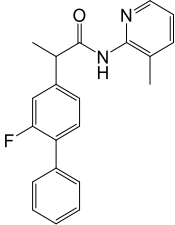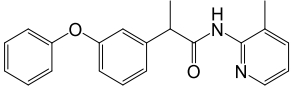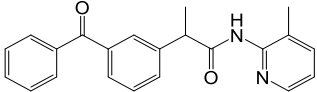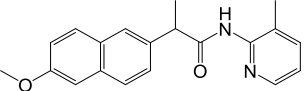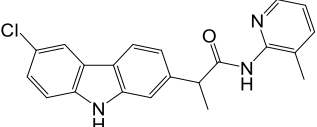
Compound	Formula	Max inhibition (%)	IC$_{50}$ (μM)
Ibu-AM5		100	0.52
Flu-AM1		100	0.44
Feno-AM1		100	51
Keto-AM1		100	19
Napr-AM1		100	0.74
Carpr-AM1		100	0.034

Table 12. Maximum percentage and IC$_{50}$ values for inhibition of rat brain AEA hydrolysis by compounds **Flu-AM1**, **Feno-AM1**, **Keto-AM1**, **Napr-AM1** and **Carpr-AM1**.

Based on these results we prepared the amides of these two profens with the amines that gave the best results in the Ibu-AM series.

In particular Carprofen was condensed with 2-amino-3-trifluoromethylpyridine **(Carpr-AM5)**, 2-amino-3-bromopyridine **(Carpr-AM4)** and 2-methyl-4-hydroxyaniline **(Carpr-AM2)** and 2-amino-3-iodopyridine **(Carpr-AM3)** (Scheme14); the corresponding flurbiprofen amides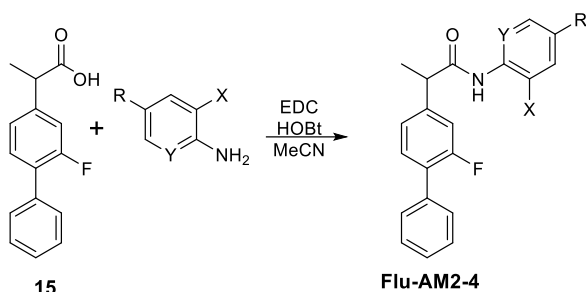 were prepared except the iodine analog (Scheme 15). As expected flurbiprofen amides showed similar behave of Ibuprofen derivatives (Table 13). Conversely, preliminary data of Carprofen amides indicate a different activity profile (Table 14).
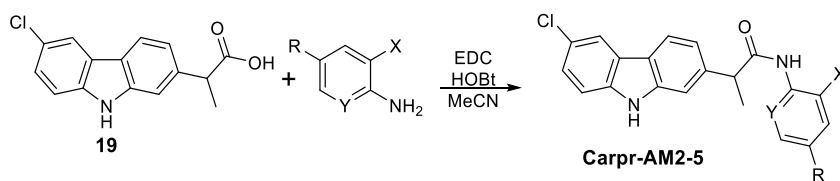
Scheme 14. Synthesis of **Carpr-AM2-5**.

Scheme 15. Synthesis of **Flu-AM2-4**.
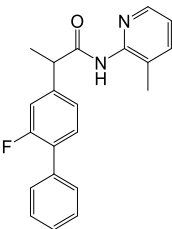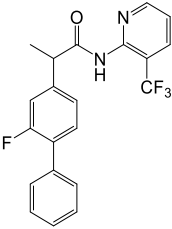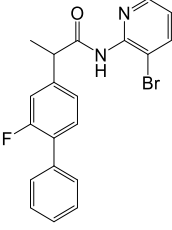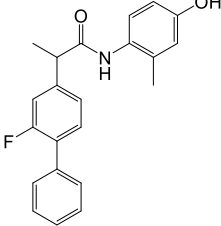
Compound	Formula	Max inhibition (%)	IC$_{50}$ (µM)
Flu-AM1		100	0.44
Flu-AM2		100	0.11
Flu-AM3		100	0.021
Flu-AM4		100	0.15

Table 13. Maximum percentage and IC$_{50}$ values for inhibition of rat brain AEA hydrolysis by compounds **Flu-AM2-4.**
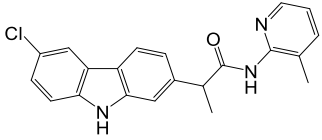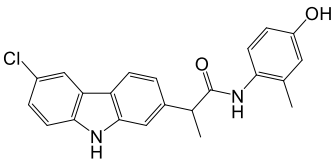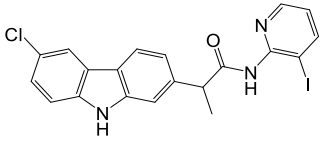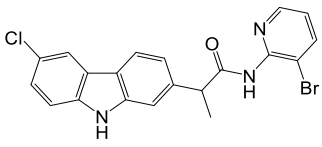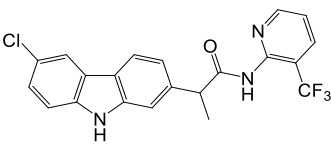
Compound	Formula	Max inhibition (%)	IC$_{50}$ (µM)
Carpr-AM1		100	0.034
Carpr-AM2		100	<0.05
Carpr-AM3		90	>5
Carpr-AM4		100	>10
Carpr-AM5		100	>15

Table 14. Maximum percentage and IC$_{50}$ values for inhibition of rat brain AEA hydrolysis by compounds **Carpr-AM2-5.**

Being the C-α to the carbonyl a chiral center we were interested to understand if as well as the presence of this methyl even its configuration is important. Therefore, we prepared the single enantiomers of **Ibu-AM5** and **Flu-AM1** and the inhibitor activity against FAAH of these was tested. As reported on the table 15 the (*S*)-(+)enantiomer of **Ibu-AM5** is almost ten times more active than **(*R*)-(-)-Ibu-AM5**. Conversely, (*R*)-(-)-ibuprofen is better FAAH inhibitor than (*S*)-(+)-ibuprofen.[106] While the enantiomers of **Flu-AM1** exhibit similar inhibitory activity, being the **(*S*)-(+)-Flu-AM1** slight less potent than the *R*-enantiomer according to the corresponding acids.
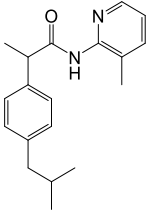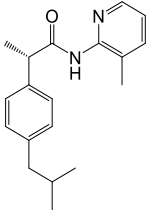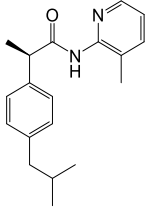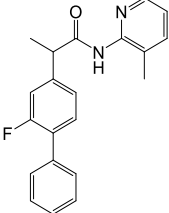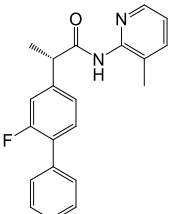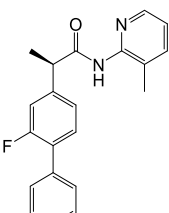
Compound	Formula	Max inhibition (%)	IC$_{50}$ (μM)
Ibu-AM5 (Racemate)		100	0.52
(S)-(+)-Ibu-AM5		100	0.59
(R)-(-)-Ibu-AM5		92±4	5.7
Flu-AM1 (Racemate)		100	0.44
(S)-(+)-Flu-AM1		100	0.99
(R)-(-)-Flu-AM1		100	0.74

Table 15. Maximum percentage and IC$_{50}$ values for inhibition of rat brain AEA hydrolysis by enantiomers of **Ibu-AM5** and **Flu-AM1.**

As highlighted by computational studies performed at the Dr. Catalanotti and Prof. Luque computational laboratories, University Federico II of Naples and University of Barcelona, Flu-AM1 and Ibu-AM5 bind a region located between the acyl chain binding (ACB) and the entrance of the membrane access channel (MAC), as well as other non-covalent FAAH inhibitors, such as carprofen[107] and (3-((3R)-1-(4-(1-benzothiophen-2-yl)pyrimidin-2-yl)piperidin-3-yl)-2-methyl-1H pyrrolo(2,3- b)pyridin-1-yl)acetonitrile.[108]

Docking experiments indicated two possible binding modes, which differ in the molecule orientation, the A-mode presents the amide moiety pointing toward the catalytic triad, while the B-mode pointing toward the membrane interacting helices α18-α19. Nevertheless, molecular dynamics (MD) studies suggested that the B-mode is the most probable binding mode in terms of stability and of the convergence of different runs. The MD simulations result were experimentally validated by testing **(R)-Flu-AM1** in rat FAAH^{T488A} mutant, in collaboration with the group of Dr. E. Pedone (IBB-CNR, Naples). The lower activity showed in the mutant FAAH^{T488A} with respect to the wild type supported the proposed binding mode, since only in the B-mode there is a relevant interaction between ligand and the FAAH residue Thr-488.

The comparison of the best representative poses of the **Flu-AM1** enantiomers (Figure 31) highlighted that they bind the enzyme in two very different ways. (S)-enantiomer, conversely to the **(R)-Flu-AM1** that binds the receptor near the catalytic site, has the binding site deeper in the MAC, suggesting that chirality is a main determinant of the binding mode.

As suggested by the inhibition results the difference on the binding modes have a much greater influence for the enantiomers of **Ibu-AM5** than for those of **Flu-AM1**. In agreement with the similar inhibitor activities, both **(R)-** and **(S)-Flu-AM1** binding mode were characterized by a similar pattern of hydrophobic interactions and two hydrogen bonds. Conversely, **(R)-Ibu-AM5** (Figure 30) showed

less hydrogen bond and less flexibility of the isobutyl moiety than (*S*)-enantiomer in full agreement with their different activities.
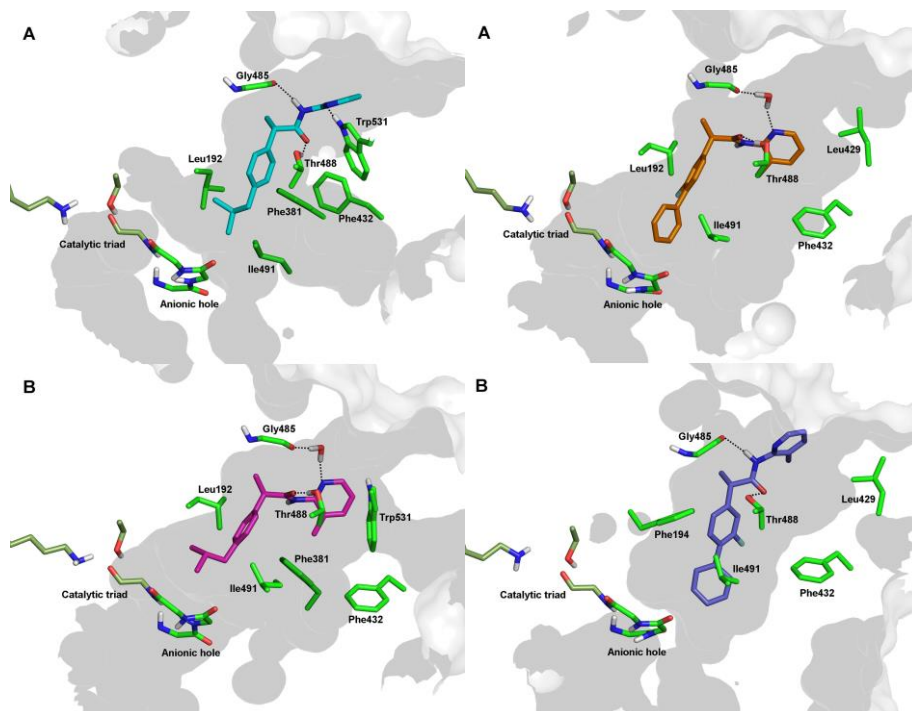
Figure 30. Representation of (*R*)- (A) and (*S*)-Ibu-AM5 (B) in the Competitive Bonding Site of the Dimeric FAAH.

Figure 31. Representation of (*R*)- (A) and (*S*)-Flu-AM1 (B) in the Competitive Bonding Site of the Dimeric FAAH.

2.8.2 Results and Discussion: TPA

The Ibu-AM derivatives are characterized by the presence of the isobutyl chain of the parent Ibuprofen. MD studies on the Ibu-AM5 enantiomers binding modes, showed that in both (*S*)- and (*R*) Ibu-AM5 the isobutyl chain fail into a wide task within the ACB channel, allowing two main populated and opposite positions of the isobutyl chain resulting in a great flexibility and freedom (Figure 32). With the aim to reduce both rotation freedom and lipophilicity, we explored the possibility to substitute the isobutyl group of **Ibu-AM5** with 2-(trifuoromethyl)pyridin-4-ylamino group, obtaining a new series of 2-(4-((2-(**T**rifluoromethyl)**P**yridin-4-yl)amino)phenyl)propan **A**mides (TPA) (Figure 33).
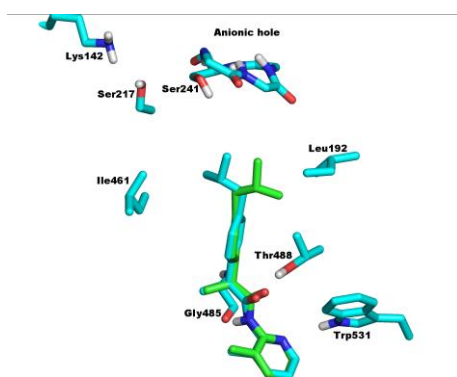
Figure 32. (*R*)-Ibu-AM5 MD.
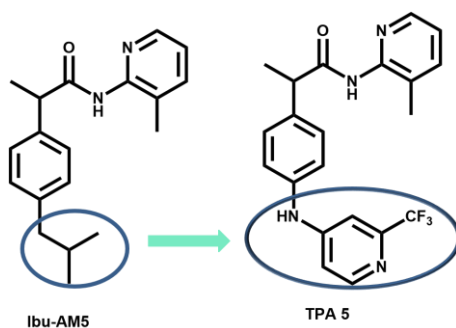
Figure 33. Design of TPA5.

The new series derive from the acid 2-(4-((2-(trifluoromethyl)pyridin-4-yl)amino)phenyl)propanoic acid **(TPA0)**. The starting material used for the synthesis of **TPA0** is 2-(4-nitrophenyl)propionic acid which is first converted into its methyl ester and subsequently submitted to reduction of the nitro group. Then the resulting methyl 2-(4-aminophenyl)propionate was treated with 1,1,1-trifluoro-4-methoxypent-3-en-2-one **(22)** at reflux in acetonitrile solution to obtain the enaminone **23**, which was reacted with N,N-dimethylformamide dimethyl acetal (DMF-DMA), thus obtaining the dienaminone **24**. Next step was the cyclization of the dienaminone **24**

with ammonium acetate to obtain the ester **25**, which was hydrolyzed to the corresponding acid **TPA0** (Scheme 16).
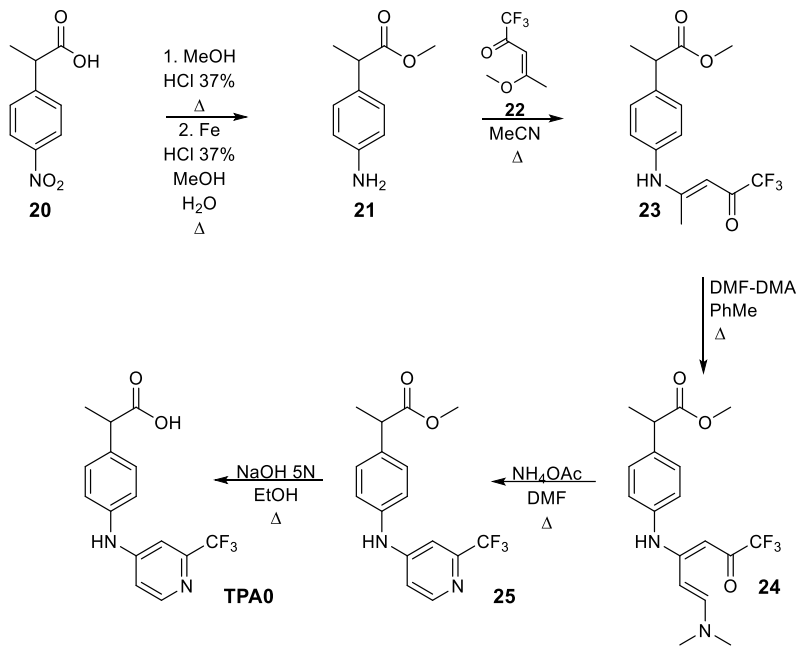
Scheme 16. Synthesis of **TPA0**.

The **TPA0** was converted in its amide with 2-amino-3-methylpyridine **TPA5** (Scheme 17), which show an IC_{50} value of 0.59 μM, very similar to that of **Ibu-AM5** (0.52 μM) (Table 16).
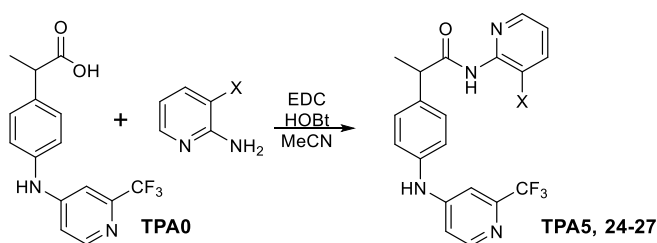
Scheme 17. Synthesis of **TPA5, 24-27.**

In order to better understand the structure-activity relationship of TPAs and to discover the better modification to improve the activity as FAAH inhibitors, we made modification to all moieties of the molecule (Figure 34).

Figure 34. SAR scheme of the **TPA5** modifications.
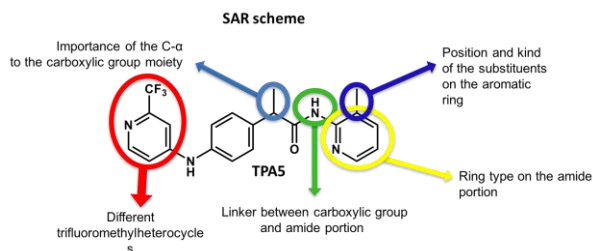
First we dedicate our attention to extension of the distance between the carbonyl group and the pyridine ring. To this purpose **TPA0** was condensed with 2-picolylamine and 3-picolylamine to obtain the amides **TPA8** and **TPA9** respectively (Scheme 18). Confirming the data of the analog Ibu-AMs the presence of a longer linker between the carbonyl and the pyridine ring caused a considerable decrease in activity (IC_{50} more than 20 µM) (Table 16).

Scheme 18. Synthesis of **TPA8-9.**
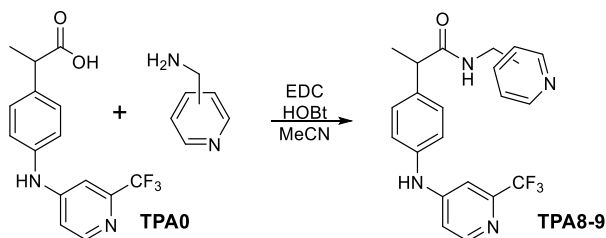
The further linker extension was the introduction of second amide moiety to give **TPA10 (IbuAM9** analog**)**. This compound was prepared starting from condensation between **TPA0** and ethyl glycinate hydrochloride using the EDC method. The obtained ester **26** was hydrolyzed under basic conditions to obtain compound **27**. This acid was finally condensed with the 2-amino-3-methylpiridine using the EDC to obtain the amide **TPA10** (Scheme 19). **TPA10** showed a slight reduction of the activity (IC_{50} value of 2.4 µM) as compared to **TPA5** (Table 16).
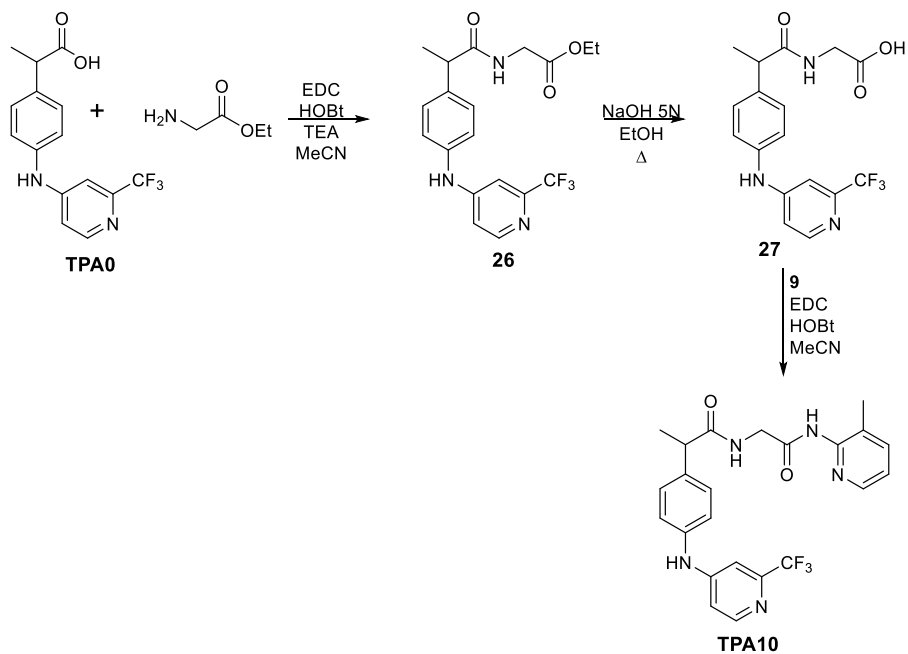
Scheme 19. Synthesis of **TPA10.**
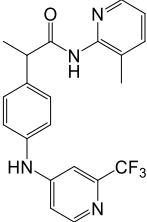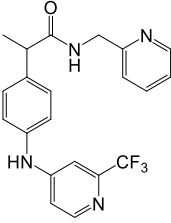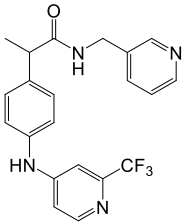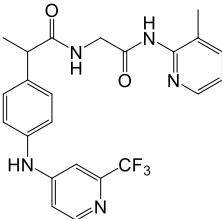
Compound	Formula	Max inhibition (%)	IC50 (μM)
TPA5		100	0.59
TPA8		100	23.0
TPA9		100	32.0
TPA10		100	2.4

Table 16. Maximum percentage and IC_{50} values for inhibition of rat brain AEA hydrolysis by compounds **TPA5, 8-10.**

Then we modified the 3-methylpyridoamido moiety: **TPA11** and **TPA12** are **TPA5** analogs bearing the methyl group in different position of the pyridine ring, respectively in 5-position and 4-position (Scheme 20); both showed a highest IC_{50} as compared to **TPA5**, respectively of 11.0 and 4.0 μM (Table 17). The activity reduction in both cases indicates that the position of the methyl on the pyridine ring is crucial for the inhibitory activity.
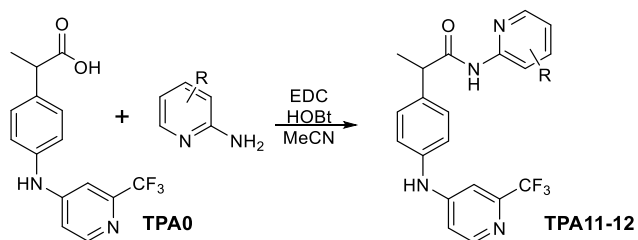
Scheme 20. Synthesis of **TPA11-12.**

To evaluate the influence of the position of the pyridine nitrogen on the activity, we prepared **TPA13**, **TPA14** and **TPA15**, through condensation of **TPA0** with 2-aminopyridine, 3-aminopyridine and 4-aminopyridine respectively (Scheme 21). The pharmacological results indicate that the 3-aminopyridine derivative **TPA14** shows the better IC_{50} (6.4 μM), followed by **TPA13** (2-aminopyridine substituted) showing an IC_{50} value of 12 μM and last by **TPA15** (4-aminopyridine substituted) showing an IC_{50} 52 μM. Interestingly **TPA13** displays inhibitory activity about 20 folds lower than **TPA5** confirming the greater importance of the presence of the 3-methyl pyridine substituent than nitrogen atom position. This is also emphasized by **TPA16**, the phenyl analog of **TPA5** (Scheme 22), this compound showed an IC_{50} value of 0.74 μM (Table 17).
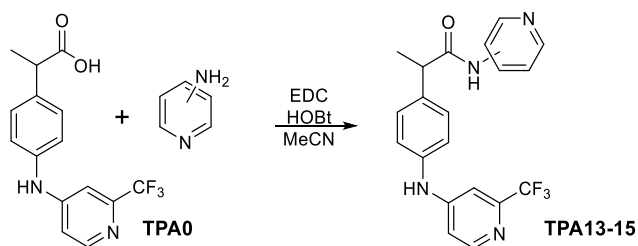
Scheme 21. Synthesis of **TPA13-15.**
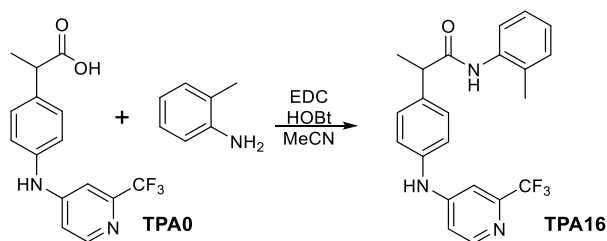
Scheme 22. Synthesis of **TPA16.**

Based on the results just described we replaced the pyridine ring with pyrimidine **(TPA17)** and pyrazine ring **(TPA18)** (Scheme 23). As displayed on the table 17 both the compounds show an activity increased in particular **TPA17** displaying an IC_{50} value of 0.99 µM.
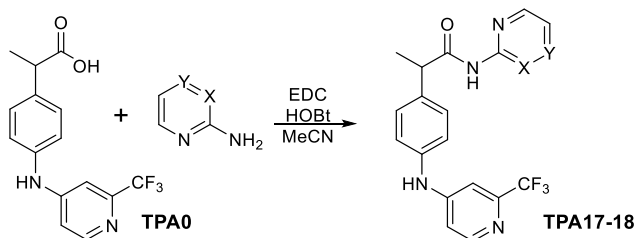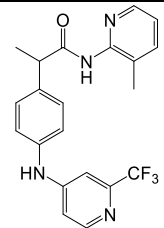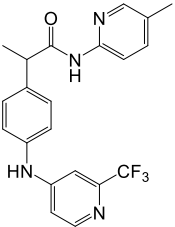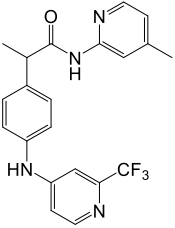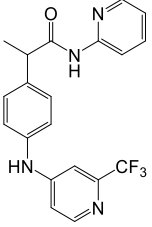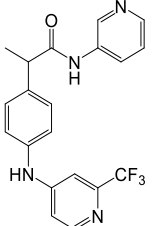
Scheme 23. Synthesis of **TPA17-18**.

To evaluate how a larger and more lipophilic ring influenced the activity, **TPA0** was condensed with 8-aminoquinoline (Scheme 24). The obtained amide **TPA19**, has an activity about seven times lower than the reference compound **TPA5**, indicating that the increase in size and lipophilicity of the amide region does not improve the FAAH inhibitory activity (Table 17).
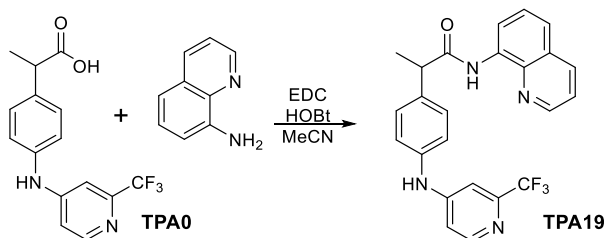
Scheme 24. Synthesis of **TPA19**.

Compound	Formula	Max inhibition (%)	IC50 (µM)
TPA5		100	0.59
TPA11		68±4	11.0
TPA12		100	4.0
TPA13		93±3	12.0
TPA14		86±2	6.4
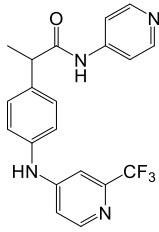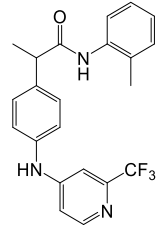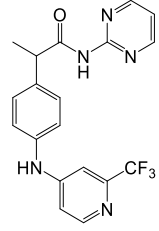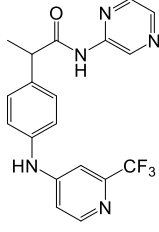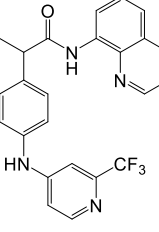
TPA15		100	52.0
TPA16		100	0.74
TPA17		100	0.99
TPA18		100	2.0
TPA19		75±7	4.3

Table 17. Maximum percentage and IC$_{50}$ values for inhibition of rat brain AEA hydrolysis by compounds **TPA11-19.**

Based on the best results obtained for Ibuprofen phenylpiperazine derivatives, we prepared the **TPA20**, **TPA21**, **TPA22**, and **TPA23** deriving from 1-(3-chlorophenyl)piperazine, 1-(4-chlorophenyl) piperazine, 1-(2,3-dimethylphenyl)piperazine and 1-(2-methylphenyl)

piperazine respectively (Scheme 25). Even in these cases, the phenylpiperazine derivatives showed inhibitor activity lower than the reference compound **TPA5**. That is particularly evident for compounds **TPA22** and **TPA23**, which completely lose the inhibitory activity (Table 18). However, the different behavior between the halogenated and the methyl phenylpiperazines compared to the Ibu-AM analogues may, again, suggests a different interaction with FAAH of TPA and Ibu-AM derivatives.
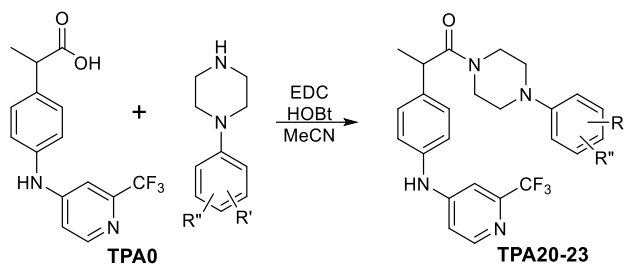
Scheme 25. Synthesis of **TPA20-23.**

Compound	Formula	Max inhibition (%)	IC50 (µM)
TPA20		100	27
TPA21		65±8	17
TPA22		24±2% inhibition @100 µM	
TPA23		24±3% inhibition @ 100 µM	

Table 18. Maximum percentage and IC_{50} values for inhibition of rat brain AEA hydrolysis by compounds **TPA20-23.**

In order to evaluate the characteristics of the substituent in *ortho* to the amidic nitrogen we replaced the methyl with halogen such as bromine, iodine, trifluoromethyl and chlorine (Scheme 26). All these amides showed a very good activity, in every case better than **TPA5**, with IC_{50} values of 0.13 µM for **TPA24**, 0.10 µM for **TPA25**, 0.33 µM for **TPA26** and even 0.058 µM for the chlorine derivative **TPA27**, which is the best of the series (Table 19).

As for the **Ibu-AM52** even in this case we prepared the derivative with the 2-methyl-4-hydroxyaniline in order to evaluate the effect of the presence of a group that can give hydrogen bonds **(TPA28)** (Scheme 26). Also in this case the compound with the hydroxyl group has an IC_{50} lower than the **TPA16**, as well as **Ibu-AM48** and **Ibu-AM52** (Table 19).
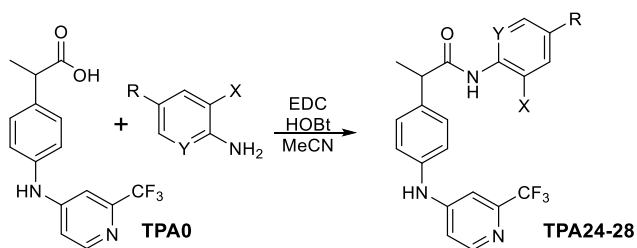
Scheme 26. Synthesis of **TPA24-28**.

Compound	Formula	Max inhibition (%)	IC50 (μM)
TPA5		100	0.59
TPA24		100	0.13
TPA25		100	0.10
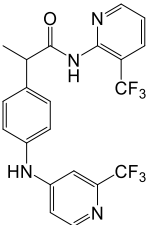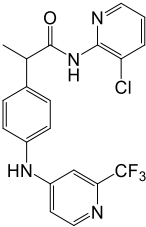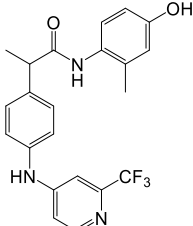
TPA26		100	0.33
TPA27		100	0.058
TPA28		100	0.63

Table 19. Maximum percentage and IC_{50} values for inhibition of rat brain AEA hydrolysis by compounds **TPA24-28.**

TPA5 and **TPA27** were also tested in kinetics experiments in order to get some information in the mechanism of action of this novel class of FAAH inhibitors. **TPA5** resulted a competitive inhibitor while **TPA27** showed different inhibition kinetics, with Ki and alfa values of 0.28 µM and 1.03, respectively (Chart 2 and 3). Therefore **TPA27** behaves as a non-competitive inhibitor. Further experiments highlighted that **TPA27** is fully reversible. Taken into account these considerations we hypothesized that **TPA5** and **TPA27** both behave as FAAH inhibitors, exerting their effect by binding two different binding sites on the enzyme.
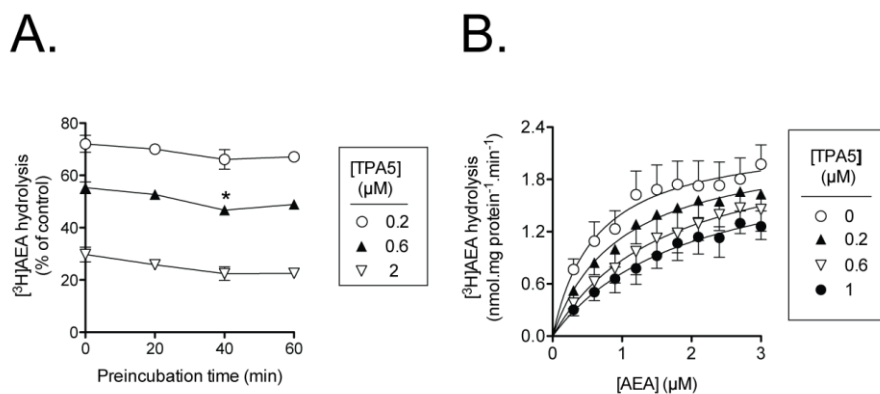
Chart 2. Mode of inhibition of rat brain FAAH by **TPA5**. Panel A: homogenates were preincubated with the compounds for the times shown prior to addition of 0.5 μM [3H]AEA and assay for FAAH activity (means and s.e.m., n=3-4)Panel B: AEA hydrolysis at the substrate and inhibitor concentrations shown (means and s.e.m, n=3).
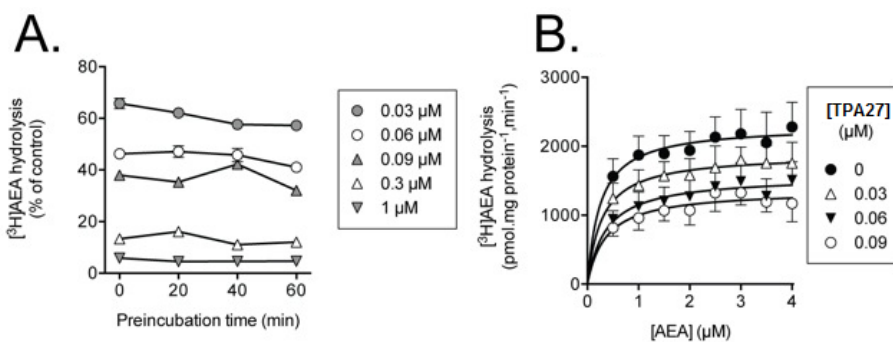
Chart 3. Mode of inhibition of rat brain FAAH by **TPA27**. Panel A: homogenates were preincubated with the compounds for the times shown prior to addition of 0.5 μM [3H]AEA and assay for FAAH activity (means and s.e.m., n=3-4)Panel B: AEA hydrolysis at the substrate and inhibitor concentrations shown (means and s.e.m, n=3).

Therefore the kinetics experiments highlighted that even small modifications on the TPA scaffold may influence dramatically the binding preference and therefore the inhibition mechanism. In the light of such considerations, caution should be taken in order to derive the structure activity relationships, since structure modifications could influence a single or more binding mode.

Conformational studies on **TPA5** and **TPA27** (Maestro, MM3 forcefield, ε=4) revealed a different conformational behavior for **TPA5** and **TPA27** (Figure 35), thus suggesting a potential explanation for this finding.
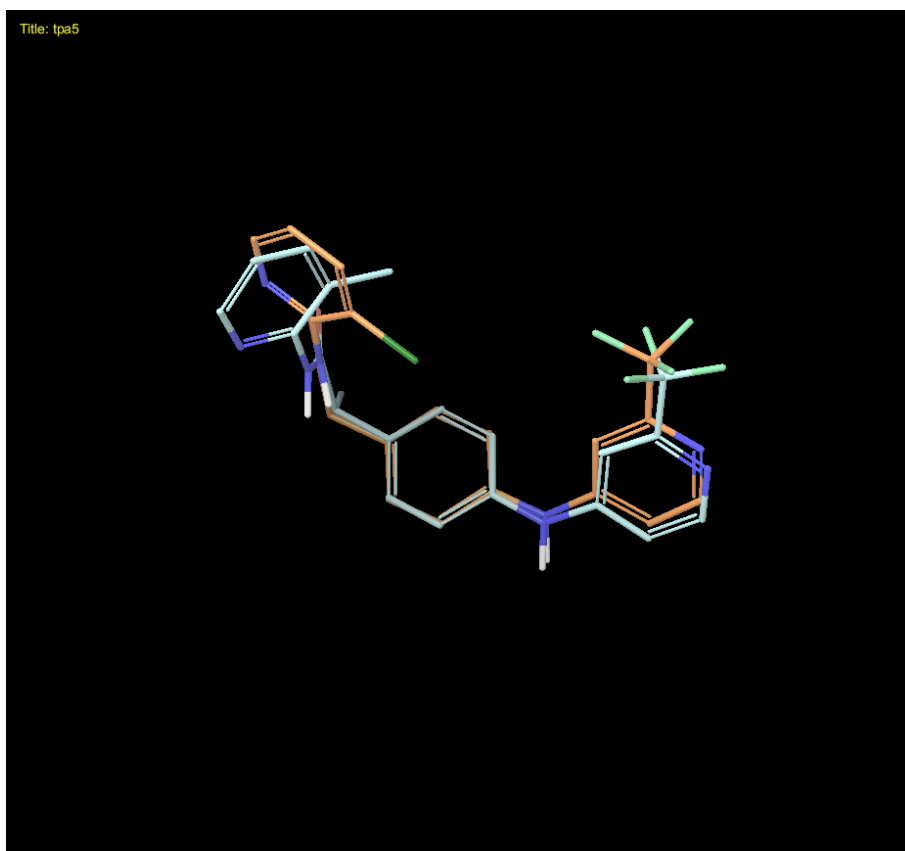
Figure 35. Superimposition of global minumum conformers of TPA5 (grey) and TPA27 (orange).

Docking and MD studies allowed us to get preliminary information about the putative binding mode for **(S)-TPA5**. The pure competitive inhibition kinetic showed by **(S)-TPA5** addressed us to perform docking calculations in the substrate-binding site. As previously found for **Ibu-AM5** and **Flu-AM1** enantiomers, docking indicated two possible orientation, namely the A-mode showing the amide moiety pointing toward the catalytic triad, and the B-mode with the amide pointing toward the membrane interacting helices α18- α 19. MD simulations of 100 ns were run on the best four poses (2 for A-mode and two for B-mode). The analysis of the MD run suggested that the A-mode is the most stable binding mode as shown by the analysis of the RMSD during the MD run, showing convergence among different MD run. Moreover, QM/MM calculations also demonstrated a lower

ΔG for the A-mode (-78 kcal/mol) compared to the B mode (-59.25 kcal/mol).
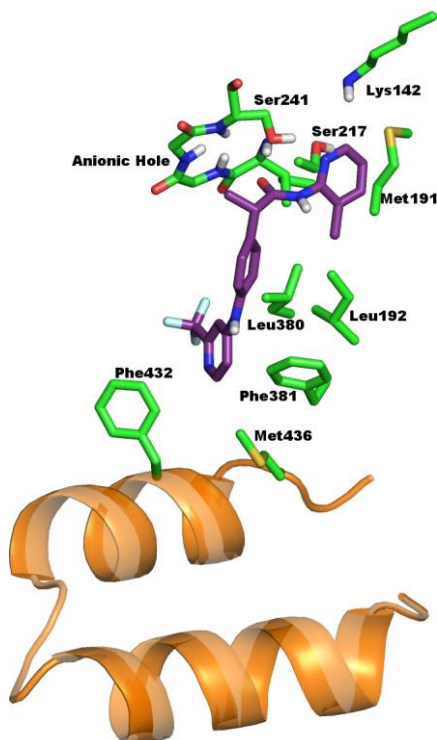
Figure 36. Representation of (*S*)-TPA5 (violet) in the competitive binding site of the dimeric FAAH (green) as obtained from MD simulations. The membrane interacting helices α18- α19 are highlighted in orange.

The analysis of the most relevant frame in the only cluster resulting by the A-mode run (Figure 36), showed the carbonyl moiety interacting with to the oxyanion hole, composed of four main chain amide N-H groups, including those of Ile238, Gly239, Gly240, Ser241, while the methyl pyridine moiety established hydrophobic contacts with Met191, Ile238 and Leu192. The central core of **TPA5** elongated along the ACB channel and the trifluoromethylpyridinamine moiety interacted with residues at the gorge of the MAC, establishing face to edge π-π interactions with Phe381 and Phe432, and hydrophobic contacts with Met436 and Leu380. No interactions with the Thr488 were observed. To further confirm the putative binding mode, experiments on mutated FAAH are currently in progress.

As for the Ibu-AM series, we explored the importance of the substituent on C-α to the carbonyl group; firstly, we deleted the methyl **(TPA29)**. To prepare this compound we utilized the same synthetic procedure used to prepare **TPA0** starting from the methyl ester of the 2-(4-aminophenyl)acetic acid **(28)**, the obtained acid **31** was subsequently condensed with 2-amino-3-methylpyridine using EDC method (Scheme 27). As expected, the activity greatly reduced (Table 20). After that, we evaluated how the insertion of a second methyl group influenced the activity. To prepare **TPA30** (Scheme 28) 2-(4-nitrophenyl)acetic acid was converted into its methyl ester derivative **33**, which was treated with iodomethane in DMF solution in presence of NaH to obtain compound **34**. The nitro group of **34** was reduced into its corresponding amine **(35)**. This last was converted into **TPA30** with the same procedure used to obtain **TPA29** (Scheme 28). Enzymatic assays showed **TPA30** to be slightly less potent than **TPA5**. Taken together, results of **TPA29** and **TPA30** suggested that the presence of a lipophilic group on C-α to the carbonyl group is essential (Table 20).
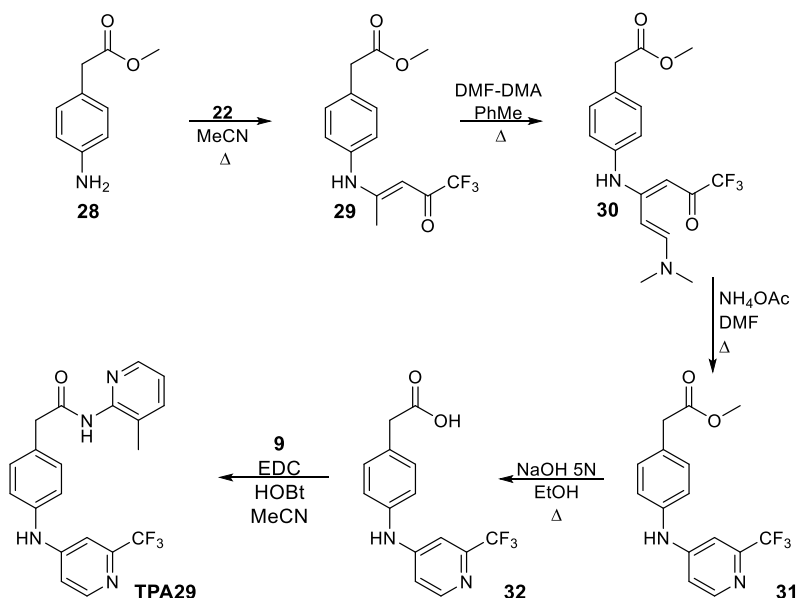
Scheme 27. Synthesis of **TPA29**.
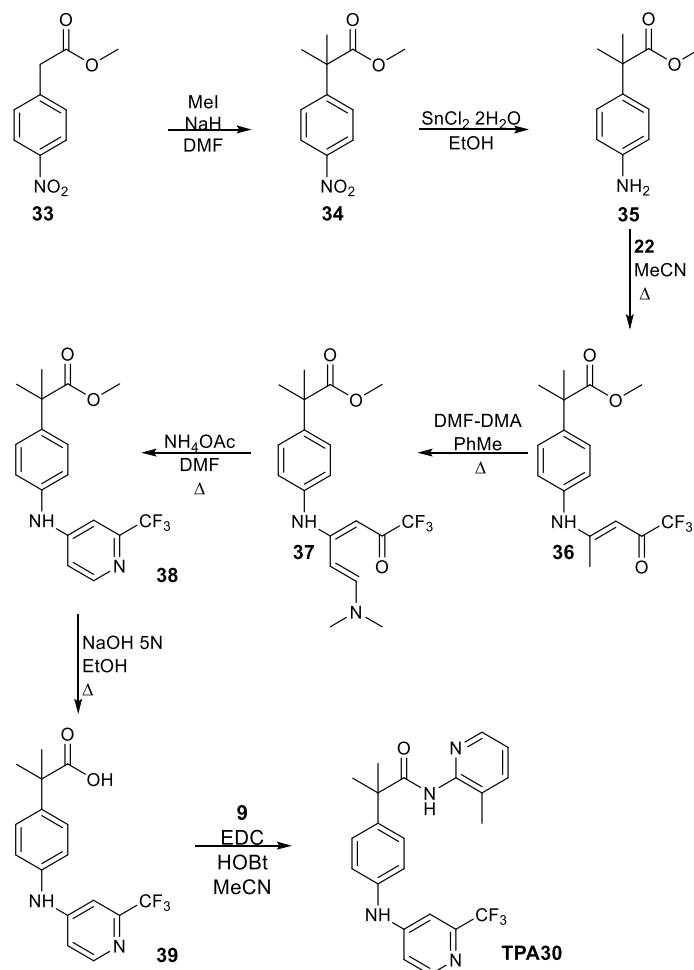
Scheme 28. Synthesis of **TPA30.**
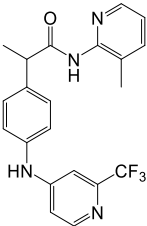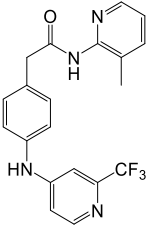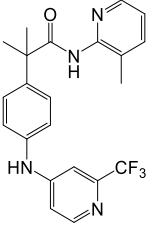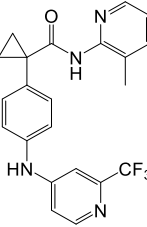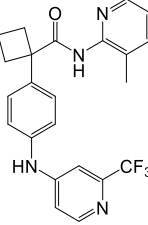
We therefore tried to increase the steric hindrance at the C-α to the carbonyl group, by inserting three, four, five and six atom rings. **TPA31**, **TPA32**, **TPA33** and **TPA34** were prepared with the same procedure described to prepare **TPA30**, using the appropriate di-halogen derivatives, namely 1,2-dibromoethane, 1,3-diiodopropane, 1,4-diiodobutane, 1,5-diiodopentane respectively (Scheme 29); all the obtained amides show IC_{50} higher than **TPA5**. With the exception of the compound bearing the cyclopropyl group **(TPA31),** the increase in size of the cycle causes a progressive reduction of the activity (Table 20). Therefore it is concluded that the chiral center is

not a critical requisite, but the presence of small lipophilic group is essential, more likely due to reduction of the region flexibility.
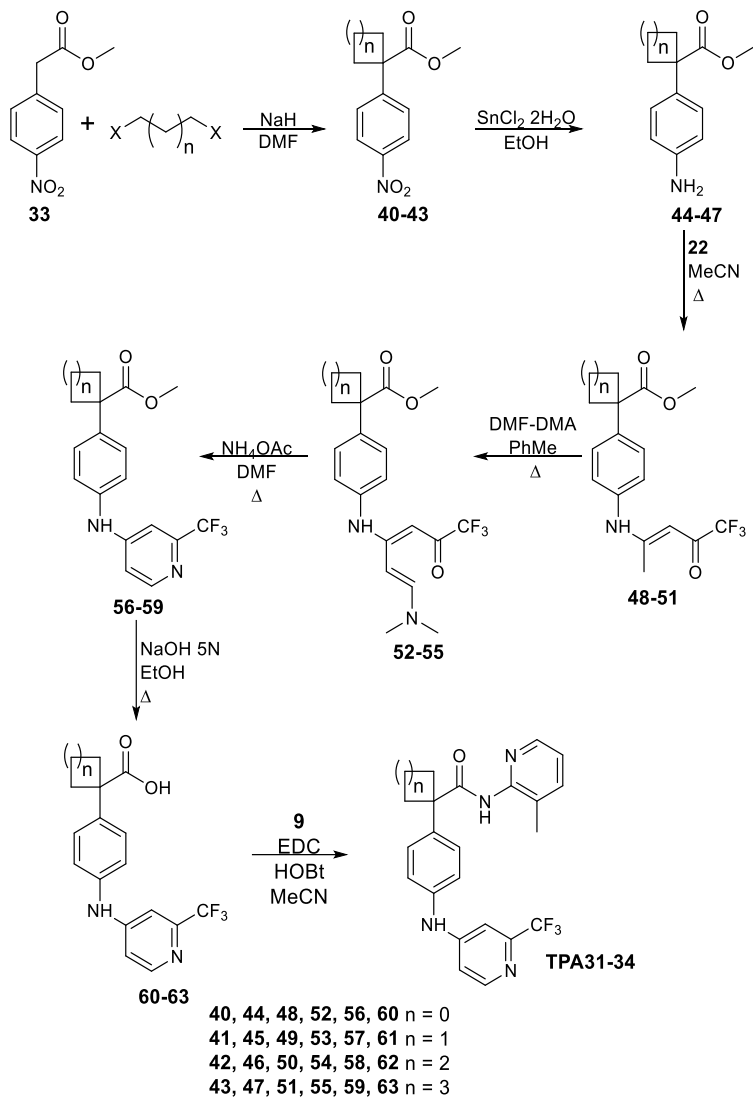
Scheme 29. Synthesis of **TPA31-34**.

40, 44, 48, 52, 56, 60 n = 0
41, 45, 49, 53, 57, 61 n = 1
42, 46, 50, 54, 58, 62 n = 2
43, 47, 51, 55, 59, 63 n = 3

Compound	Formula	Max inhibition (%)	IC50 (µM)
TPA5		100	0.59
TPA29		100	48
TPA30		100	1.8
TPA31		100	14
TPA32		100	9.1
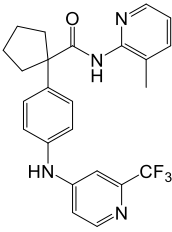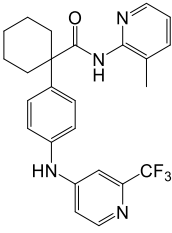
TPA33		100	60

TPA34		30±3	>100

Table 20. Maximum percentage and IC$_{50}$ values for inhibition of rat brain AEA hydrolysis by compounds **TPA29-34.**

To further extend the SAR we also evaluated the importance of the heterocyclic moiety bearing the trifluoromethyl group, preparing the compounds **TPA35** and **TPA36**, where a trifluoromethyl quinoline replace the trifluoromethylpyridine ring. To prepare these compounds the ester **21** was hydrolyzed to the acid **40**. That is subsequently treated with 4-chloro-8-trifluoromethylquinoline and 4-chloro-7-trifluoromethylquinoline to obtain the corresponding acids **65** and **66**, which are condensed with 2-amino-3-methylpyridine by EDC method to obtain **TPA35** and **TPA36**, respectively (Scheme 30). In both cases there is a reduction in the activity, more pronounced when the trifluoromethyl group is in 8-position (Table 21).
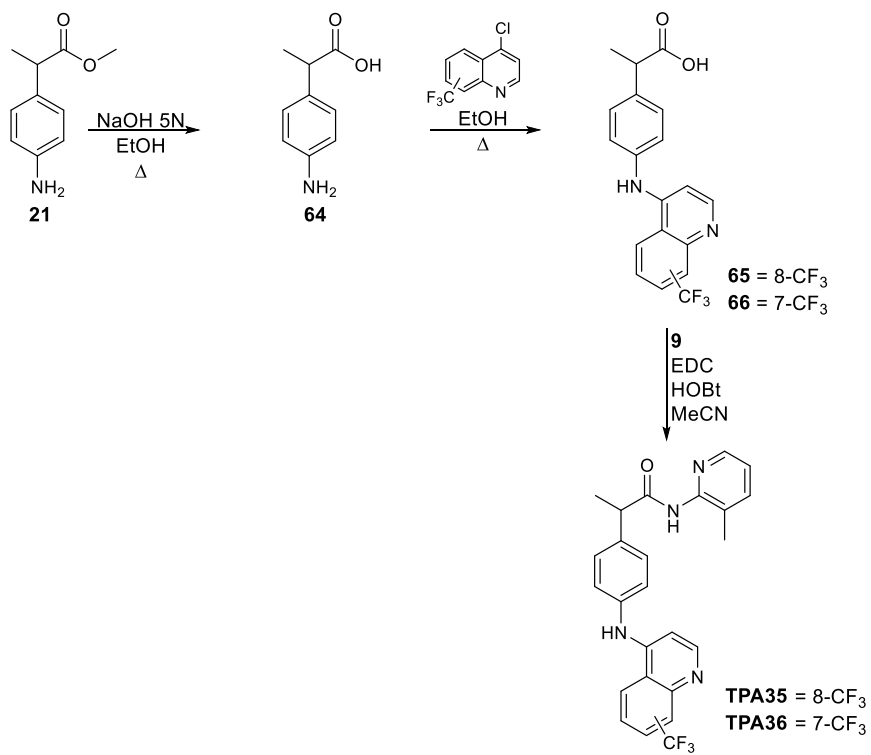
Scheme 30. Synthesis of **TPA35-36.**
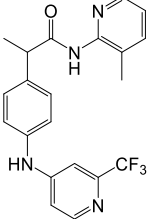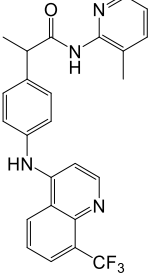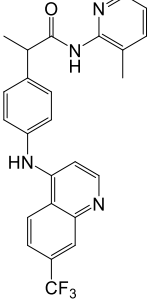
Compound	Formula	Max inhibition (%)	IC50 (µM)
TPA5		100	0.59
TPA35		100	27
TPA36		100	3.1

Table 21. Maximum percentage and IC_{50} values for inhibition of rat brain AEA hydrolysis by compounds **TPA35-36.**

2.9 Experimental[102,103]

Commercially available solvents and reagents were used without further purification unless otherwise stated. Tetrahydrofuran (THF) was freshly distilled from sodium/benzophenone. Reactions requiring anhydrous conditions were performed in oven-dried glassware under argon atmosphere. ^{1}H NMR spectra were recorded on a Varian Inova 500 spectrometer. The chemical shifts (δ) are reported in part per million downfield from tetramethylsilane (TMS), which was used as internal standard, and the spectra were recorded in DMSO-d_6. Infrared spectra were recorded on a Bruker Vector 22 spectrometer. The main bands are given in cm^{-1}. Optical rotation were assessed at 10 mg/mL concentrations using a Perkin Elmer 241 polarimeter in a 10 cm water-jacketed cell at 25 °C. Melting points (m.p.) were determined on a Stuart Scientific Melting point SMP1 apparatus and are uncorrected. All products reported showed NMR spectra in agreement with the assigned structures. The purity of tested compounds was determined by combustion elemental analyses conducted by the Microanalytical Laboratory of the Chemistry Department of the University of Ferrara with a Yanagimoto MT-5 CHN recorder elemental analyzer. All tested compounds yielded data consistent with a purity of at least 95% as compared with the theoretical.

Analytical thin layer chromatography was performed using 0.25 mm silica gel 60-F plates. Flash chromatography was performed using 200-400 mesh silica gel (Merk KGaA). Unless otherwise stated, yields refer to chromatography and spectroscopically pure materials.

Ethyl (2-(4-isobutylphenyl)propanoyl)glycinate (2)
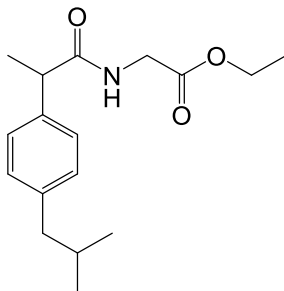
Ibuprofen (0.41 g, 2 mmol), EDC (0.39 g, 2.2 mmol) and HOBt (0.27 g, 2 mmol) were dissolved in MeCN (10 mL). The mixture was stirred at r.t. for 30 minutes, then were added triethylamine (TEA) (0.4 mL, 4 mmol) and ethylglicinate hydrochloride (0.56 g, 4 mmol). The mixture was stirred at r.t. for 4 hours. After the solvent was removed under vacuum. The residue was dissolved in ethyl acetate (AcOEt) (20 mL) and washed sequentially with brine (2x5 mL), 10% citric acid (2x5 mL), saturated NaHCO$_3$ aqueous solution (2x5 mL) and water (2x5 mL). The organic layer was dried over anhydrous sodium sulfate (Na$_2$SO$_4$) and evaporated under vacuum. The residue was treated with isopropyl ether (iPr$_2$O); the precipitate was then filtrated and purified by recrystallization from 2-propanol (2-PrOH).

Yield: 70%. m.p. 132-133 °C (2-PrOH). ^{1}H NMR (DMSO-d_6) δ 0.91 (d, J= 6.6, 6H, CH$_3$), 1.30 (t, J= 7.8, 3H, CH$_3$), 1.44 (d, J= 7.0, 3H, CH$_3$), 1.52 (d, J= 7.0, 2H, CH$_2$), 1.82 (m, 1H, CH), 2.18 (m, 2H, CH$_2$), 2.43 (m, 1H, CH), 3.52 (m, 1H, CH), 4.13 (q, J = 7.8, 2H, CH$_2$), 4.16 (s, 2H, CH$_2$), 7.13 (m, 2H, Ar), 7.30 (m, 2H, Ar), 8.35 (s, 1H, NH). IR (Nujol) 3230, 2766, 1712, 1653 cm^{-1}. Elemental analysis: calculated for C$_{17}$H$_{25}$NO$_3$ (291.18) % C70.07; H 8.65; N 4.81; Found % C70.01; H 8.66; N 4.84.

Ethyl 3-(2-(4-isobutylphenyl)propanamido)propanoate (3)
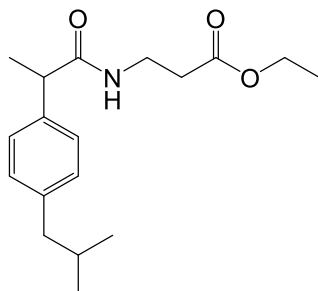
Ibuprofen (0.41 g, 2 mmol), EDC (0.39 g, 2.2 mmol) and HOBt (0.27 g, 2 mmol) were dissolved in MeCN (10 mL). The mixture was stirred at r.t. for 30 minutes, then were added TEA (0.4 mL, 4 mmol) and ethyl 3-aminopropionate (0.61 g, 4 mmol). The mixture was stirred at r.t. for 4 hours. After the solvent was removed under vacuum. The residue was dissolved in AcOEt (20 mL) and washed sequentially with brine (2x5 mL), 10% citric acid (2x5 mL), saturated $NaHCO_3$ aqueous solution (2x5 mL) and water (2x5 mL). The organic layer was dried over anhydrous Na_2SO_4 and evaporated under vacuum. The residue was treated with iPr_2O; the precipitate was then filtrated and purified by recrystallization from 2-PrOH.

Yield: 85%. m.p. 128-130 °C (2-PrOH). ^{1}H NMR (DMSO-d_6) δ 0.92 (d, J= 6.6, 6H, CH_3), 1.28 (t, J= 7.8, 3H, CH_3), 1.46 (d, J= 7.0, 3H, CH_3), 1.49 (d, J= 7.0, 2H, CH_2), 1.82 (m, 1H, CH), 2.19 (m, 2H, CH_2), 2.40 (m, 1H, CH), 2.65 (m, 2H, CH_2), 3.52 (m, 1H, CH), 4.12 (q, J = 7.8, 2H, CH_2), 4.15 (s, 2H,CH_2), 7.17 (m, 2H, Ar), 7.33 (m, 2H, Ar), 8.32 (s, 1H, NH). IR (Nujol) 3244, 2754, 1718, 16547 cm^{-1}. Elemental analysis: calculated for $C_{18}H_{27}NO_3$ (320.22) % C70.79; H 8.91; N 4.59; found % C70.84; H 8.88; N 4.56.

(2-(4-Isobutylphenyl)propanoyl)glycine (4)
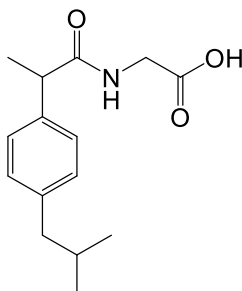
To a solution of the ester **2** (0.29 g, 1 mmol) in ethanol (EtOH) (10 mL) 5N solution of sodium hydroxide (NaOH) (2mL) and water (2 mL) were added. The resulting mixture was stirred at r.t. for 24h. After removing EtOH under vacuum to the resulting solution was ice added and then acidified with aqueous 20% hydrochloric acid (HCl) solution until pH 3-4. The formed precipitate was filtrated, washed with water and re-crystallized from EtOH.

Yield 76%. m.p. 160-161 °C (2-PrOH). ^{1}H NMR (DMSO-d_6) δ 0.91 (d, J= 6.6, 6H, CH$_3$), 1.44 (d, J= 7.0, 3H, CH$_3$), 1.52 (d, J= 7.0, 2H, CH$_2$), 1.82 (m, 1H, CH), 2.19 (m, 2H, CH$_2$), 2.43 (m, 1H, CH), 3.52 (m, 1H, CH), 4.14(s, 2H, CH$_2$), 7.13 (m, 2H, Ar), 7.30 (m, 2H, Ar), 8.35 (s, 1H, NH), 10.82 (s, 1H, OH). IR (Nujol) 3317, 1770, 1661 cm^{-1}. Elemental analysis: calculated for C$_{15}$H$_{21}$NO$_3$ (263.15) % C 68.42; H 8.04; N 5.32; found % C 68.37; H 8.06; N 5.35.

3-(2-(4-Isobutylphenyl)propanamido)propanoic acid (5)
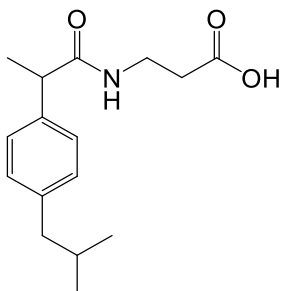
To a solution of the ester **3** (0.32 g, 1mmol) in EtOH (10 mL) 5N solution of NaOH (2mL) and water (2 mL) were added. The resulting

mixture was stirred at r.t. for 24h. After removing EtOH under vacuum to the resulting solution was ice added and then acidified with aqueous 20% HCl solution until pH 3-4. The formed precipitate was filtrated, washed with water and re-crystallized from 2-PrOH.

Yield 84 %. m.p. 147-149 °C (2-PrOH). ^{1}H NMR (DMSO-d_6) δ 0.91 (d, J= 6.5, 6H, CH$_3$), 1.46 (d, J= 7.0, 3H, CH$_3$), 1.52 (d, J= 6.9, 2H, CH$_2$), 1.84 (m, 1H, CH), 2.19 (m, 2H, CH$_2$), 2.42 (m, 1H, CH), 2.66 (m, 2H, CH$_2$), 3.52 (m, 1H, CH), 4.16 (s, 2H, CH$_2$), 7.17 (m, 2H, Ar), 7.35 (m, 2H, Ar), 8.40 (s, 1H, NH), 10.78 (s, 1H, OH). IR (Nujol) 3307, 3061, 1698, 1643 cm^{-1}. Elemental analysis: calculated for C$_{16}$H$_{23}$NO$_3$ (277.17) % C 69.29; H 8.36; N 5.05; found % C 68.24; H 8.38; N 5.02

General procedure for the synthesis of amides Ibu-AM9-13

A mixture of the appropriate acid **4**, **5** (1 mmol), EDC (0.19 g, 1.1 mmol) and HOBt (0.13 g, 1 mmol) in anhydrous MeCN (10 mL) was stirred at r.t. for 30 minutes. After then the appropriate amine (1 mmol) was added. The mixture was then stirred for other 24h. After, the solvent was removed under vacuum; the residue was dissolved in AcOEt (20 mL) and washed sequentially with brine (2x5 mL), 10% citric acid (2x5 mL), NaHCO$_3$ 10% aqueous solution (2x5 mL) and water (2x5 mL). The organic layer was dried over anhydrous Na$_2$SO$_4$ and evaporated under vacuum to obtain the compounds **Ibu-AM9-13**.

2-(4-Isobutylphenyl)-N-(2-((3-methylpyridin-2-yl)amino)-2-oxoethyl)propanamide (Ibu-AM9)
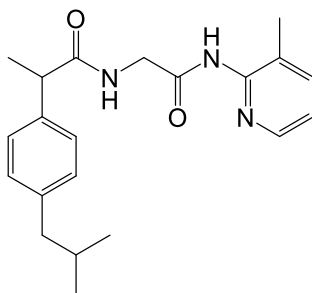
Obtained following the general procedure, by the condensation between the acid **2** and 2-amino-3-methylpyridine **(9)**.

Yield 68%. Oil. ^{1}H NMR (DMSO-d_6) δ 0.95 (d, J= 6.6, 6H, CH$_3$), 1.45 (d, J= 7.0, 3H, CH$_3$), 1.90 (m, 1H, CH), 2.14 (s, 2H, CH$_2$), 2.20 (s, 3H, CH$_3$), 2.50 (s, 3H, CH$_3$), 3.60 (m, 1H, CH), 4.04 (m, 2H, CH$_2$), 7.19-7.74 (m, 7H, Ar), 8.34 (s, 1H, NH), 10.05 (s, 1H, NH). IR (Film) 3264, 1660 cm^{-1}. Elemental analysis: calculated for C$_{21}$H$_{27}$N$_3$O$_2$ (353.21) % C 71.36; H 7.70; N 11.89; found % C 71.41; H 7.68; N 11.93.

2-(4-Isobutylphenyl)-N-(2-((6-methylpyridin-2-yl)amino)-2-oxoethyl)propanamide (Ibu-AM10)
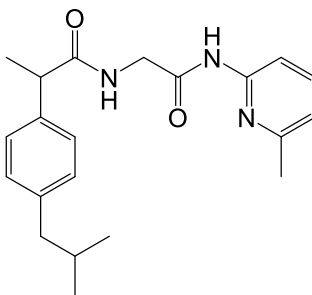
Obtained following the general procedure, by the condensation between the acid **2** and 2-amino-6-methylpyridine.

Yield 55%. m.p. 121-123 °C (cyclohexane). ^{1}H NMR (DMSO-d_6) δ 0.96 (d, J= 6.3, 6H, CH$_3$), 1.44 (d, J= 6.9, 3H, CH$_3$), 1.92 (m, 1H, CH), 2.42 (m, 2H, CH$_2$), 2.50 (s, 3H, CH$_3$), 3.54 (m, 1H, CH), 4.10 (s, 2H, CH$_2$), 7.07-7.93 (m, 7H, Ar), 8.34 (s, 1H, NH), 10.43 (s, 1H). IR (Nujol) 3284,

3069, 1682, 1645 cm^{-1}. Elemental analysis: calculated for $C_{21}H_{27}N_3O_2$ (353.21) % C 71.36; H 7.70; N 11.89; found % C 71.30; H 7.72; N 11.86

2-(4-Isobutylphenyl)-N-(3-((3-methylpyridin-2-yl)amino)-3-oxopropyl)propanamide (Ibu-AM11)
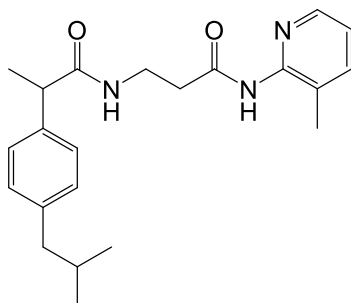
Obtained following the general procedure, by the condensation between the acid **3** and 2-amino-3-methylpyridine.

Yield 62%; Oil. ^{1}H NMR (CDCl$_3$) δ 0.85 (d, J= 5.5, 6H, CH$_3$), 1.45 (d, J= 7.3, 3H, CH$_3$), 1.79 (m, 1H, CH), 2.14 (m, 1H, CH), 2.42 (m, 2H, CH$_2$), 2.48 (m, 2H, CH$_2$), 2.70 (m, 2H, CH$_2$), 3.50 (m, 3H, CH$_3$), 6.98–7.78 (m, 7H, Ar), 8.11 (s, 1H, NH), 9.13 (s, 1H, NH). IR (Film) 3307, 1779, 1669, 1650 cm^{-1}. Elemental analysis: calculated for $C_{22}H_{29}N_3O_2$ (367.23) % C 71.90; H 7.95; N 11.43; found % C 71.96; H 7.92; N 11.45.

2-(4-isobutylphenyl)-N-(2-oxo-2-((pyridin-2-ylmethyl)amino)ethyl)propanamide (Ibu-AM12)
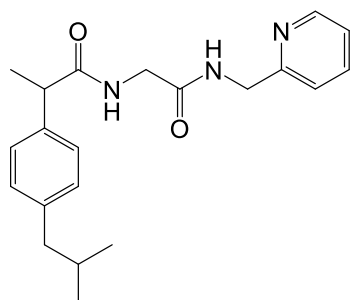
Obtained following the general procedure, by the condensation between the acid **2** and 2-picolylamine.

Yield 68%. Oil. ^{1}H NMR (DMSO-d_6) δ 0.95 (d, J = 6.5, 6H), 1.44 (d, J = 7.0, 3H), 1.89 (hept, J = 6.5, 1H), 2.49 (m, 2H), 3.54 (m, 1H), 4.10 (s, 2H), 4.48 (m, 2H), 7.16, 7.40, 7.88, 8.37, 8.50 (m, 8H), 8.60 (s, 1H), 10.45 (s, 1H).IR (Film) 3320, 1704, 1672, 1645 cm^{-1}. Elemental analysis: calculated for $C_{21}H_{27}N_3O_2$ (353.21) % C 71.36; H 7.70; N 11.89; found % C 71.43; H 7.71; N 11.85.

2-(4-isobutylphenyl)-N-(2-oxo-2-((pyridin-3-ylmethyl)amino)ethyl)propanamide (Ibu-AM13)
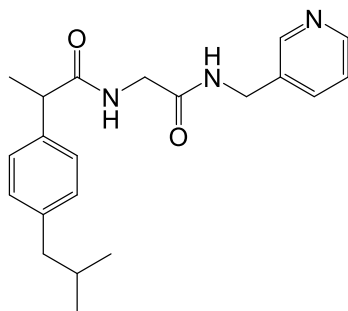
Obtained following the general procedure, by the condensation between the acid **2** and 3-picolylamine.

Yield 75%. Oil. ^{1}H NMR (CDCl$_3$) δ 0.84 (d, J= 5.9, 6H, CH$_3$), 1.41 (d, J= 6.5, 3H, CH$_3$), 1.92 (hept, J= 6.5, 2H, CH), 2.38 (t, J= 7.2, 2H, CH$_2$), 3.56 (m, 1H, CH), 4.14 (s, 2H, CH$_2$), 4.32 (s, 2H, CH$_2$), 7.30-7.65 (m, 8H, Ar), 8.43 (s, 1H, NH), 8.47 (s, 1H, NH). IR (Film) 3298, 3069, 1692, 1654 cm^{-1}. Elemental analysis: calculated for $C_{21}H_{27}N_3O_2$ (353.21) % C 71.36; H 7.70; N 11.89; found % C 71.31; H 7.73; N 11.94.

General procedure for the synthesis of benzylamide derivatives Ibu-AM14-27

A solution of ibuprofen (0.21 g, 1 mmol), EDC (0.19 g, 1.1 mmol) and HOBt (0.13 g, 1 mmol) in anhydrous MeCN (10 mL) was stirred at r.t. for 30 minutes. Then the appropriate benzylamine (1 mmol) was added. The mixture was then stirred for 24h at r.t. After, the solvent was removed under vacuum; the residue was dissolved in AcOEt (20 mL) and washed sequentially with brine (2x5 mL), 10% citric acid (2x5

mL), NaHCO$_3$ 10% aqueous solution (2x5 mL) and water (2x5 mL). The organic layer was dried over anhydrous Na$_2$SO$_4$ and evaporated under vacuum. The obtained residue was tritured with iPr$_2$O; the precipitate was then filtrated to obtain the compounds **Ibu-AM14-27.**

N-Benzyl-2-(4-isobutylphenyl)propanamide (Ibu-AM14)
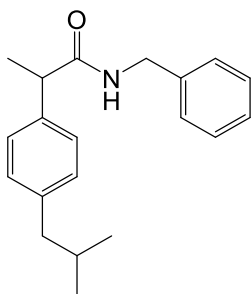
Obtained following the general procedure by the condensation between ibuprofen and benzylamine.

Yield 78%. m.p. 60-62 °C. ^{1}H NMR (DMSO-d$_6$) δ 0.85 (d, J= 6.5 Hz, 6H, CH$_3$), 1.34 (d, J= 7.0 Hz, 3H, CH$_3$), 1.81 (hept, J= 6.5-7.0 Hz, 1H, CH), 2.41 (d, J= 6.5 Hz, 2H, CH$_2$), 3.62 (q, J= 7 Hz, 1H, CH), 4.23 (d, J= 5.5 Hz, 2H, CH$_2$) 7.07-7.30 (m, 9H, Ar), 8.39 (t, J= 5.5 Hz, 1H, NH). IR (Nujol) 3311, 1645, 1546, 1466, 1378, 1230 cm^{-1}. Elemental analysis: calculated for C$_{20}$H$_{25}$NO (295.43) % C 81.31; H 8.53; N 4.74; found % C 81.36; H 8.51; N 4.73.

N-(4-Fluorobenzyl)-2-(4-isobutylphenyl)propanamide (Ibu-AM15)

Obtained following the general procedure by the condensation between ibuprofen and 4-fluorobenzylamine.

Yield 83%. m.p. 58-61 °C. ^{1}H NMR (DMSO-d$_6$) δ 0.85 (d, J= 6.5 Hz, 6H, CH$_3$), 1.34 (d, J= 7.0 Hz, 3H, CH$_3$), 1.81 (hept, J= 6.5-7.0 Hz, 1H, CH), 2.41 (d, J= 6.5 Hz, 2H, CH$_2$), 3.62 (q, J= 7.0 Hz, 1H, CH), 4.23 (d, J= 5.5 Hz, 2H, CH$_2$) 7.04-7.22 (m, 8H, Ar), 8.39 (t, J= 5.5 Hz, 1H, NH). IR (Nujol) 3308, 1638, 1538, 1512, 1463 cm^{-1}. Elemental analysis: calculated for C$_{20}$H$_{24}$FNO (313.42) % C 76.60; H 7.72; N 4.47; found % C 76.70; H 7.70; N 4.45.

N-(4-Chlorobenzyl)-2-(4-isobutylphenyl)propanamide (Ibu-AM16)

Obtained following the general procedure by the condensation between ibuprofen and 4-chlorobenzylamine.

Yield 82%. m.p. 65-68 °C. ^{1}H NMR (DMSO-d$_6$) δ 0.85 (d, J= 6.5 Hz, 6H, CH$_3$), 1.34 (d, J= 7.3 Hz, 3H, CH$_3$), 1.81 (hept, J= 6.5-7.0 Hz, 1H, CH), 2.41 (d, J= 6.5 Hz, 2H, CH$_2$), 3.62 (q, J= 7.0 Hz, 1H, CH), 4.23 (d, J= 5.5 Hz, 2H, CH$_2$) 7.07-7.30 (m, 8H, Ar), 8.42 (t, J=5.0 Hz, 1H, NH). IR (Nujol) 3270, 3084, 1904, 1709, 1646, 1560, 1463, 1422 cm$^{-1.}$ Elemental analysis: calculated for C$_{20}$H$_{24}$ClNO (329.87) % C 72.82; H 7.33; N 4.25; found % C 72.88; H 7.32; N 4.24.

N-(4-(tert-Butyl)benzyl)-2-(4-isobutylphenyl)propanamide (Ibu-AM17)

Obtained following the general procedure by the condensation between ibuprofen and 4-(tertbuthyl)benzylamine.

Yield 80%. Oil. ^{1}H NMR (DMSO-d$_6$) δ 0.85 (d, J= 6.5 Hz, 6H, CH$_3$), 1.23 (s, 9H, CH$_3$) 1.34 (d, J= 7.0 Hz, 3H, CH$_3$), 1.81 (m, 1H, CH), 2.41 (d, J= 6.5 Hz, 2H, CH$_2$), 3.62 (q, J= 7.0 Hz, 1H, CH), 4.23 (d, J= 5.5 Hz, 2H, CH$_2$) 7.07-7.26 (m, 8H, Ar), 8.39 (t, J= 5.5 Hz, 1H, NH). IR (Film) 3291, 1649, 1547, 1514 cm^{-1}. Elemental analysis: calculated for C$_{24}$H$_{33}$NO (351.53) % C 82.00; H 9.46; N 3.98; found % C 82.07; H 9.44; N 3.97.

2-(4-Isobutylphenyl)-N-(4-(trifluoromethyl)benzyl)propanamide (Ibu-AM18)

Obtained following the general procedure by the condensation between ibuprofen and 4-(trifluoromethyl)benzylamine.

Yield 82%. m.p. 62-64 °C. ^{1}H NMR (DMSO-d$_6$) δ 0.85 (d, J= 6.5 Hz, 6H, CH$_3$), 1.34 (d, J= 7.0 Hz, 3H, CH$_3$), 1.81 (hept, J= 6.5-7.0 Hz, 1H, CH), 2.41 (d, J= 6.5 Hz, 2H, CH$_2$), 3.62 (q, J= 7.0 Hz, 1H, CH), 4.23 (d, J= 5.5 Hz, 2H, CH$_2$) 7.07-7.60 (m, 8H, Ar), 8.49 (t, J= 5.5 Hz, 1H, NH). IR

(Nujol) 3332, 3274, 1639, 1541, 1462 cm^{-1}. Elemental analysis: calculated for $C_{21}H_{24}F_3NO$ (363.42) % C 69.40; H 6.66; N 3.85; found % C 69.48; H 6.64; N 3.83.

2-(4-Isobutylphenyl)-N-(4-methoxybenzyl)propanamide (Ibu-AM19)

Obtained following the general procedure by the condensation between ibuprofen and 4-methoxybenzylamine.

Yield 81%. m.p. 78-80 °C. ^{1}H NMR (DMSO-d_6) δ 0.85 (d, J= 6.5 Hz, 6H, CH$_3$), 1.34 (d, J= 7.0 Hz, 3H, CH$_3$), 1.81 (hept, J= 6.5-7.0 Hz, 1H, CH), 2.41 (d, J= 6.5 Hz, 2H, CH$_2$), 3.62 (q, J= 7.0 Hz, 1H, CH), 3.68 (s, 3H, OCH$_3$) 4.23 (d, J= 5.5 Hz, 2H, CH$_2$) 6.08-7.23 (m, 8H, Ar), 8.31 (t, J= 5.5 Hz, 1H, NH). IR (Nujol) 3284, 2360, 1710, 1648, 1462 cm^{-1}. Elemental analysis: calculated for $C_{21}H_{27}NO_2$ (325,45) % C 77.50; H 8.36; N 4.30; found % C 77.56; H 8.34; N 4.28.

2-(4-Isobutylphenyl)-N-(3-(trifluoromethyl)benzyl)propanamide (Ibu-AM20)
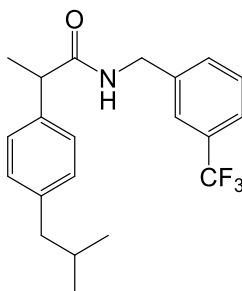
Obtained following the general procedure by the condensation between ibuprofen and 3-(trifluoromethyl)benzylamine.

Yield 83%. m.p. 53-55 °C. ^{1}H NMR (DMSO-d$_6$) δ 0.85 (d, J= 6.5 Hz, 6H, CH$_3$), 1.34 (d, J= 7.0 Hz, 3H, CH$_3$), 1.81 (hept, J= 6.5-7.0 Hz, 1H, CH), 2.41 (d, J= 6.5 Hz, 2H, CH$_2$), 3.62 (q, J= 7.0 Hz, 1H, CH), 4.23 (d, J= 5.5 Hz, 2H, CH$_2$) 7.04-7.41 (m, 8H, Ar), 8.35 (t, J= 5.5 Hz, 1H, NH). IR (Nujol) 3288, 3073, 1651, 1584, 1452, 1329, 1165 cm^{-1}. Elemental analysis: calculated for C$_{21}$H$_{24}$F$_3$NO (363.42) % C 69.40; H 6.66; N 3.85; found % C 69.47; H 6.64; N 3.84.

2-(4-Isobutylphenyl)-N-(2-methoxybenzyl)propanamide (Ibu-AM21)
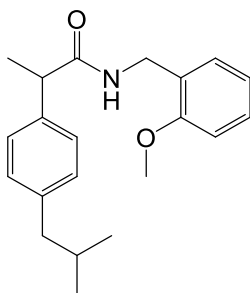
Obtained following the general procedure by the condensation between ibuprofen and 2-methoxybenzylamine.

Yield 82%. m.p. 61-63 °C. ^{1}H NMR (DMSO-d$_6$) δ 0.85 (d, J= 6.5 Hz, 6H, CH$_3$), 1.34 (d, J= 7.0 Hz, 3H, CH$_3$), 1.81 (hept, J= 6.5-7.0 Hz, 1H, CH), 2.41 (d, J= 6.5 Hz, 2H, CH$_2$), 3.62 (q, J= 7.0 Hz, 1H, CH), 3.68 (s, 3H, OCH$_3$) 4.23 (d, J= 5.5 Hz, 2H, CH$_2$) 6.75-7.24 (m, 8H, Ar), 8.15 (t, J= 5.5 Hz, 1H, NH). IR (Nujol) 3275, 1777, 1641, 1564, 1462, cm^{-1}. Elemental analysis: Calculated for C$_{21}$H$_{27}$NO$_2$ (325.45) % C 77.50; H 8.36; N 4.30; found % C 77.57; H 8.34; N 4.28.

N-(2-Chlorobenzyl)-2-(4-isobutylphenyl)propanamide (Ibu-AM22)
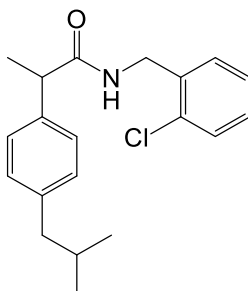
Obtained following the general procedure by the condensation between ibuprofen and 2-chlorobenzylamine.

Yield 85%. m.p. 60-63 °C. ^{1}H NMR (DMSO-d_6) δ 0.85 (d, J= 6.5 Hz, 6H, CH$_3$), 1.34 (d, J= 7.0 Hz, 3H, CH$_3$), 1.81 (hept, J= 6.5-7.0 Hz, 1H, CH), 2.41 (d, J= 6.5 Hz, 2H, CH$_2$), 3.62 (q, J= 7.0 Hz, 1H, CH), 4.23 (d, J= 5.5 Hz, 2H, CH$_2$) 7.08-7.04 (m, 8H, Ar), 8.39 (t, J= 5.5 Hz, 1H, NH). IR (Nujol): 3270, 1710, 1666, 1641, 1562 cm^{-1}. Elemental analysis: calculated for C$_{20}$H$_{24}$ClNO (329.87) % C 72.82; H 7.33; N 4.25; found % C 72.88; H 7.32; N 4.24.

N-(3-Hydroxy-4-methoxybenzyl)-2-(4-isobutylphenyl)propanamide (Ibu-AM23)
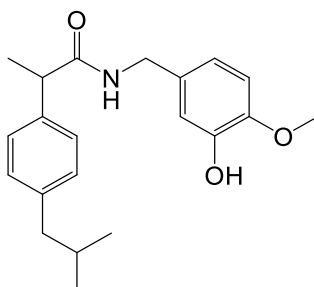
Obtained following the general procedure by the condensation between ibuprofen and 3-hydroxy-4-methoxybenzylamine.

Yield 80%. m.p. 82-85 °C. ^{1}H NMR (DMSO-d_6) δ 0.85 (d, J= 6.5 Hz, 6H, CH$_3$), 1.34 (d, J= 7.0 Hz, 3H, CH$_3$), 1.81 (hept, J= 6.5-7.0 Hz, 1H, CH), 2.41 (d, J= 6.5 Hz, 2H, CH$_2$), 3.62 (q, J= 7.0 Hz, 1H, CH), 3.72 (s, 3H, OCH$_3$) 4.23 (d, J= 5.5 Hz, 2H, CH$_2$) 6.62-7.21 (m, 7H, Ar), 8.39 (t, J= 5.5

Hz, 1H, NH) 9.45 (s, 1H, OH). IR (Nujol) 3334, 3276, 1642, 1564, 1462 cm^{-1}. Elemental analysis: calculated for $C_{21}H_{27}NO_3$ (341.45) % C 73.87; H 7.97; N 4.10; found % C 73.90; H 7.95; N 4.08.

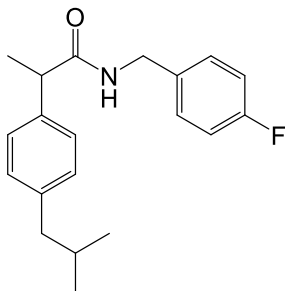### N-(3,4-Dichlorobenzyl)-2-(4-isobutylphenyl)propanamide (Ibu-AM24)
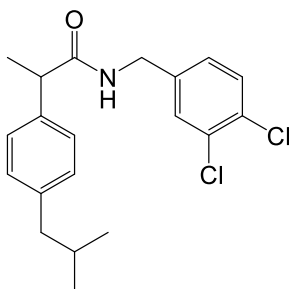
Obtained following the general procedure to by the condensation between ibuprofen and 3,4-dichlorobenzylamine.

Yield 83%. m.p. 78-82 °C. ^{1}H NMR (DMSO-d$_6$) δ 0.85 (d, J= 6.5 Hz, 6H, CH$_3$), 1.34 (d, J= 7.0 Hz, 3H, CH$_3$), 1.81 (hept, J= 6.5-7.0 Hz, 1H, CH), 2.41 (d, J= 6.5 Hz, 2H, CH$_2$), 3.62 (q, J= 7.0 Hz, 1H, CH), 4.23 (d, J= 5.5 Hz, 2H, CH$_2$), 7.07-7.60 (m, 7H, Ar), 8.39 (t, J= 5.5 Hz, 1H, NH). IR (Nujol) 3268, 3072, 1647, 1549, 1428 cm^{-1}. Elemental analysis: calculated for $C_{20}H_{23}Cl_2NO$ (364.31) % C 65.94; H 6.36; N 3.84; found % C 66.03; H 6.35; N 3.82.
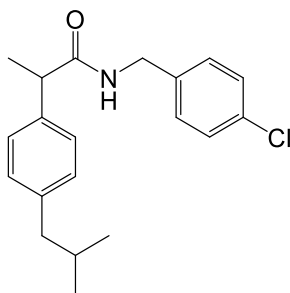
N-(2,4-Dichlorobenzyl)-2-(4-isobutylphenyl)propanamide (Ibu-AM25)
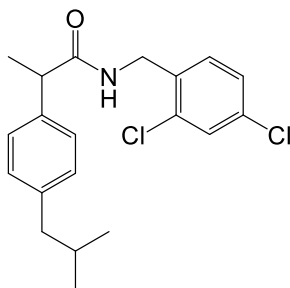
Obtained following the general procedure by the condensation between ibuprofen and 2,4-dichlorobenzylamine.

Yield 79%. m.p. 73-75 °C. ^{1}H NMR (DMSO-d_6) δ 0.85 (d, J= 6.5 Hz, 6H, CH$_3$), 1.34 (d, J= 7.0 Hz, 3H, CH$_3$), 1.81 (hept, J= 6.5-7.0 Hz, 1H, CH), 2.41 (d, J= 6.5 Hz, 2H, CH$_2$), 3.62 (q, J= 7.0 Hz, 1H, CH), 4.23 (d, J= 5.5 Hz, 2H, CH$_2$) 7.07-7.60 (m, 7H, Ar), 8.39 (t, J= 5.5 Hz, 1H, NH). IR (Nujol) 3274, 3083, 1646, 1557 cm^{-1}. Elemental analysis: calculated for C$_{20}$H$_{23}$Cl$_2$NO (364.31) % C 65.94; H 6.36; N 3.84; found % C 66.03; H 6.35; N 3.82.

N-(2,5-Dichlorobenzyl)-2-(4-isobutylphenyl)propanamide (Ibu-AM26)
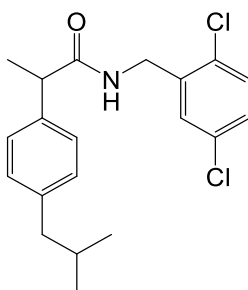
Obtained following the general procedure by the condensation between ibuprofen and 2,5-dichlorobenzylamine.

Yield 82%. m.p. 93-96 °C. ^{1}H NMR (DMSO-d_6) δ 0.85 (d, J= 6.5 Hz, 6H, CH$_3$), 1.34 (d, J= 7.3 Hz, 3H, CH$_3$), 1.81 (hept, J= 6.5-7.0 Hz, 1H, CH), 2.41 (d, J= 6.5 Hz, 2H, CH$_2$), 3.62 (q, J= 7.0 Hz, 1H, CH), 4.23 (d, J= 5.5

Hz, 2H, CH_2) 7.06-7.40 (m, 7H, Ar), 8.39 (t, J= 5.5 Hz, 1H, NH). IR (Nujol) 3268, 3072, 1647, 1549, 1428 cm^{-1}. Elemental Analysis: calculated for $C_{20}H_{23}Cl_2NO$ (363.42) % C 65.94; H 6.36; N 3.84; found % C 66.03; H 6.35; N 3.82.
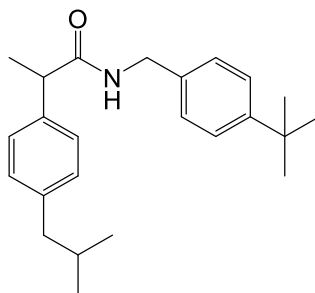
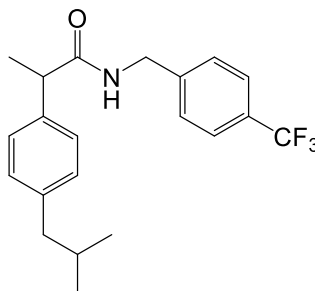## N-(2,6-Dichlorobenzyl)-2-(4-isobutylphenyl)propanamide (Ibu-AM27)
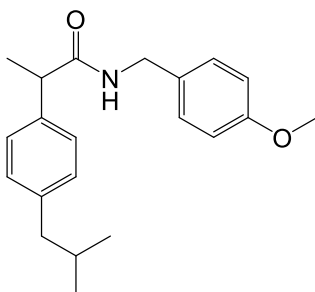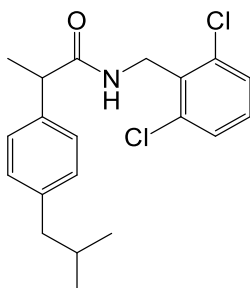

Obtained following the general procedure by the condensation between ibuprofen and 2,6-dichlorobenzylamine.

Yield 82%. m.p. 130-135 °C. ^{1}H NMR (DMSO-d_6) δ 0.85 (d, J= 6.5 Hz, 6H, CH_3), 1.34 (d, J= 7.0 Hz, 3H, CH_3), 1.81 (hept, J= 6.5-7.0 Hz, 1H, CH), 2.41 (d, J= 6.5 Hz, 2H, CH_2), 3.62 (q, J= 7.0 Hz, 1H, CH), 4.23 (d, J= 5.5 Hz, 2H, CH_2) 7.04-7.45 (m, 7H, Ar), 8.39 (t, J= 5.5 Hz, 1H, NH). IR (Nujol) 3310, 1641, 1534, 1437 cm^{-1}. Elemental analysis: calculated for $C_{20}H_{23}Cl_2NO$ (363.42) % C 65.94; H 6.36; N 3.84; found % C 66.00; H 6.35; N 3.82.

General procedure for the synthesis of phenylpiperazine derivatives Ibu-AM28-37

A solution of ibuprofen (0.21 g, 1 mmol), EDC (0.19 g, 1.1 mmol) and HOBt (0.13 g, 1 mmol) in anhydrous MeCN (10 mL) was stirred at r.t. for 30 minutes, then the appropriate phenylpiperazine (1 mmol). was added The mixture was then stirred for 12h at r.t. After, the solvent was removed under vacuum; the residue was dissolved in AcOEt (20 mL) and washed sequentially with brine (2x5 mL), 10% citric acid (2x5 mL), $NaHCO_3$ 10% aqueous solution (2x5 mL) and water (2x5 mL). The

organic layer was dried over anhydrous Na_2SO_4 and evaporated under vacuum. The obtained residue was tritured with iPr_2O; the precipitate was then filtrated to obtain the compounds **Ibu-AM28-37.**

2-(4-Isobutylphenyl)-1-(4-phenylpiperazin-1-yl)propan-1-one (Ibu-AM28)
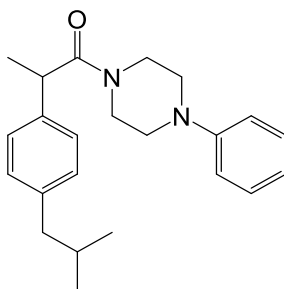
Obtained following the general procedure by the condensation between ibuprofen and 1-phenylpiperazine.

Yield 97 %. m.p. 75-80 °C. ^{1}H NMR (DMSO-d_6) δ 0.83 (d, J= 7.0 Hz, 6H, CH_3), 1.30 (d, J= 7.0 Hz, 3H, CH_3), 1.80 (hept, J= 7.0 Hz, 1H, CH), 2.42 (d, J= 7.0 Hz, 2H, CH_2), 3.16 (m, 2H, CH_2), 3.20 (m, 2H, CH_2), 3.40 (m, 1H, CH), 3.48-3.65 (m, 4H, CH_2), 6.81 (m, 1H Ar), 7.04-7.45 (m, 6H, Ar), 7.53 (m, 1H Ar), 7.59 (m, 1H Ar). IR (Nujol) 3273, 1741, 1631, 1600, 1508, 1465 cm^{-1}. Elemental analysis: calculated for $C_{23}H_{30}N_2O$ (350.51) % C 78.82; H 8.63; N 7.99; found % C 78.89; H 8.67; N 7.85.

## 1-(4-(3-Chlorophenyl)piperazin-1-yl)-2-(4-isobutylphenyl)propan-1-one (Ibu-AM29)
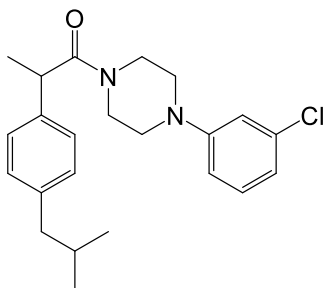
Obtained following the general procedure by the condensation between ibuprofen and 1-(3-chlorophenyl)piperazine.

Yield 95%. Oil. ^{1}H NMR (DMSO-d$_6$) δ 0.84 (d, J= 6.5 Hz, 6H, CH$_3$), 1.32 (d, J= 7.0 Hz, 3H, CH$_3$), 1.81 (hept, J= 6.5-7.0 Hz, 1H, CH), 2.43 (d, J= 7.0 Hz, 2H, CH$_2$), 2.89 (m, 2H, CH$_2$), 3.23 (m, 2H, CH$_2$), 3.41 (q, J= 7.0 Hz, 1H, CH), 3.45-3.68 (m, 4H, CH$_2$), 6.70 (m, 1H Ar), 7.06-7.43 (m, 6H, Ar), 7.50 (m, 1H Ar). IR (Film) 3437, 1732, 1646, 1594, 1486, 1463, 1384, 1231 cm^{-1}. Elemental analysis: calculated for C$_{23}$H$_{29}$ClN$_2$O (384.95) % C 71.76; H 7.59; N 7.28; found % C 71.75; H 7.60; N 7.35.

1-(4-(4-Chlorophenyl)piperazin-1-yl)-2-(4-isobutylphenyl)propan-1-one (Ibu-AM30)
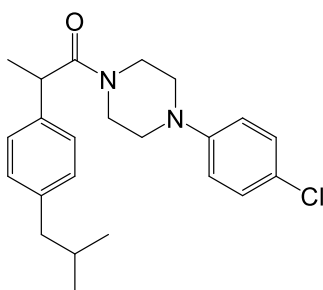
Obtained following the general procedure by the condensation between ibuprofen and 1-(4-chlorophenyl)piperazine.

Yield 83%. Oil. ^{1}H NMR (DMSO-d$_6$) δ 0.94 (d, J= 7.0 Hz, 6H, CH$_3$), 1.32 (d, J=6.5 Hz, 3H, CH$_3$), 1.81 (hept, J= 7.0 Hz, 1H, CH), 2.66 (m, 2H, CH$_2$), 2.95 (m, 2H, CH$_2$), 3.11 (m, 2H, CH$_2$), 3.50-3.68 (m, 4H, CH$_2$),

4.17 (q, J=6.5Hz, 1H, CH), 6.89 (m, 1H, Ar), 7.03 (m, 1H, Ar), 7.16-7.21 (m, 5H, Ar), 7.30 (m, 1H, Ar). IR (Film) 3421, 2955, 1731, 1645, 1497, 1463, 1384 cm^{-1}. Elemental analysis: calculated for $C_{23}H_{29}ClN_2O$ (384.95) % C 71.76; H 7.59; N 7.28; found % C 71.70; H 7.65; N 7.30.

1-(4-(3,4-Dichlorophenyl)piperazin-1-yl)-2-(4-isobutylphenyl)propan-1-one (Ibu-AM31)

Obtained following the general procedure by the condensation between ibuprofen and 1-(3,4-dichlorophenyl)piperazine.

Yield 90%. Oil. ^{1}H NMR (DMSO-d$_6$) δ 0.86 (d, J= 6.5 Hz, 6H, CH$_3$), 1.33 (d, J= 7.0 Hz, 3H, CH$_3$), 1.80 (hept, J= 6.5-7.0 Hz, 1H, CH), 2.41 (d, J= 7.0 Hz, 2H, CH$_2$), 2.92 (m, 2H, CH$_2$), 3.17 (m, 2H, CH$_2$), 3.22 (m, 1H, CH), 3.40-3.71 (m, 4H, CH$_2$), 6.88 (m, 1H Ar), 7.06-7.43 (m, 5H, Ar), 7.53 (m, 1H Ar). IR (Film) 3433, 1728, 1645, 1594, 1555, 1484, 1230 cm^{-1}. Elemental analysis: calculated for $C_{23}H_{28}Cl_2N_2O$ (419.39) % C 64.87; H 6.73; N 6.68; found % C 64.78; H 6.68; N 6.59.

1-(4-(4-Fluorophenyl)piperazin-1-yl)-2-(4-isobutylphenyl)propan-1-one (Ibu-AM32)

Obtained following the general procedure by the condensation between ibuprofen and 1-(4-fluorophenyl)piperazine.

Yield 97 %. m.p. 45-50 °C. ^{1}H NMR (DMSO-d_6) δ 0.90 (d, J= 7.0 Hz, 6H, CH_3), 1.36 (d, J=6.5 Hz, 3H, CH_3), 1.87 (hept, J= 6.5-7.0 Hz, 1H, CH), 2.61 (m, 2H, CH_2), 2.99 (m, 2H, CH_2), 3.06 (m, 2H, CH_2), 3.44-3.61 (m, 4H, CH_2), 4.19 (q, J=6.5Hz, 1H, CH), 6.97 (m, 1H, Ar), 7.02 (m, 1H, Ar), 7.10-7.27 (m, 5H, Ar), 7.34 (m, 1H, Ar). IR (Nujol) 3445, 2955, 2929, 1644, 1510, 1441, 1230 cm^{-1}. Elemental analysis: calculated for $C_{23}H_{29}FN_2O$ (368.23) % C 74.97; H 7.93; N 7.60; found % C 75.01; H 7.90; N 7.55.

2-(4-Isobutylphenyl)-1-(4-(4-methoxyphenyl)piperazin-1-yl)propan-1-one (Ibu-AM33)
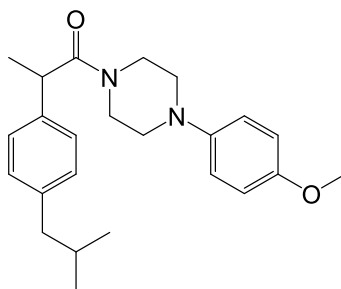
Obtained following the general procedure by the condensation between ibuprofen and 1-(4-methoxyphenyl)piperazine.

Yield 95 %. Oil. ^{1}H NMR (DMSO-d_6) δ 0.95 (d, J= 7.0 Hz, 6H, CH_3), 1.30 (d, J=6.5 Hz, 3H, CH_3), 1.83 (hept, J= 6.5-7.0 Hz, 1H, CH), 2.62 (m, 2H,

CH$_2$), 3.03 (m, 2H, CH$_2$), 3.09 (m, 2H, CH$_2$), 3.40-3.59 (m, 4H, CH$_2$), 3.66 (s, 3H, CH$_3$), 4.22 (q, J=6.5Hz, 1H, CH), 7.01 (m, 1H, Ar), 7.04 (m, 1H, Ar), 7.12-7.23 (m, 5H, Ar), 7.38 (m, 1H, Ar). IR (Film) 3440, 2954, 2930, 1732, 1644, 1464, 1442, 1246 cm^{-1}. Elemental analysis: calculated for C$_{24}$H$_{32}$N$_2$O$_2$ (380.53) % C 75.75; H 8.48; N 7.36; found % C 75.80; H 8.53; N 7.30.

2-(4-Isobutylphenyl)-1-(4-(3-methoxyphenyl)piperazin-1-yl)propan-1-one (Ibu-AM34)
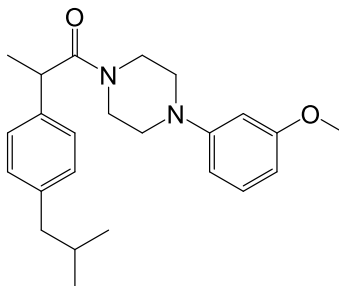
Obtained following the general procedure by the condensation between ibuprofen and 1-(3-methoxyphenyl)piperazine.

Yield 92%. Oil. ^{1}H NMR (DMSO-d$_6$) δ 0.82 (d, J= 7.0 Hz, 6H, CH$_3$), 1.28 (d, J=6.0 Hz, 3H, CH$_3$), 1.79 (hept, J= 6.0-7.0 Hz, 1H, CH), 2.87 (m, 2H, CH$_2$), 3.01 (m, 2H, CH$_2$), 3.13 (m, 2H, CH$_2$), 3.44-3.54 (m, 4H, CH$_2$), 3.68 (s, 3H, CH$_3$), 4.08 (q, J= 6.5Hz, 1H, CH), 6.34 (m, 2H, Ar), 6.42 (m, 1H, Ar), 7.05-7.10 (m, 3H, Ar), 7.16 (m, 2H, Ar). IR (Film) 2956, 2928, 1734, 1647, 16071460,1203 cm^{-1}. Elemental analysis: calculated for C$_{24}$H$_{32}$N$_2$O$_2$ (380.53) % C 75.75; H 8.48; N 7.36; found % C 75.70; H 8.50; N 7.34.

2-(4-Isobutylphenyl)-1-(4-(m-tolyl)piperazin-1-yl)propan-1-one

(Ibu-AM35)
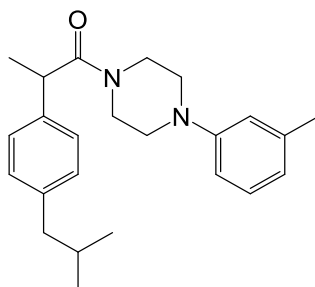
Obtained following the general procedure by the condensation between ibuprofen and 1-(3-methylphenyl)piperazine.

Yield 91 %. Oil. ^{1}H NMR (DMSO-d$_6$) δ 0.81 (d, J= 7.0 Hz, 6H, CH$_3$), 1.27 (d, J= 6.0 Hz, 3H, CH$_3$), 1.78 (hept, J= 6.0-7.0 Hz, 1H, CH), 2.20 (s, 3H, CH$_3$), 2.50 (d, J= 7.0 Hz, 2H, CH$_2$), 2.83 (m, 1H, CH$_2$), 2.98 (m, 1H, CH$_2$), 3.13 (m, 1H, CH$_2$), 3.46-3.53 (m, 4H, CH$_2$), 3.73 (m, 1H, CH$_2$), 4.09 (q, J= 6.5 Hz, 1H, CH), 6.58-6.64 (m, 3H, Ar), 7.05 (m, 1H, Ar), 7.09 (d, J= 8.0, 2H, Ar), 7.16 (d, J= 8.0 Hz, 2H, Ar). IR (Film) 3483, 2955, 1926, 1644, 1602, 1494, 1434, 1233,1185 cm^{-1}. Elemental analysis: calculated for C$_{24}$H$_{32}$N$_2$O (364.25) % C 79.08; H 8.85; N 7.68; found % C 79.15; H 8.92; N 7.60.

1-(4-(2,3-Dimethylphenyl)piperazin-1-yl)-2-(4-isobutylphenyl)propan-1-one (Ibu-AM36)
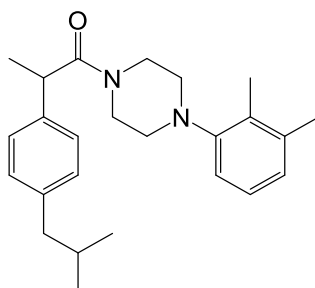
Obtained following the general procedure by the condensation between ibuprofen and 1-(2,3-dimethylphenyl)piperazine.

Yield 90%. Oil. ^{1}H NMR (DMSO-d$_6$) δ 0.83 (d, J= 7.0 Hz, 6H, CH$_3$), 1.30 (d, J=7.0 Hz, 3H, CH$_3$), 1.78 (hept, J= 7.0 Hz, 1H, CH), 2.12 (m, 3H, CH$_3$), 2.18 (m, 3H, CH$_3$), 2.40 (m, 2H, CH$_2$) 2.12 (m, 2H, CH$_2$), 2.50 (m, 2H, CH$_2$), 2.72 (m, 2H, CH$_2$), 3.56 (m, 2H, CH$_2$), 4.09 (q, J= 7 Hz, 1H, CH), 6.76 (m, 1H, Ar), 6.69 (m, 1H, Ar), 6.99 (m, 1H, Ar), 7.11 (m, 2H, Ar), 7.17 (m, 2H, Ar). IR (Film) 2959, 1731, 1644, 15111471, 1367, 1235 cm^{-1}. Elemental analysis: calculated for C$_{25}$H$_{34}$N$_2$O (378.56) % C 79.32; H 9.05; N 7.40; found % C 79.28; H 9.02; N 7.50.

2-(4-Isobutylphenyl)-1-(4-(o-tolyl)piperazin-1-yl)propan-1-one (Ibu-AM37)
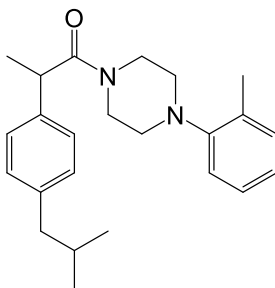
Obtained following the general procedure by the condensation between ibuprofen and 1-(2-chlorophenyl)piperazine.

Yield 91%. Oil. ^{1}H NMR (DMSO-d$_6$) δ 0.83 (d, J= 6.5 Hz, 6H, CH$_3$), 1.29 (d, J= 7.0 Hz, 3H, CH$_3$), 1.81 (hept, J= 6.5-7.0 Hz, 1H, CH), 2.21 (s, 3H, CH$_3$), 2.24 (m, 1H, CH$_2$), 2.41 (d, J= 6.0 Hz, 2H, CH$_2$), 2.63 (m, 2H, CH$_2$), 2.76 (m, 1H, CH$_2$), 3.43 (m, 1H, CH$_2$), 3.56 (m, 2H, CH$_2$), 3.69 (m, 1H, CH$_2$), 4.10 (q, J= 7.0 Hz, 1H, CH), 6.82 (m, 1H, Ar), 6.93 (m, 1H, Ar), 7.07-7.14 (m, 4H, Ar), 7.42 (d, J= 7.5, 2H, Ar). IR (Film) 2923, 1639, 1600, 1494, 14631377,1224, 1147 cm^{-1}. Elemental analysis: calculated for C$_{25}$H$_{32}$N$_2$O (364.25) % C 79.32; H 8.85; N 7.68; found % C 79.27; H 9.00; N 7.59.

2-(4-Isobutylphenyl)-1-(piperazin-1-yl)propan-1-one
(ibupiperazine 7)
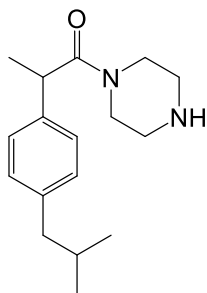
Ibuprofen (2.06 g, 10 mmol), EDC (2.09 g, 11 mmol) and HOBt (1.35 g, 10 mmol) were dissolved in MeCN (10mL). The mixture was stirred at r.t. for 30 minutes, BOC-piperazine (1.86 g, 10 mmol). The mixture was stirred at r.t. for 12 hours. After the solvent was removed under vacuum. The residue was dissolved in AcOEt (20 mL) and washed sequentially with brine (2x5 mL), 10% citric acid (2x5 mL), saturated $NaHCO_3$ aqueous solution (2x5 mL) and water (2x5 mL). The organic layer was dried over anhydrous Na_2SO_4 and evaporated under vacuum. The obtained residue was dissolved in dichloromethane without further purification, added trifluoroacetic acid (TFA) (20 mL) and stirred at r.t. for 24h. Then the solvent was removed under vacuum and to the obtained residue diethyl ether (Et_2O) (20 mL) was added leading to formation of a solid that was filtered to give the title compound.

Yield 97%. Oil. ^1H NMR (DMSO-d_6) δ 0.84 (d, J= 5.0 Hz, 6H, CH_3), 1.28 (d, J= 5.0 Hz, 3H, CH_3), 1.81 (m, 1H, CH), 2.41 (d, J= 6.0 Hz, 2H, CH_2), 2.56 (m, 1H, CH_2), 3.00 (m, 3H, CH_2), 3.34 (m, 1H, CH_2), 3.58 (m, 1H, CH_2), 3.74 (m, 2H, CH_2), 4.09 (m, 1H, CH), 7.11 (m, 2H, Ar), 7.18 (d, 2H, Ar), 8.88 (s, 1H, NH). IR (Film) 2957, 2925, 2854, 1674, 16361461, 1442, 1367, 1199, 1082 cm^{-1}. Elemental analysis: calculated for $C_{17}H_{26}N_2O$ (274.20) % C 74.41; H 9.55; N 10.21; found % C 74.35; H 9.58; N 10.29.

General procedure for the synthesis of benzylpiperazine Ibu-AM38-42

To a solution of ibupiperazine **(7)** (0.39 g, 1 mmol) in CH_2Cl_2 (10 mL) the appropriate benzaldehyde (1.6 mmol), sodium $NaHCO_3$ (0.10 g, 1.2 mmol) and sodium triacetoxyborohydride ($NaBHAc_3$) (0.32 g, 1.5 mmol) were added; the mixture was then stirred for h at r.t. for 24h. After the mixture was basified to pH 10 with a solution of NaOH 0.1 N, then extracted with CH_2Cl_2 (3x20 mL). The organic phases were collected, dried over sodium Na_2SO_4, filtrated and the solvent removed to obtain the desired compound.

1-(4-Benzylpiperazin-1-yl)-2-(4-isobutylphenyl)propan-1-one (Ibu-AM38)
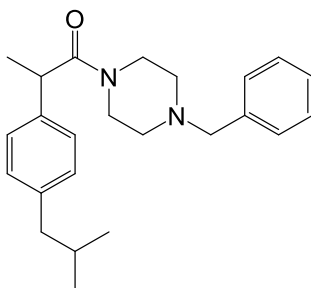
Obtained following the general procedure by the reductive alkylation between **7** and benzaldehyde.

Yield 91%. Oil. ^{1}H NMR (DMSO-d_6) δ 0.85 (d, J= 7.0 Hz, 6H, CH_3), 1.25 (d, J= 7.0 Hz, 3H, CH_3), 1.78 (m, 1H, CH_2), 1.81 (q, J= 6.0 Hz, 1H, CH), 2.21 (m, 1H, CH_2), 2.34 (m, 1H, CH_2), 2.41 (d, J= 7.5 Hz, 2H, CH_2), 2.50 (s, 1H, CH_2), 3.36 (m, 3H, CH_2), 3.38 (s, 2H, CH_2), 3.60 (m, 1H, CH_2), 4.03 (m, 1H, CH), 7.08 (m, 2H, Ar), 7.13 (d, 2H, Ar), 7.23 (m, 3H, Ar), 7.29 (d, 2H, Ar). IR (Film) 3448, 2954, 2929, 2645, 1462, 1230, 1032, 1000 cm^{-1}. Elemental analysis: calculated for $C_{24}H_{32}N_2O$ (364.25) % C 79.08; H 8.85; N 7.68; found % C 79.15; H 8.80; N 7.65.

1-(4-(2-Chlorobenzyl)piperazin-1-yl)-2-(4-isobutylphenyl)propan-1-one (Ibu-AM39)
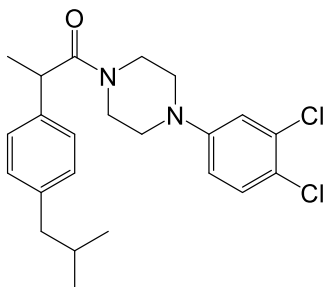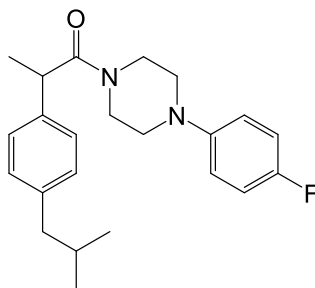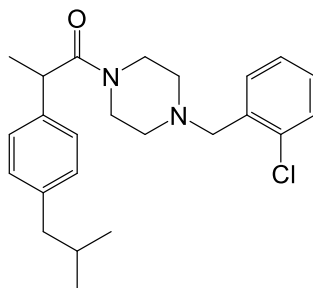

Obtained following the general procedure by the reductive alkylation between **7** and 2-chlorobenzaldehyde.

Yield 87%. Oil. ^{1}H NMR (DMSO-d_6) δ 0.83 (d, J= 7.0 Hz, 6H, CH$_3$), 1.23 (d, J= 7.0 Hz, 3H, CH$_3$), 1.79 (q, J= 6.0 Hz, 1H, CH), 2.40 (d, J= 7.5 Hz, 2H, CH$_2$), 3.32-3.75 (m, 8H, CH$_2$), 4.00 (m, 1H, CH), 4.56 (s, 2H, CH$_2$), 6.99-7.56 (m, 8H, Ar). IR (Film) 3416, 2955, 2927, 1628, 1060, 1033 cm^{-1}. Elemental analysis: calculated for C$_{24}$H$_{31}$ClN$_2$O (398.98) % C 72.25; H 7.83; N 7.02; found % C 72.30; H 7.81; N 7.08.

## 1-(4-(3-Chlorobenzyl)piperazin-1-yl)-2-(4-isobutylphenyl)propan-1-one (Ibu-AM40)
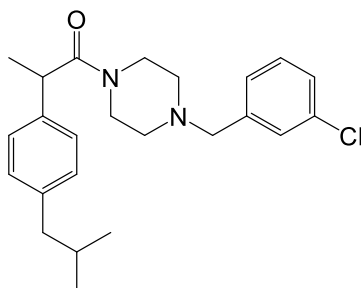
Obtained following the general procedure by the reductive alkylation between **7** and 3-chlorobenzaldehyde.

Yield 90 %. Oil. ^{1}H NMR (DMSO-d_6) δ 0.96 (d, J= 6.5 Hz, 6H, CH$_3$), 1.36 (d, J= 7.5 Hz, 3H, CH$_3$), 1.94 (q, J= 6.5-7.5 Hz, 1H, CH), 2.52 (d, J= 7.5 Hz, 2H, CH$_2$), 3.37-3.85 (m, 8H, CH$_2$), 4.14 (m, 1H, CH), 4.62 (s, 2H, CH$_2$), 7.13-7.55 (m, 8H, Ar). IR (Film) 3414, 2955, 2928,1702, 1631,

1464, 1434, 1228, 1196 cm^{-1}. Elemental analysis: calculated for C$_{24}$H$_{31}$ClN$_2$O (398.98) % C 72.25; H 7.83; N 7.02; found % C 72.38; H 7.85; N 7.00.

2-(4-Isobutylphenyl)-1-(4-(4-(trifluoromethyl)benzyl)piperazin-1-yl)propan-1-one (Ibu-AM41)
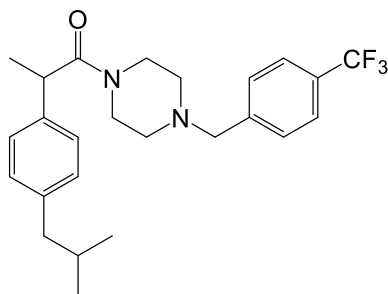
Obtained following the general procedure by the reductive alkylation between **7** and 4-(trifluoromethyl)benzaldehyde.

Yield 50 %. Oil. ^{1}H NMR (DMSO-d$_6$) δ 0.96 (d, J= 6.5 Hz, 6H, CH$_3$), 1.37 (d, J= 6.5 Hz, 3H, CH$_3$), 1.90 (q, J= 6.5 Hz, 1H, CH), 2.53 (s, 2H, CH$_2$), 2.61 (d, J= 6.5 Hz, 2H, CH$_2$), 3.43-3.70 (m, 8H, CH$_2$), 4.12 (m, 1H, CH), 7.13-7.27 (m, 8H, Ar). IR (Film) 3332, 2955, 32868, 1644, 1510, 1462, 1367, 1228, 1164, 1125, 1066 cm^{-1}. Elemental analysis: calculated for C$_{25}$H$_{31}$F$_3$N$_2$O (432.53) % C 69.42; H 7.22; N 6.48; found % C 69.48; H 7.21; N 6.53.

1-(4-(3-Fluorobenzyl)piperazin-1-yl)-2-(4-isobutylphenyl)propan-1-one (Ibu-AM42)
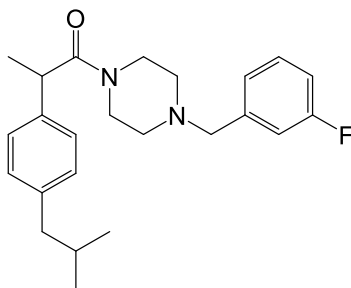
Obtained following the general procedure by the reductive alkylation between **7** and 3-fluorobenzaldehyde.

Yield 49 %. Oil. ^{1}H NMR (DMSO-d$_6$) δ 0.96 (d, J= 6.5 Hz, 6H, CH$_3$), 1.36 (d, J= 6.5 Hz, 3H, CH$_3$), 1.89 (q, J= 6.5 Hz, 1H, CH), 2.51 (s, 2H, CH$_2$), 2.61 (d, J= 6.5 Hz, 2H, CH$_2$), 3.32-3.52 (m, 8H, CH$_2$), 4.12 (m, 1H, CH), 7.15-7.25 (m, 8H, Ar). IR (Film) 3407, 2955, 2926, 1713, 1696, 1631, 1591, 1254, 1001 cm^{-1}. Elemental analysis: calculated for C$_{24}$H$_{31}$FN$_2$O (382.52) % C 75.36; H 8.17; N 7.32; found % C 75.40; H 8.05; N 7.40.

General procedure for the synthesis of amides Ibu-AM43-58

A solution of Ibuprofen (0.21 g, 1 mmol), EDC (0.19 g, 1.1 mmol) and HOBt (0.13 g, 1 mmol) in anhydrous MeCN (10 mL) was stirred at r.t. for 30 minutes, after the appropriate amine (1 mmol) was added. The mixture was then stirred for 24h at r.t. After the solvent was removed under vacuum; the residue was dissolved in AcOEt (20 mL) and washed sequentially with brine (2x5 mL), 10% citric acid (2x5 mL), NaHCO$_3$ 10% aqueous solution (2x5 mL) and water (2x5 mL). The organic layer was dried over anhydrous Na$_2$SO$_4$ and evaporated under vacuum. The obtained residue was triture with iPr$_2$O; the precipitate was then filtrated to obtain the compounds **Ibu-AM 43-58**.

## 2-(4-Isobutylphenyl)-N-(2-methylpyridin-3-yl)propanamide (Ibu-AM43)
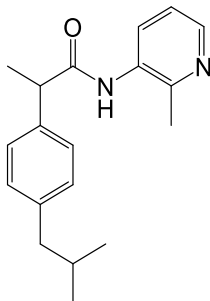
Obtained following the general procedure by the condensation between ibuprofen and 3-amino-2-methylpyridine.

Yield 61 %. Oil. ^{1}H NMR (DMSO-d$_6$) δ 0.85 (d, J= 7.0 Hz, 6H, CH$_3$), 1.34 (d, J= 7.0 Hz, 3H, CH$_3$), 1.40 (d, J= 7.0 Hz, 2H, CH$_2$), 1.80 (m, 1H, CH), 2.42 (s, 3H, CH$_3$), 3.89 (m, 1H, CH), 7.11-7.71 (m, 7H, Ar), 9.52 (s, 1H, NH). IR (Film) 3295, 1708, 1560, 1513, 1464 cm^{-1}. Elemental analysis: calculated for C$_{19}$H$_{24}$N$_2$O (296.41) % C 76.99; H 8.16; N 9.45; found % C 77.03; H 8.07; N 9.50.

2-(4-Isobutylphenyl)-1-(2-methyl-1H-indol-1-yl)propan-1-one

(Ibu-AM44)
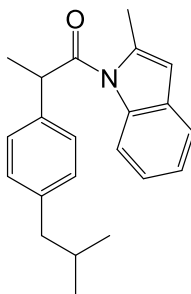
Obtained following the general procedure by the condensation between ibuprofen and 2-methylindole.

Yield 54 %. m.p. 28-30 °C. ^{1}H NMR (DMSO-d$_6$) δ 0.86 (d, J= 6.0 Hz, 6H, CH$_3$), 1.34(d, J= 6.0 Hz, 3H, CH$_3$), 1.82 (q, J= 6.0 Hz, 1H, CH), 2.41 (s, 3H, CH$_3$), 2.50 (m, 2H, CH$_2$), 3.63 (m, 1H, CH), 6.10 (s, 1H, Ar), 6.91-

6.98 (m, 2H, Ar), 7.10 (m, 2H, Ar), 7.18 (m, 2H, Ar), 7.25 (m, 1H, Ar), 7.38 (m, 1H, Ar). IR (Nujol) 3385, 2924, 1719, 1549, 1456, 1421 cm^{-1}. Elemental analysis: calculated for $C_{22}H_{25}NO$ (319.45) % C 82.72; H 7.89; N 4.38; found % C 82.75; H 7.92; N 4.44.

2-(4-Isobutylphenyl)-N-(thiazol-2-yl)propanamide (Ibu-AM45)
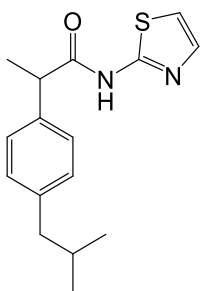
Obtained following the general procedure by the condensation between ibuprofen and 2-aminothiazole.

Yield 47 %. m.p. 150-153 °C. ^{1}H NMR (DMSO-d$_6$) δ 0.86 (d, J= 6.6 Hz, 6H, CH$_3$), 1.43 (d, J= 7.0 Hz, 3H, CH$_3$), 1.81 (m, J= 6.6 Hz, 1H, CH), 2.42 (d, J= 7.0 Hz, 2H, CH$_2$), 3.96 (m, 1H, CH), 7.12-7.46 (m, 6H, Ar), 12.25 (s, 1H, NH). IR (Nujol) 3167, 1682, 1575, 1507 cm^{-1}. Elemental analysis: calculated for $C_{16}H_{20}N_2OS$ (288.41) % C 66.63; H 6.99; N 9.71; found % C 66.70; H 7.06; N 9.75.

2-(4-Isobutylphenyl)-N-(1,3,4-thiadiazol-2-yl)propanamide

(Ibu-AM46)
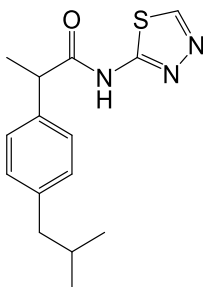
Obtained following the general procedure by the condensation between ibuprofen and 2-aminothiadiazole.

Yield 62 %. m.p. 174-176 °C. ^{1}H NMR (DMSO-d$_6$) δ 0.84 (d, J=7.0 Hz, 6H, CH$_3$), 1.44 (d, J= 7.0 Hz, 3H, CH$_3$), 1.80 (m, J= 7.0 Hz, 1H, CH), 2.40 (d, J= 7.0 Hz, 2H, CH$_2$), 4.0 (d, J= 7.0 Hz, 1H, CH), 7.12 (d, J= 7.5 Hz, 2H, Ar), 7.27 (d, J= 7.5 Hz, 2H, Ar), 9.15 (s, 1H, Ar). IR (Nujol) 1685, 1564, 1457 cm^{-1}. Elemental analysis: calculated for C$_{15}$H$_{19}$N$_3$OS (289.40) % C 62.26; H 6.62; N 14.52; found % C 62.30; H 6.60; N 14.60.

2-(4-Isobutylphenyl)-N-(5-(trifluoromethyl)-1,3,4-thiadiazol-2-yl)propanamide (Ibu-AM47)
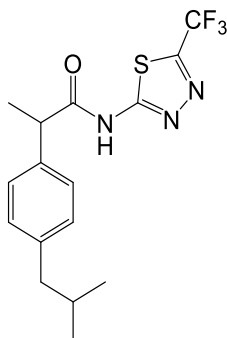
Obtained following the general procedure by the condensation between ibuprofen and 2-amino-5-trifluoromethylthiadiazole.

Yield 34 %. m.p. 186-190 °C. ^{1}H NMR (DMSO-d$_6$) δ 0.85 (d, J= 6.5 Hz, 6H, CH$_3$), 1.45 (d, J= 7.0 Hz, 3H, CH$_3$), 1.80 (q, J= 6.5 Hz, 1H, CH), 2.40 (d, J= 7.0 Hz, 2H, CH$_2$), 4.0 (m, 1H, CH), 7.13 (d, J= 7.7 Hz, 2H, Ar), 7.27 (d, J= 7.7 Hz, 2H, Ar), 13.42 (s, 1H, NH). IR (Nujol) 3136, 1696, 1534, 1467 cm^{-1}. Elemental analysis: calculated for C$_{16}$H$_{18}$F$_3$N$_3$OS (357.40) % C 53.77; H 5.08; N 11.76; found % C 53.80; H 5.05; N 11.80.

2-(4-Isobutylphenyl)-N-(o-tolyl)propanamide (Ibu-AM48)
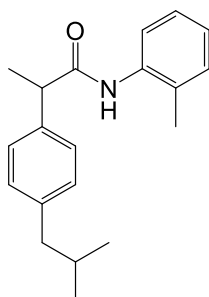
Obtained following the general procedure by the condensation between ibuprofen and 2-methylaniline.

Yield 95 %. Oil. ^{1}H NMR (DMSO-d$_6$) δ 0.85 (d, J= 7.0 Hz, 6H, CH$_3$), 1.41 (d, J= 7.0 Hz, 3H, CH$_3$), 1.83 (q, J= 7.0 Hz 1H, CH), 2.04 (s, 3H, CH$_3$), 2.42 (q, J= 7.0 Hz, 2H, CH$_2$), 3.88 (q, J= 7.0 Hz, 1H, CH), 7.04-7.10 (m, 6H, Ar), 7.31 (m, 2H, Ar), 9.30 (s, 1H, NH). IR (Film) 3265, 2955, 2929, 1738, 1659, 1528, 1456, 1367, 1170 cm^{-1}. Elemental analysis: calculated for C$_{20}$H$_{25}$NO (295.43) % C 81.31; H 8.53; N 4.74; found % C 81.35; H 8.56; N 4.70.

N-(2-Fluorophenyl)-2-(4-isobutylphenyl)propanamide (Ibu-AM49)
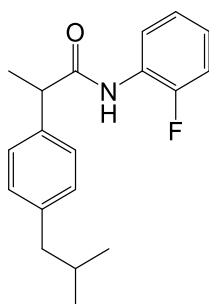
Obtained following the general procedure by the condensation between ibuprofen and 2-fluoroaniline.

Yield 55 %. m.p. 87 °C. ^{1}H NMR (DMSO-d$_6$) δ 0.84 (d, J= 6.5 Hz, 6H, CH$_3$), 1.39 (d, J= 7.0 Hz, 3H, CH$_3$), 1.80 (q, J= 7.0 Hz 1H, CH), 2.40 (q, J= 6.5 Hz, 2H, CH$_2$), 3.97 (q, J= 6.5 Hz, 1H, CH), 7.09-7.84 (m, 8H, Ar), 9.74 (s, 1H, NH). IR (Nujol) 3297, 1666, 1616, 1534, 1454, 1376 cm^{-1}.

Elemental analysis: calculated for $C_{19}H_{22}FNO$ (299.39) % C 76.22; H 7.41; N 6.53; found % C 76.30; H 7.50; N 6.55.

N-(2-Hydroxyphenyl)-2-(4-isobutylphenyl)propanamide (Ibu-AM50)
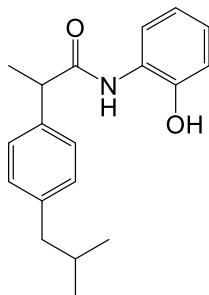
Obtained following the general procedure by the condensation between ibuprofen and 2-hydroxyaniline.

Yield 52 %. m.p. 120-125 °C. ^{1}H NMR (DMSO-d$_6$) δ 0.85 (d, J= 7.0 Hz, 6H, CH$_3$), 1.40 (d, J= 6.5 Hz, 3H, CH$_3$), 1.82 (hept, J= 6.5-7.0 Hz 1H, CH), 2.40 (q, J= 6.5 Hz, 2H, CH$_2$), 4.00 (q, J= 6.5 Hz, 1H, CH), 6.72 (m, 1H, Ar), 6.82 (m, 1H, Ar), 6.91 (m, 1H, Ar), 7.10 (m, 2H, Ar), 7.30 (m, 2H, Ar), 7.79 (m, 1H, Ar), 9.12 (s, 1H, OH), 9.73 (s, 1H, NH). IR (Nujol) 3359, 3091, 2733, 1654, 1592, 1541, 1454, 1380, 1282 cm^{-1}. Elemental analysis: calculated for $C_{19}H_{23}NO_2$ (297.17) % C 76.74; H 7.80; N 4.71; found % C 76.71; H 7.86; N 4.76.

N-(4-Hydroxyphenyl)-2-(4-isobutylphenyl)propanamide (Ibu-AM51)
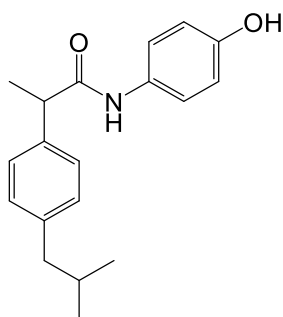
Obtained following the general procedure by the condensation between ibuprofen and 4-hydroxyaniline.

Yield 47 %. m.p. 112-115 °C. ^{1}H NMR (DMSO-d$_6$) δ 0.85 (d, J= 7.0 Hz, 6H, CH$_3$), 1.37 (d, J= 7.0 Hz, 3H, CH$_3$), 1.80 (q, J= 7.0 Hz, 1H, CH), 2.40 (d, J= 7.0 Hz, 2H, CH$_2$), 3.72 (q, J= 7.0 Hz, 1H, CH), 6.66 (d, J= 8.5 Hz, 2H Ar), 7.01 (d, J= 8.0 Hz, 2H, Ar), 7.28 (d, J= 8.0 Hz, 2H, Ar), 7.35 (d, J= 8.5 Hz, 2H, Ar), 9.14 (s, 1H, OH), 9.77 (s, 1H, NH). IR (Nujol) 3299, 1653, 1609, 1538 cm^{-1}. Elemental analysis: calculated for C$_{19}$H$_{23}$NO$_2$ (297.17) % C 76.74; H 7.80; N 4.71; found % C 76.72; H 7.84; N 4.73.

N-(4-Hydroxy-2-methylphenyl)-2-(4-isobutylphenyl)propanamide (Ibu-AM52)
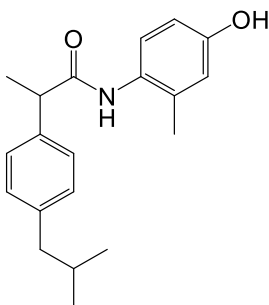
Obtained following the general procedure by the condensation between ibuprofen and 4-hydroxy-2-methylaniline.

Yield 63 %. m.p. 133-135 °C. ^{1}H NMR (DMSO-d$_6$) δ 0.83 (d, J= 7.0 Hz, 6H, CH$_3$), 1.35 (d, J= 7.0 Hz, 3H, CH$_3$), 1.77 (hept, J= 7.0 Hz, 1H, CH), 1.90 (s, 3H, CH$_3$), 2.40 (d, J= 7.0 Hz, 2H, CH$_2$), 3.75 (q, J= 7.0 Hz, 1H, CH), 6.48-7.28 (m, 7H, Ar), 9.09 (s, 1H, OH). (MANCA UN CH3) IR (Nujol) 3398, 3292, 1656, 1610 cm^{-1}. Elemental analysis: calculated for C$_{20}$H$_{25}$NO$_2$ (311.43) % C 77.14; H 8.09; N 4.50; found % C 77.10; H 8.11; N 4.58.

2-(4-Isobutylphenyl)-N-(4-methoxy-2-methylphenyl)propanamide (Ibu-AM53)
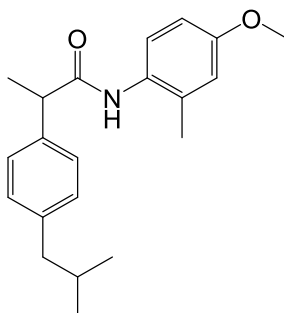
Obtained following the general procedure by the condensation between ibuprofen and 4-methoxy-2-methylaniline.

Yield 49 %. m.p. 100-102 °C. ^{1}H NMR (DMSO-d$_6$) δ 0.85 (d, J= 7.0 Hz, 6H, CH$_3$), 1.40 (d, J= 7.0 Hz, 3H, CH$_3$), 1.81 (hept, J= 7.0 Hz, 1H, CH), 1.99 (s, 3H, CH$_3$), 2.42 (d, J= 7.0 Hz, 2H, CH$_2$), 3.70 (s, 3H, CH$_3$), 3.81 (d, J= 7.0 Hz, 1H, CH), 6.69-7.31 (m, 7H, Ar), 9.21 (s, 1H, NH). IR (Nujol) 3298, 1655, 1613, 1521, 1458 cm^{-1}. Elemental analysis: calculated for C$_{21}$H$_{27}$NO$_2$ (325.45) % C 77.50; H 8.36; N 4.30; found % C 77.55; H 8.40; N 4.25.

N-(3-Chloropyridin-2-yl)-2-(4-isobutylphenyl)propanamide (Ibu-AM54)

Obtained following the general procedure by the condensation between ibuprofen and 2-amino-3-chloropyridine.

Yield 39 %. Oil. ^{1}H NMR (DMSO-d$_6$) δ 0.85 (d, J= 6.5 Hz, 6H, CH$_3$), 1.34 (d, J= 7.0 Hz, 3H, CH$_3$), 1.41 (d, J= 7.0 Hz, 2H, CH$_2$), 1.82 (m, J= 7.0 Hz, 1H, CH), 3.88 (m, 1H, CH), 7.09-8.37 (m, 7H, Ar), 10.25 (s, 1H, NH). IR (Film) 1707, 1512, 1462 cm^{-1}. Elemental analysis: calculated for C$_{18}$H$_{21}$ClN$_2$O (316.83) % C 68.24; H 6.68; N 8.84; found % C 68.33; H 6.74; N 8.80.

2-(4-Isobutylphenyl)-N-(3-(trifluoromethyl)pyridin-2-yl)propanamide (Ibu-AM55)
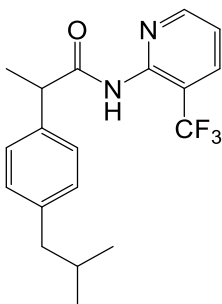
Obtained following the general procedure by the condensation between ibuprofen and 2-amino-3-(trifluoromethyl)pyridine.

Yield 59 %. m.p. 110-114 °C. ^{1}H NMR (DMSO-d$_6$) δ 0.85 (d, J= 6.0 Hz, 6H, CH$_3$), 1.39 (d, J= 7.0 Hz, 3H, CH$_3$), 1.81 (q, J= 6.5 Hz, 1H, CH), 2.42 (d, J= 7.0 Hz, 2H, CH$_2$), 3.87 (q, J= 7.0 Hz, 1H, CH), 7.10-8.71 (m, 7H, Ar), 10.25 (s, 1H, NH). IR (Nujol) 3253, 1670, 1583, 1516, 1441 cm^{-1}. Elemental analysis: calculated for C$_{19}$H$_{21}$F$_3$N$_2$O (350.16) % C 65.13; H 6.04; N 8.00; found % C 65.15; H 6.08; N 7.95.

## N-(3-Bromopyridin-2-yl)-2-(4-isobutylphenyl)propanamide (Ibu-AM56)

Obtained following the general procedure by the condensation between ibuprofen and 2-amino-3-bromopyridine.

Yield 67 %. Oil. ^{1}H NMR (DMSO-d_6) δ 0.85 (d, J= 6.0 Hz, 6H, CH$_3$), 1.34 (d, J= 7.5 Hz, 3H, CH$_3$), 1.42 (d, J= 7.0 Hz, 2H, CH$_2$), 1.81 (m, 1H, CH), 3.86 (q, J= 7.0 Hz, 1H, CH), 7.1-8.41 (m, 7H, Ar), 10.22 (s, 1H, NH). IR (Film) 3240, 1703, 1580, 1509, 1444 cm^{-1}. Elemental analysis: calculated for C$_{18}$H$_{21}$BrN$_2$O (360.08) % C 59.84; H 5.86; N 7.75; found % C 59.96; H 5.80; N 7.81.

N-(3-Iodopyridin-2-yl)-2-(4-isobutylphenyl)propanamide (Ibu-AM57)
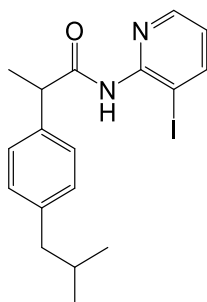
Obtained following the general procedure by the condensation between ibuprofen and 2-amino-3-iodopyridine.

Yield 53 %. Oil. ^{1}H NMR (DMSO-d_6) δ 0.85 (d, J=7Hz, 6H, CH$_3$), 1.42 (d, J=7Hz, 3H, CH$_3$), 1.80 (m, J=7Hz, 1H, CH), 2.41 (m, 2H, CH$_2$), 3.84 (m, J=7Hz, 1H, CH), 7.02-8.40 (m, 7H Ar e Py), 10.18 (s, 1H, NH). IR (Film) 3233, 1701, 1574, 1509, 1425 cm^{-1}. Elemental analysis: calculated for

___

$C_{18}H_{21}IN_2O$ (408.28) % C 52.95; H 5.18; N 6.86; found % C 53.01; H 5.25; N 6.92.

N-(3-Hydroxypyridin-2-yl)-2-(4-isobutylphenyl)propanamide (Ibu-AM58)
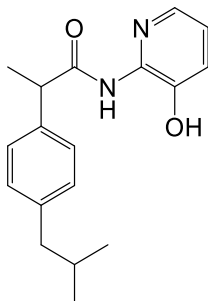
Obtained following the general procedure by the condensation between ibuprofen and 2-amino-3-hydroxypyridine.

Yield 38 %. Oil. ^{1}H NMR (DMSO-d$_6$) δ 0.85 (d, J= 7.0 Hz, 6H, CH$_3$), 1.42 (d, J= 7.5 Hz, 3H, CH$_3$), 1.79 (hept, J= 7.0 Hz, 1H, CH), 2.40 (d, J= 7.0 Hz, 2H, CH$_2$), 3.62 (q, J= 7.0 Hz, 1H, CH), 7.09-7.88 (m, 7H, Ar), 10.24 (s, 1H, NH), 10.75 (s, 1H, OH). IR (Film) 1622, 1512, 1458, 1366 cm^{-1}. Elemental analysis: calculated for $C_{18}H_{22}N_2O_2$ (298.39) % C 72.46; H 7.43; N 9.39; found % C 72.49; H 7.45; N 9.42.

Methyl 2-(4-isobutylphenyl)acetate (10)
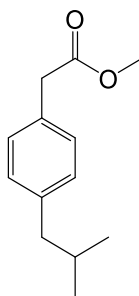
A solution of Ibufenac (1.92 g, 10mmol) in methanol (MeOH) (10 mL) was treated at room temperature with 37 % HCl (0.5mL) and refluxed for 4 h. The solvent was removed under vacuum and the crude methyl ester was used for without purification in the further step.

___

Yield 85 %. Oil. ^{1}H NMR (DMSO-d$_6$) δ 0.98 (d, J= 7.0 Hz, 6H, CH$_3$), 1.93 (m, 1H, CH), 2.42 (d, J= 7.0 Hz, 2H, CH$_2$), 3.65 (s, 2H, CH$_2$), 3.78 (s, 3H, CH$_3$), 7.15 (m, 2H, Ar), 7.19 (m, Hz, 2 H, Ar). Elemental analysis: calculated for C$_{13}$H$_{18}$O$_2$ (206.29) % C 75.69; H 8.80; found % C 75.71; H 8.86. Physical and spectral data were in accordance with literature values.[109]

General procedure for the synthesis of esters 11 and 13

Lithium bis-(trimethylsilyl)amide (4.00 g, 24 mmol) was added to a solution of ester **10** (2.00 g, 9.7 mmol) in dry THF (40 mL) under argon at -78 °C, the mixture was stirred at this temperature for 45 minutes. Then MeI (3.40 g, 24 mmol) or 1,2 dibromoethane (4.51 g, 12 mmol) was added dropwise to the stirred solution for an additional 1h. The mixture was poured in water and the desired product was extracted with Et$_2$O (2x30 mL). The solvent was dried over Na$_2$SO$_4$, and then the solvent was evaporated under reduced pressure and the residue purified by silica gel column chromatography with petroleum ether 40-60 °C and AcOEt 20:1.

Methyl 2-(4-isobutylphenyl)-2-methylpropanoate (11)
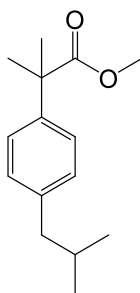
Yield 80 %. Oil. ^{1}H NMR (DMSO-d$_6$) δ 0.95 (d, J= 7.0 Hz, 6H, CH$_3$), 1.63 (s, 6H, CH$_3$), 1.82 (m, 1H, CH), 2.42 (d, J= 7.0 Hz, 2H, CH$_2$), 3.66 (s, 3H, CH$_3$), 7.07 (d, J= 7.5 Hz, 2H, Ar), 7.25 (d, J= 7.5 Hz, 2 H, Ar). Elemental analysis: calculated for C$_{15}$H$_{22}$O$_2$ (234.16) % C 76.88; H 9.46; found % C 76.92; H 9.52. Physical and spectral data were in accordance with literature values.[110]

Methyl 1-(4-isobutylphenyl)cyclopropane-1-carboxylate (13)
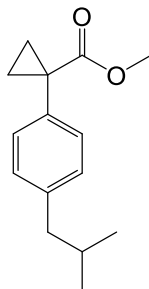
Yield 60 %. Oil. ^{1}H NMR (DMSO-d$_6$) δ 0.91 (d, J= 7.0 Hz, 6H, CH$_3$), 1.25 (m, 2H, CH$_2$), 1.58 (m, 2H, CH$_2$), 1.84 (m, 1H, CH), 2.43 (d, J= 7.0 Hz, 2H, CH$_2$), 3.69 (s, 3H, CH$_3$), 7.15 (d, J= 7.5 Hz, 2 H, Ar), 7.23 (d, J= 7.5 Hz, 2 H, Ar). Elemental analysis: calculated for C$_{15}$H$_{20}$O$_2$ (232.32) % C 77.55; H 8.68; found % C 77.62; H 8.72. Physical and spectral data were in accordance with literature values.[110]

2-(4-Isobutylphenyl)-2-methylpropanoic acid (12)
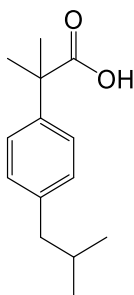
Obtained following the procedure used to obtain acid **5** starting from ester **11**.

Yield 90%. m.p. 70-72 °C. ^{1}H NMR (DMSO-d$_6$) δ 0.90 (d, J= 7.0 Hz, 6H, CH$_3$), 1.64 (s, 6H, CH$_3$), 1.90 (m, 1H, CH), 2.55 (d, J= 7.0 Hz, 2H, CH$_2$), 7.09 (d, J= 7.5 Hz, 2H, Ar), 7.33 (d, J= 7.5 Hz, 2 H, Ar). Elemental analysis: calculated for C$_{14}$H$_{20}$O (220.15) % C 76.33; H 9.15; found % C 76.33; H 9.03. Physical and spectral data were in accordance with literature values.[110]

1-(4-Isobutylphenyl)cyclopropane-1-carboxylic acid (14)
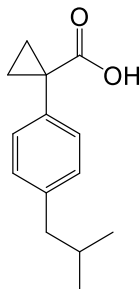
Obtained following the procedure used to obtain acid **5** starting from ester **13**.

Yield 90 %. 74-76 °C. ^{1}H NMR (DMSO-d_6) δ 0.87 (d, J= 7.0 Hz, 6H, CH$_3$), 1.08 (m, 2H, CH$_2$), 1.41 (m, 2H, CH$_2$), 1.80 (m, 1H, CH), 2.42 (d, J= 7.0 Hz, 2H, CH$_2$), 7.06 (d, J= 7.5 Hz, 2 H, Ar), 7.21 (d, J= 7.5 Hz, 2 H, Ar). Elemental analysis: calculated for C$_{14}$H$_{18}$O$_2$ (218.30) % C 77.03; H 8.31; found % C 77.10; H 8.25. Physical and spectral data were in accordance with literature values.[110]

General procedure for the synthesis of amides Ibu-AM59 and Ibu-AM60

The solution of acid **12** or acid **14** (1 mmol), EDC (0.19 g, 1.1 mmol) and HOBt (0.13 g, 1 mmol) in anhydrous MeCN (10 mL) was stirred at r.t. for 30 minutes, after that was added the 2-amino-3-methylpyridine (0.108 g, 1 mmol). The mixture was stirred at r.t. for 36 hours. After the solvent was removed under vacuum. The residue was dissolved in AcOEt (20 mL) and washed sequentially with brine (2x5 mL), 10% citric acid (2x5 mL), saturated NaHCO$_3$ aqueous solution (2x5 mL) and water (2x5 mL). The organic layer was dried over anhydrous Na$_2$SO$_4$ and evaporated under vacuum. The obtained residue was tritured with iPr$_2$O and filtered to obtain **Ibu-AM59** or **Ibu-AM60** respectively.

2-(4-Isobutylphenyl)-2-methyl-N-(3-methylpyridin-2-yl)propanamide (Ibu-AM59)
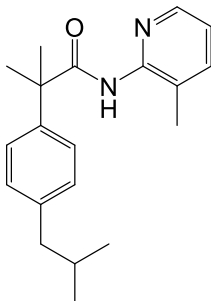
Yield 70 %. Oil. ^{1}H NMR (DMSO-d$_6$) δ 0.86 (d, J= 7.0 Hz, 6H, CH$_3$), 1.57 (s, 6H, CH$_3$), 2.02 (m, 1H, CH), 2.03 (s, 3H, CH$_3$), 2.44 (d, J= 7.0 Hz, 2H, CH$_2$), 7.12-7.20 (m, 3H, Ar), 7.30-7.35 (m, 2H, Ar), 7.62 (m, 1H, Ar), 8.22 (m, 1H, Ar), 9.27 (s, 1H, NH). IR (Film) 3167, 2956, 1731, 1686, 1583, 1448, 1384, 1366 cm^{-1}. Elemental analysis: calculated for C$_{20}$H$_{26}$N$_2$O (310.44) % C 77.38; H 8.44; N 9.02; found % C 77.34; H 8.50; N 9.07.

3-Methylpyridin-2-yl 1-(4-isobutylphenyl)cyclopropane-1-carboxylate (Ibu-AM60)
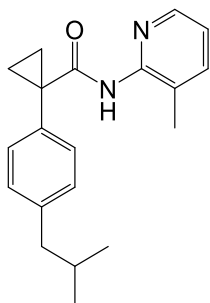
Yield 73 %. Oil.^{1}H NMR (DMSO-d$_6$) δ 0.87 (d, J= 7.0 Hz, 6H, CH$_3$), 1.10 (m, 2H, CH$_2$), 1.44 (m, 2H, CH$_2$), 1.82 (m, 1H, CH), 2.03 (s, 3H, CH$_3$), 2.42 (d, J= 7.0 Hz, 2H, CH$_2$), 7.07-7.25 (m, 4H, Ar), 7.37 (m, 1H, Ar), 7.62 (m, 1H, Ar), 8.19 (m, 1H, Ar), 8.59 (s, 1H, NH). IR (Film) 3397, 1774, 1687, 1582, 1489, 1446, 1338, 1290, 1192 cm^{-1}. Elemental

analysis: calculated for $C_{20}H_{24}N_2O$ (308.43) % C 77.89; H 7.84; N 9.08; found % C 77.34; H 8.50; N 9.07.

General procedure for the synthesis of Ibuf-AM1, Feno-AM1, Keto-AM1, Napr-AM1, Flu-AM1-4, Carpr-AM1-5

The solution of the appropriate acid (1 mmol), EDC (0.19 g, 1.1 mmol) and HOBt (0.13 g, 1 mmol) in anhydrous MeCN (10 mL) was stirred at r.t., after 30 minutes the opportune amine (1 mmol). The mixture was stirred at r.t. for 36 hours. After the solvent was removed under vacuum. The residue was dissolved in AcOEt (20 mL) and washed sequentially with brine (2x5 mL), 10% citric acid (2x5 mL), saturated NaHCO$_3$ aqueous solution (2x5 mL) and water (2x5 mL). The organic layer was dried over anhydrous Na$_2$SO$_4$ and evaporated under vacuum. To give the title amides.

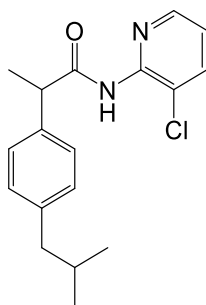### 2-(4-Isobutylphenyl)-N-(3-methylpyridin-2-yl)acetamide (Ibuf-AM1)
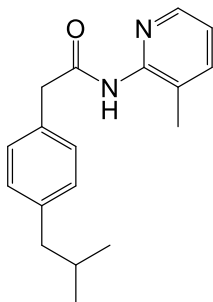
Obtained following the general procedure by the condensation between ibufenac and 2-amino-3-methylpyridine.

Yield 77 %. Oil. ^{1}H NMR (DMSO-d$_6$) δ 0.86 (d, J= 7.0 Hz, 6H, CH$_3$), 1.82 (m, 1H, CH), 2.42 (s, 3H, CH$_3$), 2.50 (d, J= 7.0 Hz, 2H, CH$_2$), 3.55 (s, 2H, CH$_2$), 7.09-7.64 (m, 7H, Ar). IR (Nujol) 3310, 3270, 3070, 3050, 1668, 1620, 1569 cm^{-1}. Elemental analysis: calculated for $C_{18}H_{22}N_2O$ (282.17) % C 76.56; H 7.85; N 9.92; found % C 76.44; H 7.96; N 9.99.

2-(2-Fluoro-(1,1'-biphenyl)-4-yl)-N-(3-methylpyridin-2-yl)propanamide (Feno-AM1)
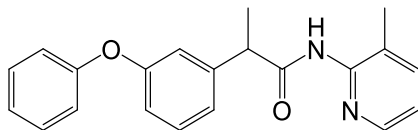
Obtained following the general procedure by the condensation between fenoprofen and 2-amino-3-methylpyridine.

Yield 82 %. Oil. ^{1}H NMR (DMSO-d$_6$) δ 1.57 (d, J= 7.0 Hz, 3H, CH$_3$), 2.15 (s, 3H, CH$_3$), 3.83 (q, J= 7.0 Hz, 1H, CH), 7.10-8.18 (m, 12H, Ar). IR (Film) 3198, 1698 cm^{-1}. Elemental analysis: calculated for C$_{21}$H$_{20}$N$_2$O$_2$ (332.40) % C 75.88; H 6.06; N 8.43; found % C 75.96; H 6.03; N 8.56.
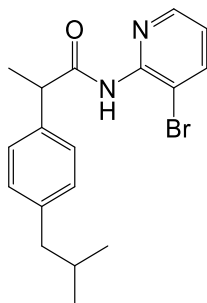
2-(3-Benzoylphenyl)-N-(3-methylpyridin-2-yl)propanamide (Keto-AM2)
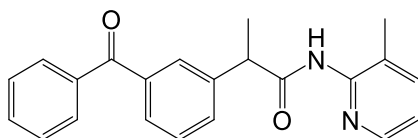
Obtained following the general procedure by the condensation between ketoprofen and 2-amino-3-methylpyridine.

Yield 87 %. Oil. ^{1}H NMR (DMSO-d$_6$) δ 1.58 (d, J= 7.0 Hz, 3H, CH$_3$), 2.16 (s, 3H, CH$_3$), 3.84 (q, J= 7.0 Hz, 1H, CH), 7.12-8.16 (m, 12H, Ar). IR (Film) 3180, 1708, 1659 cm^{-1}. Elemental analysis: calculated for C$_{22}$H$_{20}$N$_2$O$_2$ (344.41) % C 76.72; H 5.85; N 8.13; found % C 76.72; H 5.85; N 8.13.

2-(6-Methoxynaphthalen-2-yl)-N-(3-methylpyridin-2-yl)propanamide (Napr-AM1)
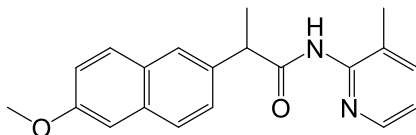
Obtained following the general procedure by the condensation between naproxen and 2-amino-3-methylpyridine.

Yield 40 %. Oil. ^{1}H NMR (DMSO-d$_6$) δ 1.50 (d, J= 7.0 Hz, 3H, CH$_3$), 1.96 (s, 3H, CH$_3$), 3.86 (s, 3H, CH$_3$) 4.05 (q, J= 7.0 Hz, 1H, CH), 7.14-8.21 (m, 9H, Ar), 10.15 (s, 1H, NH). IR (Film) 3243, 2971, 2934, 1697, 1633, 1505, 1392, 1217 cm^{-1}. Elemental analysis: calculated for C$_{20}$H$_{20}$N$_2$O$_2$ (320.39) % C 74.98; H 6.29; N 8.74; found % C 75.01; H 6.25; N 8.76.

## 2-(2-Fluoro-(1,1'-biphenyl)-4-yl)-N-(3-methylpyridin-2-yl)propanamide (Flu-AM1)
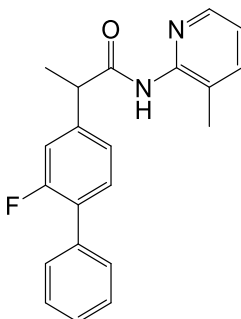
Obtained following the general procedureby the condensation between flurbiprofen and 2-amino-3-methylpyridine.

Yield 52 %. Oil. ^{1}H NMR (DMSO-d$_6$) δ 1.56 (d, J= 7.0 Hz, 3H, CH$_3$), 2.05 (s, 3H, CH$_3$), 3.79 (m, 1H, CH), 7.15-7.51 (m, 9H, Ar), 7.98 (m, 1H, Ar), 8.14 (m, 1H, Ar). IR (Film) 3034, 2979, 2934, 1736, 1669, 1581, 1484, 1418, 1388, 1200 cm^{-1}. Elemental analysis: calculated for C$_{21}$H$_{19}$FN$_2$O (334.39) % C 75.43; H 5.73; N 8.38; found % C 75.41; H 5.71; N 8.31.

2-(2-Fluoro-(1,1'-biphenyl)-4-yl)-N-(3-(trifluoromethyl)pyridin-2-yl)propanamide (Flu-AM2)
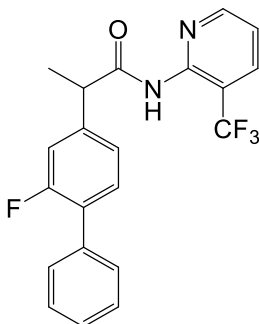
Obtained following the general procedure by the condensation between flurbiprofen and 2-amino-3-(trifluoromethyl)pyridine.

Yield 45 %. m.p. 112 °C. ^{1}H NMR (DMSO-d$_6$) δ 1.45 (d, J= 7.0 Hz, 3H, CH$_3$), 3.99 (m, 1H, CH), 7.28-8.73 (m, 11H, Ar e Py), 10.39 (s, 1H, NH). IR (Nujol) 3267, 1673, 1583, 1515 cm^{-1}. Elemental analysis: calculated for C$_{21}$H$_{16}$F$_4$N$_2$O (388.37) % C 64.95; H 4.15; N 7.21; found % C 65.00; H 4.10; N 7.22.

N-(3-Bromopyridin-2-yl)-2-(2-fluoro-(1,1'-biphenyl)-4-yl)propanamide (Flu-AM3)
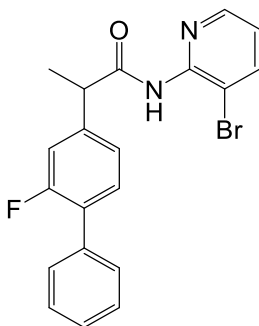
Obtained following the general procedure by the condensation between flurbiprofen and 2-amino-3-bromopyridine.

Yield 60 %. m.p. 90 °C. ^{1}H NMR (DMSO-d$_6$) δ 1.45 (d, J= 7.0 Hz, 3H, CH$_3$), 3.99 (q, J= 7.0 Hz, 1H, CH), 7.23-8.42 (m, 11H, Ar), 10.35 (s, 1H, NH). IR (Nujol) 3265, 1667, 1511, 1460, 1377 cm^{-1}. Elemental analysis:

calculated for $C_{20}H_{16}BrFN_2O$ (398.26) % C 60.17; H 4.04; N 7.02; found % C 60.20; H 4.10; N 7.08.

2-(2-Fluoro-(1,1'-biphenyl)-4-yl)-N-(4-hydroxy-2-methylphenyl)propanamide (Flu-AM4)

Obtained following the general procedure by the condensation between flurbiprofen and 4-hydroxy-2-methylaniline.

Yield 30 %. m.p. 123 °C. ^{1}H NMR (DMSO-d$_6$) δ 1.43 (s, 3H, CH$_3$), 1.99 (s, 3H, CH$_3$), 3.90 (s, 1H, CH), 6.52-7.53 (m, 11H, Ar), 9.18 (s, 1H, OH), 9.27 (s, 1H, NH). IR (Nujol) 3282, 1655, 1461, 1377, 1223 cm^{-1}. Elemental analysis: calculated for $C_{22}H_{20}FNO_2$ (349.41) % C 75.63; H 5.77; N 4.01; found % C 75.65; H 5.80; N 3.98.

2-(6-Chloro-*9H*-carbazol-2-yl)-N-(3-methylpyridin-2-yl)propanamide (Carpr-AM1)
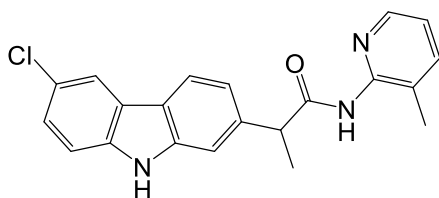
Obtained following the general procedure by the condensation between carprofen and 2-amino-3-methylpyridine.

Yield 44 %. m.p. 208 °C. ^{1}H NMR (DMSO-d$_6$) δ 1.42 (d, J= 7.0 Hz, 1H, CH), 1.48 (d, J= 7.0 Hz, 3H, CH$_3$) 1.95 (s, 3H, CH$_3$) 7.07-7.58 (m, 6H, Ar), 8.05-8.19 (m, 3H, Ar), 10.12 (s, 1H, NH). IR (Nujol) 3204, 1727,

1650, 1516 cm^{-1}. Elemental analysis: calculated for $C_{21}H_{18}ClN_3O_2$ (363.85) % C 69.32; H 4.99; N 11.55; found % C 69.36; H 5.02; N 11.60.

2-(6-Chloro-9H-carbazol-2-yl)-N-(4-hydroxy-2-methylphenyl)propanamide (Carpr-AM2)

Obtained following the general procedure by the condensation between carprofen and 4-hydroxy.2-methylaniline.

Yield 26 %. m.p. 126 °C. ^{1}H NMR (DMSO-d$_6$) δ 1.52 (d, J= 6.5 Hz, 3H, CH$_3$), 4.04(d, J= 7.0 Hz, 1H, CH), 7.03-8.40 (m, 9H, Ar), 10.25 (s, 1H, NH), 11.35 (s, 1H, NH). IR (Nujol) 1659, 1569, 1460, 1377 cm^{-1}. Elemental analysis: calculated for $C_{22}H_{19}ClN_2O_2$ (378.86) % C 69.75; H 5.06; N 7.39; found % C 69.80; H 5.08; N 7.42.

2-(6-Chloro-9H-carbazol-2-yl)-N-(3-iodopyridin-2-yl)propanamide (Carpr-AM3)
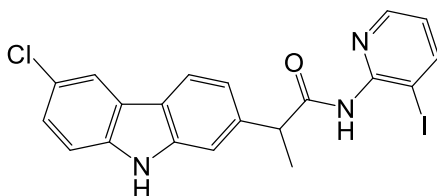
Obtained following the general procedure for the synthesis of amides derivatives, by the condensation between carprofen and 2-amino-3-iodopyridine.

Yield 17 %. m.p. 191 °C. ^{1}H NMR (DMSO-d$_6$) δ 1.52 (d, J= 6.5 Hz, 3H, CH$_3$), 4.04 (d, J= 7.0 Hz, 1H, CH), 7.03-8.40 (m, 9H, Ar), 10.25 (s, 1H, NH), 11.35 (s, 1H, NH). IR (Nujol) 1659, 1569, 1460, 1377 cm^{-1}. Elemental analysis: calculated for $C_{20}H_{15}ClIN_3O$ (474.71) % C 50.50; H 3.18; N 8.83; found % C 50.55; H 3.15; N 8.96.

N-(3-Bromopyridin-2-yl)-2-(6-chloro-9H-carbazol-2-yl)propanamide (Carpr-AM4)
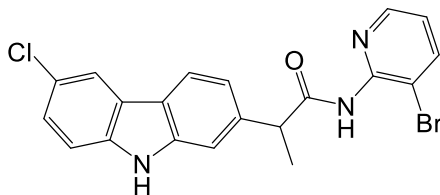
Obtained following the general procedure by the condensation between carprofen and 2-amino-3-bromopyridine.

Yield 23 %. m.p. 118 °C. ^{1}H NMR (DMSO-d_6) δ 1.43 (d, J= 6.5 Hz, 3H, CH$_3$), 3.82(q, J= 7.0 Hz, 1H, CH), 6.58-8.10 (m, 9H, Ar), 11.34 (s, 1H, NH). IR (Nujol) 1648, 1562, 1461, 1377, 1273, 1212 cm^{-1}. Elemental analysis: calculated for C$_{20}$H$_{15}$BrClN$_3$O (428.71) % C 56.03; H 3.53; N 9.80; found % C 50.96; H 3.60; N 9.96.

2-(6-Chloro-9H-carbazol-2-yl)-N-(3-(trifluoromethyl)pyridin-2-yl)propanamide (Carpr-AM5)
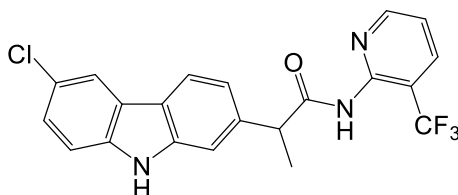
Obtained following the general procedure by the condensation between carprofen and 2-amino-3-(trifluoromethyl)pyridine.

Yield 31 %. m.p. 115 °C. ^{1}H NMR (DMSO-d_6) δ 1.44 (d, J= 6.5 Hz, 3H, CH$_3$), 3.82(d, J= 7.0 Hz, 1H, CH), 6.58-8.16 (m, 9H, Ar e Py), 11.34 (s, 1H, NH). IR (Nujol) 1688, 1648, 1561, 1461, 1377, 1341, 1273, 1212 cm^{-1}. Elemental analysis: calculated for C$_{21}$H$_{15}$ClF$_3$N$_3$O (417.82) % C 60.37; H 3.62; N 10.06; found % C 60.40; H 3.60; N 10.10.

(*S*)-(+)-2-(4-Isobutylphenyl)-N -(3-methylpyridin-2-yl)propanamide ((*S*)-(+)-Ibu-AM5)
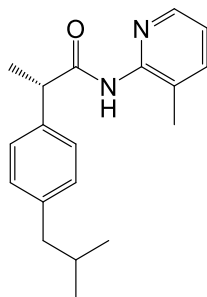
Obtained following the general procedure by the condensation between (*S*)-Ibuprofen and 2-amino-3-methylpyridine.

Yield 57%. m.p. 93-94 °C. ^{1}H NMR (DMSO-d$_6$) δ 0.86 (d, J= 6.5 Hz, 6H, CH$_3$), 1.47 (d, J= 7.0 Hz, 3H, CH$_3$), 1.83 (hept, J= 6.5 Hz, 1H, CH), 2.03 (s, 3H, CH$_3$), 2.41 (d, J= 7.0 Hz, 2H, CH$_2$), 3.88 (q, J= 7.0 Hz, 1H, CH), 6.15 (s, 1H, NH), 6.70 (m, 1H, Ar), 7.22 (d, J= 8.0 Hz, 2H, Ar), 7.26 (d, J= 8.0 Hz, 2H, Ar), 7.35 (m, 1H, Ar), 7.90 (m, 1H, Ar). IR (Nujol) 3309, 3245, 3098, 3054, 1666, 1615, 1592 cm^{-1}. Optical rotation [α]= +60.8°. Elemental analysis: calculated for C$_{19}$H$_{24}$N$_2$O (296.41) % C 76.99; H 8.16; N 9.45; found % C 76.94; H 8.19; N 8.20.

(*R*)-(-)-2-(4-Isobutylphenyl)-N -(3-methylpyridin-2-yl)propanamide ((*R*)-(-)-Ibu-AM5)
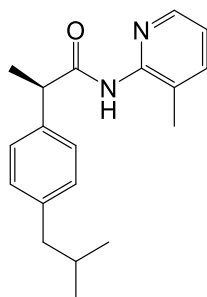
Obtained following the general procedure by the condensation between (*R*)-Ibuprofen and 2-amino-3-methylpyridine.

Yield 58%. m.p. 94-95 °C. ^{1}H NMR (DMSO-d$_6$) δ 0.84 (d, J= 6.5 Hz, 6H, CH$_3$), 1.50 (d, J= 7.0 Hz, 3H, CH$_3$), 1.78 (hept, J= 6.5 Hz, 1H, CH), 2.07 (s, 3H, CH$_3$), 2.44 (d, J= 7.0 Hz, 2H, CH$_2$), 3.90 (q, J= 7.0 Hz, 1H, CH), 6.11 (s, 1H, NH), 6.72 (m, 1H, Ar), 7.28 (d, J= 8.0 Hz, 2H, Ar), 7.35 (d, J= 8.0 Hz, 2H, Ar), 7.41 (m, 1H, Ar), 7.87 (m, 1H, Ar). IR (Nujol) 3297, 3253, 3087, 3050, 1672, 1620, 1579 cm^{-1}. Optical rotation [α]= -60.9°. Elemental analysis: calculated for C$_{19}$H$_{24}$N$_2$O (296.41) % C 76.99; H 8.16; N 9.45; found % C 77.05; H 8.18; N 8.13.

(*S*)-(+)- 2-(2-Fluoro-(1,1'-biphenyl)-4-yl)-N-(3-methylpyridin-2-yl)propanamide ((*S*)-(+)-Flu-AM1)
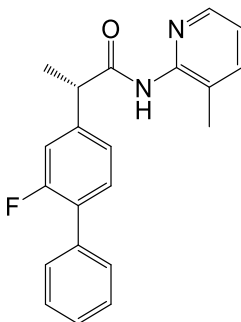
Obtained following the general procedure by the condensation between (*S*)-Flurbiprofen and 2-amino-3-methylpyridine.

Yield 52%. Oil. ^{1}H NMR (DMSO-d$_6$) δ 1.42 (d, J= 7.0 Hz, 3H, CH$_3$), 2.10 (s, 3H, CH$_3$), 3.91 (q, J= 7.0 Hz, 1H, CH), 7.21-7.52 (m, 10H, Ar), 7.98 (s, 1H, Ar), 10.03 (s, 1H, NH). IR (Film) 3330, 3020, 2965, 1675, 1638, 1576 cm^{-1}. Optical rotation [α]= +11.5°. Elemental analysis: calculated for C$_{21}$H$_{19}$FN$_2$O (334.39) % C 75.37; H 5.75; N 8.90; found % C 75.47; H 5.72; N 8.89.

(R)-(-)- 2-(2-Fluoro-(1,1'-biphenyl)-4-yl)-N-(3-methylpyridin-2-yl)propanamide ((R)-(-)-Flu-AM1)
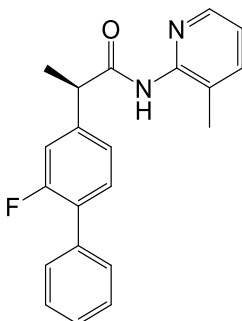
Obtained following the general procedure by the condensation between (R)-Flurbiprofen and 2-amino-3-methylpyridine.

Yield 54%. Oil. ^{1}H NMR (DMSO-d$_6$) δ 1.48 (d, J= 7.0 Hz, 3H, CH$_3$), 2.14 (s, 3H, CH$_3$), 3.87 (q, J= 7.0 Hz, 1H, CH), 7.25-7.50 (m, 10H, Ar), 7.99 (s, 1H, Ar), 10.10 (s, 1H, NH). IR (Film) 3333, 3018, 2978, 1665, 1631, 1570 cm^{-1}. Optical rotation [α]= -11.2°. Elemental analysis: calculated for C$_{21}$H$_{19}$FN$_2$O (334.39) % C 75.43; H 5.73; N 8.83; found % C 75.40; H 5.77; N 8.85.

Methyl 2-(4-aminophenyl)propanoate (21)
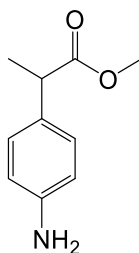
A solution of 2-(4-nitrophenyl)propionic acid (20) (5g, 26 mmol) in MeOH (25 mL) was treated at room temperature with 37 % HCl (1 mL) and then refluxed for 4 h. The solvent was removed under vacuum and crude methyl ester was used for the further step.

Iron powder (14 g, 256 mmol) was suspended in a mixture of MeCN (50 mL) and water (4 mL); the mixture was treated with 37% HCl (0.1 mL), than refluxed for 1h. After cooling at room temperature a

solution of crude methyl ester in MeOH (5 mL) was added dropwise in 30 minutes and the resulting solution was refluxed overnight. The hot suspension was filtered on a celite pad and the filtrate evaporated to afford an orange oil (4 g) that was dissolved in CH_2Cl_2 (40 mL) and extracted with a saturated $NaHCO_3$ aqueous solution (3 x 35 mL), dried over anhydrous Na_2SO_4 and evaporated under vacuum to give the methyl-2-(4-aminophenyl)propanoate **(21)** as orange oil.

Yield 75%. Oil. ^{1}H NMR (DMSO-d_6) δ 1.45 (d, J= 7 Hz, 3H, CH_3), 3.60 (s, 3H, CH_3), 3.75 (s, 2H, NH_2), 3.80 (m, 1H, CH), 6.65 (d, J= 7.0 Hz, 2H, Ar), 7.05 (d, J= 7.0 Hz, 2H, Ar). IR (Film) 3458, 3374, 2979, 2951, 1729, 1626, 1517, 1455, 1435, 1339, 1267, 1210, 1168 cm^{-1}. Elemental analysis: calculated for $C_{10}H_{13}NO_2$ (179.22) % C 67.02; H 7.31; N 7.82; found % C 67.06; H 7.36; N 8.86. Physical and spectral data were in accordance with literature values.[111]

Methyl (*E*)-2-(4-((5,5,5-trifluoro-4-oxopent-2-en-2-yl)amino)phenyl)propanoate (23)
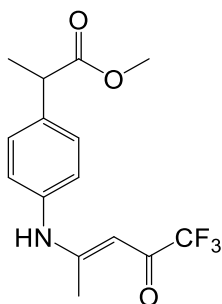
A mixture of methyl ester **21** (1.79 g, 10 mmol), and enol ether **22** (2.52 g, 15 mmol) in anhydrous MeCN (10 mL) was refluxed for 2 h. After cooling, the formed precipitate was collected by filtration, washed with iPr$_2$O, dried, and used without further purification.

Yield 78 %. m.p. 43-45 °C. ^{1}H NMR (DMSO-d_6) δ 1.45 (d, J= 5.0 Hz, 3H, CH_3), 2.24 (s, 3H, CH_3), 3.70 (s, 3H, CH_3), 3.98 (m, 1H, CH), 5.74 (s, 1H, CH), 6.94 (d, J= 8.4 Hz, 2H, Ar), 7.73 (d, J= 8.4 Hz, 2H, Ar), 12.48 (s, 1H, NH). IR (Nujol) 3376, 2981, 2936, 1729 cm^{-1}. Elemental analysis:

calculated for $C_{15}H_{16}F_3NO_3$ (315.29) % C 57.14; H 5.12; N 4.44; found % C 57.19; H 5.20; N 4.50.

Methyl 2-(4-(((1*E*,3*E*)-1-(dimethylamino)-6,6,6-trifluoro-5-oxohexa-1,3-dien-3-yl)amino)phenyl)propanoate (24)
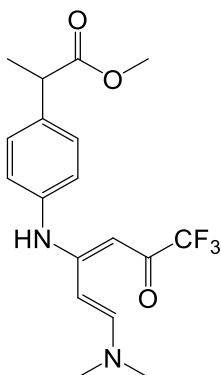
A mixture of **23** (1.58 g, 5 mmol), and DMF-DMA (1.79 g, 15 mmol) in anhydrous toluene (20 mL) was refluxed for 1 h, then was allowed to reach the room temperature and stirred for additional 24 h. The mixture was carefully concentrated in vacuum to give **24**.

Yield 88 %. Oil. ^{1}H NMR (DMSO-d_6) δ 1.41 (d, J= 6.5 Hz, 3H, CH$_3$), 2.75 (s, 3H, CH$_3$), 3.10 (s, 3H, CH$_3$), 3.60 (s, 3H, CH$_3$), 3.85 (m, 1H, CH), 4.98 (d, J= 10.5 Hz, 1H, CH), 5.74 (s, 1H, CH), 7.25 (d, J= 7.5 Hz, 2H, Ar), 7.33 (d, J= 7.5 Hz, 2H, Ar), 7.91 (d, J= 10.5 Hz, 1H, CH), 12.76 (s, 1H, NH). IR (Film) 1722, 1671 cm^{-1}. Elemental analysis: calculated for $C_{18}H_{21}F_3N_2O_3$ (377.37) % C 58.37; H 5.72; N 7.56; found % C 58.45; H 5.80; N 7.60.

Methyl 2-(4-((2-(trifluoromethyl)pyridin-4-yl)amino)phenyl)propanoate (25)
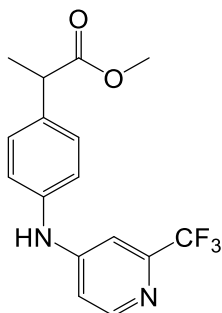
To a solution of **24** (0.74 g, 2 mmol) in dry DMF (5 mL), ammonium acetate (0.31 g, 4 mmol) was added and the mixture was gently refluxed for 1.5 h. The mixture was carefully concentrated in vacuum, and then ice-water (15 mL) was added. The formed solid was filtered off, washed with water, air-dried, and then recrystallized with iPr$_2$O to give **25**.

Yield 75 %. m.p. 36-39 °C. ^{1}H NMR (DMSO-d$_6$) δ 1.57 (d, J= 6.5 Hz, 3H, CH$_3$), 3.92 (m, 1H, CH), 3.98 (s, 3H, CH$_3$), 6.50 (m, 2H, Ar), 6.75 (m, 2H, Ar), 7.02 (m, 2H, Ar), 8.48 (m, 1H, Ar), 9.69 (s, 1H, NH). IR (Nujol) 3346, 3312, 1737, 1670 cm^{-1}. Elemental analysis: calculated for C$_{16}$H$_{15}$F$_3$N$_2$O$_2$ (324.11) % C 59.26; H 4.66; N 8.64; found % C 59.30; H 4.25; N 8.70.

2-(4-((2-(Trifluoromethyl)pyridin-4-yl)amino)phenyl)propanoic acid (TPA0)
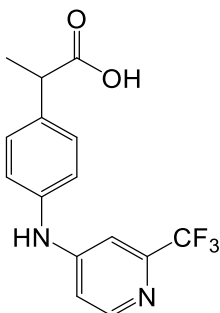
To a solution of the ester **25** (0.65 g; 2mmol) in EtOH (20mL) 5N solution of NaOH (4 mL) and water (4 mL) were added. The resulting mixture was stirred at r.t. for 24h. After removing EtOH under vacuum, ice was added to the residue and then acidified with aqueous 20% HCl solution until pH 3-4. The formed precipitate was filtered, washed with water and re-crystallized with EtOH to obtain the title compound.

Yield 69 %. m.p. 36-39 °C. ^{1}H NMR (DMSO-d_6) δ 1.37 (d, J= 7.0 Hz, 3H, CH$_3$), 3.67 (q, J= 7.0 Hz, 1H, CH), 7.08 (m, 1H, Ar), 7.20 (m, 3H, Ar), 7.30 (m, 2H, Ar), 8.30 (m, 1H, Ar), 9.22 (s, 1H, NH), 12.28 (s, 1H, OH). IR (Nujol) 3336, 3296, 2485, 1683, 1603, 1520, 1462, 1413, 1359, 1310 cm^{-1}. Elemental analysis: calculated for C$_{15}$H$_{13}$F$_3$N$_2$O$_2$ (310.28) % C 58.07; H 4.22; N 9.03; found % C 58.10; H 4.25; N 8.90.

General procedure for the synthesis of amides TPA5, 8-9, 11-28

A solution of **TPA0** (0.31 g, 1 mmol), EDC (0.19 g, 1.1 mmol) and HOBt (0.13 g, 1 mmol) in anhydrous MeCN (10 mL) was stirred at r.t. for 30 minutes, then the appropriate amine (1 mmol)was added. The mixture was stirred at r.t. for 36 hours. After the solvent was removed under vacuum. The residue was dissolved in AcOEt (20 mL) and washed sequentially with brine (2x5 mL), 10% citric acid (2x5 mL), saturated NaHCO$_3$ aqueous solution (2x5 mL) and water (2x5

mL). The organic layer was dried over anhydrous Na_2SO_4 and evaporated under vacuum to give the title amides.

N-(3-Methylpyridin-2-yl)-2-(4-((2-(trifluoromethyl)pyridin-4-yl)amino)phenyl)propanamide (TPA5)
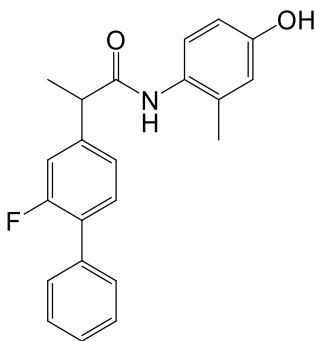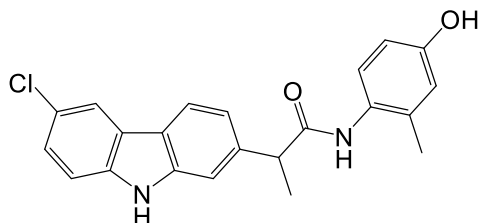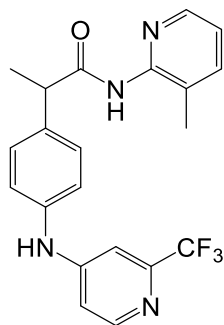

Obtained following the general procedure by the condensation between **TPA0** and 2-amino-3-methylpyridine.

Yield 79 %. m.p. 110 °C. ^{1}H NMR (DMSO-d$_6$) δ 1.15 (d, J= 6.2 Hz, 3H, CH$_3$), 1.50 (s, 3H, CH$_3$), 3.79 (q, J= 6.2 Hz, 1H, CH), 7.18-7.53(m, 8H, Ar), 8.40 (m, 2H, Ar), 9.28 (s, 1H, NH), 10.26 (s, 1H, NH). IR (Nujol) 1674, 1620, 1603, 1521, 1459, 1360 cm^{-1}. Elemental analysis: calculated for $C_{21}H_{19}F_3N_4O$ (400.15) % C 62.99; H 4.78; N 13.99; found % C 63.05; H 4.70; N 13.90.

N-(Pyridin-2-ylmethyl)-2-(4-((2-(trifluoromethyl)pyridin-4-yl)amino)phenyl)propanamide (TPA8)

Obtained following the general procedure by the condensation between **TPA0** and 2-picolylamine.

Yield 71 %. m.p. 70-75 °C. ^{1}H NMR (DMSO-d$_6$) δ 1.49 (m, 3H, CH$_3$), 3.29 (m, 1H, CH), 4.47 (s, 2H, CH$_2$), 7.19-7.49 (m, 7H, Ar), 7.83 (m, 1H, Ar), 8.41 (m, 1H, Ar), 8.59 (m, 1H, Ar), 8.76 (m, 1H, Ar), 9.39 (s, 1H, NH). IR (Nujol) 2924, 1600, 1532, 1459, 1360, 1325, 1218 cm^{-1}. Elemental analysis: calculated for C$_{21}$H$_{19}$F$_3$N$_4$O (400.15) % C 62.99; H 4.78; N 13.99; found % C 62.90; H 4.77; N 13.95.

N-(Pyridin-3-ylmethyl)-2-(4-((2-(trifluoromethyl)pyridin-4-yl)amino)phenyl)propanamide (TPA9)

Obtained following the general procedure by the condensation between **TPA0** and 3-picolylamine.

Yield 58 %. m.p. 140-145 °C. ^{1}H NMR (DMSO-d$_6$) δ 1.14 (m, 3H, CH$_3$), 2.64 (s, 2H, CH$_2$), 4.39 (m, 1H, CH), 7.16-7.66 (m, 8H, Ar), 8.40-8.71 (m, 3H, Ar), 9.36 (s, 1H, NH). IR (Nujol) 2906, 1657, 1601, 1521, 1463, 1360, 1321 cm^{-1}. Elemental analysis: calculated for C$_{21}$H$_{19}$F$_3$N$_4$O (400.15) % C 62.99; H 4.78; N 13.99; found % C 62.95; H 4.82; N 13.94.

N-(2-((3-Methylpyridin-2-yl)amino)-2-oxoethyl)-2-(4-((2-(trifluoromethyl)pyridin-4-yl)amino)phenyl)propanamide (TPA11)

Obtained following the general procedure by the condensation between **TPA0** and 2-amino-5-methylpyridine.

Yield 25 %. m.p. 145-150 °C. ^{1}H NMR (DMSO-d_6) δ 1.46 (m, 3H, CH$_3$), 2.64 (s, 3H, CH$_3$), 3.90 (m, 1H, CH), 7.19-7.69 (m, 9H, Ar), 8.39 (m, 1H, Ar), 9.39 (s, 1H, NH). IR (Nujol) 1666, 1601, 1514, 1461, 1377cm^{-1}. Elemental analysis: calculated for C$_{21}$H$_{19}$F$_3$N$_4$O (400.15) % C 62.99; H 4.78; N 13.99; found % C 63.01; H 4.80; N 13.94.

N-(4-Methylpyridin-2-yl)-2-(4-((2-(trifluoromethyl)pyridin-4-yl)amino)phenyl)propanamide (TPA12)

Obtained following the general procedure by the condensation between **TPA0** and 2-amino-4-methylpyridine.

Yield 31 %. m.p. 50-55 °C. ^{1}H NMR (DMSO-d_6) δ 1.47 (m, 3H, CH$_3$), 2.65 (s, 3H, CH$_3$), 3.94 (m, 1H, CH), 7.06-7.56 (m, 9H, Ar), 8.40 (m, 1H, Ar), 9.40 (s, 1H, NH). IR (Nujol) 2923, 1681, 1601, 1462, 1320 cm^{-1}.

Elemental analysis: calculated for $C_{21}H_{19}F_3N_4O$ (400.15) % C 62.99; H 4.78; N 13.99; found % C 62.90; H 4.75; N 13.90.

N-(Pyridin-2-yl)-2-(4-((2-(trifluoromethyl)pyridin-4-yl)amino)phenyl)propanamide (TPA13)
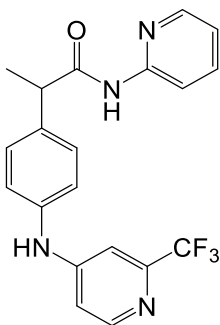
Obtained following the general procedure by the condensation between **TPA0** and 2-aminopyridine.

Yield 30 %. m.p. 130-135 °C. ^{1}H NMR (DMSO-d_6) δ 1.14 (m, 3H, CH$_3$), 4.22 (m, 1H, CH), 7.18-7.84 (m, 10H, Ar), 8.39 (m, 1H, Ar), 9.34 (s, 1H, NH). IR (Nujol) 3298, 2924, 1668, 1602, 1517, 1463, 1377, 1182, 1140 cm^{-1}. Elemental analysis: calculated for $C_{20}H_{17}F_3N_4O$ (386.38) % C 62.17; H 4.44; N 14.50; found % C 62.20; H 4.50; N 14.60.

N-(Pyridin-3-yl)-2-(4-((2-(trifluoromethyl)pyridin-4-yl)amino)phenyl)propanamide (TPA14)
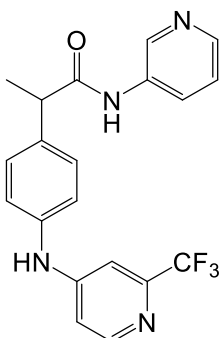
Obtained following the general procedure by the condensation between **TPA0** and 3-aminopyridine.

Yield 44 %. m.p. 156-152 °C. ^{1}H NMR (DMSO-d$_6$) δ 1.44 (m, 3H, CH$_3$), 3.99 (m, 1H, CH), 7.13-8.33 (m, 11H, Ar). IR (Nujol) 3274, 2955, 1695, 1603, 1522, 1462, 1376, 1322 cm^{-1}. Elemental analysis: calculated for C$_{20}$H$_{17}$F$_3$N$_4$O (386.38) % C 62.17; H 4.44; N 14.50; found % C 62.22; H 4.45; N 14.55.

N-(Pyridin-4-yl)-2-(4-((2-(trifluoromethyl)pyridin-4-yl)amino)phenyl)propanamide (TPA15)
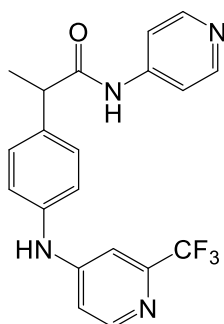
Obtained following the general procedure by the condensation between **TPA0** and 4-aminopyridine.

Yield 22 %. m.p. 120-130 °C. ^{1}H NMR (DMSO-d$_6$) δ 1.15 (d, J= 5.5 Hz, 3H, CH$_3$), 3.61 (q, J= 5.5 Hz, 1H, CH), 7.06 (m, 2H, Ar), 7.19 (m, 4H, Ar), 7.31 (m, 2H, Ar), 7.57 (m, 1H, Ar), 8.28 (m, 2H, Ar), 9.24 (s, 1H, NH), 10.54 (s, 1H, NH). IR (Nujol) 1602, 1515, 1460, 1361, 1181 cm^{-1}. Elemental analysis: calculated for C$_{20}$H$_{17}$F$_3$N$_4$O (386.38) % C 62.17; H 4.44; N 14.50; found % C 62.15; H 4.40; N 14.60.

N-(o-Tolyl)-2-(4-((2-(trifluoromethyl)pyridin-4-yl)amino)phenyl)propanamide (TPA16)
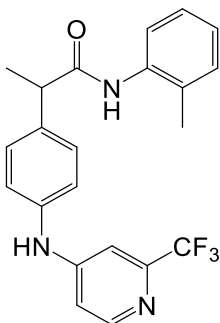
Obtained following the general procedure by the condensation between **TPA0** and 2-methylaniline.

Yield 60 %. m.p. 210-215 °C. ^{1}H NMR (DMSO-d$_6$) δ 1.03 (d, J= 6.0 Hz, 3H, CH$_3$), 2.08 (s, 3H, CH$_3$), 3.92 (q, J= 7.0 Hz, 1H, CH), 7.07 (m, 2H, Ar), 7.13-7.23 (m, 5H, Ar), 7.32 (m, 1H, Ar), 7.44 (m, 2H, Ar), 8.29 (m, 1H, Ar), 9.22 (s, 1H, NH), 9.38 (s, 1H, NH). IR (Nujol) 1667, 1604, 1532, 1456, 1362, 1181 cm^{-1}. Elemental analysis: calculated for C$_{22}$H$_{20}$F$_3$N$_3$O (399.16) % C 66.16; H 5.05; N 10.52; found % C 66.20; H 5.10; N 10.63.

N-(Pyrimidin-2-yl)-2-(4-((2-(trifluoromethyl)pyridin-4-yl)amino)phenyl)propanamide (TPA17)
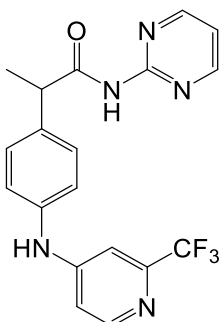
Obtained following the general procedure by the condensation between **TPA0** and 2-aminopyrimidine.

Yield 31 %. m.p. 95-100 °C. ^{1}H NMR (DMSO-d_6) δ 1.40 (d, J= 7.0 Hz, 3H, CH$_3$), 4.10 (q, J= 7.0 Hz, 1H, CH), 7.17 (m, 1H, Ar), 7.20 (m, 4H, Ar), 7.40 (m, 2H, Ar), 8.28 (m, 1H, Ar), 8.64 (m, 2H, Ar), 9.21 (s, 1H, NH), 10.71 (s, 1H, NH). IR (Nujol) 1701, 1602, 1519, 1459, 1360, 1181 cm^{-1}. Elemental analysis: calculated for C$_{19}$H$_{16}$F$_3$N$_5$O (387.37) % C 58.91; H 4.16; N 18.08; found % C 58.99; H 4.20; N 18.12.

N-(pyrazin-2-yl)-2-(4-((2-(trifluoromethyl)pyridin-4-yl)amino)phenyl)propanamide (TPA18)
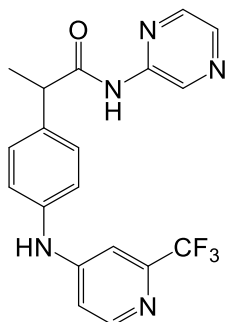
Obtained following the general procedure by the condensation between **TPA0** and 2-aminopyrazine.

Yield 46 %. m.p. 80-85 °C. ^{1}H NMR (DMSO-d_6) δ 1.44 (d, J= 7.0 Hz, 3H, CH$_3$), 4.06 (q, J= 7.0 Hz, 1H, CH), 7.07 (m, 1H, Ar), 7.21-7.22 (m, 3H, Ar), 7.32 (m, 1H, Ar), 7.43 (m, 2H, Ar), 8.27-8.39 (m, 2H, Ar), 9.22 (s, 1H, CH), 9.34 (s, 1H, NH), 10.95 (s, 1H, NH). IR (Nujol) 1701, 1602, 1511, 1460, 1378, 1180 cm^{-1}. Elemental analysis: calculated for C$_{19}$H$_{16}$F$_3$N$_5$O (387.37) % C 58.91; H 4.16; N 18.08; found % C 58.96; H 4.22; N 18.10.

N-(Quinolin-8-yl)-2-(4-((2-(trifluoromethyl)pyridin-4-yl)amino) phenyl)propanamide (TPA19)
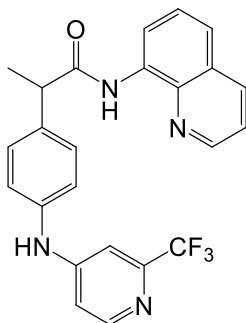
Obtained following the general procedure by the condensation between **TPA0** and 8-aminoquinoline.

Yield 69 %. m.p. 187 °C. ^{1}H NMR (DMSO-d$_6$) δ 1.50 (d, J= 7.0 Hz, 3H, CH$_3$), 3.57 (m, J= 7.0 Hz, 1H, CH), 7.15 (m, J= 8.0 Hz, 4H, Ar), 7.57 (m, J= 8.5 Hz, 5H, Ar), 8.26 (d, 1H, Ar), 8.37 (d, J= 8.5 Hz, 1H, Ar), 8.63 (d, J= 8.0 Hz, 1H, Ar), 8.85 (s, 1H, Ar), 9.21 (s, 1H, NH). IR (Nujol) 1657, 1600, 1523, 1487 cm^{-1}. Elemental analysis: calculated for C$_{24}$H$_{19}$F$_3$N$_4$O (436.44) % C 66.05; H 4.39; N 12.84; found % C 66.00; H 4.30; N 12.95.

1-(4-(3-Chlorophenyl)piperazin-1-yl)-2-(4-((2-(trifluoromethyl)pyridin-4-yl)amino)phenyl)propan-1-one (TPA20)
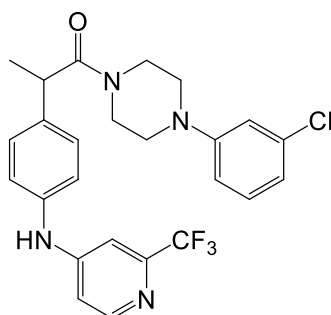
Obtained following the general procedure by the condensation between **TPA0** and 1-(3-chlorophenyl)piperazine.

Yield 67 %. m.p. 75-80 °C. ^{1}H NMR (DMSO-d$_6$) δ 1.44 (d, J= 7.5 Hz, 3H, CH$_3$), 2.66 (m, 1H, CH$_2$), 2.99 (m, 1H, CH$_2$), 3.18 (m, 2H, CH$_2$), 3.50-3.68 (m, 4H, CH$_2$), 4.16 (q, J= 7.0 Hz, 1H, CH), 6.78 (m, 1H, Ar), 6.83 (m, 1H, Ar), 6.89 (m, 1H, Ar), 7.03 (m, 1H, Ar), 7.18 (m, 4H, Ar), 7.31 (m, 2H, Ar), 8.26 (m, 1H, Ar), 9.18 (s, 1H, NH). IR (Nujol) 1596, 1519, 1463, 1377, 1228, 1182 cm^{-1}. Elemental analysis: calculated for C$_{25}$H$_{24}$ClF$_3$N$_4$O (488.94) % C 61.41; H 4.95; N 11.46; found % C 61.46; H 4.91; N 11.50.

1-(4-(4-Chlorophenyl)piperazin-1-yl)-2-(4-((2-(trifluoromethyl)pyridin-4-yl)amino)phenyl)propan-1-one (TPA21)
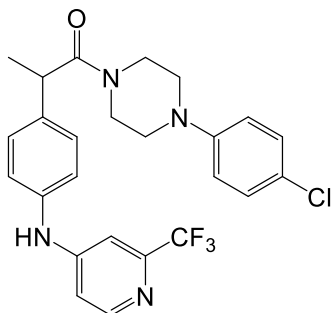
Obtained following the general procedure by the condensation between **TPA0** and 1-(4-chlorophenyl)piperazine.

Yield 82 %. m.p. 80-85 °C. ^{1}H NMR (DMSO-d$_6$) δ 1.32 (d, J= 6.5 Hz, 3H, CH$_3$), 2.66 (m, 1H, CH$_2$), 2.95 (m, 1H, CH$_2$), 3.11 (m, 2H, CH$_2$), 3.50-3.68 (m, 4H, CH$_2$), 4.17 (q, J= 6.5 Hz, 1H, CH), 6.89 (d, J= 8.0 Hz, 2H, Ar), 7.03 (m, 1H,Ar), 7.16-7.21 (m, 5H, Ar), 7.30 (d, J= 8.0 Hz, 2H, Ar), 8.27 (m, 1H, Ar), 9.18 (s, 1H, NH). IR (Nujol) 1645, 1600, 1519, 1496, 1461, 1365 cm^{-1}. Elemental analysis: calculated for C$_{25}$H$_{24}$ClF$_3$N$_4$O (488.94) % C 61.41; H 4.95; N 11.46; found % C 61.36; H 4.85; N 11.40.

1-(4-(2,3-Dimethylphenyl)piperazin-1-yl)-2-(4-((2-(trifluoromethyl)pyridin-4-yl)amino)phenyl)propan-1-one (TPA22)
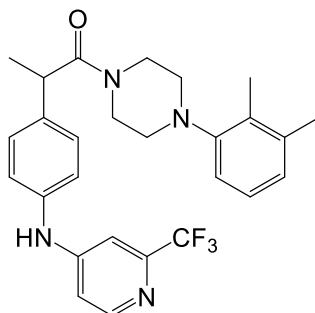
Obtained following the general procedure by the condensation between **TPA0** and 1-(2,3-dimethylphenyl)piperazine.

Yield 62 %. m.p. 85 °C. ^{1}H NMR (DMSO-d$_6$) δ 1.33 (d, J= 6.0 Hz, 3H, CH$_3$), 2.14 (s, 3H, CH$_3$), 2.19 (s, 3H, CH$_3$), 2.31 (m, 1H, CH$_2$), 2.65 (m, 2H, CH$_2$), 2.73 (m, 1H, CH$_2$), 3.48-3.64 (m, 4H, CH$_2$), 4.16 (q, J= 6.0 Hz, 1H, CH), 6.74 (d, J= 7.5 Hz, 1H, Ar), 6.86 (d, J= 7.0 Hz, 1H, Ar), 6.98 (m, 1H, Ar), 7.05 (m, 1H, Ar), 7.18-7.21 (m, 3H, Ar), 7.31 (d, J= 8.0 Hz, 2H, Ar), 8.28 (m, 1H, Ar), 9.20 (s, 1H, NH). IR (Nujol) 3280, 2924, 1601, 1518, 1461, 1377, 1137 cm^{-1}. Elemental analysis: calculated for C$_{27}$H$_{29}$F$_3$N$_4$O (482.55) % C 67.20; H 6.06; N 11.61; found % C 67.22; H 6.08; N 11.56.

1-(4-(o-Tolyl)piperazin-1-yl)-2-(4-((2-(trifluoromethyl)pyridin-4-yl)amino)phenyl)propan-1-one (TPA23)
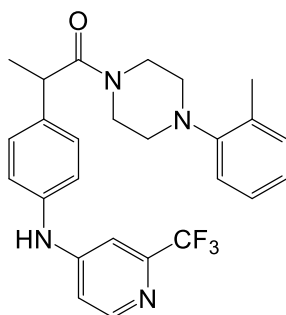
Obtained following the general procedure by the condensation between **TPA0** and 1-(2-methylphenyl)piperazine.

Yield 68 %. m.p. 80 °C. ^{1}H NMR (DMSO-d$_6$) δ 1.33 (d, J= 6.5 Hz, 3H, CH$_3$), 2.22 (s, 3H, CH$_3$), 2.36 (m, 1H, CH$_2$), 2.69 (m, 2H, CH$_2$), 2.78 (m, 1H, CH$_2$), 3.60-3.67 (m, 4H, CH$_2$), 4.16 (q, J= 6.5 Hz, 1H, CH), 6.87 (m, 1H, Ar), 6.94 (m, 1H, Ar), 7.05-7.22 (m, 5H, Ar), 7.31 (m, 1H, Ar), 7.31 (m, 2H, Ar), 8.28 (m, 1H, Ar), 9.21 (s, 1H, NH). IR (Nujol) cm^{-1}. Elemental analysis: calculated for C$_{26}$H$_{27}$F$_3$N$_4$O (468.21) % C 66.65; H 5.81; N 11.96; found % C 66.70; H 5.89; N 11.90.

N-(3-Bromopyridin-2-yl)-2-(4-((2-(trifluoromethyl)pyridin-4-yl)amino)phenyl)propanamide (TPA24)
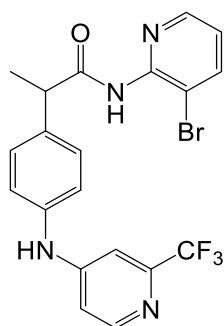
Obtained following the general procedure by the condensation between **TPA0** and 2-amino-3-bromopyridine.

Yield 77 %. m.p. 200 °C. ^{1}H NMR (DMSO-d$_6$) δ 1.43 (d, J= 6.5 Hz, 3H, CH$_3$), 3.88 (q, J= 6.5 Hz, 1H, CH), 7.05 (m, 1H, Ar), 7.18 (d, J= 8.5 Hz, 2H, Ar), 7.21-7.24 (m, 2H, Ar), 7.41 (d, J= 8.0 Hz, 2H, Ar), 8.10 (m, 1H, Py), 8.28 (m, 1H, Py), 8.41 (m, 1H, Py), 9.19 (s, 1H, NH), 10.26 (s, 1H, NH). IR (Nujol) 1670, 1603, 1532, 1462, 1377 cm^{-1}. Elemental analysis: calculated for C$_{20}$H$_{16}$BrF$_3$N$_4$O (464.05) % C 51.63; H 3.47; N 12.04; found % C 51.70; H 3.50; N 11.99.

N-(3-Iodopyridin-2-yl)-2-(4-((2-(trifluoromethyl)pyridin-4-yl)amino)phenyl)propanamide (TPA25)
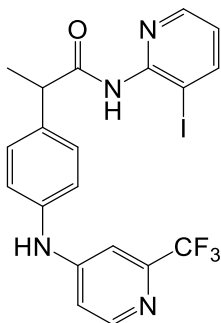
Obtained following the general procedure by the condensation between **TPA0** and 2-amino-3-iodopyridine.

Yield 33 %. m.p. 210 °C. ^{1}H NMR (DMSO-d_6) δ 1.44 (d, J= 7.0 Hz, 3H, CH$_3$), 3.88 (q, J= 7.5 Hz, 1H, CH), 7.05 (m, 2H, Ar), 7.18 (m, 1H, Ar), 7.19 (d, J= 8.0 Hz, 2H, Ar), 7.41 (d, J= 8.5 Hz, 2H, Ar), 8.28 (m, 2H, Ar), 8.41 (m, 1H, Ar), 9.19 (s, 1H, NH), 10.23 (s, 1H, NH). IR (Nujol) 1667, 1602, 1531, 1459, 1424 cm^{-1}. Elemental analysis: calculated for C$_{20}$H$_{16}$F$_3$IN$_4$O (512.03) % C 46.89; H 3.15; N 10.94; found % C 46.90; H 3.21; N 11.02.
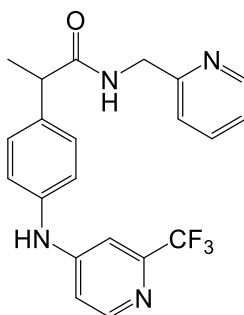
N-(3-(Trifluoromethyl)pyridin-2-yl)-2-(4-((2-(trifluoromethyl)pyridin-4-yl)amino)phenyl)propanamide (TPA26)
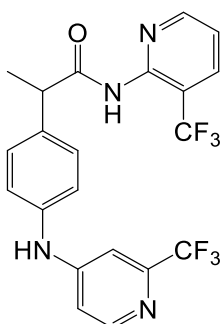
Obtained following the general procedure by the condensation between **TPA0** and 2-amino-3-(trifluoromethyl)pyridine.

Yield 59 %. m.p. 190 °C. ^{1}H NMR (DMSO-d$_6$) δ 1.42 (d, J= 7.0 Hz, 3H, CH$_3$), 3.91 (q, J= 7.0 Hz, 1H, CH), 7.05 (m, 1H, Ar), 7.17 (s, 1H, Ar), 7.20 (d, J= 6.5 Hz, 2H, Ar), 7.39 (d, J= 7.0 Hz, 2H, Ar), 7.53 (m, 1H, Ar), 8.20 (m, 1H, Ar), 8.28 (m, 1H, Ar), 8.72 (m, 1H, Ar), 9.20 (s, 1H, NH), 10.28 (s, 1H, NH). IR (Nujol) 1671, 1603, 1533, 1460, 1376, 1321, 1144 cm^{-1}. Elemental analysis: calculated for C$_{21}$H$_{16}$F$_6$N$_4$O (454.38) % C 55.51; H 3.55; N 12.33; found % C 55.58; H 3.52; N 12.36.

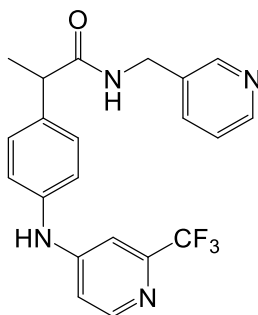### N-(3-Chloropyridin-2-yl)-2-(4-((2-(trifluoromethyl)pyridin-4-yl)amino)phenyl)propanamide (TPA27)
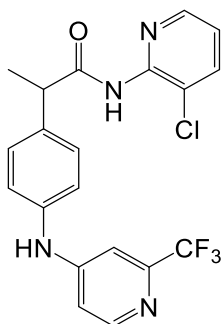
Obtained following the general procedure by the condensation between **TPA0** and 2-amino-3-chloropyridine.

Yield 78 %. m.p. 145-150 °C. ^{1}H NMR (DMSO-d$_6$) δ 1.44 (d, J= 5.5 Hz, 3H, CH$_3$), 3.93 (q, J= 5.5 Hz, 1H, CH), 7.07 (m, 1H, Ar), 7.21 (m, 3H, Ar), 7.32 (m, 1H, Ar), 7.41 (m, 2H, Ar), 7.96 (m, 1H, Ar), 8.29 (m, 1H, Ar), 8.38 (m, 1H, Ar), 9.22 (s, 1H, NH), 10.32 (s, 1H, NH). IR (Nujol) 1670, 1603, 1531, 1462, 1364, 1187 cm^{-1}. Elemental analysis: calculated for C$_{20}$H$_{16}$ClF$_3$N$_4$O (420.82) % C 57.08; H 3.83; N 13.31; found % C 57.12; H 3.91; N 13.35.

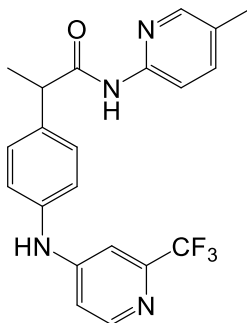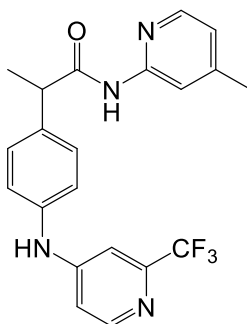### N-(4-hydroxy-2-methylphenyl)-2-(4-((2-(trifluoromethyl)pyridin-4-yl)amino)phenyl)propanamide (TPA28)
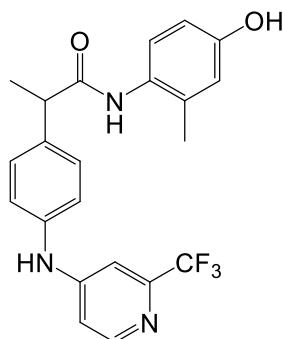
Obtained following the general procedure by the condensation between **TPA0** and 4-hydroxy-2-methylaniline.

Yield 87 %. m.p. 218 °C. ^{1}H NMR (DMSO-d_6) δ 1.41 (d, J= 7.0 Hz, 3H, CH_3), 1.94 (s, 3H, CH_3), 3.81 (q, J= 6.5 Hz, 1H, CH), 6.50-8.28(m, 10H, Ar), 9.18 (m, 3H, NH OH). IR (Nujol) 3266, 1654, 1605, 1526, 1460, 1365, 1322, 1227, 1186 cm^{-1}. Elemental analysis: calculated for $C_{22}H_{20}F_3N_3O_2$ (415.15) % C 63.61; H 4.85; N 10.12; found % C 63.66; H 4.91; N 10.16.

(2-(4-((2-(Trifluoromethyl)pyridin-4-yl)amino)phenyl)propanoyl)glycine (27)
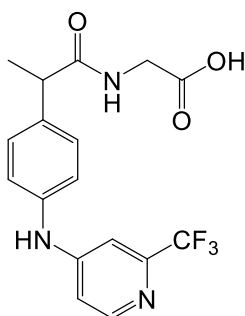
TPA0 (0.62 g, 2 mmol), EDC (0.39 g, 2.2 mmol) and HOBt (0.27 g, 2mmol) were dissolved in MeCN (10mL). The mixture was stirred at r.t. for 30 minutes, then TEA (0.4 mL, 4 mmol) and ethylglicinate hydrochloride (0.56 g, 4 mmol) were added. The mixture was stirred

at r.t. for 4 hours. After the solvent was removed under vacuum. The residue was dissolved in AcOEt (20 mL) and washed sequentially with brine (2x5 mL), 10% citric acid (2x5 mL), saturated NaHCO$_3$ aqueous solution (2x5 mL) and water (2x5 mL). The organic layer was dried over anhydrous Na$_2$SO$_4$ and evaporated under vacuum. The residue was treated with iPr$_2$O; the precipitate was then filtrated and purified by crystallization with 2-PrOH to obtain the ester **26** at almost pure state. The ester **26** (0.40 g, 1 mmol) was dissolved in EtOH (10 mL). To this solution a 5N solution of NaOH (2mL) and water (2 mL) were added. The resulting mixture was stirred at r.t. for 24h. After removing EtOH under vacuum ice and then aqueous 20% HCl solution until pH 3-4 were added. The formed precipitate was filtrated, washed with water and re-crystallized with EtOH.

Yield 94 %. m.p. 230 °C. ^{1}H NMR (DMSO-d$_6$) δ 1.33 (d, J= 7.5, 3H, CH$_3$), 3.66-3.79 (m 3H, CH$_2$ CH), 7.04 (m, 1H, Ar), 7.17 (m, 3H, Ar), 7.34 (m, 2H, Ar), 8.28 (m, 2H, Ar NH), 9.19 (s, 1H, NH), 12.46 (s, 1H, OH). IR (Nujol) 3350, 3281, 2854, 2522, 1900, 1707, 1657, 1606, 1538, 1454, 1364 cm^{-1}. Elemental analysis: calculated for C$_{17}$H$_{16}$F$_3$N$_3$O$_3$ (367.33) % C 55.59; H 4.39; N 11.44; found % C 55.63; H 4.35; N 11.52.

N-(2-((3-Methylpyridin-2-yl)amino)-2-oxoethyl)-2-(4-((2-(trifluoromethyl)pyridin-4-yl)amino)phenyl)propanamide (TPA10)
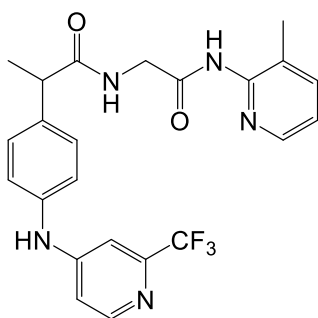
A solution of acid **27** (0.37 g, 1 mmol), EDC (0.19 g, 1.1 mmol) and HOBt (0.13 g, 1 mmol) in anhydrous MeCN (10 mL) was stirred at r.t. for 30 minutes, then 2-amino-3-methylpyridine (0.108 g, 1 mmol) was added. The mixture was stirred at r.t. for 36 hours. After the

solvent was removed under vacuum. The residue was dissolved in AcOEt (20 mL) and washed sequentially with brine (2x5 mL), 10% citric acid (2x5 mL), saturated NaHCO$_3$ aqueous solution (2x5 mL) and water (2x5 mL). The organic layer was dried over anhydrous Na$_2$SO$_4$ and evaporated under vacuum. The obtained residue was washed with iPr$_2$O and filtered to obtain the title compound.

Yield 76 %. m.p. 225-230 °C. ^{1}H NMR (DMSO-d$_6$) δ 1.38 (m, 3H, CH$_3$), 2.62 (s, 3H, CH$_3$), 3.85-4.05 (m 3H, CH$_2$ CH), 7.19-8.53 (m, 10H, Ar). IR (Nujol) 1658, 1602, 1524, 1377, 1181 cm^{-1}. Elemental analysis: calculated for C$_{23}$H$_{22}$F$_3$N$_5$O$_2$ (457.17) % C 60.39; H 4.85; N 15.31; found % C 60.45; H 4.90; N 15.36.

Methyl (E)-2-(4-((5,5,5-trifluoro-4-oxopent-2-en-2-yl)amino)phenyl)acetate (29)
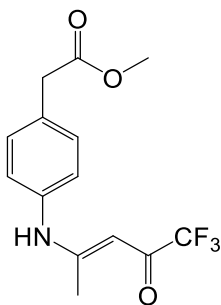
Ester **29** was prepared using the same procedure used for the synthesis of the compound **23**, starting from methyl 2-(4-aminophenyl)acetate.

Yield 96 %. m.p. 164-165 °C. ^{1}H NMR (DMSO-d$_6$) δ 2.24 (s, 3H, CH$_3$), 3.54 (s, 2H, CH$_2$), 3.98 (s, 3H, CH$_3$), 5.82 (s, 1H, CH), 7.34 (d, J= 7.6 Hz, 2H, Ar), 7.81 (d, J= 7.6 Hz, 2H, Ar), 12.52 (s, 1H, NH). IR (Nujol) 3260, 1717 cm^{-1}. Elemental analysis: calculated for C$_{14}$H$_{14}$F$_3$NO$_3$ (301.27) % C 55.82; H 4.68; N 4.65; found % C 55.86; H 4.70; N 4.70.

Methyl 2-(4-(((1E,3E)-1-(dimethylamino)-6,6,6-trifluoro-5-oxohexa-1,3-dien-3-yl)amino)phenyl)acetate (30)
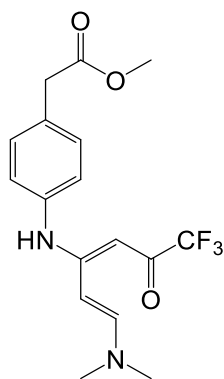
Ester **30** was prepared using the same procedure used for the synthesis of the compound **24**, starting from ester **29**.

Yield 95 %. m.p. 105-106 °C (n-hexane). ^{1}H NMR (DMSO-d$_6$) δ 2.77 (s, 3H, CH$_3$), 3.28 (s, 3H, CH$_3$), 3.92 (s, 3H, CH$_3$), 4.03 (s, 2H, CH$_2$), 5.02 (d, J=12.8, 1H, CH), 5.96 (s, 1H, CH), 7.49 (m, 2H, Ar), 8.03 (m, 3H, Ar CH), 12.86 (s, 1H, NH). IR (Nujol) 1724, 1661 cm^{-1}. Elemental analysis: calculated for C$_{17}$H$_{19}$F$_3$N$_2$O$_3$ (356.35) % C 57.30; H 5.37; N 7.86; found % C 57.36; H 5.45; N 7.90.

Methyl 2-(4-((2-(trifluoromethyl)pyridin-4-yl)amino)phenyl)acetate (31)
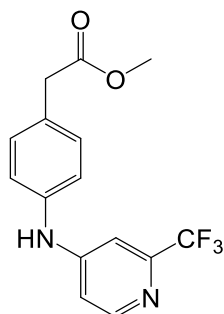
Ester **31** was prepared using the same procedure used for the synthesis of compound **25**, starting from ester **30**.

Yield 90 %. m.p. 48-50 °C (n-hexane). ^{1}H NMR (DMSO-d$_6$) δ 3.58 (s, 2H, CH$_2$), 3.93 (s, 3H, CH$_3$), 6.93 (m, 1H, Ar), 7.18 (m, 2H, Ar), 7.59 (m, 2H, Ar), 7.72 (m, 1H, Ar), 8.48 (m, 1H, Ar), 9.70 (s, 1H, NH). IR (Nujol) 3362, 3205, 1717 cm^{-1}. Elemental analysis: calculated for C$_{15}$H$_{13}$F$_3$N$_2$O$_2$ (310.28) % C 58.07; H 4.22; N 9.03; found % C 58.10; H 4.22; N 9.10.

2-(4-((2-(trifluoromethyl)pyridin-4-yl)amino)phenyl)acetic acid (32)
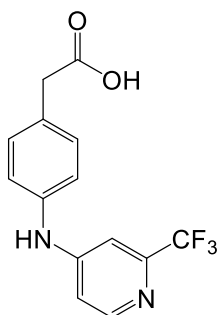
Acid **32** was prepared using the same procedure used for the synthesis of TPA0, starting from ester **31**.

Yield 84 %. m.p. 219-220 °C. ^{1}H NMR (DMSO-d$_6$) δ 3.67 (s, 2H, CH$_2$), 7.19 (m, 1H, Ar), 7.31 (m, 3H, Ar), 7.40 (d, J= 8.4 Hz, 2H, Ar), 8.40 (d, J= 5.8 Hz, 1H, Ar), 9.33 (s, 1H, NH). IR (Nujol) 3325, 2495, 1898, 1693 cm^{-1}. Elemental analysis: calculated for C$_{14}$H$_{11}$F$_3$N$_2$O$_2$ (296.25) % C 56.76; H 3.74; N 9.46; found % C 56.85; H 3.82; N 9.38.

N-(3-Methylpyridin-2-yl)-2-(4-((2-(trifluoromethyl)pyridin-4-yl)amino)phenyl)acetamide (TPA29)
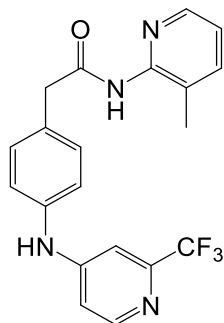
A solution of acid **32** (0.30 g, 1 mmol), EDC (0.19 g, 1.1 mmol) and HOBt (0.13 g, 1 mmol) in anhydrous MeCN (10 mL) was stirred at r.t. for 30 minutes, after 2-amino-3-methylpyridine (0.108 g, 1 mmol) was added. The mixture was stirred at r.t. for 36 hours. After the solvent was removed under vacuum. The residue was dissolved in AcOEt (20 mL) and washed sequentially with brine (2x5 mL), 10% citric acid (2x5 mL), saturated NaHCO$_3$ aqueous solution (2x5 mL) and water (2x5 mL). The organic layer was dried over anhydrous Na$_2$SO$_4$ and evaporated under vacuum. The obtained residue was washed with iPr$_2$O and the resulting precipitate filtered.

Yield 78 %. m.p. 135-140 °C. ^{1}H NMR (DMSO-d$_6$) δ 2.08 (s, 3H, CH$_3$), 3.67 (s, 2H, CH$_2$), 7.05-7.37(m, 9H, Ar), 8.28 (m, 1H, Ar), 9.25 (s, 1H, NH), 10.20 (s, 1H, NH). IR (Nujol) 1602, 1518, 1462, 1377, 1180, 1135 cm^{-1}. Elemental analysis: calculated for C$_{20}$H$_{17}$F$_3$N$_4$O (386.38) % C 62.17; H 4.44; N 14.50; found % C 62.20; H 4.46; N 14.60.

Methyl 2-methyl-2-(4-nitrophenyl)propanoate (34)
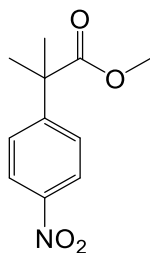
Methyl ester **33** (1.56 g, 8 mmol) was dissolved in anhydrous DMF (20 mL). The solution was cooled to 0° C. Sodium hydride (0.63 g, 16 mmol; 60% dispersion in oil) was added slowly and cautiously. The resulting mixture was allowed to warm to r.t. and then stirred for additional 20 min. The solution was cooled again to 0 °C. Iodomethane (2 mL, 32 mmol) was added dropwise, and the resulting solution was allowed to stir at 0 °C. for about 30 min. The solution was warmed to r.t. and stirred for additional 1 h. The solution was cooled to 0 °C and quenched with water, maintaining 0 °C throughout the quenching process. The obtained mixture was extracted with dichloromethane (2 x 15 mL). The combined organic layers were washed with water (2 x 5 mL) and brine (2 x 5 mL); dried over sodium Na_2SO_4. After removing the Na_2SO_4 by filtration, the filtrate was concentrated under vacuum. The residue was purified by column chromatography (silica gel, 8:1 petrolium ether: AcOEt) and gave the title compound as a yellow solid material.

Yield 80 %. Oil. ^{1}H NMR (DMSO-d_6) δ 1.69 (s, 6H, CH_3), 3.74 (s, 3H, CH_3), 7.45 (d, J= 8.5 Hz, 2H, Ar), 8.13 (d, J= 8.5 Hz, 2H, Ar). Elemental analysis: calculated for $C_{11}H_{13}NO_4$ (223.23) % C 59.19; H 5.87; N 6.27; found % C 59.15; H 5.90; N 6.28. Physical and spectral data were in accordance with literature values.[112]

Methyl 2-(4-aminophenyl)-2-methylpropanoate (35)
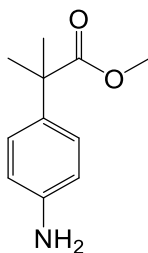
To a solution of ester **34** (1.34 g, 6 mmol) in EtOH (15 mL) tin (II) chloride dihydrate (5.5 g, 24 mmol) was added. The resulting solution was stirred at 85 °C for 4 h. After cooling, the pH was adjusted to with 40% aqueous NaOH. The mixture was extracted with AcOEt (3 x 5 mL). The combined organic layers were washed with water (2 x 5mL) and brine (2 x 5 mL) and dried over Na_2SO_4. After removing of the Na_2SO_4 the filtrate was concentrated under vacuum to obtain the title compound as yellow oil.

Yield 87%. Oil. ^{1}H NMR (DMSO-d_6) δ 0.63 (s, 3H, CH_3), 0.91 (s, 3H, CH_3), 3.54 (s, 3H, CH_3), 4.96 (s, 2H, NH_2), 6.49 (d, J= 8.5 Hz, 2H, Ar), 6.91 (d, J= 8.5 Hz, 2H, Ar). IR (Film) 3435, 3349, 2956, 1723, 1626, 1517, 1468, 1433 cm^{-1}. Elemental analysis: calculated for $C_{11}H_{15}NO_2$ (193.25) % C 68.37; H 7.82; N 7.25; found % C 68.40; H 7.90; N 7.28.

Methyl (E)-2-methyl-2-(4-((5,5,5-trifluoro-4-oxopent-2-en-2-yl)amino)phenyl)propanoate (36)
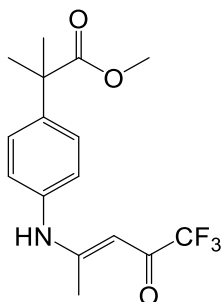
Ester **36** was prepared using the same procedure used for the synthesis of the compound **23**, starting from ester **35**.

Yield 87%. Oil. ^{1}H NMR (DMSO-d$_6$) δ 1.53 (s, 6H, CH$_3$), 2.27 (s, 3H, CH$_3$), 3.77 (s, 3H, CH$_3$), 5.77 (s, 1H, CH), 7.01 (d, J= 8.5 Hz, 2H, Ar), 7.77 (d, J= 8.5 Hz, 2H, Ar), 12.58 (s, 1H, NH). IR (Film) 2925, 1721, 1571, 1515, 1436, 1365, 1247, 1188, 1139 cm^{-1}. Elemental analysis: calculated for C$_{16}$H$_{18}$F$_3$NO$_3$ (329.32) % C 58.36; H 5.51; N 4.25; found % C 58.40; H 5.60; N 4.28.

2-Methyl-2-(4-((2-(trifluoromethyl)pyridin-4-yl)amino)phenyl)propanoic acid (39)
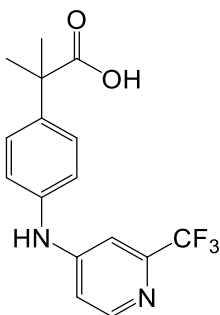
A mixture of **36** (1.65 g, 5 mmol) and DMF-DMA (1.79 g, 15 mmol) in anhydrous toluene (20 mL) was refluxed for 1 h, then allowed to reach the room temperature and stirred for additional 24 h. The mixture was carefully concentrated in vacuum. Without isolate it the dienaminone intermediate was dissolved in dry DMF (5 mL), ammonium acetate (0.308 g, 4 mmol) was added and the mixture was gently heated for 1.5 h. The mixture was carefully concentrated in vacuum, and then ice-water (15 mL) was added. The formed solid was filtered off and washed with water. The obtained trifluoromethylpyridine ester was dissolved in EtOH (20 mL), 5N solution of NaOH (4 mL) and water (4 mL) were added. The resulting mixture was stirred at r.t. for 24h. After removing EtOH under vacuum, the residue was ice added and then acidified with aqueous 20% HCl solution until pH 3-4. The formed precipitate was filtered and washed with water.

Yield 42 %. m.p. 170-175 °C. ^{1}H NMR (DMSO-d$_6$) δ 1.48 (s, 6H, CH$_3$), 7.02 (m, 1H, Ar), 7.17 (m, 3H, Ar), 7.52 (m, 2H, Ar), 8.28 (m, 1H, Ar),

9.25 (s, 1H, NH). IR (Nujol) 3285, 2924, 1690, 1623, 1602, 1534, 1464, 1368, 1186 cm^{-1}. Elemental analysis: calculated for $C_{16}H_{15}F_3N_2O_2$ (324.30) % C 59.26; H 4.66; N 8.64; found % C 59.30; H 4.70; N 8.60.

2-Methyl-N-(3-methylpyridin-2-yl)-2-(4-((2-(trifluoromethyl)pyridin-4-yl)amino)phenyl)propanamide (TPA30)
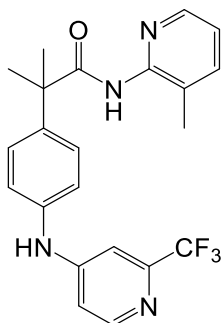
A solution of acid **39** (0.32 g, 1 mmol), EDC (0.19 g, 1.1 mmol) and HOBt (0.13 g, 1 mmol) in anhydrous MeCN (10 mL) was stirred at r.t. for 30 minutes, then 2-amino-3-methylpyridine (0.108 g, 1 mmol) was added. The mixture was stirred at r.t. for 36 hours. After the solvent was removed under vacuum. The residue was dissolved in AcOEt (20 mL) and washed sequentially with brine (2x5 mL), 10% citric acid (2x5 mL), saturated NaHCO$_3$ aqueous solution (2x5 mL) and water (2x5 mL). The organic layer was dried over anhydrous Na$_2$SO$_4$ and evaporated under vacuum. The obtained residue was tritured with iPr$_2$O and the obtained precipitate filtered off.

Yield 61 %. m.p. 220 °C. ^{1}H NMR (DMSO-d$_6$) δ 1.60 (s, 6H, CH$_3$), 2.06 (s, 3H, CH$_3$), 7.09 (s, 1H, Ar), 7.23 (m, 4H, Ar), 7.46 (s, 2H, Ar), 7.64 (s, 1H, Ar), 8.24 (s, 1H, Ar), 8.30 (s, 1H, Ar), 9.24 (s, 1H, NH). IR (Nujol) 3290, 1661, 1605, 1534 cm^{-1}. Elemental analysis: calculated for $C_{22}H_{21}F_3N_4O$ (414.43) % C 63.76; H 5.11; N 13.52; found % C 63.80; H 5.16; N 13.60.

General procedure for the synthesis of esters 40-43

33 (2.50 g, 12.8 mmol) was dissolved in anhydrous DMF (20 mL). The solution was cooled to 0° C. NaH (1.02 g, 25.6 mmol; 60% dispersion in oil) was added slowly and cautiously. The resulting mixture was allowed to warm to r.t. and was stirred for additional 20 min. The solution was cooled again to 0 °C The appropriate dihaloalkane (25.6 mmol) was added dropwise, and the resulting solution was allowed to stir at 0 °C. for 30 min. The solution was warmed to r.t. and stirred for additional 1 h. The solution was cooled to 0 °C and quenched with water, maintaining 0 °C throughout the quenching process. The obtained mixture was extracted with dichloromethane (2x20 mL). The combined organic layers were washed with water and brine and dried over Na_2SO_4. This was removed by filtration and the filtrate concentrated under vacuum to give product.[113]

Methyl 1-(4-nitrophenyl)cyclopropane-1-carboxylate (40)
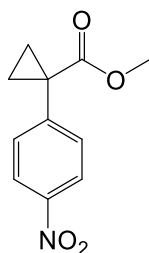
Compound **40** was prepared following the general procedure starting from 1,2-dibromoethane. The obtained product was purified by column chromatography (silica gel, 8:1 petrolium ether:AcOEt).

Yield 45 %. m.p. 96-98 °C. ^{1}H NMR (DMSO-d6) δ 1.24-1.27 (m, 2H, CH_2), 1.65-1.69 (m, 2H, CH_2), 3.62 (s, 3H, CH_3), 7.53-7.58 (m, 2H, Ar), 8.17-8.19 (m, 2H, Ar). IR (Nujol) 2915, 1713, 1603, 1517, 1460, 1305 cm^{-1}. Elemental analysis: calculated for $C_{11}H_{11}NO_4$ (221.21) % C 59.73; H 5.01; N 6.33; found % C 59.75; H 5.05; N 6.42. Analytical and spectral data were in accordance with literature values.[113]

Methyl 1-(4-nitrophenyl)cyclobutane-1-carboxylate (41)
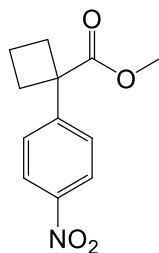
Compound **41** was prepared following the general procedure starting from 1,3-diiodopropane. The obtained product was purified by column chromatography (silica gel, 15:1 petrolium ether:AcOEt).

Yield 45 %. Oil. ^{1}H NMR (DMSO-d_6) δ 1.83-2.18 (m, 2H, CH$_2$), 2.44-2,52 (m, 2H, CH$_2$), 2.90-3.01 (m, 2H, CH$_2$), 3.69 (s, 3H, CH$_3$), 7.44 (m, 2H, Ar), 8.20 (m, 2H, Ar). Elemental analysis: calculated for C$_{12}$H$_{13}$NO$_4$ (235.08) % C 61.27; H 5.57; N 5.95; found % C 61.32; H 5.60; N 5.88. Analytical and spectral data were in accordance with literature values.[113]

Methyl 1-(4-nitrophenyl)cyclopentane-1-carboxylate (42)
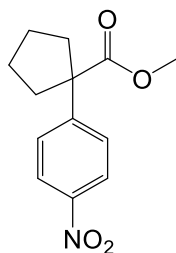
Compound **42** was prepared following the general procedure starting from 1,4-diiodobutane. The obtained product was purified by column chromatography (silica gel, 15:1 petrolium ether:AcOEt).

Yield 60 %. Oil. ^{1}H NMR (DMSO-d_6) δ 1.70-1.86 (m, 6H, CH$_2$), 2.58 (m, 2H, CH$_2$), 3.55 (s, 3H, CH$_3$), 6.66 (m, 2H, Ar), 7.25 (m, 2H, Ar). Elemental analysis: calculated for C$_{13}$H$_{15}$NO$_4$ (249.27) % C 62.64; H 6.07; N 5.62; found % C 62.68; H 6.10; N 5.63. Physical and spectral data were in accordance with literature values.[113]

Methyl 1-(4-nitrophenyl)cyclohexane-1-carboxylate (43)
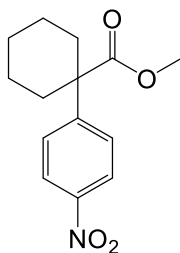
Compound **43** was prepared following the general procedure starting from 1,5-diiodopentane. The obtained product was purified by column chromatography (silica gel, 15:1 petrolium ether:AcOEt).

Yield 40 %. Oil. ^{1}H NMR (DMSO-d$_6$) δ 1.39–1.68 (m, 6H, CH$_2$), 1.75 (t, J = 13.0 Hz, 2H, CH$_2$), 2.49 (d, J = 13.0 Hz, 2H, CH$_2$), 3.66 (s, 3H, CH$_3$), 7.56 (d, J = 9.0Hz, 2H, Ar), 8.17 (d, J = 9.0 Hz, 2H, Ar). Elemental analysis: calculated for C$_{14}$H$_{17}$NO$_4$ (263.29) % C 63.87; H 6.51; N 5.32; found % C 71.20; H 7.75; N 6.42.

General procedure for the synthesis of esters 44-47

To a solution of ester **40-43** (9.78 mmol) in AcOEt (230 mL) stannous chloride hydrate (110 g, 48.9 mmol was added). The reaction mixture was stirred at 75 °C for 4 h. Reaction mixture was cooled at r.t and then diluted with AcOEt (100 mL) and made alkaline (pH 10) using aqueous ammonia chloride solution 25 %. Organic layer was separated out, dried over Na$_2$SO$_4$ and the solvent evaporated under vacuum to obtain the desired compound **44-47**.

Methyl 1-(4-aminophenyl)cyclopropane-1-carboxylate (44)
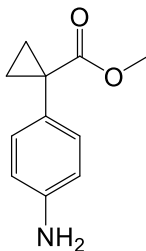
Compound **44** was prepared following the general procedure starting from compound **40**.

Yield 89 %. Oil. ^{1}H NMR (DMSO-d$_6$) δ 1.12-1.16 (m, 2H, CH$_2$), 1.50-1.57 (m, 2H, CH$_2$), 3.66 (s, 3H, CH$_3$), 6.63 (m, 2H, Ar), 7.10 (m, 2H, Ar). IR (Film) 3359, 3301, 2926, 1706, 1660, 1637, 1522, 1459, 1376, 1297 cm^{-1}. Elemental analysis: calculated for C$_{11}$H$_{13}$NO$_2$ (263.29) % C 69.09; H 6.85; N 7.32; found % C 69.09; H 6.89; N 7.40.

Methyl 1-(4-aminophenyl)cyclobutane-1-carboxylate (45)
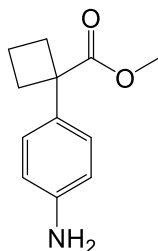
Compound **45** was prepared following the general procedure starting from compound **41**.

Yield 90 %. Oil. ^{1}H NMR (DMSO-d$_6$) δ 2.00 (m, 2H, CH$_2$), 2.41 (m, 2H, CH$_2$), 2.78 (m, 2H, CH$_2$), 3.64 (s, 3H, CH$_3$), 6.65 (m, 2H, Ar), 7.08 (m, 2H, Ar). Elemental analysis: calculated for C$_{12}$H$_{15}$NO$_2$ (263.29) % C 70.22; H 7.37; N 6.82; found % C 70.25; H 7.38; N 6.80.

Methyl 1-(4-aminophenyl)cyclopentane-1-carboxylate (46)
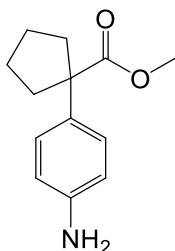
Compound **46** was prepared following the general procedure starting from compound **42**.

Yield 94 %. Oil. ^{1}H NMR (DMSO-d$_6$) δ 1.70 (m, 6H, CH$_2$), 2.58 (m, 2H, CH$_2$), 3.62 (s, 3H, CH$_3$), 6.57 (m, 2H, Ar), 7.20 (m, 2H, Ar). Elemental analysis: calculated for C$_{13}$H$_{17}$NO$_2$ (219.28) % C 71.21; H 7.81; N 6.39; found % C 71.20; H 7.83; N 6.40.

Methyl 1-(4-aminophenyl)cyclohexane-1-carboxylate (47)
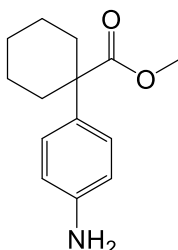
Compound **47** was prepared following the general procedure starting from compound **43**.

Yield 90 %. Oil. ^{1}H NMR (DMSO-d$_6$) δ 1.28-1.62 (m, 6H, CH$_2$), 2.10 (m, 2H, CH$_2$), 2.50 (m, 2H, CH$_2$), 3.64 (s, 3H, CH$_3$), 6.32 (m, 2H, Ar), 7.02 (m, 2H, Ar). Elemental analysis: calculated for C$_{14}$H$_{19}$NO$_2$ (233.31) % C 72.07; H 8.21; N 6.00; found % C 72.08; H 8.30; N 6.08.

Methyl (*E*)-1-(4-((5,5,5-trifluoro-4-oxopent-2-en-2-yl)amino)phenyl)cyclopropane-1-carboxylate (48)
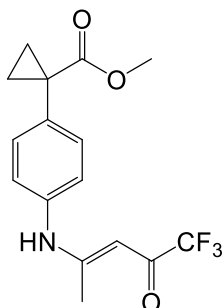
Ester **48** was prepared using the same procedure used to prepare the compound **23**, starting from ester **44**.

Yield 45 %. m.p. 158-160 °C. ^{1}H NMR (DMSO-d$_6$) δ 1.15 (m, 2H, CH$_2$), 1.55 (m, 2H, CH$_2$), 2.23 (s, 3H, CH$_3$), 3.80 (s, 3H, CH$_3$), 5.70 (s, 1H, CH), 7.05 (d, J= 8.0 Hz, 2H, Ar), 7.70 (d, J= 8.0 Hz, 2H, Ar), 12.58 (s, 1H, NH). IR (Nujol) 1729, 1617, 1572, 1461, 1295, 1249, 1171, 1139 cm^{-1}. Elemental analysis: calculated for C$_{16}$H$_{16}$F$_3$NO$_3$ (327.30) % C 58.71; H 4.93; N 4.28; found % C 58.73; H 5.01; N 4.30.

Methyl (*E*)-1-(4-((5,5,5-trifluoro-4-oxopent-2-en-2-yl)amino)phenyl)cyclobutane-1-carboxylate (49)
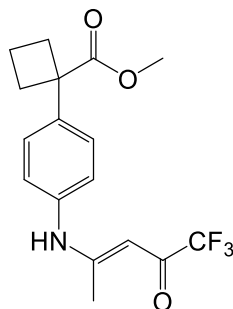
Ester **49** was prepared using the same procedure used to prepare the compound **23**, starting from ester **45**.

Yield 52 %. m.p. 153-157 °C. ^{1}H NMR (DMSO-d$_6$) δ 2.20 (m, 2H, CH$_2$), 2.31 (s, 3H, CH$_3$), 2.49 (m, 2H, CH$_2$), 2.73 (m, 2H, CH$_2$), 3.59 (s, 3H, CH$_3$), 5.64 (s, 1H, CH), 7.23-7.35 (m, 4H, Ar), 12.47 (s, 1H, NH). IR

(Nujol) 3423, 1721, 1571, 1524, 1437, 1366, 1319, 1295, 1248 cm^{-1}.
Elemental analysis: calculated for $C_{17}H_{18}F_3NO_3$ (341.33) % C 59.82; H 5.32; N 4.10; found % C 59.86; H 5.30; N 4.15.

Methyl (*E*)-1-(4-((5,5,5-trifluoro-4-oxopent-2-en-2-yl)amino)phenyl)cyclopentane-1-carboxylate (50)
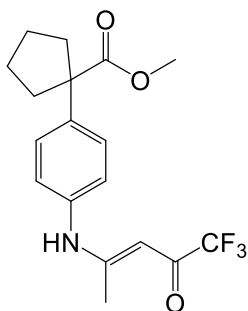
Ester **50** was prepared using the same procedure used to prepare the compound **23**, starting from ester **46**.

Yield 80 %. m.p. 148-152 °C. ^{1}H NMR (DMSO-d$_6$) δ 1.63 (m, 4H, CH$_2$), 1.87 (m, 2H, CH$_2$), 2.49 (m, 2H, CH$_2$), 2.53 (s, 3H, CH$_3$), 3.59 (s, 3H, CH$_3$), 5.64 (s, 1H, CH), 7.31-7.41 (m, 4H, Ar), 12.46 (s, 1H, NH). IR (Nujol) 1720, 1631, 1585, 1525, 1456, 1379, 1364, 1299, 1247 cm^{-1}. Elemental analysis: calculated for $C_{18}H_{20}F_3NO_3$ (355.36) % C 60.84; H 5.67; N 3.94; found % C 60.86; H 5.70; N 4.00.

Methyl (*E*)-1-(4-((5,5,5-trifluoro-4-oxopent-2-en-2-yl)amino)phenyl)cyclohexane-1-carboxylate (51)
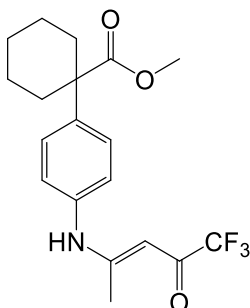
Ester **51** was prepared using the same procedure used to prepare the compound **23**, starting from ester **47**.

Yield 72 %. m.p. 145-147 °C. ^{1}H NMR (DMSO-d$_6$) δ 1.24-1.70 (m, 8H, CH$_2$), 2.19 (m, 2H, CH$_2$) 2.49 (s, 3H, CH$_3$), 3.60 (s, 3H, CH$_3$), 5.64 (s, 1H, CH), 7.33-7.42 (m, 4H, Ar), 12.46 (s, 1H, NH). Elemental analysis: calculated for C$_{19}$H$_{22}$F$_3$NO$_3$ (369.38) % C 61.78; H 6.00; N 3.79; found % C 61.86; H 6.05; N 3.80.

General procedure for the synthesis of esters 52-55

A mixture of ester **48-51** (5 mmol), and DMF-DMA (1.79 g, 15 mmol) in anhydrous toluene (20 mL) was refluxed for 1 h, then allowed to reach the room temperature and stirred for additional 8 h. The mixture was carefully concentrated in vacuum to give the desired dienaminone **52-55**.

Methyl 1-(4-(((1*E*,3*E*)-1-(dimethylamino)-6,6,6-trifluoro-5-oxohexa-1,3-dien-3-yl)amino)phenyl)cyclopropane-1-carboxylate (52)
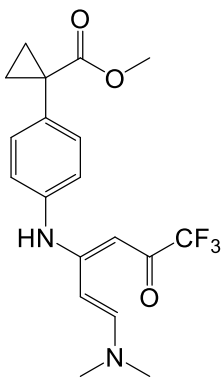
Dienaminone **52** was prepared using the general procedure starting from enaminone **48**.

Yield 70 %. m.p. 100-103 °C. ^{1}H NMR (DMSO-d$_6$) δ 1.45 (m, 2H, CH$_2$), 2.68 (m, 2H, CH$_2$), 2.54 (s, 6H, CH$_3$), 3.79 (s, 3H, CH$_3$), 5.12 (m, 1H, CH), 5.67 (s, 1H, CH), 7.29 (m, 2H, Ar), 7.43 (m, 2H, Ar), 7.78 (m, 1H, CH), 12.56 (s, 1H, NH). IR (Nujol) 3583, 2923, 1691, 1604, 1522, 1461, 1377, 1308, 1183, 1078 cm^{-1}. Elemental analysis: calculated for C$_{19}$H$_{21}$F$_3$N$_2$O$_3$ (382.38) % C 59.68; H 5.54; N 7.33; found % C 59.61; H 5.50; N 7.36.

Methyl 1-(4-(((1*E*,3*E*)-1-(dimethylamino)-6,6,6-trifluoro-5-oxohexa-1,3-dien-3-yl)amino)phenyl)cyclobutane-1-carboxylate (53)
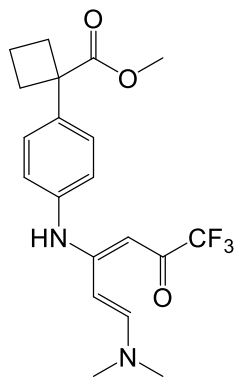
Dienaminone **53** was prepared using the general procedure starting from enaminone **49**.

Yield 64 %. m.p. 93-97 °C. ^{1}H NMR (DMSO-d$_6$) δ 1.82 (m, 2H, CH$_2$), 2.49 (s, 6H, CH$_3$), 3.16 (m, 4H, CH$_2$), 3.59 (s, 3H, CH$_3$), 5.01 (m, 1H, CH), 5.73 (s, 1H, CH), 7.26 (d, J= 7.5 Hz, 2H, Ar), 7.31 (d, J= 7.5 Hz, 2H, Ar), 7.91 (m, 1H, CH), 12.76 (s, 1H, NH). IR (Nujol) 3345, 2855, 1734, 1633, 1572, 1459, 1397, 1272, 1253, 1211 cm^{-1}. Elemental analysis: calculated for C$_{20}$H$_{23}$F$_3$N$_2$O$_3$ (396.41) % C 60.60; H 5.85; N 7.07; found % C 60.65; H 5.90; N 7.10.

Methyl 1-(4-(((1*E*,3*E*)-1-(dimethylamino)-6,6,6-trifluoro-5-oxohexa-1,3-dien-3-yl)amino)phenyl)cyclopentane-1-carboxylate (54)
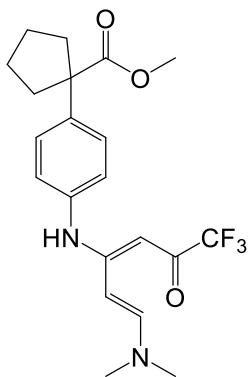
Dienaminone **54** was prepared using the general procedure starting from enaminone **50**.

Yield 62 %. m.p. 90-92 °C. ^{1}H NMR (DMSO-d$_6$) δ 1.60 (m, 2H, CH$_2$), 1.68 (m, 2H, CH$_2$), 1.88 (m, 2H, CH$_2$), 2.53 (m, 2H, CH$_2$), 2.74 (s, 3H, CH$_3$), 3.15 (s, 3H, CH$_3$), 3.56 (s, 3H, CH$_3$), 4.99 (m, 1H, CH), 5.72 (s, 1H, CH), 7.24 (d, J= 8.0 Hz, 2H, Ar), 7.36 (d, J= 8.0 Hz, 2H, Ar), 7.90 (m, 1H, CH), 12.76 (s, 1H, NH). IR (Nujol) 3346, 2924, 1732, 1634, 1574, 1452, 1398, 1273, 1253, 1212 cm^{-1}. Elemental analysis: calculated for C$_{21}$H$_{25}$F$_3$N$_2$O$_3$ (410.44) % C 61.45; H 6.14; N 6.83; found % C 61.50; H 6.20; N 6.88.

Methyl 1-(4-(((1*E*,3*E*)-1-(dimethylamino)-6,6,6-trifluoro-5-oxohexa-1,3-dien-3-yl)amino)phenyl)cyclohexane-1-carboxylate (55)
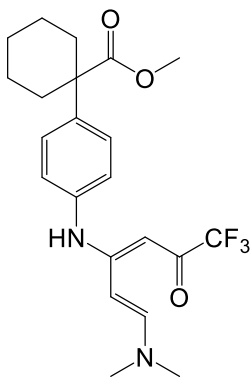
Dienaminone **55** was prepared using the general procedure starting from enaminone **51**.

Yield 53 %. m.p. 88-90 °C. ^{1}H NMR (DMSO-d$_6$) δ 1.35 (m, 4H, CH$_2$), 1.70 (m, 4H, CH$_2$), 2.37 (m, 2H, CH$_2$), 2.74 (s, 3H, CH$_3$), 3.16 (s, 3H, CH$_3$), 3.60 (s, 3H, CH$_3$), 4.98 (m, 1H, CH), 5.72 (s, 1H, CH), 7.25 (d, J= 8.0 Hz, 2H, Ar), 7.38 (d, J= 8.0 Hz, 2H, Ar), 7.90 (m, 1H, CH), 12.74 (s, 1H, NH). IR (Nujol) 3354, 2855, 1731, 1633, 1574, 1459, 1274, 1253, 1214 cm^{-1}. Elemental analysis: calculated for C$_{22}$H$_{27}$F$_3$N$_2$O$_3$ (426.46) % C 62.25; H 6.41; N 6.60; found % C 62.30; H 6.50; N 6.55.

General procedure for the synthesis of acids 60-63

To a solution of dienaminone **52-55** (2 mmol) in dry DMF (5 mL), ammonium acetate (0.308 g, 4 mmol) was added and the mixture was gently refluxed for 1.5 h. The mixture was carefully concentrated in vacuum, and then ice-water (15 mL) was added. The formed solid was dissolved in EtOH (20mL), this solution was added with 5N solution of NaOH (4 mL) and water (4 mL). The resulting mixture was stirred at r.t. for 20 h. After removing EtOH under vacuum ice was added and then aqueous 20% HCl solution until pH 3-4. The formed precipitate was filtered and washed with water and dried.

1-(4-((2-(Trifluoromethyl)pyridin-4-yl)amino)phenyl)cyclopropane-1-carboxylic acid (60)
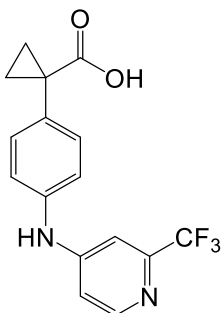
Acid **60** was prepared using the general procedure starting from dienaminone **52**.

Yield 59 %. m.p. 210 °C. ^{1}H NMR (DMSO-d$_6$) δ 1.13 (m, 2H, CH$_2$), 1.45 (m, 2H, CH$_2$), 7.10 (m, 1H, Ar), 7.16 (m, 2H, Ar), 7.23 (m, 1H, Ar), 7.33 (m, 2H, Ar), 8.29 (s, 1H, Ar), 9.34 (s, 1H, NH). IR (Nujol) 3285, 2924, 1677, 1602, 1521, 1480, 1458, 1349, 1307, 1188, 1140 cm^{-1}. Elemental analysis: calculated for C$_{16}$H$_{13}$F$_3$N$_2$O$_2$ (322.29) % C 59.63; H 4.07; N 8.69; found % C 59.66; H 4.09; N 8.72.

1-(4-((2-(Trifluoromethyl)pyridin-4-yl)amino)phenyl)cyclobutane-1-carboxylic acid (61)
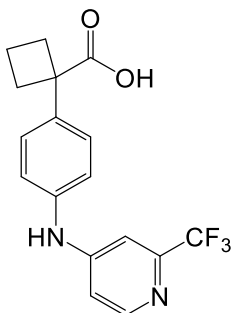
Acid **61** was prepared using the general procedure starting from dienaminone **53**.

Yield 78 %. m.p. 185 °C. ^{1}H NMR (DMSO-d$_6$) δ 1.75-1.96 (m, 2H, CH$_2$), 2.38 (m, 2H, CH$_2$), 2.70 (m, 2H, CH$_2$), 7.08 (m, 1H, Ar), 7.21 (m, 3H, Ar), 7.30 (m, 2H, Ar), 8.28 (s, 1H, Ar), 9.26 (s, 1H, NH). IR (Nujol) 3319,

2855, 1671, 1622, 1606, 1519, 1463, 1302 cm^{-1}. Elemental analysis: calculated for C$_{17}$H$_{15}$F$_3$N$_2$O$_2$ (336.31) % C 60.71; H 4.50; N 8.33; found % C 60.75; H 4.58; N 8.40.

1-(4-((2-(Trifluoromethyl)pyridin-4-yl)amino)phenyl)cyclopentane-1-carboxylic acid (62)
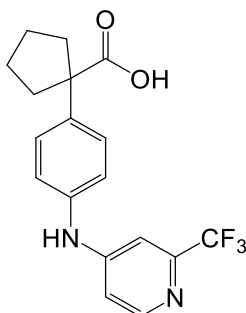
Acid **62** was prepared using the general procedure starting from dienaminone **44**.

Yield 86 %. m.p. >250 °C. ^{1}H NMR (DMSO-d$_6$) δ 1.65 (m, 4H, CH$_2$), 1.79 (m, 4H, CH$_2$), 7.07 (m, 1H, Ar), 7.18 (m, 3H, Ar), 7.34 (m, 2H, Ar), 8.27 (s, 1H, Ar), 9.27 (s, 1H, NH), 12.24 (s, 1H, NH). IR (Nujol) 3301, 2921, 1691, 1618, 1601, 1518, 1462, 1377, 1353 cm^{-1}. Elemental analysis: calculated for C$_{18}$H$_{17}$F$_3$N$_2$O$_2$ (350.34) % C 61.71; H 4.89; N 8.00; found % C 61.75; H 4.92; N 8.10.

1-(4-((2-(Trifluoromethyl)pyridin-4-yl)amino)phenyl)cyclohexane-1-carboxylic acid (63)
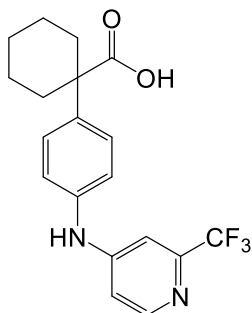
Acid **63** was prepared using the general procedure starting from dienaminone **55**.

Yield 88 %. m.p. >250 °C. ^{1}H NMR (DMSO-d_6) δ 1.22-1.59 (m, 8H, CH$_2$), 2.64 (m, 2H, CH$_2$), 7.07 (m, 1H, Ar), 7.18 (m, 3H, Ar), 7.39 (m, 2H, Ar), 8.27 (s, 1H, Ar), 9.28 (s, 1H, NH). IR (Nujol) 3305, 1687, 1622, 1603, 1523, 1459, 1364, 1320, 1229, 1178 cm^{-1}. Elemental analysis: calculated for C$_{19}$H$_{19}$F$_3$N$_2$O$_2$ (364.37) % C 62.63; H 5.26; N 7.69; found % C 62.65; H 5.29; N 7.70.

N-(3-Methylpyridin-2-yl)-1-(4-((2-(trifluoromethyl)pyridin-4-yl)amino)phenyl)cyclopropane-1-carboxamide (TPA31)
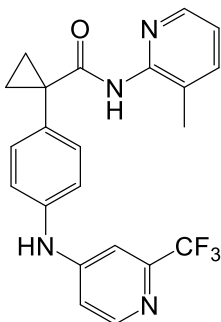
Amide **TPA31** was prepared using the same procedure used for the synthesis of **TPA30**, starting from the acid **60**.

Yield 78 %. m.p. 210 °C. ^{1}H NMR (DMSO-d_6) δ 1.20 (m, 2H, CH$_2$), 1.46 (m, 2H, CH$_2$), 2.10 (s, 3H, CH$_3$), 7.18 (m, 1H, Ar), 7.21 (m, 1H, Ar), 7.24

(m, 3H, Ar), 7.48 (m, 2H, Ar), 7.63 (m, 1H, Ar), 8.19 (s, 1H, Ar), 8.30 (m, 1H, Ar), 8.79 (s, 1H, NH), 9.28 (s, 1H, NH). IR (Nujol) 3401, 3244, 2924, 1688, 1599, 1525, 1445, 1359, 1321, 1175 cm^{-1}. Elemental analysis: calculated for $C_{22}H_{19}F_3N_4O$ (412.42) % C 64.07; H 4.64; N 13.59; found % C 64.09; H 4.70; N 13.50.

N-(3-Methylpyridin-2-yl)-1-(4-((2-(trifluoromethyl)pyridin-4-yl)amino)phenyl)cyclobutane-1-carboxamide (TPA32)
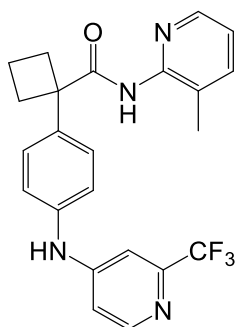
Amide **TPA32** was prepared using the same procedure used to prepare **TPA30**, starting from acid **61**.

Yield 21 %. m.p. 185 °C. ^{1}H NMR (DMSO-d$_6$) δ 1.83-1.98 (m, 6H, CH$_2$), 2.88 (s, 3H, CH$_3$), 7.06 (m, 1H, Ar), 7.19 (m, 2H, Ar), 7.22 (m, 2H, Ar), 7.47 (m, 2H, Ar), 7.61 (m, 1H, Ar), 8.21 (s, 1H, Ar), 8.30 (m, 1H, Ar), 9.22 (s, 1H, NH), 9.70 (s, 1H, NH). IR (Nujol) 3583, 2925, 1652, 1606, 1536, 1462 cm^{-1}. Elemental analysis: calculated for $C_{23}H_{21}F_3N_4O$ (426.44) % C 64.78; H 4.96; N 13.14; found % C 64.82; H 4.92; N 13.20.

N-(3-Methylpyridin-2-yl)-1-(4-((2-(trifluoromethyl)pyridin-4-yl)amino)phenyl)cyclopentane-1-carboxamide (TPA33)
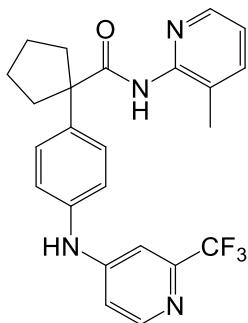
Amide **TPA33** was prepared using the same procedure used for the synthesis of **TPA30**, starting from acid **62**.

Yield 27 %. m.p. >250 °C. ^{1}H NMR (DMSO-d_6) δ 1.69 (m, 4H, CH$_2$), 1.92 (m, 4H, CH$_2$), 2.72 (s, 3H, CH$_3$), 7.05 (m, 1H, Ar), 7.20 (m, 4H, Ar), 7.46 (m, 2H, Ar), 7.58 (m, 1H, Ar), 8.19 (s, 1H, Ar), 8.27 (m, 1H, Ar), 9.22 (s, 1H, NH), 9.51 (s, 1H, NH). IR (Nujol) 3583, 3201, 2926, 1650, 1607, 1535, 1460, 1377, 1185 cm^{-1}. Elemental analysis: calculated for C$_{24}$H$_{23}$F$_3$N$_4$O (440.47) % C 65.44; H 5.26; N 12.72; found % C 65.46; H 5.20; N 12.76.

N-(3-Methylpyridin-2-yl)-1-(4-((2-(trifluoromethyl)pyridin-4-yl)amino)phenyl)cyclohexane-1-carboxamide (TPA34)
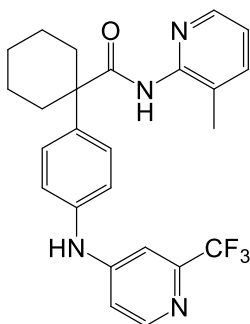
Amide **TPA34** was prepared using the same procedure used for the synthesis of **TPA30**, starting from acid **63**.

Yield 55 %. m.p. >250 °C. ^{1}H NMR (DMSO-d$_6$) δ 1.53-1.75 (m, 8H, CH$_2$), 1.97 (s, 3H, CH$_3$), 2.59 (m, 2H, CH$_2$), 7.07-7.24 (m, 5H, Ar), 7.49 (m, 2H, Ar), 7.62 (m, 1H, Ar), 8.20 (s, 1H, Ar), 8.27 (m, 1H, Ar), 9.45 (s, 1H, NH), 9.47 (s, 1H, NH). IR (Nujol) 3583, 3288, 2925, 1645, 1606, 1462, 1377, 1180 cm^{-1}. Elemental analysis: calculated for C$_{25}$H$_{25}$F$_3$N$_4$O (454.50) % C 66.07; H 5.54; N 12.33; found % C 66.10; H 5.60; N 12.42.

2-(4-Aminophenyl)propanoic acid (64)
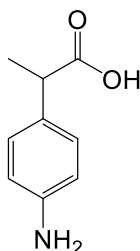
To a solution of the ester **21** (1.79 g, 10 mmol) in EtOH (50 mL) 5N solution of NaOH (20 mL) and water (20 mL) were added. The resulting mixture was stirred at r.t. for 24h. After removing EtOH under vacuum to the resulting solution ice was added and then aqueous 20% HCl solution until pH 3-4. The formed precipitate was filtered, washed with water, dried and re-crystallized from EtOH.

Yield 97 %. m.p. 120-125 °C. ^{1}H NMR (DMSO-d$_6$) δ 1.26 (d, J= 7.0 Hz, 3H, CH$_3$), 3.43 (q, J= 7.0 Hz, 1H, CH), 6.48 (d, J= 8.5 Hz, 2H, Ar), 6.90 (d, J= 8.5 Hz, 2H, Ar). IR (Nujol) 2854, 2610, 2188, 1632, 1591, 1514, 1460, 1380, 1361 cm^{-1}. Elemental analysis: calculated for C$_9$H$_{11}$NO$_2$ (165.19) % C 65.44; H 6.71; N 8.48; found % C 65.50; H 6.72; N 8.52.

General procedure for the synthesis of acids 65-66

A solution of acid **64** (0.34 g, 2 mmol) in EtOH (40 mL) was added with the appropriate 4-chloroquinoline (2 mmol) and refluxed for 24 h. Then the solvent was removed under vacuum and the formed solid was filtered treated with iPr$_2$O, filtered and dried.

2-(4-((8-(Trifluoromethyl)quinolin-4-yl)amino)phenyl)propanoic acid (65)
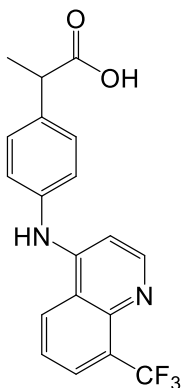
Obtained with the general procedure starting from 4-chloro-8-trifluoromethylquinoline.

Yield 89 %. m.p. 155-160 °C. ^{1}H NMR (DMSO-d$_6$) δ 1.42 (m, 3H, CH$_3$), 4.09 (m, 1H, CH), 6.93 (m, 1H, Ar), 7.45 (m, 4H, Ar), 7.87 (m, 1H, Ar), 8.38 (m, 1H, Ar), 8.46 (m, 1H, Ar), 9.08 (m, 1H, Ar). IR (Nujol) 2926, 1726, 1619, 1589, 1544, 1511, 1463, 1377, 1343, 1315 cm^{-1}. Elemental analysis: calculated for C$_{19}$H$_{15}$F$_3$N$_2$O$_2$ (360.34) % C 63.33; H 4.20; N 7.77; found % C 63.40; H 4.22; N 7.80.

2-(4-((7-(Trifluoromethyl)quinolin-4-yl)amino)phenyl)propanoic acid (66)
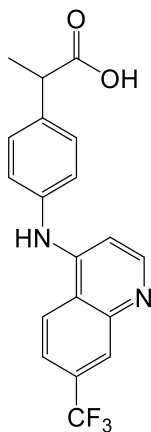
Obtained with the general procedure starting from 4-chloro-7-trifluoromethylquinoline.

Yield 87 %. m.p. 160-165 °C. ^{1}H NMR (DMSO-d_6) δ 1.41 (m, 3H, CH$_3$), 3.80 (m, 1H, CH), 6.90 (m, 1H, Ar), 7.44 (m, 2H, Ar), 7.49 (m, 2H, Ar), 8.12 (m, 1H, Ar), 8.45 (m, 1H, Ar), 8.60 (m, 1H, Ar), 9.03 (m, 1H, Ar), 11.16, (s, 1H, NH), 12.40 (s, 1H, OH). IR (Nujol) 2960, 1720, 1598, 1542, 1511, 1459, 1377, 1319, 1212 cm^{-1}. Elemental analysis: calculated for C$_{19}$H$_{15}$F$_3$N$_2$O$_2$ (360.34) % C 63.33; H 4.20; N 7.77; found % C 63.30; H 4.25; N 7.71.

General procedure for the synthesis of amides TPA35-36

A solution of acid **65-66** (0.36 g, 1 mmol), EDC (0.19 g, 1.1 mmol) and HOBt (0.13 g, 1 mmol) in anhydrous MeCN (10 mL) was stirred at r.t. for 30 minutes, then 2-amino-3-methylpyridine (0.108 g, 1 mmol) was added. The mixture was stirred at r.t. for 36 hours. The solvent was removed under vacuum. The residue was dissolved in AcOEt (20 mL) and washed sequentially with brine (2x5 mL), 10% citric acid (2x5 mL), saturated NaHCO$_3$ aqueous solution (2x5 mL) and water (2x5 mL). The organic layer was dried over anhydrous Na$_2$SO$_4$ and evaporated under vacuum. The obtained residue was treated with iPr$_2$O and the obtained solid filtered off.

N-(3-Methylpyridin-2-yl)-2-(4-((7-(trifluoromethyl)quinolin-4-yl)amino)phenyl)propanamide (TPA35)
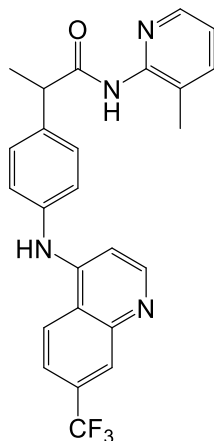
Obtained with the procedure used for the synthesis of **TPA30** starting from acid **65**.

Yield 83 %. m.p. 113 °C. ^{1}H NMR (DMSO-d$_6$) δ 1.45 (d, J= 6.5 Hz, 3H, CH$_3$), 2.01 (s, 3H, CH$_3$), 3.96 (q, J= 6.5 Hz, 1H, CH), 6.95-9.20 (m, 12H, Ar), 10.17 (s, 1H, NH). IR (Nujol) 1671, 1587, 1514, 1460, 1377, 1311 cm^{-1}. Elemental analysis: calculated for C$_{25}$H$_{21}$F$_3$N$_4$O (450.17) % C 66.66; H 4.70; N 12.44; found % C 66.70; H 4.75; N 12.50.

N-(3-Methylpyridin-2-yl)-2-(4-((8-(trifluoromethyl)quinolin-4-yl)amino)phenyl)propanamide (TPA36)
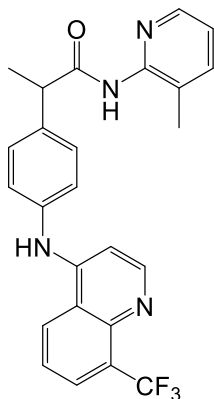
Obtained with the procedure used for the synthesis of **TPA30** starting from acid **66**.

Yield 78 %. m.p. 231 °C. ^{1}H NMR (DMSO-d_6) δ 1.40 (d, J= 6.5 Hz, 3H, CH$_3$), 2.02 (s, 3H, CH$_3$), 3.97 (q, J= 6.5 Hz, 1H, CH), 6.98-9.19 (m, 12H, Ar), 10.16 (s, 1H, NH), 12.31 (s, 1H, NH). IR (Nujol) 1663, 1583, 1536, 1460, 1378, 1329, 1155, 1121 cm^{-1}. Elemental analysis: calculated for C$_{25}$H$_{21}$F$_3$N$_4$O (450.17) % C 66.66; H 4.70; N 12.44; found % C 66.69; H 4.72; N 12.42.

2.10 References

1 Gaoni, Y. & Mechoulam, R. Isolation and structure of .DELTA.+-tetrahydrocannabinol and other neutral cannabinoids from hashish. *Journal of the American Chemical Society* **93**, 217-224, doi:10.1021/ja00730a036 (1971).

2 Devane, W. A., Dysarz, F. A., Johnson, M. R., Melvin, L. S. & Howlett, A. C. Determination and characterization of a cannabinoid receptor in rat brain. *Molecular Pharmacology* **34**, 605-613 (1988).

3 Matsuda, L. A., Lolait, S. J., Brownstein, M. J., Young, A. C. & Bonner, T. I. Structure of a cannabinoid receptor and functional expression of the cloned cDNA. *Nature* **346**, 561-564 (1990).

4 Munro, S., Thomas, K. L. & Abu-Shaar, M. Molecular characterization of a peripheral receptor for cannabinoids. *Nature* **365**, 61-65 (1993).

5 Ameri, A. The effects of cannabinoids on the brain. *Progress in Neurobiology* **58**, 315-348, doi:http://dx.doi.org/10.1016/S0301-0082(98)00087-2 (1999).

6 Mackie, K. & Hille, B. Cannabinoids inhibit N-type calcium channels in neuroblastoma-glioma cells. *Proceedings of the National Academy of Sciences of the United States of America* **89**, 3825-3829 (1992).

7 Mackie, K., Lai, Y., Westenbroek, R. & Mitchell, R. Cannabinoids activate an inwardly rectifying potassium conductance and inhibit Q-type calcium currents in AtT20 cells transfected with rat brain cannabinoid receptor. *The Journal of Neuroscience* **15**, 6552-6561 (1995).

8 Howlett, A. C. Efficacy in CB1 receptor-mediated signal transduction. *British Journal of Pharmacology* **142**, 1209-1218, doi:10.1038/sj.bjp.0705881 (2004).

9 Chen, J., Matias, I., Dinh, T., Lu, T., Venezia, S., Nieves, A., Woodward, D. F. & Di Marzo, V. Finding of endocannabinoids in human eye tissues: Implications for glaucoma. *Biochemical and Biophysical Research Communications* **330**, 1062-1067, doi:http://dx.doi.org/10.1016/j.bbrc.2005.03.095 (2005).

10 Farquhar-Smith, W. P., Egertová, M., Bradbury, E. J., McMahon, S. B., Rice, A. S. C. & Elphick, M. R. Cannabinoid CB1 Receptor Expression in Rat Spinal Cord. *Molecular and Cellular Neuroscience* **15**, 510-521, doi:http://dx.doi.org/10.1006/mcne.2000.0844 (2000).

11   Pertwee, R. G. Evidence for the presence of CB1 cannabinoid receptors on peripheral neurones and for the existence of neuronal non-CB1 cannabinoid receptors. *Life Sciences* **65**, 597-605, doi:http://dx.doi.org/10.1016/S0024-3205(99)00282-9 (1999).

12   Herkenham, M., Lynn, A., Johnson, M., Melvin, L., de Costa, B. & Rice, K. Characterization and localization of cannabinoid receptors in rat brain: a quantitative in vitro autoradiographic study. *The Journal of Neuroscience* **11**, 563-583 (1991).

13   Parolaro, D. Presence and functional regulation of cannabinoid receptors in immune cells. *Life Sciences* **65**, 637-644, doi:http://dx.doi.org/10.1016/S0024-3205(99)00286-6 (1999).

14   Cabral, G. A., Raborn, E. S., Griffin, L., Dennis, J. & Marciano-Cabral, F. CB2 receptors in the brain: role in central immune function. *British Journal of Pharmacology* **153**, 240-251, doi:10.1038/sj.bjp.0707584 (2008).

15   Van Sickle, M. D., Duncan, M., Kingsley, P. J., Mouihate, A., Urbani, P., Mackie, K., Stella, N., Makriyannis, A., Piomelli, D., Davison, J. S., Marnett, L. J., Di Marzo, V., Pittman, Q. J., Patel, K. D. & Sharkey, K. A. Identification and Functional Characterization of Brainstem Cannabinoid CB2 Receptors. *Science* **310**, 329-332, doi:10.1126/science.1115740 (2005).

16   Di Marzo, V., Breivogel, C. S., Tao, Q., Bridgen, D. T., Razdan, R. K., Zimmer, A. M., Zimmer, A. & Martin, B. R. Levels, Metabolism, and Pharmacological Activity of Anandamide in CB1 Cannabinoid Receptor Knockout Mice. *Journal of Neurochemistry* **75**, 2434-2444, doi:10.1046/j.1471-4159.2000.0752434.x (2000).

17   Penumarti, A. & Abdel-Rahman, A. A. The Novel Endocannabinoid Receptor GPR18 Is Expressed in the Rostral Ventrolateral Medulla and Exerts Tonic Restraining Influence on Blood Pressure. *The Journal of Pharmacology and Experimental Therapeutics* **349**, 29-38, doi:10.1124/jpet.113.209213 (2014).

18   Moriconi, A., Cerbara, I., Maccarrone, M. & Topai, A. GPR55: Current Knowledge and Future Perspectives of a Purported “Type-3” Cannabinoid Receptor. *Current Medicinal Chemistry* **17**, 1411-1429, doi:10.2174/092986710790980069 (2010).

19   Devane, W., Hanus, L., Breuer, A., Pertwee, R., Stevenson, L., Griffin, G., Gibson, D., Mandelbaum, A., Etinger, A. & Mechoulam, R. Isolation and structure of a brain constituent that binds to the cannabinoid receptor. *Science* **258**, 1946-1949, doi:10.1126/science.1470919 (1992).

20   Mechoulam, R., Ben-Shabat, S., Hanus, L., Ligumsky, M., Kaminski, N. E., Schatz, A. R., Gopher, A., Almog, S., Martin, B. R., Compton, D. R., Pertwee, R. G., Griffin, G., Bayewitch, M., Barg, J. & Vogel, Z. Identification of an endogenous 2-monoglyceride, present in canine gut, that binds to cannabinoid receptors. *Biochemical Pharmacology* **50**, 83-90, doi:http://dx.doi.org/10.1016/0006-2952(95)00109-D (1995).

21   Hanuš, L., Abu-Lafi, S., Fride, E., Breuer, A., Vogel, Z., Shalev, D. E., Kustanovich, I. & Mechoulam, R. 2-Arachidonyl glyceryl ether, an endogenous agonist of the cannabinoid CB1 receptor. *Proceedings of the National Academy of Sciences* **98**, 3662-3665, doi:10.1073/pnas.061029898 (2001).

22   Porter, A. C., Sauer, J.-M., Knierman, M. D., Becker, G. W., Berna, M. J., Bao, J., Nomikos, G. G., Carter, P., Bymaster, F. P., Leese, A. B. & Felder, C. C. Characterization of a Novel Endocannabinoid, Virodhamine, with Antagonist Activity at the CB1 Receptor. *Journal of Pharmacology and Experimental Therapeutics* **301**, 1020-1024, doi:10.1124/jpet.301.3.1020 (2002).

23   Rodriguez de Fonseca, F., Navarro, M., Gomez, R., Escuredo, L., Nava, F., Fu, J., Murillo-Rodriguez, E., Giuffrida, A., LoVerme, J., Gaetani, S., Kathuria, S., Gall, C. & Piomelli, D. An anorexic lipid mediator regulated by feeding. *Nature* **414**, 209-212, doi:http://www.nature.com/nature/journal/v414/n6860/suppinfo/414209a0_S1.html (2001).

24   Bisogno, T., Melck, D., Bobrov, M. Y., Gretskaya, N. M., Bezuglov, V. V., De Petrocellis, L. & Di Marzo, V. N-acyl-dopamines: novel synthetic CB1 cannabinoid-receptor ligands and inhibitors of anandamide inactivation with cannabimimetic activity in vitro and in vivo. *Biochemical Journal* **351**, 817-824, doi:10.1042/bj3510817 (2000).

25   Huang, S. M., Bisogno, T., Trevisani, M., Al-Hayani, A., De Petrocellis, L., Fezza, F., Tognetto, M., Petros, T. J., Krey, J. F., Chu, C. J., Miller, J. D., Davies, S. N., Geppetti, P., Walker, J. M. & Di Marzo, V. An endogenous capsaicin-like substance with high potency at recombinant and native vanilloid VR1 receptors. *Proceedings of the National Academy of Sciences* **99**, 8400-8405, doi:10.1073/pnas.122196999 (2002).

26   Christie, M. J. & Vaughan, C. W. Neurobiology: Cannabinoids act backwards. *Nature* **410**, 527-530 (2001).

27   Tian, X., Guo, J., Yao, F., Yang, D.-P. & Makriyannis, A. The Conformation, Location, and Dynamic Properties of the

Endocannabinoid Ligand Anandamide in a Membrane Bilayer. *Journal of Biological Chemistry* **280**, 29788-29795, doi:10.1074/jbc.M502925200 (2005).

28   Hermann, A., Kaczocha, M. & Deutsch, D. G. 2-Arachidonoylglycerol (2-AG) membrane transport: History and outlook. *The AAPS Journal* **8**, E409-E412, doi:10.1007/BF02854913 (2006).

29   Cravatt, B. F., Giang, D. K., Mayfield, S. P., Boger, D. L., Lerner, R. A. & Gilula, N. B. Molecular characterization of an enzyme that degrades neuromodulatory fatty-acid amides. *Nature* **384**, 83-87 (1996).

30   Goparaju, S., Ueda, N., Taniguchi, K. & Yamamoto, S. Enzymes of porcine brain hydrolyzing 2-arachidonoylglycerol, an endogenous ligand of cannabinoid receptors. *Biochemical Pharmacology* **57**, 417-423, doi:http://dx.doi.org/10.1016/S0006-2952(98)00314-1 (1999).

31   Yu, M., Ives, D. & Ramesha, C. S. Synthesis of Prostaglandin E2 Ethanolamide from Anandamide by Cyclooxygenase-2. *Journal of Biological Chemistry* **272**, 21181-21186, doi:10.1074/jbc.272.34.21181 (1997).

32   Kozak, K. R., Prusakiewicz, J. J. & Marnett, L. J. Oxidative Metabolism of Endocannabinoids by COX-2. *Current Pharmaceutical Design* **10**, 659-667, doi:10.2174/1381612043453081 (2004).

33   Burkey, T. H., Quock, R. M., Consroe, P., Ehlert, F. J., Hosohata, Y., Roeske, W. R. & Yamamura, H. I. Relative efficacies of cannabinoid CB1 receptor agonists in the mouse brain. *European Journal of Pharmacology* **336**, 295-298, doi:http://dx.doi.org/10.1016/S0014-2999(97)01255-7 (1997).

34   Glass, M. & Northup, J. K. Agonist Selective Regulation of G Proteins by Cannabinoid CB1 and CB2 Receptors. *Molecular Pharmacology* **56**, 1362-1369, doi:10.1124/mol.56.6.1362 (1999).

35   Di Marzo, V., Fontana, A., Cadas, H., Schinelli, S., Cimino, G., Schwartz, J.-C. & Piomelli, D. Formation and inactivation of endogenous cannabinoid anandamide in central neurons. *Nature* **372**, 686-691 (1994).

36   Sun, Y.-X., Tsuboi, K., Okamoto, Y., Tonai, T., Murakami, M., Kudo, I. & Ueda, N. Biosynthesis of anandamide and N-palmitoylethanolamine by sequential actions of phospholipase A2 and lysophospholipase D. *Biochemical Journal* **380**, 749-756, doi:10.1042/bj20040031 (2004).

37   Sugiura, T., Kondo, S., Sukagawa, A., Tonegawa, T., Nakane, S., Yamashita, A., Ishima, Y. & Waku, K. Transacylase-Mediated and

Phosphodiesterase-Mediated Synthesis of N-Arachidonoylethanolamine, an Endogenous Cannabinoid-Receptor Ligand, in Rat Brain Microsomes. *European Journal of Biochemistry* **240**, 53-62, doi:10.1111/j.1432-1033.1996.0053h.x (1996).

38   Bisogno, T., Sepe, N., Melck, D., Maurelli, S., De Petrocellis, L. & Di Marzo, V. Biosynthesis, release and degradation of the novel endogenous cannabimimetic metabolite 2-arachidonoylglycerol in mouse neuroblastoma cells. *Biochemical Journal* **322**, 671-677 (1997).

39   Stella, N., Schweitzer, P. & Piomelli, D. A second endogenous cannabinoid that modulates long-term potentiation. *Nature* **388**, 773-778 (1997).

40   Bisogno, T., Melck, D., De Petrocellis, L. & Di Marzo, V. Phosphatidic Acid as the Biosynthetic Precursor of the Endocannabinoid 2-Arachidonoylglycerol in Intact Mouse Neuroblastoma Cells Stimulated with Ionomycin. *Journal of Neurochemistry* **72**, 2113-2119, doi:10.1046/j.1471-4159.1999.0722113.x (1999).

41   Thomas, E. A., Cravatt, B. F., Danielson, P. E., Gilula, N. B. & Sutcliffe, J. G. Fatty acid amide hydrolase, the degradative enzyme for anandamide and oleamide, has selective distribution in neurons within the rat central nervous system. *Journal of Neuroscience Research* **50**, 1047-1052, doi:10.1002/(SICI)1097-4547(19971215)50:6<1047::AID-JNR16>3.0.CO;2-1 (1997).

42   Chebrou, H., Bigey, F., Arnaud, A. & Galzy, P. Study of the amidase signature group. *Biochimica et Biophysica Acta (BBA) - Protein Structure and Molecular Enzymology* **1298**, 285-293, doi:http://dx.doi.org/10.1016/S0167-4838(96)00145-8 (1996).

43   Patricelli, M. P. & Cravatt, B. F. Characterization and Manipulation of the Acyl Chain Selectivity of Fatty Acid Amide Hydrolase†. *Biochemistry* **40**, 6107-6115, doi:10.1021/bi002578r (2001).

44   Lodola, A., Mor, M., Hermann, J. C., Tarzia, G., Piomelli, D. & Mulholland, A. J. QM/MM modelling of oleamide hydrolysis in fatty acid amide hydrolase (FAAH) reveals a new mechanism of nucleophile activation. *Chemical Communications*, 4399-4401, doi:10.1039/B503887A (2005).

45   Tubert-Brohman, I., Acevedo, O. & Jorgensen, W. L. Elucidation of Hydrolysis Mechanisms for Fatty Acid Amide Hydrolase and Its Lys142Ala Variant via QM/MM Simulations. *Journal of the American Chemical Society* **128**, 16904-16913, doi:10.1021/ja065863s (2006).

46   Starowicz, K. & Di Marzo, V. Non-psychotropic analgesic drugs from the endocannabinoid system: "Magic bullet" or "multiple-target"

strategies? *European Journal of Pharmacology* **716**, 41-53, doi:http://dx.doi.org/10.1016/j.ejphar.2013.01.075 (2013).

47   Manzanares, J., Julian, M. D. & Carrascosa, A. Role of the Cannabinoid System in Pain Control and Therapeutic Implications for the Management of Acute and Chronic Pain Episodes. *Current Neuropharmacology* **4**, 239-257 (2006).

48   Di Marzo, V., Hill, M. P., Bisogno, T., Crossman, A. R. & Brotchie, J. M. Enhanced levels of endogenous cannabinoids in the globus pallidus are associated with a reduction in movement in an animal model of Parkinson's disease. *The FASEB Journal* **14**, 1432-1438, doi:10.1096/fj.14.10.1432 (2000).

49   Pazos, M. R., Núñez, E., Benito, C., Tolón, R. M. & Romero, J. Role of the endocannabinoid system in Alzheimer's disease: New perspectives. *Life Sciences* **75**, 1907-1915, doi:http://dx.doi.org/10.1016/j.lfs.2004.03.026 (2004).

50   Pacher, P., Bátkai, S. & Kunos, G. The Endocannabinoid System as an Emerging Target of Pharmacotherapy. *Pharmacological Reviews* **58**, 389-462, doi:10.1124/pr.58.3.2 (2006).

51   Walker, J. M. & Hohmann, A. G. in *Cannabinoids* Vol. 168 *Handbook of Experimental Pharmacology* (ed RogerG Pertwee) Ch. 17, 509-554 (Springer Berlin Heidelberg, 2005).

52   Jimenez-Del-Rio, M., Daza-Restrepo, A. & Velez-Pardo, C. The cannabinoid CP55,940 prolongs survival and improves locomotor activity in Drosophila melanogaster against paraquat: Implications in Parkinson's disease. *Neuroscience Research* **61**, 404-411, doi:http://dx.doi.org/10.1016/j.neures.2008.04.011 (2008).

53   Bridges, D., Ahmad, K. & Rice, A. S. C. The synthetic cannabinoid WIN55,212-2 attenuates hyperalgesia and allodynia in a rat model of neuropathic pain. *British Journal of Pharmacology* **133**, 586-594, doi:10.1038/sj.bjp.0704110 (2001).

54   Justinova, Z., Solinas, M., Tanda, G., Redhi, G. H. & Goldberg, S. R. The Endogenous Cannabinoid Anandamide and Its Synthetic Analog R(+)-Methanandamide Are Intravenously Self-Administered by Squirrel Monkeys. *The Journal of Neuroscience* **25**, 5645-5650, doi:10.1523/jneurosci.0951-05.2005 (2005).

55   Berlach, D. M., Shir, Y. & Ware, M. A. Experience with the Synthetic Cannabinoid Nabilone in Chronic Noncancer Pain. *Pain Medicine* **7**, 25-29, doi:10.1111/j.1526-4637.2006.00085.x (2006).

56   Calhoun, S. R., Galloway, G. P. & Smith, D. E. Abuse Potential of Dronabinol (Marinol®). *Journal of Psychoactive Drugs* **30**, 187-196, doi:10.1080/02791072.1998.10399689 (1998).

_____

57   Atwood, B. K., Straiker, A. & Mackie, K. CB(2): Therapeutic target-in-waiting. *Progress in neuro-psychopharmacology & biological psychiatry* **38**, 16-20, doi:10.1016/j.pnpbp.2011.12.001 (2012).

58   Kohnz, R. A. & Nomura, D. K. Chemical approaches to therapeutically target the metabolism and signaling of the endocannabinoid 2-AG and eicosanoids. *Chemical Society Reviews* **43**, 6859-6869, doi:10.1039/C4CS00047A (2014).

59   Deutsch, D. G. & Chin, S. A. Enzymatic synthesis and degradation of anandamide, a cannabinoid receptor agonist. *Biochemical Pharmacology* **46**, 791-796, doi:http://dx.doi.org/10.1016/0006-2952(93)90486-G (1993).

60   Deutsch, D. G., Omeir, R., Arreaza, G., Salehani, D., Prestwich, G. D., Huang, Z. & Howlett, A. Methyl arachidonyl fluorophosphonate: a potent irreversible inhibitor of anandamide amidase. *Biochemical Pharmacology* **53**, 255-260, doi:http://dx.doi.org/10.1016/S0006-2952(96)00830-1 (1997).

61   Bracey, M. H., Hanson, M. A., Masuda, K. R., Stevens, R. C. & Cravatt, B. F. Structural Adaptations in a Membrane Enzyme That Terminates Endocannabinoid Signaling. *Science* **298**, 1793-1796 (2002).

62   Koutek, B., Prestwich, G. D., Howlett, A. C., Chin, S. A., Salehani, D., Akhavan, N. & Deutsch, D. G. Inhibitors of arachidonoyl ethanolamide hydrolysis. *Journal of Biological Chemistry* **269**, 22937-22940 (1994).

63   Boger, D. L., Fecik, R. A., Patterson, J. E., Miyauchi, H., Patricelli, M. P. & Cravatt, B. F. Fatty acid amide hydrolase substrate specificity. *Bioorganic & Medicinal Chemistry Letters* **10**, 2613-2616, doi:http://dx.doi.org/10.1016/S0960-894X(00)00528-X (2000).

64   Boger, D. L., Sato, H., Lerner, A. E., Hedrick, M. P., Fecik, R. A., Miyauchi, H., Wilkie, G. D., Austin, B. J., Patricelli, M. P. & Cravatt, B. F. Exceptionally potent inhibitors of fatty acid amide hydrolase: The enzyme responsible for degradation of endogenous oleamide and anandamide. *Proceedings of the National Academy of Sciences of the United States of America* **97**, 5044-5049 (2000).

65   Boger, D. L., Miyauchi, H., Du, W., Hardouin, C., Fecik, R. A., Cheng, H., Hwang, I., Hedrick, M. P., Leung, D., Acevedo, O., Guimarães, C. R. W., Jorgensen, W. L. & Cravatt, B. F. Discovery of a Potent, Selective, and Efficacious Class of Reversible α-Ketoheterocycle Inhibitors of Fatty Acid Amide Hydrolase Effective as Analgesics. *Journal of Medicinal Chemistry* **48**, 1849-1856, doi:10.1021/jm049614v (2005).

_____

66   Hardouin, C., Kelso, M. J., Romero, F. A., Rayl, T. J., Leung, D., Hwang, I., Cravatt, B. F. & Boger, D. L. Structure−Activity Relationships of α-Ketooxazole Inhibitors of Fatty Acid Amide Hydrolase. *Journal of Medicinal Chemistry* **50**, 3359-3368, doi:10.1021/jm061414r (2007).

67   Lichtman, A. H., Leung, D., Shelton, C. C., Saghatelian, A., Hardouin, C., Boger, D. L. & Cravatt, B. F. Reversible Inhibitors of Fatty Acid Amide Hydrolase That Promote Analgesia: Evidence for an Unprecedented Combination of Potency and Selectivity. *Journal of Pharmacology and Experimental Therapeutics* **311**, 441-448, doi:10.1124/jpet.104.069401 (2004).

68   Bisogno, T., Melck, D., De Petrocellis, L., Bobrov, M. Y., Gretskaya, N. M., Bezuglov, V. V., Sitachitta, N., Gerwick, W. H. & Marzo, V. D. Arachidonoylserotonin and Other Novel Inhibitors of Fatty Acid Amide Hydrolase. *Biochemical and Biophysical Research Communications* **248**, 515-522, doi:http://dx.doi.org/10.1006/bbrc.1998.8874 (1998).

69   Di Marzo, V., Bisogno, T., De Petrocellis, L., Melck, D., Orlando, P., Wagner, J. A. & Kunos, G. Biosynthesis and inactivation of the endocannabinoid 2-arachidonoylglycerol in circulating and tumoral macrophages. *European Journal of Biochemistry* **264**, 258-267, doi:10.1046/j.1432-1327.1999.00631.x (1999).

70   Jarrahian, A., Manna, S., Edgemond, W. S., Campbell, W. B. & Hillard, C. J. Structure—Activity Relationships Among N-Arachidonylethanolamine (Anandamide) Head Group Analogues for the Anandamide Transporter. *Journal of Neurochemistry* **74**, 2597-2606, doi:10.1046/j.1471-4159.2000.0742597.x (2000).

71   Maione, S., De Petrocellis, L., de Novellis, V., Moriello, A. S., Petrosino, S., Palazzo, E., Rossi, F. S., Woodward, D. F. & Di Marzo, V. Analgesic actions of N-arachidonoyl-serotonin, a fatty acid amide hydrolase inhibitor with antagonistic activity at vanilloid TRPV1 receptors. *British Journal of Pharmacology* **150**, 766-781, doi:10.1038/sj.bjp.0707145 (2007).

72   Jonsson, K.-O., Vandevoorde, S., Lambert, D. M., Tiger, G. & Fowler, C. J. Effects of homologues and analogues of palmitoylethanolamide upon the inactivation of the endocannabinoid anandamide. *British Journal of Pharmacology* **133**, 1263-1275, doi:10.1038/sj.bjp.0704199 (2001).

73   Di Marzo, V., Griffin, G., De Petrocellis, L., Brandi, I., Bisogno, T., Williams, W., Grier, M. C., Kulasegram, S., Mahadevan, A., Razdan, R. K. & Martin, B. R. A Structure/Activity Relationship Study on

Arvanil, an Endocannabinoid and Vanilloid Hybrid. *Journal of Pharmacology and Experimental Therapeutics* **300**, 984-991, doi:10.1124/jpet.300.3.984 (2002).

74   Mor, M., Rivara, S., Lodola, A., Plazzi, P. V., Tarzia, G., Duranti, A., Tontini, A., Piersanti, G., Kathuria, S. & Piomelli, D. Cyclohexylcarbamic Acid 3'- or 4'-Substituted Biphenyl-3-yl Esters as Fatty Acid Amide Hydrolase Inhibitors: Synthesis, Quantitative Structure–Activity Relationships, and Molecular Modeling Studies. *Journal of Medicinal Chemistry* **47**, 4998-5008, doi:10.1021/jm031140x (2004).

75   Alexander, J. P. & Cravatt, B. F. Mechanism of Carbamate Inactivation of FAAH: Implications for the Design of Covalent Inhibitors and In Vivo Functional Probes for Enzymes. *Chemistry & biology* **12**, 1179-1187, doi:10.1016/j.chembiol.2005.08.011 (2005).

76   Jayamanne, A., Greenwood, R., Mitchell, V. A., Aslan, S., Piomelli, D. & Vaughan, C. W. Actions of the FAAH inhibitor URB597 in neuropathic and inflammatory chronic pain models. *British Journal of Pharmacology* **147**, 281-288, doi:10.1038/sj.bjp.0706510 (2006).

77   Kathuria, S., Gaetani, S., Fegley, D., Valino, F., Duranti, A., Tontini, A., Mor, M., Tarzia, G., Rana, G. L., Calignano, A., Giustino, A., Tattoli, M., Palmery, M., Cuomo, V. & Piomelli, D. Modulation of anxiety through blockade of anandamide hydrolysis. *Nat Med* **9**, 76-81 (2003).

78   Moore, S. A., Nomikos, G. G., Dickason-Chesterfield, A. K., Schober, D. A., Schaus, J. M., Ying, B.-P., Xu, Y.-C., Phebus, L., Simmons, R. M. A., Li, D., Iyengar, S. & Felder, C. C. Identification of a high-affinity binding site involved in the transport of endocannabinoids. *Proceedings of the National Academy of Sciences of the United States of America* **102**, 17852-17857, doi:10.1073/pnas.0507470102 (2005).

79   Alexander, J. P. & Cravatt, B. F. The Putative Endocannabinoid Transport Blocker LY2183240 Is a Potent Inhibitor of FAAH and Several Other Brain Serine Hydrolases. *Journal of the American Chemical Society* **128**, 9699-9704, doi:10.1021/ja062999h (2006).

80   Matsumoto, T., Kori, M., Miyazaki, J. & Kiyota, Y. Preparation of piperidinecarboxamides and piperazinecarboxamides as fatty acid amide hydrolase (FAAH) inhibitors. WO2006054652A1 (2006).

81   Apodaca, R., Breitenbucher, J. G., Pattabiraman, K., Seierstad, M. & Xiao, W. Preparation of thiadiazolylpiperazinecarboxamides as modulators of fatty acid amide hydrolase (FAAH). US20070004741A1 (2007).

82   Keith, J. M., Apodaca, R., Xiao, W., Seierstad, M., Pattabiraman, K., Wu, J., Webb, M., Karbarz, M. J., Brown, S., Wilson, S., Scott, B., Tham, C.-S., Luo, L., Palmer, J., Wennerholm, M., Chaplan, S. & Breitenbucher, J. G. Thiadiazolopiperazinyl ureas as inhibitors of fatty acid amide hydrolase. *Bioorganic & Medicinal Chemistry Letters* **18**, 4838-4843, doi:http://dx.doi.org/10.1016/j.bmcl.2008.07.081 (2008).

83   Ahn, K., Johnson, D. S., Fitzgerald, L. R., Liimatta, M., Arendse, A., Stevenson, T., Lund, E. T., Nugent, R. A., Nomanbhoy, T. K., Alexander, J. P. & Cravatt, B. F. Novel Mechanistic Class of Fatty Acid Amide Hydrolase Inhibitors with Remarkable Selectivity†. *Biochemistry* **46**, 13019-13030, doi:10.1021/bi701378g (2007).

84   Leung, D., Hardouin, C., Boger, D. L. & Cravatt, B. F. Discovering potent and selective reversible inhibitors of enzymes in complex proteomes. *Nat Biotech* **21**, 687-691, doi:http://www.nature.com/nbt/journal/v21/n6/suppinfo/nbt826_S1.html (2003).

85   Huggins, J. P., Smart, T. S., Langman, S., Taylor, L. & Young, T. An efficient randomised, placebo-controlled clinical trial with the irreversible fatty acid amide hydrolase-1 inhibitor PF-04457845, which modulates endocannabinoids but fails to induce effective analgesia in patients with pain due to osteoarthritis of the knee. *Pain* **153**, 1837-1846, doi:http://dx.doi.org/10.1016/j.pain.2012.04.020 (2012).

86   http://www.nature.com/news/scientists-in-the-dark-after-french-clinical-trial-proves-fatal-1.19189. *scientists in the dark after french clinical trial proves fatal*, 2016).

87   Kiss, L. E., Learmonth, D. A., Rosa, C. P. D. C. P., Gusmao de Noronha, R., Palma, P. N. L., Soares da Silva, P. M. V. A. & Beliaev, A. Pharmaceutical compounds inhibiting fatty acid amide hydrolase for treating and preventing diseases. WO2010074588A2 (2010).

88   NCT02498392, C. g. I. *An Efficacy, Safety and Tolerability Study of JNJ-42165279 in Participants With Major Depressive Disorder With Anxious Distress*, 2015).

89   Kozak, K. R., Prusakiewicz, J. J., Rowlinson, S. W., Prudhomme, D. R. & Marnett, L. J. Amino Acid Determinants in Cyclooxygenase-2 Oxygenation of the Endocannabinoid Anandamide†. *Biochemistry* **42**, 9041-9049, doi:10.1021/bi034471k (2003).

90   Kozak, K. R., Crews, B. C., Morrow, J. D., Wang, L.-H., Ma, Y. H., Weinander, R., Jakobsson, P.-J. & Marnett, L. J. Metabolism of the Endocannabinoids, 2-Arachidonylglycerol and Anandamide, into

_____

Prostaglandin, Thromboxane, and Prostacyclin Glycerol Esters and Ethanolamides. *Journal of Biological Chemistry* **277**, 44877-44885, doi:10.1074/jbc.M206788200 (2002).

91   Matias, I., Chen, J., De Petrocellis, L., Bisogno, T., Ligresti, A., Fezza, F., Krauss, A. H.-P., Shi, L., Protzman, C. E., Li, C., Liang, Y., Nieves, A. L., Kedzie, K. M., Burk, R. M., Di Marzo, V. & Woodward, D. F. Prostaglandin Ethanolamides (Prostamides): In Vitro Pharmacology and Metabolism. *Journal of Pharmacology and Experimental Therapeutics* **309**, 745-757, doi:10.1124/jpet.103.061705 (2004).

92   Naidu, P. S., Booker, L., Cravatt, B. F. & Lichtman, A. H. Synergy between Enzyme Inhibitors of Fatty Acid Amide Hydrolase and Cyclooxygenase in Visceral Nociception. *The Journal of Pharmacology and Experimental Therapeutics* **329**, 48-56, doi:10.1124/jpet.108.143487 (2009).

93   Sasso, O., Bertorelli, R., Bandiera, T., Scarpelli, R., Colombano, G., Armirotti, A., Moreno-Sanz, G., Reggiani, A. & Piomelli, D. Peripheral FAAH inhibition causes profound antinociception and protects against indomethacin-induced gastric lesions. *Pharmacological Research* **65**, 553-563, doi:http://dx.doi.org/10.1016/j.phrs.2012.02.012 (2012).

94   Sasso, O., Migliore, M., Habrant, D., Armirotti, A., Albani, C., Summa, M., Moreno-Sanz, G., Scarpelli, R. & Piomelli, D. Multitarget fatty acid amide hydrolase/cyclooxygenase blockade suppresses intestinal inflammation and protects against nonsteroidal anti-inflammatory drug-dependent gastrointestinal damage. *The FASEB Journal* **29**, 2616-2627, doi:10.1096/fj.15-270637 (2015).

95   Migliore, M., Habrant, D., Sasso, O., Albani, C., Bertozzi, S. M., Armirotti, A., Piomelli, D. & Scarpelli, R. Potent multitarget FAAH-COX inhibitors: Design and structure-activity relationship studies. *European Journal of Medicinal Chemistry* **109**, 216-237, doi:http://dx.doi.org/10.1016/j.ejmech.2015.12.036 (2016).

96   Ates, M., Hamza, M., Seidel, K., Kotalla, C. E., Ledent, C. & Gühring, H. Intrathecally applied flurbiprofen produces an endocannabinoid-dependent antinociception in the rat formalin test. *European Journal of Neuroscience* **17**, 597-604, doi:10.1046/j.1460-9568.2003.02470.x (2003).

97   Guindon, J., De Léan, A. & Beaulieu, P. Local interactions between anandamide, an endocannabinoid, and ibuprofen, a nonsteroidal anti-inflammatory drug, in acute and inflammatory pain. *Pain* **121**, 85-93, doi:http://dx.doi.org/10.1016/j.pain.2005.12.007 (2006).

_____

98   Fowler, C. J., Tiger, G. & Stenström, A. Ibuprofen Inhibits Rat Brain Deamidation of Anandamide at Pharmacologically Relevant Concentrations. Mode of Inhibition and Structure-Activity Relationship. *Journal of Pharmacology and Experimental Therapeutics* **283**, 729-734 (1997).

99   Cipriano, M., Björklund, E., Wilson, A. A., Congiu, C., Onnis, V. & Fowler, C. J. Inhibition of fatty acid amide hydrolase and cyclooxygenase by the N-(3-methylpyridin-2-yl)amide derivatives of flurbiprofen and naproxen. *European Journal of Pharmacology* **720**, 383-390, doi:http://dx.doi.org/10.1016/j.ejphar.2013.09.065 (2013).

100   Teresa Cocco, M., Congiu, C., Onnis, V., Morelli, M. & Cauli, O. Synthesis of ibuprofen heterocyclic amides and investigation of their analgesic and toxicological properties. *European Journal of Medicinal Chemistry* **38**, 513-518, doi:http://dx.doi.org/10.1016/S0223-5234(03)00074-6 (2003).

101   Holt, S., Paylor, B., Boldrup, L., Alajakku, K., Vandevoorde, S., Sundström, A., Cocco, M. T., Onnis, V. & Fowler, C. J. Inhibition of fatty acid amide hydrolase, a key endocannabinoid metabolizing enzyme, by analogues of ibuprofen and indomethacin. *European Journal of Pharmacology* **565**, 26-36, doi:http://dx.doi.org/10.1016/j.ejphar.2007.02.051 (2007).

102   Alessandro, D. *Derivatives of Ibuprofen as Dual Inhibitor FAAH and COX* Master Degree thesis, University of Cagliari, (2012).

103   Fowler, C. J., Björklund, E., Lichtman, A. H., Naidu, P. S., Congiu, C. & Onnis, V. Inhibitory properties of ibuprofen and its amide analogues towards the hydrolysis and cyclooxygenation of the endocannabinoid anandamide. *Journal Of Enzyme Inhibition And Medicinal Chemistry* **28**, 172-182, doi:10.3109/14756366.2011.643304 (2013).

104   Prusakiewicz, J. J., Duggan, K. C., Rouzer, C. A. & Marnett, L. J. Differential Sensitivity and Mechanism of Inhibition of COX-2 Oxygenation of Arachidonic Acid and 2-Arachidonoylglycerol by Ibuprofen and Mefenamic Acid. *Biochemistry* **48**, 7353-7355, doi:10.1021/bi900999z (2009).

105   Favia, A. D., Habrant, D., Scarpelli, R., Migliore, M., Albani, C., Bertozzi, S. M., Dionisi, M., Tarozzo, G., Piomelli, D., Cavalli, A. & De Vivo, M. Identification and Characterization of Carprofen as a Multitarget Fatty Acid Amide Hydrolase/Cyclooxygenase Inhibitor. *Journal of Medicinal Chemistry* **55**, 8807-8826, doi:10.1021/jm3011146 (2012).

_____

106   Fowler, C. J., Janson, U., Johnson, R. M., Wahlström, G., Stenström, A., Norström, Å. & Tiger, G. Inhibition of Anandamide Hydrolysis by the Enantiomers of Ibuprofen, Ketorolac, and Flurbiprofen. *Archives of Biochemistry and Biophysics* **362**, 191-196, doi:http://dx.doi.org/10.1006/abbi.1998.1025 (1999).

107   Bertolacci, L., Romeo, E., Veronesi, M., Magotti, P., Albani, C., Dionisi, M., Lambruschini, C., Scarpelli, R., Cavalli, A., De Vivo, M., Piomelli, D. & Garau, G. A Binding Site for Nonsteroidal Anti-inflammatory Drugs in Fatty Acid Amide Hydrolase. *Journal of the American Chemical Society* **135**, 22-25, doi:10.1021/ja308733u (2013).

108   Gustin, D. J., Ma, Z., Min, X., Li, Y., Hedberg, C., Guimaraes, C., Porter, A. C., Lindstrom, M., Lester-Zeiner, D., Xu, G., Carlson, T. J., Xiao, S., Meleza, C., Connors, R., Wang, Z. & Kayser, F. Identification of potent, noncovalent fatty acid amide hydrolase (FAAH) inhibitors. *Bioorganic & Medicinal Chemistry Letters* **21**, 2492-2496, doi:http://dx.doi.org/10.1016/j.bmcl.2011.02.052 (2011).

109   Adams, A. D., Jones, A. B., Berger, J. P., Dropinski, J. F., Elbrecht, A., Liu, K., Macnaul, K. L., Shi, G.-q., Von, L. D. J. & Zhou, G. Preparation of 2-aryloxy-2-arylalkanoic acids for diabetes and lipid disorders. WO2002064094A2 (2002).

110   Windsor, M. A., Hermanson, D. J., Kingsley, P. J., Xu, S., Crews, B. C., Ho, W., Keenan, C. M., Banerjee, S., Sharkey, K. A. & Marnett, L. J. Substrate-Selective Inhibition of Cyclooxygenase-2: Development and Evaluation of Achiral Profen Probes. *ACS Medicinal Chemistry Letters* **3**, 759-763, doi:10.1021/ml3001616 (2012).

111   Allegretti, M., Aramini, A., Bianchini, G. & Cesta, M. C. 2-Arylpropionic acids and derivatives and pharmaceutical compositions containing them. WO2010031835A2 (2010).

112   Kevin B. Bahnck, A. S., Yong Tao, Susan C. Lilley, Melissa P. Andrews, Gary E. Aspnes, David J. Bernhardson, David R. Bill, Mark W. Bundesmann, Robert L. Dow, Kapil Karki, Tung Le, Qifang Li, Michael J. Munchhof, Asaad Nematalla, Mohammed Nihlawi, Leena Patel, Christian Perreault, Michael Waldo. Efficient Synthesis of 4-Amino-2-methoxy-7,8-dihydropyrido[4,3-d]pyrimidin-5-ones: Practical Access to a Novel Chemotype in the Development of DGAT-1 Inhibitors. *Synthesis* **44**, 3152-3157 (2012).

113   Alexander, C. W., De, D., Khanna, I. K. & Pillarisetti, S. Preparation of novel heterocyclic compounds as GATA modulators. WO2010028179A1 (2010).

_____
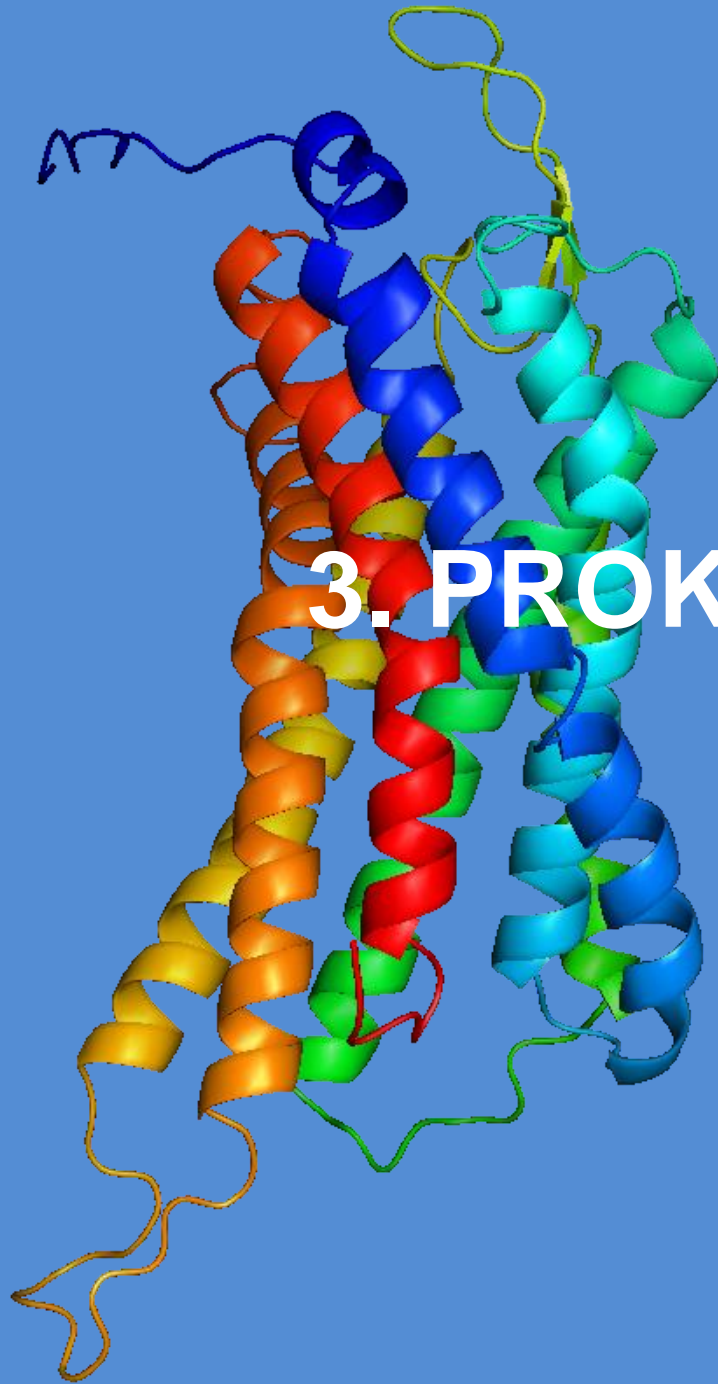
3. PROKINETICIN SYSTEM

3. Prokineticin System

3.1 Prokineticin System: A brief overview

From skin secretion of the frog *Bombina variegata* (Figure 1) in 1999

Figure 1. Bombina Variegata.

was isolated a small peptide (77 amino acids) rich in cysteine residues, named Bv8. The name was chosen to indicate its provenience and its molecular weight, 8KDa.[1] Afterward Bv8 homologues were identified on other amphibian like lizard, in Takifugu fish species as intestinal toxin and as venom component (MIT-1 or VRPA) of the snake black mamba.[2]
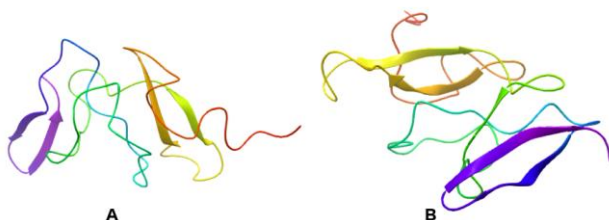
Figure 2. 3D structure of prokineticin 1 (A) and prokineticin 2 (B).

In numerous other species, including mammals analogs of this peptide have been found. Variants of MIT-1 and Bv8 in mammals are called respectively PK1 (Figure 2A) or endocrine gland-derived vascular endothelial growth factor (EG-VEGF) and PK2 (Figure 2B) or mammalian Bv8 (mBv8).[3] Their name, prokineticin, comes from their ability to contract the guinea pig ileum. A variant of PK2 has been identified and called PK2β, it differs for the presence of additional 21 amino acids respect to the base sequence.[4]

PK1 and PK2 are constituted by 80-90 amino acids, they belong to the protein family AVIT rich in cysteine, especially in the C-terminal portion, and both have the same N-terminal sequence.[2,5] In addition to the N-terminal hexapeptide sequence another structural feature in common is the presence of five disulphide bonds among ten cysteines. Evidence suggests that both this characteristics are essential for their biological activity.[6]
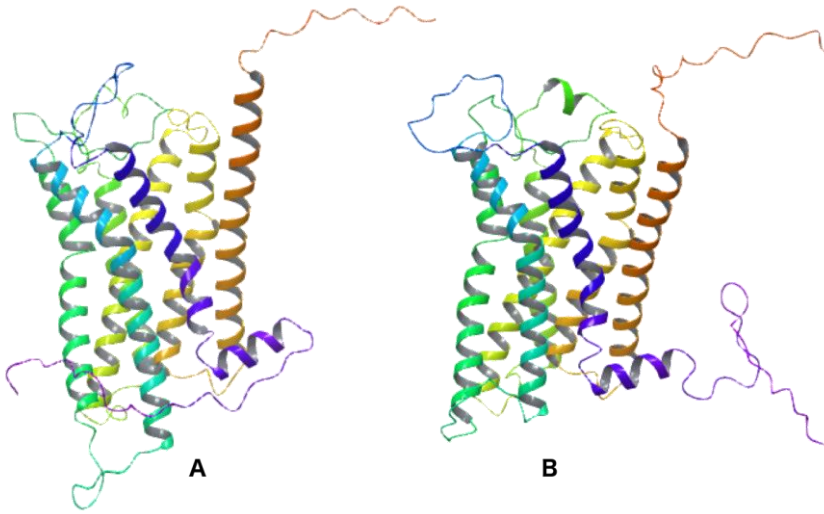
Figure 3. 3D structure of prokineticin receptor 1 (A) and prokineticin receptor 2 (B).

PKs exert their activity binding two specific receptors coupled with different kinds of G proteins, G_q, G_i and G_s, the activation of each of these proteins determines respectively the increased mobilization of intracellular calcium, phosphorylation of p44-p42 MAPK, phosphorylation of serine/threonine kinase and increase of cAMP levels.[4]

PK receptors, PKR1 (Figure 3A) and PKR2 (Figure 3B), as all GPCRs, are characterized by seven α-helix transmembrane segments separated by three intra- and three extracellular loops. They have an 85% of sequence homology, the major differences are on the N-terminal region, on the second intracellular loop and on the C-terminal.[6]

PK1, PK2 and PK2β do not display the same affinity to the two receptors, for PKR1 the best ligand is PK2 the other two have approximately the same affinity. The best ligand for PKR2 is PK2 followed by PK1, whereas PK2β has a much lower affinity.[4]

3.2 Prokineticin System: PKRs localization

PKs and PKRs are expressed differently in different tissues thus increasing the functional complexity of the system as well as the PKRs coupling with the various G proteins. These facts are determinant to guarantee that in different cells there is a different response after the stimulation given by a same ligand.[7]

The presence of mRNA of both PKR1 and PKR2 in the gastrointestinal tract (in particular, PKR1 is mainly expressed in the stomach, small intestine and other parts of the digestive tract, whereas PKR2 is only expressed in the ileum-cecum) suggest that PKR1 is the prokineticin receptor mainly involved in the intestinal motility regulation.[8] The activity of prokineticin system on gastrointestinal tract could be therapeutically useful to increase the gastric motility after surgery.[9]

PKR1 are localized in other peripheral tissues like lungs, spleen, pancreas, testicles, salivary and endocrine glands.[10,11]

PKR2 and PK2 are abundantly expressed on suprachiasmatic nucleus where they are involved in the regulation of circadian rhythms;[12] in the olfactory bulb they regulate morphogenesis.[13]

Studies in cultured mouse cells suggest that the PKR2 are expressed primarily in neurons, while the PKR1 are predominantly expressed in astrocytes and microglia.[14]

PK2 is an important modulator of biological processes in CNS, in mouse brain it is found in high concentrations and acts on neuronal survival as neurotrophic endogenous factor.[12]

In various tissues PKs actively participate to physiological angiogenesis and in some cases also to the neoplastic one.[15] More precisely PK1 is implicated in the recruitment of the precursor cells,

induces proliferation and stabilizes the nascent blood vessels, while PK2 leads to endothelium destabilization that promotes the integration and proliferation of endothelial cells.[15] PK1 is also known as EG-VEGF for its ability to induce angiogenesis in the endocrine glands, ovaries and testicles, also it induces proliferation, migration and fenestration of endothelial cells derived from the adrenergic glands.[16,17]

The PK1 is found in small amounts in healthy prostate tissue and its increases in tumor tissue appear to be a signal for the development of prostate cancer. It is important to emphasize that only the PKR2 expression is increased in the malignant cells of the prostate, the same goes for PK2 than PK1. [18] A high expression of PK1 is also one of the characteristics of human neuroblastoma. Conversely, PK1 expression decreases in endometrial and liver carcinomas.[19,20]

PKs are implicated also in the development of hepatocellular carcinoma, in liver PK2 is very abundant but much less PK1, however their expression vary in the presence of the tumor.[20]

PKs are also important on the regulation of other numerous processes like alimentation, thirst, circadian rhythms, hyperalgesia and inflammation.[15]

The PK2/PKR1 system expression on inflamed tissues suggests that there is a connection between the cells which infiltrate these tissues and the inflammatory pain.[21]

Diminution of pain threshold given by the action of PK2 on its sensitive neurons receptors implies that the prokineticin system play a role on inflammation and neuropathic pain. PK2 released from inflammatory cells can bind the PKR1 on primary sensitive neurons and contributes in this way to the inflammatory pain signaling.[21] According to this, blocking the activity of PK2 and/or PKR1 might have benefits both for treatment of pain and cancer.[22]

Furthermore PKs released by tissue damage act as autocrine/paracrine regulator of immunoinflammatory response and

with a stimulation of the neuronal PKs increase the nociception responsiveness.[23]

PKRs are expressed on DRG and when PK2 binds the receptors on these neurons caused hyperalgesia with different intracellular mechanism; included the activation of TRPV1 by phosphorylation, which results in reduction of pain threshold to thermal and mechanical stimuli.[23]

Studies on mice lacking the PKRs have shown the involvement of this system in modulation of pain. These mice showed a higher threshold for thermal and mechanical pain, and are less sensitive to chronic inflammatory pain also.[24-26]

Other studies showed that administration of amphibians Bv8 in PAG have pro-nociceptive effects due to the intrinsic GABAergic tone increase that in turn is responsible for the inhibition of efferent antinociceptive neurons from PAG to medullary and rostral ventromedial neurons.[27]

3.3 Prokineticin System: PKRs exogenous modulators

To date there are few reported compounds that interact with PKRs. The first patents on the synthesis and activity of small non-peptide molecule endowed with triazinedione structure (Figure 4A) active on these receptors date back to 2006-2007.[28-30] In the same years it has been filed a patent that describes the PKR inhibitory activity of compounds endowed with morpholine structure (Figure 4B).[31] Even more recently, in 2013 and in 2015 two patents disclosing molecules endowed with piperidine/piperazine structure (Figure 4C-D) active on these receptors were filed.[32,33]
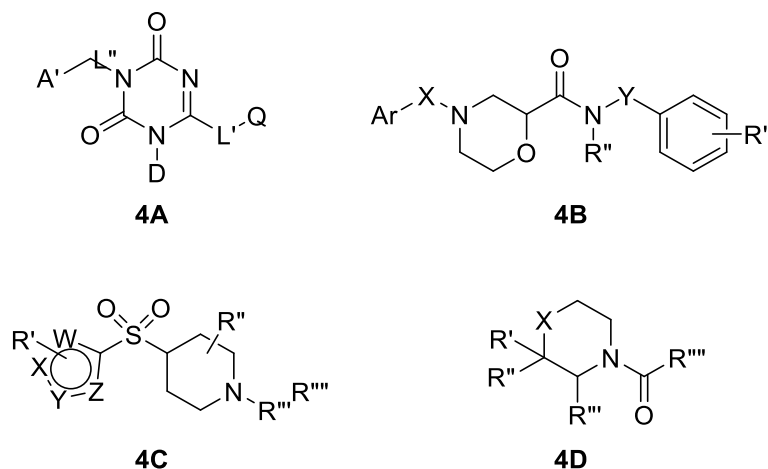
Figure 4. General scaffolds of patented PKR inhibitors.

The synthesis of triazinedione compounds reported in the Janssen Pharmaceutica's patent[28] starts from the formation of the isothiourea derivatives by the reaction between the sulfonic salt of 2-methyl-isothiourea and benzyl isocyanate. The isothioureas were then acylated with methyl chloroformiate in the presence of triethylamine. The obtained compounds were cyclized to obtain triazinediones functionalized on the N-1 and C-2 in very low overall yields.

3.4 Prokineticin System: Results and Discussion

Based on these considerations, we set up a new simpler and high yielding synthetic method that can give easy access to new triazinediones as potential ligands for prokineticin receptors.

This new synthetic procedure started from the conversion of variously substituted benzylamines into the corresponding ureas **2**, using potassium cyanate (KOCN) in water in the presence of HCl. Ureas were functionalized on the free amino group by treatment with ethoxycarbonyl isothiocyanate in refluxing toluene.

Cyclization of the obtained thioureas **3** was carried out in MeOH solution in the presence of sodium methoxide (NaOMe). Triazines **4** were then methylated on the sulfur with MeI in MeOH solution (route A). These last two steps can be performed one pot to improve yields (route B).

Then the thiomethyltriazines **6** were alkylated on the N-1 with the appropriate benzyl halide, in DMF solution in the presence of potassium carbonate (K_2CO_3).

The final step was the replacement of the thiomethyl group with a side chain in position 2. Triazinediones **7** were first reacted with ethylendiamine in refluxing toluene solution and then the obtained intermediates **8** were reacted with 1H-pyrazole-1-carboxamidine in MeCN solution in presence of diisopropylethylamine (DIPEA).

This synthetic procedure allowed obtaining triazinediones **PC** in about 50% overall yields (Scheme 1).
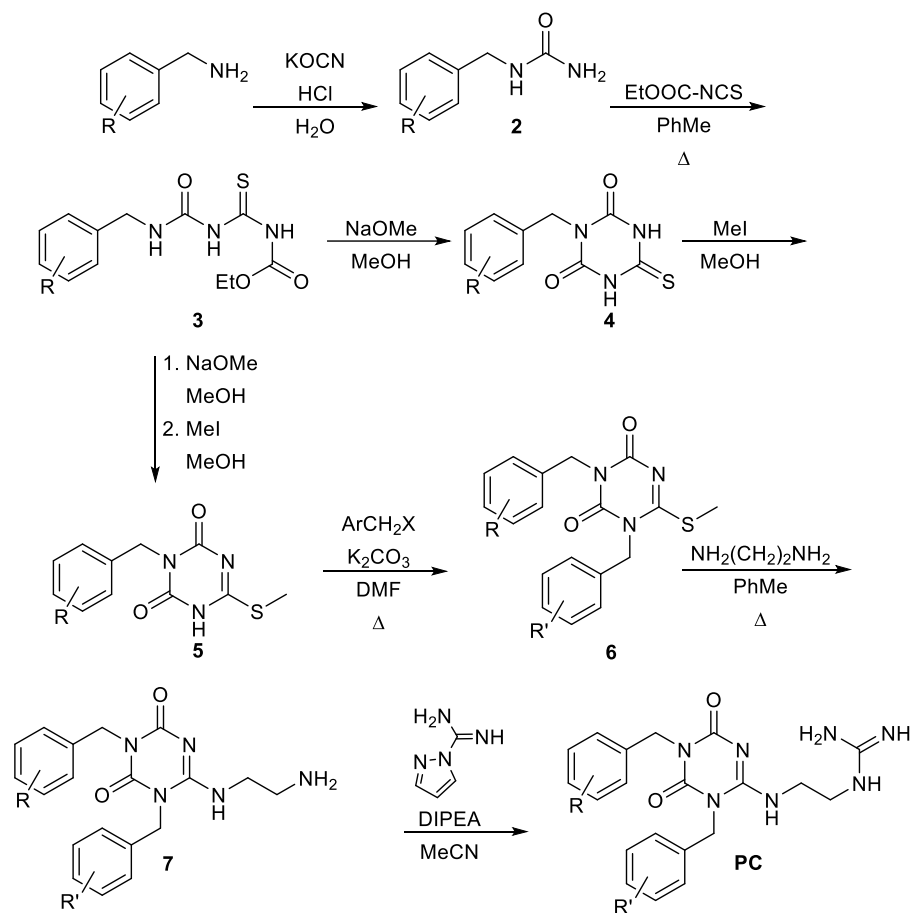
Scheme 1. Synthesis of PCs.

All triazinediones were *in vivo* screened by the group of Prof. Negri, University of Rome La Sapienza, to evaluate their ability to antagonize the hyperalgesia induced by administration of Bv8 in mice paw. The pain threshold was determined with the test of immersion of the paw in 48 °C water, measured as the latency to paw withdrawal from water.

To evaluate the ability to antagonize the Bv8-induced decrease of nociceptive threshold to thermal pain the triazinediones have been injected, in the same paw region where Bv8 was injected, 5 minutes before. The results are showed in table 1.

For the structure-activity relationship study of these compounds, with reference to the substituents on the benzylic groups, **PC1** which displays an EC_{50} value of 5.8 pM, was used as reference compound.

The substitution of the ethyl group with chlorine (**PC18**) or methyl group (**PC15**) did not produce significant influence on the EC_{50} values as well as the inversion of the position on triazine core of the corresponding benzylic groups (**PC29** and **PC31**).
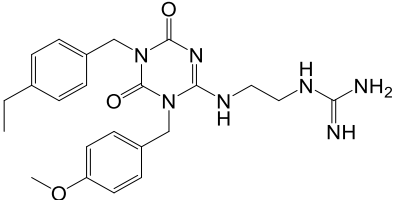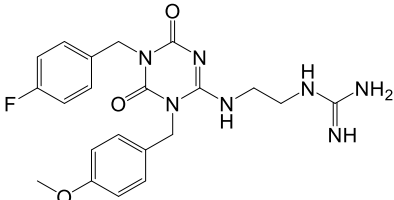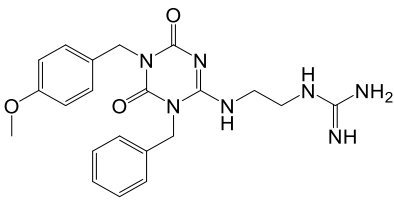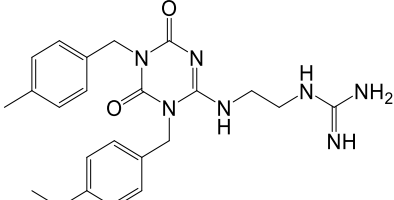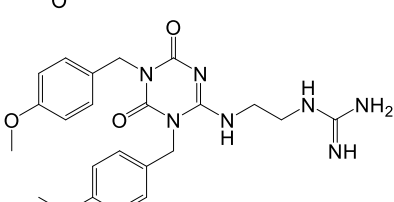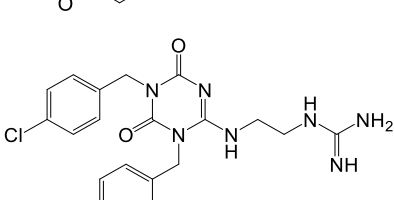
While the substitutions with bromine (**PC25**), fluorine (**PC7**) and methoxy group (**PC17**) led to more than 10 times increase in the activity as compared to the reference compound. Conversely, the presence of iodine (**PC35**) or trifluoromethyl group (**PC23**) greatly reduced the activity. The replacement of the methoxy group of **PC23** with a methyl switches from the compound less active to the more active, **PC27**, displaying an EC_{50} value of 0.033 pM.
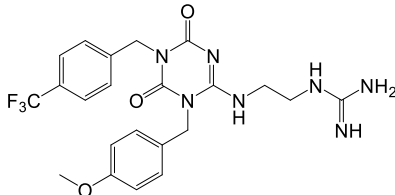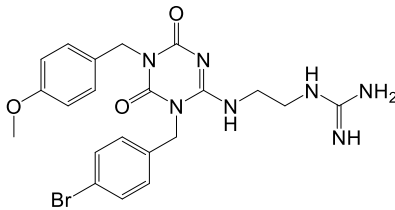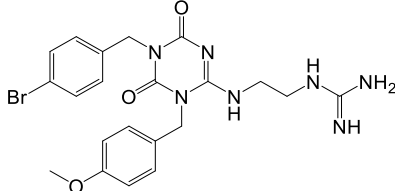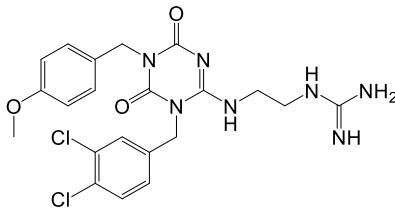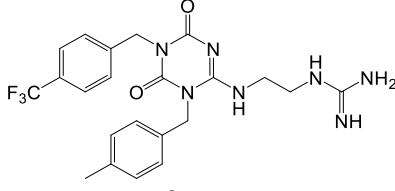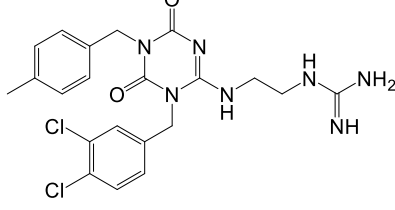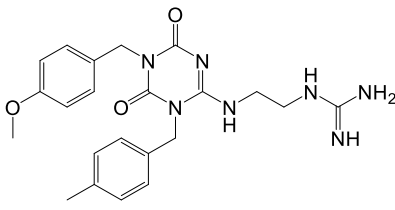
Inversion of the substituents on the two aromatic rings of the compounds **PC25** and **PC7** to obtain respectively **PC24** and **PC30** led to decrease in activity. On the contrary, activity is slightly improved in the compounds **PC32** and **PC34** as compared to the corresponding analogs **PC27** and **PC35** respectively, even if their EC_{50} values remain far from reference compound **PC1**.

The substitution of ethyl group with 3,4-methylenedioxy moiety (**PC33**) or nitro (**PC36**) group led to a considerable reduction in the activity. The replacement of the ethyl with a methoxy group afforded the poorest compound of the series (**PC8**).

Lastly the replacement of the methoxybenzyl with a 3,4-dichlorobenzyl and the ethyl group with a methoxy (**PC26**) or a methyl (**PC28**) group did not lead to significant changes in the activity compared to the reference compound.

Name	Compound	EC$_{50}$ (pM)	95% Confidence intervals
PC1		5.8	3.6 - 9.1
PC7		0.31	0.16 – 0.59
PC8		63	44 – 90
PC15		4.4	2.5 – 7.8
PC17		0.053	0.038 – 0.067
PC18		4.0	2.9 – 5.7

PC23		51	27 – 83
PC24		4.3	2.7 – 6.8
PC25		0.36	0.17 – 0.78
PC26		4.5	2.9 – 6.4
PC27		0.033	0.018 – 0.061
PC28		5.1	3.8 – 6.8
PC29		4.5	3.4 – 5.6
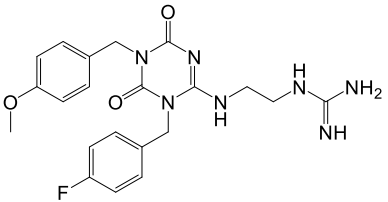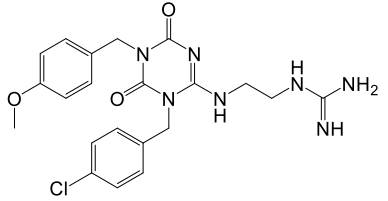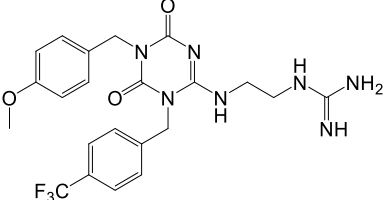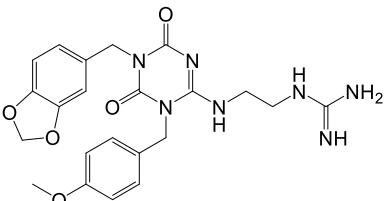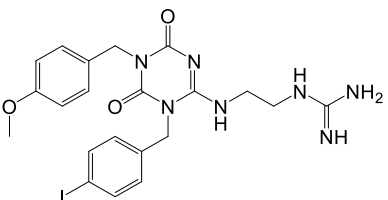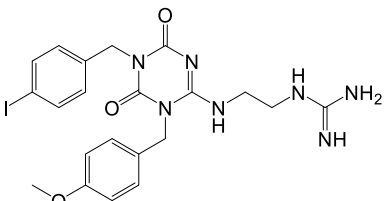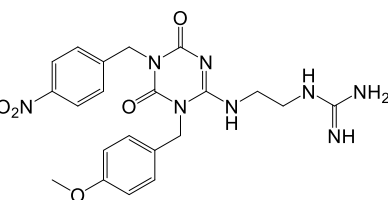
PC30		36	24 – 59
PC31		4.4	3.1 – 5.9
PC32		48	33 – 70
PC33		39	29 – 53
PC34		39	27 – 52
PC35		51	32 – 80
PC36		48	35 – 69

Table 1. In vivo analgesic activity of triazinedione derivatives.

Based on these *in vivo* activities to evaluate the activity and selectivity for PKR1 and PKR2, selected PC halogenated derivatives were screened *in vitro* and *in vivo* tests. These studies were carried out *in vitro*, using Bioluminescence Resonance Energy Transfer (BRET) technology, and in vivo, in transgenic mice expressing only one of the PKRs.

PC7, bearing a 4-fluorobenzyl group, in *in vitro* assay resulted about 100 times more selective for PKR1 than PKR2 and it is a 4 times better inhibitor than **PC1**. The chlorine substituted **PC18** and the iodine substituted **PC35**, as well as **PC7** displayed lower affinity for PKR2 than PKR1. However the 4-bromine analog **PC25** was the best compound for both PKR1 affinity (about 18 times better than **PC1**) and selectivity (about 300 times than for PKR2).

As further confirmation in *in vivo* assays on transgenic mice all halogenated triazinediones abolished the Bv8-induced thermal hyperalgesia with a dose 10 times lower in PKR2(-/-) (15 pmol) than PKR1(-/-)mice (150 pmol). The selectivity was more evident in compounds **PC7** and **PC25**, which were approximately 100 and 300 times more selective towards PKR2(-/-) (0.15 and 0.04 pmol) than PKR1(-/-) (15 and 14 pmol) respectively. Despite **PC18** and **PC35** appeared less active than **PC7** and **PC25**, the selectivity (about 100 times) for PKR1 was confirmed in these cases also.

At laboratory of computational medicine, biostatistics unit, Faculty of Medicine, Autonomous University of Barcelona (Bellaterra, Spain), some computational studies were made. In particular, using a flexible docking method the binding mode of **PC1** and **PC25** on both PKR1 and PKR2 was evaluated to better understand the reasons of the different affinity on the two receptors. The difference in affinity may be due to the presence of a different residue in the binding site, in PKR1 there is a threonine, which interact with the ethyl benzene group of **PC1**, conversely, in PKR2 the threonine is substituted by alanine. This residue may also be the responsible of the different activity of **PC1** and **PC25**, because the presence of bromine instead of

ethyl group allows a more stable interaction by halogen bonding with this residue.

Further computational studies were conducted in the research group of Dr. Stefano Costanzi, at American University (Washington DC, USA), with the aim of identifying models putatively endowed with an accurate representation of the ligand-binding cavity. In particular we focused our attention on the PKR1 receptor.

Due to the absence of crystal structures for the PKR1 receptor, we resorted to the homology modeling technique for the construction of the models. Subsequently, was employed the models in controlled virtual screening experiments, meant to study their ability to distinguish between ligand and non-ligands of the PKR1 receptor. Notably, it has been shown by Costanzi and others the models that best discriminate between ligands and non-ligands of a given receptor tend to be those with the most structurally accurate representation of the binding site.[34,35]

For the selection of templates to be employed in the construction of the models, we clustered the Class A GPCRs for which structures have been solved to through X-ray crystallography on the basis of their amino acid sequence and, for each branch of the resulting tree, we selected the receptor that showed the highest percentage of sequence identity with the PKR1 subtype. Namely, the receptors selected as templates were the κ-opioid receptor (κ-OPR), the neurotensin receptor 1 (NTS$_1$), the β-1 adrenergic receptor (β$_1$), the chemokine receptor type 4 (CXCR4), the protease-activated receptor 1 (PAR1), rhodopsin receptor (RHOR). After aligning the amino acid sequence the PKR1 receptor with those of the templates, were built homology models following a protocol similar to that recently described by Costanzi.[36]

In order to conduct the controlled virtual screening experiments, we assembled a database containing all known PKR ligands endowed with a triazine structure. After calculating the fingerprints of these compounds, thousands of molecules were computationally screened

to identify structurally related compounds to be employed as "decoys" in the subsequent docking-based virtual screening experiment. As a result, a set of about 9000 compounds was gathered.
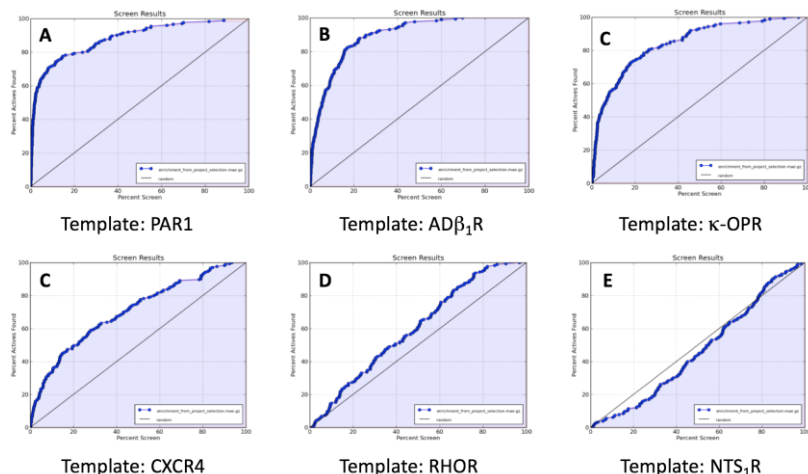
Figure 5. Receiver operating characteristic (ROC) analyses.

The following step entailed docking-based controlled virtual screening analyses intended to evaluate the ability of the various models to discriminate between ligands and decoys. After each docking experiment, the results were studied through *Receiver operating characteristic* (ROC) *analyses*. Another criterion that was considered to evaluate the reliability of the models was the consistency of the docking poses of the ligands within the models of the PKR1 receptor.

As the ROC curves shown in Figure 1 illustrate, the model that best discriminated between ligand and decoys was the one build on the basis of the PAR1 receptor. The PAR1-based models were also deemed satisfactory according to the consistency of the binding poses, since the known ligands docked within its binding cavity adopted very similar positions and conformations (Figure 2).
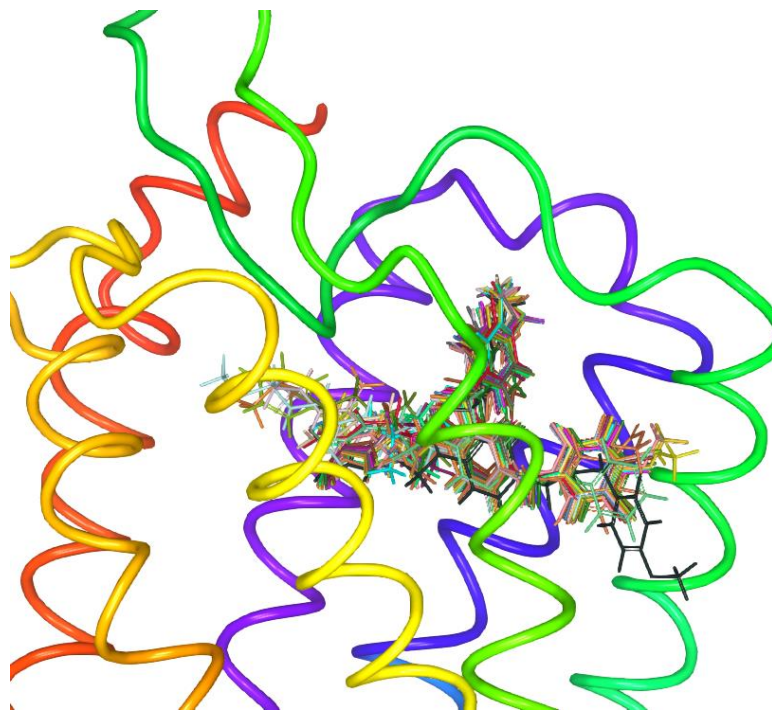
Figure 6. Example of pose conservation of the first 22 ligands

3.3 Experimental Section

Commercially available solvents and reagents were used without further purification unless otherwise stated. ^{1}H NMR spectra were recorded on a Varian Inova 500 spectrometer. The chemical shifts (δ) are reported in part per million downfield from TMS, which was used as internal standard, and the spectra were recorded in DMSO-d6. Infrared spectra were recorded on a Bruker Vector 22 spectrometer. The main bands are given in cm^{-1}. M.p. were determined on a Stuart Scientific Melting point SMP1 apparatus and are uncorrected. All products reported showed NMR spectra in agreement with the assigned structures. The purity of tested compounds was determined by combustion elemental analyses conducted by the Microanalytical Laboratory of the Chemistry Department of the University of Ferrara with a Yanagimoto MT-5 CHN recorder elemental analyzer. All tested compounds yielded data consistent with a purity of at least 95% as compared with the theoretical values.

General procedure for the synthesis of benzylureas 2

The appropriate benzylamine (2 mmol) was suspended in water (5 mL) and solubilized trough formation of the corresponding salt by adding an equimolar amount of 37% aqueos HCl (0.17 mL). To the obtained solution KOCN (0.16 g, 2 mmol) was added, the mixture was heated at 60 °C for 30 minutes. After cooling at r.t. the formed precipitated was filtered, washed with ice water and dried.

4-Ethylbenzylurea (2a)
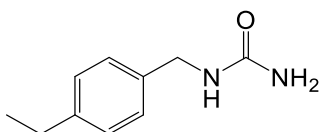
Yield 82%. m.p. 199-203 °C (2-PrOH). ^{1}H NMR (DMSO-d_6) δ 1.25 (m, 3H, CH$_3$), 2.60 (m, 2H, CH$_2$), 4.25 (s, 2H, CH$_2$), 6.32 (s, 1H, NH), 6.98 (m, 2H, Ar), 7.18 (m, 2H, Ar), 9.21 (s, 2H, NH$_2$). IR (Nujol) 3439, 3336,

1653 cm^{-1}. Elemental analysis: Calculated for C$_{10}$H$_{14}$N$_2$O (178.23) % C 67.39; H 7.92; N 15.72; found % C 67.38; H 7.90; N 15.74.

4-Fluorobenzylurea (2b)
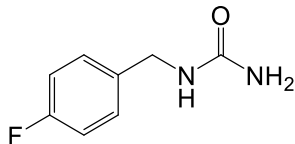
Yield 78%. m.p. 172-174 °C. ^{1}H NMR (DMSO-d$_6$) δ 4.20 (s, 2H, CH$_2$), 6.17 (s, 1H, NH), 7.12 (d, J= 8.5 Hz, 2H, Ar), 7.39 (d, J= 8.5 Hz, 2H, Ar), 8.99 (s, 2H, NH$_2$). IR (Nujol) 3412, 3320, 1659 cm^{-1}. Elemental analysis: calculated for C$_8$H$_9$FN$_2$O (168.17) % C 57.14; H 5.39; N 16.66; found % C 57.13; H 5.40; N 16.66. Physical and spectral data were in accordance with literature values.[37]

4-Methoxybenzylurea (2c)
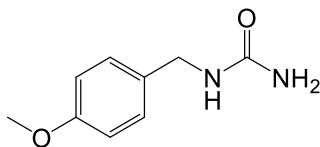
Yield 90%. m.p. 164-165 °C. ^{1}H NMR (400 MHz, CDCl$_3$), δ 3.80 (s, 3H, CH$_3$), 4.29 (s, 2H, CH$_2$), 7.21–7.27 (m, 4H, Ar). IR (Nujol) 3427, 3336, 1651 cm^{-1}. Elemental Analysis: calculated for C$_9$H$_{12}$N$_2$O$_2$ (180.20) % C 59.99; H 6.71; N 15.55; found % C 60.01; H 6.70; N 15.50. Physical and spectral data were in accordance with literature values.[37]

4-Methylbenzylurea (2d)
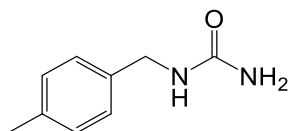
Yield 88%. m.p. 185-186 °C. ^{1}H NMR (400 MHz, CDCl$_3$), δ 2.95 (s, 3H, CH$_3$), 4.25 (s, 2H, CH$_2$), 7.18–7.25 (m, 4H, Ar). IR (Nujol) 3438, 3336, 1655 cm^{-1}. Elemental analysis: calculated for C$_9$H$_{12}$N$_2$O (164.20) % C

65.83; H 7.37; N 17.06; found % C 65.80; H 7.38; N 17.05. Physical and spectral data were in accordance with literature values.[38]

4-Chlorobenzylurea (2e)
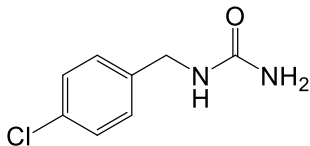
Yield 82%. m.p. 192-193 °C. ^{1}H NMR (400 MHz, CDCl$_3$), δ 4.31 (s, 2H, CH$_2$), 7.23–7.29 (m, 4H, Ar). IR (Nujol) 3440, 3333, 1655 cm^{-1}. Elemental analysis: calculated for C$_8$H$_9$ClN$_2$O (184.62) % C 52.04; H 4.91; N 15.17; found % C 52.01; H 4.90; N 15.18. Physical and spectral data were in accordance with literature values.[39]

4-Trifluoromethylbenzylurea (2f)
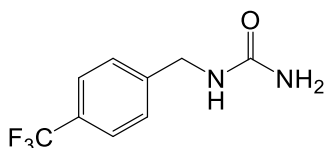
Yield 79%. m.p. 195-199 °C. ^{1}H NMR (DMSO-d$_6$) δ 4.24 (s, 2H, CH$_2$), 5.60 (s, 2H, NH$_2$), 6.52 (m, 1H, NH), 7.42 (d, J= 8.3 Hz, 2H, Ar), 7.66 (d, J= 8.3, 2H, Ar). IR (Nujol) 3440, 3345, 1652 cm^{-1}. Elemental analysis: calculated for C$_9$H$_9$F$_3$N$_2$O (218.18) % C 49.55; H 4.16; N 12.84; found % C 49.49; H 4.17; N 12.87. Physical and spectral data were in accordance with literature values.[37]

4-Bromobenzylurea (2g)
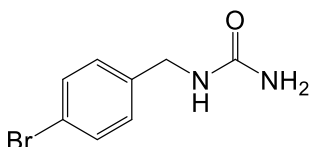
Yield 88%. m.p. 199-200 °C. ^{1}H NMR (DMSO-d$_6$) δ 4,19 (s, 2H, CH$_2$), 6,12 (s, 2H, NH$_2$), 7,12 (d, J= 8.0 Hz, 2H, Ar), 7,85 (d, J= 8.0 Hz 2H, Ar), 9,03 (s, 1H, NH). IR (Nujol) 3442, 3336, 1654 cm^{-1}. Elemental analysis:

calculated for $C_8H_9BrN_2O$ (229.07) % C 41.95; H 3.96; N 12.23; found % C 41.97; H 3.97; N 12.24. Physical and spectral data were in accordance with literature values.[40]

1-(1,3-Benzodioxo-5-yl)methylurea (2h)
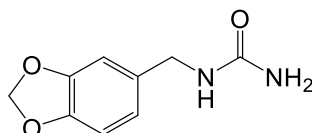
Yield 83%. m.p. 180-182 °C. ^1H NMR (DMSO-d_6) δ 4.20 (s, 2H, CH₂), 6.02 (s, 1H, NH), 6.07 (s, 2H, CH₂), 6.76 (m, 1H, Ar), 6.81 (m, 1H, Ar), 7.03 (m, 1H, Ar), 8.99 (s, 2H, NH₂). IR (Nujol) 3416, 3359, 1647 cm^{-1}. Elemental analysis: calculated for $C_9H_{10}N_2O_3$ (194.19) % C 55.67; H 5.19; N 14.43; found % C 55.6O; H 5.21; N 14.44.

4-Iodobenzylurea (2i)
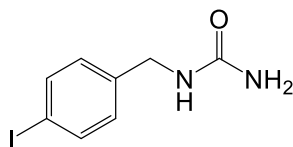
Yield 65%. m.p. 202-204 °C. ^1H NMR (DMSO-d_6) δ 4.26 (s, 2H, CH₂), 6.34 (s, 1H, NH), 7.00 (d, 8.5 Hz, 2H, Ar), 7.56 (d, 8.5 Hz, 2H, Ar), 9.15 (s, 2H, NH₂). IR (Nujol) 3425, 3352, 1652 cm^{-1}. Elemental analysis: calculated for $C_8H_9IN_2O$ (276.07) % C 34.80; H 3.29; N 10.15; found % C 34.87; H 3.27; N 10.12. Physical and spectral data were in accordance with literature values.[41]

4-Nitrobenzylurea (2l)
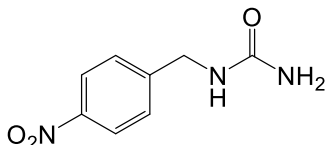
Yield 88%. m.p. 199-201 °C. ^1H NMR (DMSO-d_6) δ 4.25 (s, 2H, CH₂), 6.17 (s, 1H, NH), 7.95 (d, J= 8.5 Hz, 2H, Ar), 8.14 (d, J= 8.5 Hz, 2H, Ar),

9.21 (s, 2H, NH$_2$). IR (Nujol) 3460, 3307, 1649 cm^{-1}. Elemental analysis: calculated for C$_8$H$_9$N$_3$O$_3$ (195.18) % C 49.23; H 4.65; N 21.53; found % C 49.25; H 4.66; N 21.53. Physical and spectral data were in accordance with literature values.[37]

General procedure for the synthesis of ethyl ((benzylcarbamoyl)carbamathioyl)carbamates (3)

A mixture of benzylurea **(2)** (2 mmol) and ethoxycarbonyl isothiocyanate (0.28 mL, 2.4 mmol) was refluxed in dry toluene (5 mL) for 2.5 h. After elimination of the solvent under vacuum, the solid residue was suspended in i-Pr$_2$O, filtered, dried and used for the next reaction step.

Ethyl ((4-ethyl-benzylcarbamoyl)carbamathioyl)carbamate (3a)
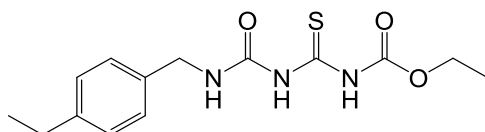
Yield 93%. m.p. 118-124 °C. ^{1}H NMR (DMSO-d$_6$) δ 1.14 (m, 3H, CH$_3$), 2.22 (m, 3H, CH$_3$), 2.55 (m, 2H, CH$_2$), 4.16 (m, 2H, CH$_2$), 4.32 (m, 2H, CH$_2$) 7.1 (m, 4H, Ar), 8.58 (s, 1H, NH), 11.02 (s, 1H, NH), 12.19 (s, 1H, NH). IR (Nujol) 3317, 3202, 1748, 1734, 1718, 1697 cm^{-1}. Elemental analysis: calculated for C$_{14}$H$_{19}$N$_3$O$_3$S (309.39) % C 54.35; H 6.19; N 13.58; found % C 54.40; H 6.18; N 13.56.

Ethyl ((4-fluoro-benzylcarbamoyl)carbamathioyl)carbamate (3b)
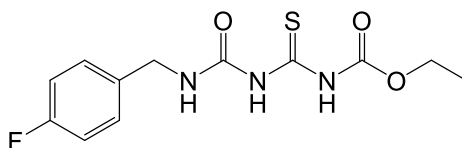
Yield 78%. m.p. 130-135 °C. ^{1}H NMR (DMSO-d$_6$) δ 1.38 (t, J= 7.2 Hz, 3H, CH$_3$), 4.27 (q, J= 7.2 Hz, 2H, CH$_2$), 4.50 (m, 2H, CH$_2$), 7.52-7.48 (m, 4H, Ar), 8.80 (s, 1H, NH), 11.20 (s, 1H, NH), 12.30 (s, 1H, NH). IR (Nujol) 3317, 1744, 1702 cm^{-1}. Elemental analysis: calculated for

$C_{12}H_{14}FN_3O_3S$ (299.32) % C 48.15; H 4.71; N 14.04; found % C 48.21; H 4.70; N 14.02.

Ethyl ((4-methoxy-benzylcarbamoyl)carbamathioyl)carbamate (3c)
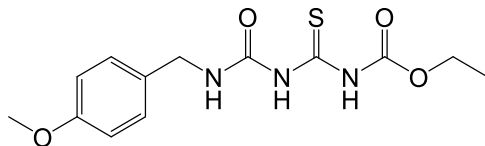
Yield 96%. m.p. 139-141 °C. ^{1}H NMR (DMSO-d$_6$) δ 1.20 (t, 3H, CH$_3$), 3.83 (s, J= 7.2 Hz, 3H, CH$_3$), 4.13 (q, J= 7.2 Hz, 2H, CH$_2$), 4.25 (s, 2H, CH$_2$), 6.87 (d, 8.5 Hz, 2H, Ar), 7.25 (d, 8.5 Hz, 2H, Ar), 8.90 (s, 1H, NH), 11.09 (s, 1H, NH), 12.15 (s, 1H, NH). IR (Nujol) 3315, 1747, 1698 cm^{-1}. Elemental analysis: calculated for $C_{13}H_{17}N_3O_4S$ (311.36) % C 50.5; H 5.50; N 13.50; found % C 50.14; H 5.5; N 13.52.

Ethyl ((4-methyl-benzylcarbamoyl)carbamathioyl)carbamate (3d)
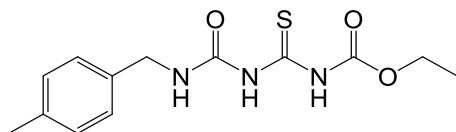
Yield 72%. m.p. 140-142 °C. ^{1}H NMR (DMSO-d$_6$) δ 1.29 (t, J= 7.0 Hz, 3H, CH$_3$), 2.34 (s, 3H, CH$_3$), 4.13 (q, J= 7.2 Hz, 2H, CH$_2$), 4.25 (s, 2H, CH$_2$), 7.11 (m, 4H, Ar), 9.27 (s, 1H, NH), 11.34 (s, 1H, NH), 12.10 (S, 1H, NH). IR (Nujol) 3324, 1745, 1700 cm^{-1}. Elemental analysis: calculated for $C_{13}H_{17}N_3O_3S$ (295.36) % C 52.86; H 5.80; N 14.23; % C 52.87; H 5.82; N 14.20.

Ethyl ((4-chloro-benzylcarbamoyl)carbamathioyl)carbamate (3e)
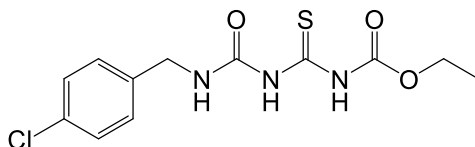
Yield 95%. m.p. 132-137 °C. ^{1}H NMR (DMSO-d$_6$) δ 1.20 (t, J= 7.2 Hz, 3H, CH$_3$), 4.09 (q, J= 7.2 Hz, 2H, CH$_2$), 4.25 (s, 2H, CH$_2$), 7.32 (d, J= 8.2

Hz, 2H, Ar), 7.37 (d, J= 8.2 Hz, 2H, Ar), 9.30 (s, 1H, NH), 11.60 (s, 1H, NH), 12.20 (s, 1H, NH). IR (Nujol) 3189, 1736, 1701 cm^{-1}. Elemental analysis: calculated for $C_{12}H_{14}ClN_3O_3S$ (315.78) % C 454; H 47; N 13.31; % C 45.60; H 4.48; N 13.29.

Ethyl ((4-trifluoromethyl-benzylcarbamoyl)carbamathioyl)carbamate (3f)
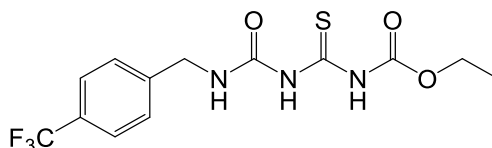
Yield 51%. m.p. 122-125 °C. ^{1}H NMR (DMSO-d$_6$) δ 1.27 (t, J= 7.5 Hz, 3H, CH$_3$), 4.10 (q, J= 7.5 Hz, 2H, CH$_2$), 4.26 (s, 2H, CH$_2$), 7.16 (d, 8.5 Hz, 2H, Ar), 7.50 (d, 8.5 Hz, 2H, Ar), 9.50 (s, 1H, NH), 10.97 (s, 1H, NH), 12.00 (s, 1H, MH). IR (Nujol) 3302, 3177, 1734, 1638 cm^{-1}. Elemental analysis: calculated for $C_{13}H_{14}F_3N_3O_3S$ (349.33) % C 44.70; H 4.04; N 12.03; % C 44.77; H 4.05; N 12.00.

Ethyl ((4-bromo-benzylcarbamoyl)carbamathioyl)carbamate (3g)
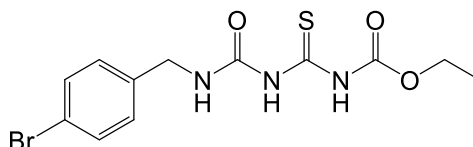
Yield 61%. m.p. 129-130 °C. ^{1}H NMR (DMSO-d$_6$) δ 1.30 (t, J= 7.2 Hz, 3H, CH$_3$), 4.13 (q, J= 7.2 Hz, 2H, CH$_2$), 4.24 (s, 2H, CH$_2$), 7.12 (m, 2H, Ar), 7.85 (m, 2H, Ar), 9.14 (s, 1H, NH), 11.22 (s, 1H, NH), 12.10 (s, 1H, NH). IR (Nujol) 3582, 3439, 3320, 1745, 1731, 1700 cm^{-1}. Elemental analysis: calculated for $C_{12}H_{14}BrN_3O_3S$ (360.23) % C 40.01; H 3.92; N 11.66; found % C 40.03; H 3.94; N 11.65.

Ethyl (((1,3-benzodioxo-5-yl-methyl)carbamoyl)carbamathioyl)carbamate (3h)
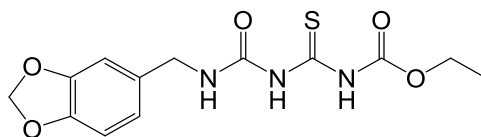
Yield 44%. m.p. 143-147 °C. ^{1}H NMR (DMSO-d$_6$) δ 1.29 (t, J= 7.0 Hz, 3H, CH$_3$), 4.13 (q, J= 7.0 Hz, 2H, CH$_2$), 4.25 (s, 2H, CH$_2$), 6.07 (s, 2H, CH$_2$), 6.76 (m, 1H, Ar), 6.81 (m, 1H, Ar), 7.03 (m, 1H, Ar), 9.15 (s, 1H, NH), 11.30 (s, 1H, NH), 12.02 (s, 1H, NH). IR (Nujol) 3582, 3423, 3312, 1747, 1697, 1649 cm^{-1}. Elemental analysis: calculated for C$_{13}$H$_{15}$N$_3$O$_5$S (325.34) % C 47.99; H 4.65; N 12.92; found % C 48.03; H 4.66; N 12.91.

Ethyl ((4-iodo-benzylcarbamoyl)carbamathioyl)carbamate (3i)
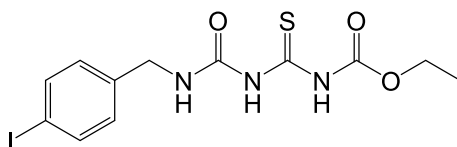
Yield 76%. m.p. 135-139 °C. ^{1}H NMR (DMSO-d$_6$) δ 1.29 (t, J= 7.2 Hz, 3H, CH$_3$), 4.13 (q, J= 7.2 Hz, 2H, CH$_2$), 4.25 (s, 2H, CH$_2$), 7.00 (d, J= 8.0 Hz, 2H, Ar), 7.56 (d, J= 8.0 Hz, 2H,Ar), 9.01 (s, 1H, NH), 11.42 (s, 1H, NH), 12.19 (s, 1H, NH). IR (Nujol) 3440, 3320, 1745, 1731, 1696, 1651 cm^{-1}. Elemental analysis: calculated for C$_{12}$H$_{14}$IN$_3$O$_3$S (407.23) % C 35.39; H 3.47; N 10.32; found % C 35.38; H 3.49; N 10.30.

Ethyl ((4-nitro-benzylcarbamoyl)carbamathioyl)carbamate (3l)
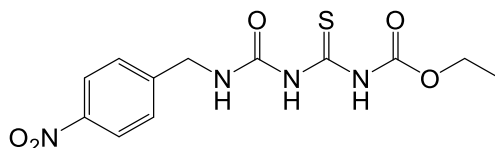
Yield 71%. m.p. 140-141 °C. ^{1}H NMR (DMSO-d$_6$) δ 1.34 (t, J= 7.5 Hz, 3H, CH$_3$), 4.28 (q, J= 7.5 Hz, 2H, CH$_2$), 4.65 (s, 2H, CH$_2$), 7.68 (d, 8.5 Hz, 2H, Ar), 8.33 (d, 8.5 Hz, 2H, Ar), 8.91 (s, 1H, NH), 11.31 (s, 1H, NH),

12.28 (s, 1H, NH). IR (Nujol) 3212, 3170, 3080, 1728, 1694 cm^{-1}. Elemental analysis: calculated for $C_{12}H_{14}N_4O_5S$ (326.33) % C 44.17; H 4.32; N 17.17; found % C 44.20; H 4.33; N 17;16.

General procedure for the synthesis of 3-benzyl-6-methylthio-1,3,5-triazin-2,4-diones (5)

Route A:

Step I: General procedure for the synthesis of 3-benzyl-6-thioxo-1,3,5-trihydro-triazin-2,4-diones (4)

To a mixture of thiourea **(3)** (2 mmol) in dry MeOH (5 mL) NaOMe (0.11 g, 2 mmol) was added. The mixture was heated at 50 °C for 30 minutes. After solvent elimination under vacuum, the obtained solid was dissolved in water (5 mL) and the solution acidified with 10% aqueous HCl until pH 5-6. The formed precipitate was filtered, washed with Et$_2$O and dried.

3-(4-Ethylbenzyl)-6-thioxo-1,3,5-triazin-2,4-dione (4a)
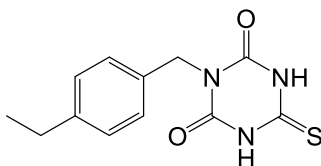
Yield 72%. m.p. >250 °C. ^{1}H NMR (DMSO-d$_6$) δ 1.25 (t, J= 7.2 Hz, 3H, CH$_3$), 2.60 (q, J= 7.2 Hz, 2H, CH$_2$), 5.02 (s, 2H, CH$_2$), 6.98 (d, 8.3 Hz, 2H, Ar), 7.18 (d, 8.3 Hz, 2H, Ar), 11.93 (s, 2H, NH). IR (Nujol) 3069, 1743, 1680 cm^{-1}. Elemental analysis: calculated for $C_{12}H_{13}N_3O_2S$ (263.32) % C 54.74; H 4.98; N 15.96; found % C 54.70; H 4.97; N 15.98.

3-(4-Fluorobenzyl)-6-thioxo-1,3,5-triazin-2,4-dione (4b)
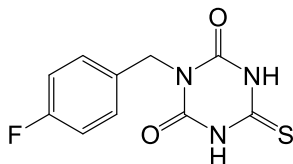
Yield 80%. m.p. 240-241 °C. ^{1}H NMR (DMSO-d_6) δ 4.91 (s, 2H, CH$_2$), 7.25 (m, 2H, Ar), 7.48 (m, 2H, Ar), 12.83 (s, 2H, NH). IR (Nujol) 3085, 1765 cm^{-1}. Elemental analysis: calculated for C$_{10}$H$_8$FN$_3$O$_2$S (253.26) % C 47.43; H 3.18; N 16.59; found % C 47.40; H 3.15; N 16.59.

3-(4-Methoxybenzyl)-6-thioxo-1,3,5-triazin-2,4-dione (4c)
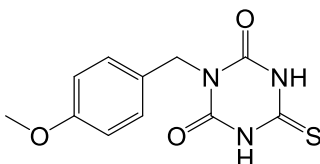
Yield 76%. m.p. >250 °C. ^{1}H NMR (DMSO-d_6) δ 3.83 (s, 3H, CH$_3$), 5.12 (s, 2H, CH$_2$), 6.87 (m, 2H, Ar), 7.25 (m, 2H, Ar), 11.88 (s, 2H, NH). IR (Nujol) 3105, 1763, 1693 cm^{-1}. Elemental analysis: calculated for C$_{11}$H$_{11}$N$_3$O$_3$S (265.29) % C 49.80; H 4.18; N 15.84; found % C 49.83; H 4.19; N 15.82.

3-(4-Chlorobenzyl)-6-thioxo-1,3,5-triazin-2,4-dione (4e)
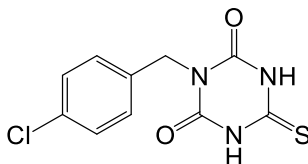
Yield 78%. m.p. >250 °C. ^{1}H NMR (DMSO-d_6) δ 5.10 (s, 2H, CH$_2$), 7.32 (d, 8.3 Hz,2H, Ar), 7.37 (d, 8.3 Hz, 2H, Ar), 10.67 (s, 2H, NH). IR (Nujol) 3075, 1763, 1689 cm^{-1}. Elemental analysis: calculated for C$_{10}$H$_8$ClN$_3$O$_2$S (269.71) % C 44.53; H 2.99; N 15.58; found % C 44.50; H 2.98; N 15.59.

6-Thioxo-3-(4-(trifluoromethyl)benzyl)-1,3,5-triazin-2,4-dione (4f)
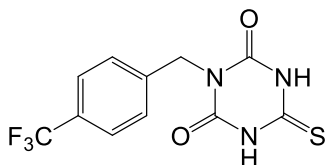
Yield 63%. m.p. >250 °C. ^{1}H NMR (DMSO-d$_6$) δ 4.99 (s, 2H, CH$_2$), 7.16 (d, J= 8.0 Hz, 2H, Ar), 7.50 (d, J= 8.0 Hz, 2H, Ar), 12.01 (s, 2H, NH). IR (Nujol) 3073, 1765, 1690 cm^{-1}. Elemental analysis: calculated for C$_{11}$H$_8$F$_3$N$_3$O$_2$S (303.26) % C 43.57; H 2.66; N 13.86; found % C 43.50; H 2.65; N 13.85.

3-(4-Bromobenzyl)-6-thioxo-1,3,5-triazin-2,4-dione (4g)
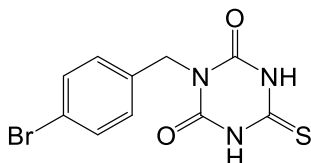
Yield 70%. m.p. >250 °C. ^{1}H NMR (DMSO-d$_6$) δ 5.20 (s, 2H, CH$_2$), 7.12 (d, 8.3 Hz, 2H, Ar), 7.85 (d, 8.3 Hz, 2H, Ar), 11.23 (s, 2H, NH). IR (Nujol) 3074, 1762, 1688 cm^{-1}. Elemental analysis: calculated for C$_{10}$H$_8$BrN$_3$O$_2$S (314.16) % C 38.23; H 2.57; N 13.38; found % C 38.20; H 2.55; N 13.39.

3-(Benzo(d)(1,3)dioxol-5-ylmethyl)-6-thioxo-1,3,5-triazin-2,4-dione (4h)
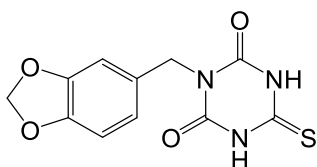
Yield 58%. m.p. >250 °C. ^{1}H NMR (DMSO-d$_6$) δ 5.18 (s, 2H, CH$_2$), 6.07 (s, 2H, CH$_2$), 6.76 (m, 1H, Ar), 6.81 (m, 1H, Ar), 7.03 (s, 1H, Ar), 11.15 (s, 2H, NH). IR (Nujol) 3447, 3347, 3262, 3177, 1713, 1647 cm^{-1}.

Elemental analysis: calculated for $C_{11}H_9N_3O_4S$ (279.27) % C 47.31; H 3.25; N 15.05; found % C 47.33; H 3.27; N 15.01.

Step II: General procedure for the synthesis of 3-benzyl-6-methylthio-1,3,5-triazin-2,4-diones (5)

To a solution of compound **(4)** (2 mmol) in dry MeOH (5 mL) MeI (0.19 mL, 3 mmol) was added. The mixture was heated for 50 °C for 3 h., then the solvent was evaporated under vacuum. Water (5 mL) was added to the resulting residue. The formed solid was filtered off, washed with water (2x 5 mL) and dried.

3-(4-Ethylbenzyl)-6-(methylthio)-1,3,5-triazin-2,4-dione (5a)
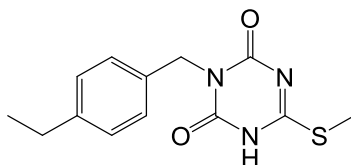
Yield 90%. m.p. 170-172 °C. ^{1}H NMR (DMSO-d_6) δ 1.25 (t, J= 7.5 Hz, 3H, CH$_3$), 2.55 (s, 3H, CH$_3$), 2.60 (q, J= 7.5 Hz, 2H, CH$_2$), 5.18 (s, 2H, CH$_2$), 6.98 (d, 8.3 Hz, 2H, Ar), 7.18 (d, 8.3 Hz, 2H, Ar), 10.47 (s, 1H, NH). IR (Nujol) 3326, 3204, 1754 cm^{-1}. Elemental analysis: calculated for $C_{13}H_{15}N_3O_2S$ (277.34) % C 56.30; H 5.45; N 15.15; found % C 56.32; H 5.46; N 15.13.

3-(4-Fluorobenzyl)-6-(methylthio)-1,3,5-triazin-2,4-dione (5b)
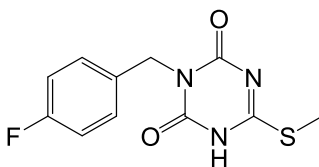
Yield 98%. m.p. 230 °C. ^{1}H NMR (DMSO-d_6) δ 2.58 (d, 3H, CH$_3$), 4.96 (s, 2H, CH$_2$), 7.25 (m, 2H, Ar), 7.45 (m, 2H, Ar), 12.90 (s, 1H, NH). IR (Nujol) 3136, 1733, 1658 cm^{-1}. Elemental analysis: calculated for $C_{11}H_{10}FN_3O_2S$ (267.28) % C 49.43; H 3.77; N 15.72; found % C 49.44; H 3.73; N 15.74.

3-(4-Methoxybenzyl)-6-(methylthio)-1,3,5-triazin-2,4-dione (5c)
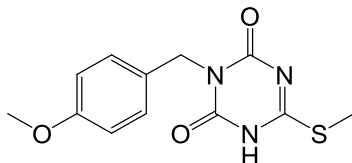
Yield 88%. m.p. 230-233 °C. ^{1}H NMR (DMSO-d$_6$) δ 2.55 (s, 3H, CH$_3$), 3.83 (s, 3H, CH$_3$), 5.20 (s, 2H, CH$_2$), 6.87 (d, 8.0 Hz, 2H, Ar), 7.25 (d, 8.0 Hz, 2H, Ar), 10.9 (s, 1H, NH). IR (Nujol) 3130, 1737 cm^{-1}. Elemental analysis: calculated for C$_{12}$H$_{13}$N$_3$O$_3$S (279.31) % C 51.60; H 4.69; N 15.04; found % C 51.62; H 4.68; N 15.05.

3-(4-Chlorobenzyl)-6-(methylthio)-1,3,5-triazin-2,4-dione (5e)
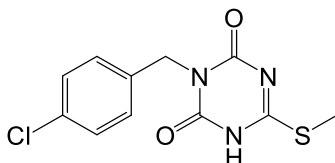
Yield 97%. m.p. 219-222 °C. ^{1}H NMR (DMSO-d$_6$) δ 2.60 (s, 3H, CH$_3$), 5.00 (s, 2H, CH$_2$), 7.45 (m, 4H, Ar), 13.0 (s, 1H, NH). IR (Nujol) 3227, 3136, 1734 cm^{-1}. Elemental analysis: calculated for C$_{11}$H$_{10}$ClN$_3$O$_2$S (283.73) % C 46.56; H 3.55; N 14.81; found % C 46.58; H 3.58; N 14.80.

6-(Methylthio)-3-(4-(trifluoromethyl)benzyl)-1,3,5-triazin-2,4-dione (5f)
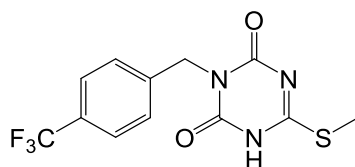
Yield 57%. m.p. 238-245 °C. ^{1}H NMR (DMSO-d$_6$) δ 2.44 (s, 3H, CH$_3$), 4.94 (s, 2H, CH$_2$), 7.48 (m, 2H, Ar), 7.65 (m, 2H, Ar), 12.80 (s, 1H, NH). IR (Nujol) 2720, 1756 cm^{-1}. Elemental analysis: calculated for

C$_{12}$H$_{10}$F$_3$N$_3$O$_2$S (317.29) % C 45.43; H 3.18; N 13.24; found % C 45.44; H 3.16; N 13.22.

3-(4-Bromobenzyl)-6-(methylthio)-1,3,5-triazin-2,4-dione (5g)
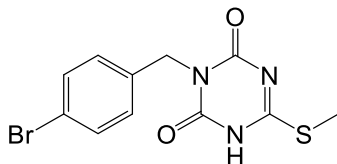
Yield 57%. m.p. 213-219 °C. ^{1}H NMR (DMSO-d$_6$) δ 2.55 (s, 3H, CH$_3$), 5.20 (s, 2H, CH$_2$), 6.05 (s, 1H, NH), 7.12 (d, 8.0 Hz, 2H, Ar), 7.85 (d, 8.0 Hz, 2H, Ar). IR (Nujol) 2178, 1756, 1736 cm^{-1}. Elemental analysis: calculated for C$_{11}$H$_{10}$BrN$_3$O$_2$S (328.18) % C 40.26; H 3.07; N 12.80; found % C 40.28; H 3.05; N 12.81.

3-(Benzo(d)(1,3)dioxol-5-ylmethyl)-6-(methylthio)-1,3,5-triazin-2,4-dione (5h)
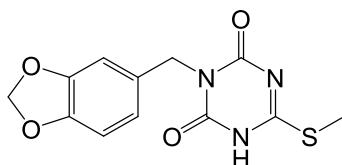
Yield 38%. m.p. 210-215 °C. ^{1}H NMR (DMSO-d$_6$) δ 2.55 (s, 3H, CH$_3$), 5.18 (s, 2H, CH$_2$), 6.02 (s, 1H, NH), 6.07 (s, 2H, CH$_2$), 6.76 (m, 1H, Ar), 6.81 (m, 1H, Ar), 7.03 (m, 1H, Ar). IR (Nujol) 2855, 1728, 1671, 1589, 1501, 1487, 1442, 1376, 1350, 1238, 1031 cm^{-1}. Elemental analysis: calculated for C$_{12}$H$_{11}$N$_3$O$_4$S (293.30) % C 49.14; H 3.78; N 14.33; found % C 49.16; H 3.79; N 14.31.

Route B:

General procedure for the synthesis of 3-benzyl-6-methylthio-1,3,5-triazin-2,4-diones (5)

To a solution of thiourea (3) (2 mmol) in dry MeOH (5 mL) NaOMe (0.11 g, 2 mmol) was added. The mixture was heated at 50 °C for 30 minutes. Then MeI (0.19 mL, 3 mmol) was added and the reaction

mixture was heated at 50 °C for additional 3 h. MeOH was evaporated under vacuum and water (5 mL) was added. The formed solid was filtered, washed with water (2x5 mL) and dried.

3-(4-Methylbenzyl)-6-(methylthio)-1,3,5-triazin-2,4-dione (5d)
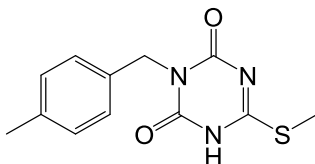
Yield 98%. m.p. 242-247 °C. ^{1}H NMR (DMSO-d$_6$) δ 2.34 (s, 3H, CH$_3$), 2.55 (s, 3H, CH$_3$), 4.99 (s, 2H, CH$_2$), 7.11-7.43 (m, 4H, Ar), 8.20 (s, 1H, NH). IR (Nujol) 3582, 2714, 1754, 1728 cm^{-1}. Elemental analysis: calculated for C$_{12}$H$_{13}$N$_3$O$_2$S (263.32) % C 54.74; H 4.98; N 15.96; found % C 54.70; H 4.96; N 15.99.

3-(4-Iodobenzyl)-6-(methylthio)-1,3,5-triazin-2,4-dione (5i)
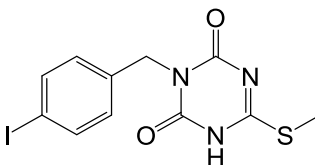
Yield 48%. m.p. 175-179 °C. ^{1}H NMR (DMSO-d$_6$) δ 2.62 (s, 3H, CH$_3$), 4.90 (s, 2H, CH$_2$), 6.83 (s, 1H, NH), 7.22 (d, 8.3 Hz, 2H, Ar), 7.78 (d, 8.3 Hz, 2H, Ar). IR (Nujol) 3582, 1665 cm^{-1}. Elemental analysis: calculated for C$_{11}$H$_{10}$IN$_3$O$_2$S (375.19) % C 35.21; H 2.69; N 11.20; found % C 35.20; H 2.68; N 11.22.

6-(Methylthio)-3-(4-nitrobenzyl)-1,3,5-triazin-2,4-dione (5l)
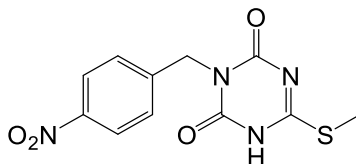
Yield 99%. m.p. 220-223 °C. ^{1}H NMR (DMSO-d$_6$) δ 2.55 (s, 3H, CH$_3$), 5.18 (s, 2H, CH$_2$), 6.02 (s, 1H, NH), 7.95 (m, 2H, Ar), 8.14 (m, 2H, Ar).

IR (Nujol) 3582, 3379, 1757, 1729 cm^{-1}. Elemental analysis: calculated for C$_{11}$H$_{10}$N$_4$O$_4$S (294.29) % C 44.89; H 3.43; N 19.04; found % C 44.87; H 3.45; N 19.07.

General procedure for the synthesis of 1,3-dibenzyl-6-methylthio-1,3,5-triazin-2,4-diones (6)

Thiomethyltriazine **(5)** (2 mmol) was treated with the appropriate benzyl substituted halide (2 mmol) in the presence of K$_2$CO$_3$ (0.55 g, 4 mmol) in dry DMF solution (1.5 mL). The mixture was stirred at r.t. for 48 h, then water (10 mL) was added and the obtained solid was filtered, washed with water (2x5 mL) and dried.

3-(4-Ethylbenzyl)-1-(4-methoxybenzyl)-6-(methylthio)-1,3,5-triazine-2,4(1H,3H)-dione (6a)
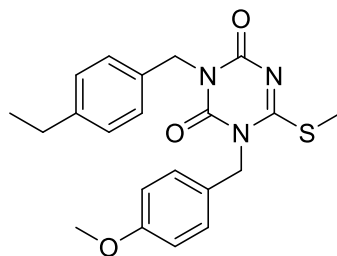
Yield 80%. m.p. 120-126 °C. ^{1}H NMR (DMSO-d$_6$) δ 1.24 (t, J= 7.2 Hz, 3H, CH$_3$), 2.45 (s, 3H, CH$_3$), 2.54 (q, J= 7.2 Hz, 2H, CH$_2$), 3.70 (s, 3H, CH$_3$), 4.89 (s, 2H, CH$_2$), 5.01 (s, 2H, CH$_2$), 6.88 (d, 8.0 Hz, 2H, Ar), 7.13 (d, 8.0 Hz, 2H, Ar), 7.19 (m, 4H, Ar). IR (Nujol) 1729 cm^{-1}. Elemental analysis: calculated for C$_{21}$H$_{23}$N$_3$O$_3$S (397.49) % C 63.45; H 5.83; N 10.57; found % C 63.47; H 5.87; N 10.50.

3-(4-Fluorobenzyl)-1-(4-methoxybenzyl)-6-(methylthio)-1,3,5-triazine-2,4(1H,3H)-dione (6b)
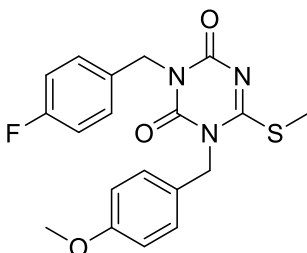
Yield 74%. m.p. 127-129 °C. ^{1}H NMR (DMSO-d$_6$) δ 2.59 (s, 3H CH$_3$), 3.85 (s, 3H, CH$_3$), 5.05 (s, 2H, CH$_2$), 5.14 (s, 2H, CH$_2$), 7.02 (d, J= 8.2 Hz, 2H, Ar), 7.26 (m, 2H, Ar), 7.36 (d, J= 8.2 Hz, 2H, Ar), 7.49 (t, 2H, Ar). IR (Nujol) 3582, 1721 cm^{-1}. Elemental analysis: calculated for C$_{19}$H$_{18}$FN$_3$O$_3$S (387,43) % C 58.90; H 4.68; N 10.85; found % C 58.95; H 4.68; N 10.80.

1-Benzyl-3-(4-methoxybenzyl)-6-(methylthio)-1,3,5-triazine-2,4(1H,3H)-dione (6c)
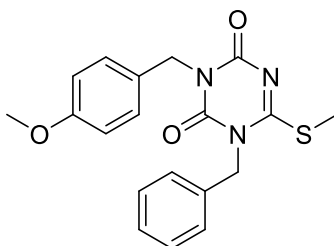
Yield 84%. m.p. 115-119 °C. ^{1}H NMR (DMSO-d$_6$) δ 2.00 (s, 3H, CH$_3$), 3.72 (s, 3H, CH$_3$), 4.42 (s, 4H, CH$_2$), 6.65 (m, 2H, Ar), 6.95 (m, 2H, Ar), 7.25 (m, 1H, Ar), 7.26 (m, 2H, Ar), 7.31 (s, 2H, Ar). IR (Nujol) 3581, 1726 cm^{-1}. Elemental analysis: calculated for C$_{19}$H$_{19}$N$_3$O$_3$S (369.44) % C 61.77; H 5.18; N 11.37; found % C 61.79; H 5.16; N 11.39.

1-(4-Methoxybenzyl)-3-(4-methylbenzyl)-6-(methylthio)-1,3,5-triazine-2,4(1H,3H)-dione (6d)
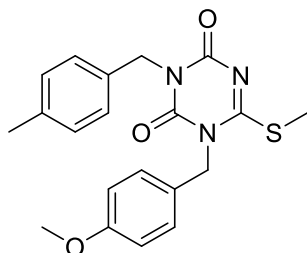
Yield 82%. m.p. 132-135 °C. ^{1}H NMR (DMSO-d$_6$) δ 2.0 (s, 3H, CH$_3$), 2.19 (s, 3H, CH$_3$), 3.72 (s, 3H, CH$_3$), 4.42 (s, 4H, CH$_2$), 6.65 (m, 2H, Ar), 6.94 (m, 2H, Ar), 6.95 (m, 2H, Ar), 7.12 (m, 2H, Ar). IR (Nujol) 3581, 1725 cm^{-1}. Elemental analysis: calculated for C$_{20}$H$_{21}$N$_3$O$_3$S (383.46) % C 62.64; H 5.52; N 10.96; found % C 62.62; H 5.53; N 10.97.

1,3-bis(4-Methoxybenzyl)-6-(methylthio)-1,3,5-triazine-2,4(1H,3H)-dione (6e)
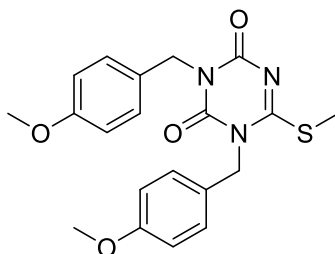
Yield 80%. m.p. 106-110 °C. ^{1}H NMR (DMSO-d$_6$) δ 2.0 (s, 3H CH$_3$). 3.72 (s, 6H, CH$_3$). 4.42 (s, 4H, CH$_2$), 6.65 (m, 4H, Ar), 6.95 (m, 4H, Ar). IR (Nujol) 3582, 1726 cm^{-1}. Elemental analysis: calculated for C$_{20}$H$_{21}$N$_3$O$_4$S (399.46) % C 60.13; H 5.30; N 10.52; found % C 60.15; H 5.30; N 10.51.

3-(4-Chlorobenzyl)-1-(4-methoxybenzyl)-6-(methylthio)-1,3,5-triazine-2,4(1H,3H)-dione (6f)
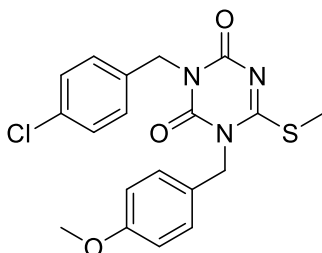
Yield 60%. m.p. 130-133 °C. ^{1}H NMR (DMSO-d_6) δ 2.0 (s, 3H CH$_3$), 3.72 (s, 3H, CH$_3$), 4.42 (s, 4H, CH$_2$), 6.65 (d, J= 8.2 Hz,2H, Ar), 6.95 (d, J= 8.0 Hz, 2H, Ar), 7.32 (d, J= 7.2 Hz, 2H, Ar), 7.39 (d, J= 8.0 Hz, 2H, Ar). IR (Nujol) 3582, 1724 cm^{-1}. Elemental analysis: calculated for C$_{19}$H$_{18}$ClN$_3$O$_3$S (403.89) % C 56.50; H 4.49; N 10.40; found % C 56.54; H 4.47; N 10.40.

1-(4-Methoxybenzyl)-6-(methylthio)-3-(4-(trifluoromethyl)benzyl)-1,3,5-triazine-2,4(1H,3H)-dione (6g)
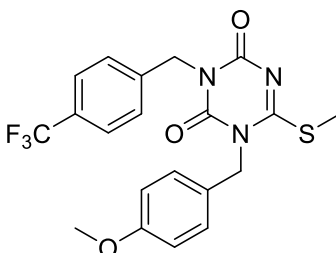
Yield 80%. m.p. 125 °C. ^{1}H NMR (DMSO-d_6) δ 2.0 (s, 3H, CH$_3$), 3.72 (s, 3H, CH$_3$), 4.42 (s, 4H, CH$_2$), 6.65 (m, 2H, Ar), 6.95 (m, 2H, Ar), 6.99 (m, 2H, Ar), 7.54 (m, 2H, Ar). IR (Nujol) 3582, 3395, 1728cm^{-1}. Elemental analysis: calculated for C$_{20}$H$_{18}$F$_3$N$_3$O$_3$S (437.44) % C 54.91; H 4.15; N 9.61; found % C 54.89; H 4.18; N 9.60.

1-(4-Bromobenzyl)-3-(4-methoxybenzyl)-6-(methylthio)-1,3,5-triazine-2,4(1H,3H)-dione (6h)
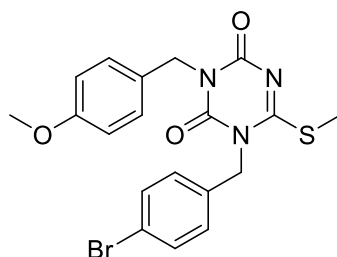
Yield 82%. m.p. 117-122 °C. ^{1}H NMR (DMSO-d_6) δ 2.01 (s, 3H, CH$_3$), 3.72 (s, 3H, CH$_3$), 4.42 (s, 4H, CH$_2$), 6.65 (m, 2H, Ar), 6.95 (m, 4H, Ar), 7.31 (m, 2H, Ar). IR (Nujol) 3582, 3493, 1724 cm^{-1}. Elemental analysis: calculated for $C_{19}H_{18}BrN_3O_3S$ (448.33) % C 50.90; H 4.05; N 9.37; found % C 50.94; H 4.02; N 9.39.

3-(4-Bromobenzyl)-1-(4-methoxybenzyl)-6-(methylthio)-1,3,5-triazine-2,4(1H,3H)-dione (6i)
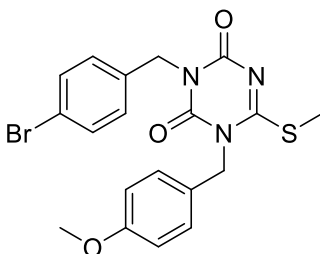
Yield 36%. m.p. 123-126 °C. ^{1}H NMR (DMSO-d_6) δ 2.0 (s, 3H, CH$_3$), 3.72 (s, 3H, CH$_3$), 4.42 (s, 4H, CH$_2$), 6.65 (m, 2H, Ar), 6.95 (m, 4H, Ar), 7.31 (m, 2H, Ar). IR (Nujol) 3582, 1725 cm^{-1}. Elemental analysis: calculated for $C_{19}H_{18}BrN_3O_3S$ (448.33) % C 50.90; H 4.05; N 9.37; found % C 50.92; H 4,05; N 9.36.

1-(3,4-Dichlorobenzyl)-3-(4-methoxybenzyl)-6-(methylthio)-1,3,5-triazine-2,4(1H,3H)-dione (6l)
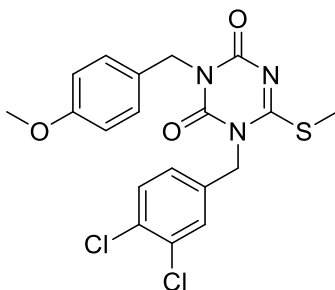
Yield 43%. m.p. 136-138 °C. ^{1}H NMR (DMSO-d_6) δ 2.0 (s, 3H, CH$_3$), 3.72 (s, 3H, CH$_3$), 4.42 (s, 4H, CH$_2$), 6.65 (m, 2H, Ar), 6.95 (m, 2H, Ar), 6.88 (s, 1H, Ar), 7.01 (m, 1H, Ar), 7.09 (m, 1H, Ar). IR (Nujol) 3582, 3478, 1731 cm^{-1}. Elemental analysis: calculated for C$_{19}$H$_{17}$Cl$_2$N$_3$O$_3$S (438.33) % C 52.06; H 3.91; N 9.59; found % C 52.08; H 3.90; N 9.57.

1-(4-Methylbenzyl)-6-(methylthio)-3-(4-(trifluoromethyl)benzyl)-1,3,5-triazine-2,4(1H,3H)-dione (6m)
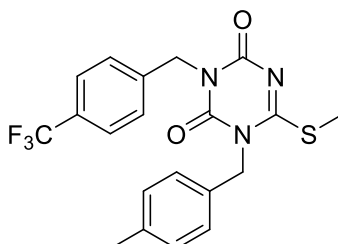
Yield 22%. m.p. 115-120 °C. ^{1}H NMR (DMSO-d_6) δ 2.03 (s, 3H, CH$_3$), 2.19 (s, 3H, CH$_3$), 4.42 (s, 4H, CH$_2$), 6.94 (d, J= 8.2 Hz, 2H, Ar), 6.99 (d, J= 8.0 Hz,2H, Ar), 7.12 (d, J= 8.2 Hz, 2H, Ar), 7.54 (d, J= 8.0 Hz, 2H, Ar). IR (Nujol) 3582, 1735 cm^{-1}. Elemental analysis: calculated for C$_{20}$H$_{18}$F$_3$N$_3$O$_2$S (421.44) % C 57.00; H 4.31; N 9.97; found % C 57.02; H 4.33; N 9.92.

1-(3,4-Dichlorobenzyl)-3-(4-methylbenzyl)-6-(methylthio)-1,3,5-triazine-2,4(1H,3H)-dione (6n)
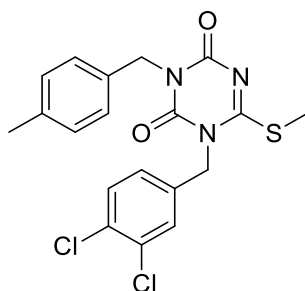
Yield 84%. m.p. 134-139 °C. ^{1}H NMR (DMSO-d$_6$) δ 2.0 (s, 3H, CH$_3$), 2.19 (s, 3H, CH$_3$), 4.42 (s, 4H, CH$_2$), 6.88 (m, 1H, Ar), 6.94 (m, 2H, Ar), 7.01 (s, 1H, Ar), 7.09 (s, 1H, Ar), 7.12 (m, 2H, Ar). IR (Nujol) 3582, 1730 cm^{-1}. Elemental analysis: calculated for C$_{19}$H$_{17}$Cl$_2$N$_3$O$_2$S (422.33) % C 54.03; H 4.06; N 9.95; found % C 54.03; H 4.05; N 9.97.

3-(4-Methoxybenzyl)-1-(4-methylbenzyl)-6-(methylthio)-1,3,5-triazine-2,4(1H,3H)-dione (6o)
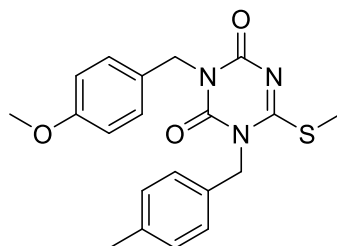
Yield 45%. m.p. 119-123 °C. ^{1}H NMR (DMSO-d$_6$) δ 2.0 (s, 3H, CH$_3$), 2.19 (s, 3H, CH$_3$), 3.72 (s, 3H, CH$_3$), 4.42 (s, 4H, CH$_2$), 6.65 (d, J= 8.0 Hz, 2H, Ar), 6.94 (d, J= 8.3 Hz, 2H, Ar), 6.95 (d, J= 8.3 Hz, 2H, Ar), 7.12 (d, J= 8.0 Hz, 2H, Ar). IR (Nujol) 3582, 1727 cm^{-1}. Elemental analysis: calculated for C$_{20}$H$_{21}$N$_3$O$_3$S (383.46) % C 62.64; H 5.52; N 10.96; found % C 62.61; H 5.53; N 10.98.

1-(4-Fluorobenzyl)-3-(4-methoxybenzyl)-6-(methylthio)-1,3,5-triazine-2,4(1H,3H)-dione (6p)
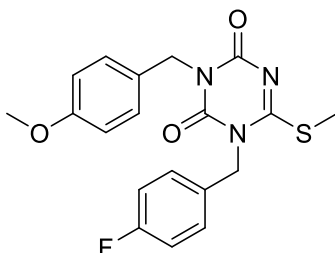
Yield 50 %. m.p. 109-112 °C. ^{1}H NMR (DMSO-d$_6$) δ 2.0 (s, 3H, CH$_3$), 3.72 (s, 3H, CH$_3$), 4.42 (s, 4H, CH$_2$), 6.65 (m, 2H, Ar), 6.95 (m, 2H, Ar), 7.07 (m, 2H, Ar), 7.39 (m, 2H, Ar). IR (Nujol) 3582, 1729 cm^{-1}. Elemental analysis: calculated for C$_{19}$H$_{18}$FN$_3$O$_3$S (387.43) % C 58.90; H 4.68; N 10.85; found % C 58.94; H 4.67; N 10.80.

1-(4-Chlorobenzyl)-3-(4-methoxybenzyl)-6-(methylthio)-1,3,5-triazine-2,4(1H,3H)-dione (6q)
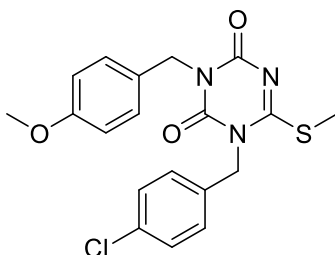
Yield 25%. m.p. 116-122 °C. ^{1}H NMR (DMSO-d$_6$) δ 2.0 (s, 3H, CH$_3$), 3.72 (s, 3H, CH$_3$), 4.42 (s, 4H, CH$_2$), 6.65 (d, J= 8.0 Hz, 2H, Ar), 6.95 (d J= 8.0 Hz,, 2H, Ar), 7.32 (d, J= 8.0 Hz, 2H, Ar), 7.39 (d, J= 8.0 Hz, 2H, Ar). IR (Nujol) 3582, 1731 cm^{-1}. Elemental analysis: calculated for C$_{19}$H$_{18}$ClN$_3$O$_3$S (403.89) % C 56.50; H 4.49; N 10.40; found % C 56.52; H 4.47; N 10.41.

3-(4-Methoxybenzyl)-6-(methylthio)-1-(4-(trifluoromethyl)benzyl)-1,3,5-triazine-2,4(1H,3H)-dione (6r)
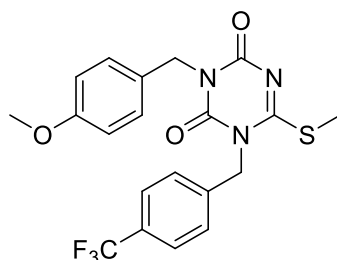
Yield 41%. m.p. 130-132 °C. ^{1}H NMR (DMSO-d$_6$) δ 2.0 (s, 3H, CH$_3$), 3.72 (s, 3H, CH$_3$), 4.42 (s, 4H, CH$_2$), 6.65 (m, 2H, Ar), 6.95 (m, 2H, Ar), 6.99 (m, 2H, Ar), 7.54 (m, 2H, Ar). IR (Nujol) 3582, 3384, 1735 cm^{-1}. Elemental analysis: calculated for C$_{20}$H$_{18}$F$_3$N$_3$O$_3$S (437.44) % C 54.91; H 4.15; N 9.61; found % C 54.88; H 4.18; N 9.60.

3-(Benzo(d)(1,3)dioxol-5-ylmethyl)-1-(4-methoxybenzyl)-6-(methylthio)-1,3,5-triazine-2,4(1H,3H)-dione (6s)
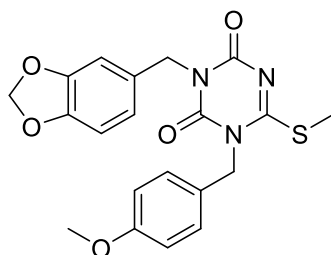
Yield 24%. m.p. 123-125 °C. ^{1}H NMR (DMSO-d$_6$) δ 2.0 (s, 3H, CH$_3$), 3.72 (s, 3H, CH$_3$), 4.42 (s, 4H, CH$_2$), 6.06 (s, 2H, CH$_2$), 6.51 (m, 1H, Ar), 6.65 (s, 2H, Ar), 6.86 (m, 1H, Ar), 6.95 (m, 2H, Ar), 7.03 (m, 1H, Ar). IR (Nujol) 3582, 3312, 1721, 1662 cm^{-1}. Elemental analysis: calculated for C$_{20}$H$_{19}$N$_3$O$_5$S (413.45) % C 58.10; H 4.63; N 10.16; found % C 58.11; H 4.65; N 10.12.

1-(4-Iodobenzyl)-3-(4-methoxybenzyl)-6-(methylthio)-1,3,5-triazine-2,4(1H,3H)-dione (6t)
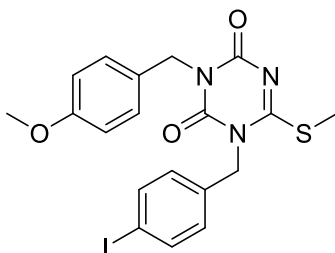
Yield 30%. m.p. 129-132 °C. ^{1}H NMR (DMSO-d_6) δ 2.0 (s, 3H, CH$_3$), 3.72 (s, 3H, CH$_3$), 4.42 (s, 4H, CH$_2$), 6.65 (m, 2H, Ar), 6.83 (m, 2H, Ar), 6.95 (m, 2H, Ar), 7.52 (m, 2H, Ar). IR (Nujol) 3582, 1733, 1673, 1608 cm^{-1}. Elemental analysis: calculated for C$_{19}$H$_{18}$IN$_3$O$_3$S (495.33) % C 46.07; H 3.66; N 8.48; found % C 46.08; H 3.62; N 8.49.

3-(4-Iodobenzyl)-1-(4-methoxybenzyl)-6-(methylthio)-1,3,5-triazine-2,4(1H,3H)-dione (6u)
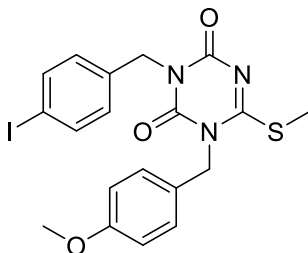
Yield 80%. m.p. 110-116 °C. ^{1}H NMR (DMSO-d_6) δ 2.0 (s, 3H, CH$_3$), 3.72 (s, 3H, CH$_3$), 4.42 (s, 4H, CH$_2$), 6.65 (d, J= 8.0 Hz, 2H, Ar), 6.83 (d, J= 8.0 Hz, 2H, Ar), 6.95 (d, J= 8.0 Hz, 2H, Ar), 7.52 (d, J= 8.0 Hz, 2H, Ar). IR (Nujol) 3582, 1726 cm^{-1}. Elemental analysis: calculated for C$_{19}$H$_{18}$IN$_3$O$_3$S (495.33) % C 46.07; H 3.66; N 8.48; found % C 46.09; H 3.62; N 8.47.

1-(4-Methoxybenzyl)-6-(methylthio)-3-(4-nitrobenzyl)-1,3,5-triazine-2,4(1H,3H)-dione (6v)
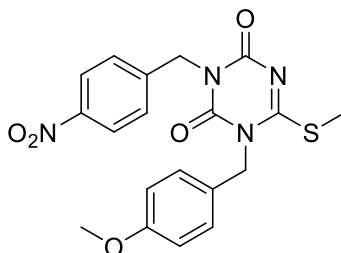
Yield 44%. 129-131 °C. ^{1}H NMR (DMSO-d$_6$) δ 2.0 (s, 3H, CH$_3$), 3.72 (s, 3H, CH$_3$), 4.42 (s, 4H, CH$_2$), 6.65 (d, J= 8.2 Hz, 2H, Ar), 6.95 (d, J= 8.0 Hz, 2H, Ar), 7.32 (d, J= 8.2 Hz, 2H, Ar), 8.17 (d, J= 8.0 Hz, 2H, Ar). IR (Nujol) 3582, 3457, 1732 cm^{-1}. Elemental analysis: calculated for C$_{19}$H$_{18}$N$_4$O$_5$S (414.44) % C 55.06; H 4.38; N 13.52; found % C 55.08; H 4.37; N 13.53.

General procedure for the synthesis of 6-((2-aminoethyl)amino)-1,3-dibenzyl-1,3,5-triazine- 2,4(1*H*,3*H*)-dione (7)

To a solution of S-methyl-triazinedione **(6)** (2 mmol) in dry toluene (10 mL) ethylenediamine (0.7 mL, 10 mmol) was added. The mixture was refluxed for 16 h. After solvent elimination under vacuum, the residue was suspended in iPr$_2$O (10 mL) and the obtained solid was filtered, washed with iPr$_2$O (2x2.5 mL) and dried.

6-((2-Aminoethyl)amino)-3-(4-ethylbenzyl)-1-(4-methoxybenzyl)-1,3,5-triazine-2,4(1H,3H)-dione (7a)
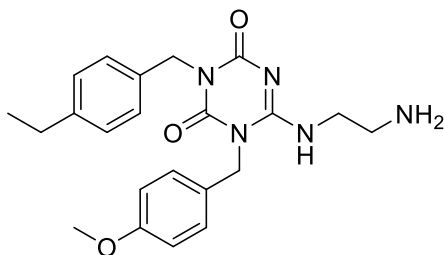
Yield 99%. m.p. 183-185 °C. ^{1}H NMR (DMSO-d$_6$) δ 1.24 (t, J= 7.0 Hz, 3H, CH$_3$), 2.59 (q, J= 7.0 Hz, 2H, CH$_2$), 2.91 (m, 4H, CH$_2$), 3.72 (s, 3H, CH$_3$), 4.42 (s, 4H, CH$_2$), 5.80 (s, 2H, NH$_2$), 6.65 (m, 2H, Ar), 6.95 (m, 2H, Ar), 7.00 (m, 2H, Ar), 7.01 (m, 2H, Ar), 8.12 (s, 1H, NH). IR 3378, 3196, 1687, 1560 cm^{-1}. Elemental analysis: calculated for C$_{22}$H$_{27}$N$_5$O$_3$ (409.48) % C 64.53; H 6.65; N 17.10; found % C 64.55; H 6.66; N 17.06.

6-((2-Aminoethyl)amino)-3-(4-fluorobenzyl)-1-(4-methoxybenzyl)-1,3,5-triazine-2,4(1H,3H)-dione (7b)
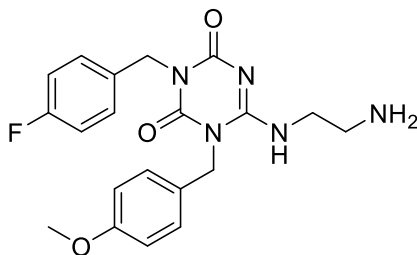
Yield 17%. m.p. 182-186 °C. ^{1}H NMR (DMSO-d$_6$) δ 2.91 (m, 4H, CH$_2$), 3.72 (s, 3H, CH$_3$), 4.42 (s, 4H, CH$_2$), 5.92 (s, 2H, NH$_2$), 6.65 (d, J= 8.0 Hz, 2H, Ar), 6.95 (d, J= 8.0 Hz, 2H, Ar), 7.07 (d, J= 8.0 Hz, 2H, Ar), 7.39 (d, J= 8.0 Hz, 2H, Ar), 7.89 (s, 1H, NH). IR (Nujol) 3331, 1720, 1561 cm^{-1}. Elemental analysis: calculated for C$_{20}$H$_{22}$FN$_5$O$_3$ (399.42) % C 60.14; H 5.55; N 17.53; found % C 60.15; H 5.53; N 17.52.

6-((2-Aminoethyl)amino)-1-benzyl-3-(4-methoxybenzyl)-1,3,5-triazine-2,4(1H,3H)-dione (7c)
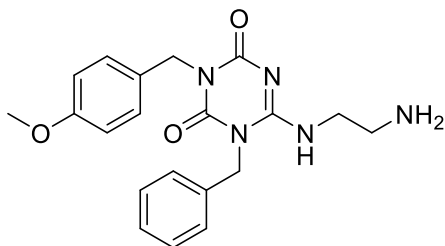
Yield 88 %. m.p. 192-195 °C. ^{1}H NMR (DMSO-d$_6$) δ 2,91 (t, J= 7.5 Hz, 4H, CH$_2$), 3,72 (s, 3H, CH$_3$), 4,42 (s, 4H, CH$_2$), 5.82 (s, 2H, NH$_2$), 6,65 (d, J= 8.0 Hz, 2H, Ar), 6,95 (d, J= 8.5 Hz, 2H, Ar), 7,25 (d, J= 8.0 Hz, 1H, Ar), 7,26 (t, J= 8.5 Hz, 2H, Ar), 7,31 (d, 2H, Ar), 8.04 (s, 1H, NH). IR 3342, 1705, 1570 cm^{-1}. Elemental analysis: calculated for C$_{20}$H$_{23}$N$_5$O$_3$ (381,43) % C 62.98; H 6.08; N 18.36; found % C 62.99; H 6.05; N 18.35.

6-((2-Aminoethyl)amino)-1-(4-methoxybenzyl)-3-(4-methylbenzyl)-1,3,5-triazine-2,4(1H,3H)-dione (7d)
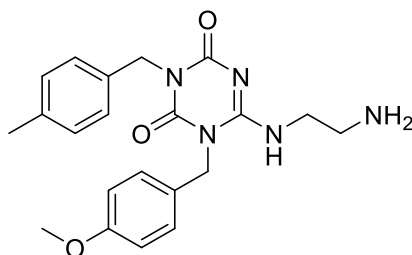
Yield 83%. m.p. 179-183 °C. ^{1}H NMR (DMSO-d$_6$) δ 2.19 (s, 3H, CH$_3$), 2.91 (m, 4H, CH$_2$), 3.72 (s, 3H, CH$_3$), 4.42 (s, 4H, CH$_2$), 5.77 (s, 2H, NH$_2$), 6.65 (d, J= 8.5 Hz, 2H, Ar), 6.94 (d, J= 8.2 Hz, 2H, Ar), 6.95 (d, J= 8.2 Hz, 2H, Ar), 7.12 (d, J= 8.5 Hz, 2H, Ar), 8.13 (s, 1H, NH). IR 3328, 1712, 1587 cm^{-1}. Elemental analysis: calculated for C$_{21}$H$_{25}$N$_5$O$_3$ (395.45) % C 63.78; H 6.37; N 17.71; found % C 63.76; H 6.35; N 17.76.

6-((2-Aminoethyl)amino)-1,3-bis(4-methoxybenzyl)-1,3,5-triazine-2,4(1H,3H)-dione (7e)
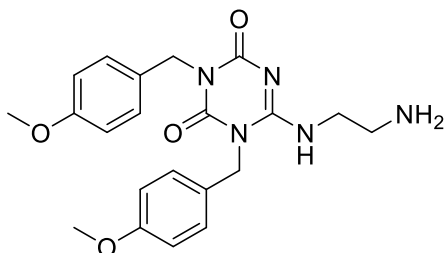
Yield 78%. m.p. 198-200 °C. ^{1}H NMR (DMSO-d$_6$) δ 2.91 (t, J= 7.5 Hz, 4H, CH$_2$), 3.72 (s, 6H, CH$_3$), 4.42 (s, 4H, CH$_2$), 5.78 (s, 2H, NH$_2$), 6.65 (m, 4H, Ar), 6.95 (m, 4H, Ar), 7.99 (s, 1H, NH). IR 3298, 1703, 1580 cm^{-1}. Elemental analysis: calculated for C$_{21}$H$_{25}$N$_5$O$_4$ (411.45) % C 61.30; H 6.12; N 17.02; found % C 61.32; H 6.13; N 17.00.

6-((2-Aminoethyl)amino)-3-(4-chlorobenzyl)-1-(4-methoxybenzyl)-1,3,5-triazine-2,4(1H,3H)-dione (7f)
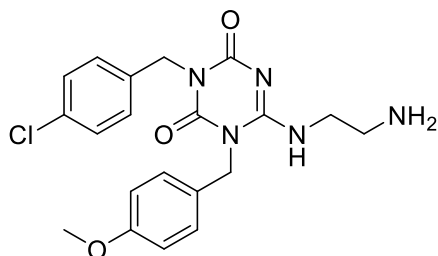
Yield 88%. m.p. 185-187 °C. ^{1}H NMR (DMSO-d$_6$) δ 2.91 (t, J= 7.0 Hz, 4H, CH$_2$), 3.72 (s, 3H, CH$_3$), 4.42 (s, 4H, CH$_2$), 5.67 (s, 2H, NH$_2$), 6.65 (d, J= 8.0 Hz, 2H, Ar), 6.95 (d, J= 8.0 Hz, 2H, Ar), 7.32 (d, J= 8.0 Hz, 2H, Ar), 7.39 (d, J= 8.0 Hz, 2H, Ar), 8.59 (s, 1H, NH). IR 3348, 1696, 1571 cm^{-1}. Elemental analysis: calculated for C$_{20}$H$_{22}$ClN$_5$O$_3$ (415.87) % C 57.76; H 5.33; N 16.84; found % C 57.77; H 5.30; N 16.86.

6-((2-Aminoethyl)amino)-1-(4-methoxybenzyl)-3-(4-(trifluoromethyl)benzyl)-1,3,5-triazine-2,4(1H,3H)-dione (7g)

Yield 75%. m.p. 180-183 °C. ^{1}H NMR (DMSO-d$_6$) δ 2.91 (t, J= 7.0 Hz, 4H, CH$_2$), 3.72 (s, 3H, CH$_3$), 4.42 (s, 4H, CH$_2$), 5.93 (s, 2H, NH$_2$), 6.65 (m, 2H, Ar), 6.95 (m, 2H, Ar), 6.99 (m, 2H, Ar), 7.54 (m, 2H, Ar), 8.23 (s, 1H, NH). IR 3323, 1694, 1570 cm^{-1}. Elemental analysis: calculated for C$_{21}$H$_{22}$F$_3$N$_5$O$_3$ (449.43) % C 56.12; H 4.93; N 15.58; found % C 56.10; H 4.94; N 15.59.

6-((2-Aminoethyl)amino)-1-(4-bromobenzyl)-3-(4-methoxybenzyl)-1,3,5-triazine-2,4(1H,3H)-dione (7h)
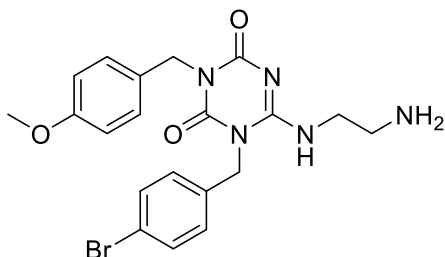
Yield 82%. m.p. 192-196 °C. ^{1}H NMR (DMSO-d$_6$) δ 2.91 (m, 4H, CH$_2$), 3.72 (s, 3H, CH$_3$), 4.42 (s, 4H, CH$_2$), 5.85 (s, 2H, NH$_2$), 6.65 (d, J= 8.5 Hz, 2H, Ar), 6.95 (m, 4H, Ar), 7.31 (d, J= 8.5 Hz, 2H, Ar), 7.89 (s, 1H, NH). IR 3326, 1717, 1566 cm^{-1}. Elemental analysis: calculated for C$_{20}$H$_{22}$BrN$_5$O$_3$ (460.32) % C 52.18; H 4.82; N 15.21; found % C 52.19; H 4.80; N 15.24.

6-((2-Aminoethyl)amino)-3-(4-bromobenzyl)-1-(4-methoxybenzyl)-1,3,5-triazine-2,4(1H,3H)-dione (7i)

Yield 80%. m.p. 170-172 °C. ^{1}H NMR (DMSO-d_6) δ 2.91 (t, J= 7.0 Hz, 4H, CH$_2$), 3.72 (s, 3H, CH$_3$), 4.42 (s, 4H, CH$_2$), 5.80 (s, 2H, NH$_2$), 6.65 (d, J= 8.0 Hz, 2H, Ar), 6.95 (m, 4H, Ar), 7.31 (d, J= 8.0 Hz, 2H, Ar), 7.77 (s, 1H, NH). IR 3337, 1702, 1570 cm^{-1}. Elemental analysis: calculated for C$_{20}$H$_{22}$BrN$_5$O$_3$ (460.32) % C 52.18; H 4.82; N 15.21; found % C 52.17; H 4.83; N 15.21.

6-((2-Aminoethyl)amino)-1-(3,4-dichlorobenzyl)-3-(4-methoxybenzyl)-1,3,5-triazine-2,4(1H,3H)-dione (7l)
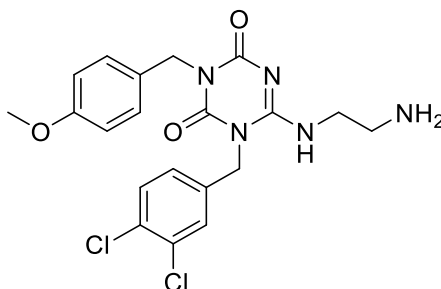
Yield 78%. m.p. 188-192 °C. ^{1}H NMR (DMSO-d_6) δ 2.91 (m, 4H, CH$_2$), 3.72 (s, 3H, CH$_3$), 4.42 (s, 4H, CH$_2$), 5.84 (s, 2H, NH$_2$), 6.65 (d, J= 8.0 Hz, 2H, Ar), 6.95 (d, J= 8.0 Hz, 2H, Ar), 6.88 (m, 1H, Ar), 7.01 (m,, 1H, Ar), 7.09 (s, 1H, Ar), 8.07 (s, 1H, NH). IR 3340, 1708, 1582 cm^{-1}. Elemental analysis: calculated for C$_{20}$H$_{21}$Cl$_2$N$_5$O$_3$ (450.32) % C 53.34; H 4.70; N 15.55; found % C 53.35; H 4.74; N 15.55.

6-((2-Aminoethyl)amino)-1-(4-methylbenzyl)-3-(4-(trifluoromethyl)benzyl)-1,3,5-triazine-2,4(1H,3H)-dione (7m)
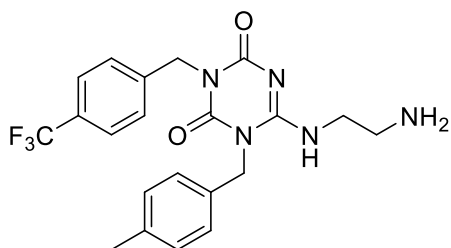
Yield 67%. m.p. 203-205 °C. ^{1}H NMR (DMSO-d$_6$) δ 2.19 (s, 3H, CH$_3$), 2.91 (t, J= 7.5 Hz, 4H, CH$_2$), 4.42 (s, 4H, CH$_2$), 5.67 (s, 2H, NH$_2$), 6.94 (m, 2H, Ar), 6.99 (m, 2H, Ar), 7.12 (m, 2H, Ar), 7.54 (m, 2H, Ar), 7.89 (s, 1H, NH). IR 3298, 1697, 1588 cm^{-1}. Elemental analysis: calculated for C$_{21}$H$_{22}$F$_3$N$_5$O$_2$ (433.43) % C 58.19; H 5.12; N 16.16; found % C 58.15; H 5.13; N 16.12.

6-((2-Aminoethyl)amino)-1-(3,4-dichlorobenzyl)-3-(4-methylbenzyl)-1,3,5-triazine-2,4(1H,3H)-dione (7n)
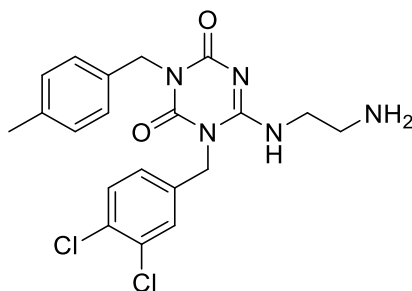
Yield 68%. m.p. 199-201 °C. ^{1}H NMR (DMSO-d$_6$) δ 2.19 (s, 3H, CH$_3$), 2.91 (m, 4H, CH$_2$), 4.42 (s, 4H, CH$_2$), 5.92 (s, 2H, NH$_2$), 6.88 (m, 1H, Ar), 6.94 (m, 2H, Ar), 7.01 (s, 1H, Ar), 7.09 (s, 1H, Ar), 7.12 (m, 2H, Ar), 7.78 (s, 1H, NH). IR 3315, 1702, 1567 cm^{-1}. Elemental analysis: calculated for C$_{20}$H$_{21}$Cl$_2$N$_5$O$_2$ (434.32) % C 55.31; H 4.87; N 16.12; found % C 55.30; H 4.85; N 16.18.

6-((2-Aminoethyl)amino)-3-(4-methoxybenzyl)-1-(4-methylbenzyl)-1,3,5-triazine-2,4(1H,3H)-dione (7o)
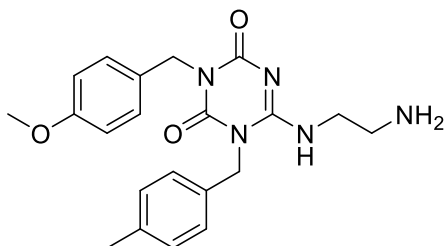
Yield 89%. m.p. 176-179 °C. ^{1}H NMR (DMSO-d$_6$) δ 2.19 (s, 3H, CH$_3$), 2.91 (t, J= 7.0 Hz, 4H, CH$_2$), 3.72 (s, 3H, CH$_3$), 4.42 (s, 4H, CH$_2$), 5.76 (s, 2H, NH$_2$), 6.65 (d, J= 8.0 Hz, 2H, Ar), 6.94 (d, J= 8.0 Hz, 2H, Ar), 6.95 (d, J= 8.0 Hz, 2H, Ar), 7.12 (d, J= 8.0 Hz, 2H, Ar), 8.00 (s, 1H, NH). IR 3330, 3124, 1698, 1577 cm^{-1}. Elemental analysis: calculated for C$_{21}$H$_{25}$N$_5$O$_3$ (395.46) % C 63.78; H 6.37; N 17.71; found % C 63.79; H 6.34; N 17.72.

6-((2-Aminoethyl)amino)-1-(4-fluorobenzyl)-3-(4-methoxybenzyl)-1,3,5-triazine-2,4(1H,3H)-dione (7p)
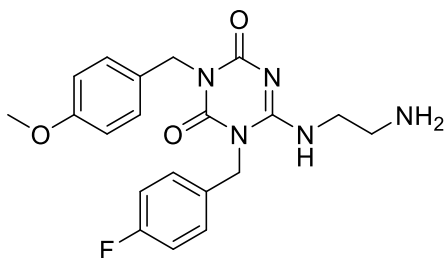
Yield 83%. m.p. 193-196 °C. ^{1}H NMR (DMSO-d$_6$) δ 2.91 (t, J= 7.5 Hz, 4H, CH$_2$), 3.72 (s, 3H, CH$_3$), 4.42 (s, 4H, CH$_2$), 5.76 (s, 2H, NH$_2$), 6.65 (d, J= 8.0 Hz, 2H, Ar), 6.95 (d, J= 8.0 Hz, 2H, Ar), 7.07 (m, 2H, Ar), 7.39 (m, 2H, Ar), 7.98 (s, 1H, NH). IR 3327, 3290, 1699, 1575 cm^{-1}. Elemental analysis: calculated for C$_{20}$H$_{22}$FN$_5$O$_3$ (399.42) % C 60.14; H 5.55; N 17.53; found % C 60.17; H 5.52; N 17.50.

6-((2-Aminoethyl)amino)-1-(4-chlorobenzyl)-3-(4-methoxybenzyl)-1,3,5-triazine-2,4(1H,3H)-dione (7q)
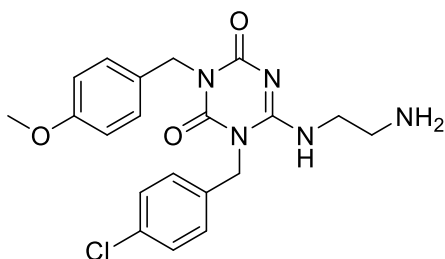
Yield 86%. m.p. 183-187 °C. ^{1}H NMR (DMSO-d_6) δ 2.91 (t, J= 7.0 Hz, 4H, CH$_2$), 3.72 (s, 3H, CH$_3$), 4.42 (s, 4H, CH$_2$), 5.89 (s, 2H, NH$_2$), 6.65 (m, 2H, Ar), 6.95 (m, 2H, Ar), 7.32 (m, 2H, Ar), 7.39 (m, 2H, Ar), 7.99 (s, 1H, NH). IR 3339, 3287, 1702, 1568 cm^{-1}. Elemental analysis: calculated for C$_{20}$H$_{22}$ClN$_5$O$_3$ (415.87) % C 57.76; H 5.33; N 16.84; found % C 57.70; H 5.33; N 16.84.

6-((2-Aminoethyl)amino)-3-(4-methoxybenzyl)-1-(4-(trifluoromethyl)benzyl)-1,3,5-triazine-2,4(1H,3H)-dione (7r)
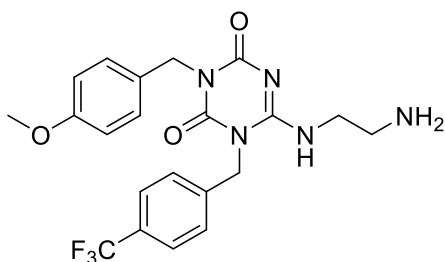
Yield 89%. m.p. 181-183 °C. ^{1}H NMR (DMSO-d_6) δ 2.91 (m, 4H, CH$_2$), 3.72 (s, 3H, CH$_3$), 4.42 (s, 4H, CH$_2$), 5.91 (s, 2H, NH$_2$), 6.65 (d, J= 8.0 Hz, 2H, Ar), 6.95 (d, J= 8.0 Hz, 2H, Ar), 6.99 (d, J= 8.0 Hz, 2H, Ar), 7.54 (d, J= 8.0 Hz, 2H, Ar), 7.86 (s, 1H, NH). IR 3320, 1699, 1586 cm^{-1}. Elemental analysis: calculated for C$_{21}$H$_{22}$F$_3$N$_5$O$_3$ (449.43) % C 56.12; H 4.93; N 15.58; found % C 56.14; H 4.95; N 15.53.

6-((2-Aminoethyl)amino)-3-(benzo(d)(1,3)dioxol-5-ylmethyl)-1-(4-methoxybenzyl)-1,3,5-triazine-2,4(1H,3H)-dione (7s)
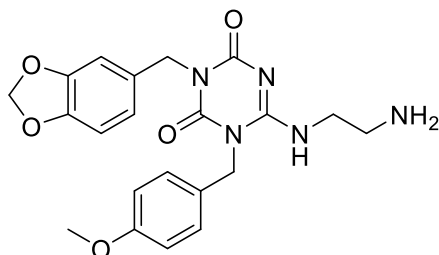
Yield 78%. m.p. 196-199 °C. ^{1}H NMR (DMSO-d_6) δ 2.91 (t, J= 7.0 Hz, 4H, CH_2), 3.72 (s, 3H, CH_3), 4.42 (s, 4H, CH_2), 4.50 (s, 2H, CH_2), 5.86 (s, 2H, NH_2), 6.06 (s, 2H, Ar), 6.51 (m, 1H, Ar), 6.65 (s, 2H, Ar), 6.86 (m, 1H, Ar), 6.95 (m, 1H, Ar), 7.03 (d, 1H, NH), 7.84 (s, 1H). IR 3341, 3120, 1710, 1601 cm^{-1}. Elemental analysis: calculated for $C_{21}H_{23}N_5O_5$ (425.44) % C 59.29; H 5.45; N 16.46; found % C 59.30; H 5.44; N 16.48.

6-((2-Aminoethyl)amino)-1-(4-iodobenzyl)-3-(4-methoxybenzyl)-1,3,5-triazine-2,4(1H,3H)-dione (7t)
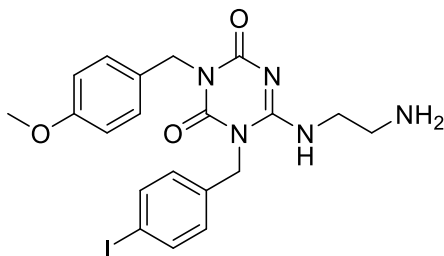
Yield 84%. m.p. 182-185 °C. ^{1}H NMR (DMSO-d_6) δ 2.91 (m, 4H, CH_2), 3.72 (s, 3H, CH_3), 4.42 (s, 4H, CH_2), 5.97 (s, 2H, NH_2), 6.65 (d, J= 8.5 Hz, 2H, Ar), 6.83 (d, J= 8.5 Hz, 2H, Ar), 6.95 (d, J= 8.5 Hz, 2H, Ar), 7.52 (d, J= 8.5 Hz, 2H, Ar), 8.01 (s, 1H, NH). IR 3333, 1712, 1580 cm^{-1}. Elemental analysis: calculated for $C_{20}H_{22}IN_5O_3$ (507.32) % C 47.35; H 4.37; N 13.80; found % C 47.37; H 4.32; N 13.81.

6-((2-Aminoethyl)amino)-3-(4-iodobenzyl)-1-(4-methoxybenzyl)-1,3,5-triazine-2,4(1H,3H)-dione (7u)
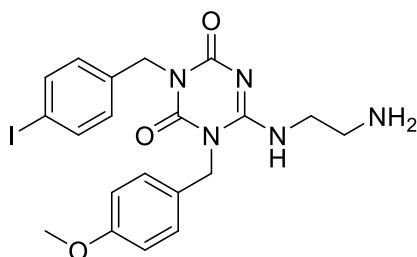
Yield 78%. m.p. 195-196 °C. ^{1}H NMR (DMSO-d$_6$) δ 2.91 (t, J= 7.0 Hz, 4H, CH$_2$), 3.72 (s, 3H, CH$_3$), 4.42 (s, 4H, CH$_2$), 5.87 (s, 2H, NH$_2$), 6.65 (d, J= 8.0 Hz, 2H, Ar), 6.83 (d, J= 8.0 Hz, 2H, Ar), 6.95 (d, J= 8.0 Hz, 2H, Ar), 7.52 (d, J= 8.0 Hz, 2H, Ar), 7.98 (s, 1H, NH). IR 3337, 1702, 1570 cm^{-1}. Elemental analysis: calculated for C$_{20}$H$_{22}$IN$_5$O$_3$ (507.32) % C 47.35; H 4.37; N 13.80; found % C 47.34; H 4.37; N 13.83.

6-((2-Aminoethyl)amino)-1-(4-methoxybenzyl)-3-(4-nitrobenzyl)-1,3,5-triazine-2,4(1H,3H)-dione (7v)
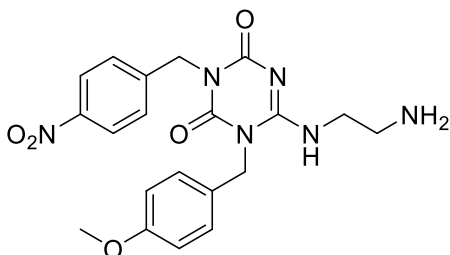
Yield 80%. m.p. 177-179 °C. ^{1}H NMR (DMSO-d$_6$) δ 2.91 (m, 4H, CH$_2$), 3.72 (s, 3H, CH$_3$), 4.42 (s, 4H, CH$_2$), 5.99 (s, 2H, NH$_2$), 6.65 (d, J= 8.0 Hz, 2H, Ar), 6.95 (d, J= 8.5 Hz, 2H, Ar), 7.32 (d, J= 8.5 Hz, 2H, Ar), 7.99 (s, 1H, NH), 8.17 (d, J= 8.0 Hz, 2H, Ar). IR 3345, 1700, 1582 cm^{-1}. Elemental analysis: calculated for C$_{20}$H$_{22}$N$_6$O$_5$ (426.43) % C 56.33; H 5.20; N 19.71; found % C 56.34; H 5.26; N 19.65.

___

General procedure for the synthesis of 1-(2-((1,5-dibenzyl-4,6-dioxo-1,4,5,6-tetrahydro-1,3,5-triazin-2-yl)amino)ethyl)guanidine (PC)

A mixture of compound **(7)** (2 mmol), 1*H*-pyrazole-1-carboxyamidine hydrochloride (0.29 g, 2 mmol) and DIPEA (0.70 mL, 4 mmol) in dry MeCN (10 mL) was refluxed for 18 h. After solvent elimination under vacuum the obtained residue was suspended in water (10 mL), filtered and washed with water (2 x 2.5 mL) and dried.

1-(2-((5-(4-Ethylbenzyl)-1-(4-methoxybenzyl)-4,6-dioxo-1,4,5,6-tetrahydro-1,3,5-triazin-2-yl)amino)ethyl)guanidine (PC1)
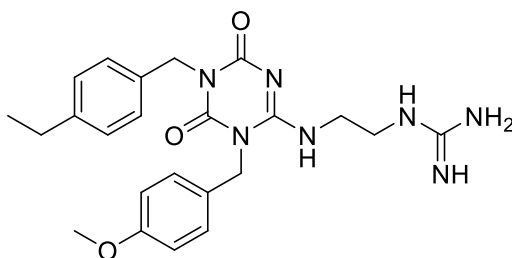
Yield 92 %. m.p. >250 °C. ^{1}H NMR (DMSO-d$_6$) δ 1.24 (t, J= 7.2 Hz, 3H, CH$_3$), 2.59 (q, J= 7.2 Hz, 2H, CH$_2$), 2.91 (t, J= 7.0 Hz, 4H, CH$_2$), 3.72 (s, 3H, CH$_3$), 4.42 (s, 4H, CH$_2$), 6.63 (s, 2H, NH$_2$), 6.65 (m, 2H, Ar), 6.95 (m, 2H, Ar), 7.00 (m, 2H, Ar), 7.01 (m, 2H, NH), 7.60 (s, 1H, NH), 8.02 (s, 1H, NH), 11.20 (s, 1H). IR 3389, 3153, 1720, 1654, 1580 cm^{-1}. Elemental analysis: calculated for C$_{23}$H$_{29}$N$_7$O$_3$ (451.52) % C 61.18; H 6.47; N 21.71; found % C 61.13; H 6.49; N 21.70

___

1-(2-((5-(4-Fluorobenzyl)-1-(4-methoxybenzyl)-4,6-dioxo-1,4,5,6-tetrahydro-1,3,5-triazin-2-yl)amino)ethyl)guanidine (PC7)
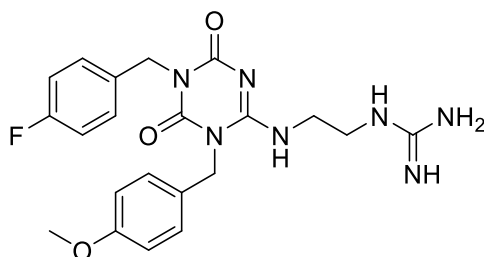
Yield 95%. m.p. >250 °C. ^{1}H NMR (DMSO-d$_6$) δ 2.89 (t, J= 7.0 Hz, 4H, CH$_2$), 3.70 (s, 3H, CH$_3$), 4.43 (s, 4H, CH$_2$), 6.63 (s, 2H, NH$_2$) 6.65 (d, J= 8.0 Hz, 2H, Ar), 6.95 (d, J= 8.0 Hz, 2H, Ar), 7.07 (d, J= 8.0 Hz, 2H, Ar), 7.39 (d, J= 8.0 Hz, 2H, Ar), 7.48 (s, 1H, NH), 9.43 (s, 1H, NH), 11.23 (s, 1H, NH). IR (Nujol) 3405, 3157, 1719, 1661, 1572 cm^{-1}. Elemental analysis: calculated for C$_{21}$H$_{24}$FN$_7$O$_3$ (441.46) % C 57.13; H 5.48; N 22.21; found % C 57.16; H 5.46; N 22.21.

1-(2-((1-Benzyl-5-(4-methoxybenzyl)-4,6-dioxo-1,4,5,6-tetrahydro-1,3,5-triazin-2-yl)amino)ethyl)guanidine (PC8)
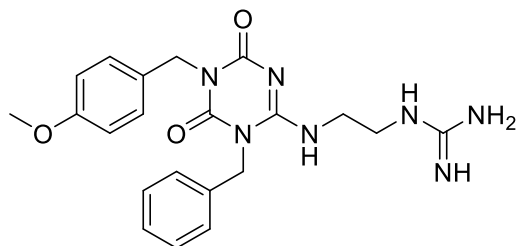
Yield 98%. m.p. >250 °C. ^{1}H NMR (DMSO-d$_6$) δ 2.87 (m, 4H, CH$_2$), 3.80 (s, 3H, CH$_3$), 4.38 (s, 4H, CH$_2$), 6.58 (s, 2H, NH$_2$), 6.65 (m, 2H, Ar), 6.95 (m, 2H, Ar), 7.25 (m, 1H, Ar), 7.26 (m, 2H, Ar), 7.31 (m, 2H, Ar), 7.62 (s, 1H, NH), 9.43 (s, 1H, NH), 11.49 (s, 1H, NH). IR 3385, 3142, 1716, 1669, 1570 cm^{-1}. Elemental analysis: calculated for C$_{21}$H$_{25}$N$_7$O$_3$ (423.47) % C 59.56; H 5.95; N 23.15; found % C 59.58; H 5.94; N 23.19.

1-(2-((1-(4-Methoxybenzyl)-5-(4-methylbenzyl)-4,6-dioxo-1,4,5,6-tetrahydro-1,3,5-triazin-2-yl)amino)ethyl)guanidine (PC15)
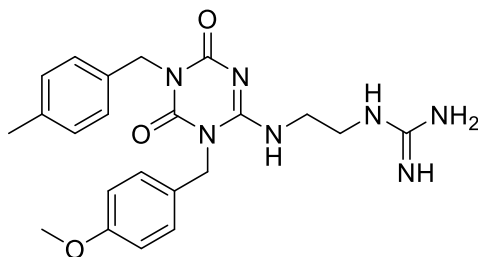
Yield 89%. m.p. >250 °C. ^{1}H NMR (DMSO-d_6) δ 2.19 (s, 3H, CH$_3$), 2.93 (t, J= 7.5 Hz, 4H, CH$_2$), 3.77 (s, 3H, CH$_3$), 4.40 (s, 4H, CH$_2$), 6.65 (d, J= 8.0 Hz, 2H, Ar), 6.73 (s, 2H, NH$_2$), 6.94 (d, J= 8.0 Hz, 2H, Ar), 6.95 (d, J= 8.0 Hz, 2H, Ar), 7.12 (d, J= 8.0 Hz, 2H, Ar), 7.81 (s, 1H, NH), 9.50 (s, 1H, NH), 11.11 (s, 1H, NH). IR 3420, 3170, 1722, 1597, 1594 cm^{-1}. Elemental analysis: calculated for C$_{22}$H$_{27}$N$_7$O$_3$ (437.49) % C 60.40; H 6.22; N 22.41; % C 60.43; H 6.22; N 22.38.

1-(2-((1,5-bis(4-Methoxybenzyl)-4,6-dioxo-1,4,5,6-tetrahydro-1,3,5-triazin-2-yl)amino)ethyl)guanidine (PC17)
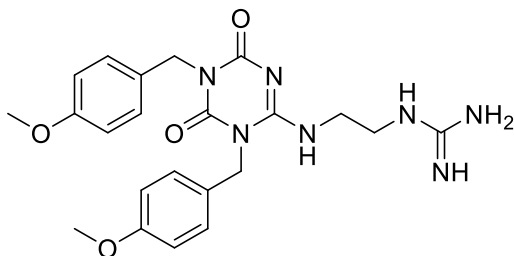
Yield 93%. m.p. >250 °C. ^{1}H NMR (DMSO-d_6) δ 2.87 (m, 4H, CH$_2$), 3.72 (s, 6H, CH$_3$), 4.45 (s, 4H, CH$_2$), 6.60 (s, 2H, NH$_2$), 6.65 (m, 4H, Ar), 6.95 (m, 4H, Ar), 7.84 (s, 1H, NH), 9.38 (s, 1H, NH), 11.32 (s, 1H, NH). IR 3412, 3190, 1725, 1652, 1583 cm^{-1}. Elemental analysis: calculated for C$_{22}$H$_{27}$N$_7$O$_4$ (453.49) % C 58.27; H 6.00; N 21.62; found % C 58.29; H 6.03; N 21.60.

1-(2-((5-(4-Chlorobenzyl)-1-(4-methoxybenzyl)-4,6-dioxo-1,4,5,6-tetrahydro-1,3,5-triazin-2-yl)amino)ethyl)guanidine (PC18)
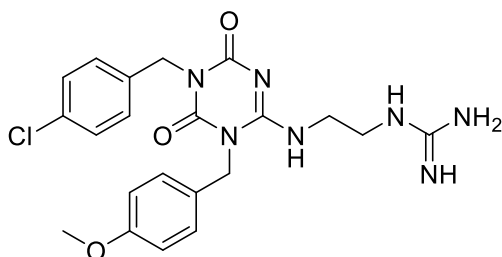
Yield 91%. m.p. >250 °C. ^{1}H NMR (DMSO-d$_6$) δ 2.94 (t, J= 7.2 Hz, 4H, CH$_2$), 3.81 (s, 3H, CH$_3$), 4.39 (s, 4H, CH$_2$), 6.60 (s, 2H, NH$_2$), 6.65 (d, J= 8.5 Hz, 2H, Ar), 6.95 (d, J= 8.0 Hz, 2H, Ar), 7.32 (d, J= 8.0 Hz, 2H, Ar), 7.39 (d, J= 8.5 Hz, 2H, Ar), 7.81 (s, 1H, NH), 9.42 (s, 1H, NH), 11.45 (s, 1H, NH). IR 3408, 3163, 1721, 1655, 1580 cm^{-1}. Elemental analysis: calculated for C$_{21}$H$_{24}$ClN$_7$O$_3$ (457.91) % C 55.08; H 5.28; N 21.41; found % C 55.09; H 5.26; N 21.47.

1-(2-((1-(4-Methoxybenzyl)-4,6-dioxo-5-(4-(trifluoromethyl)benzyl)-1,4,5,6-tetrahydro-1,3,5-triazin-2-yl)amino)ethyl)guanidine (PC23)
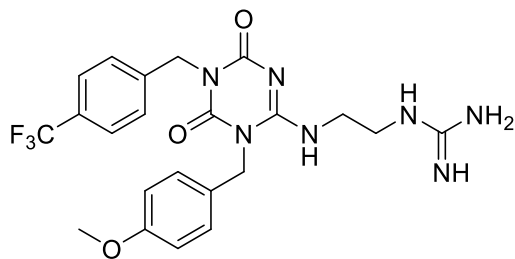
Yield 84%. m.p. >250 °C. ^{1}H NMR (DMSO-d$_6$) δ 2.91 (t, J= 7.0 Hz, 4H, CH$_2$), 3.69 (s, 3H, CH$_3$), 4.40 (s, 4H, CH$_2$), 6.65 (d, J= 8.2 Hz, 2H, Ar), 6.95 (d, J= 8.5 Hz, 2H, Ar), 6.84 (s, 2H, NH$_2$), 6.99 (d, J= 8.2 Hz, 2H, Ar), 7.54 (d, J= 8.5 Hz, 2H, Ar), 7.78 (s, 1H, NH), 9.35 (s, 1H, NH), 11.23 (s, 1H, NH). IR 3389, 3190, 1729, 1669, 1561 cm^{-1}. Elemental analysis: calculated for C$_{22}$H$_{24}$F$_3$N$_7$O$_3$ (491.47) % C 53.76; H 4.92; N 19.95; found % C 53.72; H 4.93; N 19.97.

1-(2-((1-(4-Bromobenzyl)-5-(4-methoxybenzyl)-4,6-dioxo-1,4,5,6-tetrahydro-1,3,5-triazin-2-yl)amino)ethyl)guanidine (PC24)
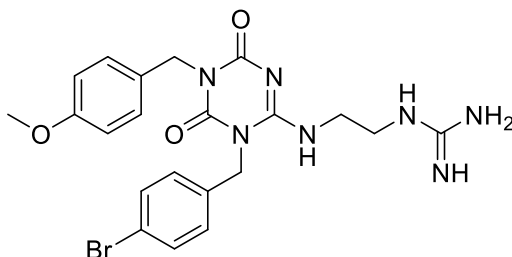
Yield 78%. m.p. >250 °C. ^{1}H NMR (DMSO-d_6) δ 2.88 (m, 4H, CH$_2$), 3.77 (s, 3H, CH$_3$), 4.41 (s, 4H, CH$_2$), 6.58 (s, 2H, NH$_2$), 6.65 (d, J= 8.0 Hz, 2H, Ar), 6.95 (m, 4H, Ar), 7.31 (d, J= 8.0 Hz, 2H, Ar), 7.68 (s, 1H, NH), 9.38 (s, 1H, NH), 11.16 (s, 1H, NH). IR 3415, 3166, 1710, 1660, 1585 cm^{-1}. Elemental analysis: calculated for C$_{21}$H$_{24}$BrN$_7$O$_3$ (502.36) % C 50.21; H 4.82; N 19.52; found % C 50.20; H 4.86; N 19.51.

1-(2-((5-(4-Bromobenzyl)-1-(4-methoxybenzyl)-4,6-dioxo-1,4,5,6-tetrahydro-1,3,5-triazin-2-yl)amino)ethyl)guanidine (PC25)
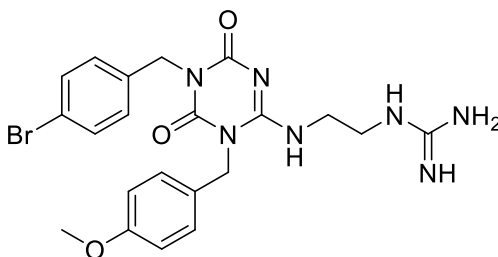
Yield 98%. m.p. >250 °C. ^{1}H NMR (DMSO-d_6) δ 2.91 (t, J= 7.2 Hz, 4H, CH$_2$), 3.81 (s, 3H, CH$_3$), 4.37 (s, 4H, CH$_2$), 6.65 (m, 2H, Ar), 6.73 (s, 2H, NH$_2$), 6.95 (m, 4H, Ar), 7.31 (m, 2H, Ar), 7.56 (s, 1H, NH), 9.42 (s, 1H, NH), 11.32 (s, 1H, NH). IR 3396, 3149, 1724, 1666, 1578 cm^{-1}. Elemental analysis: calculated for C$_{21}$H$_{24}$BrN$_7$O$_3$ (502.36) % C 50.21; H 4.82; N 19.52; found % C 50.20; H 4.79; N 19.53.

1-(2-((1-(3,4-Dichlorobenzyl)-5-(4-methoxybenzyl)-4,6-dioxo-1,4,5,6-tetrahydro-1,3,5-triazin-2-yl)amino)ethyl)guanidine (PC26)
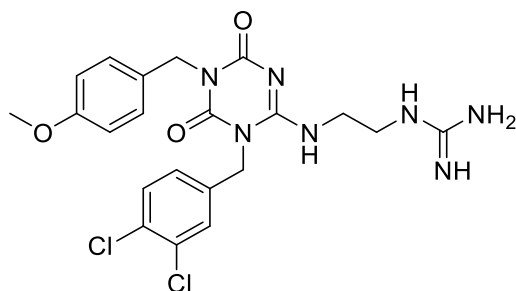
Yield 89%. m.p. >250 °C. ^{1}H NMR (DMSO-d$_6$) δ 2.86 (m, 4H, CH$_2$), 3.76 (s, 3H, CH$_3$), 4.40 (s, 4H, CH$_2$), 6.59 (s, 2H, NH$_2$), 6.65 (d, J= 8.0 Hz, 2H, Ar), 6.95 (d, J= 8.0 Hz, 2H, Ar), 6.88 (m, 1H, Ar), 7.01 (m, 1H, Ar), 7.09 (m, 1H, Ar), 7.86 (s, 1H, NH), 9.38 (s, 1H, NH), 11.40 (s, 1H, NH). IR 3410, 3172, 1708, 1670, 1584 cm^{-1}. Elemental analysis: calculated for C$_{21}$H$_{23}$Cl$_2$N$_7$O$_3$ (492.36) % C 51.23; H 4.7; N 19.91; found % C 51.25; H 4.74; N 19.87.

1-(2-((1-(4-Methylbenzyl)-4,6-dioxo-5-(4-(trifluoromethyl)benzyl)-1,4,5,6-tetrahydro-1,3,5-triazin-2-yl)amino)ethyl)guanidine (PC27)
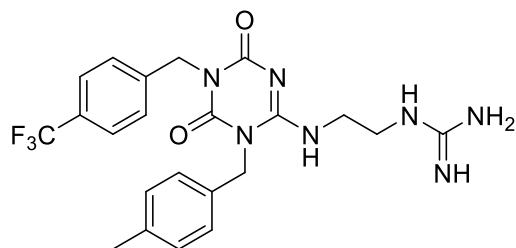
Yield 83%. m.p. >250 °C. ^{1}H NMR (DMSO-d$_6$) δ 2.17 (s, 3H, CH$_3$), 2.90 (t, J= 7.3 Hz, 4H, CH$_2$), 4.39 (s, 4H, CH$_2$), 6.94 (m, 2H, NH$_2$), 6.99 (m, 2H, Ar), 7.02 (s, 2H, NH$_2$), 7.12 (m, 2H, Ar), 7.54 (m, 2H, Ar), 7.83 (s, 1H, NH), 9.41 (s, 1H, NH), 11.32 (s, 1H, NH). IR 3397, 3166, 1721, 1660, 1579 cm^{-1}. Elemental analysis: calculated for C$_{22}$H$_{24}$F$_3$N$_7$O$_2$ (475.47) % C 55.57; H 5.09; N 20.62; found % C 55.59; H 5.04; N 20.67.

1-(2-((1-(3,4-Dichlorobenzyl)-5-(4-methylbenzyl)-4,6-dioxo-1,4,5,6-tetrahydro-1,3,5-triazin-2-yl)amino)ethyl)guanidine (PC28)
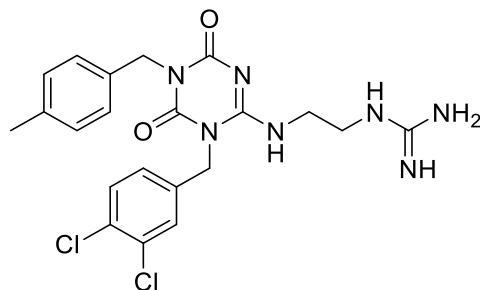
Yield 87%. m.p. >250 °C. ^{1}H NMR (DMSO-d$_6$) δ 2.19 (s, 3H, CH$_3$), 2.91 (m, 4H, CH$_2$), 4.42 (s, 4H, CH$_2$), 6.88 (d, 1H, Ar), 6.94 (s, 2H, NH$_2$), 6.99 (s, 2H, Ar), 7.01 (s, 1H, Ar), 7.09 (s, 1H, Ar), 7.12 (m, 2H, Ar), 7.82 (s, 1H, NH), 9.38 (s, 1H, NH), 11.25 (s, 1H, NH). IR 3412, 3172, 1718, 1661, 1570 cm^{-1}. Elemental analysis: calculated for C$_{21}$H$_{23}$Cl$_2$N$_7$O$_2$ (476.36) % C 52.95; H 4.87; N 20.58; found % C 52.97; H 4.82; N 20.57.

1-(2-((5-(4-Methoxybenzyl)-1-(4-methylbenzyl)-4,6-dioxo-1,4,5,6-tetrahydro-1,3,5-triazin-2-yl)amino)ethyl)guanidine (PC29)
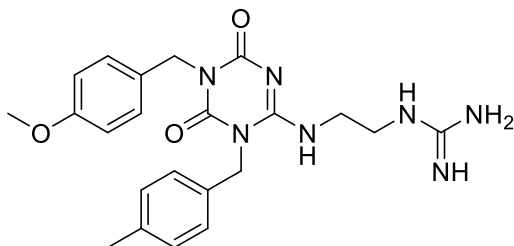
Yield 89%. m.p. >250 °C. ^{1}H NMR (DMSO-d$_6$) δ 2.19 (s, 3H, CH$_3$), 2.91 (t, J= 7.0 Hz, 4H, CH$_2$), 3.72 (s, 3H, CH$_3$), 4.42 (s, 4H, CH$_2$), 6.59 (s, 2H, NH$_2$), 6.65 (d, J= 8.0 Hz, 2H, Ar), 6.94 (d, J= 8.0 Hz, 2H, Ar), 6.95 (d, J= 8.0 Hz, 2H, Ar), 7.12 (d, J= 8.0 Hz, 2H, Ar), 7.81 (s, 1H, NH), 9.40 (s, 1H, NH), 11.36 (s, 1H, NH). IR 3422, 3133, 1709, 1667, 1570 cm^{-1}. Elemental analysis: calculated for C$_{22}$H$_{27}$N$_7$O$_3$ (437.50) % C 60.40; H 6.22; N 22.41; found % C 60.40; H 6.22; N 22.41.

1-(2-((1-(4-Fluorobenzyl)-5-(4-methoxybenzyl)-4,6-dioxo-1,4,5,6-tetrahydro-1,3,5-triazin-2-yl)amino)ethyl)guanidine (PC30)
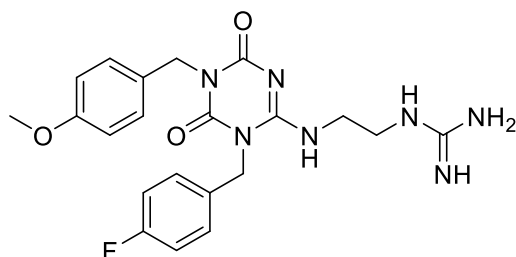
Yield 87%. m.p. >250 °C. ^{1}H NMR (DMSO-d_6) δ 2.94 (m, 4H, CH_2), 3.82 (s, 3H, CH_3), 4.39 (s, 4H, CH_2), 6.65 (d, J= 8.0 Hz, 2H, Ar), 6.84 (s, 2H, NH_2), 6.95 (d, J= 8.0 Hz, 2H, Ar), 7.07 (m, 2H, Ar), 7.39 (m, 2H, Ar), 7.66 (s, 1H, NH), 9.47 (s, 1H, NH), 11.20 (s, 1H, NH). IR 3405, 3157, 1719, 1661, 1572 cm^{-1}. Elemental analysis: calculated for $C_{21}H_{24}FN_7O_3$ (441.46) % C 57.13; H 5.48; N 22.21; found % C 57.10; H 5.49; N 22.26.

1-(2-((1-(4-Chlorobenzyl)-5-(4-methoxybenzyl)-4,6-dioxo-1,4,5,6-tetrahydro-1,3,5-triazin-2-yl)amino)ethyl)guanidine (PC31)
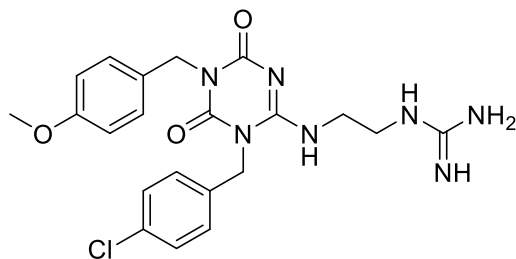
Yield 90% .m.p. >250 °C. ^{1}H NMR (DMSO-d_6) δ 2.91 (t, J= 7.5 Hz, 4H, CH_2), 3.72 (s, 3H, CH_3), 4.42 (s, 4H, CH_2), 6.63 (s, 2H, NH_2), 6.65 (d, J= 8.2 Hz, 2H, Ar), 6.95 (d, J= 8.2 Hz, 2H, Ar), 7.32 (d, J= 8.0 Hz, 2H, Ar), 7.39 (d, J= 8.0 Hz, 2H, Ar), 7.80 (s, 1H, NH). IR 3407, 3125, 1718 cm^{-1}. Elemental analysis: calculated for $C_{21}H_{24}ClN_7O_3$ (457.91) % C 55.08; H 5.28; N 21.41; found % C 55.09; H 5.26; N 21.46.

1-(2-((5-(4-Methoxybenzyl)-4,6-dioxo-1-(4-(trifluoromethyl)benzyl)-1,4,5,6-tetrahydro-1,3,5-triazin-2-yl)amino)ethyl)guanidine (PC32)
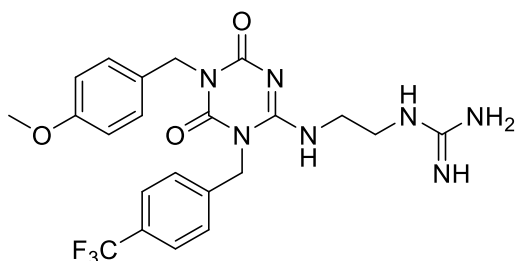
Yield 93%. m.p. >250 °C. ^{1}H NMR (DMSO-d_6) δ 2.91 (m, 4H, CH$_2$), 3.72 (s, 3H, CH$_3$), 4.42 (s, 4H, CH$_2$), 6.65 (m, 2H, NH$_2$), 6.95 (m, 2H, Ar), 6.99 (m, 2H, Ar), 7.23 (s, 2H, NH$_2$), 7.54 (m, 2H, Ar), 7.89 (s, 1H, NH), 9.14 (s, 1H, NH), 11.45 (s, 1H, NH). IR 3388, 3150, 1719, 1667, 1560 cm^{-1}. Elemental analysis: calculated for $C_{22}H_{24}F_3N_7O_3$ (491.47) % C 53.76; H 4.92; N 19.95; % C 53.76; H 4.92; N 19.95.

1-(2-((5-(Benzo(d)(1,3)dioxol-5-ylmethyl)-1-(4-methoxybenzyl)-4,6-dioxo-1,4,5,6-tetrahydro-1,3,5-triazin-2-yl)amino)ethyl)guanidine (PC33)
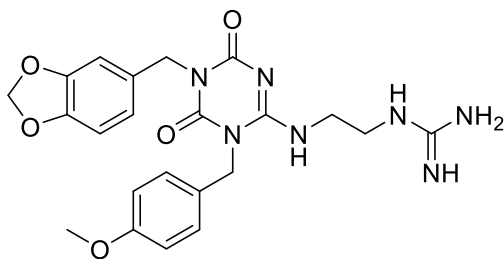
Yield 89%. m.p. >250 °C. ^{1}H NMR (DMSO-d_6) δ 2.91 (m, 4H, CH$_2$), 3.72 (s, 3H, CH$_3$), 4.42 (s, 4H, CH$_2$), 6.51 (m, 1H, Ar), 6.63 (s, 2H, NH$_2$), 6.65 (s, 2H, CH$_2$), 6.76 (s, 2H, Ar), 6.86 (m, 1H, Ar), 6.95 (m, 2H, Ar), 7.03 (m, 1H, Ar), 7.86 (s, 1H, NH), 9.38 (s, 1H, NH), 11.24 (s, 1H, NH). IR 3405, 3157, 1719, 1661, 1572 cm^{-1}. Elemental analysis: calculated for $C_{22}H_{25}N_7O_5$ (467,48) % C 56.52; H 5.39; N 20.97; found % C 56.50; H 5.38; N 20.98.

1-(2-((1-(4-iodobenzyl)-5-(4-methoxybenzyl)-4,6-dioxo-1,4,5,6-tetrahydro-1,3,5-triazin-2-yl)amino)ethyl)guanidine (PC34)
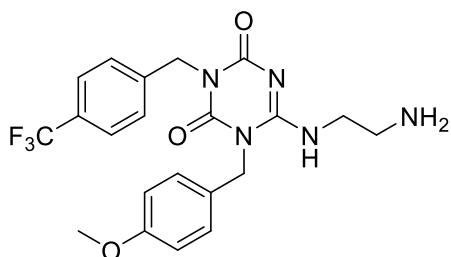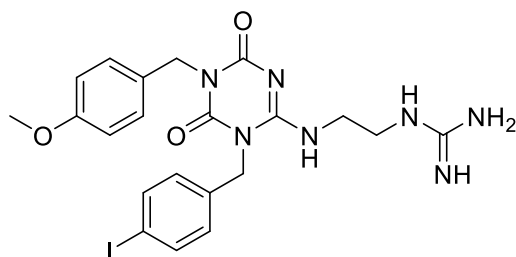

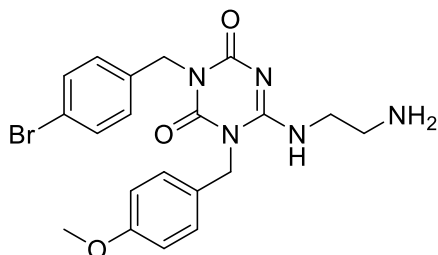Yield 90%. m.p. >250 °C. ^{1}H NMR (DMSO-d_6) δ 2.91 (t, J= 7.0 Hz, 4H, CH$_2$), 3.72 (s, 3H, CH$_3$), 4.42 (s, 4H, CH$_2$), 6.59 (s, 2H, NH$_2$), 6.65 (d, J= 8.0 Hz, 2H, Ar), 6.83 (d, J= 8.0 Hz, 2H, Ar), 6.95 (d, J= 8.0 Hz, 2H, Ar), 7.52 (d, J= 8.0 Hz, 2H, Ar), 7.84 (s, 1H, NH), 9.36 (s, 1H, NH), 11.41 (s, 1H, NH). IR 3390, 3153, 1723, 1647, 1584 cm^{-1}. Elemental analysis: calculated for C$_{21}$H$_{24}$IN$_7$O$_3$ (549.36) % C 45.91; H 4.40; N 17.85; found % C 45.93; H 4.40; N 17.87.

1-(2-((5-(4-Iodobenzyl)-1-(4-methoxybenzyl)-4,6-dioxo-1,4,5,6-tetrahydro-1,3,5-triazin-2-yl)amino)ethyl)guanidine (PC35)
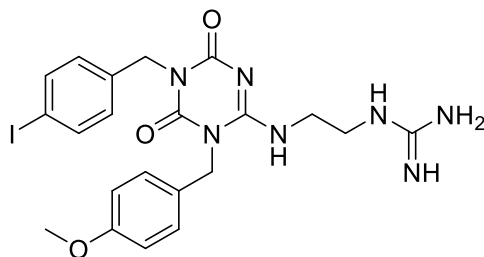
Yield 95%. m.p. >250 °C. ^{1}H NMR (DMSO-d_6) δ 2.91 (m, 4H, CH$_2$), 3.72 (s, 3H, CH$_3$), 4.42 (s, 4H, CH$_2$), 6.65 (d, J= 8.2 Hz, 2H, NH$_2$), 6.83 (d, J= 8.2 Hz, 2H, Ar), 6.95 (d, J= 8.2 Hz, 2H, Ar), 7.23 (s, 2H, NH$_2$), 7.52 (d, J= 8.2 Hz, 2H, Ar), 7.81 (s, 1H, NH), 9.25 (s, 1H, NH), 11.56 (s, 1H). IR 3405, 3157, 1719, 1661, 1572 cm^{-1}. Elemental analysis: calculated for C$_{21}$H$_{24}$IN$_7$O$_3$ (549.36) % C 45.91; H 4.40; N 17.85; found % C 45.90; H 4.45; N 17.82.

1-(2-((1-(4-Methoxybenzyl)-5-(4-nitrobenzyl)-4,6-dioxo-1,4,5,6-tetrahydro-1,3,5-triazin-2-yl)amino)ethyl)guanidine (PC36)
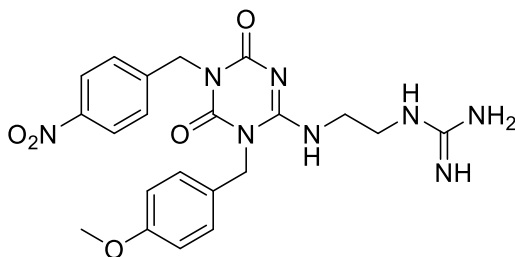

Yield 97%. m.p. >250 °C. ^{1}H NMR (DMSO-d$_6$) δ 2.91 (t, J= 7.5 Hz, 4H, CH$_2$), 3.72 (s, 3H, CH$_3$), 4.42 (s, 4H, CH$_2$), 6.63 (s, 2H, NH$_2$), 6.65 (d, J= 8.2 Hz, 2H, Ar), 6.95 (d, J= 8.0 Hz, 2H, Ar), 7.32 (d, J= 8.0 Hz, 2H, Ar), 7.85 (s, 1H, NH), 8.17 (d, J= 8.2 Hz, 2H, Ar), 9.42 (s, 1H, NH), 11.12 (s, 1H, NH). IR 3405, 3157, 1719, 1661, 1572 cm^{-1}. Elemental analysis: calculated for C$_{21}$H$_{24}$N$_8$O$_5$ (468.47) % C 53.84; H 5.16; N 23.92; found % C 53.85; H 5.16; N 23.97.

.

3.6 References

1   Mollay, C., Wechselberger, C., Mignogna, G., Negri, L., Melchiorri, P., Barra, D. & Kreil, G. Bv8, a small protein from frog skin and its homologue from snake venom induce hyperalgesia in rats. *European Journal of Pharmacology* **374**, 189-196, doi:http://dx.doi.org/10.1016/S0014-2999(99)00229-0 (1999).

2   Kaser, A., Winklmayr, M., Lepperdinger, G. & Kreil, G. The AVIT protein family: Secreted cysteine-rich vertebrate proteins with diverse functions. *EMBO Reports* **4**, 469-473, doi:10.1038/sj.embor.embor830 (2003).

3   Bullock, C., Li, J. & Zhou, Q. Structural determinants required for the bioactivities of prokineticins and identification of prokineticin receptor antagonists. *Molecular Pharmacology* **65**, 582 - 588 (2004).

4   Chen, J., Kuei, C., Sutton, S., Wilson, S., Yu, J., Kamme, F., Mazur, C., Lovenberg, T. & Liu, C. Identification and Pharmacological Characterization of Prokineticin 2β as a Selective Ligand for Prokineticin Receptor 1. *Molecular Pharmacology* **67**, 2070-2076, doi:10.1124/mol.105.011619 (2005).

5   Li, M., Bullock, C. M., Knauer, D. J., Ehlert, F. J. & Zhou, Q. Y. Identification of Two Prokineticin cDNAs: Recombinant Proteins Potently Contract Gastrointestinal Smooth Muscle. *Molecular Pharmacology* **59**, 692-698, doi:10.1124/mol.59.4.692 (2001).

6   Levit, A., Yarnitzky, T., Wiener, A., Meidan, R. & Niv, M. Y. Modeling of Human Prokineticin Receptors: Interactions with Novel Small-Molecule Binders and Potential Off-Target Drugs. *PLoS ONE* **6**, e27990, doi:10.1371/journal.pone.0027990 (2011).

7   Maldonado-Pérez, D., Evans, J., Denison, F., Millar, R. P. & Jabbour, H. N. Potential roles of the prokineticins in reproduction. *Trends in Endocrinology & Metabolism* **18**, 66-72, doi:http://dx.doi.org/10.1016/j.tem.2006.12.002 (2007).

8   Lin, D. C.-H., Bullock, C. M., Ehlert, F. J., Chen, J.-L., Tian, H. & Zhou, Q.-Y. Identification and Molecular Characterization of Two Closely Related G Protein-coupled Receptors Activated by Prokineticins/Endocrine Gland Vascular Endothelial Growth Factor. *Journal of Biological Chemistry* **277**, 19276-19280, doi:10.1074/jbc.M202139200 (2002).

9   AGA abstracts W1190–W1748. *Gastroenterology* **126**, A586-A659, doi:http://dx.doi.org/10.1016/S0016-5085(04)80015-5 (2004).

10   Lin, D., Bullock, C., Ehlert, F., Chen, J., Tian, H. & Zhou, Q. Identification and molecular characterization of two closely related G protein-coupled receptors activated by prokineticins/endocrine gland vascular endothelial growth factor. *The Journal of Biological Chemistry* **277**, 19276 - 19280 (2002).

11   Zhou, Q.-Y. The Prokineticins: A Novel Pair of Regulatory Peptides. *Molecular interventions* **6**, 330-338, doi:10.1124/mi.6.6.6 (2006).

12   Cheng, M., Bullock, C., Li, C., Lee, A., Bermak, J., Belluzzi, J., Weaver, D., Leslie, F. & Zhou, Q. Prokineticin 2 transmits the behavioural circadian rhythm of the suprachiasmatic nucleus. *Nature* **417**, 405 - 410 (2002).

13   Ng, K. L., Li, J.-D., Cheng, M. Y., Leslie, F. M., Lee, A. G. & Zhou, Q.-Y. Dependence of Olfactory Bulb Neurogenesis on Prokineticin 2 Signaling. *Science* **308**, 1923-1927, doi:10.1126/science.1112103 (2005).

14   Koyama, Y., Kiyo-oka, M., Osakada, M., Horiguchi, N., Shintani, N., Ago, Y., Kakuda, M., Baba, A. & Matsuda, T. Expression of prokineticin receptors in mouse cultured astrocytes and involvement in cell proliferation. *Brain Research* **1112**, 65-69, doi:http://dx.doi.org/10.1016/j.brainres.2006.07.013 (2006).

15   Monnier, J. & Samson, M. Prokineticins in angiogenesis and cancer. *Cancer Letters* **296**, 144-149, doi:http://dx.doi.org/10.1016/j.canlet.2010.06.011 (2010).

16   LeCouter, J., Kowalski, J., Foster, J., Hass, P., Zhang, Z., Dillard-Telm, L., Frantz, G., Rangell, L., DeGuzman, L., Keller, G., Peale, F., Gurney, A., Hillan, K. & Ferrara, N. Identification of an angiogenic mitogen selective for endocrine gland endothelium. *Nature* **412**, 877 - 884 (2001).

17   LeCouter, J., Lin, R., Tejada, M., Frantz, G., Peale, F., Hillan, K. J. & Ferrara, N. The endocrine-gland-derived VEGF homologue Bv8 promotes angiogenesis in the testis: Localization of Bv8 receptors to endothelial cells. *Proceedings of the National Academy of Sciences* **100**, 2685-2690, doi:10.1073/pnas.0337667100 (2003).

18   Pasquali, D., Rossi, V., Staibano, S., Rosa, G. D., Chieffi, P., Prezioso, D., Mirone, V., Mascolo, M., Tramontano, D., Bellastella, A. & Sinisi, A. A. The Endocrine-Gland-Derived Vascular Endothelial Growth Factor (EG-VEGF)/Prokineticin 1 and 2 and Receptor Expression in Human Prostate: Up-Regulation of EG-VEGF/Prokineticin 1 with Malignancy. *Endocrinology* **147**, 4245-4251, doi:doi:10.1210/en.2006-0614 (2006).

19 Ngan, E. S. W., Lee, K. Y., Yeung, W. S. B., Ngan, H. Y. S., Ng, E. H. Y. & Ho, P. C. Endocrine Gland-Derived Vascular Endothelial Growth Factor Is Expressed in Human Peri-implantation Endometrium, But Not in Endometrial Carcinoma. *Endocrinology* **147**, 88-95, doi:doi:10.1210/en.2005-0543 (2006).

20 Monnier, J., Piquet-Pellorce, C., Feige, J.-J., Musso, O., Clément, B., Turlin, B., Théret, N. & Samson, M. Prokineticin 2/Bv8 is expressed in Kupffer cells in liver and is down regulated in human hepatocellular carcinoma. *World Journal of Gastroenterology : WJG* **14**, 1182-1191, doi:10.3748/wjg.14.1182 (2008).

21 Giannini, E., Lattanzi, R., Nicotra, A., Campese, A. F., Grazioli, P., Screpanti, I., Balboni, G., Salvadori, S., Sacerdote, P. & Negri, L. The chemokine Bv8/prokineticin 2 is up-regulated in inflammatory granulocytes and modulates inflammatory pain. *Proceedings of the National Academy of Sciences* **106**, 14646-14651, doi:10.1073/pnas.0903720106 (2009).

22 Jacobson, O., Weiss, I. D., Niu, G., Balboni, G., Congiu, C., Onnis, V., Kiesewetter, D. O., Lattanzi, R., Salvadori, S. & Chen, X. Prokineticin Receptor 1 Antagonist PC-10 as a Biomarker for Imaging Inflammatory Pain. *Journal of Nuclear Medicine* **52**, 600-607, doi:10.2967/jnumed.110.084772 (2011).

23 Negri, L., Lattanzi, R., Giannini, E. & Melchiorri, P. Bv8/Prokineticin proteins and their receptors. *Life Sciences* **81**, 1103-1116, doi:http://dx.doi.org/10.1016/j.lfs.2007.08.011 (2007).

24 Negri, L., Lattanzi, R., Giannini, E., Colucci, M., Margheriti, F., Melchiorri, P., Vellani, V., Tian, H., De Felice, M. & Porreca, F. Impaired nociception and inflammatory pain sensation in mice lacking the prokineticin receptor PKR1: focus on interaction between PKR1 and the capsaicin receptor TRPV1 in pain behavior. *The Journal of Neuroscience* **26**, 6716 - 6727 (2006).

25 Vellani, V., Colucci, M., Lattanzi, R., Giannini, E., Negri, L., Melchiorri, P. & McNaughton, P. A. Sensitization of Transient Receptor Potential Vanilloid 1 by the Prokineticin Receptor Agonist Bv8. *The Journal of Neuroscience* **26**, 5109-5116, doi:10.1523/jneurosci.3870-05.2006 (2006).

26 Lattanzi, R., Sacerdote, P., Franchi, S., Canestrelli, M., Miele, R., Barra, D., Visentin, S., DeNuccio, C., Porreca, F., De Felice, M., Guida, F., Luongo, L., de Novellis, V., Maione, S. & Negri, L. Pharmacological activity of a Bv8 analogue modified in position 24. *British Journal of Pharmacology* **166**, 950-963, doi:10.1111/j.1476-5381.2011.01797.x (2012).

27 De Novellis, V., Negri, L., Lattanzi, R., Rossi, F., Palazzo, E., Marabese, I., Giannini, E., Vita, D., Melchiorri, P. & Maione, S. The prokineticin receptor agonist Bv8 increases GABA release in the periaqueductal grey and modifies RVM cell activities and thermoceptive reflexes in the rat. *European Journal of Neuroscience* **26**, 3068-3078, doi:10.1111/j.1460-9568.2007.05910.x (2007).

28 Coats, S. J., Dyatkin, A. B., He, W., Lisko, J., Ralbovsky, J. L. & Schultz, M. J. Preparation of triazinediones and pyrimidinediones as prokineticin 2 receptor antagonists. WO2006104713A1 (2006).

29 Coats, S. J., Dyatkin, A. B., He, W., Lisko, J., Ralbovsky, J. L. & Schultz, M. J. Preparation of pyrimidinediones and triazinediones as prokineticin 1 (PK1) receptor antagonists. WO2006104715A1 (2006).

30 Coats, S. J., Dyatkin, A. B., He, W., Lisko, J., Miskowski, T. A., Ralbovsky, J. L. & Schulz, M. Preparation of triazine-2,4-dione derivatives as prokineticin 2 receptor antagonists. WO2007079214A2 (2007).

31 Thompson, W. J. & Melamed, J. Y. Preparation of morpholinecarboxamides as prokineticin 2 receptor antagonists. WO2007067511A2 (2007).

32 Carroll, C., Goldby, A. & Teall, M. Preparation of sulfonylpiperidine derivatives and their use for treating prokineticin mediated diseases. WO2013179024A1 (2013).

33 Bousba, S., Goldby, A., Jenkins, K., Kinsella, N. & Teall, M. Preparation of piperidine and azepine derivatives as prokineticin receptor modulators. WO2015019103A1 (2015).

34 Vilar, S., Ferino, G., Phatak, S. S., Berk, B., Cavasotto, C. N. & Costanzi, S. Docking-based virtual screening for ligands of G protein-coupled receptors: Not only crystal structures but also in silico models. *Journal of Molecular Graphics and Modelling* **29**, 614-623, doi:http://dx.doi.org/10.1016/j.jmgm.2010.11.005 (2011).

35 Costanzi, S. in *G Protein-Coupled Receptors: From Structure to Function* 359-374 (The Royal Society of Chemistry, 2011).

36 Costanzi, S. in *Homology Modeling: Methods and Protocols* (eds W. Andrew J. Orry & Ruben Abagyan) 259-279 (Humana Press, 2012).

37 Breitler, S., Oldenhuis, N. J., Fors, B. P. & Buchwald, S. L. Synthesis of Unsymmetrical Diarylureas via Pd-Catalyzed C–N Cross-Coupling Reactions. *Organic Letters* **13**, 3262-3265, doi:10.1021/ol201210t (2011).

38 Tang, Q., Zhang, G., Du, X., Zhu, W., Li, R., Lin, H., Li, P., Cheng, M., Gong, P. & Zhao, Y. Discovery of novel 6,7-disubstituted-4-

phenoxyquinoline derivatives bearing 5-(aminomethylene)pyrimidine-2,4,6-trione moiety as c-Met kinase inhibitors. *Bioorganic & Medicinal Chemistry* **22**, 1236-1249, doi:http://dx.doi.org/10.1016/j.bmc.2014.01.014 (2014).

39 Nasrollahzadeh, M. Application of TiO2 nanoparticles for the synthesis of N-arylureas in water at room temperature. *RSC Advances* **4**, 29089-29093, doi:10.1039/C4RA03580A (2014).

40 Liao, W., Hu, G., Guo, Z., Sun, D., Zhang, L., Bu, Y., Li, Y., Liu, Y. & Gong, P. Design and biological evaluation of novel 4-(2-fluorophenoxy)quinoline derivatives bearing an imidazolone moiety as c-Met kinase inhibitors. *Bioorganic & Medicinal Chemistry* **23**, 4410-4422, doi:http://dx.doi.org/10.1016/j.bmc.2015.06.026 (2015).

41 Bew, S. P., Brimage, R. A., Hiatt-Gipson, G., Sharma, S. V. & Thurston, S. Hybrid Calix[4]arenes via Ionic Hydrogenation and Transition-Metal-Mediated Processes. *Organic Letters* **11**, 2483-2486, doi:10.1021/ol900714n (2009).

4. TRPV1 CHANNEL

4. TRPV1 Channel

4.1 TRPV1: The Channel
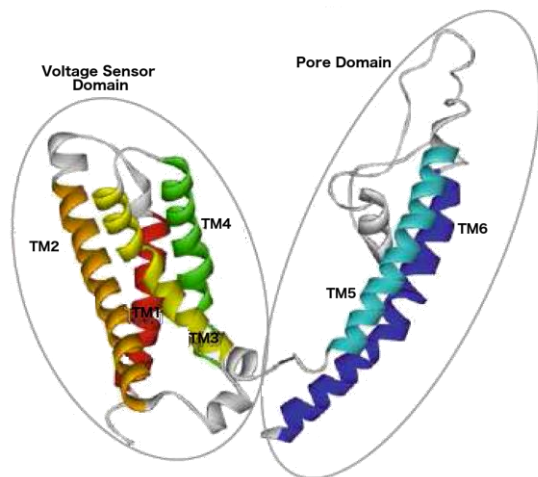
Figure 1. TRPV1 Channel 3D structure.

Transient Receptor Potential Channel Vanilloid type 1, or TRPV1 (Figure 1), is a non-selective cation channel receptor. It is directly activated by numerous external stimuli, both physical (such as low pH and high temperature) and chemicals like capsaicin (Figure 2A) and resiniferatoxin (RTX) (Figure 2B). These last are two natural active components contained in chili pepper and in the latex of a cactus-like plant the *Euphorbia resinifera* commonly found in Morocco, respectively.[1,2]

TRPV1 belong to the Transient Receptor Potential (TRP) family; these receptors are constituted by six transmembrane domains, TM1-TM4 are voltage sensing while TM5-TM6 constitute the pore.[3] TRPV1 is a non-selective cation channel with a better permeability to Ca^{2+}.

Both N and C terminal domains are intracellular. The N domain has three ankyrin repeated domains, important to bind multiple ligands and to modulate channel
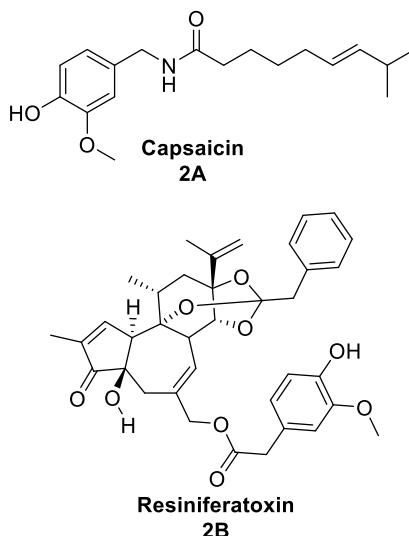
Figure 2. Capsaicine (2A) and Resiniferatoxin (2B).

sensitivity.[4] The C domain presents the binding sites for calmodulin and PIP$_2$.[5]

TRPV1 is localized in DRG on both nociceptive C and Aδ fibers;[6] in brain it is located in dopaminergic neurons, in substantia nigra, in hippocampal pyramidal neurons, in hypothalamic neurons, in the locus coeruleus and in the cortex.[7]

TRPV1 is present also in non-neuronal structures like epidermal keratinocytes, urothelium, liver, bladder, smooth muscle, polymorphonuclear granulocytes and macrophages.

In DRG, TRPV1 is co-localized with both CBRs and δ opioid receptor, the activation of these two caused a diminution of vanilloid channels activity by down-regulation of PKA activity.

4.2 Role of TRPV1 in pain

TRPV1 is an important component of pain information transmission, its activation enhances the channel Ca^{2+} permeability with consequent increase of Ca^{2+} intracellular concentration, which results in neuronal depolarization and transmission of the pain information to the supraspinal center.

As illustrated above numerous pain mediators influence the activity of this channel, some of these such as bradykinin and prostanoids promote its opening, other like ECs and opioids induce its closure.

Generally, the activation is followed by a desensitized state, which makes fibers insensitive to further stimulation.

The TRPV1 expressed in hypothalamus are responsible for increase in body temperature during inflammatory state.

In addition to endogenous compounds that interact via second messengers with the receptor, the endovanilloids (EV) cause directly the channel opening. The principal EVs acting on TRPV1 are: AEA (Figure 3A),[8] NADA (Figure 3B), which is the most potent known EV,[9] and AA metabolites of lipoxygenase action like 12-(*S*)- and 15-(*S*)-hydroperoxyeicosatetraenoic acid (HPETE) (Figure 3C).
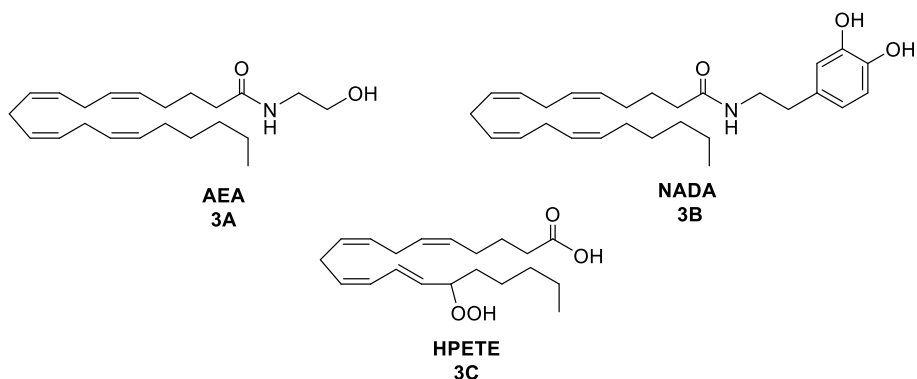
Figure 3. Three endogenous TRPV1 ligands: Anandamide (3A), N-Arachidonoyl dopamine (3B) and 15-(S) hydroperoxyeicosatetraenoic acid (3C).

TRPV1 is modulated by PKA and PKC phosphorylation.[10] The PKA phosphorylation makes the receptor more sensitive to the AEA, while the PKC enhances the receptor response to capsaicin.

4.3 TRPV1 exogenous modulators

The importance of this receptor in nociception information transmission makes it a promising target for pain treatment. As mentioned above, both the activation with consequent desensitization and the inhibition of TRPV1 have as effect the blocking of the neuron depolarization and consequent progression of the pain information. Thus compound like capsaicin and, the more powerful, RTX, produce analgesic effects by desensitization.[11]

The problem with the use of agonists is that before desensitization effect there is the activation of the TRPV1, which results in an initial neuronal excitation, causing pain before having the analgesic effect.

For this reason the antagonists are preferred. In tests carried out on neuronal cell cultures the synthetic analogue of

Capsazepine

Figure 4. Structure of the TRPV1 antagonist Capsazepine.

capsaicin, capsazepine (Figure 4), has been shown to reduce directly

the calcium influx induced by an agonist thus blocking the depolarization of the cell. *In vivo* studies confirmed the ability of capsazepine to counteract the hyperalgesic effect induced by administration of Freund's adjuvant on paw.[12,13]

Pain therapy with TRPV1 antagonist is considered broad-spectrum analgesia, lacking the typical side effects of both NSAIDs and opioids.[14]

In recent years, the interest on TRPV1, as potential target for pain therapy, is increased.
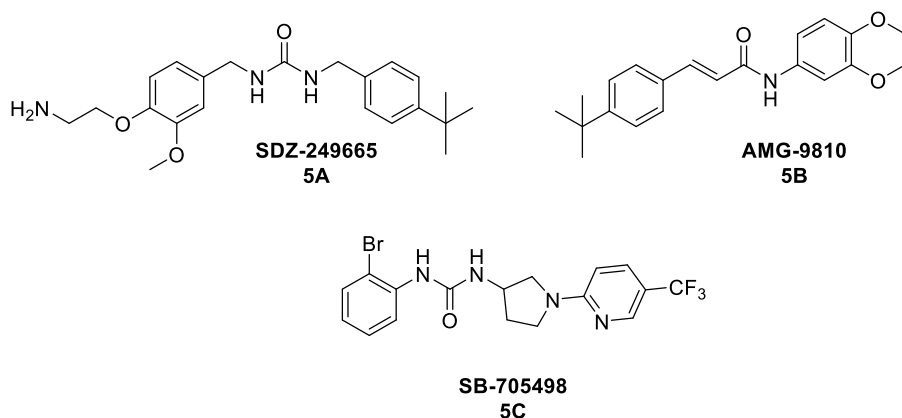
Figure 5. Structure of three different TRPV1 modulators.

Recently Novartis developed a new agonist, SDZ-249665 (Figure 5A), which was shown to be more potent than capsaicin orally.[15] Another interesting compound is the amide AMG-9810 (Figure 5B) that showed *in vitro* interesting characteristic as TRPV1 antagonist, and that *in vivo* demonstrated good anti-inflammatory and analgesic properties.[16]

The ureido derivative SB-705498 (Figure 5C) is a TRPV1 antagonist actually is in phase II of clinical trials and is a promising compound for the treatment of acute migraine.[17]

Another class of compounds developed by Merck and Princeton University are characterized by the presence of a heterocycle ring.

The further development of this collaboration led to the discovery of the isoxazole derivative (Figure 6), which showed analgesic property

on Hargreaves test. In this assay it was injected capsaicin into the paw, which causes thermal hyperalgesia.[18]
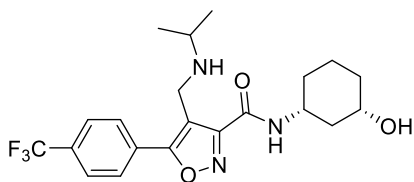
Figure 6. Isoxazole TRPV1 modulator.

4.4 TRPV1 Channels: Results and Discussion

Recently a new compound endowed with triazine core, namely N^2-(3-(dimethylamino)propyl)-N^4,N^6-bis(4-fluorophenethyl)-1,3,5-triazine-2,4,6-triamine also known as **8aA**, has been reported as the most potent TRPV1 blocker known.[19]

This compound acts as uncompetitive antagonist of TRPV1. The goal of the compounds inhibiting TRPV1 with this mechanism is the activity-dependent binding that occurs only when the receptor is complexed with the agonist or when the channel is in the open state, blocking only highly activated receptors.

Triazine **8aA** binds a site located deep within the pore, accessible only when the channel is open. This antagonism strategy is better than a complete pharmacological block of TRPV1 because the TRPV1 inhibition with high affinity irreversible, competitive vanilloid antagonists can result in hyperthermia and other side effects.[20]

On these bases and considering the connections between prokineticin system and vanilloid receptors,[21] the in vivo antinociceptive activity of the triazinedione PCs described on the chapter 3 might be produced at least in part by the inhibition of TRPV1. As consequence we decided to evaluate the triazinedione PCs TRPV1-blocking propriety. To this purpose were selected two of the most active PCs, **PC7** and **PC27** as well as the reference **PC1**.

The first evaluation made was about the protonation states of these compounds. The pK$_a$ value for these PCs, calculated with Epik [22,23] was 12.44, indicating that at physiological pH they can be protonated more than **8aA**, which showed a pK$_a$ value of 9.51.

Both agonistic and antagonistic activity of these compounds was evaluated on TRPV1 measuring the effect of the influx of Ca^{2+} on HEK-23 cells, which overexpress the human TRPV1 receptor (hTRPV1). All tested compounds showed no or very low agonist activity (**PC27** EC$_{50}$ > 50 μM with an efficacy at 100 μM at 20%) (Table 1).

PC1 and **PC27** inhibited the capsaicin (0.1 µM)-induced response in hTRPV1-HEK-23 cells, but their antagonist activity was weaker than 8aA, while **PC7** was not able to inhibit the capsaicin effect (Table 1).

These results indicate that the substitution of the ethyl group with a fluorine atom in 4-position on the N-5-benzyl was not tolerated, conversely the contemporary substitution of the ethyl with a trifluoromethyl group in 4-position of the N-5-benzyl and of methoxy with a methyl group on the N-1-benzyl group, causes an increase in activity, from 40.8 ± 0.9 µM of **PC1** to 27.2 ± 1.9 µM of **PC27** (Table 1).
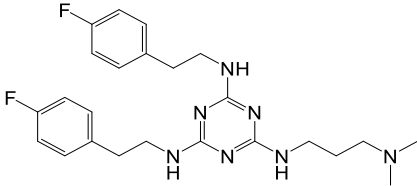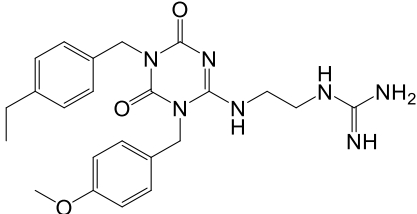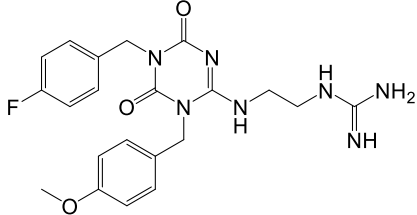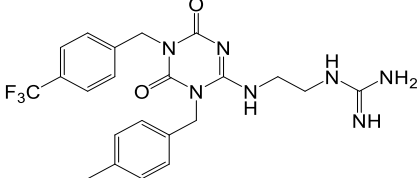
Name	Compound	TRPV1 IC$_{50}$ µM (cells pre-treated with capsaicin 0.1 µM)	TRPV1 EC$_{50}$ µM (efficacy at 100 µM)
8aA		21.7±0.7 (20.5±1.9)	NA (<10)
PC1		40.8±0.9 (40.5±1.1)	NA (<10)
PC7		>100 (>100)	NA (<10)
PC27		27.2±1.9 (31.0±1.0)	NA (<10)

Table 1. In vitro TRPV1 activity of selected triazine derivatives.

As previously described, TRPV1 and PKR are often co-located with the TRPA1; suggesting that the pro-inflammatory activity mediated by the TRPA1 might be due in part to release of PK and activation of PKR1 receptors. For this connection it appeared interesting to study if the triazinedione PCs and 8aA interact also with TRPA1, however none of the tested compounds showed any activity on this channel (Table 2).
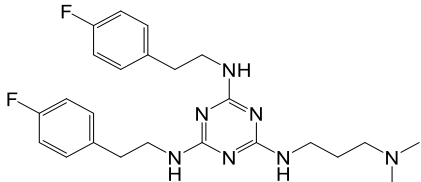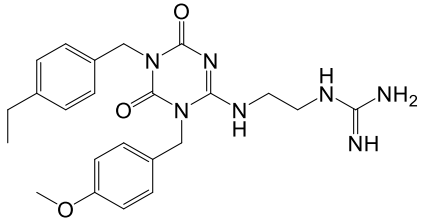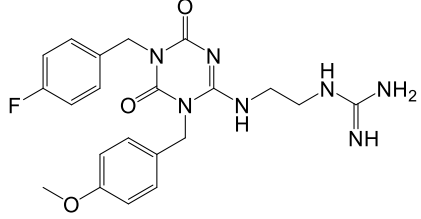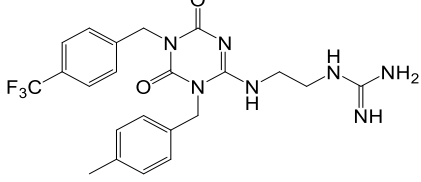
Name	Compound	TRPA1 IC$_{50}$ μM vs AITC 100 μM	TRPA1 EC$_{50}$ μM (efficacy at 100 μM vs AITC 100 μM)
8aA		>100	NA (52.7±2.4)
PC1		>100	NA (18.2±0.1)
PC7		>100	NA (0)
PC27		>100	>50 (42.6±2.6)

Table 2. In vitro TRPA1 activity of selected triazine derivatives.

To evaluate the selectivity of these compounds, triazinodione PCs and **8aA** were also tested against TRPM8 by measuring their effect on TRPM8-mediated elevation of intracellular Ca^{2+} in HEK-293 cells stably transfected with the rat recombinant TRPM8 channel.

Both agonistic and antagonistic properties of these compounds were tested (Table 3); **PC1** and **PC7** did not show any agonist activity, conversely to **PC27** displayed a weak activity, causing desensitization of TRPM8 after activation with icilin 0.25 μM. In addition, **PC1** showed a weak antagonist activity.

Name	Compound	TRPM8 IC$_{50}$ μM vs icilin 0.25 μM	TRPM8 EC$_{50}$ μM (efficacy at 100 μM vs AITC 100 μM)
8aA		0.95±0.03	1.1±0.1 (70.2±1.1)
PC1		57.5±0.8	NA (<10)
PC7		>100	NA (<10)
PC27		34.2±1.5	57.0±4.7 (31.1±1.7)

Table 3. In vitro TRPM8 activity of selected triazine derivatives.

4.5 References

1   Caterina, M., Schumacher, M., Tominaga, M., Rosen, T., Levine, J. & Julius, D. The capsaicin receptor: a heat-activated ion channel in the pain pathway. *Nature* **389**, 816 - 824 (1997).

2   Maggi, C. A., Patacchini, R., Tramontana, M., Amann, R., Giuliani, S. & Santicioli, P. Similarities and differences in the action of resiniferatoxin and capsaicin on central and peripheral endings of primary sensory neurons. *Neuroscience* **37**, 531-539, doi:http://dx.doi.org/10.1016/0306-4522(90)90421-Y (1990).

3   Planells-Cases, R., Garcìa-Sanz, N., Morenilla-Palao, C. & Ferrer-Montiel, A. Functional aspects and mechanisms of TRPV1 involvement in neurogenic inflammation that leads to thermal hyperalgesia. *Pflugers Arch - European Journal of Physiology* **451**, 151-159, doi:10.1007/s00424-005-1423-5 (2005).

4   Lishko, P. V., Procko, E., Jin, X., Phelps, C. B. & Gaudet, R. The Ankyrin Repeats of TRPV1 Bind Multiple Ligands and Modulate Channel Sensitivity. *Neuron* **54**, 905-918, doi:10.1016/j.neuron.2007.05.027.

5   Lau, S.-Y., Procko, E. & Gaudet, R. Distinct properties of Ca(2+)–calmodulin binding to N- and C-terminal regulatory regions of the TRPV1 channel. *The Journal of General Physiology* **140**, 541-555, doi:10.1085/jgp.201210810 (2012).

6   Ferrer-Montiel, A., García-Martínez, C., Morenilla-Palao, C., García-Sanz, N., Fernández-Carvajal, A., Fernández-Ballester, G. & Planells-Cases, R. Molecular architecture of the vanilloid receptor. *European Journal of Biochemistry* **271**, 1820-1826, doi:10.1111/j.1432-1033.2004.04083.x (2004).

7   van der Stelt, M. & Di Marzo, V. Endovanilloids. *European Journal of Biochemistry* **271**, 1827-1834, doi:10.1111/j.1432-1033.2004.04081.x (2004).

8   Smart, D., Gunthorpe, M. J., Jerman, J. C., Nasir, S., Gray, J., Muir, A. I., Chambers, J. K., Randall, A. D. & Davis, J. B. The endogenous lipid anandamide is a full agonist at the human vanilloid receptor (hVR1). *British Journal of Pharmacology* **129**, 227-230, doi:10.1038/sj.bjp.0703050 (2000).

9   Huang, S. M., Bisogno, T., Trevisani, M., Al-Hayani, A., De Petrocellis, L., Fezza, F., Tognetto, M., Petros, T. J., Krey, J. F., Chu, C. J., Miller, J. D., Davies, S. N., Geppetti, P., Walker, J. M. & Di Marzo, V. An endogenous capsaicin-like substance with high potency at recombinant and native vanilloid VR1 receptors.

Proceedings of the National Academy of Sciences **99**, 8400-8405, doi:10.1073/pnas.122196999 (2002).

10   De Petrocellis, L., Harrison, S., Bisogno, T., Tognetto, M., Brandi, I., Smith, G. D., Creminon, C., Davis, J. B., Geppetti, P. & Di Marzo, V. The vanilloid receptor (VR1)-mediated effects of anandamide are potently enhanced by the cAMP-dependent protein kinase. *Journal of Neurochemistry* **77**, 1660-1663, doi:10.1046/j.1471-4159.2001.00406.x (2001).

11   Szallasi, A. & Blumberg, P. M. Vanilloid (Capsaicin) Receptors and Mechanisms. *Pharmacological Reviews* **51**, 159-212 (1999).

12   Caterina, M. J., Leffler, A., Malmberg, A. B., Martin, W. J., Trafton, J., Petersen-Zeitz, K. R., Koltzenburg, M., Basbaum, A. I. & Julius, D. Impaired Nociception and Pain Sensation in Mice Lacking the Capsaicin Receptor. *Science* **288**, 306-313, doi:10.1126/science.288.5464.306 (2000).

13   Davis, J. B., Gray, J., Gunthorpe, M. J., Hatcher, J. P., Davey, P. T., Overend, P., Harries, M. H., Latcham, J., Clapham, C., Atkinson, K., Hughes, S. A., Rance, K., Grau, E., Harper, A. J., Pugh, P. L., Rogers, D. C., Bingham, S., Randall, A. & Sheardown, S. A. Vanilloid receptor-1 is essential for inflammatory thermal hyperalgesia. *Nature* **405**, 183-187, doi:http://www.nature.com/nature/journal/v405/n6783/suppinfo/405183a0_S1.html (2000).

14   Cui, M., Honore, P., Zhong, C., Gauvin, D., Mikusa, J., Hernandez, G., Chandran, P., Gomtsyan, A., Brown, B., Bayburt, E. K., Marsh, K., Bianchi, B., McDonald, H., Niforatos, W., Neelands, T. R., Moreland, R. B., Decker, M. W., Lee, C.-H., Sullivan, J. P. & Faltynek, C. R. TRPV1 Receptors in the CNS Play a Key Role in Broad-Spectrum Analgesia of TRPV1 Antagonists. *The Journal of Neuroscience* **26**, 9385-9393, doi:10.1523/jneurosci.1246-06.2006 (2006).

15   Urban, L., Campbell, E. A., Panesar, M., Patel, S., Chaudhry, N., Kane, S., Buchheit, K.-H., Sandells, B. & James, I. F. In vivo pharmacology of SDZ 249-665, a novel, non-pungent capsaicin analogue. *Pain* **89**, 65-74, doi:http://dx.doi.org/10.1016/S0304-3959(00)00349-3 (2000).

16   Gavva, N. R., Tamir, R., Qu, Y., Klionsky, L., Zhang, T. J., Immke, D., Wang, J., Zhu, D., Vanderah, T. W., Porreca, F., Doherty, E. M., Norman, M. H., Wild, K. D., Bannon, A. W., Louis, J.-C. & Treanor, J. J. S. AMG 9810 [(E)-3-(4-t-Butylphenyl)-N-(2,3-dihydrobenzo[b][1,4]dioxin-6-yl)acrylamide], a Novel Vanilloid Receptor 1 (TRPV1) Antagonist with Antihyperalgesic Properties. *Journal of*

Pharmacology and Experimental Therapeutics **313**, 474-484, doi:10.1124/jpet.104.079855 (2005).

17   Meents, J., Hoffmann, J., Chaplan, S., Neeb, L., Schuh-Hofer, S., Wickenden, A. & Reuter, U. Two TRPV1 receptor antagonists are effective in two different experimental models of migraine. *The Journal of Headache and Pain* **16**, 57 (2015).

18   Ratcliffe, P. *et al.* Discovery of potent, soluble and orally active TRPV1 antagonists. Structure–activity relationships of a series of isoxazoles. *Bioorganic & Medicinal Chemistry Letters* **21**, 4652-4657, doi:http://dx.doi.org/10.1016/j.bmcl.2011.01.051 (2011).

19   Vidal-Mosquera, M., Fernández-Carvajal, A., Moure, A., Valente, P., Planells-Cases, R., González-Ros, J. M., Bujons, J., Ferrer-Montiel, A. & Messeguer, A. Triazine-Based Vanilloid 1 Receptor Open Channel Blockers: Design, Synthesis, Evaluation, and SAR Analysis. *Journal of Medicinal Chemistry* **54**, 7441-7452, doi:10.1021/jm200981s (2011).

20   Gavva, N. R. Body-temperature maintenance as the predominant function of the vanilloid receptor TRPV1. *Trends in Pharmacological Sciences* **29**, 550-557, doi:http://dx.doi.org/10.1016/j.tips.2008.08.003 (2008).

21   Hu, W.-P., Zhang, C., Li, J.-D., Luo, Z. D., Amadesi, S., Bunnett, N. & Zhou, Q.-Y. Impaired pain sensation in mice lacking prokineticin 2. *Molecular Pain* **2**, 35 (2006).

22   Greenwood, J., Calkins, D., Sullivan, A. & Shelley, J. Towards the comprehensive, rapid, and accurate prediction of the favorable tautomeric states of drug-like molecules in aqueous solution. *Journal of Computer-Aided Molecular Design* **24**, 591-604, doi:10.1007/s10822-010-9349-1 (2010).

23   Shelley, J., Cholleti, A., Frye, L., Greenwood, J., Timlin, M. & Uchimaya, M. Epik: a software program for pK a prediction and protonation state generation for drug-like molecules. *Journal of Computer-Aided Molecular Design* **21**, 681-691, doi:10.1007/s10822-007-9133-z (2007).

5. FULL PAPERS

PLOS | ONE

RESEARCH ARTICLE

Characterisation of (R)-2-(2-Fluorobiphenyl-4-yl)-N-(3-Methylpyridin-2-yl)Propanamide as a Dual Fatty Acid Amide Hydrolase: Cyclooxygenase Inhibitor

Sandra Gouveia-Figueira[1,2], Jessica Karlsson[1], Alessandro Deplano[3], Sanaz Hashemian[1], Mona Svensson[1], Marcus Fredriksson Sundbom[1], Cenzo Congiu[3], Valentina Onnis[3], Christopher J. Fowler[1]*

1 Department of Pharmacology and Clinical Neuroscience, Pharmacology Unit, Umeå University, Umeå, Sweden, 2 Department of Chemistry, Umeå University, Umeå, Sweden, 3 Department of Life and Environmental Sciences, Unit of Pharmaceutical, Pharmacological and Nutraceutical Sciences, University of Cagliari, via Ospedale 72, Cagliari, Italy

* cf@pharm.umu.se

Abstract

Background

Increased endocannabinoid tonus by dual-action fatty acid amide hydrolase (FAAH) and substrate selective cyclooxygenase (COX-2) inhibitors is a promising approach for pain-relief. One such compound with this profile is 2-(2-fluorobiphenyl-4-yl)-N-(3-methylpyridin-2-yl)propanamide (Flu-AM1). These activities are shown by Flu-AM1 racemate, but it is not known whether its two single enantiomers behave differently, as is the case towards COX-2 for the parent flurbiprofen enantiomers. Further, the effects of the compound upon COX-2-derived lipids in intact cells are not known.

Methodology/Principal Findings

COX inhibition was determined using an oxygraphic method with arachidonic acid and 2-arachidonoylglycerol (2-AG) as substrates. FAAH was assayed in mouse brain homogenates using anandamide (AEA) as substrate. Lipidomic analysis was conducted in unstimulated and lipopolysaccharide + interferon γ- stimulated RAW 264.7 macrophage cells. Both enantiomers inhibited COX-2 in a substrate-selective and time-dependent manner, with IC_{50} values in the absence of a preincubation phase of: (R)-Flu-AM1, COX-1 (arachidonic acid) 6 μM; COX-2 (arachidonic acid) 20 μM; COX-2 (2-AG) 1 μM; (S)-Flu-AM1, COX-1 (arachidonic acid) 3 μM; COX-2 (arachidonic acid) 10 μM; COX-2 (2-AG) 0.7 μM. The compounds showed no enantiomeric selectivity in their FAAH inhibitory properties. (R)-Flu-AM1 (10 μM) greatly inhibited the production of prostaglandin D_2 and E_2 in both unstimulated and lipopolysaccharide + interferon γ- stimulated RAW 264.7 macrophage cells. Levels of 2-AG were not affected either by (R)-Flu-AM1 or by 10 μM flurbiprofen, either alone or in combination with the FAAH inhibitor URB597 (1 μM).

5. Full Papers

Conclusions/Significance

Both enantiomers of Flu-AM1 are more potent inhibitors of 2-AG compared to arachidonic acid oxygenation by COX-2. Inhibition of COX in lipopolysaccharide + interferon γ- stimulated RAW 264.7 cells is insufficient to affect 2-AG levels despite the large induction of COX-2 produced by this treatment.

Introduction

According to the textbooks, non-steroidal anti-inflammatory drugs (NSAIDs) produce their effects upon pain and inflammation as a result of the inhibition of cyclooxygenase (COX)-derived prostaglandin production [1]. There is, however, evidence that NSAIDs also involve the endocannabinoid (eCB) system in their actions. Thus, for example, the effects of spinal administration of the NSAID indomethacin in the formalin test of prolonged pain is blocked by a CB_1 receptor antagonist and is not seen in $CB_1^{-/-}$ mice [2], and similar effects have been seen with other spinally administered NSAIDs (review, see [3]). In 2010, Bishay et al. [4] reported that the (R)-enantiomer of flurbiprofen produced CB receptor-mediated effects in a model of neuropathic pain. Given that the COX-inhibitory properties of the profens such as flurbiprofen are traditionally considered to reside in the (S)-enantiomer [5], this is an important result and may have bearing upon the analgesic properties of this compound.

The two most well-studied endogenous ligands for the eCB system are anandamide (AEA) and 2-arachidonoylglycerol (2-AG). AEA and 2-AG are effectively metabolised both by hydrolytic and other pathways [6]. With respect to the former, AEA is hydrolysed by both fatty acid amide hydrolase (FAAH) and N-acylethanolamine acid amidase (NAAA), whilst 2-AG is hydrolysed by monoacylglycerol lipase, α/β-hydrolase domain 6/12 and FAAH to form arachidonic acid [6]. However, AEA and 2-AG are also substrates for COX-2 [7,8]. In 2009, Prusakiewicz et al. [9] reported that ibuprofen and mefenamic acid were more potent inhibitors of the oxygenation of 2-AG by COX-2 than of the oxygenation of arachidonic acid by this enzyme isoform. COX-2 is a homodimeric enzyme, and the authors suggested that the selectivity was due to the fact that 2-AG oxygenation was blocked when the inhibitor had bound to one of the monomers, whereas blockade of arachidonic acid metabolism required binding to both monomers [9]. This type of substrate-selective inhibition may be therapeutically useful: an indomethacin analogue, LM-4131, has also been identified as a substrate-selective inhibitor of COX-2. The compound increases brain 2-AG levels, and produces potentially beneficial effects in models of anxiety [10]. This group has also investigated the (R)-enantiomers of the profens and found them to be potent inhibitors of AEA and 2-AG oxygenation without affecting arachidonic acid oxidation [11]. They showed further that in dorsal root ganglion cells cultured under inflammatory conditions, the (R)-enantiomers of ibuprofen, naproxen and flurbiprofen increased AEA and 2-AG levels without affecting arachidonic acid levels [11]. It is not known, however, whether substrate-selective COX-2 inhibitors increase AEA and 2-AG in other cells, such as macrophages, when they are cultured under inflammatory conditions.

An important unwanted property of NSAIDs is their propensity to cause gastric lesions. In a key study, Naidu et al. [12] showed that not only did the FAAH inhibitor URB597 reduce the gastrointestinal damage produced by the NSAID diclofenac, but also acted synergistically with this compound in a model of visceral pain. This and other findings has led to the suggestion that dual-action FAAH-COX inhibitors may be useful for the treatment of pain [13]. Recently, Sasso et al. [14] reported the synthesis of a compound, ARN2508. The compound inhibited

324

FAAH and both COX isoforms in an irreversible manner and reduced concentrations in the plasma of the prostaglandin metabolite 6-keto $PGF_{1\alpha}$ whilst increasing levels of the FAAH substrates PEA and OEA. ARN2508 showed efficacy in a model of inflammatory pain without producing gastric lesions [14]. It is not known, however, whether the compound inhibits COX-2 in a substrate-selective manner.

In 2003, two of us (C.C., V.O.) reported that the amide derivative of ibuprofen with 2-amino-3-methylpyridine was more potent than ibuprofen in a model of visceral pain, but had a considerably lower ulcerogenic potency [15]. This compound was subsequently shown to inhibit FAAH with a potency approximately 2–3 orders of magnitude greater than ibuprofen itself, whilst retaining its COX-inhibitory properties [16,17]. We have also reported that the corresponding amide analogue of flurbiprofen (Flu-AM1) is a potent inhibitor of rat brain FAAH and additionally shows a substrate-selective inhibition of COX-2, whereby lower concentrations were needed to block the oxygenation of 2-AG than of arachidonic acid [18]. As with flurbiprofen, Flu-AM1 has a chiral centre. In view of the clear enantiomeric difference seen with flurbiprofen towards the inhibition of COX-2 [11], it is important to investigate whether the profile of Flu-AM1 as a dual action FAAH: substrate-selective COX-2 inhibitor can be further refined by selection of the (R)-enantiomer.

Thus from the above discussion, two distinct questions can be formulated:

a. Do the amide derivatives of flurbiprofen with 2-amino-3-methylpyridine show enantiomeric differences with respect to inhibition of COX-2 and FAAH?

b. Is COX-2 inhibition *per se* sufficient to affect endocannabinoid levels in macrophage cells cultured under inflammatory conditions?

These questions have been investigated in the present study.

Materials and Methods

Compounds and materials

Radioactive arachidonoyl ethanolamide[1-^{3}H] ([^{3}H]-AEA) was obtained from American Radiolabeled Chemicals, Inc (St Louis, MO, USA). (R)(-)-Flurbiprofen and (S)(+)-Flurbiprofen were purchased from Santa Cruz Biotechnology Inc. (Dallas, Texas, USA). Ovine COX-1 (cat. no. 60100), human recombinant COX-2 (cat. no. 60122), COX-2 polyclonal antibody (rabbit anti-mouse, cat #: 160106), arachidonic acid, 2-AG, AEA and URB597 (cyclohexylcarbamic acid 3′-carbamoylbiphenyl-3-yl ester) were purchased from the Cayman Chemical Co. (Ann Arbor, MI, USA). Substrates were dissolved in ethanol or DMSO as appropriate. Polyclonal goat anti-rabbit immunoglobulin/HRP was obtained from Dako (Glostrup, Denmark). Protease inhibitor cocktail set III was obtained from Merck Millipore (Darmstadt, Germany). For the lipid quantification experiments, the following native and deuterated standards were purchased from the Cayman Chemical Co.: AEA, 2-AG, PEA, OEA, DEA, LEA, SEA, 2-LG, AEA-d^8, 2-AG-d^8, PEA-d^4, SEA-d^3, OEA-d^4, PGF$_{2\alpha}$, PGE$_2$, TXB$_2$, PGD$_2$, 12(13)-EpOME, 9(10)-DiHOME, 12(13)-DiHOME, 11-HETE, 12-HETE, 15-HETE, 9-HODE, 13-HODE, 12-HEPE, 12-[[(cyclohexylamino)carbonyl]amino]-dodecanoic acid (CUDA), 12(13)-DiHOME-d^4, 12(13)-EpOME-d^4, 9-HODE-d^4, PGE$_2$-d^4 and PGD$_2$-d^4. 9,10,13-TriHOME and 9,12,13-TriHOME were obtained from Larodan (Sweden, Malmö). For list of lipid abbreviations, see S1 Table.

Synthesis of the enantiomers of Flu-AM1

Enantiomerically pure (R)(-)-Flu-AM1 and (S)(+)-Flu-AM1 were synthesized using a slight modification of the procedure previously described for the racemate [18]. Briefly, commercially

available (*R*)(-)-Flurbiprofen and (*S*)(+)-Flurbiprofen (0.24 g, 1 mmol) in dry acetonitrile solution (10 mL) were added with 1-(3-dimethylaminopropyl)-3-ethylcarbodiimide hydrochloride (0.21 g, 1.1 mmol) and hydroxybenzotriazole (0.13 g, 1 mmol). This mixture was stirred at room temperature for 30 min and then treated with 2-amino-3-methylpyridine (0,11 g, 1 mmol), after which the mixture was stirred at room temperature for additional 24 h. Solutions were evaporated to dryness *in vacuo* and the residues were dissolved in ethyl acetate (20 mL) and washed sequentially with brine (2 x 5 mL), 10% aqueous sodium carbonate (2 x 5 mL), 10% aqueous citric acid (2 x 5 mL), and water (2 x 5 mL). The organic layer was dried over anhydrous magnesium sulphate, filtered, and concentrated to dryness under reduced pressure. The respective (*R*)(+)-Flu-AM1 or (*S*)(-)-Flu-AM1 was obtained (54 and 52% yield respectively) in analytically pure form. ^{1}H NMR (DMSO-d_6, recorded on a Varian Inova 500 spectrometer in DMSO-d_6 solution, with chemical shifts (δ) given in part per million downfield from the internal standard, tetramethylsilane): δ 1.42 (d, J = 7.0 Hz, 3H, CH$_3$), 2.10 (s, 3H, CH$_3$), 3.91 (q, J = 7.0 Hz, 1H, CH), 7.21–7.52 (m, 10H, Ar and Py), 7.98 (s, 1H, Ar), 10.03 (s, 1H, NH). Infrared spectra (recorded on a Bruker Vector 22 spectrometer in Nujol mull): 3330, 3020, 2965, 1675, 1638, 1576 cm^{-1}. Optical rotation (assessed at 10 mg/mL concentrations using a Perkin Elmer 241 polarimeter in a 10 cm water-jacketed cell at 25°C): [α] = -11.2° for (*R*)(-)-Flu-AM1 and [α] = +11.5° for (*S*)(+)-Flu-AM1. MS (positive-ion electrospray ionization (ESI) mass spectra recorded on a double-focusing Finnigan MAT 95 instrument with BE geometry): m/z 335 (M + H)$^+$. Combustion elemental analyses (conducted with a Yanagimoto MT-5 CHN recorder elemental analyzer): Anal. Calcd. for C$_{21}$H$_{19}$FN$_2$O: C, 75.43; H, 5.73; N, 8.83. Found: C, 75.47; H, 5.72; N, 8.89 for (*R*)(-)-Flu-AM1 and C, 75.37; H, 5.75; N, 8.90 for (*S*)(+)-Flu-AM1.

COX-1 and 2 inhibition experiments

The assay was performed according to Meade *et al.* [19] with minor modifications [20]. An oxygen electrode chamber with integral stirring (Oxygraph System, Hansatech Instruments, King´s Lynn, U.K.) was calibrated daily to ambient temperature and air pressure. The assay buffer contained 0.1 M Tris-HCl buffer pH 7.4, 1 µM haematin, 2 mM phenol, 5 mM EDTA, 10 µM substrate (arachidonic acid or 2-AG) (final assay volume was 2 ml). After addition of (*R*)- or (*S*)-Flu-AM1 dissolved in ethanol (final assay concentration 1%), a baseline was established for 5 min before initiation of reaction by addition of 200 units ovine COX-1 or human recombinant COX-2. The change in oxygen consumption as a measurement of enzyme activity was monitored for approximately 5 min.

FAAH assay

Brains from male B6CBAF1/J mice, stored at -80°C, were thawed, weighed and homogenized in cold buffer (20 mM HEPES, 1 mM MgCl$_2$ pH 7.0). Homogenates were centrifuged (35,000 g at 4°C for 20 min) before the pellet was resuspended in cold homogenization buffer. Centrifugation and resuspension was repeated twice. The suspension was incubated at 37°C for 15 min to degrade any endogenous substrate able to interfere with the FAAH assay. After centrifugation (35,000 g at 4°C for 20 min), the pellet was resuspended in cold buffer (50 mM Tris-HCl, 1mM EDTA, 3 mM MgCl$_2$, pH 7.4). The protein concentration was determined according to the Bradford assay [21] after which the samples were frozen in aliquots at -80°C. Ethical permission for the animal experiments was obtained from the local animal research ethical committee (Umeå Ethical Committee for Animal Research, Umeå, Sweden). FAAH was assayed using the method of Boldrup et al. [22], whereby homogenates (0.3 µg protein / assay) in assay buffer (10 mM Tris-HCl, 1mM EDTA, pH 7.4), test compounds and substrate ([^{3}H]AEA in

10 mM Tris-HCl, 1mM EDTA, pH 7.4 containing 10 mg/ml fatty acid-free bovine serum, assay concentration 0.5 μM unless otherwise stated) were incubated for 10 min at 37°C. Thereafter, 400 μL activated charcoal (80 μL activated charcoal + 320 μL 0.5 M HCl) was added and the samples were placed on ice and centrifuged at 2500 rpm for 10 min. Aliquots (200 μL) of the supernatant was analyzed for tritium content by liquid scintillation spectroscopy with quench correction.

LPS/INF-γ treatment of RAW 264.7 cells

RAW264.7 mouse leukemic monocyte/macrophage cells (European collection of cell cultures, Port Down, UK) were cultured in DMEM medium containing 4 mM glutamine, 10% foetal bovine serum and 100 U/mL penicillin and 100 μg/mL streptomycin. The cells were cultured in a 75 cm^2 flasks at 37°C with 5% CO$_2$ at humidified atmospheric pressure and split (ratio 1:3–6) approximately twice a week. LPS/INF-γ treatment was undertaken on RAW 264.7 cells seeded in 6 well plates. For the lipid measurements, 2.5 x 10^5 cells/well were seeded and either phosphate-buffered saline (unstimulated) or LPS (0.1 μg/mL) + INF-γ (100 U/mL) were added immediately and the cells cultured for 24 h. Medium was then discarded. Test compounds (1 μM URB597, 10 μM flurbiprofen, 1 μM URB597 + 10 μM flurbiprofen, 10 μM (R)-Flu-AM1 or vehicle) were added, and the cells were incubated for 30 min at 37°C. When indicated, the calcium ionophore ionomycin (5 μM) was added at the same time as the test compounds. The plates were placed on ice and after removal of medium, the cells were washed twice with ice-cold PBS (2x1mL). One mL of methanol was added to the wells and the mixture was scraped using a rubber policeman and the extract pipetted into Falcon tubes. An additional 1 mL of methanol was added to the wells, the mixture was scraped and the mixture was pipetted into the same tubes. These were then centrifuged at 2000 x g for 15 min (4°C) to sediment cell debris, and the methanol phase collected and stored at -80°C until used for analysis of prostaglandins, 2-AG, AEA and related lipids.

[3H]AEA hydrolysis by intact RAW 264.7 cells

For the studies of [3H]AEA hydrolytic capacity of RAW 264.7 cells, initial experiments indicated that low activities were seen. In consequence, 2.5 x 10^6 cells/well were seeded and cultured overnight prior to addition of either phosphate-buffered saline or LPS (0.1 μg/mL) + INF-γ (100 U/mL) and incubation for a further 24 h. [3H]AEA hydrolytic capacity was then measured as described previously [23]. Briefly, the cells were washed twice with 400 μL of pre-warmed KRH buffer (120mM NaCl, 4.7mM KCl, 2.2 mM CaCl$_2$, 10mM 4-(2-hydroxyethyl)-piperazineethane-sulfonic acid (HEPES), 0.12 mM KH$_2$PO$_4$, 0.12 mM MgSO$_4$, pH 7.4) with 1% BSA prior to addition of 340 μL of pre-warmed KRH buffer with 0.1% fatty acid-free BSA and 10 μL of test compound (final concentrations as above) or vehicle (0.05% DMSO + 0.1% ethanol). After preincubation for 10 min at 37°C, [3H]AEA (50 μL, final concentration 0.1 μM, in KRH buffer with 0.1% fatty acid-free BSA) was added and the cells were incubated for a further 60 min at 37°C. Reactions were stopped by addition of 600 μL of activated charcoal buffer (120 μL activated charcoal + 480 μL 0.5 M HCl) and the samples were then worked up as described above for the FAAH assay.

Western blot for COX-2

RAW 264.7 cells (2.5 x 10^6 cells/well) were seeded into 6 well plate and incubated for 24 h at 37°C prior to treatment with either phosphate-buffered saline or LPS (0.1 μg/mL) + INF-γ (100 U/mL). Following incubation for 1.5–24 h at 37°C, medium was aspirated, 400 μl ice-cold phosphate-buffered saline was added, and the cells were scraped using a rubber policeman.

5. Full Papers

This procedure was repeated, and the samples were centrifuged for 4 min at 1000 r.p.m., 4°C to sediment the cells. A mixture of 150mM NaCl, 50mM Tris, 1% Triton-X100, pH 8.0 + Protease Inhibitor III (1:200 v.v^{-1}, 500 μL) was added to the cells in Eppendorf tubes, which were then shaken for 30 min at 750 r.p.m., 4°C. Samples were then centrifuged at 14,000 g for 5 min at 4°C, and the supernatants then frozen at -80°C until used. Proteins in samples (20 μL, containing 3 μg of the samples and 1 x Laemmli buffer) were separated by gel electrophoresis using Mini Protean TGX stain free gels (BioRad, Hercules, CA, USA, cat # 456–8093; 200 V x 35 min). Human recombinant COX-2 (750 ng) was used as positive control. Proteins were transferred to PVDF mini membranes using a Trans-Blot Turbo Transfer System (BioRad). The membranes were treated with blocking solution (5% dried milk in 1 x tris-Buffered saline / Tween-20 [TBST] solution, 1 hour at room temperature) after which the primary antibody (COX-2 polyclonal antibody, rabbit anti-mouse, 1:1000, in 5% dried milk / TBST) was added and the membranes were left overnight at 4°C on a rotating table. After five washes with TBST, the membranes were treated with the secondary antibody (HRP-conjugated goat anti-rabbit, 1:2000) for 1 h at room temperature on a rotating table. After five washes, the membranes were treated with Clarity Western ECL substrate and photographed in a Molecular Imager Gel Doc XR system (BioRad) and quantified using ImageLab software 5.1 according to the manufacturers instructions (http://www.bio-rad.com/webroot/web/pdf/lsr/literature/Bulletin_6434.pdf).

Cell viability experiments

RAW 264.7 cells (2.5 x 10^6 cells/well) were seeded into 6 well plate and incubated for 24 h at 37°C prior to treatment with either phosphate-buffered saline or LPS (0.1 μg/mL) + INF-γ (100 U/mL). Following incubation for 1.5–24 h at 37°C, medium was aspirated, 400 μL ice-cold phosphate-buffered saline was added, and the cells were scraped using a rubber policeman. Cell viability was assessed using trypan blue and a TC20 automated cell counter (Bio-Rad).

Assay of prostaglandins, 2-AG, AEA and related lipids in extracts from RAW 264.7 cells

Cell extracts were thawed on ice and milliQ water was added to give a final methanol concentration of 5% (v/v). After samples were spiked with 10 μL internal standard solutions (800 ng/mL 2-AG-d$_8$, 40 ng/mL PGF$_{2\alpha}$-EA-d4 and PGE$_2$-EA-d4, 20 ng/mL AEA-d$_4$ and OEA-d$_4$, PEA-d$_4$ and SEA-d$_3$, 50 ng/mL 12(13)-DiHOME-d$_4$ and 12(13)-EpOME-d$_4$ and 25 ng/mL 20-HETE-d$_6$, 5(S)-HETE-d$_8$, 9(S)-HODE-d$_4$, PGE$_2$-d$_4$, PGD$_2$-d$_4$ and TXB$_2$-d$_4$, 10 μL antioxidant solution (0.2 mg/mL BHT/EDTA in methanol/water (1:1)) and then applied directly to the solid phase extraction cartridge. Briefly, compounds were extracted using Waters Oasis HLB cartridges (60 mg of sorbent, 30 μm particle size). Cartridges were washed with 2 mL of ethyl acetate, followed by 2x2 mL of MeOH, and then conditioned with 2x2 mL of wash solution (95:5 v/v water/methanol with 0.1% acetic acid). After loading the sample containing internal standard and antioxidant solution, the cartridges were washed with 2x4 mL of wash solution, dried under high vacuum for about 1 minute, and eluted with 3 mL acetonitrile, followed by 2 mL of methanol and 1 mL of ethyl acetate into polypropylene tubes containing 6 μL of a glycerol solution (30% in methanol). Eluates were concentrated with a MiniVac system (Farmingdale, NY, U.S.A.) and reconstituted in 100 μL of methanol and vortexed. If necessary, samples were centrifuged to remove any residuals. Solutions were then transferred to LC vials with low-volume inserts, 10 μL of a recovery standard (CUDA, 50 ng/mL) was added, to normalise for changes in volume and instrument variability, and UPLC-MS/MS analysis was performed immediately.

Chromatographic separation of the analytes was performed using an Agilent ultra-perfor-mance (UP)LC system (Infinity 1290) was coupled with an electrospray ionization source (ESI) to an Agilent 6490 Triple Quadrupole system equipped with the iFunnel Technology (Agilent Technologies, Santa Clara, CA, USA) [24]. Separate injections for subsequent ioniza-tion in positive (for 2-AG, AEA and related N-acylethanolamines) and negative mode (for the prostaglandins and other oxylipins) were undertaken. Analyte separation was performed using a Waters BEH C18 column (2.1 mm x 150 mm, 2.5 μm particle size), and 10 μL injection vol-umes were employed for each run. The mobile phase consisted of (A) 0.1% acetic acid in MilliQ water and (B) acetonitrile:isopropanol (90:10). The following gradients were employed: 0.0–3.5 min 10–35% B, 3.5–5.5 min 40% B, 5.5–7.0 min 42%B, 7.0–9.0 min 50% B, 9.0–15.0 min 65% B, 15.0–17.0 min 75% B, 17.0–18.5 min 85% B, 18.5–19.5 min 95% B, 19.5–21 min 10% B, 21.0–25.0 min 10% B (prostaglandins and other oxylipins); and 0.0–2.0 min 30–45% B, 2.0–2.5 min 45–79% B, 2.5–11.5 min 79% B, 11.5–12 min 79–90% B, 12–14 min 90% B, 14–14.5 min 90–79% B, 14.5–15.5 min 79% B, 15.6–19 min 30% B (2-AG, AEA and related N-acylethanolamines).

Precursor ions, $[M+H]^+$ and $[M-H]^-$, product ions, multiple reaction monitoring (MRM) transitions and optimal collision energies were established for each analyte. ESI conditions were: capillary and nozzle voltage at 4000 V and 1500 V, drying gas temperature 230°C with a gas flow of 15 L/min, sheet gas temperature 400°C with a gas flow of 11 L/min, the nebulizer gas flow was 35 psi, and iFunnel high and low pressure RF at 90 and 60 V (negative mode) and 150 and 60 V (positive mode). The dynamic MRM option was performed for all compounds with optimized transitions and collision energies. The MassHunter Workstation software was used manually to integrate all peaks. The limits of quantification (LOQ) for compounds in the eCB metabolome were in the range 0.5–1000 fg on column, intraday accuracy and precision ranges (%) were 83–125 and 0.3–17, respectively, and interday accuracy and precision ranges (%) were 80–119 and 1.2–20, respectively, dependent upon the compound and the concentra-tion studied. Corresponding values for the oxylipins were LOQ 0.5 fg– 4.2 pg on column (LOQ), 85–115% (inter- and intraday accuracy) and < 5% (precision) [24].

Internal standard recovery rates were established for RAW264.7 cells pellet methanolic extracts (5 replicates, test samples) and PBS (100 mM, 5 replicates). Briefly, samples were spiked with 10 μL of internal standard solutions and extracted by SPE as described above. To calculate recovery rates, internal standard calibration curves obtained at five different concen-trations normalized against CUDA were used and expressed as the percentage of the expected value. Matrix-dependent recovery was established by spiking 10 μL internal standards in a sim-ilar manner to human plasma.

Statistical analyses

pI_{50} and IC_{50} values were calculated using log(inhibitor) vs. response with variable slope (four parameters) algorithm in the GraphPad Prism computer program (GraphPad Software Inc., San Diego, CA. USA). The best fit was chosen by Akaike's informative criteria. K_i values were obtained in two ways: 1) using the enzyme kinetics competitive model algorithm available in the GraphPad Prism programme; 2) from the intersection of the lines in a Dixon plot. The regression lines were determined by the robust analysis, rather than the least squares analysis, available in the GraphPad Prism programme. Oxygen consumption time courses were fitted to the"plateau followed by one phase delay" algorithms available in the GraphPad Prism pro-gramme. Kruskal-Wallis testing and post-hoc testing used Dunn's multiple comparison test were undertaken using the same computer programme. The rank-based two-way ANOVAs

329

5. Full Papers

(two-way robust Wilcoxon analysis [25]) were calculated using the function raov in the Rfit package of the R computer programme [26,27].

Results

Inhibition of COX isoforms *in vitro* by the enantiomers of Flu-AM1

The inhibition of ovine COX-1 and recombinant human COX-2 by the enantiomers of Flu-AM1 are shown in Fig 1. Both compounds were effective inhibitors of arachidonic acid oxidation by both isoform, and of 2-AG oxidation by COX-2. The curves in the figure were fitted to the built-in equation "plateau followed by one phase delay" in the GraphPad Prism programme, where the initial y value was set to zero and the x_o value (the length of the initial lag phase) was allowed to be in the range 0–120 s. From the mean values returned from the equation, initial values (at $x_0 + 1$ s) were calculated and these were used to derive approximate IC_{50} values of: (R)-Flu-AM1, COX-1 (arachidonic acid) 6 µM; COX-2 (arachidonic acid) 20 µM; COX-2 (2-AG) 1 µM; (S)-Flu-AM1, COX-1 (arachidonic acid) 3 µM; COX-2 (arachidonic acid) 10 µM; COX-2 (2-AG) 0.7 µM. Thus, the (S)-enantiomer is roughly twice as potent as the (R)-enantiomer, but both enantiomers show substrate-selective inhibition of COX-2, whereby the oxygenation of 2-AG is inhibited at concentrations an order of magnitude lower than required for inhibition of the oxygenation of arachidonic acid.

Flurbiprofen inhibits COX in a time-dependent manner [28]. In order to determine whether the two enantiomers of Flu-AM1 also exhibited this property, the effect of sub-maximal concentrations of the compounds were investigated either without preincubation (where the reactions are started by addition of the enzyme) or following a five minute preincubation with enzyme prior to starting the reactions by addition of substrate. For both COX-1-catalysed oxygenation of arachidonic acid and COX-2-catalysed oxygenation of 2-AG, the inhibition was more prominent following the preincubation period (Fig 2).

Inhibition of mouse brain FAAH by the enantiomers of Flu-AM1

The inhibition of [^{3}H]AEA hydrolysis in mouse brain homogenates by the two enantiomers of Flu-AM1 is shown in Fig 3A. The potencies of the two enantiomers were very similar, with IC_{50} values of 8.8 and 11 µM for the (R)- and (S)-enantiomer, respectively. In kinetic experiments, (R)-Flu-AM1 behaved as a competitive inhibitor of FAAH with a K_i value of 20±8 µM (Fig 3B). A Dixon plot of the data gave the same K_i value (19 µM; Fig 3C). Further analysis of the Dixon plot for (R)-Flu-AM1 confirmed the assumption that, under the conditions used, the added AEA concentration is directly proportional to the free AEA concentration available to the enzyme (S1 Fig).

Comparison of URB597, flurbiprofen, their combination and (R)-Flu-AM1 upon the lipid profile of RAW 264.7 cells

Treatment of RAW 264.7 cells, a mouse macrophage cell line, with bacterial lipopolysaccharide (LPS) results in the induction of COX-2 [29]. This cell line thus allows investigation of the effects of (R)-Flu-AM1 upon prostaglandin production in unstimulated and activated cells, and to determine whether COX-2-catalysed metabolism of 2-AG is a major metabolic route in the activated cells. Initial experiments indicated that the recovery rates of the lipids from RAW 264.7 cell extracts were very good (S2 Fig; see S1 Table for list of lipid abbreviations). Additionally, preliminary studies using LPS + INF-γ - treated RAW 264.7 cells were undertaken whereby all the medium from vehicle and ionomycin-treated conditions was collected, the lipids extracted and assayed. For the vehicle-treated cells, no lipid signal above the detection
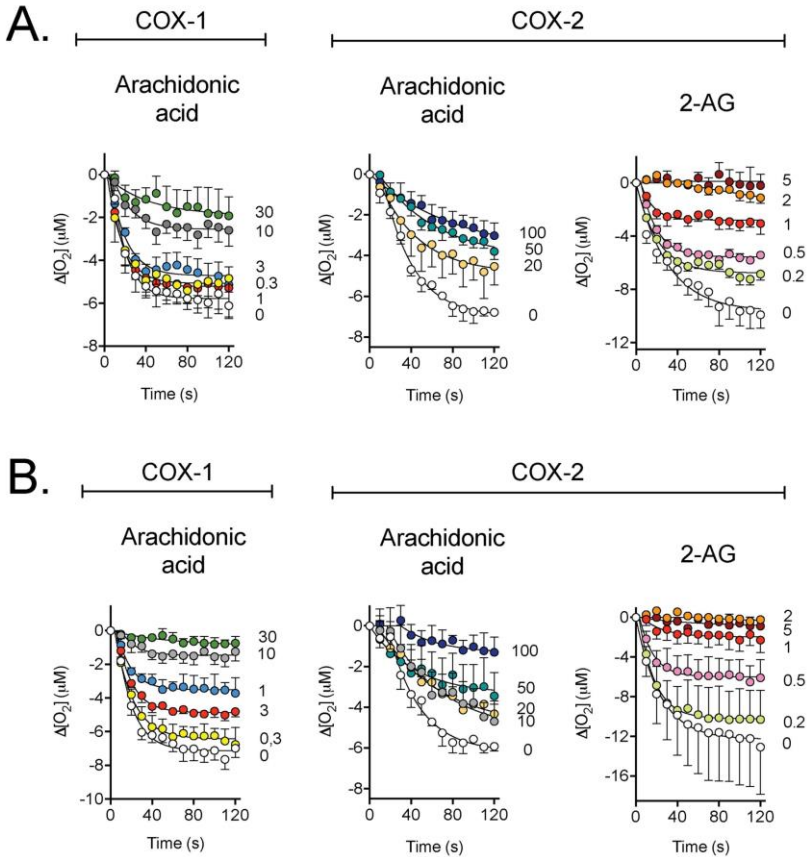
Fig 1. Inhibition of COX isoforms by the enantiomers of Flu-AM1. Shown are means ± s.e.m., n = 3 for the change in oxygen tension following addition of enzyme in the presence of the concentrations of Panel A, (R)-Flu-AM1 and Panel B, (S)-Flu-AM1. The concentrations, in µM, of the inhibitors are shown on the right of each panel, and the enzyme isoform and substrate (10 µM concentration) used above each panel.

331

5. Full Papers
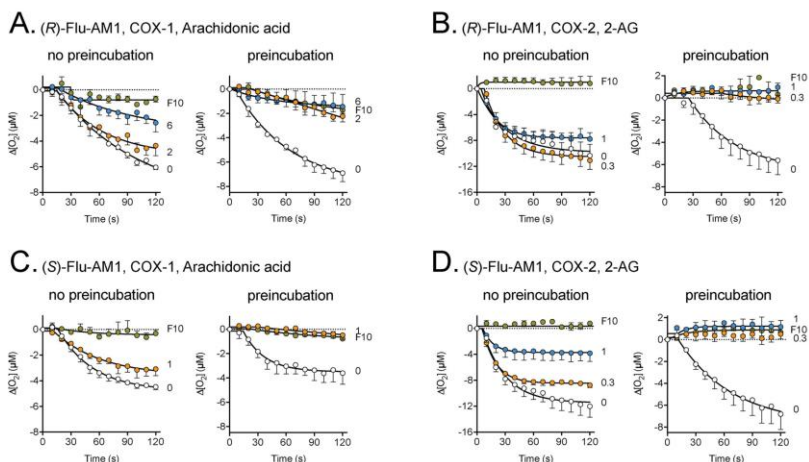
Fig 2. Effect of a preincubation phase on the inhibition of COX by the enantiomers of Flu-AM1. The concentrations, in μM, of the inhibitors are shown on the right of each panel (F10 refers to 10 μM racemic flurbiprofen, used as a positive control). The Flu-AM enantiomer, enzyme isoform and substrate (10 μM concentration) used is shown above each panel. The preincubation time was 5 min. Shown are means ± s.e.m., n = 3, except for the flurbiprofen curves in the no preincubation conditions in panels A and D, where n = 2.

doi:10.1371/journal.pone.0139212.g002
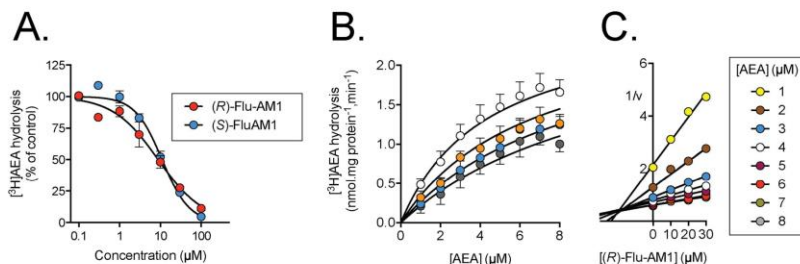
Fig 3. Inhibition of mouse brain FAAH by the enantiomers of Flu-AM1. Panel A. Concentration response curves for the inhibition of 0.5 μM [^{3}H]AEA (means ± s.e.m., n = 3, when not enclosed by the symbols). Panel B. Kinetic experiments using 1–8 μM [^{3}H]AEA (means ± s.e.m., n = 3, when not enclosed by the symbols). The curves were better fitted by a model assuming a competitive interaction (75% probability that it was correct, Akaike's informative criteria) than a model assuming a mixed-type interaction (25% probability that it was correct, Akaike's informative criteria). Panel C. Dixon replot of the mean data from Panel B. The intersection point of the regression lines projected onto the x-axis gives-K_i.

doi:10.1371/journal.pone.0139212.g003

Design, synthesis and SAR of small molecules acting on pain pathways

limit was observed in the medium extracts. For medium extracts from the ionomycin-treated cells, small peaks were seen for PEA, SEA, OEA, 13-HODE and 9(S)-HODE, but these were very close to the quantification limit. This would suggest that release of the lipids is limited under the conditions used here.

The combination of 0.1 μg/mL of LPS + 100 U/mL of INF-γ produced the expected induction of COX-2 and robust increases in the levels of PGD$_2$ and PGE$_2$ following a 24 h incubation (Fig 4). There was a variable effect of the treatment upon cell viability (Fig 4B), so that the 24 h time-point used is a trade-off between the levels of COX-2 induction required for the study and effects upon cell viability. Increasing the LPS concentration to 1 μg/mL did not increase further the expressed level of COX-2, nor did increasing the incubation time to 48 h (data not shown).

Given that both enantiomers of Flu-AM1 had relatively similar properties towards COX (Figs 1 and 2), we focussed upon the (R)-enantiomer. An almost complete inhibition of both basal and LPS +INF-γ-stimulated PGD$_2$ and PGE$_2$ production was seen with the highest concentration of (R)-Flu-AM1 tested (10 μM), whereas more variable effects were seen with lower concentrations (Fig 4C and 4D). The effects of flurbiprofen (10 μM, either *per se* or together with 1 μM URB597) and (R)-Flu-AM1 (10μM) upon the levels of prostaglandins, 2-AG and related oxylipins were investigated in a series of experiments. For some of the lipids, not least the prostaglandins, there was a large variation in levels observed between batches, and so we have normalised the data to the corresponding vehicle controls. In the initial experiments, flurbiprofen and (R)-Flu-AM1 (10μM) blocked, as expected, both unstimulated and LPS + INF-γ - induced PGD$_2$ and PGE$_2$ in the cell extracts (Table 1). LPS + INF-γ treatment also increased 11-HETE and possibly 15-HETE levels in a manner sensitive to inhibition by flurbiprofen and (R)-Flu-AM1 (Table 1). This is consistent with the report that COX-2 in activated macrophages is capable of producing these oxylipins [30]. In contrast to the robust effects of flurbiprofen and (R)-Flu-AM1 upon prostaglandin levels in the cell extracts, the levels of 2-AG were not affected (Table 1). Similar results were seen in a larger series of LPS + INF-γ –treated cells where the calcium ionophore ionomycin was also added (Fig 5). Linoleic acid-derived oxylipins were also analysed, in order to shed light on possible off-targets for (R)-Flu-AM1. No significant effects of this compound upon the linoleic acid-derived oxylipins were seen (Table 1; S3 Fig).

To determine the ability of LPS + INF-γ –treated RAW 264.7 cells to hydrolyse exogenous [³H]AEA (100 nM), the cells were incubated with this substrate for 60 min in the absence or presence of the compounds. As expected, 1 μM URB597, either *per se* or with flurbiprofen, completely blocked [³H]AEA hydrolysis (Fig 6A). Given the potencies of flurbiprofen and (R)-Flu-AM1 towards mouse FAAH are modest, clear effects of these compounds at the concentration of 10 μM upon [³H]AEA hydrolysis by the intact mouse RAW 264.7 cells would not be expected, and this was found to be the case (Fig 6A). Surprisingly, however, URB597 only produced modest effects upon the levels of AEA and related N-acylethanolamines in the cells (Table 1, Fig 6B–6H). Thus, at a concentration of URB597 causing complete inhibition of the hydrolysis of exogenous AEA, endogenous levels are only marginally affected. Flurbiprofen and (R)-Flu-AM1 did not affect the levels of these lipids in the ionomycin treated cells (Fig 6).

Discussion

In the present study, the enantiomers of Flu-AM1 were investigated in order to shed light on two questions that were asked at the end of the introduction. These questions are recapitulated below, to aid the discussion:

333
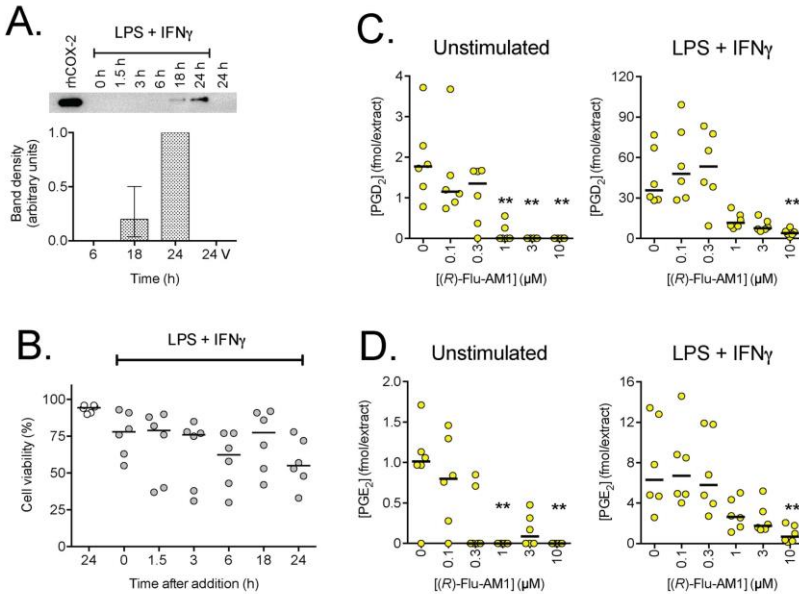
Fig 4. Effects of (R)-Flu-AM1 upon prostaglandin levels in basal and LPS + INF-γ-stimulated RAW 264.7 cells. Cells were either untreated ("unstimulated") or treated for 24 h, unless otherwise shown, with 0.1 μg/mL LPS + 100 U/ml INF-γ. Panel A shows the expression of COX-2 at different treatment times. A representative gel is shown above the bar graph, where the intensities have been normalised to the values for 24 h (median and range, n = 3). rhCOX-2 refers to human recombinant COX-2 as a positive control. The bands shown in the gel were the only bands on the gels, and they were seen at a molecular weight of ~75 kDa. Panel B shows the viability of the cells at different times after treatment for different times (n = 6). In Panels C and D, the levels of PGD_2 and PGE_2, respectively, are shown (n = 6, expressed as fmol in the extract from two wells, with the bars showing the median values) following treatment with the compounds for 30 min. For both prostaglandins, two-way robust Wilcoxon analyses [25] indicated significant (P<0.001) effects of LPS + INF-γ treatment, of (R)-Flu-AM1, and of the interaction (R)-Flu-AM1 x LPS + INF-γ treatment. In view of the significant interaction, the curves shown in the figures were analysed separately for the unstimulated and stimulated cells. **P<0.01 (otherwise not significant) vs. vehicle-treated samples, Dunn's multiple comparison test, following significant P value in the Kruskal-Wallis test.

doi:10.1371/journal.pone.0139212.g004

Do the amide derivatives of flurbiprofen with 2-amino-3-methylpyridine show enantiomeric differences with respect to inhibition of COX-2 and FAAH?

This question was motivated by previous studies showing that (R)-profens (ibuprofen, flurbiprofen, naproxen) retained the substrate-selective inhibition of COX-2 seen in the enantiomers, but lacked significant effect upon arachidonic acid oxygenation by either COX isoform [11]. Mutagenesis and computer modelling approaches have been very informative in

PLOS | ONE

Table 1. Lipid profile of RAW264.7 cells treated with or without LPS + IFNγ for 24 h. Effects of FAAH and/or COX inhibitors.

Lipid	Treatment	Vehicle	URB597	Flurbiprofen	URB + Flu	(R)FluAM1	P values
Arachidonic acid derivatives							
PGD$_2$	None	1 (0.38–2.69)	1.37 (0.79–2.48)	0 (0–0.28)	0 (0–0)	0 (0–0.25)	**L: <0.0001**
[77; 2610]	LPS + IFNγ	38.0 (12.0–69.6)	35.1 (19.4–117)	1.32 (1.04–4.76)	1.60 (1.22–3.72)	3.14 (1.51–4.13)	**I: <0.0001**
							L x I: <0.0001
PGE$_2$	None	1 (0.46–1.58)	0.98 (0.49–1.81)	0 (0–0)	0.04 (0–0.23)	0 (0–0.25)	**L: <0.0001**
[22; 172]	LPS + IFNγ	7.89 (2.10–20.4)	10.6 (7.33–33.5)	1.21 (0.91–4.54)	1.68 (0.64–2.36)	2.89 (1-28-3.30)	**I: <0.0001**
							L x I: <0.0001
11-HETE	None	1 (0.39–1.32)	1.12 (0–2.69)	0.67 (0.23–0.76)	0.83 (0–1.12)	0.55 (0.12–2.43)	**L: <0.0001**
[9.8; 112]	LPS + IFNγ	11.8 (6.68–39.5)	13.0 (4.82–25.7)	2.06 (1.67–7.71)	2.52 (1.73–3.48)	2.29 (0.92–7.87)	**I: <0.0001**
							L x I: <0.0001
12-HETE	None	1 (0.22–1.42)	0.94 (0.33–1.48)	0.65 (0.46–2.01)	0.64 (0.58–1.18)	0.94 (0.27–1.82)	L: 0.020
[98; 62]	LPS + IFNγ	0.59 (0.31–1.63)	0.61 (0.41–0.96)	0.43 (0.18–0.63)	0.78 (0.26–1.59)	0.32 (0.10–1.05)	I: 0.61
							L x I: 0.79
15-HETE	None	1 (0.71–1.58)	1.02 (0.25–2.16)	1.18 (0.15–1.85)	1.11 (0.72–2.06)	1.37 (0–2.72)	**L: 0.00011**
[23; 40]	LPS + IFNγ	2.30 (1.20–8.30)	4.58 (0.97–5.29)	1.37 (0.51–8.43)	1.42 (0.97–1.75)	1.33 (0.67–3.37)	I: 0.035
							L x I: 0.020
AEA	None	1 (0.54–1.36)	0.85 (0.45–1.18)	0.74 (0.35–1.60)	0.99 (0.59–1.51)	0.65 (0.39–0.86)	**L: 0.00010**
[18; 33]	LPS + IFNγ	1.15 (0.91–2.11)	1.39 (1.26–1.58)	1.17 (0.99–1.86)	1.19 (0.99–1.62)	1.01 (0.37–1.16)	I: 0.039
							L x I: 0.54
2-AG	None	1 (0.96–1.27)	1.10 (0.61–1.47)	1.10 (0.74–1.42)	1.09 (0.88–1.42)	0.94 (0.62–1.52)	**L: 0.00049**
[1980; 1600]	LPS + IFNγ	0.83 (0.33–1.30)	0.90 (0.70–1.11)	0.65 (0.26–1.02)	1.03 (0.82–1.35)	0.81 (0.64–0.98)	I: 0.16
							L x I: 0.40
Linoleic acid derivatives							
9-HODE	None	1 (0.92–1.13)	1.14 (0.72–2.07)	1.12 (0.50–1.89)	1.41 (0.80–7.53)	0.99 (0.66–2.11)	L: 0.99
	LPS + IFNγ	1.40 (0.70–2.74)	1.11 (0.49–1.20)	0.96 (0.62–8.38)	1.18 (0.74–1.54)	1.06 (0.50–1.64)	I: 0.67
							L x I: 0.78
13-HODE	None	1 (0.79–1.13)	1.42 (0.79–1.75)	1.19 (0.52–1.72)	1.57 (1.15–2.36)	0.97 (0.71–2.66)	L: 0.79
	LPS + IFNγ	1.53 (0.81–2.94)	1.16 (0.49–1.43)	0.88 (0.76–7.61)	1.41 (1.10–1.92)	1.21 (0.55–1.75)	I: 0.38
							L x I: 0.54
9,10-DiHOME	None	1 (0.85–1.28)	1.10 (0.65–1.32)	0.89 (0.62–1.07)	0.99 (0.40–1.63)	1.05 (0.64–1.66)	L: 0.071

(Continued)

335

_____

PLOS | ONE   Flu-AM1 Enantiomers, COX and FAAH

Table 1. (*Continued*)

Lipid	Treatment	Vehicle	URB597	Flurbiprofen	URB + Flu	(R)FluAM1	P values
	LPS + IFNγ	0.92 (0.85–1.04)	0.76 (0.69–1.05)	1.04 (0.64–1.32)	0.92 (0.72–1.01)	0.82 (0.65–1.09)	I: 0.93
							L x I: 0.10
12,13-DiHOME	None	1 (0.65–1.07)	1.15 (1.04–1.39)	0.89 (0.66–1.19)	1.32 (0.70–1.44)	1.12 (0.73–1.53)	L: 0.19
	LPS + IFNγ	1.06 (0.90–1.21)	0.93 (0.85–1.26)	1.11 (0.64–2.30)	1.00 (0.79–1.35)	0.93 (0.76–1.04)	I: 0.39
							L x I: 0.034
9,10,13-TriHOME	None	1 (0.71–1.29)	1.13 (0.44–2.51)	1.20 (0.77–2.28)	1.41 (0.85–1.89)	1.04 (0.81–1.41)	L: 0.17
	LPS + IFNγ	1.17 (0.69–1.44)	1.08 (0.68–1.89)	1.34 (0.80–1.40)	1.75 (1.13–2.09)	1.18 (0.90–1.49)	I: 0.0043
							L x I: 0.88
9,12,13-TriHOME	None	1 (0.69–1.32)	1.23 (0.51–2.53)	1.10 (0.90–1.93)	1.49 (0.98–1.77)	1.08 (0.76–1.57)	L: 0.37
	LPS + IFNγ	1.15 (0.75–1.42)	1.08 (0.66–1.79)	1.33 (0.91–1.48)	1.65 (0.92–2.00)	1.22 (0.79–1.60)	I: 0.0089
							L x I: 0.85
13-oxo-ODE	None	1 (0.55–2.30)	1.40 (0.76–2.27)	1.33 (1.14–2.51)	1.53 (0.68–4.01)	1.97 (0.59–3.00)	L: 0.19
	LPS + IFNγ	1.92 (1.09–7.10)	1.52 (0.34–2.87)	2.14 (0.66–17.3)	1.72 (1.07–5.21)	1.49 (0.31–2.85)	I: 0.73
							L x I: 0.48
12(13)-EpOME	None	1 (0.27–1.61)	1.07 (0.66–1.66)	0.84 (0.75–1.81)	1.14 (0.78–8.48)	1.03 (0.51–5.45)	L: 0.60
	LPS + IFNγ	1.03 (0.53–2.71)	1.24 (0.92–1.72)	0.99 (0.50–5.76)	1.40 (0.47–2.48)	1.02 (0.53–1.98)	I: 0.74
							L x I: 0.95
Eicosapentaneoic acid derivative							
12(S)-HEPE	None	1 (0.79–2.48)	0.59 (0–0.85)	0.44 (0.23–0.81)	0.48 (0.18–0.57)	0.90 (0.17–1.43)	L: 0.020
	LPS + IFNγ	0.35 (0–0.89)	0.59 (0.28–1.36)	0.58 (0.14–0.82)	0.44 (0–0.62)	0.27 (0–0.74)	I: 0.16
							L x I: 0.011
Other N-acyl ethanolamimes							
PEA	None	1 (0.80–1.25)	1.07 (0.87–1.28)	0.94 (0.75–1.20)	1.06 (0.89–1.53)	0.89 (0.74–1.06)	L: 0.24
	LPS + IFNγ	0.91 (0.56–1.26)	0.97 (0.88–1.31)	0.99 (0.53–1.12)	0.95 (0.65–1.16)	0.91 (0.49–1.15)	I: 0.39
							L x I: 0.87
SEA	None	1 (0.85–1.52)	0.80 (0.65–1.27)	0.83 (0.76–1.41)	1.11 (0.86–1.34)	0.90 (0.52–1.02)	L: 0.15
	LPS + IFNγ	0.90 (0.65–1.25)	0.79 (0.67–1.28)	0.88 (0.62–1.10)	0.90 (0.74–1.09)	0.86 (0.65–1.11)	I: 0.046
							L x I: 0.36
OEA	None	1 (0.79–1.30)	0.94 (0-81–1.29)	0.87 (0.81–2.16)	1.14 (0.87–6.23)	1.01 (0.79–1.11)	L: 0.86
	LPS + IFNγ	0.94 (0.80–1.22)	0.97 (0.74–1.96)	0.99 (0.86–1.43)	1.11 (0.91–1.23)	1.03 (0.87–1.22)	I: 0.19
							L x I: 0.69

(*Continued*)

_____

_____

Table 1. (*Continued*)

Lipid	Treatment	Vehicle	URB597	Flurbiprofen	URB + Flu	(R)FluAM1	P values
LEA	None	1 (0.81–1.81)	0.79 (0.68–1.15)	1.01 (0.72–1.99)	1.15 (0.94–12.8)	1.07 (0.21–1.26)	L: 0.84
	LPS + IFNγ	0.96 (0.69–1.09)	1.06 (0.79–1.87)	0.91 (0.32–1.59)	1.11 (0.83–1.66)	1.13 (0.33–1.60)	I: 0.43
							L x I: 0.49

RAW264 mouse leukemic cells (2.5×10^5 per well) were added to 6 well-plates and incubated with either vehicle ("None") or LPS (0.1 μg/mL well) + INF-γ (100 U/mL) for 24 h. at 37°C prior to incubation for 30 min with either vehicle, URB597 (1 μM), flurbiprofen (10 μM), URB597 + flurbiprofen or (R)-Flu-AM1 (10 μM). The samples were assayed in two batches. In order to minimise effects of inter-batch variations, which were seen for some of the lipids, the median value for each lipid and batch under vehicle-treated "None" conditions were set to unity and all other values for the batch were expressed relative to these median values. Data are given as medians, n = 5–6, with the range in brackets, and the statistical test used was a two-way robust Wilcoxon analysis [25]. L: main effect LPS treatment, I: main effect inhibitor treatment, T x I, interaction term. Note that since there are multiple analysis, a case can be made that the Bonferroni correction should be used. Significance levels below 0.0025 (= 0.05/20, i.e. Bonferroni-corrected) are shown in bold.

doi:10.1371/journal.pone.0139212.t001

elucidating the interaction of NSAIDs with both COX and FAAH [31,32]. The interaction of profen enantiomers with COX has been studied using both approaches [11,33], and crystallographic studies have suggested that a critical interaction for the (*R*)-profens is the ability of the carboxyl group to ion pair with the Arg[120] residue in COX-2 [11], whilst molecular modeling of the binding of (*R*)-flurbiprofen suggests that the phenolic group of Tyr[355] would interact with the α-methyl group of this inhibitor so as to interfere with the binding of the carboxylate group to Arg[120], thereby accounting for the poor potencies of the (*R*)-enantiomers towards the oxygenation of arachidonic acid [33]. The two enantiomers of Flu-AM1 retain the time-dependency of COX inhibition seen with flurbiprofen [28] but do not show marked differences in their COX-inhibitory properties. This latter finding presumably reflects the fact that they contain an uncharged amide group instead of the negatively charged carboxyl group of flurbiprofen and suggests interaction with COX different from ion pair formation with the Arg[120] residue. It would clearly be of interest to investigate using computational and mutagenesis techniques the interaction of the compounds with COX isoforms, and, indeed, with FAAH.

The two compounds show a degree of substrate-selectivity towards the inhibition of 2-AG oxygenation by COX-2 *vs.* arachidonic acid oxygenation by this isoform. For comparative purposes, recalculation by the method used here of data for racemic flurbiprofen obtained using the same method [18] gave IC_{50} values for this NSAID of: COX-1 (arachidonic acid) 4 μM; COX-2 (arachidonic acid) 95 μM; COX-2 (2-AG) 2 μM. Thus, the compounds are approximately equipotent to flurbiprofen as inhibitors of COX-1, but more potent inhibitors of 2-AG oxygenation by COX-2. The enantiomers of Flu-AM1 showed very similar potencies towards inhibition of mouse brain FAAH, a result also seen for flurbiprofen enantiomers and rat brain FAAH [34]. It was noted that the potencies were lower than previously reported for racemic Flu-AM1 (IC_{50} value 0.44 μM [18]). This seems to reflect a species difference, since the racemate was studied in rat brain homogenates, whereas mouse brain homogenates were used here. Indeed, in rat brain homogenates, (*R*)- and (*S*)-Flu-AM1 inhibit [³H]AEA hydrolysis with IC_{50} values of 0.74 and 0.99 μM, respectively (current authors, unpublished data). We have elected to present the mouse data here, since the lipidomic work described below was conducted on RAW264.7 cells, which are murine in origin.

_____

_____

337
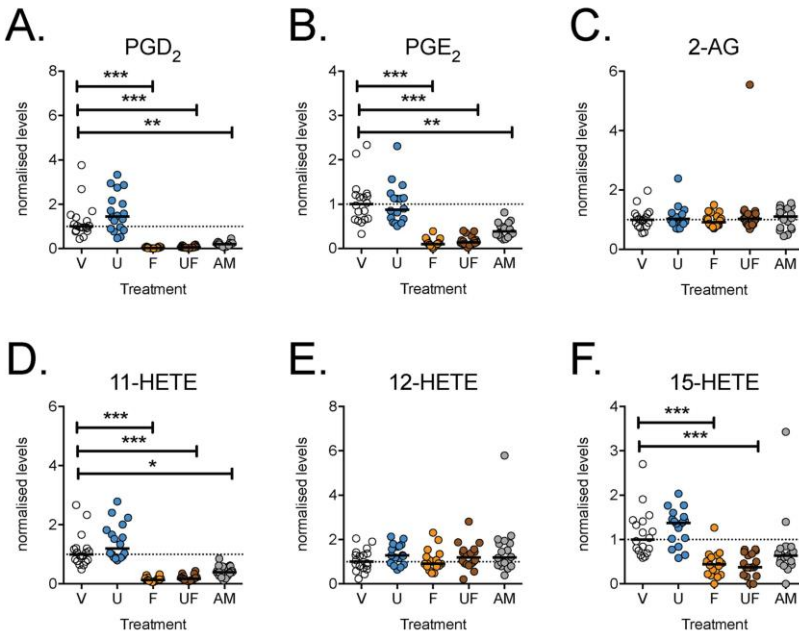
Fig 5. Effects of FAAH and/or COX inhibitors upon the levels of arachidonic acid-derivatives in ionomycin-treated RAW264.7 cells pretreated with LPS + IFNγ for 24 h. RAW264.7 mouse leukemic cells (2.5×10^5 per well) were added to 6 well-plates with LPS (0.1 µg/mL well) and INF-γ (100 U/mL) and cultured at 37°C for 24 h prior to incubation for 30 min with ionomycin (5 µM) and either vehicle (V), URB597 (U, 1 µM) or (R)-Flu-AM1 (AM, 10 µM). The median value for each lipid and batch for vehicle-treated conditions were set to unity and all other values for the batch were expressed relative to these median values. Data are shown as scatter plots (n = 18), with the median values shown as bars. *P<0.05, **P<0.01, ***P<0.001, Dunn's Multiple Comparison test vs. vehicle (otherwise not significant) following significant Kruskal-Wallis test.

doi:10.1371/journal.pone.0139212.g005

Is COX-2 inhibition sufficient to affect endocannabinoid levels in macrophage cells cultured under inflammatory conditions?

Duggan et al. [11] reported that in primary cultures of mouse dorsal root ganglia cells stimulated with granulocyte-macrophage colony-stimulating factor followed by LPS, IRN-γ and 15 (S)-HETE, resulting in the induction of COX-2, the inhibition of AEA and 2-AG oxygenation by (R)-profens increased the levels of these eCBs in the cell extracts, without affecting arachidonic acid levels. This would suggest that in these cells (which lack FAAH [11], in contrast to the situation for the dorsal root ganglia *in vivo* [35]), COX-2 is an important determinant of
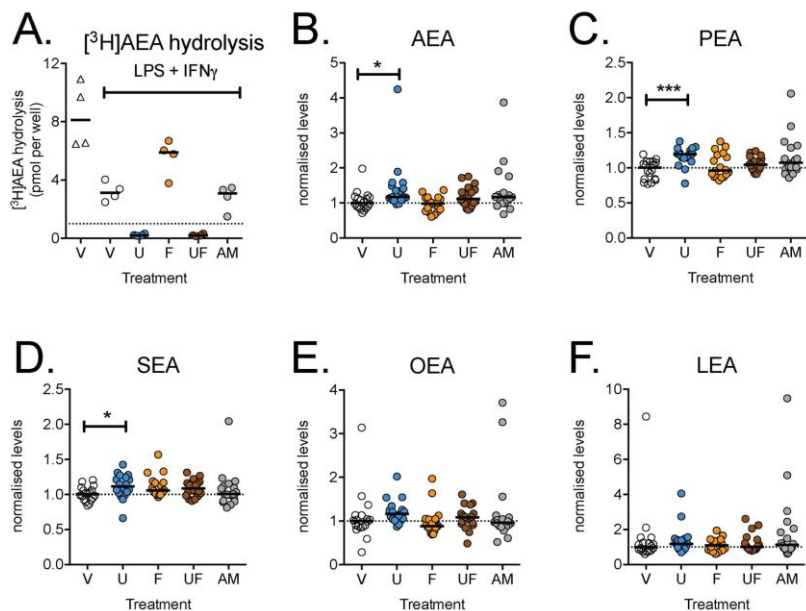
Fig 6. Effects of FAAH and/or COX inhibitors upon A. the hydrolysis of exogenously added [³H]AEA and B-F the levels of AEA and related *N*-acylethanolamines in RAW 264.7 cells. In Panel A, 2.5 x 10⁶ cells/well were seeded and cultured overnight prior to addition of either phosphate-buffered saline or LPS (0.1 µg/mL) + INF-γ (100 U/mL) and incubation for a further 24 h. The hydrolysis of 100 µM [³H]AEA is shown for the different treatments (following 1 h of incubation. In Panels B-F, cells (2.5x10⁵ per well) were added to 6 well-plates with LPS (0.1 µg/mL well) and INF-γ (100 U/mL) and cultured at 37°C for 24 h. prior to incubation for 30 min with ionomycin (5 µM) and either vehicle (V), URB597 (U, 1 µM) or (R)-Flu-AM1 (AM, 10 µM). The median value for each lipid and batch for vehicle-treated conditions were set to unity and all other values for the batch were expressed relative to these median values. Data are shown as scatterplots (n = 18) with medians as bars. *P<0.05,***P<0.001, Dunn's Multiple Comparison test *vs.* vehicle (otherwise not significant) following significant Kruskal-Wallis test.

doi:10.1371/journal.pone.0139212.g006

eCB metabolism. We found that at concentrations of 10 µM, both flurbiprofen and (R)-Flu-AM1 completely blocked prostaglandin production by both unstimulated and LPS + IFN-γ-treated RAW 264.7 macrophage cells, indicating that under these conditions the compounds block arachidonic acid oxygenation by both COX isoforms. However, this blockade did not affect the observed levels of either 2-AG or AEA. Thus, COX-2 appears to play a minor role in gating the catabolism of these eCBs in the RAW 264.7 cells, in contrast to the stimulated primary cultures of mouse dorsal root ganglia cells [11].

The present study has allowed us to answer an additional question: does FAAH inhibition affect endocannabinoid levels in macrophage cells cultured under inflammatory conditions?

339

5. Full Papers

We found that URB597 produces significant, but rather small changes in the levels of AEA and related N-acylethanolamines that are FAAH substrates in the LPS + IFN-γ-treated RAW 264.7 cells despite the essentially complete inhibition of the hydrolysis of exogenously added [^{3}H] AEA at the concentration of the compound used (1 μM). There are two explanations for this finding. It is possible that in the LPS + IFN-γ-treated RAW 264.7 cells, the turnover of the N-acylethanolamines is so slow that blockade of FAAH produces little effect. This would be the case, for example, if the synthetic pathways were the rate-limiting step in the life cycle of these lipids. There is evidence in the literature that LPS treatment increases the rate of AEA synthesis and concentration in RAW 264.7 cells despite a reduction in the expression at the mRNA level of the N-acylethanolamine synthetic enzyme N-arachidonoyl phosphatidylethanolamine-phospholipase D [36–38]. The primary pathway for AEA synthesis in the cells was instead identified as the production and then dephosphorylation of phospho-AEA [37]. In our hands, we found a modest, albeit significant, increase in AEA, but not the other N-acylethanolamines, levels following LPS + IFN-γ-treatment (Table 1). It is possible that under the conditions used here, the phospho-AEA pathway is less active than in the study of Liu et al. [37], and this results in the synthesis rather than hydrolysis being rate-limiting, even following ionomycin treatment.

An alternative (or additional) explanation is that the metabolism of endogenous AEA in the cells is less dependent upon FAAH than the hydrolysis of exogenously added AEA and that other catabolic enzymes are of greater importance. Given that the combination of flurbiprofen + URB597 did not affect levels of AEA in the RAW 264.7 cells, COX-2 can be ruled out as a candidate. The most likely enzyme is NAAA, given that it is highly expressed in macrophages [39]. NAAA inhibitors are beginning to appear in the literature, and one of these, 1-(2-biphenyl-4-yl)ethyl-carbonyl pyrrolidine, has been reported to restore PEA levels that were decreased in LPS-treated RAW 264.7 cells [40] Hopefully, more data will emerge on the effects of NAAA inhibitors on AEA as well as PEA levels in RAW 264.7 cells in the future.

Conclusions

There are two main conclusions to the present study. Firstly, we find that in contrast to the profens, the two enantiomers of Flu-AM1 show little difference with respect to their ability to inhibit COX isoforms. The compounds also inhibit FAAH with similar potencies. Thus, there is little advantage in using one or other of the enantiomers over using the racemate. Secondly, our data show that in activated RAW 264.7 cells, COX-2 plays a relatively minor role in regulating eCB levels, and that the importance of FAAH for the hydrolysis of endogenous AEA may be less pronounced than for exogenously added AEA.

Supporting Information

S1 Fig. Estimated relationship between the added AEA concentration and the free substrate concentration available to the enzyme. Values are calculated from the data shown in Fig 2C as follows: for the general case, a linear mixed-type inhibition, the intersection point in the Dixon plot projected onto the y-axis ("y_i") corresponds to $(1/V_{max})/(1-(1/\alpha))$ (Segel, 1975; $\alpha \rightarrow \infty$ for competitive inhibition). Since, in the absence of inhibitor, the observed velocity $v_o = V_{max}/(1 + K_m/[S_f])$, where $[S_f]$ in this case is the free AEA concentration presented to the enzyme, the two equations can be used to express $[S_f]/K_m$ in terms of the observed velocity, α and y_i: $[S_f]/K_m = y_i/[(1/v_o)(1-(1/\alpha))-y_i]$. This has been used here to generate a plot of different values of $[S_f]/K_m$ *vs.* the added AEA concentration for different given values of α. When $(1/v)(1-(1/\alpha)) \approx y_i$, very small differences in y_i have a large effect on $[S_f]/K_m$, and so we have limited the lowest value of α in the graph to 15. The data indicate that under the conditions used, the added AEA concentration is proportional to the free AEA concentration presented to the

340

enzyme.
(TIF)

S2 Fig. Recovery rates of lipids used as internal standards spiked to RAW 264.7 cell extracts and to phosphate-buffered saline (PBS). Internal standard recovery rates were determined as described in Materials and Methods. Shown are means ± s.e.m. for five determinations.
(TIF)

S3 Fig. Effects of FAAH and/or COX inhibitors upon the levels of linoleic acid-derivatives in ionomycin-treated RAW264.7 cells pretreated with LPS + IFNγ for 24 h. RAW264.7 mouse leukemic cells (2.5×10^5 per well) were added to 6 well-plates with LPS (0.1 µg/mL well) and INF-γ (100 U/mL) and cultured at 37°C for 24 h. prior to incubation for 30 min with iono-mycin (5 µM) and either vehicle (V), URB597 (U, 1 µM) or (R)-Flu-AM1 (AM, 10 µM). The median value for each lipid and batch for vehicle-treated conditions were set to unity and all other values for the batch were expressed relative to these median values. Data are shown as scatter plots (n = 18), with the median values shown as bars. $^+P<0.05$, Dunn's Multiple Comparison test *vs.* vehicle (otherwise not significant) following significant Kruskal-Wallis test.
(TIF)

S1 Table. List of abbreviations of the lipids reported for the RAW264.7 cells.
(DOCX)

Author Contributions

Conceived and designed the experiments: VO CJF. Performed the experiments: SGF JK AD SH MS MFS CC. Analyzed the data: SGF JK VO CJF. Wrote the paper: SGF JK SH VO CJF.

References

1. Vane JR. Inhibition of prostaglandin synthesis as a mechanism of action for aspirin-like drugs. Nat New Biol. 1971; 231:232–5. PMID: 5284360
2. Gühring H, Hamza M, Sergejeva M, Ates M, Kotalla C, Ledent C, et al. A role for endocannabinoids in indomethacin-induced spinal antinociception. Eur J Pharmacol. 2002; 454:153–63. PMID: 12421642
3. Fowler CJ. NSAIDs: eNdocannabinoid stimulating anti-inflammatory drugs? Trends Pharmacol Sci. 2012; 33:468–73. doi: 10.1016/j.tips.2012.05.003 PMID: 22664342
4. Bishay P, Schmidt H, Marian C, Häussler A, Wijnvoord N, Ziebell S, et al. R-flurbiprofen reduces neuro-pathic pain in rodents by restoring endogenous cannabinoids. PLoS ONE. 2010; 5:e10628. doi: 10.1371/journal.pone.0010628 PMID: 20498712
5. Geisslinger G, Schaible H-G. New insights into the site and mode of antinociceptive action of flurbipro-fen enantiomers. J Clin Pharmacol. 1996; 36:513–20. PMID: 8809636
6. Ueda N, Tsuboi K, Uyama T. Metabolism of endocannabinoids and related *N*-acylethanolamines: Canonical and alternative pathways. FEBS J. 2013; 280:1874–94. doi: 10.1111/febs.12152 PMID: 23425575
7. Yu M, Ives D, Ramesha C. Synthesis of prostaglandin E₂ ethanolamide from anandamide by cyclooxy-genase-2. J Biol Chem. 1997; 272:21181–6. PMID: 9261124
8. Kozak K, Rowlinson S, Marnett L. Oxygenation of the endocannabinoid, 2-arachidonoylglycerol, to glyceryl prostaglandins by cyclooxygenase-2. J Biol Chem. 2000; 275:33744–9. PMID: 10931854
9. Prusakiewicz JJ, Duggan KC, Rouzer CA, Marnett LJ. Differential sensitivity and mechanism of inhibi-tion of COX-2 oxygenation of arachidonic acid and 2-arachidonoylglycerol by ibuprofen and mefenamic acid. Biochemistry. 2009; 48:7353–5. doi: 10.1021/bi900999z PMID: 19603831
10. Hermanson DJ, Hartley ND, Gamble-George J, Brown N, Shonesy BC, Kingsley PJ, et al. Substrate-selective COX-2 inhibition decreases anxiety via endocannabinoid activation. Nat Neurosci. 2013; 16:1291–8. doi: 10.1038/nn.3480 PMID: 23912944
11. Duggan KC, Hermanson DJ, Musee J, Prusakiewicz JJ, Scheib JL, Carter BD, et al. (*R*)-Profens are substrate-selective inhibitors of endocannabinoid oxygenation by COX-2. Nat Chem Biol. 2011; 7:803–9. PMID: 22053353

5. Full Papers

―――

12. Naidu P, Booker L, Cravatt B, Lichtman A. Synergy between enzyme inhibitors of fatty acid amide hydrolase and cyclooxygenase in visceral nociception. J Pharmacol Exp Ther. 2009; 329:48–56. doi: 10.1124/jpet.108.143487 PMID: 19118134

13. Fowler CJ, Naidu PS, Lichtman A, Onnis V. The case for the development of novel analgesic agents targeting both fatty acid amide hydrolase and either cyclooxygenase or TRPV1. Br J Pharmacol. 2009; 156:412–9. doi: 10.1111/j.1476-5381.2008.00029.x PMID: 19226258

14. Sasso O, Migliore M, Habrant D, Armirotti A, Albani C, Summa M, et al. Multitarget fatty acid amide hydrolase/cyclooxygenase blockade suppresses intestinal inflammation and protects against nonsteroidal anti-inflammatory drug-dependent gastrointestinal damage. FASEB J. 2015; 29:2616–27. doi: 10.1096/fj.15-270637 PMID: 25757568

15. Cocco M, Congiu C, Onnis V, Morelli M, Cauli O. Synthesis of ibuprofen heterocyclic amides and investigation of their analgesic and toxicological properties. Eur J Med Chem. 2003; 38:513–8. PMID: 12767601

16. Holt S, Paylor B, Boldrup L, Alajakku K, Vandevoorde S, Sundström A, et al. Inhibition of fatty acid amide hydrolase, a key endocannabinoid metabolizing enzyme, by analogues of ibuprofen and indomethacin. Eur J Pharmacol. 2007; 565(1–3):26–36. PMID: 17397826

17. Fowler CJ, Björklund E, Lichtman AH, Naidu PS, Congiu C, Onnis V. Inhibitory properties of ibuprofen and its amide analogues towards the hydrolysis and cyclooxygenation of the endocannabinoid anandamide. J Enzyme Inhib Med Chem. 2013; 28:172–82. doi: 10.3109/14756366.2011.643304 PMID: 22225576

18. Cipriano M, Björklund E, Wilson AA, Congiu C, Onnis V, Fowler CJ. Inhibition of fatty acid amide hydrolase and cyclooxygenase by the N-(3-methylpyridin-2-yl)amide derivatives of flurbiprofen and naproxen. Eur J Pharmacol. 2013; 720:383–90. doi: 10.1016/j.ejphar.2013.09.065 PMID: 24120370

19. Meade EA, Smith WL, DeWitt DL. Differential inhibition of prostaglandin endoperoxide synthase (cyclooxygenase) isozymes by aspirin and other non-steroidal anti-inflammatory drugs. J Biol Chem. 1993; 268:6610–4. PMID: 8454631

20. Onnis V, Congiu C, Björklund E, Hempel F, Söderström E, Fowler CJ. Synthesis and evaluation of paracetamol esters as novel fatty acid amide hydrolase inhibitors. J Med Chem. 2010; 53:2286–98. doi: 10.1021/jm901891p PMID: 20143779

21. Bradford MM. A rapid and sensitive method for the quantitation of microgram quantities of protein utilizing the principle of protein-dye binding. Anal Biochem. 1976; 72:248–54. PMID: 942051

22. Boldrup L, Wilson SJ, Barbier AJ, Fowler CJ. A simple stopped assay for fatty acid amide hydrolase avoiding the use of a chloroform extraction phase. J Biochem Biophys Methods. 2004; 60:171–7. PMID: 15262451

23. Björklund E, Larsson TNL, Jacobsson SOP, Fowler CJ. Ketoconazole inhibits the cellular uptake of anandamide via inhibition of FAAH at pharmacologically relevant concentrations. PLoS One. 2014; 9: e87542. doi: 10.1371/journal.pone.0087542 PMID: 24466356

24. Gouveia-Figueira S, Nording ML. Validation of a tandem mass spectrometry method using combined extraction of 37 oxylipins and 14 endocannabinoid-related compounds including prostamides from biological matrices. Prostaglandins Other Lipid Mediat., in press. doi: 10.1016/j.prostaglandins.2015.06.003

25. McKean JW. Robust analysis of linear models. Stat Sci. 2004; 19(4):562–70.

26. Kloke JD, McKean JW. Rfit: Rank-based estimation for linear models. The R Journal 4: 57–64. The R Journal. 2012; 4:57–64.

27. R Core Team: R: A language and environment for statistical computing. R Foundation for Statistical Computing, Vienna, Austria. ISBN 3-900051-07-0, URL http://www.R-project.org/201

28. Rome LH, Lands WEM. Structural requirements for time-dependent inhibition of prostaglandin biosynthesis by anti-inflammatory drugs. Proc Natl Acad Sci USA. 1975; 72:4863–5. PMID: 1061075

29. Hwang D, Fischer NH, Jang BC, Tak H, Kim JK, Lee W. Inhibition of the expression of inducible cyclooxygenase and proinflammatory cytokines by sesquiterpene lactones in macrophages correlates with the inhibition of MAP kinases. Biochem Biophys Res Commun. 1996; 226:810–8. PMID: 8831694

30. Norris PC, Reichart D, Dumlao DS, Glass CK, Dennis EA. Specificity of eicosanoid production depends on the TLR-4-stimulated macrophage phenotype. J Leukoc Biol. 2011; 90:563–74. doi: 10.1189/jlb.0311153 PMID: 21653236

31. Blobaum AL, Marnett LJ. Structural and functional basis of cyclooxygenase inhibition. J Med Chem. 2007; 50:1425–41. PMID: 17341061

32. Favia AD, Habrant D, Scarpelli R, Migliore M, Albani C, Bertozzi SM, et al. Identification and characterization of carprofen as a multitarget Fatty Acid amide hydrolase/cyclooxygenase inhibitor. J Med Chem. 2012; 55:8807–26. doi: 10.1021/jm3011146 PMID: 23043222

―――

342

33. Bhattacharyya DK, Lecomte M, Rieke CJ, Garavito M, Smith WL. Involvement of arginine 120, glutamate 524, and tyrosine 355 in the binding of arachidonate and 2-phenylpropionic acid inhibitors to the cyclooxygenase active site of ovine prostaglandin endoperoxide H synthase-1. J Biol Chem. 1996; 271:2179–84. PMID: 8567676

34. Fowler CJ, Janson U, Johnson RM, Wahlström G, Stenström A, Norström Å, et al. Inhibition of anandamide hydrolysis by the enantiomers of ibuprofen, ketorolac, and flurbiprofen. Arch Biochem Biophys. 1999; 362:191–6. PMID: 9989926

35. Lever I, Robinson M, Cibelli M, Paule C, Santha P, Yee L, et al. Localization of the endocannabinoid-degrading enzyme fatty acid amide hydrolase in rat dorsal root ganglion cells and its regulation after peripheral nerve injury. J Neurosci. 2009; 29:3766–80. doi: 10.1523/JNEUROSCI.4071-08.2009 PMID: 19321773

36. Pestonjamasp V, Burstein S. Anandamide synthesis is induced by arachidonate mobilizing agonists in cells of the immune system. Biochim Biophys Acta. 1998; 1394:249–60. PMID: 9795237

37. Liu J, Wang L, Harvey-White J, Osei-Hyiaman D, Razdan R, Gong Q, et al. A biosynthetic pathway for anandamide. Proc Natl Acad Sci USA. 2006; 103:13345–50. PMID: 16938887

38. Murakami T, Yomogida S, Someya A, Kuwahara-Arai K, Tamura H, Nagaoka I. Antibacterial cathelicidin peptide CAP11 suppresses the anandamide production from lipopolysaccharide-stimulated mononuclear phagocytes. FEBS Lett. 2007; 581:140–4. PMID: 17184778

39. Tsuboi K, Zhao L-Y, Okamoto Y, Araki N, Ueno M, Sakamoto H, et al. Predominant expression of lysosommal N-acylethanolamine-hydrolysing acid amidase in macrophages revealed by immunochemical studies. Biochim Biophys Acta. 2007; 1771:623–32. PMID: 17462942

40. Li Y, Yang L, Chen L, Zhu C, Huang R, Zheng X, et al. Design and synthesis of potent N-acylethanolamine-hydrolyzing acid amidase (NAAA) inhibitor as anti-inflammatory compounds. PLoS One. 2012; 7: e43023. doi: 10.1371/journal.pone.0043023 PMID: 22916199

343

PLOS | ONE

Interaction of the *N*-(3-Methylpyridin-2-yl) amide Derivatives of Flurbiprofen and Ibuprofen with FAAH: Enantiomeric Selectivity and Binding Mode

Jessica Karlsson[1☯], Carmine M. Morgillo[2☯], Alessandro Deplano[3], Giovanni Smaldone[4], Emilia Pedone[4], F. Javier Luque[5], Mona Svensson[1], Ettore Novellino[2], Cenzo Congiu[3], Valentina Onnis[3], Bruno Catalanotti[2], Christopher J. Fowler[1] *

1 Department of Pharmacology and Clinical Neuroscience, Pharmacology Unit, Umeå University, Umeå, Sweden, 2 Department of Pharmacy, Università degli Studi di Napoli Federico II, Napoli, Italy, 3 Department of Life and Environmental Sciences, Unit of Pharmaceutical, Pharmacological and Nutraceutical Sciences, University of Cagliari, via Ospedale 72, Cagliari, I-09124, Italy, 4 Institute of Biostructures and Bioimaging, CNR, Naples, Italy, 5 Departament de Fisicoquímica and Institut de Biomedicina (IBUB), Facultat de Farmàcia, Universitat de Barcelona, Santa Coloma de Gramenet, Spain

☯ These authors contributed equally to this work.
* cf@pharm.umu.se

CrossMark
click for updates

Abstract

Background

Combined fatty acid amide hydrolase (FAAH) and cyclooxygenase (COX) inhibition is a promising approach for pain-relief. The Flu-AM1 and Ibu-AM5 derivatives of flurbiprofen and ibuprofen retain similar COX-inhibitory properties and are more potent inhibitors of FAAH than the parent compounds. However, little is known as to the nature of their interaction with FAAH, or to the importance of their chirality. This has been explored here.

Methodology/Principal Findings

FAAH inhibitory activity was measured in rat brain homogenates and in lysates expressing either wild-type or FAAH[T488A]-mutated enzyme. Molecular modelling was undertaken using both docking and molecular dynamics. The (*R*)- and (*S*)-enantiomers of Flu-AM1 inhibited rat FAAH with similar potencies (IC$_{50}$ values of 0.74 and 0.99 μM, respectively), whereas the (*S*)-enantiomer of Ibu-AM5 (IC$_{50}$ 0.59 μM) was more potent than the (*R*)-enantiomer (IC$_{50}$ 5.7 μM). Multiple inhibition experiments indicated that both (*R*)-Flu-AM1 and (*S*)-Ibu-AM5 inhibited FAAH in a manner mutually exclusive to carprofen. Computational studies indicated that the binding site for the Flu-AM1 and Ibu-AM5 enantiomers was located between the acyl chain binding channel and the membrane access channel, in a site overlapping the carprofen binding site, and showed a binding mode in line with that proposed for carprofen and other non-covalent ligands. The potency of (*R*)-Flu-AM1 was lower towards lysates expressing FAAH mutated at the proposed carprofen binding area than in lysates expressing wild-type FAAH.

Conclusions/Significance

The study provides kinetic and structural evidence that the enantiomers of Flu-AM1 and Ibu-AM5 bind in the substrate channel of FAAH. This information will be useful in aiding the design of novel dual-action FAAH: COX inhibitors.

Introduction

Fatty acid amide hydrolase (FAAH) is a hydrolytic enzyme belonging to the family of serine hydrolases. It has a wide substrate specificity, capable of hydrolysing N-acylethanolamines and N-acyltaurines. Structurally, the enzyme is a membrane-bound homodimer, whereby the substrate accesses its catalytic active site via a membrane channel [1]. The catalysis of the most-well studied substrate, the endogenous cannabinoid ligand anandamide (arachidonoylethanolamide, AEA) is brought about by the formation of an acyl-enzyme intermediate in association with substrate binding to a triad of amino acids, Lys^{142}, Ser^{217} and Ser^{241} [2,3]. Knowledge of the structure of rat FAAH, and subsequent studies using humanised rat FAAH, have resulted in a series of computational, mutagenesis and structural studies investigating the different classes of FAAH inhibitors with the enzyme (see e.g. [3–13]; for a review, see [14]).

In 1996, Paria *et al.* [15] reported that the non-steroidal anti-inflammatory drug (NSAID) indomethacin reduced the ability of uterine microsomes to hydrolyse AEA following treatment both *ex vivo* (100 μg/mouse s.c.) and *in vitro* (10 μM; [15]). The ability of indomethacin to inhibit FAAH is shared by a number of other NSAIDs including ibuprofen [16], flurbiprofen [17] and carprofen [18]. In an X-ray crystallography study of FAAH complexed with carprofen, Bertolacci *et al.* [11] reported that this NSAID was able to bind to an area at the entrance of the channel allowing the substrate access to the active site. In support of this model, the authors showed further that the potency of carprofen was lower in mutant FAAH^{T488A} (a key residue in the interaction of carprofen with the enzyme) than in the wild-type FAAH [11].

Although the NSAIDs like ibuprofen, flurbiprofen and carprofen inhibit FAAH, their potencies are modest (in the middle to high micromolar concentrations) at physiological pH values. However, a number of structure-activity relationship studies have identified more potent compounds [13,19–22]. Of these, the amide derivative of ibuprofen with 2-amino-3-methylpyridine (Ibu-AM5) is particularly interesting, since it retains the cyclooxygenase-inhibitory properties of the parent compound, and *in vivo* can alleviate visceral pain without producing overt ulcerogenic effects [19,21,23], as can the combination of an NSAID with an FAAH inhibitor [24]. The corresponding amide analogue of flurbiprofen (Flu-AM1) can also inhibit FAAH in submicromolar concentrations and retains the cyclooxygenase (COX)-inhibitory properties of the parent compound [22]. Most recently, a compound with elements of flurbiprofen and a carbamate-based FAAH inhibitor, that inhibits both FAAH and COX and which shows anti-inflammatory and gastroprotective properties, has been disclosed [25].

FAAH shows pronounced enantioselectivity towards inhibition by chiral irreversible phenyl alkylcarbamates, azetidine urea inhibitors and slowly reversible 1,3,4-oxadiazol-2-one inhibitors and by ibuprofen itself [8,9,13,17]. Both Ibu-AM5 and Flu-AM1 retain the chiral centre of the parent profens, and in a recent study published in this Journal [26], we reported that the two enantiomers of Flu-AM1 had similar potencies towards mouse brain FAAH. That paper was primarily focussed upon the COX-inhibitory properties of the Flu-AM1 enantiomers rather than upon FAAH, and the Ibu-AM5 enantiomers were not investigated. In the present study, we have investigated in detail the interaction between the enantiomers of Ibu-AM5,

5. Full Papers

Flu-AM1 and rat FAAH using biochemical, molecular biological, and molecular modelling methodologies.

Materials and Methods

Ethics statement

Ethical permission for the animal experiments was obtained from the local animal research ethical committee (Umeå Ethical Committee for Animal Research, Umeå, Sweden).

Compounds and materials

Radioactive arachidonoyl ethanolamide[1-^{3}H] ([^{3}H]-AEA) was obtained from American Radiolabeled Chemicals, Inc (St Louis, MO, USA). (R)(-)-Ibuprofen and (S)(+)-ibuprofen, were purchased from Santa Cruz Biotechnology Inc. (Dallas, Texas, USA). The enantiomers of Flu-AM1 (structures, see Fig 1) were synthesised as described elsewhere [26]. AEA and URB597 (cyclohexylcarbamic acid 3′-carbamoylbiphenyl-3-yl ester) were purchased from Cayman Chemical Co. (Ann Arbor, MI, USA). Carprofen was obtained from Sigma-Aldrich Inc, St. Louis, (MO, U.S.A.). Substrates were dissolved in ethanol or DMSO as appropriate.

Synthesis of the enantiomers of Ibu-AM5 and ibufenac-AM1

Enantiomerically pure (R)(-)-Ibu-AM5 and (S)(+)-Ibu-AM5 (see Fig 1) were synthesized using a slight modification of the procedure previously described for the racemate [23]. Commercial (R)(-)-ibuprofen and (S)(+)-ibuprofen were coupled with 2-amino-3-methylpyridine in the presence of 1-(3-dimethylaminopropyl)-3-ethylcardodiimide hydrochloride (EDC) and hydroxybenzotriazole (HOBt) in acetonitrile solution.
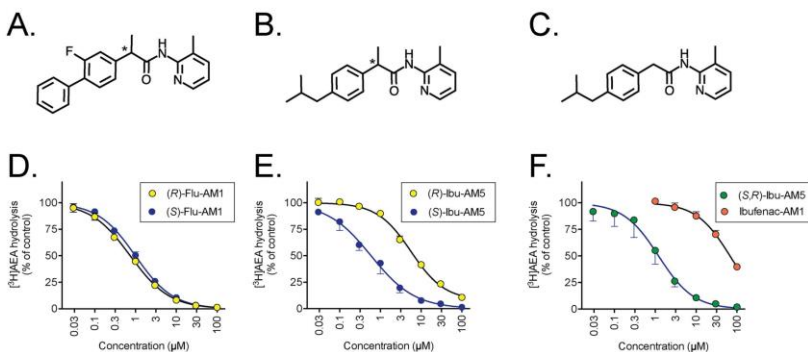
Fig 1. Inhibition of FAAH by the enantiomers of Flu-AM1 and Ibu-AM5 and by Ibufenac-AM1. Structures of the compounds are shown in Panels A-C: A, Flu-AM1; B, Ibu-AM5; C, ibufenac-AM1. The asterisks show the chiral centres. In Panels D-F, the inhibition of 0.5 μM [^{3}H]AEA hydrolysis in rat brain homogenates by the compounds is shown. Data are means ± SEM (when not enclosed by the symbols), N = 3 for the enantiomers of D, Flu-AM1; E, Ibu-AM5 and F, racemic Ibu-AM5 and ibufenac-AM1.

doi:10.1371/journal.pone.0142711.g001

346

Melting points were determined on a Stuart Scientific Melting point SMP1 and are uncorrected. ^{1}H NMR spectra were recorded on a Varian Inova 500 spectrometer. The chemical shifts (δ) are reported in part per million downfield from tetramethylsilane (TMS), which was used as internal standard. Infrared spectra were recorded on a Bruker Vector 22 spectrometer in Nujol mull. The main bands are given in cm^{-1}. Positive-ion electrospray ionization (ESI) mass spectra were recorded on a double-focusing Finnigan MAT 95 instrument with BE geometry. All products reported showed ^{1}H NMR spectra in agreement with the assigned structures. The purity of tested compounds was determined by combustion elemental analyses conducted by the Microanalytical Laboratory of the Chemistry Department of the University of Ferrara, Italy, with a Yanagimoto MT-5 CHN recorder elemental analyzer. All tested compounds yielded data consistent with a purity of at least 95% as compared with the theoretical values. Optical rotations were assessed at 10 mg/mL in methanol with a Perkin Elmer 241 polarimeter in a 10 cm water-jacketed cell at 25°C. Reaction courses and product mixtures were routinely monitored by TLC on silica gel (precoated F$_{254}$ Merck plates), and compounds were visualized using an UV lamp. Reagents and solvents were purchased from the Sigma Chemical Co (St. Louis, MO, USA).

(R) or (S) 2-(4-Isobutylphenyl)-N-(3-methylpyridin-2-yl)propanamide (Ibu-AM5). The respective (R)(-)-ibuprofen or (S)(+)-ibuprofen (0.21 g, 1 mmol), EDC (0.21 g, 1.1 mmol), and HOBt (0.13 g, 1 mmol) in dry acetonitrile (10 mL) was stirred at room temperature for 30 min and then treated with 2-amino-3-methylpyridine (0.11 g, 1 mmol). The mixture was stirred at room temperature for additional 48 h. Then the solution was evaporated to dryness *in vacuo*. The residue was taken up with brine (15 mL) and extracted with AcOEt (2 x 10 mL). The organic layer was washed sequentially with 10% aqueous sodium carbonate (2 x 5 mL), 10% aqueous citric acid (2 x 5 mL) and water (2 x 5 mL). The organic layer was dried over anhydrous magnesium sulphate, filtered and concentrated to dryness under reduced pressure. The respective (R)(+)-Ibu-AM5 or (S)(-)-Ibu-AM5 was obtained (58 and 57% yield respectively) in analytically pure form. ^{1}H NMR (CDCl$_3$): δ 0.86 (d, J = 6.5Hz, 6H, CH$_3$), 1.47 (d, J = 7.0 Hz, 3H, CH$_3$), 1.83 (hept, J = 6.5 Hz, 1H, CH), 2.03 (s, 3H, CH$_3$), 2.41 (d, J = 7.0 Hz, 2H, CH$_2$), 3.88 (q, J = 7.0 Hz, 1H, CH), 6.15 (s, 1H, NH), 6.70 (m, 1H, Py), 7.22 (d, J = 8.0 Hz, 2H, Ar), 7.26 (d, J = 8.0 Hz, 2H, Ar), 7.35 (m, 1H, Py), 7.90 (m, 1H, Py). NMR spectra agree with literature report for the racemate [23]. IR (nujol) 3297, 3253, 3087, 3050, 1672, 1620, 1579 cm^{-1}. Optical rotation [α] = -60.9° for (R)(-)-Ibu-AM5 and [α] = +60.8° for (S)(+)-Ibu-AM5. *m/z* 297 (M + H)$^+$ Anal. Calcd. for C$_{19}$H$_{24}$N$_2$O: C, 76.99; H, 8.16; N, 9.45. Found: C, 77.05; H, 8.18; N, 8.13 for (R)(-)-Ibu-AM5 and C, 76.94; H, 8.19; N, 8.20 for (S)(-)-Ibu-AM5.

2-(4-Isobutylphenyl)-N-(3-methylpyridin-2-yl)acetamide (Ibufenac-AM1). A mixture of ibufenac (0.19 g, 1 mmol), EDC (0.21 g, 1.1 mmol), and HOBt (0.13 g, 1 mmol) in dry acetonitrile (10 mL) was stirred at room temperature for 30 min and then treated with 2-amino-3-methylpyridine (0.11 g, 1 mmol). The mixture was stirred at room temperature for an additional 24 h. Then the solution was evaporated to dryness *in vacuo*. The residue was taken up with brine (15 mL) and extracted with AcOEt (2 x 10 mL). The organic layer was washed sequentially with 10% aqueous sodium carbonate (2 x 5 mL), 10% aqueous citric acid (2 x 5 mL) and water (2 x 5 mL). Concentration of the dried extracts yielded the title compound in analytically pure form. Yield 64%; ^{1}H NMR (DMSO-d$_6$) δ 0.86 (d, J = 6.5Hz, 6H, CH$_3$), 1.82 (hept, J = 6.5Hz, 1H, CH), 2.11 (s, 3H, CH$_3$), 2.48 (d, J = 7.0 Hz, 2H, CH$_2$), 3.85 (s, 2H, CH$_2$), 7.08–8.25 (m, 7H, Ar and Py), 10.16 (s, 1H, NH). IR (nujol) 3310, 3270, 3070, 3050, 1668, 1620, 1569 cm^{-1}. *m/z* 283 (M + H)$^+$ Anal. Calcd. for C$_{18}$H$_{22}$N$_2$O: C, 76.56; H, 7.85; N, 9.92. Found: C, 76.64; H, 7.87; N, 9.87.

347

5. Full Papers

Preparation of rat and mouse brain homogenates

Brains (minus cerebella) from adult Wistar or Sprague-Dawley rats (killed by decapitation) and from male B6CBAF1/J mice (killed by cervical dislocation), stored at -80°C, were thawed, weighed and homogenized in cold buffer (20 mM HEPES, 1 mM $MgCl_2$ pH 7.0). Homogenates were centrifuged (35,000 g at 4°C for 20 min) before the pellet was resuspended in cold homogenization buffer. Centrifugation and resuspension was repeated twice. The suspension was incubated at 37°C for 15 min to degrade any endogenous substrate able to interfere with the FAAH assay. After centrifugation (35,000 g at 4°C for 20 min), the pellet was resuspended in cold buffer (50 mM Tris-HCl, 1mM EDTA, 3 mM $MgCl_2$, pH 7.4). The protein concentration was determined according to [27] after which the samples were frozen in aliquots at -80°C.

Cloning and expression of FAAH^{wt} and FAAH^{T488A} in HeLa cells

The recombinant plasmid (pcDNA4) containing rat Flag-FAAH gene was kindly provided by Prof. Dale Deutsch (Department of Biochemistry and Cell Biology, Stony Brook University). The single mutant FAAH (T488A) was obtained using a Quick Change site directed mutagenesis kit (Agilent Technologies). The insertion of the corrected mutation was confirmed by DNA sequencing. The recombinant plasmids pcDNA-FAAH^{wt} and -FAAH^{T488A} were used to transfect HeLa cells by Lipofectamine Ltx (Life Technologies). After 24h of expression, HeLa cells were detached from the flask with trypsin, washed twice with phosphate buffered saline and resuspendin 0.5 mL of the same buffer. Then, the cells were homogenized by means of a pellet pestle (Sigma). Particulate matter was removed by centrifuging at 3500 g for 20 min. Protein content was determined by [27] and wt or T488A FAAH expression was visualized by Western Blot analysis using an anti-FLAG antibody (Sigma Aldrich).

Assay of [^{3}H]AEA hydrolysis in the homogenates and lysates

The assays were performed according to [28] with minor modifications. Briefly, homogenates or cell lysates in assay buffer (10 mM Tris-HCl, 1mM EDTA, pH 7.4) were mixed with substance dissolved in ethanol on ice. Hydrolysis reactions were initiated by addition of substrate ([^{3}H]AEA in 10 mM Tris-HCl, 1mM EDTA, pH 7.4 containing 10 mg ml^{-1} fatty acid-free bovine serum, assay concentration 0.5 μM unless otherwise stated) and incubation at 37°C. For the brain homogenates, hydrolysis at 37°C was allowed to proceed for 10 min (assay volume was 200 μL, with 1 and 0.3 μg/assay protein concentrations of the rat and mouse homogenates, respectively). For the transfected cells, assay conditions are given in the Figure legend. For the kinetic experiments, the AEA: fatty acid-free bovine serum albumin ratio was kept constant at 1: ~4.5 (μM). Following incubation, reactions were stopped by addition of 400 μL activated charcoal (80 μL activated charcoal + 320 μL 0.5 M HCl) and placement of samples on ice before centrifugation at 2500 rpm for 10 min. Aliquots (200 μL) of the supernatant were analyzed for tritium content by liquid scintillation spectroscopy with quench correction. Sample sizes were chosen on the basis of previous data investigating FAAH inhibitory properties of compounds.

Computational studies

Direct interactions between compounds and FAAH were investigated combining molecular docking studies with molecular dynamics simulations. The simulations were performed with deprotonated Lys^{142}, as proposed for the catalytic mechanism of FAAH [1]. A preliminary validation of the computational protocol was performed by reproducing the experimentally determined binding mode of the pyrrolopyridine inhibitor found in the crystal structure 3QK5,

348

which showed the reliability of the procedure not only to reproduce the ligand binding, but also the position of key water molecules within the active site.

Molecular docking. Rigid docking calculations were performed using the software Autodock 4.2 [29]. The 3D structures of compounds were generated with pymol. Docking was performed on a single monomer of rat FAAH (PDB code: 3QK5 [30], monomer A), after crystallized ligand removal. Rigid docking was performed using a cubic docking box of 60^3 grid points, centred on the position of the original ligand (3-{(3R)-1-[4-(1-benzothiophen-2-yl)pyrimidin-2-yl]piperidin-3-yl}-2-methyl-1H-pyrrolo[2,3-b]pyridin-1-yl)acetonitrile. The rotatable bonds of the compounds were detected automatically by Autodock using default parameters. For each docking run, 100 iterations were performed using default parameters of Lamarckian genetic algorithm (GALS). The results were clustered on the basis of RMSD criterion (≤ 4 Å). The representative poses of the best two clusters of each system were used for further analysis.

Molecular Dynamics. MD simulations were performed with Amber12 [31] to refine best docking results. To this end, the representative poses of the best two clusters retrieved from docking calculations, representing the A- and B- mode for each ligand, were loaded in the two monomers of the dimeric form of rat FAAH (PDB code: 3QK5,) after removal of the pyrrolopyridine derivative and water molecules. Hence, a total of 8 systems were subjected to molecular dynamics analysis. A preliminary validation of the computational protocol was obtained by predicting the experimentally determined binding mode of the pyrrolopyridine derivative in the 3QK5 crystal structure. The non-covalent ligand of the X-ray structure 3QK5 was chosen as reference due to the higher structural similarity toward our compounds with respect to carprofen. It is worth noting that the computational procedure successfully reproduced the binding mode of the pyrrolopyridine inhibitor, as well as the distribution of water molecules around the ligand in the binding cavity (see S1 Fig).

Each complex was immersed in a pre-equilibrated octahedral box of TIP3P water molecules, and the system was neutralized. The final systems contained about 80000 atoms. All simulations were performed with the ff99SBildn force field [32] for the protein and the gaff force field [33] for the ligands. The charge distribution of the inhibitors was refined using RESP charges [34] fitted to the B3LYP/6-31G(d) electrostatic potential obtained with Gaussian09 [35]. For each complex, the geometry was minimized using convergence criterion for the energy gradient set to 0.01 kcal.(mol.Å)$^{-1}$ in three steps, which involve: i) hydrogen atoms in the system (5000 steps of steepest descent and 10000 steps of conjugate gradient), ii) hydrogen atoms, water molecules and counterions (2000 steps of steepest descent and 18000 steps of conjugate gradient), iii) finally the whole system (2000 steps of steepest descent and 18000 steps of conjugate gradient). Thermalization of the system was performed in four steps of 60 ps, increasing the temperature from 50 to 298 K. Concomitantly, the atoms that define the protein backbone were restrained during thermalization using a variable restraining force. Thus, a force constant of 30 kcal.mol^{-1}.Å^{-2} was used in the first stage of the thermalization and was subsequently decreased by increments of 5 kcal. mol^{-1}.Å^{-2} in the next stages. Then, an additional step of 250 ps was performed in order to equilibrate the system density at constant pressure (1 bar) and temperature (298 K). Finally, an extended trajectory was run using a time step of 2 fs. SHAKE was used for those bonds containing hydrogen atoms in conjunction with periodic boundary conditions at constant pressure and temperature, particle mesh Ewald for the treatment of long range electrostatic interactions, and a cutoff of 10 Å for non-bonded interactions. The structural analysis was performed using in-house software and standard codes of Amber 12. All the systems were subjected to 50 ns of molecular dynamics. One run for (R)-Flu-AM1 and one for (S)-Ibu-AM5 were extended to 100 ns in order to confirm the structural integrity of the proposed binding mode for the most active enantiomers.

349

Homology building. The amino acid sequence of mouse FAAH was retrieved from the Universal Protein Resource database (http://www.uniprot.org accession ID O08914). The 3D structure of the target protein was modelled using SWISSMODEL [36]. The X-ray determined structure of rat FAAH 3QK5 was used as template (covered sequence 100%; sequence identity of 91.7%).

Statistical analyses

pI_{50} and IC_{50} values were calculated using log(inhibitor) *vs.* response with variable slope (four parameters) algorithm in the GraphPad Prism computer program (GraphPad Software Inc., San Diego, CA. USA). Data was expressed as % of control and the pI_{50} and IC_{50} values determined using uninhibited (top) values set to 100% and minimum (bottom) values either fixed to zero or allowed to float. The best fit was chosen by Akaike's informative criteria. K_i and α values were obtained using the enzyme kinetics mixed model inhibition curve fitting algorithm available in the GraphPad Prism programme. This models the observed velocity v^{app} at a given substrate concentration where $v^{app} = V_{max}^{app}/(1 + K_m^{app}/[S])$, $V_{max}^{app} = V_{max}/(1+[I]/(\alpha K_i))$ and $K_m^{app} = K_m(1+[I]/K_i)/(1+[I]/(\alpha K_i))$ (http://www.graphpad.com/guides/prism/6/curve-fitting/index.htm?reg_mixered_model.htm, URL checked 16 October 2015). The model assuming competitive interactions (where $\alpha \rightarrow \infty$) was also used, and the best fit was chosen by Akaike's informative criteria. Robust linear regressions for the Dixon plots, which are less sensitive to outliers than the standard least-squares methodology [37] were undertaken using the same computer programme.

Results

Inhibition of FAAH by the enantiomers of Flu-AM1 and Ibu-AM5

The inhibition of [^{3}H]AEA hydrolysis in rat brain homogenates by the enantiomers of Flu-AM1 and Ibu-AM5 is shown in Fig 1 and summarised in Table 1. For Flu-AM1, the potencies of the two enantiomers were very similar, with IC_{50} values of 0.74 and 0.99 μM being found for the (R)- and (S)-enantiomers, respectively. In contrast, for Ibu-AM5, the (S)-enantiomer (IC_{50} value 0.59 μM) was an order of magnitude more potent than the (R)-enantiomer (IC_{50} of 5.7 μM). Ibufenac-AM1, lacking the methyl group on the C-2 carbon atom and thus lacking the chiral centre of Ibu-AM5, was a weak inhibitor of rat brain FAAH, with a pI_{50} value of 4.17±0.04 (IC_{50} value of 68 μM) as compared with the pI_{50} value of 5.92±0.09 (IC_{50} of 1.2 μM) for racemic Ibu-AM5 (Fig 1F). Time-dependency and reversibility experiments were undertaken for (R)-Flu-AM1 (Fig 2). There was a small degree of time-dependency for (R)-Flu-AM1,

Table 1. Species-dependent inhibition of FAAH by the enantiomers of Flu-AM1 and Ibu-AM5.

	Rat brain			Mouse brain		
	pI_{50}	IC_{50} (μM)	n_H	pI_{50}	IC_{50} (μM)	n_H
(R)-Flu-AM1	6.13±0.03	0.74	0.90±0.04	5.05±0.06*	8.8*	0.78±0.09
(S)-Flu-AM1	6.00±0.02	0.99	0.94±0.04	4.96±0.04*	11*	1.31±0.16
(R)-Ibu-AM5	5.25±0.05#	5.7	1.05±0.10	4.28±0.07	53	1.50±0.36
(S)-Ibu-AM5	6.23±0.06	0.59	0.81±0.08	5.16±0.11	7.0	1.33±0.38

Unless otherwise stated, the IC_{50} values were calculated using a maximum inhibition of 100%.
#Best fit was for maximum inhibition of 92±4%. Data calculated from 3–6 experiments using a [^{3}H]AEA concentration of 0.5 μM.
*Data from from [26]. n_H refers to the Hill slopes returned by the analyses.

doi:10.1371/journal.pone.0142711.t001
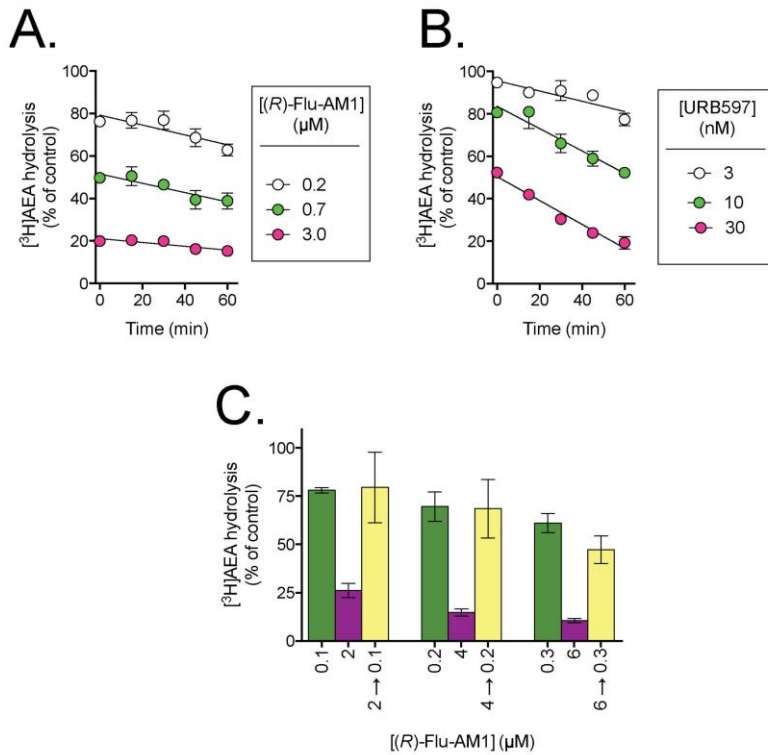
Fig 2. Time-dependency and reversibility of the inhibition of rat brain FAAH by (R)-Flu-AM1. Panels A and B show the time-dependencies of (R)-Flu-AM1 and URB597, respectively. The data are means ± SEM, N = 3. In Panel C, homogenates (at 20-fold normal strength) were preincubated with either vehicle, 2, 4 or 6 µM (R)-Flu-AM1 for 60 min. Aliquots were then diluted 20-fold and assayed for FAAH activity. These are shown as 2 →0.1, 4 →0.2 and 6 →0.3. Concomitantly, (R)-Flu-AM1 was added to vehicle-preincubated aliquots to give concentrations of 0.1, 0.2 and 0.3 µM (representing free concentrations after a 20- fold dilution), 2, 4 and 6 µM final concentrations. The panel shows the data as % of corresponding control (means ± SEM, N = 3). For a fully reversible compound, the inhibition seen in the yellow bars (i.e. following the dilution) should be lower than in the purple bars (the inhibition seen at the undiluted concentrations) but equal to the green bars (the free concentrations after the dilution).

doi:10.1371/journal.pone.0142711.g002

but it was less pronounced than for the irreversible inhibitor URB597. Thus, for example, the % activity remaining in the presence of 0.7 µM (R)-Flu-AM1 was 50±1% and 39±4% after

5. Full Papers
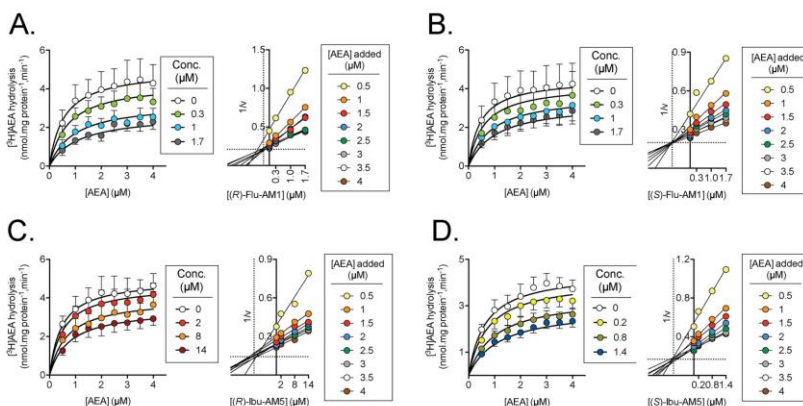
Fig 3. Kinetics of inhibition of FAAH by A, (R)-Flu-AM1; B, (S)-Flu-AM1; C, (R)-Ibu-AM5 and D, (S)-Ibu-AM5. Left panels shown are means ± SEM, N = 3–4, when not enclosed within the symbol, of the FAAH activity at the added concentrations shown of AEA. Right panels show Dixon plots of the mean data. The dotted lines show the projections of the median intersection point on the axes.

doi:10.1371/journal.pone.0142711.g003

preincubation for 0 and 60 min at 37°C, respectively. The corresponding values for 30 nM URB597 were 52±1% and 19±3%, respectively. Further, dilution experiments conducted after 60 min of preincubation indicated that the inhibition produced by (R)-Flu-AM1 was completely reversible in nature (Fig 2).

The ability of the enantiomers of Ibu-AM5 to inhibit FAAH was also investigated in mouse brain homogenates (Table 1). The pattern of enantiomeric selectivity for Ibu-AM5 was also seen in the mouse brain homogenates. However, the potencies of the enantiomers of Ibu-AM5 were about an order of magnitude lower in the mouse brain homogenates compared with the rat brain homogenates, and the same is true for the enantiomers of Flu-AM1. To aid the reader, the pI_{50} and hence IC_{50} values obtained in [26] for inhibition of mouse brain FAAH by the Flu-AM1 enantiomers are given in Table 1.

Mode of inhibition of rat brain FAAH by (R)- and (S)-enantiomers of Flu-AM1 and Ibu-AM5. The inhibition of the hydrolysis of 0.5–4 µM of added [^{3}H]AEA by the (R)- and (S)-enantiomers of Flu-AM1 are shown in Fig 3. The data for the untransformed curves (left panels for the figures) were in both cases better fitted to a model assuming a linear mixed inhibition (see Statistics section of Materials and Methods for a description of the model) than a model assuming a pure competitive interaction. For (R)-Flu-AM1, the model returned K_i and α values of 0.63±0.17 µM and 3.2±1.3, respectively (Fig 3A, left panel). For (S)-Flu-AM1, the corresponding values were 0.79±0.28 µM and 5.6±3.6, respectively (Fig 3B, left panel). Dixon plots were also constructed for the data (Fig 3A and 3B right panels). For a mixed-type inhibitor, the straight lines obtained at each substrate concentration should intersect at a value which, when projected onto the x-axis, corresponds to -K_i [38,39]. For eight substrate concentrations as here, there are 28 different intersections. In an analogous situation, the direct linear

352

plot of Eisenthal and Cornish-Bowden [40], those authors used the median values to solve the issue of undue influence of outliers on intersections. Using this approach, K_i values for (R)- and (S)-Flu-AM1 of 0.28 and 0.86 μM, respectively, were found.

The two enantiomers of Ibu-AM5 were also investigated, and again, both datasets were better fitted by the linear mixed inhibition model than by a pure competitive inhibition model. (S)-Ibu-AM5 inhibited rat brain [^{3}H]AEA hydrolysis with K_i and α values of 0.80±0.21 μM and 3.2±1.5, respectively, and the Dixon plot gave a K_i value of 0.89 μM (Fig 3C). The corresponding values for the (R)-enantiomer were 10±2.5 μM and 3.1±1.1, respectively; Dixon plot K_i value 9.8 μM (Fig 3D).

Multiple inhibition experiments. Experiments where two inhibitors are investigated together are a useful way of determining whether the compounds act in a mutually exclusive manner or in a cooperative manner [39]. In essence, the activity of the enzyme in the presence of different concentrations of both compounds is assessed and the data plotted as 1/v vs. the concentration of one of the compounds, i.e. a Dixon plot. For two compounds acting in a mutually exclusive manner, the Dixon plots should show a series of parallel lines, whereas for two compounds interacting in a co-operative manner, the lines should form a "V"-shape towards the y axis [39]. We investigated the interaction between either (R)-Flu-AM1 or (S)-Ibu-AM5 and carprofen (Fig 4). When analysing the data for carprofen per se, we noted that the Hill slope, n_H was greater than expected (see S1 Appendix). However, this can satisfactorily be explained in terms of its interaction with the fatty acid-free bovine serum albumin in the assay, whereby the free carprofen concentration available for interaction with FAAH is not directly proportional to the added concentration (for analysis see S1 Appendix). Given the uncertainty concerning the free carprofen concentrations, we have presented the data showing the -AM compound concentrations on the x-axes and with the different lines corresponding to each added carprofen concentration (Fig 4). In this way, parallel lines vs. a "V"-shape can be identified without making assumptions about the free carprofen concentrations. There was no obvious evidence of a "V"-shape in the Dixon plots, suggesting that the inhibitors act upon FAAH in a mutually exclusive manner.

Inhibition of wild-type FAAH and FAAH^{T488A} by (R)-Flu-AM1 and carprofen
The simplest explanation for the mutual exclusivity of the -AM compounds and carprofen described above is that they share a binding site on the FAAH molecule. Given the report by Bertolacci et al. [11] that the potency of carprofen was lower towards FAAH^{T488A} than wild-type FAAH, consistent with their model of carprofen interaction with the enzyme, we investigated (R)-Flu-AM1 and carprofen in HeLa cells transfected with the two recombinant FAAH proteins.

Initial time courses indicated that the catalytic activity of the FAAH^{T488A} lysates was very low. In consequence, a long incubation time (18 h at 37°C) was necessary. Under these conditions, (R)-Flu-AM1 indeed inhibited AEA hydrolysis by lysates expressing wild-type FAAH more potently than by lysates expressing FAAH^{T488A} (Fig 5A). In order to check that this difference was not a reflection of the different assay protein contents (lower for the wild type FAAH lysates than for the FAAH^{T488A} lysates in view of their different catalytic activities), the inhibition of a mixture of wild-type lysates and lysates containing the empty vector (which lacked overt AEA-hydrolytic activity) were combined to give the same protein concentration as the FAAH^{T488A} lysates. Addition of the lysates containing the empty vector did not affect the observed potency of (R)-Flu-AM1 towards wild-type FAAH (Fig 5A). Carprofen was also less potent in the FAAH^{T488A} lysates than the wild-type FAAH lysates (Fig 5B), but the steep inhibition curves for the samples will tend to minimise changes in potency, assuming that the high n_H values reflect saturation with fatty acid-free bovine serum albumin as a limiting factor (S1 Appendix). As for (R)-Flu-AM1, addition of the lysates containing the empty vector did

353

Inhibition of FAAH by the Enantiomers of Flu-AM1 and Ibu-AM5
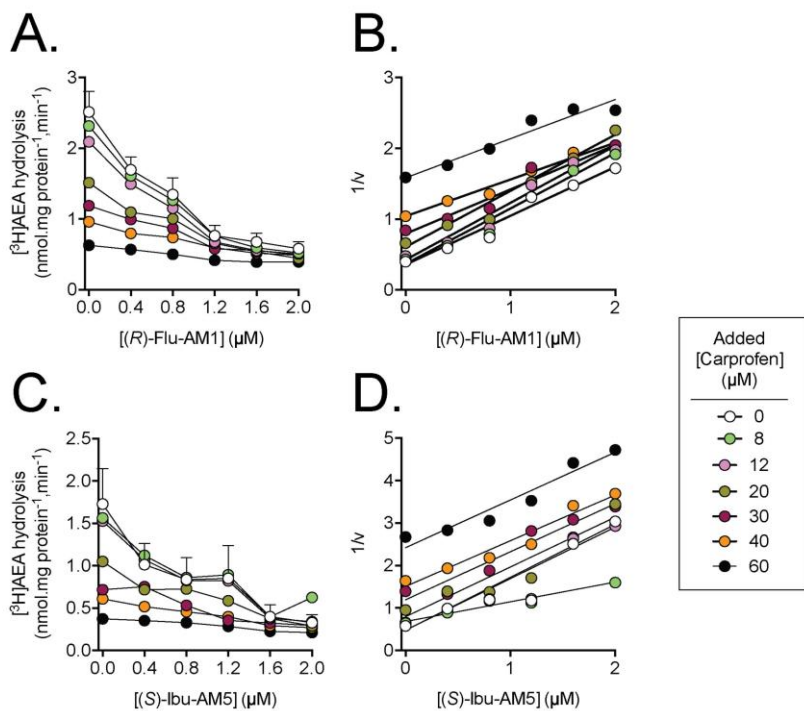
Fig 4. Multiple-inhibitor experiments for the inhibition of rat brain [³H]AEA (0.5 μM) hydrolysis using carprofen and either A, B, (R)-Flu-AM1, or C, D, (S)-Ibu-AM5. The left panels show the untransformed data and are means ± SEM, N = 3–4. The right panels show the Dixon plots of the mean data.

doi:10.1371/journal.pone.0142711.g004

not affect the observed potency of carprofen towards wild-type FAAH (Fig 5B). It was noted that the potency of (R)-Flu-AM1 towards wild type FAAH was lower than seen in the rat brain homogenates, but it is hard to compare these values given that the experimental conditions are so different. Indeed, in preliminary experiments using another batch of wild-type FAAH, 1.5–2 μg/assay and incubation times of 20 min at 37°C, the potencies of (R)- and (S)-Flu-AM1 (1.6 and 2.4 μM, respectively) and (R)- and (S)-Ibu-AM5 (8.8 and 0.53 μM, respectively, data from two experiments) were reasonably similar to the rat brain FAAH values.
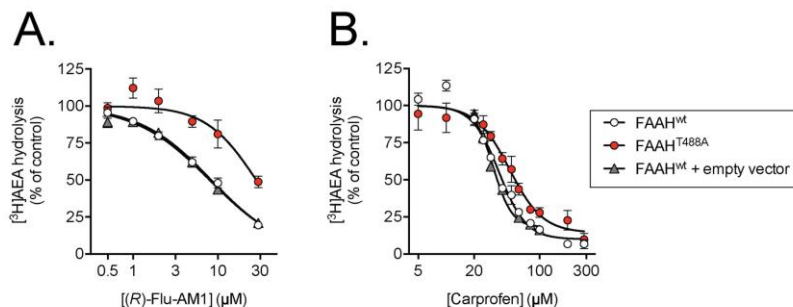
Fig 5. Inhibition of rat wild-type and FAAH^{T488A} by A. (R)-Flu-AM1 and B. carprofen. Samples were incubated for 18 h with inhibitor and substrate (0.5 μM [^{3}H]AEA). The concentrations of lysates used were FAAH^{wt}, 0.04 μg/assay, FAAH^{T488A}, 0.4 μg/assay, empty vector 0.36 μg/assay. Shown are means ± SEM, N = 3–6. The pI$_{50}$ values, with corresponding IC$_{50}$ and n$_H$ values in brackets were: (R)-Flu-AM1: FAAH^{wt}, 5.08±0.03 (8.3 μM; n$_H$ = 1.02±0.07); FAAH^{T488A}, 4.55±0.07 (28 μM; n$_H$ = 1.47±0.37), FAAH^{wt} + empty vector, 5.10±0.02 (8.0 μM; n$_H$ = 0.99±0.06). Carprofen: FAAH^{wt}, 4.43±0.02 (37 μM, n$_H$ = 3.00±0.31); FAAH^{T488A}, 4.32±0.04 (48 μM, n$_H$ = 2.43±0.37), FAAH^{wt} + empty vector, 4.50±0.01 (32 μM; n$_H$ = 4.28±0.41). Note that for carprofen and wild-type FAAH, the analyses suggested that a curve with a maximum inhibition of 82–91% fitted the data better than a curve with 100% maximum inhibition, and these values have been used here.

doi:10.1371/journal.pone.0142711.g005

Molecular dynamics studies

The binding modes of the enantiomeric forms of Flu-AM1 and Ibu-AM5 to the rat FAAH enzyme were studied by combining docking studies and MD simulations using a protocol which was successful in predicting the binding mode of non-covalent ligands (see Materials and Methods section). The docking results were ranked considering the cluster population and the binding energy. The results showed that the ligands bind to a region formed by the acyl chain binding (ACB) channel and the membrane access channel (MAC), filling the cavity experimentally found for other non-covalent ligands [10,11]. Two binding modes that differ in the orientation of the amide moiety were found. Thus, the amide moiety points toward either the catalytic triad (A-mode) or the membrane interacting helices α18-α19 (B-mode). The B-mode was found to be the most populated cluster for the two ligands, but the scores for A- and B-modes were highly similar, thus preventing a firm distinction between the ligand orientations (S1 Table).

To check the structural integrity of two binding modes, the best poses of each docking cluster were submitted to 50 ns of all atom MD simulation. As a general trend, the simulations starting from the B-mode remained stable along the whole trajectory, whilst the ligand showed significant rearrangements when the simulation started from the A-mode. As an example, this is reflected in the positional root-mean square-deviation (RMSD) profiles obtained for (R)- and (S)-Flu-AM1, which show much larger fluctuations in the A-mode binding (S2 Fig). Moreover, the B-mode binding generally led to a consistent pattern of interactions in the binding pocket, whereas the A-mode exhibited less consensus in the interactions between ligand and protein. As an additional test, an independent MD simulation was run for (R)-Flu-AM1 bound to FAAH dimer starting from the B-mode binding, and the results confirmed the structural integrity of the ligand arrangement (see below). Therefore, in the following discussion is limited to the structural features of the B-mode simulations.

Three out of the four ligand-bound systems run for (R)-Flu-AM1 converged to a common binding mode, which is characterized by a stable hydrogen bond between the hydroxyl group of Thr[488] and the carbonyl unit of (R)-Flu-AM1 (Fig 6A), as noted in the similar arrangement obtained upon superposition of representative snapshots (see S3 Fig). The ligand is closely packed in the binding site, forming interactions that are preserved along most of the trajectory (Fig 6A). The biphenyl moiety fills a hydrophobic cavity, with the distal ring pointing to the centre of the anionic hole and forming van der Waals contacts with hydrophobic residues lining the ACB channel (Ile[491], Phe[381], Leu[380], Ile[238] and Phe[194]). No specific interactions were observed for the methyl group on the chiral centre. On the other side, transient hydrogen bonds were observed between the pyridine nitrogen and either the backbone of Asp[403] or alternatively Gly[485] (through a water molecule), and between the amide NH unit and the backbone of Leu[401] (S3 Fig). Van der Waals contacts are also formed with Met[436] and Ile[407]. The structural integrity of this binding mode was maintained upon extension of the trajectory up to 100 ns (data not shown).

The MD trajectories run for (S)-Flu-AM1 led to similar ligand poses in the two monomers of FAAH. The results showed that the amide bond establishes stable hydrogen bonds between the amide NH unit and the backbone of Gly[485], and between the amide carbonyl with the Thr[488] side chain (Fig 6B). Moreover, the biphenyl system formed van der Waals contacts with hydrophobic residues in the ACB channel (Leu[192], Ile[491], Phe[381], Leu[401], Phe[432]). The methyl group on the chiral carbon pointed toward Leu[404] and Leu[401].

Comparison of (R)- and (S)-Flu-AM1 binding modes is shown in Fig 6, which highlights how the enantiomers were bound in slightly different arrangements in the same site located between ACB and the MAC channels. Nevertheless, the enantiomers showed a very similar pattern of interactions: i) the aromatic rings formed a number of van der Waals contacts mainly involving aliphatic side chains, ii) the fluorine atom weakly interacted with Phe[381], and iii) the amidopyridine moiety established hydrogen-bonds with Gly[485] and Thr[488].

MD simulations of (S)-Ibu-AM5 B-mode converged to similar binding modes in the two monomers of FAAH. Extension of the MD simulation to 100 ns confirmed the stability of the B-mode, which remained stable for the last 70 ns of the simulation. (S)-Ibu-AM5 binds at the bottom of the ACB channel and the MAC (Fig 7A) with the pyridine nitrogen fitting the position of the carprofen carboxylic group (PDB code 4DO3) (S4 Fig). The pyridine ring is firmly packed in a hydrophobic cavity in the proximity of the membrane, interacting with hydrophobic residues at the gorge of the MAC (Trp[531], Leu[429] and Ile[407]). The amide unit of the ligand formed hydrogen-bonds with the backbone carbonyl of Gly[485] and to the Thr[488] side chain (Fig 7A). The profen moiety is placed in the apolar gorge of the ACB with the methyl group on the chiral carbon pointing toward Leu[404] and Leu[401].

Simulations run for (R)-Ibu-AM5 also supported the B-mode binding, leading to similar ligand arrangements in the two monomers. Compared to the (S)-enantiomer, most of the differences arise from the pattern of interactions established by the amidopyridine moiety, since a hydrogen bond was formed between the carbonyl unit of the amide group and the hydroxyl group of Thr[488] and the pyridine nitrogen formed a water-mediated contact with Gly[485] (Fig 7B), in addition to hydrophobic contacts with Trp[531], Ile[407] and Phe[381].

Discussion

In the present study, the interaction of the enantiomers of Flu-AM1 and Ibu-AM5 with rat FAAH have been extensively studied in order to determine the importance of the presence of the chiral centre and its configuration. (R)-Flu-AM1 was marginally more potent than the corresponding (S)-enantiomer as an inhibitor of FAAH, a result also seen for flurbiprofen [17]. In
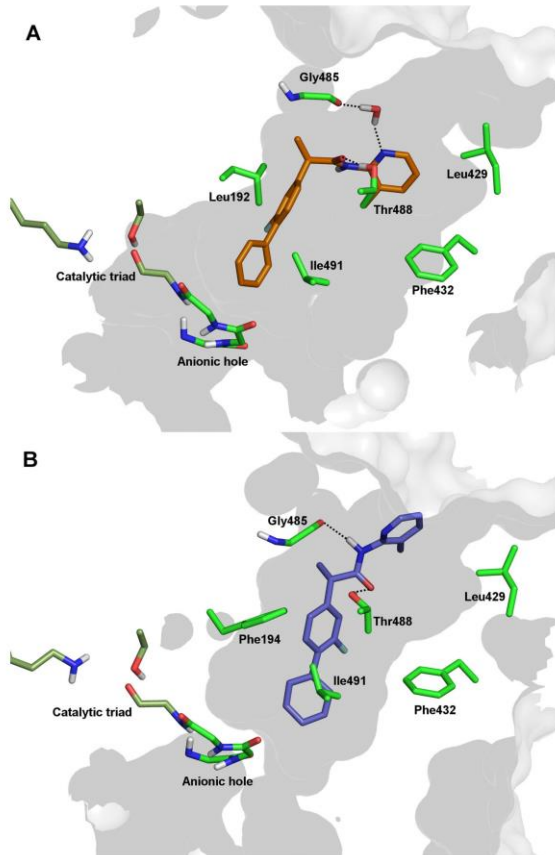
Fig 6. Representation of (R)-Flu-AM1 (A) and (S)-Flu-AM1 (B) in the competitive binding site of the dimeric FAAH as obtained from MD simulations.

357
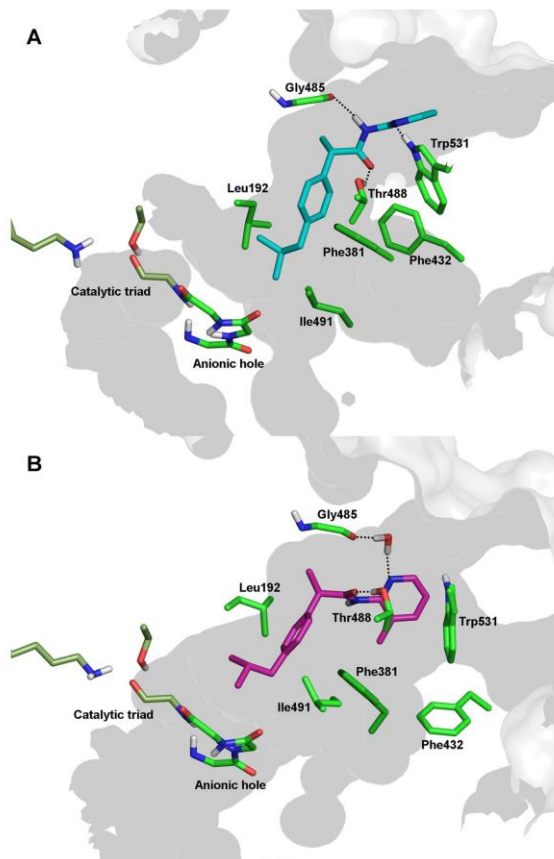
Fig 7. Representation of (S)-Ibu-AM5 (A) and (R)- Ibu-AM5 (B) in the competitive binding site of the dimeric FAAH as obtained from MD simulations.

contrast, the (R)-enantiomer of Ibu-AM5 was 10-fold less potent an inhibitor of FAAH than the (S)-enantiomer, in direct contrast to ibuprofen, where the (R)-enantiomer is more potent than the (S)-enantiomer [17]. Interestingly, the presence of the methyl at the C-2 carbon atom of Ibu-AM5 is more important than its configuration for FAAH inhibitory activity, since ibufenac-AM1 was less potent an inhibitor of FAAH than Ibu-AM5.

The computational studies suggested that Flu-AM1 and Ibu-AM5 bind a region located between the ACB channel and the entrance of the MAC, filling the binding site of other non-covalent inhibitors, such as carprofen [11] (PDB code 4DO3) and the pyrrolopyridine inhibitor in the 3QK5 crystal structure (S4 Fig). Among the two possible binding modes found in docking studies, MD simulations showed that only the B-mode forms a relevant interaction with Thr^{488}. This conclusion was supported by the finding that (R)-Flu-AM1 is a less potent inhibitor of the $FAAH^{T488A}$ mutant enzyme than of the wild-type enzyme. The data with the wild type and $FAAH^{T488A}$ mutant with carprofen are consistent with those of [11], although they found a larger shift despite a lower assay albumin concentration, and lend support to their model that carprofen interacts with Thr^{488} at the entrance to the substrate binding pocket for rat FAAH. On the other hand, the proposed binding mode differs from the one proposed for a series of 1,3,4-oxadiazol-2-ones derivatives of ibuprofen and flurbiprofen [13]. A reasonable explanation of differences in the binding mode can be found in the higher polarity of the 1,3,4-oxadiazol-2-one moiety compared to the pyridine unit, which would make the coordination with the oxyanion hole the main driving force upon binding.

The comparison of the best representative poses of (R)- and (S)-Flu-AM1 showed very different binding modes for the two enantiomers, with the (S)-enantiomer binding deeper in the MAC. The same behaviour was observed from the MD simulations of (R)- and (S)-Ibu-AM5 (S5 Fig) suggesting that chirality is a main determinant of the binding mode. Interestingly, this behaviour seems to be associated to the conformational change of Phe^{432}. In the MD trajectories of (S)-enantiomers the Phe^{432} χ_1 dihedral switched from 90° to 180°, allowing the packing of the methylpyridine ring in a hydrophobic cavity formed by Trp^{531}, Leu^{429} and Ile^{407} (S2 Table). The same Phe^{432} rotamer ($\chi_1 = 180°$) was found in the crystal structure of the rat FAAH in complex with an anandamide analogue (PDB code 1MT5). In contrast, in the binding of the (R)-enantiomers, Phe^{432} assumes the same conformation found in 3QK5 and 4DO3 crystal structures ($\chi_1 = 90°$).

The enzymatic assays showed that these differences in the binding mode slightly affected the activity of Flu-AM1 enantiomers, while it has more remarkable effect on the Ibu-AM5 enantiomers. The binding modes of (R)- and (S)-Flu-AM1 were characterized by a similar pattern of hydrophobic interactions and two hydrogen bonds that is in full agreement with the similar activities showed by these enantiomers. On the contrary, the (S)-Ibu-AM5 binding mode was more stable in the light of the higher member of H-bonds.

The above discussion has only considered a single binding site for the compounds. However, the kinetic experiments suggested a mixed type of inhibition, with a value of α in single figures. A mixed-type inhibition has often been suggested to imply an allosteric mode of inhibition, but this is not necessarily so, and there are many examples of compounds that produce kinetics that are not competitive despite their binding to the active site [41]. One possible mechanism, seen with some NSAIDs such as flurbiprofen (but not ibuprofen) and their interactions with COX, is a two-step reaction whereby an initial competitive interaction is followed by a slower tight-binding or even irreversible inhibition. However, in these cases, the time-dependency is very marked, occurring over minutes [42]. In the present case, there was some apparent time-dependency with (R)-Flu-AM1, but it was very slow, and we have previously not seen such time-dependency with racemic Flu-AM1, despite its mixed-type mode of inhibition [22]. We thus do not favour this mechanism as an explanation for our data. A simpler

5. Full Papers

mechanism for a fully reversible linear-mixed type inhibitor is for the compound to bind to two mutually exclusive sites [39]. Such a model would be consistent with the data, since all that is required in the multiple inhibition experiments with carprofen is mutual exclusivity rather than a specific locus of action [39].

We noted a difference in potencies between inhibition of rat and mouse FAAH by the enantiomers of Flu-AM1 and Ibu-AM5. Pronounced species-dependency has also been reported for carbamate and urea FAAH inhibitors [7,43], although these studies did not compare rat with mouse FAAH. Interestingly, the inhibition of mouse brain FAAH by (R)-Flu-AM1 is competitive rather than mixed [26]. In theory, differences in the amino acid compositions in the binding site of rat and mouse FAAH may account for the potency differences of the enantiomers in the two species. The alignment of the mouse and rat FAAH structures revealed only two differences within the (R)-FluAM1 binding site, Phe[194] to Tyr and Ile[407] to Val. We built a 3D model of the mouse FAAH to evaluate the effects of these mutations on the binding site. These mutations did not change the binding site shape, as shown in S6 Fig, and therefore they should not affect to a dramatic extent the inhibitory potency of (R)-FluAM1. This may mean that there is a species difference in the structure of the enzyme at this additional site. Further experiments are required to be able to identify the site on the enzyme.

Conclusions

The present study has used a range of biochemical, pharmacological, molecular biological and computational methods to explore the interaction of the enantiomers of Flu-AM1 and Ibu-AM5 with FAAH. Given the potentially useful properties of compounds with combined FAAH–COX inhibitory properties [25,44], the characterisation of the binding of the compounds to the substrate access channel of FAAH may provide vital information for the optimisation of such compounds.

Supporting Information

S1 Appendix. Difference in Hill slopes inhibition of FAAH by carprofen, flurbiprofen and the enantiomers of Flu-AM1 and Ibu-AM5: role of binding to fatty acid-free bovine serum albumin.
(DOCX)

S1 Fig. Comparison of the position of the pyrrolopiridine inhibitor and water molecules in the crystal structure 3QK5 (green), in the docking result (yellow), in the best cluster obtained after 50 ns in monomer A (cyan) and in the best cluster obtained after 50 ns in the monomer B (pink). Superimposition was made on protein backbone.
(TIFF)

S2 Fig. Time evolution (ns) of the RMSD (Å) of the (R) and (S) Flu-AM1 enantiomers in the MD run starting from A-mode best poses (left), and MD run starting from B-mode best poses (right).
(TIF)

S3 Fig. Superposition of representative snapshots taken from the two MD runs of (R)-Flu-AM1 bound to monomer A (protein in maroon, ligand in orange and pink) and monomer B (dark cyan). Alignment was obtained by superimposition of the protein backbone. For sake of clarity only polar Hydrogen were shown.
(TIF)

360

S4 Fig. Comparison of the binding modes of (*R*)-Flu-AM1, (*S*)-Ibu-AM5, carprofen and the pyrrolopyridine derivative. (A) (*R*)-Flu-AM1 (orange) compared to carprofen (white; PDB ID: 4DO3); (B) (*R*)-Flu-AM1 (orange) compared to pyrrolopyridine derivative (green; PDB ID: 3QK5); (C) (*S*)-Ibu-AM5 (cyan) compared to carprofen (white); (B) (*S*)-Ibu-AM5 (cyan) compared to pyrrolopyridine derivative (green). Alignment was obtained by superimposition of the protein backbone. For sake of clarity only polar Hydrogen were shown. (TIFF)

S5 Fig. Superimposition of the binding mode proposed for (*S*)-enantiomers (A) and (*R*)-enantiomers (B). (TIF)

S6 Fig. Superimposition of the model of mouse FAAH (green) to the binding mode of (*R*)-FluAM1 (protein in maroon and ligand in orange) complex. (TIF)

S1 Table. Docking result on Flu-AM1 and Ibu-AM5 enantiomers. [a] Autodock 4.2 evaluation of binding energy in kcal/mol. (DOCX)

S2 Table. Dihedral angles of Phe^{432} in different complexes. (DOCX)

Acknowledgments

Author Contributions

Conceived and designed the experiments: JK BC EP EN VO CJF. Performed the experiments: JK CMM AD GS EP FJL MS CC VO BC. Analyzed the data: JK CMM AD GS EP FJL MS CC VO BC CJF. Wrote the paper: JK FJL BC VO CJF.

References

1. Bracey M, Hanson M, Masuda K, Stevens R, Cravatt B. Structural adaptions in a membrane enzyme that terminates endocannabinoid signaling. Science. 2002; 298:1793–6. PMID: 12459591

2. McKinney M, Cravatt B. Evidence for distinct roles in catalysis for residues of the serine-serine-lysine catalytic triad of fatty acid amide hydrolase. J Biol Chem. 2003; 278:37393–8399. PMID: 12734197

3. Palermo G, Campomanes P, Cavalli A, Rothlisberger U, De Vivo M. Anandamide hydrolysis in FAAH reveals a dual strategy for efficient enzyme-assisted amide bond cleavage via nitrogen inversion. J Phys Chem B. 2015; 119:789–801. doi: 10.1021/jp5052276 PMID: 25205244

4. Mor M, Rivara S, Lodola A, Plazzi P, Tarzia G, Duranti A, et al. Cyclohexylcarbamic acid 3´- or 4´-substituted biphenyl-3-yl esters as fatty acid amide hydrolase inhibitors: synthesis, quantitative structure-activity relationships, and molecular modelling studies. J Med Chem. 2004; 47:4998–5008. PMID: 15456244

5. Alexander J, Cravatt B. Mechanisms of carbamate inactivation of FAAH: implications for the design of covalent inhibitors and in vivo functional probes for enzymes. Chem Biol. 2005; 12:1179–87. PMID: 16298297

6. Mei G, Di Venere A, Gasperi V, Nicolai E, Masuda K, Finazzi-Agrò A, et al. Closing the gate to the active site. Effect of the inhibitor methoxyarachidonyl fluorophosphonate on the conformation and membrane binding of fatty acid amide hydrolase. J Biol Chem. 2007; 282:3829–36. PMID: 17158103

7. Mileni M, Johnson D, Wang Z-Q, Everdeen D, Liimatta M, Pabst B, et al. Structure-guided inhibitor design for human FAAH by interspecies active site conversion. Proc Natl Acad Sci USA. 2008; 105:12820–4. doi: 10.1073/pnas.0806121105 PMID: 18753625

361

_____

8. Myllymäki MJ, Käsnänen H, Kataja AO, Lahtela-Kakkonen M, Saario SM, Poso A, et al. Chiral 3-(4,5-dihydrooxazol-2-yl)phenyl alkylcarbamates as novel FAAH inhibitors: Insight into FAAH enantioselectivity by molecular docking and interaction fields. Eur J Med Chem. 2009; 44:4179–91. doi: 10.1016/j.ejmech.2009.05.012 PMID: 19539407

9. Hart T, Macias AT, Benwell K, Brooks T, D'Alessandro J, Dokurno P, et al. Fatty acid amide hydrolase inhibitors. Surprising selectivity of chiral azetidine ureas. Bioorg Med Chem Lett. 2009; 19:4241–4. doi: 10.1016/j.bmcl.2009.05.097 PMID: 19515560

10. Gustin DJ, Ma Z, Min X, Li Y, Hedberg C, Guimaraes C, et al. Identification of potent, noncovalent fatty acid amide hydrolase (FAAH) inhibitors. Bioorg Med Chem Lett. 2011; 21:2492–6. doi: 10.1016/j.bmcl.2011.02.052 PMID: 21392988

11. Bertolacci L, Romeo E, Veronesi M, Magotti P, Albani C, Dionisi M, et al. A binding site for nonsteroidal anti-inflammatory drugs in fatty acid amide hydrolase. J Am Chem Soc. 2013; 135:22–5. doi: 10.1021/ja308733u PMID: 23240907

12. Otrubova K, Brown M, McCormick MS, Han GW, O'Neal ST, Cravatt BF, et al. Rational design of fatty acid amide hydrolase inhibitors that act by covalently bonding to two active site residues. J Am Chem Soc. 2013; 135:6289–99. doi: 10.1021/ja4014997 PMID: 23581831

13. Patel JZ, Parkkari T, Laitinen T, Kaczor AA, Saario SM, Savinainen JR, et al. Chiral 1,3,4-oxadiazol-2-ones as highly selective FAAH inhibitors. J Med Chem. 2013; 56:8484–96. doi: 10.1021/jm400923s PMID: 24083878

14. Palermo G, Rothlisberger U, Cavalli A, De Vivo M. Computational insights into function and inhibition of fatty acid amide hydrolase. Eur J Med Chem. 2015; 91:15–26. doi: 10.1016/j.ejmech.2014.09.037 PMID: 25240419

15. Paria B, Deutsch D, Dey S. The uterus is a potential site for anandamide synthesis and hydrolysis: differential profiles of anandamide synthase and hydrolase activities in the mouse uterus during the peri-implantation period. Mol Reprod Dev. 1996; 45:183–92. PMID: 8914076

16. Fowler C, Tiger G, Stenström. Ibuprofen inhibits rat brain deamidation of anandamide at pharmacologically relevant concentrations. Mode of inhibition and structure-activity relationship. J Pharmacol Exp Ther. 1997; 283:729–34. PMID: 9353392

17. Fowler CJ, Janson U, Johnson RM, Wahlström G, Stenström A, Norström Å, et al. Inhibition of anandamide hydrolysis by the enantiomers of ibuprofen, ketorolac, and flurbiprofen. Arch Biochem Biophys. 1999; 362:191–6. PMID: 9989926

18. Favia AD, Habrant D, Scarpelli R, Migliore M, Albani C, Bertozzi SM, et al. Identification and characterization of carprofen as a multitarget fatty acid amide hydrolase/cyclooxygenase inhibitor. J Med Chem. 2012; 55:8807–26. doi: 10.1021/jm3011146 PMID: 23043222

19. Holt S, Paylor B, Boldrup L, Alajakku K, Vandevoorde S, Sundström A, et al. Inhibition of fatty acid amide hydrolase, a key endocannabinoid metabolizing enzyme, by analogues of ibuprofen and indomethacin. Eur J Pharmacol. 2007; 565:26–36. PMID: 17397826

20. De Wael F, Muccioli GG, Lambert DM, Sergent T, Schneider Y-J, Rees J-F, et al. Chemistry around imidazopyrazine and ibuprofen: discovery of novel fatty acid amide hydrolase (FAAH) inhibitors. Eur J Med Chem. 2010; 45:3564–74. doi: 10.1016/j.ejmech.2010.04.040 PMID: 20570023

21. Fowler CJ, Björklund E, Lichtman AH, Naidu PS, Congiu C, Onnis V. Inhibitory properties of ibuprofen and its amide analogues towards the hydrolysis and cyclooxygenation of the endocannabinoid anandamide. J Enzyme Inhib Med Chem. 2013; 28:172–82. doi: 10.3109/14756366.2011.643304 PMID: 22225576

22. Cipriano M, Björklund E, Wilson AA, Congiu C, Onnis V, Fowler CJ. Inhibition of fatty acid amide hydrolase and cyclooxygenase by the N-(3-methylpyridin-2-yl)amide derivatives of flurbiprofen and naproxen. Eur J Pharmacol. 2013; 720:383–90. doi: 10.1016/j.ejphar.2013.09.065 PMID: 24120370

23. Cocco M, Congiu C, Onnis V, Morelli M, Cauli O. Synthesis of ibuprofen heterocyclic amides and investigation of their analgesic and toxicological properties. Eur J Med Chem. 2003; 38:513–8. PMID: 12767601

24. Naidu P, Booker L, Cravatt B, Lichtman A. Synergy between enzyme inhibitors of fatty acid amide hydrolase and cyclooxygenase in visceral nociception. J Pharmacol Exp Ther. 2009; 329:48–56. doi: 10.1124/jpet.108.143487 PMID: 19118134

25. Sasso O, Migliore M, Habrant D, Armirotti A, Albani C, Summa M, et al. Multitarget fatty acid amide hydrolase/cyclooxygenase blockade suppresses intestinal inflammation and protects against nonsteroidal anti-inflammatory drug-dependent gastrointestinal damage. FASEB J. 2015; 29:2616–27. doi: 10.1096/fj.15-270637 PMID: 25757568

26. Gouveia-Figueira S, Karlsson J, Deplano A, Hashemian S, Svensson M, Fredriksson Sundbom M, et al. Characterisation of (R)-2-(2-fluorobiphenyl-4-yl)-N-(3-methylpyridin-2-yl)propanamide as a dual

_____

_____

362

fatty acid amide hydrolase: cyclooxygenase inhibitor. PLoS ONE. 2015; 10:e0139212 doi: 10.1371/journal.pone.0139212 PMID: 26406890

27. Bradford MM. A rapid and sensitive method for the quantitation of microgram quantities of protein utilizing the principle of protein-dye binding. Anal Biochem. 1976; 72:248–54. PMID: 942051

28. Boldrup L, Wilson SJ, Barbier AJ, Fowler CJ. A simple stopped assay for fatty acid amide hydrolase avoiding the use of a chloroform extraction phase. J Biochem Biophys Methods. 2004; 60:171–7. PMID: 15262451

29. Morris GM, Huey R, Lindstrom W, Sanner MF, Belew RK, Goodsell DS, et al. Autodock4 and AutoDockTools4: automated docking with selective receptor flexiblity. J Comput Chem. 2009; 16:2785–91.

30. Gustin DJ, Ma Z, Min X, Li Y, Hedberg C, Guimaraes C, et al. (2011). Identification of potent, noncovalent fatty acid amide hydrolase (FAAH) inhibitors. Bioorg Med Chem Lett. 2011; 21:2492–6. doi: 10.1016/j.bmcl.2011.02.052 PMID: 21392988

31. Case DA, Darden TA, Cheatham TE III, Simmerling CL, Wang J, Duke RE, et al. AMBER 12, University of California, San Francisco, 2012.

32. Lindorff-Larsen K, Piana S, Palmo K, Maragakis P, Klepeis JL, Dror RO, et al. Improved side-chain torsion potentials for the Amber ff99SB protein force field. Proteins. 2010; 78:1950–8. doi: 10.1002/prot.22711 PMID: 20408171

33. Wang J, Wolf RM, Caldwell JW, Kollman PA, Case DA. Development and testing of a general amber force field. J Comput Chem. 2004; 25:1157–74. PMID: 15116359

34. Bayly CI, Cieplak P, Cornell WD, Kollman PA (1993). A well-behaved electrostatic potential based method using charge restraints for deriving atomic charges J Phys Chem. 1993; 97:10269–80.

35. Gaussian 09, Revision D.01, Frisch MJ, Trucks GW, Schlegel HB, Scuseria GE, Robb MA, Cheeseman JR, et al. Gaussian, Inc., Wallingford CT, USA, 2009.

36. Biasini M, Bienert S, Waterhouse A, Arnold K, Studer G, Schmidt T, et al. SWISS-MODEL: modelling protein tertiary and quaternary structure using evolutionary information. Nucleic Acids Res. 2014; 42:W252–8. doi: 10.1093/nar/gku340 PMID: 24782522

37. Motulsky HJ, Brown RE. Detecting outliers when fitting data with nonlinear regression—a new method based on robust nonlinear regression and the false discovery rate. BMC Bioinformatics. 2006; 7:123. PMID: 16526949

38. Dixon M. The determination of enzyme inhibitor constants. Biochem J. 1953; 55:170–1. PMID: 13093635

39. Segel IH. Enzyme kinetics. Behavior and analysis of rapid equilibrium and steady-state enzyme systems. Jhn Wiley & Sons, New York, 1975.

40. Eisenthal R, Cornish-Bowden A. The direct linear plot. A new graphical procedure for estimating enzyme kinetic parameters. Biochem J. 1974; 139:715–20. PMID: 4854723

41. Blat Y. Non-competitive inhibition by active site binders. Chem Biol Drug Des. 2010; 75:535–40. doi: 10.1111/j.1747-0285.2010.00972.x PMID: 20374252

42. Rome LH, Lands WEM. Structural requirements for time-dependent inhibition of prostaglandin biosynthesis by anti-inflammatory drugs. Proc Natl Acad Sci USA. 1975; 72:4863–5. PMID: 1061075

43. Estiarte MA, Johnson RJ, Kaub CJ, Gowlugari S, O'Mahony DJR, Nguyen MT, et al. 2-Amino-5-aryl-benzoxazole derivatives as potent inhibitors of fatty acid amide hydrolase (FAAH). Med Chem Commun. 2012; 3:611–9.

44. Fowler CJ, Naidu PS, Lichtman A, Onnis V. The case for the development of novel analgesic agents targeting both fatty acid amide hydrolase and either cyclooxygenase or TRPV1. Br J Pharmacol. 2009; 156:412–9. doi: 10.1111/j.1476-5381.2008.00029.x PMID: 19226258

363

Contents lists available at ScienceDirect

European Journal of Medicinal Chemistry

journal homepage: http://www.elsevier.com/locate/ejmech

Laboratory note

A new convenient synthetic method and preliminary pharmacological characterization of triazinediones as prokineticin receptor antagonists

Cenzo Congiu [a], Valentina Onnis [a,*], Alessandro Deplano [a], Severo Salvadori [b], Veronica Marconi [c], Daniela Maftei [c], Lucia Negri [c], Roberta Lattanzi [c], Gianfranco Balboni [a,**]

[a] Department of Life and Environmental Sciences, Unit of Pharmaceutical, Pharmacological and Nutraceutical Sciences, University of Cagliari, I-09124 Cagliari, Italy
[b] Department of Chemical and Pharmaceutical Sciences, University of Ferrara, I-44100 Ferrara, Italy
[c] Department of Physiology and Pharmacology "Vittorio Erspamer", Sapienza University of Rome, I-00185 Rome, Italy

ABSTRACT

A new efficient synthetic method to obtain prokineticin receptor antagonists based on the triazinedione scaffold is described. In this procedure the overall yield improves from 13% to about 54%, essentially for two factors: 1) N-(chlorocarbonyl) isocyanate is no more used, it represents the yield limiting step with an average yield not exceeding 30%. 2) The Mitsunobu reaction is not involved in the new synthetic scheme avoiding the use of time and solvent consuming column chromatography. All synthesized triazinediones were preliminary pharmacologically screened in vivo for their ability to reduce the Bv8-induced thermal hyperalgesia. In this assay all compounds displayed EC_{50} values in the picomolar −subpicomolar range, some triazinediones containing a 4-halogen substituted benzyl group in position 5 showed the best activity. The analogues containing a 4-fluorine atom (PC-7) and a 4-bromobenzyl group (PC-25) resulted 10 times more potent than the reference PC-1 that bears a 4-ethylbenzyl group. While the 4-trifluoromethylbenzyl substituted analog (PC-27) was 100 times more potent as compared to PC1.
© 2014 Elsevier Masson SAS. All rights reserved.

1. Introduction

The mammalian prokineticin 1 (PK1) and prokineticin 2 (PK2), also known as Endocrine Gland-derived Vascular Endothelial Growth Factor (EG-VEGF) and Bombina Variegata 8 (Bv8) are a pair of bioactive peptides highly conserved across species [1]. PK1 and PK2 make up a new family of chemokines which activate two G-protein linked receptors (prokineticin receptor 1 and 2, PKR$_1$ and PKR$_2$). Intensive research of the prokineticin system over the past decade has revealed a dazzling array of physiological functions [2]. Since their initial identification, multiple physiological roles have been discovered including: gastrointestinal motility [3,4], regulation of circadian rhythms [5], angiogenesis [6,7], olfactory bulb neurogenesis [8], neuroexcitation [9] inflammation [10,11], and reproduction [12]. In addition, the disruption of prokineticin system has been implicated in several pathological conditions, including immunological response [13] and persistent pain [14].

Recent evidences implicated PK2 in a human disease in which different point mutations in genes encoding PK2 or its receptor (PKR$_2$) lead to a type of Kallmann syndrome, a disease characterized by a deficiency in hypothalamic gonadotropin-releasing hormones [15]. Furthermore PK2 is reported as an endangering mediator of cerebral ischemia injury [16].

Considering the potential involvement of the prokineticin system in different human disease, the availability of prokineticin receptor modulators represents an important task.

At the best of our knowledge, until now only two articles describing the synthesis of triazinediones endowed with a preferential PKR$_1$ antagonist activity have been reported [17,18]. Only one unselective antagonist endowed with a morpholine scaffold is published to date [16]. On the contrary, numerous patents were filed about the synthesis and use of such antagonists endowed with triazine and morpholine scaffolds. The two most recent patents were filed in early 2012 [19,20]. Furthermore in the late 2013, Takeda Pharmaceuticals filed a patent for new PKR antagonists characterized by a sulfonylpiperidine scaffold [21].

* Corresponding author.
** Corresponding author.
E-mail addresses: vonnis@unica.it (V. Onnis), gbalboni@unica.it (G. Balboni).

In an attempt to identify one or more selective ligands for prokineticin receptors, we started the synthesis of triazinediones endowed with different substituted/unsubstituted benzyl groups at positions 1 and 5. The substitution pattern of triazine scaffold was selected taking into account the results of patent literature and the availability of the synthetic precursors. Looking at published and patented synthetic ways to triazinediones, we identified essentially two different routes clearly reported by Ralbovsky et al. and our group [18,17]. Unfortunately, each synthetic way is characterized by limiting steps which significantly lowers the overall yield. In Scheme 1 it is depicted the first of two synthetic methods published by Ralbovsky et al. [18] and also partially adopted in our previous paper [17].

The major drawback of this route is represented by the N-acylation of isothiourea 24 to give the intermediate 25. This reaction per se is not difficult, but often it is a source of side reactions and it is quite easy to obtain considerable amounts of the disubstituted isothiourea. Indeed, in our hand this step never gave yields higher than 50%. Furthermore, if the second benzyl group is introduced by a Mitsunobu reaction, a column chromatography purification is always necessary to obtain the intermediate 27 of good purity.

The second route to triazinediones is summarized in Scheme 2. In this synthetic way, the ring closure by N-(chlorocarbonyl) isocyanate (step b) to give the intermediate 30 represents the yield limiting step. The average yield of this reaction does not exceed 30%.

Taking into account these considerations, here we report a new synthetic method that can give easy access to high yield and purity new triazinediones as potential ligands for prokineticin receptors. All triazinediones were screened *in vivo* in mice to evaluate their ability to reduce the hyperalgesia induced by BV8, a selective agonist for the prokinetin receptors expressed on the peripheral endings of nociceptors.

2. Results and discussion

2.1. Chemistry

In Scheme 3 is depicted the new way we used for the synthesis of PC-25 and all the other triazinediones reported in Table 1.

Coupling 4-bromobenzylurea 31, obtained upon reaction of 4-bromobenzylamine hydrochloride with potassium cyanate [22], with the commercially available ethoxycarbonyl isothiocyanate gave the N-ethoxycarbonylthiourea 32 in 85% yield. Subsequently, 32 was cyclized under basic conditions to yield the triazine 33 (yield 93%), which was alkylated by methyl iodide under basic conditions to provide the key intermediate 34 in 90% yield (method
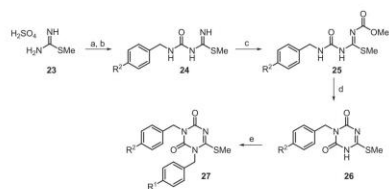
A). Alternatively, cyclization and successive methylation steps can be conveniently done one pot (Method B), avoiding the isolation and purification of 33, with a further improvement of yield up to 95%. The 4-methoxybenzyl group was introduced as a chloride in presence of potassium carbonate to give the intermediate 35. Displacement of the thiomethyl group by ethylenediamine in toluene at 90 °C yielded 36, which was converted into the final guanidine compound PC-25 with pyrazole-1-carboxamidine hydrochloride.

This synthetic method is endowed with two important features: high yield in each step, and the purification of intermediates never needs the use of time and solvent consuming column chromatography. In this way it is easy to obtain triazinediones in high amount and high purity for furthermore in deep pharmacological *in vitro* and *in vivo* studies.

2.2. Analgesic activity

All synthesized triazinediones were screened *in vivo* in mice with a quick and simple test: by injecting them into one hind paw of mice and evaluating their ability to reduce the hyperalgesia induced by BV8, a selective agonist for the prokineticin receptors expressed on the peripheral endings of nociceptors. The compounds injected into the hind paw of mice up to doses of 120 pmol never produced changes in the basal thermal sensitivity, measured as the latency to paw withdrawal from 48 °C water, indicating they do not activate any receptor involved in nociceptor sensitization. Hence we tested their antagonistic activity looking for effectiveness in antagonizing the hyperalgesic effect of Bv8, a selective PKR-1 and PKR-2 agonist which, binding these receptors, increases the nociceptor sensitization, so reducing the paw withdrawal latency. As already demonstrated [23] intraplantar (i.pl. − subcutaneous injection in the paw) injection of 63 fmol of Bv8 induced more than 50% decrease in thermal threshold of the injected paw in 30 min. We evaluated if and at which doses the new molecules were able to reduce the Bv8-induced decrease in thermal threshold when injected by intraplantar route 5 min before Bv8 injection. The ability of different doses of each compound in antagonizing the Bv8-induced hyperalgesia was evaluated. In Fig. 1 the dose–response curves of all synthesized triazinediones are reported and the corresponding EC_{50} values are showed in Table 1. Because of the high number of compounds, the dose response curves are divided in four panels. In each panel the dose–response curve of the reference PC-1 is reported. In Panel A, the most active compounds are shown while in panel B, C and D there are the compounds as/less effective than PC-1.

In this *in vivo* assay all triazinediones showed picomolar EC_{50} values. The analogues PC-7 and PC-25 displayed about 0.3 pmolar EC_{50} values and resulted 10 times more potent than the reference PC-1, while PC-27 (EC_{50} value 0.033 pmol) was 100 times more potent. The replacement of PC-1 4-ethylbenzyl group in position 5 with a 4-fluorine atom to give PC-7 or with a 4-bromobenzyl group to give PC-25 highly improved analgesic activity. The presence in 4-position of a chorine atom (PC18) produced antagonistic activity comparable with that of PC1, while its substitution with an iodine atom or a trifluoromethyl group led to reduction in activity. The opposite effect is showed by analog PC27 bearing a 4-trifluoromethylbenzyl group in position 5 and 4-methyl group in position 1, that is the most potent. The presence of a 4-methoxylbenzyl group in position 5 generally led to analogs that were less effective than the reference PC1, except PC24, PC26, PC29 and PC31 that displayed antagonistic activity comparable with that of PC1.

Peripheral nociceptors of mice contain both PKR_1 and PKR_2, hence with this test we cannot evaluate selectivity for either

Scheme 1. Reagents and conditions: (a) 3 N NaOH; (b) R^2-C_6H_4-CH_2-NCO, H_2O/MeOH/THF, 0 °C to rt; (c) methylchloroformate, NEt_3, CH_2Cl_2, −10 °C to rt; (d) NaOMe, MeOH; (e) R^1-C_6H_4-CH_2-OH, PPh_3, DEAD, THF (Mitsunobu reaction); or R^1-C_6H_4-CH_2-Cl, NaOMe, CH_3CN, heat.
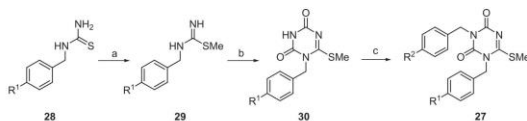
Scheme 2. Reagents: (a) MeI, MeOH; (b) ClCONCO, DIEA, CH₂Cl₂; (c) R²-C₆H₄–CH₂–OH, PPh₃, DEAD, THF (Mitsunobu reaction).
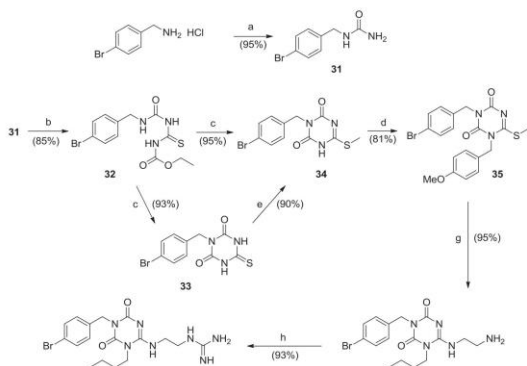
Scheme 3. Reagents and conditions: (a) KOCN, H₂O, 60 °C, 30 min; (b) ethoxycarbonyl isothiocyanate, toluene reflux, 4 h; (c) cᵃ) NaOMe, MeOH, 50 °C, 0.5 h, cᵇ) MeI, rt, 3 h; (d) NaOMe, MeOH, 50 °C, 0.5 h; (e) NaOMe, MeI, MeOH, rt, 3 h; (f) 4-MeO–C₆H₄–CH₂–Cl, K₂CO₃, DMF, rt, 48 h; (g) ethylenediamine, toluene, 90 °C; (h) pyrazole-1-carboxamidine hydrochloride, DIPEA, CH₃CN.

receptor. Because thermal nociception is mainly mediated by PKR₁ activation we might predict these compounds bind the PKR₁ however we cannot exclude they bind also PKR₂. To answer this question next step of our research will be to evaluate the affinity and selectivity for PKR₁ and PKR₂ by *in vitro* binding and *in vivo* test in mice lacking the *pkr1* or the *pkr2* gene.

3. Conclusions

We have reported a new improved synthetic method to triazinediones as potential antagonists for prokineticin receptors with an overall yield of about 54%, far better than 13% reported by us in a previous paper [17]. The advantage of this new route derives essentially by two factors: 1) the reaction of *N*-(chlorocarbonyl) isocyanate to give the intermediate **30** is not used; in fact it represents the yield limiting step with an average yield not exceeding 30%. 2) The Mitsunobu reaction is not involved in the synthetic scheme avoiding the use of time and solvent consuming column chromatography.

Using the new synthetic method we easily synthesized more than 20 triazinediones that were preliminary tested *in vivo* as potential antagonists of the hyperalgesic effect induced by Bv8. All triazinediones showed picomolar EC₅₀ values and three compounds (PC-7; PC-25 and PC-27) showed an efficacy better than the reference PC-1.

Finally, now we are able to provide large amounts of the reference PKR antagonist PC-1 for *in vivo* studies regarding the

inflammatory and neuropathic pain [14], and of PC-7 for *in vivo* studies in animal model of multiple sclerosis (manuscript in preparation) and Parkinson disease [24].
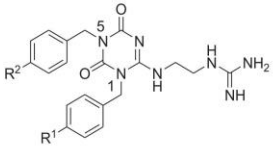
4. Experimental section

4.1. Chemistry

4.1.1. General methods

All commercially available solvents and reagents were used without further purification. ¹H and ¹³C NMR spectra were recorded on a Varian Inova 500 spectrometer. The chemical shifts (δ) are reported in part per million downfield from tetramethylsilane (TMS), which was used as internal standard, and the spectra were recorded in DMSO-d₆. Infrared spectra were recorded on a Bruker Vector 22 spectrometer in Nujol mull. The main bands are given in cm⁻¹. Positive-ion electrospray ionization (ESI) mass spectra were recorded on a double-focusing Finnigan MAT 95 instrument with BE geometry. Melting points (mp) were determined on a Stuart Scientific Melting point SMP1 apparatus and are uncorrected. All products reported showed ¹H and ¹³C NMR spectra in agreement with the assigned structures. The purity of tested compounds was determined by combustion elemental analyses conducted by the Microanalytical Laboratory of the Chemistry Department of the University of Ferrara with a Yanagimoto MT-5 CHN recorder elemental analyzer. All tested compounds yielded data consistent with a purity of at least 95% as compared with the theoretical

Table 1
Structures of new synthesized triazinediones and their EC_{50} analgesic activity values.

Compound	R^1	R^2	EC_{50} (pmol) [95% confidence intervals]
PC-1 (Reference)	OMe	Et	5.8 [3.6–9.1]
PC-7	OMe	F	0.31 [0.16–0.59]
PC-8	H	OMe	63 [44–90]
PC-15	OMe	Me	4.4 [2.5–7.8]
PC-17	OMe	OMe	0.053 [0.038–0.067]
PC-18	OMe	Cl	4.0 [2.9–5.7]
PC-23	OMe	CF₃	51 [27–83]
PC-24	Br	OMe	4.3 [2.7–6.8]
PC-25	OMe	Br	0.36 [0.17–0.78]
PC-26	3,4-diCl	OMe	4.5 [2.9–6.4]
PC-27	Me	CF₃	0.033 [0.018–0.061]
PC-28	3,4-diCl	Me	5.1 [3.8–6.8]
PC-29	Me	OMe	4.5 [3.4–5.6]
PC-30	F	OMe	36 [24–59]
PC-31	Cl	OMe	4.4 [3.1–5.9]
PC-32	CF₃	OMe	48 [33–70]
PC-33	OMe	3,4-methylenedioxy	39 [29–53]
PC-34	I	OMe	39 [27–52]
PC-35	OMe	I	51 [32–80]
PC-36	OMe	NO₂	48 [35––90]

values. Reaction courses and product mixtures were routinely monitored by TLC on silica gel (precoated F_{254} Merck plates), and compounds were visualized with aqueous $KMnO_4$, ninhydrin (1% ethanol, Merck) and chlorine spray reagents. R_f were determined in one or more of the following solvent systems: (A) AcOEt/Pe (1:9, v/v); (B) AcOEt/Pe/ammonia 30% in H_2O (1:1:0.3, v/v/v); (C) AcOEt/Pe (1:1, v/v); (D) AcOEt/Pe (1:2, v/v). Final crude compounds were purified by preparative reversed phase HPLC [Waters Delta Prep LC 40 mm assembly column C18 (30 cm × 4 cm, 15 μm particle size)] eluted at a flow rate of 20 mL/min with mobile phase solvent A (10% CH_3CN + 0.1% TFA in H_2O, v/v), and a linear gradient from 10% to 60% B (60% CH_3CN + 0.1% TFA in H_2O, v/v) in 25 min. Analytical HPLC analyses were performed on a Beckman System Gold (Beckman ultrasphere ODS column, 250 mm × 4.5 mm, 5 μm particle size). For analytical determinations and capacity factor (K') of then products were used solutions A and B as reported above, programmed at a flow rate of 1 mL/min with a linear gradient from 0% to 100% B in 25 min.

*4.1.2. 1-(4-Bromobenzyl)urea (**31**) was prepared according to the procedure of Carmellino et al. [22]*

Briefly, to a solution of 4-bromobenzylamine hydrochloride (4.45 g, 20 mmol) in H_2O (20 mL) potassium cyanate (1.62 g, 20 mmol) was added, and the mixture was heated at 60 °C for 30 min. After cooling at room temperature, the precipitate was filtered, rinsed with ice water and dried [25].

*4.1.3. 1-((4-Bromobenzyl)aminocarbonyl)-3-(ethoxycarbonyl) thiourea (**32**)*

A mixture of 1-(4-bromobenzyl)urea (**31**) (2.29 g, 10 mmol) and ethoxycarbonyl isothiocyanate (12 mmol, 1.2 mL) in toluene (15 mL) was refluxed for 4 h. The solvent was evaporated under vacuum, and the crude product was collected and washed with i-Pr_2O to give a pale-yellow solid: yield 3.06 g (85%); Rf(D) 0.66; HPLC K' 3.24; mp 180–182 °C; m/z 361 (M+H)⁺; ¹H NMR (DMSO-d_6):
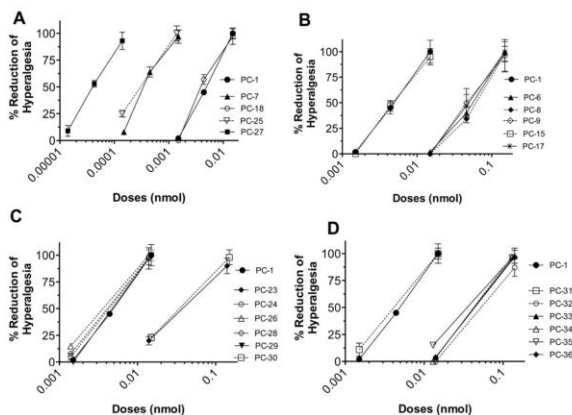
Fig. 1. Dose–response curves of all synthesized triazinediones.

δ 11,12 (s, 1H), 12.22 (s. 1H), 7.55−7.32 (m, 4H), 4.52 (d, $J = 6.0$ Hz, 2H), 4.26 (q, $J = 7.0$ Hz, 2H), 1.35 (t, $J = 7.0$ Hz, 3H); IR (nujol) 3320, 1746, 1731, 1654 cm^{-1}. Anal. Calcd. for $C_{12}H_{14}BrN_3O_3S$ (360.23): C, 40.01; H, 3.92, N, 11.66. Found: C, 40.06; H, 3.91, N, 11.64.

4.1.4. 3-(4-Bromobenzyl)-6-thioxo-1,3,5-triazine-2,4-dione (**33**)

To a solution of 1-((4-bromobenzyl)aminocarbonyl)-3-(ethoxycarbonyl)thiourea (**32**) (3.6 g, 10 mmol) in anhydrous MeOH (5 mL) 5.4 M methanolic NaOMe (1.7 mL) was added at room temperature. The reaction was heated at 50 °C for 0.5 h. The solvent was evaporated under vacuum, then H$_2$O (10 mL) was added and the solution was treated with acq. 10% hydrochloric acid to pH 5−6. The precipitate was filtered off, washed with H$_2$O (2 × 5 mL), air dried, then crystallized with EtOH to give a white solid: yield 2.92 g (93%); *Rf*(D) 0.49; HPLC *K'* 7.24; mp 236−238 °C; *m/z* 315 (M+H)$^+$; ^{1}H NMR (DMSO-d_6): δ 12.57 (s, 2H), 7.52−7.20 (m, 4H), 4.91 (s, 2H). IR (Nujol) 3075, 1763, 1570 cm^{-1}. Anal. Calcd. for $C_{10}H_8BrN_3O_2S$ (314,16): C, 38.23; H, 2.57, N, 13.38. Found: C, 38.20; H, 2.58, N, 13.41.

4.1.5. 3-(4-Bromobenzyl)-6-(methylthio)-1,3,5-triazine-2,4(1H,3H)-dione (**34**)

Method A) To a solution of 3-(4-bromobenzyl)-6-thioxo-1,3,5-triazine-2,4-dione (**33**) (3.14 g, 10 mmol) and 5.4 M methanolic NaOMe (1.7 mL) in anhydrous MeOH (5 mL) methyl iodide (1.9 mL, 30 mmol) was added at room temperature and the reaction mixture was stirred for 3 h. The solvent was evaporated under vacuum, then H$_2$O (10 mL) was added. The precipitate was filtered off, washed with H$_2$O (2 × 5 mL), then crystallized with 2-PrOH to give a pale-yellow solid: yield 2.95 g (90%); *Rf*(D) 0.28; HPLC *K'* 3.56; mp 166−168 °C; *m/z* 329 (M+H)$^+$; ^{1}H NMR (DMSO-d_6): δ 7.56−7.38 (m, 4H), 4.99 (s, 2H), 2.56 (s, 3H). IR (Nujol) 3421, 1756, 1737, 1644 cm^{-1}. Anal. Calcd. for $C_{11}H_{10}BrN_3O_2S$ (328.19): C, 40.26; H, 3.07, N, 12.80. Found: C, 40.20; H, 3.05, N, 12.83.

Method B) To a solution of 1-((4-bromobenzyl)aminocarbonyl)-3-(ethoxycarbonyl)thiourea (**32**) (3.6 g, 10 mmol) in anhydrous MeOH (5 mL) 5.4 M methanolic NaOMe (1.7 mL) was added at room temperature. The reaction was heated at 50 °C for 0.5 h. After cooling methyl iodide (0.8 mL, 12 mmol) was added at room temperature and the reaction mixture was stirred for 3 h. The title compound was isolated as described in method A: yield 3.11 g (95%).

4.1.6. 3-(4-Bromobenzyl)-1-(4-methoxybenzyl)-6-(methylthio)-1,3,5-triazine-2,4(1H,3H)-dione (**35**)

To a solution of 3-(4-bromobenzyl)-6-(methylthio)-1,3,5-triazine-2,4(1H,3H)-dione (**34**) (3.28 g, 10 mmol) in anhydrous DMF (5 mL) anhydrous potassium carbonate (2.76 g, 20 mmol) and 4-methoxybenzyl chloride (1.88 g, 12 mmol) were added. The mixture was stirred for 48 h at room temperature monitoring the reaction *via* HPLC. H$_2$O (20 mL) was added and the precipitate was filtered off, washed with H$_2$O (2 × 5 mL) and crystallized with MeCN to give a white solid: yield 3.63 g (81%); *Rf*(D) 0.53; HPLC *K'* 6.81; mp 171−173 °C; *m/z* 449 (M+H)$^+$; ^{1}H NMR (DMSO-d_6): δ 7.66−7.07 (m, 8H), 5.00 (s, 2H), 4.87 (s, 2H), 3.86 (s, 3H), 2.58 (s, 3H). IR (nujol) 1726, 1670, 1610 cm^{-1}. Anal. Calcd. for $C_{19}H_{18}BrN_3O_3S$ (448.33): C, 50.90; H, 4.05, N, 9.37. Found: C, 50.95; H, 4.06, N, 9.34.

4.1.7. 6-(2-Aminoethylamino)-3-(4-bromobenzyl)-1-(4-methoxybenzyl)-1,3,5-triazine-2,4(1H,3H)-dione (**36**)

To a solution of intermediate (**35**) (0.2 g, 0.45 mmol) in toluene (10 mL) at room temperature, ethylenediamine (0.16 mL, 2.41 mmol) was added. The reaction mixture was refluxed for 12 h. After solvent evaporation, the residue was dissolved in EtOAc and washed twice with H$_2$O (2 × 10 mL). The organic layer was dried (Na$_2$SO$_4$) and evaporated to afford (**36**) as a pale-yellow oil: yield

0.2 g (95%); *Rf*(D) 0.38; HPLC *K'* 5.41; mp 180−182 °C; *m/z* 461 (M+H)$^+$; ^{1}H NMR (DMSO-d_6): δ 7.53−6.88 (m, 8H), 4.98 (s, 2H), 4.87 (s, 2H), 3.73 (s, 3H), 3.28−3.25 (t, 2H, $J = 6.4$ Hz), 2.53−2.50 (t, 2H, $J = 6.4$ Hz); IR (nujol) 3337, 1702, 1570 cm^{-1} Anal. Calcd. for $C_{20}H_{22}BrN_5O_3$ (460.32): C, 52.18; H, 4.82, N, 15.21. Found: C, 52.12; H, 4.80, N, 15.24.

4.1.8. (2-(5-(4-Bromobenzyl)-1-(4-methoxybenzyl)-1,4,5,6-tetrahydro-4,6-dioxo-1,3,5-triazin-2-ylamino)ethyl)guanidine (**11**) [PC-25]

To a solution of intermediate (**36**) (0.17 g, 0.37 mmol) in CH$_3$CN (10 mL) at room temperature, DIPEA (0.13 mL, 0.75 mmol) and pirazole-1-carboxamidine hydrochloride (0.05 g, 0.37 mmol) were added. The reaction mixture was stirred for 12 h at room temperature. The white solid formed was collected by centrifugation and washed twice with ethyl ether (2 × 10 mL). The crude final compound was purified by reversed phase preparative HPLC. Yield 0.17 g (93%); *Rf*(D) 0.42; HPLC *K'* 5.52; mp 215−217 °C; *m/z* 503.37 (M+H)$^+$; ^{1}H NMR (DMSO-d_6): δ 7.52−6.89 (m, 8H), 4.98 (s, 2H), 4.87 (s, 2H), 3.73 (s, 3H), 3.39−3.28 (m, 4H); ^{13}C NMR (DMSO-d_6): 158.55, 156.91, 154.04, 153.27, 150.90, 136.66, 131.08 (2 carbon atoms), 129.77 (2 carbon atoms), 127.92 (2 carbon atoms), 126.99, 120.17, 113.87 (2 carbon atoms), 55.00, 44.28, 43.90, 36.98, 36.81; IR (nujol) 3396, 3149, 1724, 1666, 1578 cm^{-1}. Anal. Calcd. for $C_{25}H_{26}BrF_6N_7O_7$ (502.36) C, 50.21; H, 4.82, N, 19.52. Found: C, 50.26; H, 4.83, N, 19.55.

4.1.9. 1-((4-Fluorobenzyl)aminocarbonyl)-3-(ethoxycarbonyl)thiourea (**32-a**)

Commercially available 1-(4-fluorobenzyl)urea (**31-a**) [alternatively, it can be prepared as reported for (**31**) starting from the appropriate benzyl amine] was reacted with ethoxycarbonyl isothiocyanate as reported for (**32**): yield 2.63 g (88%); *Rf* (D) 0.55; HPLC *K'* 3.18; mp 185−187 °C; *m/z* 300 (M+H)$^+$; ^{1}H NMR (DMSO-d_6): δ 12.30 (s. 1H), 11.20 (s, 1H), 7.46 (m, 2H), 7.28 (m, 2H), 4.48 (d, $J = 6.0$ Hz, 2H), 4.26 (q, $J = 7.0$ Hz, 2H), 1.35 (t, $J = 7.0$ Hz, 3H); IR (nujol) 3317, 1744, 1702 cm^{-1}. Anal. Calcd. for $C_{12}H_{14}FN_3O_3S$ (299.32): C, 48.15; H, 4.71, N, 14.04. Found: C, 48.20; H, 4.69, N, 14.08.

4.1.10. 3-(4-Fluorobenzyl)-6-thioxo-1,3,5-triazine-2,4-dione (**33-a**)

1-((4-fluorobenzyl)aminocarbonyl)-3-(ethoxycarbonyl)thiourea (**32-a**) was reacted with NaOMe as reported for (**33**): yield 2.33 g (92%); *Rf*(D) 0.45; HPLC *K'* 6.84; mp 230−232 °C; *m/z* 254 (M+H)$^+$; ^{1}H NMR (DMSO-d_6): δ 12.84 (s, 2H), 7.48 (m, 2H), 7.26 (m, 2H), 4.91 (s, 2H). IR (nujol) 3085, 1765, 1691 cm^{-1}. Anal. Calcd. for $C_{10}H_8FN_3O_2S$ (235.25): C, 47.43; H, 3.18, N, 16.59. Found: C, 47.47; H, 3.19, N, 16.54.

4.1.11. 3-(4-Fluorobenzyl)-6-(methylthio)-1,3,5-triazine-2,4(1H,3H)-dione (**34-a**)

3-(4-Fluorobenzyl)-6-thioxo-1,3,5-triazine-2,4-dione (**33-a**) was reacted with methyl iodide as reported for (**34**): yield 2.38 g (89%); *Rf*(D) 0.31; HPLC *K'* 3.42; mp 171−173 °C; *m/z* 268 (M+H)$^+$; ^{1}H NMR (DMSO-d_6): δ 12.85 (brs, 1H), 7.26 (m, 2H), 7.46 (m, 2H), 4.97 (s, 2H), 2.57 (s, 3H); IR (nujol) 3136, 1733, 1658 cm^{-1}. Anal. Calcd. for $C_{11}H_{10}FN_3O_2S$ (267.28): C, 49.43; H, 3.77, N, 15.72. Found: C, 49.50; H, 3.75, N, 15.70.

4.1.12. 3-(4-Fluorobenzyl)-1-(4-methoxybenzyl)-6-(methylthio)-1,3,5-triazine-2,4(1H,3H)-dione (**35-a**)

3-(4-Fluorobenzyl)-6-(methylthio)-1,3,5-triazine-2,4(1H,3H)-dione (**34-a**) was reacted with 4-methoxybenzyl chloride as reported for (**35**): yield 3.21 g (83%); *Rf*(D) 0.49; HPLC *K'* 6.71; mp 175−177 °C; *m/z* 388 (M+H)$^+$; ^{1}H NMR (DMSO-d_6): δ 7.49 (m, 2H),

7.37 (d, *J* = 8.4 Hz, 2H), 7.27 (m, 2H), 7.02 (d, *J* = 8.4 Hz, 2H), 5.15 (s, 2H), 5.05 (s, 2H), 3.85 (s, 3H), 2.59 (s, 3H); IR (nujol) 1721, 1679, 1562 cm^{-1}. Anal. Calcd. for $C_{19}H_{18}FN_3O_3S$ (387.43): C, 58.90; H, 4.68, N, 10.85. Found: C, 58.85; H, 4.70, N, 10.81.

4.1.13. 6-(2-Aminoethylamino)-3-(4-fluorobenzyl)-1-(4-methoxybenzyl)-1,3,5-triazine-2,4(1H,3H)-dione (36-a)

The intermediate (**35-a**) was treated with ethylenediamine as reported for (**36**): yield 017 g (93%); *Rf*(D) 0.35; HPLC *K'* 5.28; mp 184–186 °C; *m/z* 400 (M+H)$^+$; ^{1}H NMR (DMSO-d_6): δ 7.34–6.87 (m, 8H), 4.96 (s, 2H), 4.86 (s, 2H), 3.73 (s, 3H), 3.28–3.25 (t, 2H, *J* = 6.4 Hz), 2.53–2.50 (t, 2H, *J* = 6.4 Hz); IR (nujol) 3331, 1720, 1561 cm^{-1}. Anal. Calcd. for $C_{20}H_{22}FN_5O_3$ (399.42): C, 60.14; H, 5.55, N, 17.53. Found: C, 60.10; H, 5.57, N, 17.50.

4.1.14. (2-(5-(4-Fluorobenzyl)-1-(4-methoxybenzyl)-1,4,5,6-tetrahydro-4,6-dioxo-1,3,5-triazin-2-ylamino)ethyl)guanidine (3) [PC-7]

The intermediate (**36-a**) was treated with pyrazole-1-carboxamidine hydrochloride as reported for (**11**): yield 0.15 g (92%); *Rf*(D) 0.43; HPLC *K'* 6.05; mp 221–223 °C; *m/z* 442.47 (M+H)$^+$; ^{1}H NMR (DMSO-d_6): δ 8.28 (br, 1H), 7.81 (s, 1H), 7.39 (m, 2H), 7.29 (d, *J* = 8.4 Hz, 2H), 7.17 (m, 2H), 6.94 (d, *J* = 8.6 Hz, 2H), 5.11 (s, 2H), 4.93 (s, 2H), 3.77 (s, 3H), 3.40 (m, 4H); ^{13}C NMR (DMSO-d_6): 163.01, 160.61, 159.10, 157.49, 154.60, 153.86, 151.48, 134.01, 130.26 (2 carbon atoms), 128.50 (2 carbon atoms), 115.39 (2 carbon atoms), 114.41 (2 carbon atoms), 55.56, 44.82, 44.31, 36.98, 36.81; IR (nujol) 3405, 3157, 1719, 1661, 1572 cm^{-1} Anal. Calcd. for $C_{25}H_{28}F_2N_7O_7$ (441.46): C, 57.13; H, 5.48, N, 22.21. Found: C, 57.10; H, 5.47, N, 22.25.

4.1.15. 1-((4-(Trifluoromethyl)benzyl)aminocarbonyl)-3-(ethoxycarbonyl)thiourea (32-b)

Commercially available 1-(4-(trifluoromethyl)benzyl)urea (**31-b**) (alternatively, it can be prepared as reported for **31**) starting from the appropriate benzyl amine) [26] was reacted with ethoxycarbonyl isothiocyanate as reported for (**32**): yield 2.86 g (82%); *Rf*(D) 0.51; HPLC *K'* 3.11; mp 189–191 °C; *m/z* 350 (M+H)$^+$; ^{1}H NMR (DMSO-d_6): δ 12.27 (s. 1H), 11.19 (s, 1H), 7.55–7.32 (m, 4H), 4.49 (d, *J* = 6.0 Hz, 2H), 4.28 (q, *J* = 7.0 Hz, 2H), 1.33 (t, *J* = 7.0 Hz, 3H); IR (nujol) 3303, 3177, 1734, 1683 cm^{-1}. Anal. Calcd. for $C_{13}H_{14}F_3N_3O_3S$ (349.33): C, 44.70; H, 4.04, N, 12.03. Found: C, 44.64; H, 4.05, N, 12.06.

4.1.16. 3-(4-(Trifluoromethyl)benzyl)-6-thioxo-1,3,5-triazine-2,4-dione (33-b)

1-((4-(trifluoromethyl)benzyl)aminocarbonyl)-3-(ethoxycarbonyl)thiourea (**32-b**) was reacted with NaOMe as reported for (**33**): yield 2.76 g (91%); *Rf*(D) 0.40; HPLC *K'* 6.66; mp 233–235 °C; *m/z* 304 (M+H)$^+$; ^{1}H NMR (DMSO-d_6): δ 12.70 (s, 1H), 7.70–7.54 (m, 4H), 4.90 (s, 2H); IR (nujol) 3073, 1766, 1691, 1571 cm^{-1}. Anal. Calcd. for $C_{11}H_8F_3N_3O_2S$ (303.26): C, 43.57; H, 2.66, N, 13.86. Found: C, 43.62; H, 2.65, N, 13.70.

4.1.17. 3-(4-(Trifluoromethyl)benzyl)-6-(methylthio)-1,3,5-triazine-2,4(1H,3H)-dione (34-b)

3-(4-(trifluoromethyl)benzyl)-6-thioxo-1,3,5-triazine-2,4-dione (**33-b**) was reacted with methyl iodide as reported for (**34**): yield 2.85 g (90%); *Rf*(D) 0.28; HPLC *K'* 3.39; mp 175–177 °C; *m/z* 318.29 (M+H)$^+$; ^{1}H NMR (DMSO-d_6): δ 12.80 (br s, 1H), 7.65 (d, *J* = 7.5 Hz, 2H), 7.49 (d, *J* = 7.5 Hz, 2H), 4.95 (s, 2H), 2.49 (s, 3H); IR (nujol) 1757, 1644 cm^{-1}. Anal. Calcd. for $C_{12}H_{10}F_3N_3O_2S$ (317.29): C, 45.43; H, 3.18, N, 13.24. Found: C, 45.49; H, 3.17, N, 13.20.

4.1.18. 3-(4-(Trifluoromethyl)benzyl)-1-(4-methoxybenzyl)-6-(methylthio)-1,3,5-triazine-2,4(1H,3H)-dione (35-b)

3-(4-(trifluoromethyl)benzyl)-6-(methylthio)-1,3,5-triazine-2,4(1H,3H)-dione (**34-b**) was reacted with 4-methylbenzyl chloride as reported for (**35**): yield 3.50 g (80%); *Rf*(D) 0.45; HPLC *K'* 6.56; mp 178–180 °C; *m/z* 422.44 (M+H)$^+$; ^{1}H NMR (DMSO-d_6): δ 7.69–7.11 (m, 8H), 5.02 (s, 2H), 4.99 (s, 2H), 2.58 (s, 3H), 2.27 (s, 3H). 7.49 (m, 4H), 7.28 (m, 4H), 7.17 (s, 2H), 5.05 (s, 2H), 3.86 (s, 3H), 2.58 (s, 3H); IR (nujol) 1728, 1688, 1519 cm^{-1}. Anal. Calcd. for $C_{20}H_{18}F_3N_3O_2S$ (437.44): C, 54.91; H, 4.15, N, 9.61. Found: C, 54.86; H, 4.13, N, 9.58.

4.1.19. 6-(2-Aminoethylamino)-3-(4-(trifluoromethyl)benzyl)-1-(4-methylbenzyl)-1,3,5-triazine-2,4(1H,3H)-dione (36-b)

The intermediate (**35-b**) was treated with ethylenediamine as reported for (**36**): yield 0.19 g (92%); *Rf*(D) 0.34; HPLC *K'* 5.19; mp 187–189 °C; *m/z* 434.43 (M+H)$^+$; ^{1}H NMR (DMSO-d_6): δ 7.69–7.11 (m, 8H), 5.02 (s, 2H), 4.99 (s, 2H), 3.28–3.25 (t, 2H, *J* = 6.4 Hz), 2.53–2.50 (t, 2H, *J* = 6.4 Hz). 2.27 (s, 3H); IR (nujol) 3298, 1697, 1588 cm^{-1}. Anal. Calcd. for $C_{21}H_{22}F_3N_5O_2$ (433.43): C, 58.19; H, 5.12, N, 16.16. Found: C, 58.16; H, 5.13, N, 16.18.

4.1.20. (2-(5-(4-(Trifluoromethyl)benzyl)-1-(4-methylbenzyl)-1,4,5,6-tetrahydro-4,6-dioxo-1,3,5-triazin-2-ylamino)ethyl)guanidine (13) [PC-27]

The intermediate (**36-b**) was treated with pyrazole-1-carboxamidine hydrochloride as reported for (**11**): yield 0.17 g (92%); *Rf*(D) 0.52; HPLC *K'* 6.51; mp 225–227 °C; *m/z* 476.47 (M+H)$^+$; ^{1}H NMR (DMSO-d_6): δ 7.69–7.11 (m, 8H), 5.02 (s, 2H), 4.99 (s, 2H), 3.40–3.28 (m, 4H). 2.27 (s, 3H); ^{13}C NMR (DMSO-d_6): 156.95, 154.17, 153.30, 150.95, 142.02, 136.52, 132.07 (2 carbon atoms), 129.02 (2 carbon atoms), 128.03 (2 carbon atoms), 126.24 (2 carbon atoms), 125.14 (2 carbon atoms), 125.10, 44.61, 44.15, 36.98, 36.81, 20.53; IR (nujol) 3397, 3166, 1721, 1660, 1579 cm^{-1}. Anal. Calcd. for $C_{26}H_{29}F_9N_7O_6$ (475.45): C, 55.57; H, 5.09, N, 20.62. Found: C, 55.63; H, 5.11, N, 20.68.

4.2. Biological activity

4.2.1. Animals

Male C57Bl/6 mice weighing 25–30 g were used for behaviorals experiments. Mice were housed in plastic cages (5 for each group) and maintained under 12:12 light–dark cycle at 21 ± 1 °C and 50 ± 5% humidity with food and water *ad libitum*.

All animal experiments were conducted under protocols approved by the Animal Care and Use Committee of the Italian Ministry of Health. Animal care was in compliance with the IASP and European Community (E.C.L.358/118/12/86) guidelines on the use and protection of animals in experimental research. All efforts were made to minimize animal suffering and to reduce the number of animal used.

4.2.2. Measurement of nociceptive threshold

The nociceptive threshold to thermal stimuli was evaluated by the Paw–Immersion test.

This test was performed by dipping one mouse hind-paw into hot water (48 °C) and measuring the latencies to paw withdrawal. For measurement of the nociceptive threshold, mice were trained in paw withdrawal test during the week preceding the experiment. This adaptation protocol reduced variability in threshold measurements, giving a more stable baseline and making drug-induced changes easier to detect. On the day of the experiment, nociceptive threshold was measured for 2 h at 30 min intervals before drug injection. The mean of the last three of these threshold measurements were taken as baseline nociceptive threshold (NT$_B$). Nociceptive threshold was then determined three times at 15, 30, 60, 90,

120, 150, 180 min after saline or drug administration. The mean of the three readings at each time point was defined as the nociceptive threshold at that time in the presence of the test solution (NTts). The effect of the tested drug was calculated as the percentage change in nociceptive threshold from baseline threshold (% ΔNT) according to the following equation: % $\Delta NT = 100 \times (NT_{TS} - NT_B)/NT_B$. The EC_{50} values, with 95% confidence intervals, were determined using the PRISM software (GraphPad Software 5.4, San Diego, CA, U.S.A.)

4.2.3. Drug injections

Bv8 was dissolved in saline and *injected* in a volume of 20 μl by *intraplantar* (i.pl.) *route at the dose of 63 fmol in mice*. The antagonists were dissolved in a saline and *injected* in a volume of 20 μl by *intraplantar* (i.pl.) *route* 5 min before Bv8. After drugs administration the animals were observed for 3 h at the established time intervals. For each drug dose, a different group of 5 male mice was used.

4.2.4. Statistical analysis

The data are presented as mean ± SEM. Two-way ANOVA followed by Bonferroni's post tests was performed using GraphPad PRISM 5.4.

Acknowledgment

Appendix A. Supplementary data

Supplementary data related to this article can be found at http://dx.doi.org/10.1016/j.ejmech.2014.05.030.

References

[1] A. Kaser, M. Winklmayr, G. Lepperdinger, G. Kreil, The AVIT protein family, Secreted cysteine-rich vertebrate proteins with diverse functions, EMBO Rep. 4 (2003) 469–473.
[2] L. Negri, R. Lattanzi, E. Giannini, M. Canestrelli, A. Nicotra, P. Melchiorri, Bv8/prokineticins and their receptors: a new pronociceptive system, Int. Rev. Neurobiol. 85 (2009) 145–157.
[3] P.R. Wade, J.M. Palmer, J. Mabus, P.R. Saunders, S. Prouty, K. Chevalier, M.G. Gareau, S. McKenney, P.J. Hornby, Prokineticin-1 evokes secretory and contractile activity in rat small intestine, Neurogastroenterol. Motil. 22 (2010) 152–161.
[4] R.P. Watson, E. Lilley, M. Panesar, G. Bhalay, S. Langridge, S.S. Tian, C. McClenaghan, A. Ropenga, F. Zeng, M.S. Nash, Increased prokineticin 2 expression in gut inflammation: role in visceral pain and intestinal ion transport, Neurogastroenterol. Motil. 24 (2012) 65–75.
[5] J.D. Li, W.P. Hu, L. Boehmer, M.Y. Cheng, A.G. Lee, A. Jilek, J.M. Siegel, Q.Y. Zhou, Attenuated circadian rhythms in mice lacking the prokineticin 2 gene, J. Neurosci. 26 (2006) 11615–11623.
[6] J. LeCouter, R. Lin, M. Tejada, G. Frantz, F. Peale, K.J. Hillan, N. Ferrara, The endocrine-gland-derived VEGF homologue Bv8 promotes angiogenesis in the testis: localization of Bv8 receptors to endothelial cells, Proc. Natl. Acad. Sci. USA 100 (2003) 2685–2690.
[7] F. Shojaei, X. Wu, C. Zhong, L. Yu, X.H. Liang, J. Yao, D. Blanchard, C. Bais, F.V. Peale, N. van Bruggen, et al., Bv8 regulates myeloid-celldependent tumour angiogenesis, Nature 450 (2007) 825–831.
[8] K.L. Ng, J.D. Li, M.Y. Cheng, F.M. Leslie, A.G. Lee, Q.Y. Zhou, Dependence of olfactory bulb neurogenesis on prokineticin 2 signaling, Science 308 (2005) 1923–1927.
[9] Y.C. Xiong, X.M. Li, X.J. Wang, Y.Q. Liu, F. Qiu, D. Wu, Y.B. Gan, B.H. Wang, W.P. Hu, Prokineticin 2 suppresses GABA-activated current in rat primary sensory neurons, Neuropharmacology 59 (2010) 589–594.
[10] E. Giannini, R. Lattanzi, A. Nicotra, A.F. Campese, P. Grazioli, I. Screpanti, G. Balboni, S. Salvadori, P. Sacerdote, L. Negri, The chemokine bv8/prokineticin 2 is up-regulated in inflammatory granulocytes and modulates inflammatory pain, Proc. Natl. Acad. Sci. USA 106 (2009) 14646–14651.
[11] O. Jacobson, I.D. Weiss, G. Niu, G. Balboni, C. Congiu, V. Onnis, D.O. Kiesewetter, R. Lattanzi, S. Salvadori, X. Chen, Prokineticin receptor 1 antagonist PC-10 as a biomarker for imaging inflammatory pain, J. Nucl. Med. 52 (2011) 600–607.
[12] S. Brouillet, P. Hoffmann, S. Chauvet, A. Salomon, S. Chamboredon, F. Sergent, M. Benharouga, J.J. Feige, N. Alfaidy, Revisiting the role of hCG: new regulation of the angiogenic factor EG-VEGF and its receptors, Cell. Mol. Life Sci. 69 (2012) 1537–1550.
[13] J. Monnier, M. Samson, Cytokine properties of prokineticins, FEBS J. 275 (2008) 4014–4021.
[14] L. Negri, R. Lattanzi, Bv8/PK2 and prokineticin receopros: a druggable pronociceptive system, Curr. Opin. Pharmacol. 12 (2012) 62–66.
[15] J. Sarfati, C. Dodé, J. Young, Kallmann syndrome caused by mutations in the PROK2 and PROK2 genes: pathophysiology and genotype-phenotype correlations, Front. Horm. Res. 39 (2012) 121–132.
[16] M.Y. Cheng, A.G. Lee, C. Culbertson, G. Sun, R.K. Talati, N.C. Manley, X. Li, H. Zhao, D.M. Lyons, Q.-Y. Zhou, G.K. Steinberg, R.M. Sapolsky, Prokineticin 2 is an endangering mediator of cerebral ischemic injury, Proc. Natl. Acad. Sci. USA 109 (2012) 5475–5480.
[17] G. Balboni, I. Lazzari, C. Trapella, L. Negri, R. Lattanzi, E. Giannini, A. Nicotra, P. Melchiorri, S. Visentin, C. De Nuccio, S. Salvadori, Triazine compounds as antagonists at Bv8-prokineticin receptors, J. Med. Chem. 51 (2008) 7635–7639.
[18] J.L. Ralbovsky, J.G. Lisko, J.M. Palmer, J. Mabus, K.M. Chevalier, M.J. Schulz, A.B. Dyatkin, T.A. Miskowski, S.J. Coats, P. Hornby, W. He, Triazinediones as prokineticin 1 receptor antagonists: part 1: SAR, synthesis and biological evaluation, Bioorg. Med. Chem. Lett. 19 (2009) 2661–2663.
[19] C.M. Flores, P. Wade, Prokineticin 1 Receptor Antagonists for the Treatment of Pain, Patent WO2012/006004 A1, 2012.
[20] Y.Q. Zhou, D.J. Li, Q. Huang, Prokineticin Receptor Antagonists and Uses Thereof, Patent US2012/0035149 A1, 2012.
[21] C. Carroll, A. Goldby, M. Teall, Sulfonyl Piperidine Derivatives and Their Use for Treating Prokineticin Mediated Diseases, Patent WO2013/179024 (A1), 2013.
[22] P. Borgna, L. Vicarini, M.L. Carmellino, A study on phytotoxic activity of benzylureas, Farm. Ed. Sci. 35 (1980) 1034–1038.
[23] L. Negri, R. Lattanzi, E. Giannini, A. Metere, M.A. Colucci, D. Barra, G. Kreil, P. Melchiorri, Nociceptive sensitization by the secretory protein Bv8, Br. J. Pharmacol. 137 (2002) 1147–1154.
[24] M. Neal, R. Gordon, W. Anantharam, A. Kanthasamy, Induction of prokineticin-2and its neuroprotective effect against neurotoxic insult in dopaminergic neurons, in: GLC-ASPET 25th Annual Scientific Meeting program and Abstracts, 2012, p. 21.
[25] A. Ishii, T. Kotani, Y. Nagaki, Y. Shibayama, Y. Toyomaki, N. Okukado, K.I. enaga, K. Okamoto, Highly selective aldose reductase inhibitors. 1. 3-(arylalkyl)-2,4,5-trioxoimidazolidine-1-acetic acids, J. Med. Chem. 39 (1996) 1924–1927. Supporting Information.
[26] T. Ward, R. Crossley, Compound Libraries of N-(aminocarbonyl)-piperidine-4-carboxamide Derivatives Capable of Binding to G-protein Coupled Receptors, Patent WO2004/058259 A1, 2004.

5. Full Papers

_____

INTERNATIONAL JOURNAL
OF
PHARMACEUTICAL SCIENCES
AND
RESEARCH

HALOGENATED TRIAZINEDIONES BEHAVE AS ANTAGONISTS OF PKR₁: *IN-VITRO* AND *IN-VIVO* PHARMACOLOGICAL CHARACTERIZATION

R Lattanzi [1], C Congiu [2], V Onnis [2], A Deplano [2], S Salvadori [3], V Marconi [1], D Maftei [1], A Francioso [4], C Ambrosio [5], I Casella [5], T Costa [5], G Caltabiano [6], M T Matsoukas [6], G Balboni [2], L Negri [1*]

Department of Physiology and Pharmacology [1] "Vittorio Erspamer", Sapienza University of Rome, I-00185 Rome, Italy.
Department of Life and Environmental Sciences [2], Unit of Pharmaceutical, Pharmacological and Nutraceutical Sciences, University of Cagliari, I-09124, Cagliari, Italy.
Department of Chemical and Pharmaceutical Sciences [3], University of Ferrara, I-44-100 Ferrara, Italy.
Department of Biochemical Sciences [4] "Rossi Fanelli" Sapienza University of Rome, Italy.
Dipartimento del Farmaco [5], Istituto Superiore di Sanita, I-00161 Rome, Italy.
Laboratory of Computational Medicine [6], Biostatistics Unit, Faculty of Medicine, Autonomous University of Barcelona, Bellaterra, Spain.

ABSTRACT: Different prokineticin receptor antagonists, based on the triazinedione scaffold, were synthesized by a new efficient method. Here we demonstrated that 5-benzyl triazinediones substituted in position para of the benzyl group with halogens provide compounds endowed with interesting selectivity for the Prokineticin receptor 1 (PKR₁). BRET technology indicates that such substitution results in increased affinity for the PKR₁. The affinity for PKR₂, always in μM range, was never significantly affected by the para-halogen-benzyl pharmacophores. The analog bearing a para-bromobenzyl pharmacophore (PC-25) displayed the highest affinity for PKR₁ (~18 times higher than the reference PC-1 that bears a para-ethyl benzyl group) and the highest selectivity (~300 times). The other halogen substituted analogs (PC-7, PC-18 and PC-35), showed selectivity for PKR₁ more than 100 times higher than for PKR₂. Using transgenic mice lacking one of the two PKRs we demonstrated that all these compounds were able to abolish the Bv8-induced hyperalgesia in mice still expressing the PKR₁ at doses lower than those necessary to abolish hyperalgesia in mice expressing only the PKR₂. The dose ratio reflected the *in-vitro* evaluated receptor selectivity.

INTRODUCTION: The prokineticins (among them the mammalian molecules named Prokineticin 1, PROK1, prokineticin 2, PROK2, and their Amphibian homologous, Bv8) make up a new family of chemokines [1, 2] which, in mammals, activate two G-protein linked receptors (prokineticin receptor 1 and 2, PKR₁ and PKR₂).

Intensive research of the prokineticin system over the past decade has revealed a dazzling array of physiological functions [3]. In addition, the disruption of prokineticin system has been implicated in several pathological conditions, including cancer [4], immunological response [5, 6] and persistent pain [3].

In animal models of inflammatory [7] and neuropathic [8] pain, in which the prokineticin system is highly activated, we already demonstrated that the prokineticin receptor antagonist PC-1 [9] not only abolishes pain, hindering the nociceptor sensitization, but also reduces the over expression of the endogenous

_____

mediator, the PROK2 [10]. By using mice lacking the *prokr1* or the *prokr2* gene we demonstrated that the up-regulation of PROK2 as well as its proinflammatory and immunomodulatory effects are both mediated by the receptor PKR_1 [6, 7, 11].

Our purpose is to find out molecules endowed with higher affinity and/or selectivity for the PKR_1. We foresee that these molecules might be novel drugs effective in controlling development of immuno-inflammatory processes which underlay several pathological conditions.

In previous papers we described the synthesis of a series of prokineticin-receptor antagonists endowed with PKR_1 selectivity [12]. In *in- vivo* screening we demonstrated that molecules containing a fluorine atom in para position of the benzyl pharmacophore, were effective in abolishing the Bv8-induced hyperalgesia at very low doses (fmol ranges).

Considering this behaviour it could be interesting to prepare and evaluate the affinity and selectivity of the other four halogen substituted PC1-analogs *in -vitro*, using the BRET technology, and *in- vivo*, testing the compounds in transgenic mice expressing only one of the PKRs i.e. mice lacking the *prokr1* or the *prokr2* gene.

In both experimental setting we evaluated the ability of the new compounds to quench the effects of Bv8. Bv8 is the Amphibian homologue of PROK2 which, like PROK2, displays no selectivity for either receptors, but about 10 times higher affinity, and we demonstrated to be a very good pharmacological tool to mimic the activity of the endogenous agonist PROK2 [13].

MATERIALS AND METHODS:
In- vitro experiments:
cDNA Constructs and preparation of cell lines: To prepare cDNA constructs expressing prokineticin receptors fused to the N-terminus of *Renilla* Luciferase (Rluc), PCR fragments coding for the *PROKR1* and *PROKR2* sequences were inserted into pRluc-C vectors (Packard), upstream of the Rluc-coding sequence. Each receptor-Rluc chimeric sequence was then transferred into a pQCIXN retroviral vector (Clontech) expressing the neomycin resistance gene. The preparation of bovine $G\beta_1$ tagged at the N-terminal with RGFP

(*Renilla* green fluorescent protein, Prolume) was described in Molinari *et al.* [14]

SH-SY5Y human neuroblastoma cells were grown in a 1:1 mixture of Dulbecco's modified Eagle's medium and F-12 supplemented with 10% (v/v) foetal bovine serum in a humidified atmosphere of 5% CO2 at 37 °C. Cell lines stably co-expressing each luminescent receptor (PKR_1-Rluc, PKR_2-Rluc) in association with RGFP-Gβ1 were obtained by infecting cells sequentially with retroviruses encoding the fusion proteins, followed by selection with G418 (500 µg/ml) in combination with Hygromicin B (100 µg/ml). The expression level of chimaeric proteins was determined by measuring the intrinsic luminescence and fluorescence of cell-membrane preparations [14].

BRET (Bioluminescence Resonance Energy Transfer) assays: The use of *Renilla* photoproteins as reporters of protein–protein interactions has been described previously [14]. G-protein-coupling assays were performed in membranes (prepared by differential centrifugation as described [15]) from neuroblastoma SHSY5Y cells expressing luminescent PKR_1 or PKR_2 and fluorescent $G\beta_1$. Membranes (5 mg of proteins) were incubated in sterile 96-well white plastic plates (Packard View Plate) containing 2–5 µM coelenterazine (Prolume) and different concentrations of Bv8 (10^{-12} - 10^{-6} M) in PBS for 10 min. Luminescence was recorded sequentially using two band pass filters (blue, 450/20 nm, and green, 510/20 nm, 3rd Millenium, Omega Optical, VT) in a plate luminometer (VICTOR light, PerkinElmer). To measure the effect of PKR antagonists on Bv8-induced receptor-G protein coupling, concentration-response curves of antagonists were generated in the presence of 5 nM Bv8.

Data analysis: RET ratios were calculated as the ratios of high energy (donor) and low energy (acceptor) emissions sequentially recorded through the 450 nm and 510 nm filters corrected for spectral overlap, i.e.,

RET ratio = (CPS $_{510}$× T_{450}/ CPS $_{450}$× T_{510}) − 1, where CPS indicates photon counts per second and T is the relative transmittance of the filters, as reported by the manufacturer.

In- vivo experiments:

Animals:

Male C57Bl6 PKR_1(-/-) or PKR_2(-/-) mice (Lexicon Genetics, The Woodlands, TX) weighing 25-30 g were used for behavioral experiments. Mice were housed in plastic cages (5 for each group) and maintained under 12:12 light-dark cycle at 21 ± 1 °C and $50 \pm 5\%$ humidity with food and water *ad libitum*. All animal experiments were conducted under protocols approved by the Animal Care and Use Committee of the Italian Ministry of Health. Animal care was in compliance with the IASP and European Community (E.C.L.358/118/12/86) guidelines on the use and protection of animals in experimental research. All efforts were made to minimize animal suffering and to reduce the number of animal used.

Measurement of nociceptive threshold:

The nociceptive threshold to thermal stimuli was evaluated by the Paw-Immersion test.

This test was performed by dipping one mouse hind-paw into hot water (48°C) and measuring the latencies to paw withdrawal. For measurement of the nociceptive threshold, mice were trained in paw withdrawal test during the week preceding the experiment. This adaptation protocol reduced variability in threshold measurements, giving a more stable baseline and making drug-induced changes easier to detect. On the day of the experiment, nociceptive threshold was measured for 2 h at 30 min intervals before drug injection. The mean of the last three of these threshold measurements were taken as baseline nociceptive threshold (NT_B). Nociceptive threshold was then determined three times at 15, 30, 60, 90, 120, 150, 180 min after saline or drug administration. The mean of the three readings at each time point was defined as the nociceptive threshold at that time in the presence of the test solution (NT_{TS}). The effect of the tested drug was calculated as the percentage change in nociceptive threshold from baseline threshold (%ΔNT) according to the following equation: $\%\Delta NT = 100 \times (NT_{TS} - NT_B)/ NT_B$

Drug injections:

Bv8 was extracted from the skin secretion of the frog *Bombina variegata* and purified to 98% (HPLC), as previously described [16]. Bv8 was dissolved in saline and injected in a volume of 20 µl

into one hind paw (intraplantar, i.pl.) of mice at the dose of 630 fmol .The antagonists were dissolved in a saline and injected in a volume of 20µl, i.pl., in the same paw, 5 min before Bv8. After drugs administration the animals were observed for three hours at the established time intervals. For each drug dose, a different group of 5 male mice from each genotype was used.

Statistical analysis:

The data are presented as mean $\pm$ S.E.M. Statistical analyses were performed using two-way ANOVA followed by Bonferroni post test. ** $P<0.01$ *** $P < 0.001$, Bv8+PC1 *vs.* Bv8+saline.

Molecular Modelling:

Homology modelling:

Modeller v9.13 was used to build homology models of human Prokinetin receptors PKR_1 and PKR_2 (Uniprot codes Q8TCW9 and Q8NFJ6 respectively) using the crystal structures of human kappa opioid (PDB code 4DJH) and neurotensin 1 (PDB code 4GRV) receptors as templates. The highly conserved $N^{1.50}$ in TM 1, $D^{2.50}$ in TM 2, $R^{3.50}$ in TM 3, $W^{4.50}$ in TM 4, $P^{5.50}$ in TM 5, $P^{6.50}$ in TM6, and $P^{7.50}$ in TM 7, which define the Ballesteros and Weinstein numbering scheme, were used as reference points in TM sequence alignments.

Docking of Prokineticin receptor antagonists:

All docking calculations were performed using Discovery Studio. The Flexible docking protocol was used, assigning side chains to selected residues of the orthosteric binding site using ChiFlex. The ligand docking algorithm was LibDock, and the refinement of the selected protein side-chains in the presence of the rigid ligand was made with ChiRotor. The docked poses were evaluated with the CDOCKER scoring function.

RESULTS AND DISCUSSION:

In vitro assay:

In BRET assay the Bv8-induced interaction between PKR_1 or PKR_2 and the β subunit of heterotrimeric G-proteins resulted in a dose-dependent enhancement of RET signal (**Fig. 1A, B**). Bv8-association curves with the PKR_1 (EC_{50} = 4.9 nM) and the PKR_2 (EC_{50} = 2.9 nM) were similar, confirming that Bv8, like the mammalian

ligand PROK2, binds PKR_1 and PKR_2 with the same affinity, hence is a good ligand to generate displacement curves from PKR_1- and PKR_2- preparations directly comparable. PC-1 dose-dependently reduced the Bv8-induced RET signal and displayed 20 times higher affinity for PKR_1 (IC_{50} = 144 nM) than for PKR_2 (IC_{50} = 2964 nM) (**Fig. 1C, D**) confirming the binding results measured as competition for ^{125}I MIT binding [9].
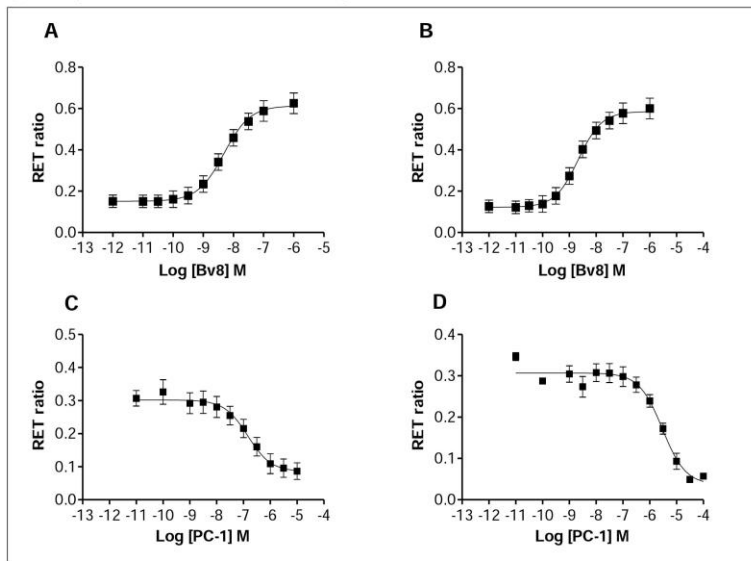
FIGURE 1: CONCENTRATION-RESPONSE CURVES FOR Bv8-INDUCED ENHANCEMENT OF RET RATIO IN MEMBRANES PREPARED FROM SHSY5Y CELLS CO-EXPRESSING FLUORESCENT Gβ AND LUMINESCENT PKR_1 (A) OR PKR_2 (B). EC_{50} VALUES ARE 4.9 ± 0.5 nM AND 2.9 ± 0.3 nM FOR PKR_1 AND PKR_2, RESPECTIVELY. CONCENTRATION-DEPENDENT INHIBITION OF 5 nM Bv8-INDUCED-RET BY PC-1 IN PKR_1 (C) OR PKR_2 (D) CELL MEMBRANES. IC_{50} VALUES ARE 144 ± 15 nM AND 2964 ± 215 nM FOR PKR_1 AND PKR_2, RESPECTIVELY. DATA POINTS ARE MEANS ± S.E.M. OF THREE EXPERIMENTS.

PC-7 (**Fig. 2A**) resulted about 100 times more selective for PKR_1 (IC_{50} = 36 nM) than for PKR_2 (IC_{50} = 4400 nM) and displayed 4 times higher affinity for PKR_1 than the lead compound PC-1. Again ^{125}I MIT-binding assay (not shown) gave affinity values for PKR_1 (IC_{50} = 50 nM) and PKR_2 (IC_{50} = 5700 nM) comparable to those obtained with BRET assay. PC-18 and PC-35 (**Fig 2 C, D**), bearing a para-iodine and para-chlorine, behaved very similar to PC-7: they maintain the same low affinity for PKR_2 and a comparable affinity for PKR_1.

PC-25 displayed the highest affinity for PKR_1 (~18 times higher than PC-1) and the highest selectivity for PKR_1 (~300 times) (**Fig. 2B** and **Table1**).

These data clearly indicate that para-halogen substitution of the benzyl group in the 5-position of triazinedione scaffold significantly increased the affinity for the PKR_1, while it did not affected the affinity for the PKR_2. The compounds containing the other halogens, chlorine, iodine and fluorine (compd. PC-18, PC-35 and PC-7, respectively) showed about 5 times lower affinity than the best compound PC-25, containing bromine.
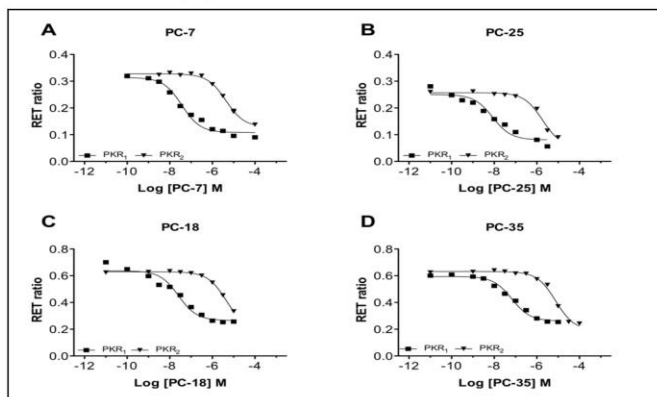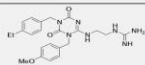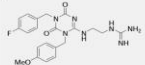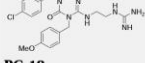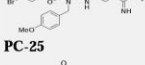
FIGURE 2: CONCENTRATION-DEPENDENT INHIBITION OF Bv8 (5 nM)-INDUCED RET SIGNAL IN PKR$_1$ (■) OR PKR$_2$ (▼) CONTAINING CELL MEMBRANES BY HALOGENATED PC-1-ANALOGS. REPRESENTATIVE CURVES OF THREE SEPARATE EXPERIMENTS. IC$_{50}$ VALUES FOR PKR$_1$ AND PKR$_2$ ARE REPORTED IN TABLE 1.

TABLE 1. AFFINITY AND SELECTIVITY OF THE HALOGENATED PC$_S$ EXPRESSED AS IC$_{50}$ VALUES. DATA ARE MEANS ± S.E.M. OF THREE EXPERIMENTS

Triazinediones	PKR$_1$ IC$_{50}$ (nM)	PKR$_2$ IC$_{50}$ (nM)	Selectivity (IC$_{50}$ PKR$_2$ / IC$_{50}$ PKR$_1$)
PC-1 *(reference)*	*144 ± 15*	*2964 ± 215*	*20.6*
PC-7	36 ± 6.1	4399 ± 340	122
PC-18	28 ± 3.2	4400 ± 310	157
PC-25	8 ± 0.5	2162 ± 180	270
PC-35	39 ± 4.9	4440 ± 385	114

In- vivo assay:

In PKR$_1$(-/-) and PKR$_2$(-/-) mice i.pl. injection of Bv8 (5 ng = 630 fmol) induced comparable hyperalgesia evaluated as decrease of the nociceptive threshold to thermal stimuli. Hyperalgesia was already evident in 15 min, peaked in 60 min and lasted for about 3 h. Pre-injection (-5 min) of the compounds, into the paw, antagonized the Bv8-induced hyperalgesia in dose-dependent manner. In PKR$_1$(-/-) mice a dose of 150 pmol of PC-1 abolished thermal hyperalgesia induced by Bv8, whereas in PKR$_2$(-/-) mice a 10

folds lower dose (15 pmol) of PC-1 was enough to obtain the same effect (**Fig. 3**).

Evaluation of the dose-effect relationship was obtained considering the area under the curves (AUC) for each tested dose. This analysis confirmed that the antihyperalgesic effect of PC-1 is more than 10 times higher in PKR$_2$(-/-) mice respect to PKR$_1$(-/-) mice accordingly with its preferential affinity for PKR$_1$, the receptor still present in PKR$_2$(-/-) mice (**Fig. 3**).
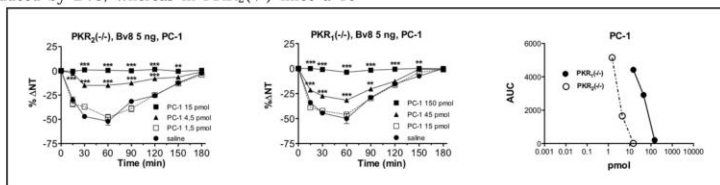
FIGURE 3: EFFECTS OF INTRAPLANTAR (i.pl.) PRE-INJECTION (-5 min) OF VARIOUS DOSES OF PC-1 ON THERMAL HYPERALGESIA INDUCED BY Bv8 (5 ng, i.pl.) IN PKR$_2$(-/-) AND PKR$_1$(-/-) MICE. THE ANTIHYPERALGESIC EFFECT WAS EVALUATED AS AUC OF THE TIME-RESPONSE CURVE FOR EACH DOSE.

As demonstrated in **Fig. 4**, PC-7 and PC-25 antagonized the Bv8-induced thermal hyperalgesia in PKR$_1$-KO mice at doses of 15 pmol and 14 pmol, but in PKR$_2$-KO mice at doses of 0.15 pmol and 0.04 pmol, respectively, confirming a selectivity of 100 and 300 times for PKR$_1$.

PC-18 and PC-35 appeared less effective than PC-7, being necessary significantly higher doses to counteract the Bv8 induced hyperalgesia, however the ratio of the effective doses in PKR$_1$ (-/-) and PKR$_2$ (-/-) mice was consistent with their selectivity: about 100 folds.
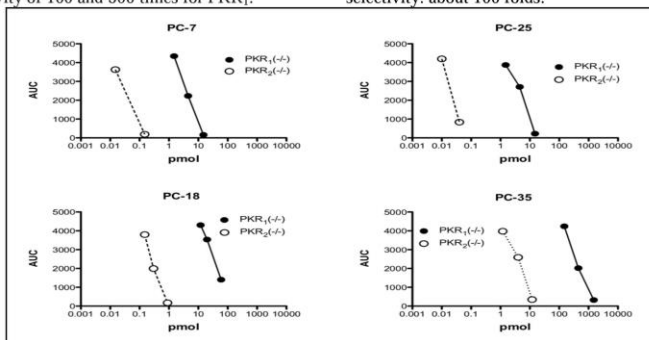
FIGURE 4: DOSE-DEPENDENT INHIBITION OF Bv8-INDUCED HYPERALGESIA BY PRETREATMENT WITH VARIOUS DOSES OF PC-7, PC-18, PC-25 AND PC-35 IN PKR$_2$(-/-) AND PKR$_1$(-/-) MICE. THE ANTIHYPERALGESIC EFFECT OF VARIOUS DOSES OF THE HALOGENATED COMPOUNDS WAS EVALUATED AS AREA UNDER THE TIME-RESPONSE CURVE (AUC).

Molecular Modelling

Using a flexible docking method (see Materials and Methods), the known antagonist PC-1 was docked to the binding site of the structural model of the PKR$_1$ receptor. Residue side chains that were considered flexible were E2.61, R3.32, T4.64, Qi+2 (at position i+2, relative to the conserved C180i engaged in a disulfide bond with C3.25 in TM 3), R6.58 and E7.39. The highest scored poses were ranked and inspected visually, to determine whether they satisfy the experimental results. Based on the docking results, as seen in **Fig. 5A**, the guanidine group interacts with E2.61 and F7.35, while one of the carbonyl oxygens interacts with R6.58. The anisole oxygen forms a hydrogen bond with N3.29 and the ethyl benzene groups is located in hydrophobic vicinity formed by T4.64 and F4.63. The interactions with PKR$_2$ are similar, with the difference of the A4.64 instead of the threonine (**Fig. 5B**). In the case of PC-25, the bromine of the benzene group is interacting with the T6.46 hydroxyl group of PKR$_1$ through a halogen bond (**Fig. 5C** see Conclusion), whereas the absence of this interaction can be seen on **Fig. 5D**.
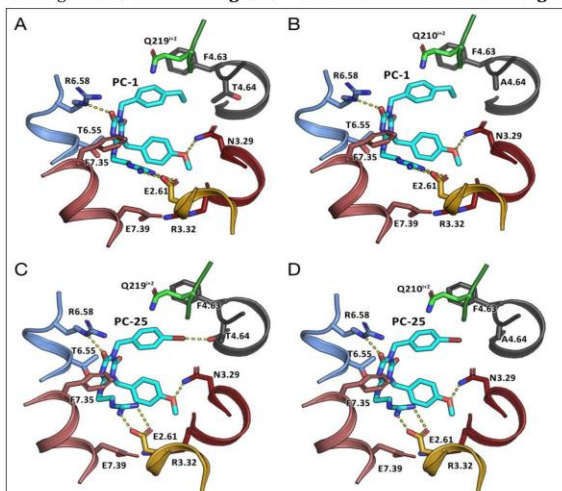
FIGURE 5. DOCKING MODELS OF PC-1 AND PC-25. DIFFERENCES IN THE BINDING OF PC-1 (CYAN STICKS) INTERACTING WITH THE BINDING SITE RESIDUES OF PKR$_1$ (PANEL A) AND PKR$_2$ (PANEL B). DIFFERENCES IN THE BINDING OF PC-25 (CYAN STICKS) INTERACTING WITH THE BINDING SITE RESIDUES OF PKR$_1$ (PANEL C) AND PKR$_2$ (PANEL D). THE COLOUR CODE OF THE HELICES IS TM 2 IN YELLOW, 3 IN RED, 4 IN GRAY, 6 IN BLUE, AND 7 IN LIGHT BROWN, WHERE EL2 IS IN GREEN

CONCLUSIONS: The primary structures of PKR$_1$ and PKR$_2$ are highly homologous, having a sequence identity of 91% and BLOSUM62 similarity of 96%. All residues that are located in the different binding pockets (mayor and minor binding pocket as well as the extracellular entrance, the latter often involved in allosteric modulation of class A GPCR) are fully conserved with the exception of position 4.64 in which PKR$_2$ has an alanine (A201 in absolute numeration) instead of a threonine (T192), featured in PKR$_1$. Most sequence variation between the PKR subtypes is concentrated in the extracellular N terminal region, which contains a nine-residue insert in PKR$_1$ compared with PKR$_2$, as well as in the second intracellular loop (ICL2) and in the C terminal tail. A conserved disulfide bridge connects the second extracellular loop (ECL2) with the extracellular end

of TM3 a characteristic shared with more than 80% of class A GPCR. Levit *et al.*[17], analyzing the human PKRs, identified a putative extracellular surface binding site, which most likely binds the endogenous PKR ligands, but also confirmed PKRs are able to use a pocket located in the upper part of the TM bundle among TMs 3,4,5,6, and 7, the extracellular entrance, were synthetic small-molecule supposedly bind.

In-vitro experiments using BRET technology confirmed results we previously obtained for PC-1 and PC-7, from competitive binding experiments labelling the PKRs with ^{125}I MIT [9].

Our docking models show residues at position 4.64 (T192 in PKR$_1$ and A201 in PKR$_2$, the only non-conserved residue of the binding sites between PKR$_1$ and PKR$_2$), are responsible of the selectivity of PC-1 towards PKR$_1$. T4.64 (T192) in PKR$_1$ potentially stabilizes the ethyl benzene group by offering an extra methyl group, enhancing the hydrophobic of this region. All the compounds containing a halogen atom instead of the ethyl group in *para*-position of the benzyl pharmacophore of the 5-position of the triazinedione scaffold resulted more selective and displayed higher affinity for PKR$_1$.

Interestingly, PC-25, which contains a bromine atom displayed the highest affinity for PKR$_1$ (~18 times higher than PC-1) and the highest selectivity (~300 times). Despite the fact PC-35, containing iodine, has not the highest affinity, the observed trend in binding is likely ascribable to the formation of a halogen bond. Halogen bond, is a specific semi-directional molecular interaction between a halogen atom, acting as a Lewis acid, and an electron-rich partner (O, N, or S acting as Lewis basis) and which strength follow the size of the positively charged σ-hole on the tips of the atoms, thus I>Br>Cl>F.

They are abundant in biological systems[18] and database surveys reveal that halogen bonding is the prevalent interaction between halogenated ligand and target protein [19, 20]. Moreover around 25% of the "top 200 brand name drugs by retail dollar in 2009" possess halogen atoms in their molecular structures [21]. Therefore, halogens have a key role in drug development. The trend in affinity of halogenated compounds to PKR$_1$ follow the halogen bond trend, I>Br>Cl>F with the exception of iodine, while no clear trend is observed in the affinity to PKR$_2$, as expected since it misses a Lewis base in position 4.64. Following and confirming the docking of PC-1, compounds PC-7, PC-18, PC-25 and P-35, are likely forming halogen bonds with the hydroxyl group of T4.64 (**Fig. 5C**) explaining both the higher affinity of these compounds to PKR$_1$ as well as their selectivity.

Despite their affinity trend is clearly following the halogen bond strength trend, no statistically difference is observed in the binding of PC-7, PC-18 and PC-35. Wilcken *et al.*[21], in an analysis of the halogen bonds found in PDB and involving threonines, observed that most of the -I···O- distances are of in the range of 5.50-6Å, while most of the Cl···O was of around 3.5Å.

The calculated distances between the halogens of PC-7, PC-18, PC-25 and P-35 and the oxygen of T4.64 are of 3.0Å±0.2, which perfectly fits with many of the observed [21] halogen bonds between Br-containing compounds and threonines, thus explaining why PC-25 is statistically binding stronger PKR$_1$ than PC-7, PC-18 and PC-35. Moreover the iodine of PC-35 is likely too close to the oxygen of T4.64 thus limiting the quality of its halogen bond.

In-vivo all these compounds were able to antagonize dose-dependently the hyperalgesia induced by the i.pl. injection of 5 ng Bv8. In PKR$_1$(-/-) mice, in which only the receptor-2 is still present, higher doses were necessary than in PKR$_2$(-/-) mice which still express the receptor-1. The dose ratio well mirrored the selectivity for the PKR$_1$. Hence this *in-vivo* test performed on mice expressing only one of two PKRs is a quick and reliable method to evaluate antagonists of the prokineticin system.

REFERENCES:

1. Lattanzi R, Giannini E, Melchiorri P and Negri L: Pharmacology of Bv8: a new peptide from amphibian skin. British Journal of Pharmacology 2001; 133: 45P.
2. Kaser A, Winklmayr M, Lepperdinger G andKreil G: The AVIT protein family. Secreted cysteine-rich vertebrate proteins with diverse functions. EMBO Reports 2003; 4: 469–473.
3. Negri L, Lattanzi R, Giannini E, Canestrelli M, Nicotra A and Melchiorri P: Bv8/prokineticins and their receptors: a new pronociceptive system. International Review of Neurobiology 2009; 85: 145-157.
4. Shojaei F, Wu X, Zhong C, Yu L, Liang XH, Yao J, Blanchard D, Bais C and Peale FV, van Bruggen N, Ho C, Ross J, Tan M, Carano RAD, Meng YG and Ferrara N: Bv8 regulates myeloid-cell-dependent tumour angiogenesis. Nature 2007; 450: 825-831.
5. Dorsh M, Qui Y, Soler D, Frank N, Duong T, Goodearl A, O'neil S, Lora J and Fraser C: PK1/EG-VEGF induces monocyte differentiation and activation. Journal of Leukocyte Biology 2005; 78: 426-434.
6. Franchi S, Giannini E, Lattuada D, Lattanzi R, Tian H, Melchiorri P, Negri L, Panerai AE and Sacerdote P: The prokineticin receptor agonist Bv8 decreases IL-10 and IL-4 production in mice splenocytes by activating prokineticin receptor-1.BMC Immunology 2008; 9: 60-73.
7. Giannini E, Lattanzi R, Nicotra A, Campese A F, Grazioli P, Screpanti I, Balboni G, Salvadori S, Sacerdote P and Negri L: The chemokine Bv8/prokineticin 2 is up-regulated in inflammatory granulocytes and modulates inflammatory pain. Proc. Natl. Acad. Sci. USA. 2009; 106: 14646-14651.
8. Maftei D, Marconi V, Florenzano F, Giancotti LA, Castelli M, Moretti S, Borsani E, Rodella LF, Balboni G, Luongo L, Maione S, Sacerdote P, Negri L and Lattanzi R: Controlling the activation of the Bv8/Prokineticin system reduces neuroinflammation and abolishes thermal and tactile hyperalgesia in neuropathic animals. British Journal of Pharmacology 2014; 171: 4850–4865.
9. Balboni G, Lazzari I, Trapella C, Negri L, Lattanzi R, Giannini E, Nicotra A, Melchiorri P, Visentin S, De Nuccio C and Salvadori S: Triazine compounds as antagonists at Bv8-prokineticin receptors. Journal of Medicinal Chemistry 2008; 51: 7635-7639.
10. Negri L and Lattanzi R: Bv8/PK2 and prokineticin recepors: a druggable pronociceptive system Current Opinion in Pharmacology 2012; 12: 62-66.
11. Martucci C, Franchi S, Giannini E, Tian H, Melchiorri P, Negri Land Sacerdote P:Bv8, the amphibian homologue of the mammalian prokineticins, induces a proinflammatory phenotype of mouse macrophages. British Journal of Pharmacology 2006; 147 (2): 225-234.
12. Congiu C, Onnis V, Deplano A, Salvadori S, Marconi V, Maftei D, Negri L, Lattanzi R and Balboni G: A new convenient synthetic method and preliminary pharmacological characterization of triazinediones as prokineticin receptor antagonists. European Journal of Medicinal Chemistry 2014; 81: 334-340.
13. Negri L and Lattanzi R: Bv8-prokineticins and their receptors: modulators of pain. Current Pharmaceutical Biotechnology 2011; 12(10):1720-1727.
14. Molinari P, Casella I and Costa T: Functional complementation of high efficiency resonance energy transfer: a new tool for the study of protein binding interactions in living cells. Biochemistry Journal 2008; 409: 251–261.
15. Molinari P, Ambrosio C, Riitano D, Sbraccia M, Gro MC and Costa T: Promiscuous coupling at receptor-Gα fusion proteins. The receptor of one covalent complex interacts with the α-subunit of another. Journal of Biological Chemistry 2003; 278: 15778-15788.
16. Mollay C, Wechsel berger C, Mignogna G, Negri L, Melchiorri P, Barra D and Kreil G: Bv8, a small protein from frog skin and its homologue from snake venom induce hyperalgesia in rats. European Journal of Pharmacology 1999; 374: 189-196.
17. Levit A, Yarnitzky T, Wiener A, Meidan R and Niv MY. Modeling of human prokineticin receptors: interactions with novel small-molecule binders and potential off-target drugs. PLoS One 2011; 6 (11): e27990.
18. Auffinger P, Hays FA, Westh of E and Ho PS: Halogen Bonds in Biological Molecules. Proc Natl Acad Sci USA 2004; 101: 16789–16794.
19. LuY, Shi T, Wang Y, Yang H, Yan X, Luo X, Jiang H and Zhu W: Halogen Bonding: A Novel Interaction for Rational Drug Design? Journal of Medicinal Chemistry 2009; 52: 2854–2862.
20. Xu Z, Liu Z, Chen T, Chen T, Wang Z, Tian G, Shi J, Wang X, Lu Y, Yan X, Wang G, Jiang H, Chen K, Wang S, Xu Y, Shen J and Zhu W: Utilization of Halogen Bond in Lead Optimization: a Case Study of Rational Design of Potent Phosphodiesterase Type 5 (PDE5) Inhibitors. Journal of Medicinal Chemistry 2011; 54: 5607–5611.
21. Wilcken R, Zimmermann MO, Lange A, Joerger AC and Boeckler FM: Principles and Applications of Halogen Bonding in Medicinal Chemistry and Chemical Biology. Journal of Medicinal Chemistry 2013; 56: 1363–1388

5. Full Papers

Inhibitory effect of positively charged triazine antagonists of prokineticin receptors on the transient receptor vanilloid type-1 (TRPV1) channel

Luciano De Petrocellis [a,*], Aniello Schiano Moriello [a], Joon Seok Byun [b], Joo Mi Sohn [b], Jae Yeol Lee [b], Ana Vázquez-Romero [c], Maria Garrido [c], Angel Messeguer [c], Fang-Xiong Zhang [d], Gerald W. Zamponi [d], Alessandro Deplano [e], Cenzo Congiu [e], Valentina Onnis [e], Gianfranco Balboni [e,**], Vincenzo Di Marzo [a,***]

[a] Endocannabinoid Research Group, Institute of Biomolecular Chemistry, National Research Council, Via Campi Flegrei 34, Comprensorio Olivetti, 80078 Pozzuoli, Naples, Italy
[b] Research Institute for Basic Sciences and Department of Chemistry, College of Sciences, Kyung Hee University, Seoul 130-701, Republic of Korea
[c] Department of Chemical and Biomolecular Nanotechnology and Department of Biological Chemistry and Molecular Modeling, Instituto de Química Avanzada de Cataluña (CSIC), Barcelona, Spain
[d] Department of Physiology and Pharmacology, Hotchkiss Brain Institute and Alberta Children's Hospital Research Institute, Cumming School of Medicine, University of Calgary, Calgary T2N 4N1, Canada
[e] Department of Life and Environmental Sciences, Unit of Pharmaceutical, Pharmacological and Nutraceutical Sciences, University of Cagliari, I-09124 Cagliari, Italy

ABSTRACT

Four positively charged compounds, previously shown to produce analgesic activity by interacting with prokineticin receptor or T-type calcium channels, were tested for their ability to inhibit capsaicin-induced elevation of intracellular Ca^{2+} in HEK-293 cells stably transfected with the human recombinant TRPV1, with the goal of identifying novel TRPV1 open-pore inhibitors. **KYS-05090** showed the highest potency as a TRPV1 antagonist, even higher than that of the open-pore triazine inhibitor **8aA**. The latter showed quite remarkable agonist/desensitizer activity at the rat recombinant TRPM8 channel. The activity of **KYS-05090** and the other compounds was selective because none of these compounds was able to modulate the rat TRPA1 channel. Open-pore inhibitors of TRPV1 may be a new class of multi-target analgesics with lesser side effects, such as loss of acute pain sensitivity and hyperthermia, than most TRPV1 antagonists developed so far.

© 2015 Published by Elsevier Ltd.

1. Introduction

The transient receptor potential vanilloid 1 (TRPV1) was the first identified member of a family of thermosensory receptors currently known as thermoTRPs, which encompass cold-, warm-, and heat-activated channels [1]. TRPV1 is a nonselective cation channel with high Ca^{2+} permeability, involved in somatosensation, chemical and thermal nociception and pain, and chronic neuroinflammatory conditions. It is also known as the 'capsaicin receptor', because capsaicin, the pungent principle of chili peppers, is a specific TRPV1 activator [2–4]. Endogenous mediators, like the endocannabinoid anandamide and 2-arachidonoyl glycerol [5–8], and some eicosanoids [9–10], also activate TRPV1 channels. The validation of TRPV1 as a therapeutic target for pain prompted the development of several TRPV1 antagonists that have entered clinical trials for the treatment of acute, chronic and neuropathic pain. [11–12]. However, complete pharmacological blocking of TRPV1 with high affinity irreversible, competitive vanilloid antagonists can result in hyperthermia and side effects [13].

Uncompetitive antagonists are activity-dependent inhibitors that specifically bind to the agonist–receptor complex or to the open state of the channel, blocking only highly activated receptors. Open-channel blockers can only access the channel when it is open, recognizing a binding site located deep within the
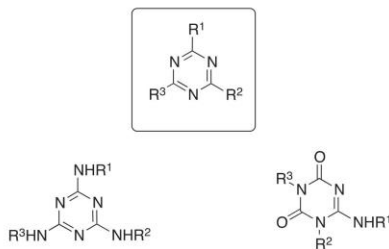

Fig. 1. General structure of triazines. On the left: triazine derivative type **8aA**. On the right: triazinedione type derivative.

pore. A class of compounds, which act as uncompetitive TRPV1 antagonists, are 1,3,5-triazine derivatives (Fig. 1). Triazine **8aA** [(2,4-bis(2′-(3″-indolyl) ethylamino)-6-(3′-(N,N-dimethylamino)-propylamino)-1,3,5-triazine)] (Fig. 1) has been recently reported as the most potent TRPV1 blocker [14]. **8aA** shares some structural features with a second family of 1,3,5-triazines derivatives (Fig. 1), which have been shown to be antagonists at prokineticin receptors (PKRs), as assessed by evaluating their inhibition of intracellular Ca^{2+} mobilization induced by the peptide Bv8 [15]. Bombina variegata 8 (Bv8) is a peptide (8 kDa) secreted by the frog skin, and acts as a selective agonist for two G-protein–coupled receptors, the prokineticin receptors of type 1 and 2, PKR1 and PKR2, expressed in dorsal root ganglia (DRG), in the outer layers of the dorsal horns of the spinal cord, and in peripheral terminals of nociceptor axons. In fact, studies in the mouse, rat, cattle, monkey, and man, identified orthologues of Bv8. Two human cDNAs have been cloned encoding two secreted proteins of 86 and 81 amino acids [16]. These two mammalian proteins were named prokineticin 1 (PK1, or EG-VEGF) and prokineticin 2 (PK2 or mBv8), which is an orthologue of amphibian Bv8 (for reviews see [17–18]), and were later shown to act as ligands for PKR1 and PKR2 [19–21]. Affinity of Bv8 for the receptors is comparable to that of PK2 and is about 40 times higher than that of PK1 [18]. Bv8/PKs are peripheral and central pain modulators: activation of nociceptor PKRs by Bv8 in rats and mice produces sensitization to thermal and mechanical stimuli, and mice lacking the PKRs or PK2 are less sensitive to noxious stimuli than wild type mice [22–23]. Very recently our group described the synthesis of compounds capable to reduce in vivo the Bv8-induced thermal hyperalgesia when injected into the hind paw of mice 5 min before Bv8. In particular, some triazinediones (Fig. 1) showed very high efficacy as prokineticin receptor antagonists [24].

The transient receptor melastatin type-8 (TRPM8) ion channel was identified as the principal sensor for environmental cold in mammals [25–26]. No endogenous agonists for the TRPM8 channel have been so far identified, although there is recent evidence that testosterone exerts an ionotropic effect on TRPM8 at picomolar concentration [27], while the endocannabinoids anandamide and N-arachidonoyldopamine produce instead antagonism [28]. Apart from its role in thermosensation, acute activation of TRPM8 can have analgesic effects [29] suggesting that neuronal TRPM8 may play a neurogenic anti-inflammatory role. Very recently it has been shown that the synthetic TRPM8 agonist icilin (i) has a potent anti-inflammatory effect, and (ii) inhibits E2F1 transcription factor-mediated cell cycle regulatory programs in prostate cancer [30], thus suggesting the potential relevance of icilin and 'icilin-like' compounds as therapeutic tools for the treatment of a variety of pathological conditions [31].

Here, we tested four positively charged compounds, previously shown to produce analgesic activity by interacting with PKRs or T-type calcium channels, for their ability to modulate TRPM8 and TRPV1 activity in vitro as potential open-pore inhibitors.

2. Material and methods

2.1. Materials

MEM medium, foetal bovine serum (FBS), Fluo-4 AM, Pluronic® F-127, Geneticin G-418 and ionomycin were obtained from Invitrogen (Carlsbad, CA, USA). Dimethyl sulfoxide (DMSO), trypsin/EDTA, penicillin, streptomycin and all other chemicals were purchased from Sigma–Aldrich (St. Louis, MO, USA).

2.2. Cell culture

Human embryonic kidney HEK-293 cells were purchased from ATCC (LGC Standards, Sesto San Giovanni, Milan, Italy).

HEK-293 and HEK-293 stably over-expressing human TRPV1, or rat TRPA1 or rat TRPM8 and selected by G-418 (Geneticin; 600 μg/ml), were grown as monolayers on 100 mm diameter Petri dishes in minimum essential medium supplemented with non-essential amino acids, 10% foetal bovine serum, and 2 mM glutamine, and maintained under 5% CO_2 at 37 °C.

2.3. TRP functional assays

Cell-based fluorescence assays of calcium influx upon TRPV1 activation were performed as described:

The effect of the substances on $[Ca^{2+}]_i$ was determined by using the selective intracellular fluorescent probe for Ca^{2+} Fluo-4. On the day of the experiment the cells were loaded for 1 h at 25 °C with 4 μM Fluo-4 methylester (Molecular Probes) in DMSO containing 0.03% Pluronic. After the loading, cells were washed with Tyrode pH 7.4 (145 mM NaCl, 2.5 mM KCl, 1.5 mM CaCl₂, 1.2 mM MgCl₂, 10 mM D-glucose, and 10 mM HEPES), resuspended in Tyrode and transferred (~100,000 cells) to the cuvette of the fluorescence detector (PerkinElmer LS50B Waltham, MA, USA) under continuous stirring. Experiments were carried out by measuring cell fluorescence at 25 °C ($\lambda_{EX} = 488$ nm, $\lambda_{EM} = 516$ nm) before and after the addition of the test compounds at various concentrations. Potency was expressed as the concentration of test compounds exerting a half-maximal agonist effect (i.e. half-maximal increases in $[Ca^{2+}]_i$) (EC_{50}). The efficacy of TRPV1 and TRPM8 agonists was determined by normalizing their effect to the maximum Ca^{2+} influx effect on $[Ca^{2+}]_i$ observed with application of 4 μM ionomycin, while the effects of TRPA1 agonists are expressed as a percentage of the effect obtained with 100 μM allylisothiocyanate (AITC). When significant, the values of the effect on $[Ca^{2+}]_i$ in wild type HEK293 (i.e. not transfected with any TRP construct) were taken as baselines and subtracted from the values obtained from transfected cells.

Antagonist/desensitizing behaviour was evaluated against capsaicin (0.1 μM) for TRPV1 against AITC (100 μM) for TRPA1 and icilin (0.25 μM) for TRPM8, by adding the test compounds in the quartz cuvette 5 min before stimulation of cells with agonists. In another set of experiments the loading cells were washed with Tyrode pH 7.4 without calcium ions (145 mM NaCl, 2.5 mM KCl, 2.7 mM MgCl₂, 10 mM D-glucose, and 10 mM HEPES), resuspended in the same buffer and treated with 1 μM capsaicin for 1 h (at the aim of dilating the pore and facilitate the entry of charged substances) in presence of different concentrations of the potential antagonist compound. After that the cells were extensively washed in order to remove capsaicin, balanced in Tyrode's buffer contained calcium and then treated with capsaicin 0.1 μM. Data are

expressed as the concentration exerting a half-maximal inhibition of agonist-induced $[Ca^{2+}]_i$ elevation (IC_{50}), which was calculated using GraphPad Prism® software. The effect on $[Ca^{2+}]_i$ exerted by agonist alone was taken as 100%. Dose–response curves were fitted by a sigmoidal regression with variable slope. All determinations were performed at least in triplicate. Statistical analysis of the data was performed by analysis of variance at each point using ANOVA followed by the Bonferroni's test.

2.4. Electrophysiological studies

DRG neurons were isolated as previously described [32]. Neurons on a glass coverslip were transferred into an external bath solution of 150 mM NaCl, 5 mM KCl, 3.5 mM MgCl$_2$, 10 mM HEPES, and 10 mM glucose at pH 7.4. Borosilicate glass pipettes (Sutter Instrument Co., Novato, CA, USA) (3–5 MΩ) were filled with internal solution containing 140 mM KCl, 2.5 mM CaCl$_2$, 1 mM MgCl$_2$, 5 mM EGTA, 10 mM HEPES, 2 mM Na-ATP and 0.3 mM Na-GTP, pH 7.3. Whole-cell patch clamp recordings were performed by using an EPC 10 amplifier (HEKA Elektronik, Bellmore, NY, USA) linked to a personal computer equipped with Pulse (V8.65) software (HEKA Elektronik). After seal formation, the membrane beneath the pipette was ruptured and the pipette solution was allowed to dialyze the cell for 3–5 min before recording. Currents were elicited by application of 1 μM capsaicin from a holding potential of −60 mV. Data were recorded at 10 kHz and filtered at 2.9 kHz.

Data analysis was performed by using online analysis built in Pulse software, and graphs were prepared by using GraphPad Prism 5 (GraphPad Software, La Jolla, CA, USA). Error bars plotted represent the mean values ± standard error.

3. Results and discussion

3.1. TRPV1 antagonist activity

The compounds were evaluated for TRPV1 antagonist activity based on their ability to block capsaicin-induced elevation of intracellular Ca^{2+} in HEK-293 cells stably transfected with the human recombinant TRPV1 (hTRPV1-HEK-293 cells). The tests were carried out with a fluorescence-based intracellular calcium detection assay for capsaicin. We started our investigation with the compound **8aA** 2,4-Bis(4′-fluorophenethylamino)-6-(3′-(N,N-dimethylamino)-propylamino)-1,3,5-triazine, a triazine-based TRPV1 receptor open channel uncompetitive antagonist, among the strongest TRPV1 open channel blockers described to date [14]. The pK_a value calculated with Epik (Epik, version 2.1, Schrödinger, L.L.C.: New York, NY, 2010) [33–34] for this compound is 9.51, indicating that it is protonated at physiological pH (7.4, at which our test is performed). Because known charged blockers have previously displayed agonistic activity, we also sought to check whether **8aA** activates TRPV1. We observed that **8aA** shows no agonist activity up to 100 μM, confirming that this compound is a pure blocker. Indeed, we calculated an inhibitory activity of the capsaicin (0.1 μM) response of **8aA** with $IC_{50} = 21.7 \pm 0.7$ μM from the corresponding dose–response curve in hTRPV1–HEK-293 cells. The IC_{50} value was therefore much higher than that measured by voltage-clamp against rat TRPV1 channels heterologously expressed in Xenopus oocytes ($IC_{50} = 0.05 \pm 0.007$ μM), as reported by Vidal-Mosquera et al. [14].

The compound **8aA** is endowed with some features in common with some prokineticin antagonists based on the triazinedione scaffold, among which compounds with EC_{50} analgesic activity values in picoM range, i.e. **PC-7** [1-(2-((5-(4-fluorobenzyl)-1-(4-methoxybenzyl)-4,6-dioxo-1,4,5,6-tetrahydro-1,3,5-triazin-2-yl)
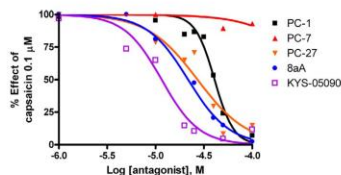

Fig. 2. Effect of a 5 min pre-incubation with the tested compound on capsaicin (100 nM)-induced Ca^{2+} elevation in HEK-293 cells over-expressing the human TRPV1. The effect on [Ca^{2+}]$_i$ exerted by capsaicin 100 nM alone was considered as 100%.

amino) ethyl) guanidine] ($EC_{50} = 0.31$ pM) and **PC-27** [1-(2-((1-(4-methylbenzyl)-5-(4-(trifluoromethyl) benzyl)-4,6-dioxo-1,4,5,6-tetrahydro-1,3,5-triazin-2-yl) amino) ethyl) guanidine] ($EC_{50} = 0.033$ pM), both containing an 4-halogen fluoride atom substituted benzyl group in position 5, which possibly explains why they are 10 and 100 times more potent, respectively than **PC-1** [1-(2-((5-(4-ethylbenzyl)-1-(4-methoxybenzyl)-4,6-dioxo-1,4,5,6-tetrahydro-1,3,5-triazin-2-yl) amino) ethyl) guanidine] ($EC_{50} = 5.8$ pM), which bears a 4-ethylbenzyl group in position 5 [22]. These compounds mimic the structural features required for Bv8 binding to PKRs [17,35], they present a triazine-guanidine moiety that mimics the N-terminal AVITGA sequence, whereas the benzyl moiety is orientated like the conserved tryptophan residue in position 24. Importantly, **PC-1**, which preferentially binds PKR1, injected intraplantar at the dose of 30 ng, significantly reduced capsaicin-induced hyperalgesia [17], suggesting that it may also inhibit TRPV1. It is to be noted that peripheral nociceptors expressing the ion channels, TRPV1 and TRPA1, co-express PKR1, which most probably contributes to the development of inflammatory hyperalgesia [22,36]. Indeed, some Bv8-responding DRG neurons also express neuromediators implicated in pain processing such as calcitonin gene-related peptide (CGRP) and substance P and release these neuropeptides upon exposure to Bv8. The glial cell line-derived neurotrophic factor (GDNF) induced 'de novo' expression of functional PKRs suggesting a possible upregulation of PKRs after the tissue damage and inflammation that cause heat hyperalgesia by sensitizing TRPV1 through PKC activation [36]. PKR1 gene deletion or PKR1 blockade with **PC-1**, markedly reduced the inflammation-induced hypersensitivity and the up-regulation of Bv8/PK2 [15,23,37]. Furthermore, the prokineticin system plays a role in neuroinflammation and in the evolution of the neuropathic pain, and **PC-1** administration at peripheral or central levels alleviates an established neuropathic hyperalgesia and prevents the activation of glia and the increased production of inflammatory cytokines [38].

In view of the above reported in vivo activity of the PKR1 antagonist **PC-1** against capsaicin-induced hyperalgesia, and of its chemical similarity with **8aA**, we extended the in vitro studies on TRPV1 to all three PKR antagonists, **PC-1**, **PC-7** and **PC-27**. The pK_a values calculated with Epik (Epik, version 2.1, Schrödinger, L.L.C.: New York, NY, 2010) [33–34] for these compounds is 12.44, indicating that they can be protonated at physiological pH more than **8aA**. The compounds showed no or very low (**PC-27** $EC_{50} > 50$ μM with an efficacy at 100 μM ∼20%) agonist activity (Table 1). However, **PC-27** and **PC-1** inhibited the capsaicin (0.1 μM)-induced response in hTRPV1-HEK-293 cells, although this effect was slightly weaker than that observed for **8aA**, whereas **PC-7** was not active as blocker (Fig. 2, Table 1).

Table 1
Structures and in vitro activity of studied compounds.

Code	Structure	TRPV1 IC$_{50}$, µM vs. capsaicin 0.1 µM (cells pre-treated with capsaicin)	TRPV1 EC$_{50}$, µM (efficacy at 100 µM)	TRPA1 IC$_{50}$, µM vs. AITC 100 µM	TRPA1 EC$_{50}$, µM (efficacy at 100 µM vs AITC 100 µM)
8aA		21.7 ± 0.7 (20.5 ± 1.9)	NA (<10)	>100	>50 (52.7 ± 2.4)
PC-1		40.8 ± 0.9 (40.5 ± 1.1)	NA (<10)	>100	NA (18.2 ± 0.1)
PC-7		>100 (>100)	NA (<10)	>100	NA (0)
PC-27		27.2 ± 1.9 (31.0 ± 1.0)	>50 (20.8 ± 0.1)	>50	>50 (42.6 ± 2.6)
KYS-05090		11.6 ± 0.7 (10.1 ± 0.5)	7.1 ± 1.9 (15.4 ± 2.0)	>50	13.3 ± 1.1 (27.6 ± 0.7)

NA = not active.

Most of the exploration so far has been focused on the 5-position benzyl group: consistent with calcium influx data from recombinant TRPV1 (Table 1), the substitution of the ethyl group with a fluorine atom in position 4 on the 5-benzyl group was not tolerated and the resulting compound did not show in vitro potency at blocking capsaicin activation of TRPV1. The introduction of a CF$_3$ in position 4 on the 5-benzyl group together with the simultaneous replacement of the methoxy group with a less polar methyl in position 4 on the 1-benzyl group resulted in the regaining in vitro activity, with slightly higher potency at blocking capsaicin activation of TRPV1 (IC$_{50}$ = 27.2 ± 1.9 µM).

3.2. TRPA1 activity

Responses to Bv8 were colocalized with responses to mustard oil, an activator of the channel TRPA1, which like TRPV1 is involved in nociception [39–41]. Furthermore, inflammatory heat hyperalgesia caused by mustard oil was also significantly lower in PKR1$^{-/-}$
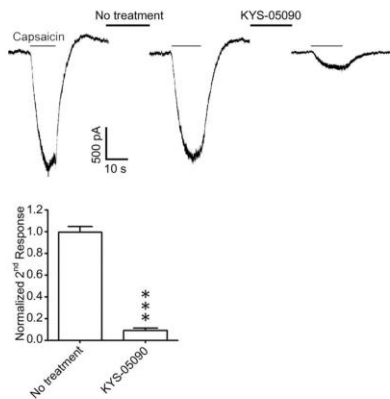
Fig. 3. KYS-05090 modulates capsaicin-evoked currents.
(Upper panel) Representative current responses to consecutive applications of 1 μM capsaicin without or with an intervening 3-min incubation of KYS-05090 (10 μM) in acutely dissociated dorsal root ganglion neurons from adult mice.
(Lower panel) Ratio of the second to the initial peak capsaicin response (mean ± SEM) in the absence or presence of an intervening KYS-05090 (10 μM) application. Capsaicin-evoked currents were significantly reduced after 3-min KYS-05090 pre-treatment ($p < 0.0001$, compared with no KYS-05090 treatment, $n = 4$).

mice [22], suggesting that these nonspecific proinflammatory stimuli act in part via release of PK and activation of PKR1 receptors. It seemed therefore interesting to study whether the test compounds interacted with TRPA1. However, none of the four compounds blocked mustard oil isothiocyanate-induced and TRPA1-mediated elevation of intracellular Ca^{2+} in HEK-293 cells stably transfected with the rat recombinant TRPA1 channel, as is shown in Table 1.

3.3. KYS-05090 activity

The T-type calcium channel blocker **KYS-05090** [2-(3-(1,1′-biphenyl-4-yl)-2-((5-(N,N-dimethylamino) pentyl)-N′-(methyl) amino)-3,4-dihydroquinazolin-4-yl)-N″-benzylacetamide] 2-hydrochloride was included in this study. Very recently the ability of **KYS-05090** to block the Ca^{2+} channel, and the dependence of **KYS-05090**-induced cell death on the $[Ca^{2+}]_i$ in a concentration- and time-dependent manner have been shown [42]. **KYS-05090** is not a trisubstituted triazine but a quite rigid dihydroquinazoline containing a cationic tertiary N,N-dimethylaminopentyl-N′-methyl- amine group (pK_a value calculated with Epik for this compound is 9.6, suggesting its protonation at physiological pH). This compound exhibited significant albeit very low agonist activity at both TRPV1 and TRPA1. However, **KYS-05090** showed the highest potency as an antagonist against TRPV1, even higher than that of **8aA**, with an IC_{50} value of 11.6 μM. Electrophysiological experiments performed on acutely dissociated dorsal root ganglion (DRG) neurons from adult mice confirmed the results of the calcium experiments. Fig. 3 shows that DRG neurons positive for TRPV1 exhibit significantly reduced capsaicin-evoked currents after a 3-min incubation with KYS-05090 (10 μM). For comparison, the IC_{50} found for **KYS-05090** when screened against TRPA1 was >50 μM.

TRPV1 is permeable by different ions with a preference for divalent species (Ca^{2+} and Mg^{2+}) over monovalent ions (Na^+, K^+ and Cs^+) [1]. Studies with ATP-gated ion channels of the P2X family suggested that prolonged agonist exposure increases the pore size, leading to enhanced permeability of the channel to cations [43–44]. In the case of TRPV1 the permeability to different cationic species varies in a time-dependent and an agonist concentration-dependent manner, allowing permeation of large organic cations [45]. During prolonged activation with vanilloids, permeability to large cations increases, although the channel continues to exclude anions. One worth noting characteristic of TRPV channels that has been proposed to explain Ca^{2+} selectivity in TRPV1 is the presence of negatively charged residues in the outer region of the selectivity filter, due to the presence of acidic residue E648 and D646, which exert an electrostatic attraction on cations [46]. It has been shown that also TRPV3 [47], and TRPA1 activation resulted in dynamic changes in permeability to cations [48–50]. Alkaline pH has been found to cause helix dilation of the pore for TRPV5 [51], whereas TRPM8 activation does not seem produce significant changes in ion selectivity [48]. The three-dimensional structure of the TRPV1 channel was recently determined by single particle electron cryo-microscopy, allowing us to explore ionic conduction in TRP channels at atomic detail [52]. Pore dilation may facilitate the entry of otherwise impermeant drugs into cells [53], although the quaternary derivative of lidocaine QX-314 seems to enter through the standard pore and does not require pore dilation [54].

3.4. Experiments on hTRPV1-HEK-293 cells pre-treated with capsaicin

When the experiments were performed on cells pre-treated with 1 μM capsaicin for 1 h with the aim of dilating the pore and facilitate the entry of charged substances, all the tested compounds inhibited the capsaicin (0.1 μM)-induced response in hTRPV1-HEK-293 cells with about the same IC_{50} exhibited without pre-treatment (Table 1).

Thus, the pore dilation previously measured in capsaicin-bound TRPV1 is still not sufficient to account for TRPV1 permeability to the large cations used in the present study. One possible explanation for our findings is that the capsaicin-bound channel represents an intermediate state, and that conformations of a flexible TRPV1 selectivity filter exhibiting even greater pore expansion are transient and possibly inducible by large cations themselves as they pass through the activated channel [55].

3.5. TRPM8 activity

To assess channel selectivity, the five compounds tested here were screened also against TRPM8 (Table 2) by measuring their effect on TRPM8-mediated elevation of intracellular Ca^{2+} in HEK-293 cells stably transfected with the rat recombinant TRPM8 channel. The triazine **8aA** activated and subsequently desensitized TRPM8 and the IC_{50} value observed desensitization was quite remarkable (0.95 ± 0.03 μM) (Fig. 4 and Table 2). This effect was surprising since it has been shown that pore dilation does not occur in TRPM8 channels [48]. The interaction of **8aA** with TRPM8 might be explained by evidence showing that this channel can be activated at the outer pore (EC_{50} 1.1 ± 0.1 μM). Menthol interacts with a hydrophobic pocket within the S1–S4 transmembrane bundle, and causes conformational rearrangements that lead to gate opening [56]. Furthermore, TRPV1 can be activated at the outer pore by a bivalent tarantula toxin involving the extracellular domains of S5 and S6 [57]. Vanillotoxins activate TRPV1 channel in the outside-out, but not inside-out configuration, consistent with an extracellular site of action, and ruling against a role for the S3-S4 domain in TRPV1-vanillotoxin interaction. Recent reports have

Table 2
Structures and in vitro TRPM8 activity of studied compounds.

Code	Structure	TRPM8 IC$_{50}$, μM vs. icilin 0.25 μM	TRPM8 EC$_{50}$, μM (efficacy at 100 μM)
8aA		0.95 ± 0.03	1.1 ± 0.1 (70.2 ± 1.1)
PC-1		57.5 ± 0.8	NA (<10)
PC-7		>100	NA (<10)
PC-27		34.2 ± 1.5	37.0 ± 4.7 (31.1 ± 1.7)
KYS-05090		11.0 ± 0.8	9.8 ± 1.2 (17.2 ± 1.3)

shown a hydrophobic binding pocket for capsaicin and anandamide that is accessible from the extracellular side [52,58], thus indicating that these compounds access TRPV1 also from the outside [59]. Our results suggest that some TRPM8 negative charged aminoacids at extracellular domains could interact with the protonated **8aA** at physiological pH. Similarly, but to a lesser extent, also **PC-27** and **KYS-05090**, but not **PC-1** and **PC-7**, activate and consequently desensitize TRPM8 (Table 2).
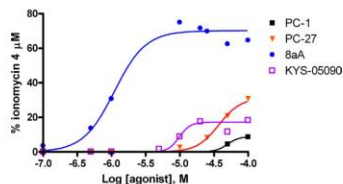
Fig. 4. Effect on intracellular Ca²⁺ elevation in HEK-293 cells over-expressing rat TRPM8. Data are expressed as % of the effect observed with 4 μM ionomycin.

4. Conclusions

Based on past evidence obtained with **8aA**, we have conducted studies on previously reported analgesic and positively charged compounds, such as three triazine inhibitors of PKRs, and a dihydroquinazoline T-type calcium selective channel blocker, with the goal of identifying novel TRPV1 open-pore inhibitors with acceptable in vitro potency and possible use as analgesics with lesser side effects than most TRPV1 antagonists developed so far. The latter compounds antagonize TRPV1 regardless of its endogenous activators, whereas TRPV1 open-pore inhibitors only act when the channel is prolongedly activated by endogenous noxious ligands, thus being potentially less prone to produce side effects such as loss of acute pain sensitivity and hyperthermia. Further chemical modification of **KYS-05090**, on the one hand, and **PC-27** and **PC-1**, on the other hand, with the aim of enhancing their potencies as potential open-pore inhibitors of TRPV1 without diminishing their capability of antagonizing T-type channels or PKRs, respectively, might lead to efficacious multi-target analgesics. None of the compounds tested showed significant activity at rat TRPA1 channels. However, we revealed that the previously developed open-pore TRPV1 antagonist, **8aA**, behaves as a relatively potent agonist/desensitizer of the rat recombinant TRPM8 channel.

Author contributions

Luciano De Petrocellis, Aniello Schiano Moriello, Joon Seok Byun, Joo Mi Sohn, Jae Yeol Lee, Ana Vázquez-Romero, Maria Garrido, Angel Messeguer, Alessandro Deplano, Cenzo Congiu, Valentina Onnis, Gianfranco Balboni and Vincenzo Di Marzo designed the study; Gerald W Zamponi and Fang-Xiong Zhang designed and performed the electrophysiological studies; Luciano De Petrocellis and Aniello Schiano Moriello performed the experiments and analyzed the data; Luciano De Petrocellis, Gianfranco Balboni and Vincenzo Di Marzo wrote the paper. All authors read and approved the final manuscript.

Conflicts of interest

The authors declare no conflict of interest.

References

[1] M.J. Caterina, M.A. Schumacher, M. Tominaga, T.A. Rosen, J.D. Levine, D. Julius, The capsaicin receptor: a heat-activated ion channel in the pain pathway, Nature 389 (1997) 816–824.

[2] A. Szallasi, P.M. Blumberg, Vanilloid (capsaicin) receptors and mechanisms, Pharmacol. Rev. 51 (1999) 159–212.

[3] J. O'Neill, C. Brock, A.E. Olesen, T. Andresen, M. Nilsson, A.H. Dickenson, Unravelling the mystery of capsaicin: a tool to understand and treat pain, Pharmacol. Rev. 64 (2012) 939–971.

[4] J. Vriens, G. Appendino, B. Nilius, Pharmacology of vanilloid transient receptor potential cation channels, Mol. Pharmacol. 75 (2009) 1262–1279.

[5] P.M. Zygmunt, J. Petersson, D.A. Andersson, H. Chuang, M. Sørgård, V. Di Marzo, D. Julius, E.D. Högestätt, Vanilloid receptors on sensory nerves mediate the vasodilator action of anandamide, Nature 400 (1999) 452–457.

[6] L. De Petrocellis, T. Bisogno, M. Maccarrone, J.B. Davis, A. Finazzi-Agrò, V. Di Marzo, The activity of anandamide at vanilloid VR1 receptors requires facilitated transport across the cell membrane and is limited by intracellular metabolism, J. Biol. Chem. 276 (2001) 12856–12863.

[7] P.M. Zygmunt, A. Ermund, P. Movahed, D.A. Andersson, C. Simonsen, B.A. Jönsson, A. Blomgren, B. Birnir, S. Bevan, A. Eschalier, C. Mallet, A. Gomis, E.D. Högestätt, Monoacylglycerols activate TRPV1—a link between phospholipase C and TRPV1, PLoS One 8 (2013) e81618.

[8] S. Petrosino, A. Schiano Moriello, S. Cerrato, M. Fusco, A. Puigdemont, L. De Petrocellis, V. Di Marzo, The anti-inflammatory mediator palmitoylethanolamide enhances the levels of 2-arachidonoyl-glycerol and potentiates its actions at transient receptor potential vanilloid type-1 channels 1, Br. J. Pharmacol. (2015). http://dx.doi.org/10.1111/bph.13084

[9] S.W. Hwang, H. Cho, J. Kwak, S.Y. Lee, C.J. Kang, J. Jung, S. Cho, K.H. Min, Y.G. Suh, D. Kim, U. Oh, Direct activation of capsaicin receptors by products of lipoxygenases: endogenous capsaicin-like substances, Proc. Natl. Acad. Sci. U. S. A. 97 (2000) 6155–6160.

[10] L. De Petrocellis, A. Schiano Moriello, R. Imperatore, L. Cristino, K. Starowicz, V. Di Marzo, A re-evaluation of 9-HODE activity at TRPV1 channels in comparison to anandamide: enantioselectivity and effects at other TRP channels and in sensory neurons, Br. J. Pharmacol. 167 (2012) 1643–1651.

[11] A. Ferrer-Montiel, A. Fernández-Carvajal, R. Planells-Cases, G. Fernández-Ballester, J.M. González-Ros, A. Messeguer, R. González-Muñiz, Advances in modulating thermosensory TRP channels, Expert Opin. Ther. Pat. 22 (2012) 999–1017.

[12] L. De Petrocellis, A. Schiano Moriello, Modulation of the TRPV1 channel: current clinical trials and recent patents with focus on neurological conditions, Recent Pat. CNS Drug Discov. 8 (2013) 180–204.

[13] N.R. Gavva, Body-temperature maintenance as the predominant function of the vanilloid receptor TRPV1, Trends Pharmacol. Sci. 29 (2008) 550–557.

[14] M. Vidal-Mosquera, A. Fernández-Carvajal, A. Moure, P. Valente, R. Planells-Cases, J.M. González-Ros, J. Bujons, A. Ferrer-Montiel, A. Messeguer, Triazine-based vanilloid 1 receptor open channel blockers: design, synthesis, evaluation, and SAR analysis, J. Med. Chem. 54 (2011) 7441–7452.

[15] G. Balboni, I. Lazzari, C. Trapella, L. Negri, R. Lattanzi, E. Giannini, A. Nicotra, P. Melchiorri, S. Visentin, C.D. Nuccio, S. Salvadori, Triazine compounds as antagonists at Bv8-prokineticin receptors, J. Med. Chem. 51 (2008) 7635–7639.

[16] M. Li, C.M. Bullock, D.J. Knauer, F.J. Ehlert, Q.Y. Zhou, Identification of two prokineticin cDNAs: recombinant proteins potently contract gastrointestinal smooth muscle, Mol. Pharmacol. 59 (2001) 692–698.

[17] L. Negri, R. Lattanzi, Bv8/PK2 and prokineticin receptors: a druggable pronociceptive system, Curr. Opin. Pharmacol. 12 (2012) 62–66.

[18] L. Negri, R. Lattanzi, E. Giannini, P. Melchiorri, Modulators of pain: Bv8 and prokineticins, Curr. Neuropharmacol. 4 (2012) 207–215.

[19] D.C. Lin, C.M. Bullock, F.J. Ehlert, J.L. Chen, H. Tian, Q.Y. Zhou, Identification and molecular characterization of two closely related G protein-coupled receptors activated by prokineticins/endocrine gland vascular endothelial growth factor, J. Biol. Chem. 277 (2002) 19276–19280.

[20] Y. Masuda, Y. Takatsu, Y. Terao, S. Kumano, Y. Ishibashi, M. Suenaga, M. Abe, S. Fukusumi, T. Watanabe, Y. Shintani, T. Yamada, S. Hinuma, N. Inatomi, T. Ohtaki, H. Onda, M. Fujino, Isolation and identification of EG-VEGF/prokineticins as cognate ligands for two orphan G-protein-coupled receptors, Biochem. Biophys. Res. Commun. 293 (2002) 396–402.

[21] T. Soga, Si. Matsumoto, T. Oda, T. Saito, H. Hiyama, J. Takasaki, M. Kamohara, T. Ohishi, H. Matsushime, K. Furuichi, Molecular cloning and characterization of prokineticin receptors, Biochim. Biophys. Acta 1579 (2002) 173–179.

[22] L. Negri, R. Lattanzi, E. Giannini, M. Colucci, F. Margheriti, P. Melchiorri, V. Vellani, H. Tian, M. De Felice, F. Porreca, Impaired nociception and inflammatory pain sensation in mice lacking the prokineticin receptor PKR1: focus on interaction between PKR1 and the capsaicin receptor TRPV1 in pain behaviour, J. Neurosci. 26 (2006) 6716–6727.

[23] E. Giannini, R. Lattanzi, A. Nicotra, A.F. Campese, P. Grazioli, I. Screpanti, G. Balboni, S. Salvadori, P. Sacerdote, L. Negri, The chemokine Bv8/prokineticin 2 is up-regulated in inflammatory granulocytes and modulates inflammatory pain, Proc. Natl. Acad. Sci. U. S. A. 106 (2009) 14646–14651.

[24] C. Congiu, V. Onnis, A. Deplano, S. Salvadori, V. Marconi, D. Maftei, L. Negri, R. Lattanzi, G. Balboni, A new convenient synthetic method and preliminary pharmacological characterization of triazinediones as prokineticin receptor antagonists, Eur. J. Med. Chem. 81 (2014) 334–340.

[25] D.D. McKemy, W.M. Neuhausser, D. Julius, Identification of a cold receptor reveals a general role for TRP channels in thermosensation, Nature 416 (2002) 52–58.

[26] A.M. Peier, A. Moqrich, A.C. Hergarden, A.J. Reeve, D.A. Andersson, G.M. Story, T.J. Earley, I. Dragoni, P. McIntyre, S. Bevan, A. Patapoutian, A TRP channel that senses cold stimuli and menthol, Cell 108 (2002) 705–715.

[27] S. Asuthkar, L. Demirkhanyan, X. Sun, P.A. Elustondo, V. Krishnan, P. Baskaran, K.K. Velpula, B. Thyagarajan, E.V. Pavlov, E. Zakharian, The TRPM8 protein is a testosterone receptor: II. Functional evidence for an ionotropic effect of testosterone on TRPM8, J. Biol. Chem. 290 (2015) 2670–2688.

[28] L. De Petrocellis, K. Starowicz, A. Schiano Moriello, M. Vivese, P. Orlando, V. Di Marzo, Regulation of transient receptor potential channels of melastatin type

8 (TRPM8): effect of cAMP, cannabinoid CB(1) receptors and endovanilloids, Exp. Cell Res. 313 (2007) 1911–1920.

[29] R. Ramachandran, E. Hyun, L. Zhao, T.K. Lapointe, K. Chapman, C.L. Hirota, S. Ghosh, D.D. McKemy, N. Vergnolle, P.L. Beck, C. Altier, M.D. Hollenberg, TRPM8 activation attenuates inflammatory responses in mouse models of colitis, Proc. Natl. Acad. Sci. U. S. A. 110 (2013) 7476–7481.

[30] S. Lee, J.N. Chun, S.-H. Kim, J.-H. Jeon, Icilin inhibits E2F1-mediated cell cycle regulatory programs in prostate cancer, Biochem. Biophys. Res. Commun. 441 (2013) 1005–1010.

[31] L. De Petrocellis, G. Ortar, A. Schiano Moriello, E.M. Serum, D.B. Rusterholz, Structure-activity relationships of the prototypical TRPM8 agonist icilin, Bioorg. Med. Chem. Lett. 25 (2015) 2285–2290.

[32] A.M. Beedle, J.E. McRory, O. Poirot, C.J. Doering, C. Altier, C. Barrere, J. Hamid, J. Nargeot, E. Bourinet, G.W. Zamponi, Agonist-independent modulation of N-type calcium channels by ORL1 receptors, Nat. Neurosci. 7 (2004) 118–125.

[33] J. Greenwood, D. Calkins, A. Sullivan, J. Shelley, Towards the comprehensive, rapid, and accurate prediction of the favorable tautomeric states of drug-like 62 molecules in aqueous solution, J. Comput.-Aided Mol. Des. 24 (2010) 591–604.

[34] J. Shelley, A. Cholleti, L. Frye, J. Greenwood, M. Timlin, M. Uchimaya, Epik: a software program for pK$_a$ prediction and protonation state generation for drug-like molecules, J. Comput.-Aided Mol. Des. 21 (2007) 681–691.

[35] R. Miele, R. Lattanzi, M.C. Bonaccorsi di Patti, A. Paiardini, L. Negri, D. Barra, Expression of Bv8 in Pichia pastoris to identify structural features for receptor binding, Protein Expression Purif. 73 (2010) 10–14.

[36] V. Vellani, M. Colucci, R. Lattanzi, E. Giannini, L. Negri, P. Melchiorri, P.A. McNaughton, Sensitization of transient receptor potential vanilloid 1 by the prokineticin receptor agonist Bv8, J. Neurosci. 26 (2006) 5109–5116.

[37] L. Negri, R. Lattanzi, Bv8-prokineticins and their receptors: modulators of pain, Curr. Pharm. Biotechnol. 12 (2011) 1720–1727.

[38] D. Maftei, V. Marconi, F. Florenzano, L.A. Giancotti, M. Castelli, S. Moretti, E. Borsani, L.F. Rodella, G. Balboni, L. Luongo, S. Maione, P. Sacerdote, L. Negri, R. Lattanzi, Controlling the activation of the Bv8/prokineticin system reduces neuroinflammation and abolishes thermal and tactile hyperalgesia in neuropathic animals, Br. J. Pharmacol. 171 (2014) 4850–4865.

[39] M. Tominaga, M.J. Caterina, Thermosensation and pain, J. Neurobiol. 61 (2004) 3–12.

[40] S.E. Jordt, D.M. Bautista, H.H. Chuang, D.D. McKemy, P.M. Zygmunt, E.D. Hogestatt, I.D. Meng, D. Julius, Mustard oils and cannabinoids excite sensory nerve fibres through the TRP channel ANKTM1, Nature 427 (2004) 260–265.

[41] L. De Petrocellis, A. Schiano Moriello, 2-Amino-4-arylthiazole compounds as TRPA1 antagonists (WO 2012085662): a patent evaluation, Expert Opin. Ther. Pat. 23 (2013) 119–147.

[42] H.K. Kim, S. Cho, D.H. Shin, K.S. Chung, Y.W. Cho, J.H. Choi, J.Y. Lee, K.T. Lee, T-type Ca2+ channel blocker, KYS05090 induces autophagy and apoptosis in A549 cells through inhibiting glucose uptake, Molecules 19 (2014) 9864–9875.

[43] B.S. Khakh, X.R. Bao, C. Labarca, H.A. Lester, Allosteric control of gating and kinetics at P2X(4) receptor channels, Nat. Neurosci. 2 (1999) 322–330.

[44] C. Virginio, A. MacKenzie, F.A. Rassendren, R.A. North, A. Surprenant, Pore dilation of neuronal P2X receptor channels, Nat. Neurosci. 2 (1999) 315–321.

[45] M.K. Chung, A.D. Güler, M.J. Caterina, TRPV1 shows dynamic ionic selectivity during agonist stimulation, Nat. Neurosci. 11 (2008) 555–564.

[46] L. Darré, S. Furini, C. Domene, Permeation and dynamics of an open-activated TRPV1 channel, J. Mol. Biol. 427 (2015) 537–549.

[47] M.K. Chung, A.D. Güler, M.J. Caterina, Biphasic currents evoked by chemical or thermal activation of the heat-gated ion channel, TRPV3, J. Biol. Chem. 280 (2005) 15928–15941.

[48] J. Chen, D. Kim, B.R. Bianchi, E.J. Cavanaugh, C.R. Faltynek, P.R. Kym, R.M. Reilly, Pore dilation occurs in TRPA1 but not in TRPM8 channels, Mol. Pain 5 (2009) 3.

[49] T.G. Banke, S.R. Chaplan, A.D. Wickenden, Dynamic changes in the TRPA1 selectivity filter lead to progressive but reversible pore dilation, Am. J. Physiol. Cell. Physiol. 298 (2010) C1457–C1468.

[50] Y. Karashima, J. Prenen, K. Talavera, A. Janssens, T. Voets, B. Nilius, Agonist-induced changes in Ca2+ permeation through the nociceptor cation channel TRPA1, Biophys. J. 98 (2010) 773–783.

[51] B.I. Yeh, Y.K. Kim, W. Jabbar, C.L. Huang, Conformational changes of pore helix coupled to gating of TRPV5 by protons, EMBO J. 24 (2005) 3224–3234.

[52] M. Liao, E. Cao, D. Julius, Y. Cheng, Structure of the TRPV1 ion channel determined by electron cryo-microscopy, Nature 504 (2013) 107–112.

[53] A.M. Binshtok, P. Gerner, S.B. Oh, M. Puopolo, S. Suzuki, D.P. Roberson, T. Herbert, C.F. Wang, D. Kim, G. Chung, A.A. Mitani, G.K. Wang, B.P. Bean, C.J. Woolf, Coapplication of lidocaine and the permanently charged sodium channel blocker QX-314 produces a long-lasting nociceptive blockade in rodents, Anesthesiology 111 (2009) 127–137.

[54] M. Puopolo, A.M. Binshtok, G.L. Yao, S.B. Oh, C.J. Woolf, B.P. Bean, Permeation and block of TRPV1 channels by the cationic lidocaine derivative QX-314, J. Neurophysiol. 109 (2013) 1704–1712.

[55] C.H. Munns, M.K. Chung, Y.E. Sanchez, L.M. Amzel, M.J. Caterina, Role of the outer pore domain in transient receptor potential vanilloid 1 dynamic permeability to large cations, J. Biol. Chem. 290 (2015) 5707–5724.

[56] M. Bandell, A.E. Dubin, M.J. Petrus, A. Orth, J. Mathur, S.W. Hwang, A. Patapoutian, High-throughput random mutagenesis screen reveals TRPM8 residues specifically required for activation by menthol, Nat. Neurosci. 9 (2006) 493–500.

[57] C.J. Bohlen, A. Priel, S. Zhou, D. King, J. Siemens, D. Julius, A bivalent tarantula toxin activates the capsaicin receptor, TRPV1, by targeting the outer pore domain, Cell 141 (2010) 834–845.

[58] E. Cao, M. Liao, Y. Cheng, D. Julius, TRPV1 structures in distinct conformations reveal activation mechanisms, Nature 504 (2013) 113–118.

[59] N.A. Hofmann, S. Barth, M. Waldeck-Weiermair, C. Klec, D. Strunk, R. Malli, W.F. Graier, TRPV1 mediates cellular uptake of anandamide and thus promotes endothelial cell proliferation and network-formation, Biol. Open 3 (2014) 1164–1172.

_____